Advances in Science, Technology & Innovation
IEREK Interdisciplinary Series for Sustainable Development

Attila Çiner · Stefan Grab · Etienne Jaillard · Domenico Doronzo · André Michard · Marina Rabineau · Helder I. Chaminé *Editors*

Recent Research on Geomorphology, Sedimentology, Marine Geosciences and Geochemistry

Proceedings of the 2nd Springer Conference of the Arabian Journal of Geosciences (CAJG-2), Tunisia 2019

IEREK
RESEARCH & KNOWLEDGE ENRICHMENT

Springer

Advances in Science, Technology & Innovation

IEREK Interdisciplinary Series for Sustainable Development

Advances in Science, Technology & Innovation (ASTI) is a series of peer-reviewed books based on important emerging research that redefines the current disciplinary boundaries in science, technology and innovation (STI) in order to develop integrated concepts for sustainable development. It not only discusses the progress made towards securing more resources, allocating smarter solutions, and rebalancing the relationship between nature and people, but also provides in-depth insights from comprehensive research that addresses the **17 sustainable development goals (SDGs)** as set out by the UN for 2030.

The series draws on the best research papers from various IEREK and other international conferences to promote the creation and development of viable solutions for a **sustainable future and a positive societal** transformation with the help of integrated and innovative science-based approaches. Including interdisciplinary contributions, it presents innovative approaches and highlights how they can best support both economic and sustainable development, through better use of data, more effective institutions, and global, local and individual action, for the welfare of all societies.

The series particularly features conceptual and empirical contributions from various interrelated fields of science, technology and innovation, with an emphasis on digital transformation, that focus on providing practical solutions to **ensure food, water and energy security to achieve the SDGs.** It also presents new case studies offering concrete examples of how to resolve sustainable urbanization and environmental issues in different regions of the world.

The series is intended for professionals in research and teaching, consultancies and industry, and government and international organizations. Published in collaboration with IEREK, the Springer ASTI series will acquaint readers with essential new studies in STI for sustainable development.

ASTI series has now been accepted for Scopus (September 2020). All content published in this series will start appearing on the Scopus site in early 2021.

More information about this series at https://link.springer.com/bookseries/15883

Attila Çiner · Stefan Grab · Etienne Jaillard · Domenico Doronzo · André Michard · Marina Rabineau · Helder I. Chaminé
Editors

Recent Research on Geomorphology, Sedimentology, Marine Geosciences and Geochemistry

Proceedings of the 2nd Springer Conference of the Arabian Journal of Geosciences (CAJG-2), Tunisia 2019

Springer

Editors
Attila Çiner
Eurasia Institute of Earth Sciences
Istanbul Technical University
Istanbul, Turkey

Etienne Jaillard
Université Grenoble Alpes
Grenoble, France

André Michard
Paris-Sud University
Paris-Sud, France

Helder I. Chaminé
Lab of Cartography and Applied Geology
School of Engineering
Instituto Superior de Engenharia do Porto
Polytechnic of Porto
Porto, Portugal

Stefan Grab
School of Geography, Archaeology
and Environmental Studies
University of the Witwatersrand (WITS)
Johannesburg, South Africa

Domenico Doronzo
Istituto Nazionale di Geofisica e Vulcanologia
Rome, Italy

Marina Rabineau
Laboratoire Géosciences Océan, Institut
Universitaire Européen de la Mer
Université Bretagne-Sud
CNRS, Univ Brest
Plouzané, France

ISSN 2522-8714 ISSN 2522-8722 (electronic)
Advances in Science, Technology & Innovation
IEREK Interdisciplinary Series for Sustainable Development
ISBN 978-3-030-72546-4 ISBN 978-3-030-72547-1 (eBook)
https://doi.org/10.1007/978-3-030-72547-1

About the 2nd Springer Conference of the Arabian Journal of Geosciences (CAJG-2), Tunisia 2019

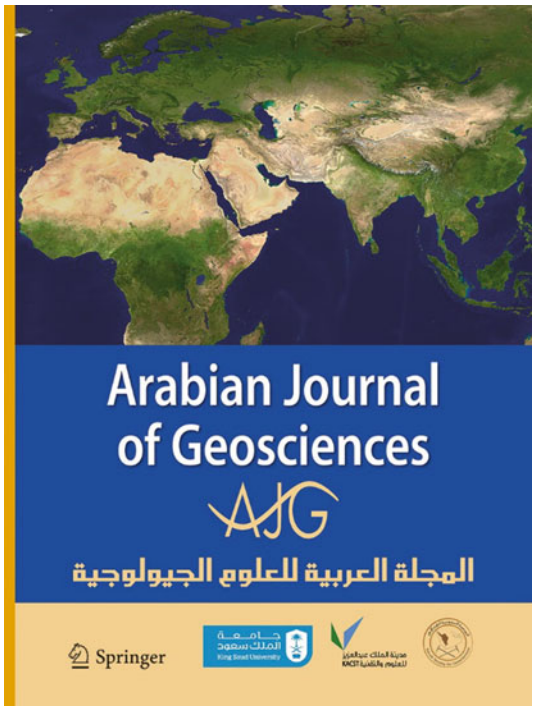

The Arabian Journal of Geosciences (AJG) is a Springer journal publishing original articles on the full range of Earth Sciences in partnership with the Saudi Society for Geosciences. The journal focuses on, but is not limited to, research themes which have regional significance for the Middle East, the Euro-Mediterranean, Africa, Asia and some other regions of the world. The journal receives on average 4000 submissions a year and accepts around 1000 papers for publication in its 24 annual issues (acceptance rate around 25%). It benefits from the participation of an editorial team of 100 international Associate Editors who generously help in evaluating and selecting the best papers.

In 2008, Prof. Abdullah Al-Amri, in close partnership with Springer, founded the Arabian Journal of Geosciences (AJGS). In 2018, the journal celebrated its 10th anniversary. To mark the event, the founder and Editor-in-Chief of the AJGS organized the 1st Conference of the Arabian Journal of Geosciences (CAJG) in close collaboration with Springer on 12–15 November 2018. The conference was an occasion to endorse the journal's long-held reputation and brought together 450 authors from 70 countries, who work in the wide-ranging fields of Earth Sciences. The dynamic 4-day conference in a stimulating environment in Hammamet, Tunisia, provided attendees with opportunities to share their latest unpublished findings and learn about the latest geosciences studies. The event also allowed attendees to meet and talk to

the journal's editors and reviewers. Three field trips were organized alongside the conference, and many participants enjoyed the wonders of the geology of Tunisia.

In a continuation of the successful 1st CAJG, the 2019's conference aimed to bring geoscientists from all over the world to present and discuss their most recent findings. The 2nd CAJG was an occasion to publish the newest findings in its proceedings by Springer and a special issue in the AJGS, with a clear mission to drive greater North–South (Europe–Africa) scientific cooperation and to open doors to new and enriching collaborations with geoscientists based in Asia and the Americas. The 2nd CAJG devoted a special session (workshop) to studies focusing on unraveling the undiscovered oil and gas resources in the Mediterranean and North Africa. Many international experts took part in the discussion.

The conference covered all cross-cutting themes of geosciences and focused principally on the following 15 tracks:

- Track 1. Atmospheric Sciences, Meteorology, Climatology, Oceanography
- Track 2. Biogeochemistry, Geobiology, Geoecology, Geoagronomy
- Track 3. Earthquake Seismology and Geodesy
- Track 4. Environmental Earth Sciences
- Track 5. Exploration & Theoretical Geophysics, Seismic & Well Logging Methods, Mathematical Geosciences
- Track 6. Geo-Informatics and Remote Sensing
- Track 7. Geochemistry, Mineralogy, Petrology, Volcanology
- Track 8. Geological Engineering, Geotechnical Engineering
- Track 9. Geomorphology, Geography, Soil Science, Glaciology, Geoarchaeology, Geoheritage
- Track 10. Hydrology, Hydrogeology, Hydrochemistry
- Track 11. Marine Geosciences, Historical Geology, Paleoceanography, Paleoclimatology
- Track 12. Numerical and Analytical Methods in Mining Sciences and Geomechanics
- Track 13. Petroleum and Energy Engineering, Petroleum Geochemistry
- Track 14. Sedimentology, Stratigraphy, Paleontology, Geochronology
- Track 15. Structural Geology, Tectonics and Geodynamics, Petroleum Geology

The dynamic 4-day conference provided more than 400 attendees with opportunities to share their latest unpublished findings and learn the newest geosciences studies. The event also allowed attendees to meet and discuss with the journal's editors and reviewers.

More than 710 short contributing papers to the conference were submitted by authors from more than 74 countries. After a pre-conference peer-review process by more than 500 reviewers, 462 papers were accepted. These papers are published as chapters in the conference proceedings which consists of four edited volumes, each edited by the following group of Arabian Journal of Geosciences (AJGS) editors and other guest editors:

Proceedings Volume 1: New Prospects in Environmental Geosciences and Hydrogeosciences

Haroun Chenchouni: University of Tebessa, Tebessa, Algeria
Helder I. Chaminé: School of Engineering - ISEP, Polytechnic of Porto, Porto, Portugal
Md Firoz Khan: Department of Chemistry, Faculty of Science, University of Malaya, Kuala Lumpur, Malaysia
Broder J. Merkel: TUBAF, Freiberg, Germany
Zhihua Zhang: Shandong University, Jinan, China
Peiyue Li: School of Water and Environment, Chang'an University, Xi'an, China

Proceedings Volume 2: Advances in Geophysics, Tectonics and Petroleum Geosciences

Proceedings Volume 3: Recent Research on Geomorphology, Sedimentology, and Geochemistry

Proceedings Volume 4: Research developments in Geotechnics, Geo-Informatics and Remote Sensing

About the Conference Steering Committee

General Chair

Abdullah Al-Amri
Founder and Editor-in-Chief
Arabian Journal of Geosciences
King Saud University, Saudi Arabia

Conference Supervisor

Nabil Khélifi
Senior Publishing Editor, MENA program
Journal Publishing Manager
Arabian Journal of Geosciences
Springer, a part of Springer Nature, Germany

Advisory Co-chair

Walter D. Mooney
Guest of Editorial Board
Arabian Journal of Geosciences
United States Geological Survey Western Region, USA

Advisory Co-chair

Dorrik Stow
Guest of Editorial Board
Arabian Journal of Geosciences
Heriot-Watt University, Edinburgh, Scotland

Scientific Committee Co-chair

François Roure
Chief Editor—Track 15
Arabian Journal of Geosciences
IFP—Energies Nouvelles, France

Scientific Committee Co-chair

Biswajeet Pradhan
Chief Editor—Track 6
Arabian Journal of Geosciences
University of Technology Sydney, Australia

Local Organizing Co-chair

Mohamed Soussi
Former Associate Editor
Arabian Journal of Geosciences
Tunis El Manar University, Tunis, Tunisia

Local Organizing Co-chair

Samir Bouaziz
Former Associate Editor
Arabian Journal of Geosciences
University of Sfax, Sfax, Tunisia

Publications Co-chair

Beatriz Bádenas
Chief Editor—Track 14
Arabian Journal of Geosciences
University of Zaragoza, Zaragoza, Spain

Publications Co-chair

Marina Rabineau
Chief Editor—Track 11
Arabian Journal of Geosciences
University of Brest, Brest, France

Program Co-chair

Amjad Kallel
Chief Editor—Track 4
Arabian Journal of Geosciences
ENIS, University of Sfax, Tunisia

Program Co-chair

Sami Khomsi
Former Associate Editor
Arabian Journal of Geosciences
King Abdulaziz University, Jeddah, Saudi Arabia

Proceedings Editorial Manager

Mourad Amer
Editor of Springer/IEREK ASTI Series
Guest of Editorial Board of AJGS
IEREK, Alexandria, Egypt

Communication Chair

Zakaria Hamimi
Associate Editor
Arabian Journal of Geosciences
Benha University, Benha, Egypt

Public Relations Chair

Faïez Gargouri
Director of the Higher Institute of Computer Science and Multimedia
President of the AIG
University of Sfax, Tunisia

Conference Manager

Mohamed Sahbi Moalla
Journal Coordinator
Arabian Journal of Geosciences
ISET, University of Sfax, Tunisia

Preface

This proceedings volume is based on 84 papers accepted and presented during the 2nd Springer Conference of the Arabian Journal of Geosciences (CAJG-2), Tunisia 2019. Major subjects treated in the volume include geomorphology, sedimentology and geochemistry. The volume presents an updated unique view in conjugating field studies and modeling to better quantify the process-product binomial unusual in geosciences. Earth systems requires a comprehensive understanding on processes and dynamics of geology, morphotectonics, sedimentology, stratigraphy and geochemistry. In the geomorphology section, 24 papers deal with topics related to fault slip and incision rates, soil science, landslides and debris flows, coastal processes, and geoarcheology and geoheritage. Under the Sedimentology section, 34 papers including stratigraphy, and environmental, tectonic and diagenetic processes, together with evolutionary, biostratigraphic and paleoenvironmental significance of paleontology are presented. Additionally, this section also contains papers on marine geosciences, from molecular proxies related to climate to geophysical surveys. Last but not least, the third section on geochemistry is composed of 26 papers that are focused on sedimentary geochemistry and mineralogical characterization, magmatic and metamorphic processes and products, and the origin and exploration of mineral deposits. This volume resumes the current situation related to the abovementioned topics mainly in the Mediterranean realm. Although more than half of the contributions come from North African countries, especially from Tunisia, other Mediterranean countries such as Turkey and Italy also actively participated in the development of this volume, testifying the geological importance of this area and surroundings. The volume is of interest to all researchers, practitioners and students in the fields of geomorphology, sedimentology, geochemistry, as well as those engaged in environmental geosciences, soil science, stratigraphy and paleontology, geoarcheology and geoheritage, marine geosciences, petrology, metallogenesis and mineral deposits.

İstanbul, Turkey — Attila Çiner
Johannesburg, South Africa — Stefan Grab
Grenoble, France — Etienne Jaillard
Naples, Italy — Domenico Doronzo
Paris, France — André Michard
Brest, France — Marina Rabineau
Porto, Portugal — Helder I. Chaminé
July 2020

Contents

About the Editors

Attila Çiner is a professor of sedimentology and quaternary geology and director of the Eurasia Institute of Earth Sciences at Istanbul Technical University, Turkey. After graduating from Middle East Technical University in Ankara (1985), he obtained his MSc degree at the University of Toledo, USA (1988) and his Ph.D. at the University of Strasbourg, France (1992). He works on the tectono-sedimentary evolution of basins and uses a process-oriented approach in order to understand the depositional environments. He also works on quaternary depositional systems such as moraines, fluvial terraces, alluvial fans and deltas, where he uses cosmogenic nuclides to date related deposits. He is mostly concentrated on the glacial deposits and landscapes and tries to understand paleoclimatic and paleoenvironmental changes since the Last Glacial Maximum. His main research fields are based in the Taurus Mountains of Turkey, Bosnia, Indonesia, Greece, Tunisia, Chile and Argentina. Lastly, he was part of the Turkish Antarctic Expedition where he spent two months to work on the site recognition and decision of the future Turkish scientific research station to be implemented on the continent. He has published more than 100 peer-reviewed articles and book chapters.

Stefan Grab Swiss by birth but grew up in Pietermaritzburg, South Africa. Studied geomorphology at the University of Natal with specialization in periglacial geomorphology. Today works in both geomorphology and historical climate change sectors. Research regions include southern and eastern Africa, the mid-Atlantic and Iran (Middle East).

Etienne Jaillard is senior researcher at the French « Institut de Recherche pour le Développement » (IRD). He is specialized in sedimentary geology and uses it for understanding continental margins and their geodynamic setting. He worked about 5 years in the Western Alps, 20 years in the Andes, and since about 20 years, he studies sedimentation, tectonics and paleoenvironments in North Africa. He is the author of about 70 international publications and contributed to the redaction of several books.

Dr. Domenico Doronzo holds a B.Sc., a M.Sc. and a Ph.D. degree (in 2011) in Earth Sciences from Università degli Studi di Bari Aldo Moro, Italy. Theses and specialties related to the degrees are physical volcanology, experimental and computational fluid dynamics, petrology, and natural hazards. Then he has worked in volcanology and sedimentology, fluid dynamics and combustion, environmental sciences and rock physics in the USA, Mexico, Spain and Italy. He is currently a contract researcher at National Institute of Geophysics and Volcanology, Italy. Particularly, he has received the Rittmann Medal (in 2014) from Associazione Italiana di Vulcanologia and Istituto Nazionale di Geofisica e Vulcanologia, which is assigned to the best young Italian volcanologist. His research interests focus on integrating theory, field, numerical modeling, experiments and laboratory to study geological processes and products in volcanic areas (Vulcano, Vesuvio, Campi Flegrei, Etna, Colli Albani, Tenerife, Altiplano Puna, Colima) from fluid dynamic and natural hazard perspectives. Particularly, he studies pyroclastic energy currents, pre-eruptive conditions, debris flows, flow-building interactions, sand and dust storms, turbidity currents, man-made environmental phenomena and georesources. He has edited the CAJG-1 proceedings on Petrogenesis and Exploration of the Earth's Interior. He is a Chief Editor of the *Arabian Journal of Geosciences* responsible for evaluating submissions in the fields of geochemistry, mineralogy, petrology and volcanology.

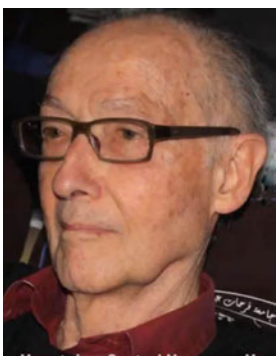

André Michard is a graduate of the Ecole Normale Supérieure, holder of the Agrégation of Natural Sciences (1955) and of a Doctorate in Earth Sciences from the University of Paris Sorbonne (1966). He is an emeritus professor from the University of Paris-Sud (Orsay) since 1999. He began his academic career in the latter university, just launched, in 1958, after a Ph.D. thesis in the Western Alps, and kept working in the Alpine belts (Alps, Oman, Taurus, Cuba) until the early 2000's. André discovered Morocco in 1966 as a professor at Mohamed-V University, Rabat, and immediately fall in love of the geology of the country. His first works concerned the Variscan metamorphic domains of the Western Meseta. Once appointed professor at the University of Strasbourg (1968), André extended his Moroccan works to the Rif belt in

connection with the Spanish geologists of the Betics. He published a first overview of Moroccan Geology in 1976 ("Eléments de Géologie marocaine"; 3d edition in 2001, also translated in Japanese), and a second one, co-authored by a large panel of Moroccan or European specialists, in 2008 ("Continental evolution: the Geology of Morocco"). In the meanwhile, André collaborated with several Moroccan academics in research programs targeting the High Atlas, Anti-Atlas and the Saharan domains. Based on this experience, he was the linchpin of the editing program of the "Nouveaux Guides géologiques et Miniers du Maroc" (2011, vol. 1–9). In the last decade, André co-authored also some 20 articles dealing with the structural geology, geodynamics, stratigraphy, paleontology or geoheritage of the various regions of Morocco. From the beginning of his academic activity, he has contributed more than a hundred articles published in prestigious international journals. The first West African Craton and Margins International Workshop (Dakhla, Apr. 2017) has been dedicated to André as a tribute for his jubilee of works in Morocco.

Marina Rabineau Education and Experience:
2017–2021 Co-chair of Laboratory LGO (100 persons)
2018-present Director of Research CNRS; Chief Editor of Arabian Journal of Geosciences "Marine Geosciences")
2001–2017 Researcher CNRS Marine Sedimentology, Plouzané
2014 Diplôme Habilitation à diriger des Recherches, Université de Brest
2001 Ph.D. in Marine Sedimentology IFREMER-Université de Rennes1 IFP
1996–1997 Research Engineer at IFP, Rueil-Malmaison
1995 Master of Science, « Petroleum Geoscience », Imperial College, London
1994 Diplôme d'Ingénieur de l'Ecole Nationale Supérieure de Géologie de Nancy

Research Interests & Expertises:
My research interests are centered on the sedimentary archives on margins. Sediments record the imprint of climate, (glacio)-eustatic cycles and vertical tectonic movements through the fluxes of materials from both land and sea. A complete decoding of the archives holds key information to understand climate, geodynamics but also ecosystem evolution. My expertise are in sedimentology, seismic and sequence stratigraphy (core description, seismic interpretation, core-log-seismic integration) and numerical stratigraphic simulation at different scales in order to understand deep earth and surface process interactions.

Helder I. Chaminé is a skilled Geologist and Professor of Engineering Geosciences at School of Engineering (ISEP) of the Polytechnic of Porto, with over 29 years' experience in multidisciplinary geosciences research, consultancy and practice. He studied geological engineering and geology (B.Sc., 1990) at the Universities of Aveiro and Porto (Portugal), respectively. He received his Ph.D. in geology at the University of Porto in 2000 and spent his postdoctoral research in applied geosciences at the University of Aveiro (2001–2003). In 2011, he received his Habilitation (D.Sc.) in geosciences from Aveiro University. Before joining academy, he worked over a decade in international projects for mining, geotechnics and groundwater industry and/or academia related to geodynamics and regional geology, hard-rock hydrogeology and water resources, engineering geosciences and applied geomorphology, rock engineering and georesources. His research interests span over fundamental to applied fields: GIS mapping techniques for applied geology, structural geology and regional geology, engineering geosciences and rock engineering, slope geotechnics, mining geology and hydrogeomechanics, hard-rock hydrogeology, exploration hydrogeology, urban groundwater and hydromineral resources. He has interests on mining geoheritage, history of cartography, military geosciences and higher-education dissemination, skills and core values. Presently, he is Head of the Laboratory of Cartography and Applied Geology (LABCARGA | ISEP), Senior Researcher at Centre GeoBioTec | U.Aveiro and Centre IDL | U.Lisbon, as well as belongs to the executive board of the M.Sc.+B.Sc. Geotechnical and Geoenvironmental Engineering (OE +EUR-ACE Label) and the Department of Geotechnical Engineering (ISEP). Currently, he belongs to the board of the Portuguese Geotechnical Society (SPG) and IAH—Portuguese Chapter. He was a board member of the APGeom—Portuguese Association of Geomorphologists (2009–2013). He was consultant and or responsible over 70 projects of rock engineering, applied geology, hydrogeomechanics, slope geotechnics, mining geology, exploration hydrogeology, hard-rock hydrogeology, water resources, urban groundwater and applied mapping (Mozambique, Portugal, and Spain). He has been co-authored over 200 publications in indexed journals, conference proceedings/full papers, book chapters, technical and professional papers. He co-edited over 13 special volumes, as well as is presently evolved in editing themed issues for three international journals (Geotechnical Research ICE, Springer Nature Applied Sciences, Water MDPI). He has a wide activity as a referee for several international journals. He served as invited Expert Evaluator of Bologna Geoscience program for DGES (Portugal) and Scientific Projects Evaluation for NCST, 2017–2019 (Kazakhstan) and NRF | RISA, 2019 (South Africa), as well as Coordinator of "Geology on Summer/ Ciência Viva" program at ISEP, since 2005, for geosciences dissemination. He has been also active with teaching and

supervising of many Ph.D., M.Sc. and undergraduate students. He has been on the editorial board, among others, of *Arabian Journal of Geosciences* (SSG+Springer), *Hydrogeology Journal* (IAH+Springer), *Euro-Mediterranean Journal for Environmental Integration* (Springer), *Springer Nature Applied Sciences* (Springer), *Mediterranean Geoscience Reviews* (Springer), *Geotechnical Research* (ICE), *Geosciences* (MDPI), *Revista Geotecnia* (Portugal), and *Geología Aplicada a la Ingeniería y al Ambiente* (Argentina). He integrates as moderator or session chair in several conferences, workshops and meetings. Currently, is Co-chair of the International Conference "Geoethics and Groundwater Management" (IAH +IAPG, Porto, May 2020) and in organizing/scientific committee of the 3rd International Workshop on Natural Hazards—NATHAZ'21 (Terceira Island, Azores, May 2021).

Geomorphology, Soil Science, Landslides, Coastal Processes, and Geoarchaeology (T9): Geomorphology: Fault Slip and Incision Rates

Cosmogenic Surface Exposure Dating Applications from Turkey; Moraines, Alluvial Fans, Fluvial Terraces, Lava Flows and Incision Rates

Attila Çiner, M. Akif Sarıkaya, and Cengiz Yıldırım

Abstract

We report our work carried out in Turkey, where various Quaternary surfaces and deposits were dated using the cosmogenic surface exposure method. Our most important applications are related to boulders collected from moraines, as they can be used to reconstruct glacier fluctuations and palaeoclimates. We have dated moraines in numerous mountains, mainly within the Taurus Mountain Range along the Mediterranean coastline, where the deposits were primarily formed during the Last Glacial Maximum (LGM; ~20 ka) and to a lesser extent during pre-LGM (~50 ka), Younger Dryas (~12 ka) and the Early Holocene (~10 ka). We also used this method to determine the timing of the abandonment/incision of alluvial fan lobes that were later cut and displaced by the left lateral strike-slip of the Ecemiş Fault. The timing of surface breaking and slip and extension rates were also calculated, permitting the evaluation of the role of these structures in terms of the regional tectonic framework. In another study, abandonment ages of river terraces based on burial and isochron-burial dating with cosmogenic ^{10}Be and ^{26}Al yielded the long-term incision rate of the Kızılırmak River (51 m/Ma since 1.9 Ma) as a proxy for the rock uplift and the long-term denudation rate of the Central Anatolia Plateau. Last but not least, by using cosmogenic nuclides, we were able to date basaltic lava flows (~5 to 10 ka) and calculate erosion rates of peculiar landforms locally known as "fairy chimneys" in Cappadocia.

Keywords

Cosmogenic surface dating • Moraines • Alluvial fans • Fluvial and marine terraces • Turkey

A. Çiner (✉) · M. A. Sarıkaya · C. Yıldırım
Eurasia Institute of Earth Sciences, Istanbul Technical University, Maslak, Istanbul, Turkey
e-mail: cinert@itu.edu.tr

1 Introduction

Increasing use of cosmogenic surface exposure dating methods in geomorphology and geology enables us to understand better the duration and extent of geomorphic processes. The exponential increase in the number of publications in high-impact journals that apply this methodology is clear evidence of its utility and necessity. For more than 15 years, we have used this methodology on several Quaternary surfaces and deposits in Turkey. Our aim is to summarise the work we carried out on different Quaternary environments, particularly in Turkey, and give very brief results from these studies.

2 Methods

Cosmogenic surface exposure dating methods are based on in situ accumulation of rare nuclides in rocks exposed to cosmic radiation. Depending on the type of cosmic ray particle and target elements in the rock, many new cosmogenic nuclides can be produced, such as radioactive ^{10}Be, ^{26}Al and ^{36}Cl. Because the production rates of these nuclides are known, their measured concentrations in rocks can be used to calculate how long these rocks were exposed at the surface (Gosse and Phillips 2001).

3 Results

3.1 Glacial Deposits and Surfaces

A glacier that flows in a valley will erode the bedrock and carry these unsorted sediments to finally deposit them to form moraines once the climate gets warmer. As the fresh boulders are exposed to cosmic radiation, nuclides will accumulate on these deposits, and the cosmogenic clock will start. We used in situ accumulation of cosmogenic nuclides

A. Çiner et al. (eds.), *Recent Research on Geomorphology, Sedimentology, Marine Geosciences and Geochemistry*, Advances in Science, Technology & Innovation, https://doi.org/10.1007/978-3-030-72547-1_1

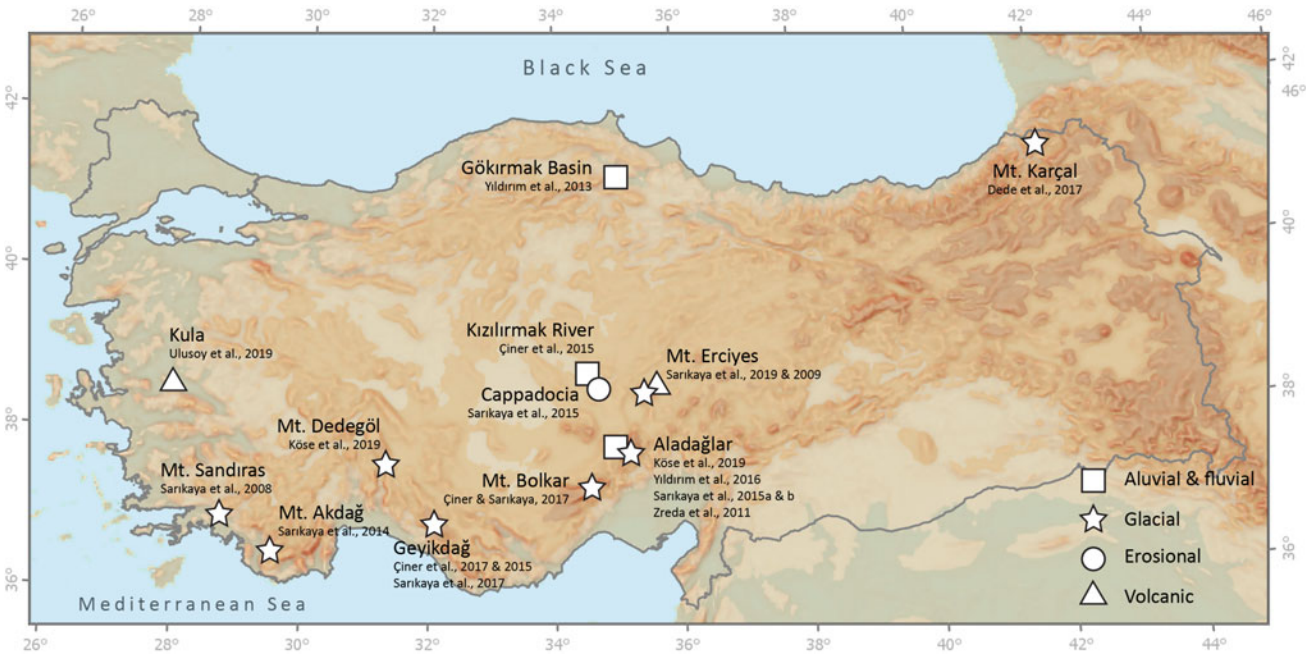

Fig. 1 Location of our study sites where cosmogenic surface dating methods were applied in Turkey

(^{36}Cl) to interpret glacial chronologies in carbonate-rich areas in the Taurus Mountain Range along the eastern Mediterranean coast of Turkey (e.g., Sarıkaya et al. 2011; Sarıkaya and Çiner 2015, 2017, 2019) (Figs. 1 and 2).

The oldest geochronological data from the region indicate glaciations before the LGM (pre-LGM). These glaciers probably developed during the beginning of the last glaciation (Marine Isotope Stage (MIS) 4; around 71 ka) and stopped advancing at the end of MIS 3 (at 29–35 ka) in the Akdağ, Bolkardağ and Dedegöl mountains (Sarıkaya et al. 2014; Çiner and Sarıkaya 2017; Köse et al. 2019). Later, glaciers reached their most extensive positions during MIS 2 (after 29 ka), particularly between 21.5 and 18.5 ka, synchronous with the global LGM. Indeed the LGM record of the Taurus Mountain Range is now clearly defined (e.g., Sarıkaya et al. 2008, 2014; Çiner et al. 2015a, 2018a). After the LGM, glaciers started to retreat to less extensive positions. They deposited their moraines in Geyikdağ and Aladağlar mountains during the Late-Glacial (~16 to 15 ka) and Younger Dryas (~12 ka) (e.g., Sarıkaya et al. 2017). Although few, Early Holocene glaciations were also reported (Zreda et al. 2011). Besides moraines, a rock glacier that we dated in Mount Geyikdağ yielded results that signal the importance of inheritance on such landforms (Çiner et al. 2017).

We also dated moraines on one of the biggest volcanoes of Turkey, Mount Erciyes (3917 m), and obtained ages that range from the LGM to Middle Holocene (Sarıkaya et al. 2009). Another non-carbonate lithology that we dated by using cosmogenic ^{36}Cl yielded the first LGM glaciation results (~20 ka) and Late-Glacial (~16 ka) rock glacier development in the Lesser Caucasus Mountains, near the border with Georgia (Dede et al. 2017). As rock glaciers provide the most reliable information on palaeo-permafrost conditions, they are more and more described and dated in high mountain areas in Turkey (see Oliva et al. 2018 for a Mediterranean perspective).

3.2 Alluvial Fans, Landslides and Faults

Another important application of the cosmogenic surface dating method was carried out on alluvial fans, where we dated the paraglacial Ecemiş River drainages on the Aladağlar Mountains to obtain the timing of alluvial fan abandonment/incision and to unravel the role of tectonic and climatic processes (Fig. 1). Our results yielded alluvial fan ages, obtained from boulders standing on the fan surface, which change between ~81 and ~136 ka, implying that they were deposited from palaeoglacier outwash during cold intervals, and, later, when glaciers started to retreat because of warming, the water released from the glaciers incised the pre-existing fan surfaces (Sarıkaya et al. 2015a, b).

These alluvial fans were later offset by the major strike-slip Ecemiş Fault Zone. From the dates we obtained, we calculated the vertical displacement, and slip and extension rate of this fault zone. Our results indicate that several fault segments deformed alluvial fan (~104 ka), moraine (~22 ka) and landslide (~81 ka) surfaces (Yıldırım et al. 2016). Accordingly, we can suggest ~1 mm/year slip rate and 0.6 mm/year extension rate for the last 104 ka, and

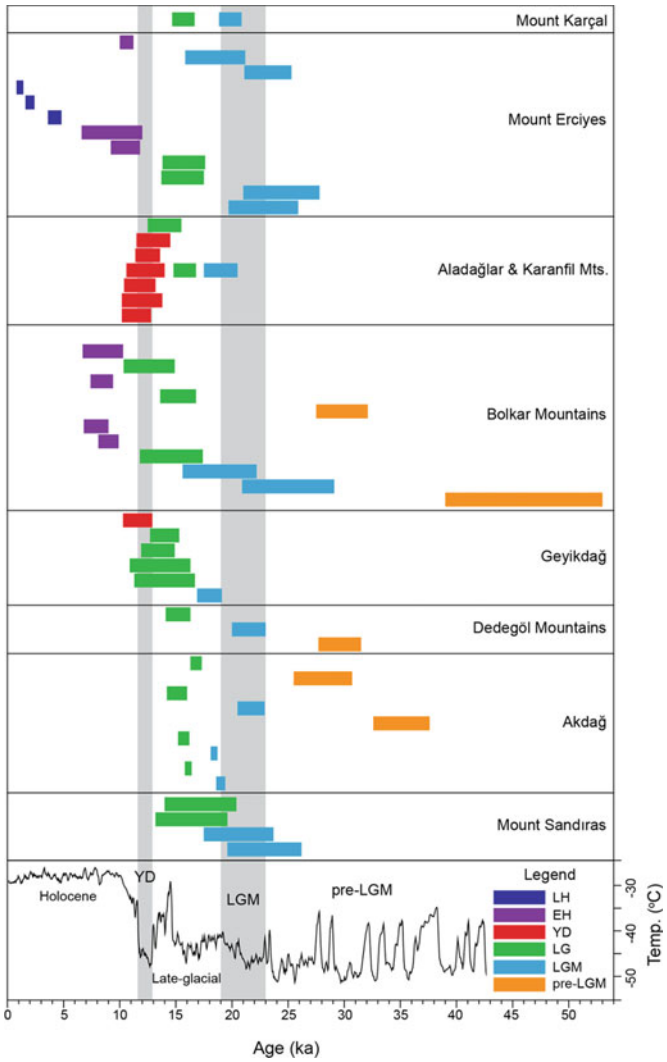

Fig. 2 Correlation of glacial chronologies in Turkey. Although only our dated sites are shown here, several works especially in the Black Sea Range (e.g., Akçar et al. 2007; Reber et al. 2014) and Mount Uludağ (Zahno et al. 2010) also confirm the presence of extensive LGM glaciation in Turkey. Reconstructed air temperatures from the Greenland Ice Sheet Project 2 ice core (Alley 2000) are shown on the bottom. The colour-coded bars reflect the age range of individual moraines from original publications, except for Sandıras, Dedegöl, Aladağlar and Erciyes mountains. We recalculated these ages based on up-to-date cosmogenic production rates by Marrero (2012). Horizontal grey shaded bars are the time frames for the LGM (19–23 ka; Mix et al. 2001) and Younger Dryas stadial (YD; 11.7–12.9 ka; Broecker et al. 2010). LH: Late Holocene, EH: Early Holocene

0.6 mm/year slip rate and 0.35 mm/year extension rate for the last 22 ka.

3.3 Fluvial Terraces

Cosmogenic nuclides are also extensively used for dating fluvial terraces. We dated the terraces of the Kızılırmak River in Cappadocia by using cosmogenic burial, isochron-burial, depth-profile and surface exposure dating methods with ^{10}Be, ^{26}Al and ^{36}Cl. A total of seven terraces indicate an average incision rate, equated to surface uplift, of 51 m/Ma since ~1.9 Ma (Çiner et al. 2015b) (Fig. 1). Additionally, along the northern margin of the Central Anatolian Plateau, fluvial terraces and pediment surfaces along the Gökırmak River, a subsidiary to Kızılırmak yielded average fluvial incision rates of 280 m/Ma over the past ~350 ka (Yıldırım et al. 2013).

3.4 Lava Flows

Although with some difficulties related to nucleogenic Chlorine contamination originating from magma, lava flows can be also dated by this method. We dated several young rhyodacite lava domes with clear exposure histories but unknown ages around Erciyes Volcano in central Turkey (Sarıkaya et al. 2019). Our results suggest an Early Holocene

(~7 to 10 ka) volcanic activity, which is also confirmed by ^{14}C age (9.7 ± 0.1 ka cal B.P) that we obtained from charcoal found in a pyroclastic flow deposit.

The Çakallar Volcano in Kula, western Turkey, is another site where cosmogenic ^{36}Cl dating (~5 ka) yielded exciting results. Prehistoric human footprints in hydrovolcanic ash near the volcano undoubtedly place the Çakallar eruption and prehistoric human footprints into the Bronze Age (Ulusoy et al. 2019).

3.5 Erosion Rates

The Cappadocia region is famous for its unique volcanic landscape and unusual rock formations. The landscape evolution starts with gently sloping plateaus, which are later dissected following the cooling fractures, to form mushroom-like structures locally known as "fairy chimneys" (Çiner and Aydar 2019). We have determined the bedrock erosion rates of the three most important stages by using cosmogenic ^{36}Cl isotopes on ignimbrites; pre-chimney (plateaus), chimney and post-chimney stages. Our results indicate that the plateaus erode at a very low rate 0.58 to 0.93 cm/ky (ky = thousand years). When dissection of a plateau starts, the erosion rate increases up to about 4.5 cm/ky. The chimneys caps have erosion rates between ~ 3.3 cm/ky, and once the chimneys disappear, erosion rates increase significantly to 28 cm/ky (Sarıkaya et al. 2015c).

4 Conclusions

Our dating efforts on Quaternary landforms and surfaces in Turkey will continue. Over the last 15 years, we concentrated our work on the dating of moraines to understand the Turkish Mountains' glacial chronologies. Now that this task is well advanced and in places accomplished, we turned towards other countries where glacial deposits require further attention. Our recent works in Patagonia (Çiner et al. 2018b, 2019a), Bosnia and Herzegovina (Çiner et al. 2019b; Žebre et al. 2019) and Antarctic Peninsula (Çiner et al. 2019c) are the first attempts of this endeavour. In the future, we also plan to use this methodology on other promising areas such as fault scarps, archaeological sites and marine terraces.

References

Akçar, N., Yavuz, V., Ivy-Ochs, S., Kubik, P.W., Vardar, M., Schluchter, C.: Paleoglacial records from Kavron Valley, NE Turkey: field and cosmogenic exposure dating evidence. Quat. Int. **164–165**, 170–183 (2007)

Alley, R.B.: The Younger Dryas cold interval as viewed from central Greenland. Quat. Sci. Rev. **19**, 213–226 (2000)

Broecker, W.S., Denton, G.H., Edwards, R.L., Cheng, H., Alley, R.B., Putnam, A.E.: Putting the Younger Dryas cold event into context. Quat. Sci. Rev. 1078–1081 (2010)

Çiner, A., Aydar, E.: A fascinating gift from volcanoes: the fairy chimneys and underground cities of Cappadocia. In: Kuzucuoğlu, C., Çiner, A., Kazancı, N. (eds.) Landforms and Landscapes of Turkey. World Geomorphological Landscapes Series, pp. 535–549. Migon, P. (ed.). Springer, Berlin. https://doi.org/10.1007/978-3-030-03515-0_31(2019)

Çiner, A., Doğan, U., Yıldırım, C., Akçar, N., Ivy-Ochs, S., Alfimov, V., Kubik, P.W., Schlüchter, C.: Quaternary uplift rates of the Central Anatolian Plateau, Turkey: insights from cosmogenic isochron-burial nuclide dating of the Kızılırmak River terraces. Quat. Sci. Rev. **107**, 81–97 (2015)

Çiner, A., Köse, O., Sarıkaya, M.A., Yıldırım, C., Candaş, A., Wilcken, K.: Late Pleistocene cosmogenic ^{36}Cl glacial chronology of the Mount Karanfil, Central Taurus Range, Turkey. In: AGU Conference, Washington D.C., 408727 (2018a)

Çiner, A., Sarıkaya, M.A.: Cosmogenic ^{36}Cl geochronology of Late Quaternary glaciers on the Bolkar Mountains, south central Turkey. In: Hughes, P., Woodward, J. (eds.) Quaternary Glaciation in the Mediterranean Mountains, vol. 433, pp. 271–287. Geological Society, London, Special Publications (2017)

Çiner, A., Sarıkaya, M.A., Todisco, D., Yıldırım, C., Girault, I. Martin, F., Borrero, L., Fabel, D.: Glacial chronology of erratic boulders on Cerro Benitez, Patagonia, Chile: implications for opening and megafauna colonization of the Mylodon Cave. International Union for Quaternary Research Conference Abstracts (INQUA) Dublin 28–31 July 2019, Ireland, p. 4476 (2019a)

Çiner, A., Sarıkaya, M.A., Yıldırım, C.: Late Pleistocene piedmont glaciations in the Eastern Mediterranean; insights from cosmogenic ^{36}Cl dating of hummocky moraines in southern Turkey. Quat. Sci. Rev. **116**, 44–56 (2015)

Çiner, A., Sarıkaya, M.A., Yıldırım, C.: Misleading old age on a young landform? The dilemma of cosmogenic inheritance in surface exposure dating: moraines vs. rock glaciers. Quat. Geochron. **42**, 76–88 (2017)

Çiner, A., Stepišnik, U., M.A., Sarıkaya, Žebre, M., Yıldırım, C.: Last Glacial Maximum and Younger Dryas piedmont glaciations in Blidinje, the Dinaric Mountains (Bosnia and Herzegovina); insights from ^{36}Cl cosmogenic dating. Mediterranean Geosci. Rev. **1**. https://doi.org/10.1007/s42990-019-0003-4(2019b)

Çiner, A., Todisco, D., Sarıkaya, M.A., Yıldırım, C., Girault, I., Martin, F., Borrero, L.A.: Chasing the erratic blocks of the last glacial maximum Patagonian ice sheet (Chile and Argentina); implications for the deglaciation, extinct megafauna land colonization and early human settlements. Turkish Quaternary Symposium (TURQUA), 2–5 May 2018, 50–51 (2018b)

Çiner, A., Yıldırım, C., Sarıkaya, M.A., Seong, Y.B., Yu, B.Y.: ^{10}Be cosmogenic dating of glacial erratic boulders on Horseshoe Island in western Antarctic Peninsula confirms rapid deglaciation in Early Holocene. Antarct. Sci. **31**(6), 319–331 (2019). https://doi.org/10.1017/S0954102019000439

Dede, V., Çiçek, İ, Sarıkaya, M.A., Çiner, A., Uncu, L.: First cosmogenic geochronology from the Lesser Caucasus: Late Pleistocene glaciation and rock glacier development in the Karçal Valley, NE Turkey. Quat. Sci. Rev. **164**, 54–67 (2017)

Gosse, J.C., Phillips, F.M.: Terrestrial in situ cosmogenic nuclides: theory and application. Quat. Sci. Rev. **20**(14), 1475–1560 (2001)

Köse, O., Sarıkaya, M.A., Çiner, A., Candaş, A.: Late Quaternary glaciations and cosmogenic 36Cl geochronology of Mount Dedegöl, Taurus Mountains, Turkey. J. Quat. Sci. **34**(1), 51–69 (2019). https://doi.org/10.1002/jqs.3080

Marrero, S.: Calibration of Cosmogenic Chlorine-36, Earth and Environmental Science, p. 365. New Mexico Ins of Mining and Techno, Socorro, New Mexico (2012)

Mix, A., Bard, A., Schneider, R.: Environmental processes of the ice age, land, oceans, glaciers (EPILOG). Quat. Sci. Rev. **20**, 627–657 (2001)

Oliva, M., et al.: The existence of permafrost conditions in the Mediterranean basin since the Last Glaciation. Earth-Sci. Rev. **185**, 397–436 (2018)

Reber, R., Akçar, N., Yesilyurt, S., Yavuz, V., Tikhomirov, D., Kubik, P.W., Schlüchter, C.: Glacier advances in northeastern Turkey before and during the global Last Glacial Maximum. Quat. Sci. Rev. **101**, 177–192 (2014)

Sarıkaya, M.A., Zreda, M., Çiner, A.: Glaciations and paleoclimate of Mount Erciyes, central Turkey, since the Last Glacial Maximum, inferred from ^{36}Cl cosmogenic dating and glacier modeling. Quat. Sci. Rev. **28**(23–24), 2326–2341 (2009)

Sarıkaya, M.A., Çiner, A.: Late Pleistocene glaciations and paleoclimate of Turkey. Bull. Mineral Res. Explor. **151**, 107–127 (2015)

Sarıkaya, M.A., Çiner, A.: The Late Quaternary glaciation in the Eastern Mediterranean. In: Hughes, P., Woodward, J. (eds.) Quaternary Glaciation in the Mediterranean Mountains, vol. 433, pp. 289–305. Geological Society, London, Special Publications (2017)

Sarıkaya, M.A., Çiner, A.: Ice in paradise: glacial heritage landscapes of Anatolia. In: Kuzucuoğlu, C., Çiner, A., Kazancı, N. (eds.) Landforms and Landscapes of Turkey. World Geomorphological Landscapes, pp. 397–411. Springer, Berlin. doi:https://doi.org/10.1007/978-3-030-03515-0_20(2019)

Sarıkaya, M.A., Çiner, A., Haybat, H., Zreda, M.: An early advance of glaciers on Mount Akdağ, SW Turkey, before the global Last Glacial Maximum; insights from cosmogenic nuclides and glacier modeling. Quat. Sci. Rev. **88**, 96–109 (2014)

Sarıkaya, M.A., Çiner, A., Yıldırım, C.: Cosmogenic ^{36}Cl glacial chronologies of the Late Quaternary glaciers on Mount Geyikdağ in the Eastern Mediterranean. Quat. Geochron. **39**, 189–204 (2017)

Sarıkaya, M.A., Çiner, A., Zreda, M.: Quaternary glaciations of Turkey. In: Ehlers, J., Gibbard, P.L., Hughes, P.D. (eds.) Quaternary Glaciations-Extent and Chronology; A Closer Look, pp. 393–403. Elsevier Publications (2011)

Sarıkaya, M.A., Çiner, A., Zreda, M.: Fairy chimney erosion rates on Cappadocia ignimbrites: insights from cosmogenic nuclides. Geomorphology **234**, 182–191 (2015)

Sarıkaya, M.A., Çiner, A., Zreda, M., Şen, E., Ersoy, O.: Chlorine degassing constrained by cosmogenic ^{36}Cl and radiocarbon dating of early Holocene rhyodacitic lava domes of Erciyes Stratovolcano, central Turkey. J. Volcan. Geother. Res. **369**, 263–275 (2019). https://doi.org/10.1016/j.jvolgeores.2018.11.029

Sarıkaya, M.A., Yıldırım, C., Çiner, A.: Late Quaternary alluvial fans of Emli Valley in the Ecemiş Fault Zone, south central Turkey: insights from cosmogenic nuclides. Geomorphology **228**, 512–525 (2015)

Sarıkaya, M.A., Yıldırım, C., Çiner, A.: No surface breaking on Ecemiş Fault, central Turkey, since Late Pleistocene (64.5 ka); new geomorphic and geochronologic data from cosmogenic dating of offset alluvial fans. Tectonophysics **649**, 33–46 (2015)

Sarıkaya, M.A., Zreda, M., Çiner, A., Zweck, C.: Cold and wet Last glacial maximum on Mount Sandıras, SW Turkey, inferred from cosmogenic dating and glacier modeling. Quat. Sci. Rev. **27**(7–8), 769–780 (2008)

Ulusoy, İ, Sarıkaya, M.A., Schmitt, A., Şen, E., Danisik, M., Gümüş, E.: Volcanic eruption eye-witnessed and recorded by prehistoric humans. Quat. Sci. Rev. **212**, 187–198 (2019)

Yıldırım, C., Sarıkaya, M.A., Çiner, A.: Late Pleistocene intraplate extension of the Central Anatolian Plateau, Turkey: Inferences from cosmogenic exposure dating of alluvial fan, landslide and moraine surfaces along the Ecemiş Fault Zone. Tectonics 35. https://doi.org/10.1002/2015TC004038(2016)

Yıldırım, C., Schildgen, T., Echtler, H., Melnick, D., Strecker, M., Bookhagen, B., Çiner, A., Niederman, S., Merchel, S., Martschini, M., Steier, P., Strecker, M.R.: Tectonic implications of fluvial incision and pediment deformation at the northern margin of the Central Anatolian Plateau based on multiple cosmogenic nuclides. Tectonics **32**, 1–14 (2013)

Zahno, C., Akçar, N., Yavuz, V., Kubik, P.W., Schlüchter, C.: Chronology of Late Pleistocene glacier variations at the Uludağ Mountain, NW Turkey. Quat. Sci. Rev. **29**, 1173–1187 (2010)

Žebre, M., Sarıkaya, M.A., Stepišnik, U., Yıldırım, C., Çiner, A.: First ^{36}Cl cosmogenic moraine geochronology of the Dinaric mountain karst: Velež and Crvanj Mountains of Bosnia and Herzegovina. Quat. Sci. Rev. **208**, 54–75 (2019). https://doi.org/10.1016/j.quascirev.2019.02.002

Zreda, M., Çiner, A., Sarıkaya, M.A., Zweck, C., Bayarı, S.: Remarkably extensive Early Holocene glaciation in Aladağlar, Turkey. Geology **39**(11), 1051–1054 (2011)

Tectonic Geomorphology and Paleoseismology of the Muğla-Yatağan Fault (SW Turkey)

Murat Ersen Aksoy, Orkun Türe, Özlem Yılmaz-Aksoy, Esra Çetin-Kasa, and Halil Kürşat Arık

Abstract

The Aegean Sea and its surroundings are considered a seismically active region due to the Hellenic arc and the westward escape of the Anatolian plate. The western section of Anatolia experiences extensional tectonics. The Muğla-Yatağan fault is a NW–SE trending ~50 km long normal fault located between the E-W trending Büyük Menderes and Gökova grabens. The fault runs through populated and industrialized settlements; however, its seismic hazard is poorly known. Empirical relations suggest that the fault may cause an earthquake reaching M7.0. Field mapping, quantitative geomorphology, and paleoseismic trenching reveal the recent tectonic activity of the fault. The Quaternary deformation of the fault is expressed as steep slopes, hanging valleys, iron flats, fault surfaces, and offset deposits. Several wine-glass shaped valleys indicate rapid and ongoing tectonic uplift. The valley floor width-to-height ratio (Vf) confirms this observation with low index values (0.09–0.40). The basin asymmetry index (AF) shows the uplift is not localized, but distributed along the fault. The hypsometric curve and the hack index attest that tectonism is the dominant processes controlling the morphology and forming steep fault scarps. Paleoseismic trenches at two sites suggest that both sites experienced at least two surface faulting events with 10–60 cm slip during the Quaternary–Holocene period. Our preliminary results show that the Muğla-Yatağan fault is potentially a source for a destructive earthquake in the region and requires further analysis to evaluate quantitatively its seismic hazard. This work has been funded by the MSKU Research Fund project 17-288.

Keywords

Extension tectonics • Normal faulting • Aegean • Quantitative geomorphology • Active tectonics • Paleoseismology

1 Introduction

The Hellenic Arc is seismically the most active region of Europe (Ambraseys 2009). The extension of tectonics to the North of the subduction zone forms several normal faults in Southern Aegean that have been a source for destructive earthquakes throughout the history (Ambraseys 2009; Guidoboni and Comastri 2005; Guidoboni et al. 1994) The Muğla-Yatağan fault is a ~50 km long normal fault, located within the Aegean-Extensional-System (Fig. 1). The fault runs through Muğla city. Many houses, public and industrial facilities are located on the fault. There are important electric power plants located close to the fault. In the last 15 years, the number of habitants in Muğla has increased by %25. The economic infrastructure of the city is continuously growing. Although, Muğla lies within the first order seismic zone of Turkey, information on the Muğla-Yatağan fault is limited. The most recent destructive earthquakes in the vicinity are the 1941 (M5.8), 1944 (M6.3), and 2017 sequence (M4.9–5.3) that caused damages to villages nearby (Sözbilir et al. 2017; Tan et al. 2008). The fault can potentially produce an M6-7 earthquake that could cause significant damage and loss in the area; therefore, it is critical to determine its seismic hazard.

2 Materials and Methods

In this study, field investigations were applied along the Muğla-Yatağan fault, and the imprint of the tectonic activity within the morphology and Quaternary deposits was

M. E. Aksoy (✉) · O. Türe · Ö. Yılmaz-Aksoy · E. Çetin-Kasa · H. K. Arık
Department of Geological Engineering, Muğla S. K. University, 4800 Muğla, Turkey
e-mail: ersenma@mu.edu.tr

A. Çiner et al. (eds.), *Recent Research on Geomorphology, Sedimentology, Marine Geosciences and Geochemistry*, Advances in Science, Technology & Innovation, https://doi.org/10.1007/978-3-030-72547-1_2

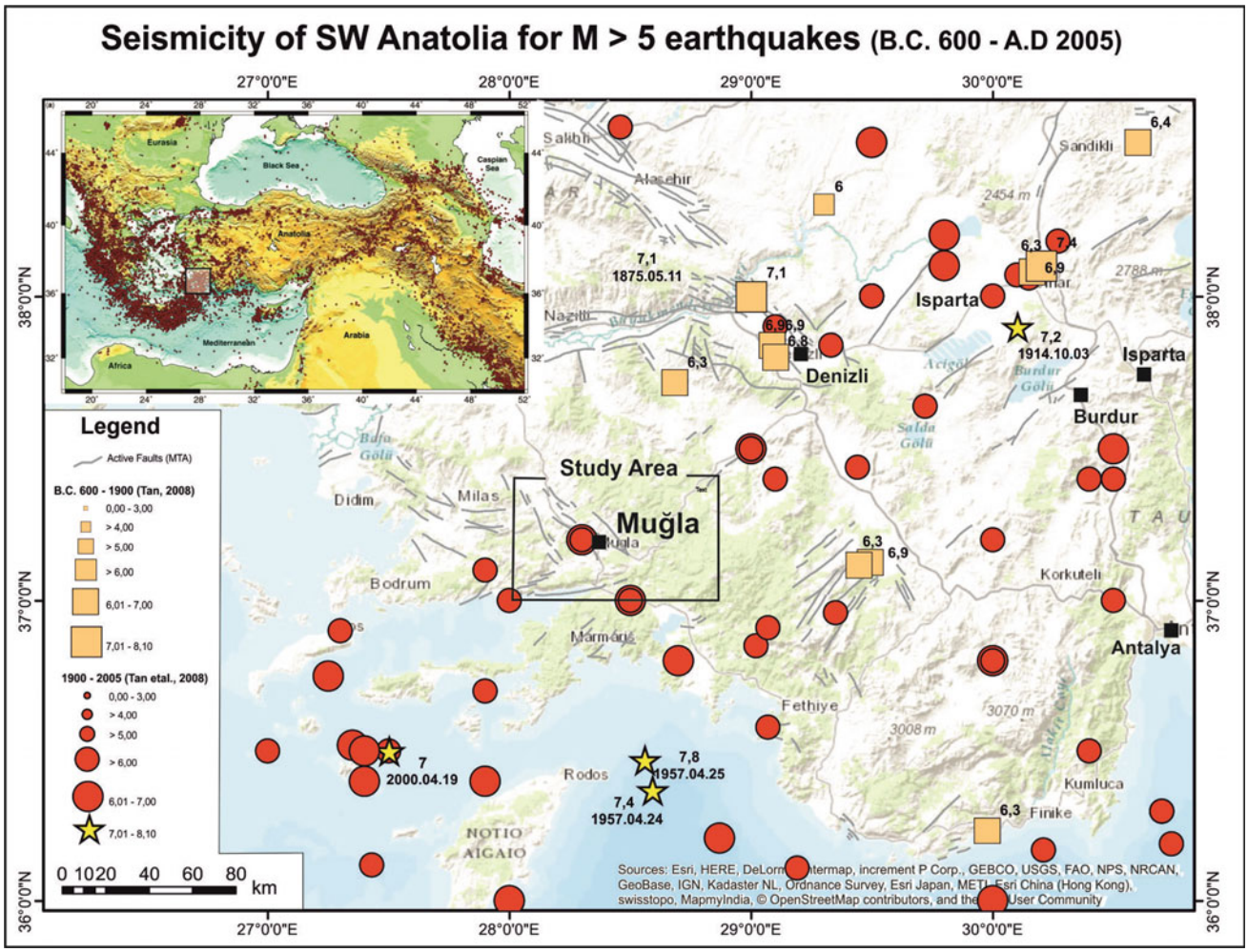

Fig. 1 Inset provides a comparison of the earthquake activity in the Eastern Mediterranean with respect to Southern Aegean (Taymaz et al. 2007). The solid black box shows SW Anatolia region laying within the seismically highly active area. Several historical and instrumental period earthquakes M > 5 hit the Muğla region (Ambraseys 2009; Guidoboni and Comastri 2005; Guidoboni et al. 1994; Tan et al. 2008)

documented. Detailed fault mapping allowed determining the segment characteristics and complexities of the fault.

In addition, morphometric indices were applied to quantitatively determine the influence of the faulting on the drainage basins and surrounding morphology of the area. Geomorphic indices such as basin asymmetry factor (AF), valley width-to-height ratio (Vf), mountain front sinuosity (Smf), hack index (SL), and hypsometric curve were used (Pinter 1996; Keller and Pinter 2002). The analysis was performed on digital elevation models that were produced from 1/25.000 scaled topographic contour maps and digital terrain models obtained from high resolution aerial photographs (10–50 cm/pixel).

Also, paleoseismic trenching was performed at two sites along the eastern section of the Mugla fault to expose the recent deformation within Quaternary deposits.

3 Results

The Quaternary deformation of the fault is expressed in both, morphology and geology as steep slopes, hanging valleys, iron flats, fault surfaces, and offset Quaternary deposits (Fig. 2). Several wine-glass shaped valleys indicate rapid and continuous tectonic uplift. The valley floor width-to-height ratio (Vf) confirms this observation with low index values (0.09–0.40) (Pinter 1996; Keller and Pinter 2002). Basin asymmetry index (AF) shows that uplift is not localized, but well distributed along the fault. The hypsometric curve and the hack index attest that tectonism is the dominant processes controlling the morphology and forming steep fault scarps (Pinter 1996; Keller and Pinter 2002).

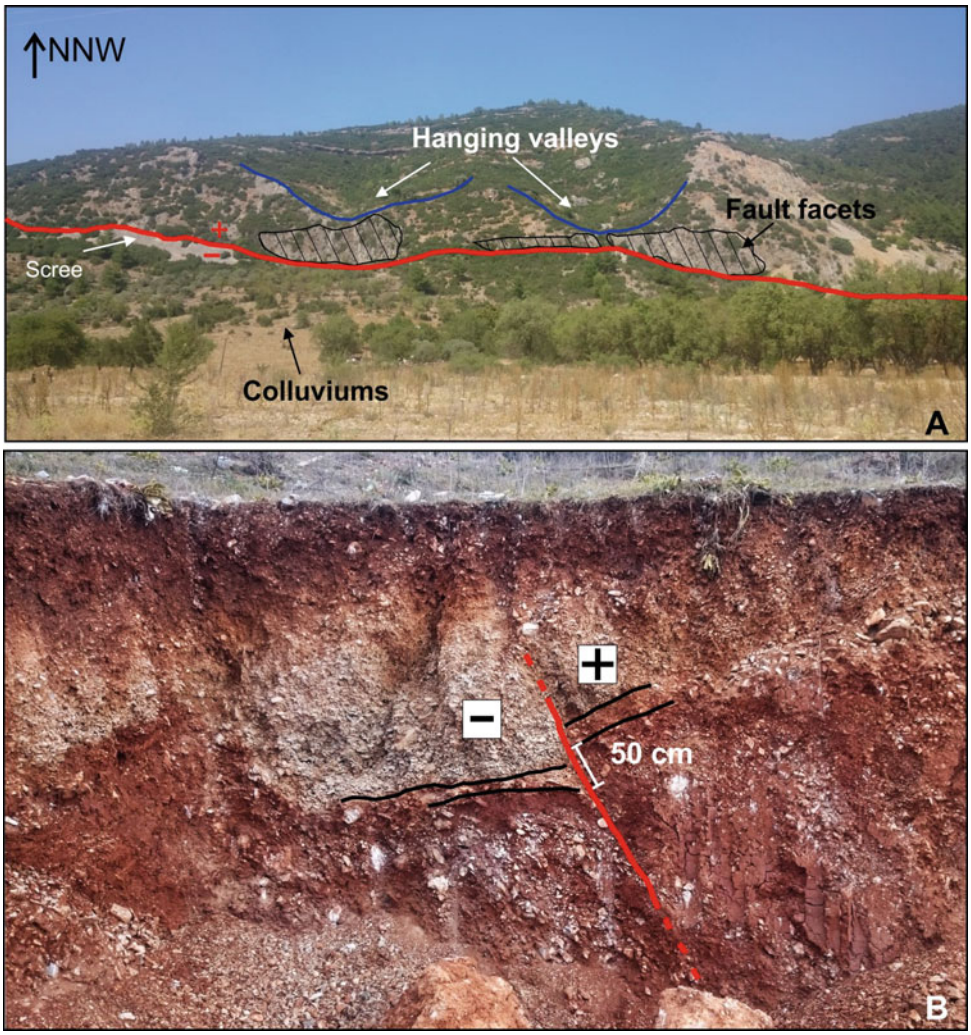

Fig. 2 **a** Escarpments of the fault that affects the present-day morphology by forming hanging valleys. **b** Quaternary–Holocene deposits displaced by the fault along the western fault section. The exposed fault line (plane) is sub-parallel to the strike of the fault and provides therefore an apparent view of the fault. The "+" is on the footwall block of the outcrop

Field investigations and paleoseismic trenching showed that the fault caused surface faulting within the Quaternary–Holocene deposits. Two trenches were opened along the eastern section of the fault. They exposed a 1–4 m wide fault zone that was overlain by colluvium and fluvial deposits in Yaras 1 and several layers of colluviums in Yaras 2. In both trenches, Quaternary–Holocene sediments were displaced by 10–60 cm vertical co-seismic displacement. Cross-cutting relationships suggest the existence of at least two events. Radiometric dating will be applied for the trench deposits in order to determine the timing of the events.

4 Conclusions

The tectonic activity of the Muğla-Yatağan fault is evident in the morphology and geology. Quantitative geomorphic analysis, field observations, and offset Quaternary–Holocene deposits exposed in the trenches are providing evidence that the fault is active and has ruptured at least twice during this time period causing 10–60 cm displacement. Radiometric dating on relevant deposits will allow a better constrain on the timing of the events. Based on empirical relations, the total fault length (~50 km) suggest that it is capable of producing a destructive earthquakes reaching M 7.0 magnitude (Wells and Coppersmith 1994). In order to properly evaluate the seismic hazard of the Muğla-Yatağan fault, further paleoseismological studies are essential.

References

Ambraseys, N.N.: Earthquakes in the Mediterranean and Middle East: A Multidisciplinary Study of Seismicity up to 1900. Cambridge University Press (2009)

Guidoboni, E., Comastri, A.: Catalogue of Earthquakes and Tsunamis in the Mediterranean Area from the 11th to the 15th Century. Istituto Nazionale di Geofisica e Vulcanologia, Rome (2005)

Guidoboni, E., Comastri, A., Traina, G.: Catalogue of ancient earthquakes in the Mediterranean area up to the 10th century: Rome, 504 p. Istituto Nazionale di Geofisica e Vulcanologia (1994)

Keller, E.A., Pinter, N.: Active tectonics: earthquakes, uplift, and landscape. Prentice Hall (2002)

Pinter, N.: Exercises in Active Tectonics An Introduction to Earthquakes and Tectonic Geomorphology. Prentice-Hall Inc., New York (1996)

Sözbilir, H., Uzel, B., Sümer, Ö., Eski, S.: Report on the 22–25 November 2017 Mugla Earthquakes and seismicity of the Mugla district. Dokuz Eylül University, Earthquake Research and Applications Centre, Active Fault Re-search Group (in Turkish), Izmir (2017)

Tan, O., Tapırdamaz, M.C., Yörük, A.: The earthquake catalogues for Turkey, Turkish. J. Earth Sci. **17**, 405–418 (2008)

Taymaz, T., Yilmaz, Y., Dilek, Y.: The geodynamics of the Aegean and Anatolia: introduction Geological Society. London, Special Publ. **291**, 1–16 (2007)

Wells, D.L., Coppersmith, K.J.: New empirical relationships among magnitude, rupture length, rupture width, rupture area, and surface displacement. Bull. Seismol. Soc. Am. **84**, 974–1002 (1994)

Slip Rate Estimation on the North Anatolian Fault Using Geomorphology and Paleoclimate Chronology: The Ganos Fault, Turkey

Murat Ersen Aksoy, Mustapha Meghraoui, Ziyadin Çakır, and Matthieu Ferry

Abstract

Offset streams are well recorders of the long-term and short-term deformation along strike-slip faults. Two independent processes act during the formation of offset streams: (1) climatic processes that support stream formation; (2) successive fault displacement across the stream channel. Field investigations are conducted along the westernmost inland segment of the North Anatolian fault; the Ganos fault; 48 right-lateral stream offsets are documented ranging 8 to 575 m. The stream offsets show five distinct groups of comparable magnitude that can be explained as episodes of new stream incisions due to high precipitation periods. Paleoclimatic studies in the region reveal the timing of these periods. Using a Black Sea sea-level curve for the last 20 ka, five subsequent sea-level rise periods are determined at 4, 10.2, 12.5, 14.5, and 17.5 ka. They can be considered as climatic periods favorable for stream incisions in the Ganos area. Linking the five offset groups with precipitation periods provides an average 17.9 mm/year slip rate for the last 20.000 years and a variability of 17.7 mm/year, 17.7 mm/year, 17.9 mm/year, and 18.9 mm/year for the last 10.2 ka, 12.5 ka, 14.5 ka, and 17.5 ka, respectively. These results are comparable with values for the eastern parts of the NAF, ranging from 15 to 25 mm/year.

Keywords

Active tectonics • Tectonic morphology • North Anatolian fault • Paleoclimate • Stream offset • Slip rate

1 Introduction

A fault's slip rate is a critical parameter in evaluating the seismic cycle of an active fault. Knowing the amount of strain accumulation since the penultimate event provides an important insight for the timing and size of the next large earthquake. Offset structures, particularly streams, are excellent markers on strike-slip faults that can record both magnitude and timing of fault movement.

The right-lateral North Anatolian Fault (NAF) in Turkey is a major continental active fault that accommodates a significant part of the present-day active deformation between Anatolia and Eurasia (Fig. 1). Co-seismic and cumulative offsets along the NAF are well documented in earlier studies (Barka 1992; Şengör et al. 2005; Zabcı et al. 2011) (and references herein). Many fluvial markers along the NAF were used to calculate an average slip rate of 15–20 mm/year for the late Holocene period (Hubert-Ferrari et al. 2002; Kozacı et al. 2009; Meghraoui et al. 2012; Zabcı 2012, and references herein).

In this study, cumulative stream offsets are documented at different scales along the Ganos fault. Using paleoclimatic proxies, we investigate how and when drainage systems respond to tectonics. A correlation of cumulative stream displacements with paleoclimatic events allows to constrain slip rates over different time scales for this segment of the NAF.

M. E. Aksoy (✉)
Department of Geological Engineering, Muğla Sıtkı Koçman University, Muğla, Turkey
e-mail: ersenma@mu.edu.tr

M. E. Aksoy · M. Meghraoui
Institut de Physique du Globe de Strasbourg, UMR 7516, Strasbourg, France

M. E. Aksoy · Z. Çakır
Department of Geological Engineering, Istanbul Technical University, Istanbul, Turkey

M. Ferry
Geoscience Montpellier, Universite Montpellier 2, UMR, 5243 Cedex 05, France

A. Çiner et al. (eds.), *Recent Research on Geomorphology, Sedimentology, Marine Geosciences and Geochemistry*, Advances in Science, Technology & Innovation, https://doi.org/10.1007/978-3-030-72547-1_3

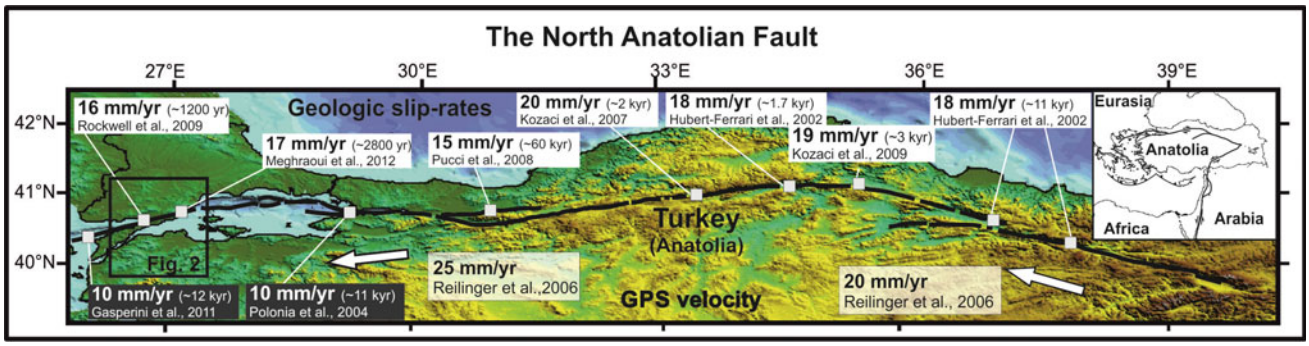

Fig. 1 Earlier estimations along the North Anatolian fault yield slip rates of 10 to 20 mm/year, while GPS velocities are at 20–25 mm/year. The western most inland section of the North Anatolian Fault is the Ganos fault (black box)

2 Geomorphological Setting and Drainage Development

The Ganos Mt. is a prominent and isolated topographic high, west to the Sea of Marmara (Fig. 1). The deformation of the westernmost section of NAF is localized within a distinct linear valley dividing the Ganos Mt. into two topographic highs. Dominant strike-slip motion is expressed by tectonomorphic structures along the 45-km-long inland section, (e.g., pressure ridges, shutter ridges, stream offsets, releasing/restraining–step-overs and–bends). Rectilinear valleys show cumulative displacements from 10 to 1000 m and verify the Holocene activity of the NAF.

A period of intense rainfall in a specific area deepens the existing stream channels and forms new incisions (streams) too. Therefore, each new stream running across a fault acts as a new counter that records fault slip (both co-seismic and aseismic). During intervals of arid climate, slip is cumulatively recorded on existing streams. Hence, groups of comparable amounts of slip represent a series of 1—periods of new stream formation and 2—periods of rainfall. Therefore, it is possible to correlate stream offsets with proxies representing climatic fluctuation; for example, sea-level curves (Ferry et al. 2007).

3 Results

The analysis of the entire inland fault section revealed 45 co-seismic (Aug. 9, 1912 Mürefte earthquake M 7.4) and 69 cumulative offsets. The values ranged from tens to hundreds of meters signifying the slip over different time spans.

We measured 48 stream offsets, which can be classified into nine groups of comparable magnitude (Fig. 2).

The Quaternary fresh water input into the Black Sea has two sources; precipitation (Karaca et al. 2000) and riverine input particularly by melt water after the LGM (Issar 2003; Huhmann et al. 2004). Both sources are shown to cause precipitation in the Balkan's (Karaca et al. 2000; Issar 2003; Huhmann et al. 2004). The sea-level change for the last 20,000 years of the Black Sea (black curve) and the Pinus pollen percentage in the Aegean Sea (gray curve) is illustrated in Fig. 2 (Dolukhanov and Arslanov 2009; Kotthoff et al. 2008). Both proxies are used as indicators of intense precipitation or arid periods. The consecutive five main periods of sea-level rises at 17.5, 14.5, 12.5, 10.2 ka, and 4.1 to 3.9 ka may correspond to such precipitation periods and correlate the offset groups consecutively to the periods with main sea-level rises after the Last Glacial Maximum.

The calculations for each offset group yield 17.5 mm/year, 18.3 mm/year, 17 mm/year, 18.4 mm/year, and 20.5 mm/year slip rate for the last 4 ka, 10.2 ka, 12.5 ka, 14.5 ka, and 17.5 ka, respectively. This implies a constant slip rate of 17.9 mm/year for the last 20,000 years and a variable slip rate of 17.7 mm/year, 17.7 mm/year, 17.9 mm/year, and 18.9 mm/year for the last 10.2 ka, 12.5 ka, 14.5 ka, and 17.5 ka, respectively (Fig. 2).

4 Conclusions

The record of successive stream offsets with systematic slip distribution attested the direct relationship of local morphotectonic features with climatic events and the associated active deformation at large scale.

The correlation of offset groups and high precipitation periods from sea-level fluctuations allowed to calculate an average slip rate of 17.9 mm/year for the last 20 k year for the westernmost section of North Anatolian Fault.

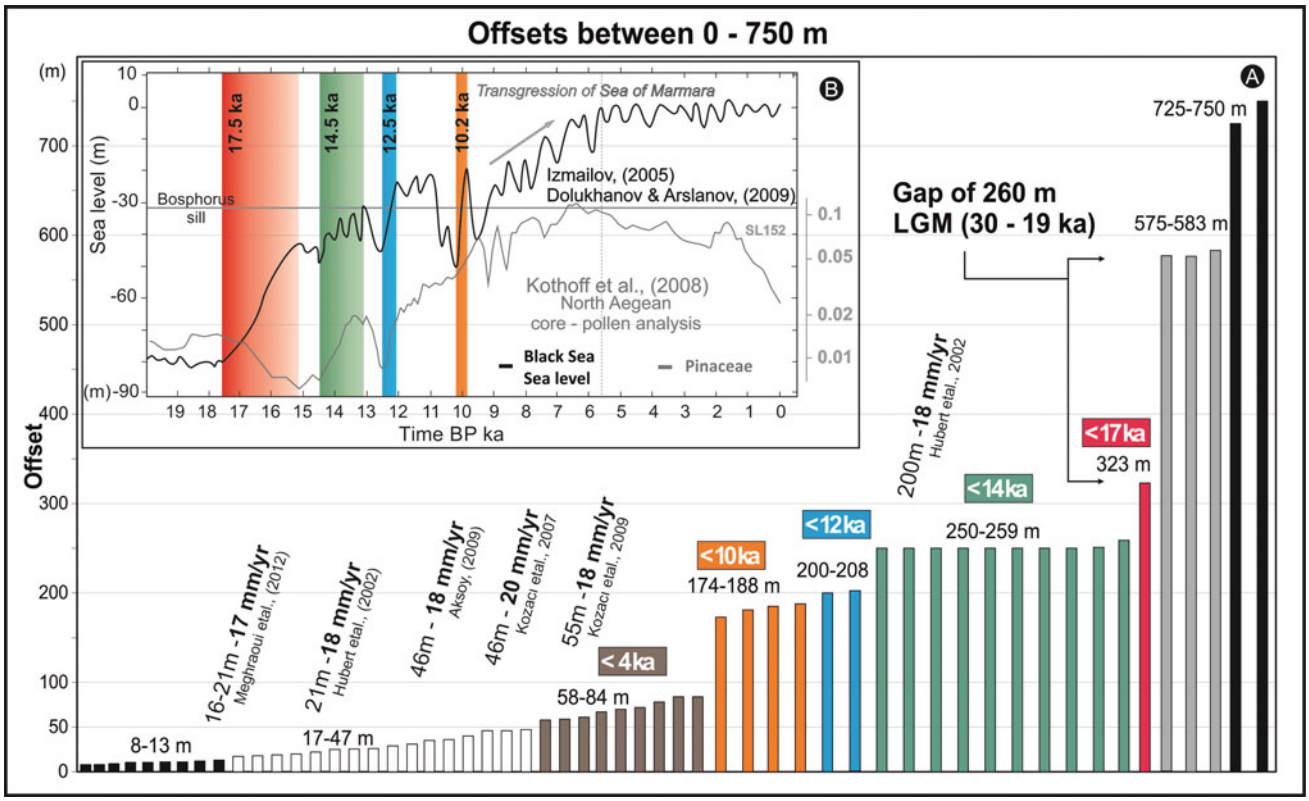

Fig. 2 **a** Histogram based on magnitude of displacement shows nine comparable groups of slip magnitudes. The amount of offsets is given above each group. **b** The inset shows the sea-level curve of the Black Sea and a pollen analysis in the Aegean Sea. The colored sections show rapid increase in sea-level rise in the Black Sea and increase of pinacea which both imply wet climate conditions. The correlation of offsets and timing of wet periods allow to calculate slip rates for this section of the NAF. Earlier slip measurements and corresponding slip rate estimations are given above the histogram (**a**)

References

Barka, A.: The North Anatolian Fault Zone Annales Tectonicae **6**, 164–195 (1992)

Dolukhanov, P.M., Arslanov, K.A.: Ecological crises and early human migrations in the Black Sea area. Quat. Int. **197**, 35–42 (2009)

Ferry, M., Meghraoui, M., Abou Karaki, N., Al-Taj, M., Amoush, H., Al-Dhaisat, S., Barjous, M.: A 48-k year-long slip rate history for the Jordan Valley segment of the Dead Sea Fault. Earth Planet. Sci. Lett. **260**, 394–406. https://doi.org/10.1016/j.epsl.2007.05.049 (2007)

Hubert-Ferrari, A., Armijo, R., King, G., Meyer, B.: Morphology, displacement, and slip rates along the North Anatolian Fault, Turkey. J. Geophys. Res. **107**(B10), 2235 (2002). https://doi.org/10.1029/2001JB000393

Huhmann, M., Kremenetski, K.V., Hiller, A., Brückner, H.: Late quaternary landscape evolution of the upper Dnister valley, western Ukraine Palaeogeography. Palaeoclimatol. Palaeoecol. **209**, 51–71 (2004)

Issar, A.: Climate Changes During the Holocene and Their Impact on Hydrological Systems. Cambridge University Press (2003)

Karaca, M., Deniz, A., Tayanç, M.: Cyclone track variability over Turkey in association with regional climate. Int. J. Climatol. **20**, 1225–1236 (2000)

Kotthoff, U., Müller, U.C., Pross, J., Schmiedl, G., Lawson, I.T., van de Schootbrugge, B., Schulz, H.: Lateglacial and Holocene vegetation dynamics in the Aegean region: an integrated view based on pollen data from marine and terrestrial archives. The Holocene **18**, 1019–1032 (2008). https://doi.org/10.1177/0959683608095573

Kozacı, Ö., Dolan, J.F., Finkel, R.C.: A late Holocene slip rate for the central North Anatolian Fault at Tahtaköprü, Turkey, from Cosmogenic 10Be geochronology: implications for fault loading and strain release rate. J. Geophys. Res. **114**, B01405 (2009). https://doi.org/10.1029/2008JB005760

Meghraoui, M., Aksoy, M.E., Akyüz, H.S., Ferry, M., Dikbaş, A., Altunel, E.: Paleoseismology of the North Anatolian Fault at Güzelköy (Ganos segment, Turkey): size and recurrence time of earthquake ruptures west of the Sea of Marmara. Geochem. Geophys. Geosyst. **13**, Q04005–Q04005 (2012)

Şengör, A.M.C., et al.: The North Anaotlian fault: a new look. Annu. Rev. Earth Planet. Sci. **33**, 37–112 (2005). https://doi.org/10.1146/annurev.earth.32.101802.120415

Zabcı: The 5 ka morphochronological slip-rate history and the paleoseismicity of the Ilgaz-Karliova section of the North Anatolian fault, Turkey. Ph.D. dissertation, Istanbul Technical University, Istanbul (2012)

Zabcı, C., Serdar, A.H., Karabacak, V., Taylan, S., Altunel, E., Gürsoy, H., Tatar, O.: Palaeoearthquakes on the Kelkit Valley segment of the North Anatolian Fault, Turkey: implications for the surface rupture of the historical 17 August 1668 Anatolian Earthquake. Turkish J. Earth Sci. **20**, 411–427. https://doi.org/10.3906/yer-0910-48(2011)

Energy Relief Analysis of the Northern Marche-Romagna Region, Northern Apennine, Central Italy

Davide Baioni

Abstract

This work deals with drainage system analysis and its evolution. Our study is carried out on the four river basins that flow in the area from the north border of Marche to Romagna region (central Italy), located on the Adriatic seaside of Apennines chain. It investigates the energy of relief (Er) along with the morphographic and morphometric parameters of drainage systems and drainage basins that are capable of supplying direct or indirect information on tectonic forcing on the landscape and field observations. The analysis reveals that drainage network anomalies, lineaments detected from satellite images and high values of energy relief, often are located in the same areas and are unrelated to local climatic conditions or lithological setting. These findings, supported by field data, indicate that this area is affected by recent neotectonic activity.

Keywords

Energy relief • Morphotectonic • Neotectonic • Northern Apennine

1 Introduction

The analysis of geomorphic indices gathered in the study of drainage basins and their integrated comparisons can contribute to the understanding of the morphotectonic structure (Ollier 1995). Also, it can be particularly useful in detecting the factors that may have influences on morphogenetic processes (Cox 1994). One of these geomorphic markers is the energy of relief (Er) also called amplitude of relief (Ar) (Ahnert 1970). Several authors studied this quantitative index as a marker of the intensity of erosion in their morpho-structural and neotectonic analyses worldwide (Cotilla Rodriguez and Cordoba Barba 2004; Gorshkov et al. 2000). In the case of central Italy, the meaning of this parameter has been tested through comparative analyses carried out in broad areas and drainage basins of the central Apennines (Della Seta et al. 2004). The area between the Apennine chain and the Adriatic Sea located in the Marche and Romagna regions is occupied by four adjacent river basins of different sizes and importance. For this area, there are no specific or detailed studies about the definition of the morphological evolutionary or morphotectonic dynamics. This study aims to identify the role of neotectonics in terms of (i) landscape evolution and (ii) the features of the drainage systems in the Northern Marche-Romagna region, through the analysis of the distribution of the energy of relief within this area.

2 Study Area

The study area (Fig. 1) is located on the Adriatic side of the northern Apennine chain in the border area between the Romagna and the Marche regions (central Italy). It covers an area of 1011 km^2 and contains four river basins named: Conca, Ventena, Tavollo and Foglia, respectively, from North toward South. This area is characterized by an arcuate shape with a main northeast vergence of asymmetric as well as thrust-faulted anticlines involving a Mesozoic-Tertiary sedimentary succession. The four river basins flow in an almost straight line from west to east crossing transversely the main anticlinal ridges before reaching the Adriatic coast. The Val Marecchia thrust-sheet influences the northwestern part represented by clays and marls and interbedded calcilutite and calcarenites. They form part of a detachment sheet tectonically overlying Miocene synorogenic strata of Umbria-Marche succession (Bonciani et al. 2007; Mayer

D. Baioni (✉)
Dipartimento di Scienze Pure e Applicate, Università di Urbino, Urbino, Italy
e-mail: davide.baioni@uniurb.it

A. Çiner et al. (eds.), *Recent Research on Geomorphology, Sedimentology, Marine Geosciences and Geochemistry*, Advances in Science, Technology & Innovation, https://doi.org/10.1007/978-3-030-72547-1_4

et al. 2003). Mio-Pliocene units of Umbria-Marche succession underlie the central part, represented by clay and sandstone. It is characterized by the occurrence of a NW–SE trending faulted anticline (Montescudo-Serrungarina). Oligo-Miocene rocks are also found in its core that is crossed transversely by the mainstream. In the downstream sector, the rivers flow on Quaternary alluvial deposits before reaching the Adriatic coast. One fascinating feature of the four basins is their asymmetry that reveals a significant change of direction. It is also worth mentioning that no recorded lithological control or localized climatic conditions could influence this phenomenon. (Baioni 2007).

3 Data and Method

An estimate of Er was obtained by subdividing the study area into square cells of 0.25 km^2, which were numbered by orthographic coordinates. Within each cell, the Er was calculated using: Er = highest elevation – lowest elevation. Highest and lowest elevation for each cell were obtained from the existing 1:25 000 topographic map and by referring to the 25 ± 10% m contours. This procedure provided detailed data, with 4,044 Er values for the entire study area. The values of Er obtained and expressed in meters were divided into several classes. Each value was associated with a different color and built, through a mosaic representation, the map of the Er (Fig. 1). In addition, the study area was divided into relatively small sectors that segmented the main axis of each river basin, from the outlet to the most distant point of the head-stream, into segments all of 700 m length. Starting from the sides of each segment, lines were created perpendicular to the main axis of the basin, terminating at the left and the right watersheds of the study area. These lines started from both extremities of each segment to enclose a sector. Further, the arithmetic average values of Er for the cells on the hydrographic left and on the right were calculated for each sector within every single river basin. Then, the values were plotted against distance along all the basins. Accordingly, four longitudinal profiles of values of Er, with the same direction (SW-NE), were created and investigated within the study area (Baioni 2007).

The Er data were integrated with field activity, analysis of satellite images, and drainage network anomalies.

4 Results

The analysis carried out provided the following findings:

(a) In the northern part of the study area, we noticed a clear band or high relief energy values. This line of high values extending in the SW-NE direction starts at the mountain sector and ends in the coastal area. This element traverses the entire area unaffected by the lithological–structural variations. It also seems to represent a limit of separation between two parts showing a different response to this geomorphic marker. (b) The values of Er show a general tendency to increase toward the south, especially in the lower sector (valley and coastal). The same tendency is also observed in the area adjacent to the coast, having practically similar characteristics (climatic, lithological, use soil, etc.). (c) In the area of Montescudo-Serrungarina anticline, the values of the Er show an anomalous trend. In fact, in correspondence of the Ventena river basin, the values of Er are higher than those of all the other adjacent basins, independently of the lithological, structural, and climatic characteristics.

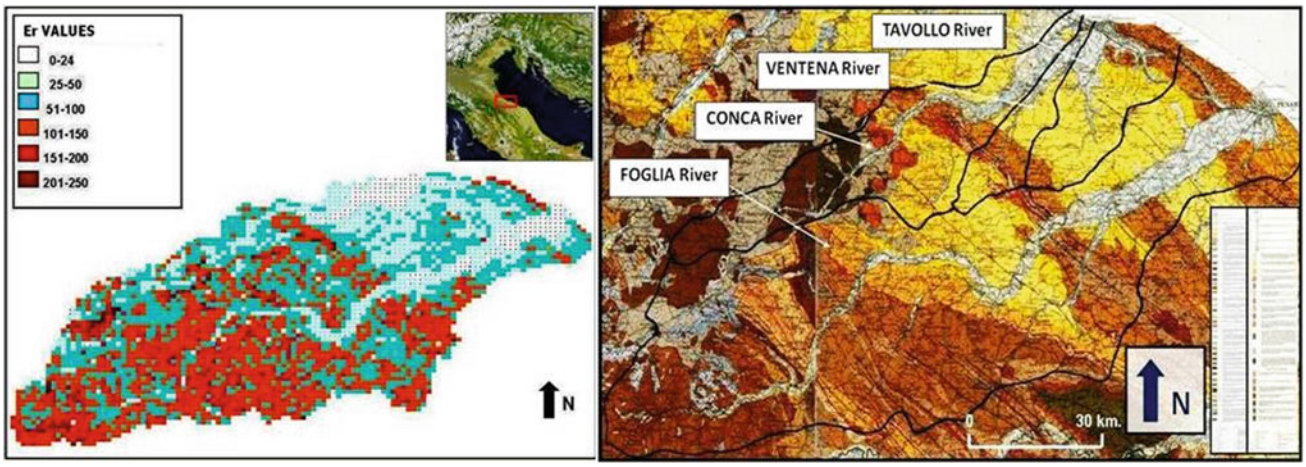

Fig. 1 Left: energy relief map of the four-river basin and location of the study area (upper right). Right: geological map of the study area with the studied four-river basin (black lines). The area is located between 43° 40–44° 00 North and 12° 21–12° 55 East

5 Discussion and Conclusions

The data analysis seems to indicate divided division of the study area into two main sectors displaying different characteristics of the energy of relief. The separation takes place according to a SW-NE direction. The extended band with SW-NE direction recorded high values of the energy of relief. This appears to divide the study area longitudinally in two sectors. The analysis of satellite images shows that the two sectors are related to a set of lineaments. Moreover, the field activity suggests that these features are normal faults that indicate an uplift of the area located to the south. Furthermore, the drainage anomalies observed, such as hook-like streams, captures, and barbed streams, are located on lineaments that coincide with those of high energy of relief detectable from satellite images. The Er data suggests the existence of areas with anomalies linked to the neotectonic activity within the study area. Some areas or blocks are also observed, subject to differentiated movements (uplift and tilting). This appears more evident in the central area of the study area, in correspondence with the part of the Montescudo-Serrungarina anticline inside the Ventena river basin. The data analyzed, supported, and integrated with field observations for this area reveal that in the central sector of the basin the right part is affected by recent uplift. The study carried out highlights the control and the role of the neotectonic due to the uplift of the study area starting from the middle-upper Pleistocene, in the morphogenetic processes of the hydrographic network and in particular on the conformation of the present drainage basins (Baioni 2007; Nesci and Savelli 2003).

References

Ahnert, F.: Functional relationships between denudation, relief, and uplift in large, mid-latitude drainage basins. Am. J. Sci. **268**, 243–263 (1970)

Baioni, D.: Drainage basin asymmetry and erosion processes relationship through a new representation of two geomorphic indices in the Conca river (northern Apennines). Italian J. Geosci. **126**, 573–579 (2007)

Bonciani, F., Cornamusini, G., Callegari, I., Conti, P., Foresi, M.L.: The role of the "Coltre della Val Marecchia"within the tectono-sedimentary evolution of the Romagnan. Marchean Appenines. Rendiconti della Società Geologica Italiana **5**, 62–62 (2007)

Cotilla Rodriguez, M.O., Cordoba Barba, D.: Morphotectonics of the Iberia Penisula. Pure Appl. Geophys. **161**, 755–815 (2004)

Cox, R.T.: Analysis of drainage-basin symmetry as a rapid technique to identify areas of possible Quaternary tilt-block tectonics: an example from Mississipi Embayment. Geol. Soc. Am. Bull. **106**, 571–581 (1994)

Della Seta, M., Del Monte, M., Fredi, P., Lupia Palmieri, E.: Quantitative morphotectonic analysis as a tool for detecting deformation patterns in soft-rock terrains: a case study from the southern Marches, Italy. Geomorphol.: Relief, Processes, Environ. **4**, 267–284 (2004)

Gorshkov, A.I., Kuznetsov, I.V., Panza, G.F., Soloviev, A.A.: Identification of future earthquake sources in the Carpatho-Balkan orogenic belt using morphostructural criteria. Pure Appl. Geophys. **157**, 79–95 (2000)

Mayer, L., Menichetti, M., Nesci, O., Savelli, D.: Morphotectonic approach to the drainage analysis in the nort Marche region, central Italy. Quatern. Int. **101–102**, 157–167 (2003)

Nesci, O., Savelli, D.: Diverging drainage in the Marche Apenines (Central Italy). Quatern. Int. **101–102**, 203–206 (2003)

Ollier, C.D.: Tectonics and landscape evolution in southeast Australia. Geomorphology **12**(3), 37–44 (1995)

Geomorphology, Soil Science, Landslides, Coastal Processes, and Geoarchaeology (T9): Soil Science

Evaluation of Electromagnetic Induction Method to Map Soil Salinity in Semiarid Tunisia

Abir Ben Slimane, Fethi Bouksila, Tarek Selim, and Farida Joumada

Abstract

Soil salinity presents a major environmental risk for soil resource degradation. In Tunisia, about 50% of irrigated lands are affected by secondary salinization. Soil salinity monitoring is essential to prevent further soil degradation. In this respect, this work aims to assess, predict, and map soil salinity by using an integrated technique that includes a non-invasive electromagnetic inductance sensor (EM38) and ESAP software. The experiment is realized in the semiarid Draa-Thammar (240 ha, Kairouan, Tunisia) district, which has been irrigated with brackish water since 1989. During 2014, EM38 readings (EM-ECa) were taken, and soil profile was sampled at 0.2 m depth intervals to 1.5 m for physical and chemical analysis. For 5 successive soil-depth intervals (0–0.4, 0–0.6, 0–0.8, 0–1, 0–1.5 m), significant and accurate relationships between EM38 readings and electrical conductivity of the soil saturated extract (lnECe) were found ($0.63 < R^2 < 0.80$, $0.11\ \text{mSm}^{-1} \leq \text{RMSE} \leq 0.18\ \text{mSm}^{-1}$). According to soil salinity maps, the temporary irrigations interruption (2010–2014) and rainfall allowed the leaching of the root zone (0–0.6 m) but were not enough to evacuate the accumulated salt in the deeper soil profile. At the spatial scale, EM38 allows a quick and accurate estimation of soil salinity which would contribute to developing appropriate water and soil management to improve soil productivity and farmers' income. To this end, ESAP software can be used as a fast tool to predict and map the soil salinity from EM38 readings.

Keywords

Soil salinity • Geophysical method • EM38 • ESAP software • Tunisia

1 Introduction

Soil salinity is one of the main problems in irrigated arid climate soils leading to land desertification. It poses a significant environmental risk by degrading soil and water quality, limiting crop growth and reducing agricultural productivity and wildlife diversity. Monitoring soil salinity is essential for the choice of crops. It also provides water and soil management recommendations to avoid or reduce the soil salinization risk (Bouksila et al. 2013).

The reference method of soil salinity measurement (electrical conductivity at 25 °C of saturated soil paste ECe) is destructive, time consuming, and expensive. The electromagnetic induction method (e.g., EM38) is considered one of the best methods for soil salinity measurements appraisal in a geospatial context (Corwin and Lesch 2003). The EM38 is designed to measure the apparent electrical conductivity (ECa) in the root zone. However, EM38 readings should be calibrated against the standard ECe used in salt-tolerance plants. The penetration depth of EM38 signal is, respectively, about 0.75 and 1.5 m in the horizontal (EMh) and vertical (EMv) dipole orientations. Several soil parameters affect the EM readings such as soil salinity, water content, porosity, soil texture, and temperature (Brevik and Fenton 2002; Friedman 2005). Thus, the objective of this study is to evaluate the electromagnetic inductance sensor (EM38) in order to estimate the soil salinity ECe in fine soil texture in Draa-Thammar (Kairouan, Tunisia), a district irrigated with brackish-treated wastewater.

A. Ben Slimane (✉) · F. Bouksila
Rural Engineering Laboratory, National Researches Institute of Rural Engineering, Water and Forests, 2080 Ariana, Tunisia
e-mail: bouksila.fethi@iresa.agrinet.tn

T. Selim
Civil Engineering Department, Faculty of Engineering, Port Said University, Port Fouad City, Egypt

F. Joumada
Commissariat Regional au Développement Agricole, 3100 Kairouan, Tunisia

A. Çiner et al. (eds.), *Recent Research on Geomorphology, Sedimentology, Marine Geosciences and Geochemistry*, Advances in Science, Technology & Innovation, https://doi.org/10.1007/978-3-030-72547-1_5

2 Materials and Methods

The experiment is realized in Draa-Thammar (35° 42′ 56.12″ N, 10° 5′ 54.94″ E) located at about 3.5 km far from Kairouan city (central Tunisia). Draa-Thammar covers 240 ha. It has been irrigated with brackish secondary-treated wastewater since 1989. The climate is semiarid with an average annual rainfall and potential evapo-transpiration (1959–2005) of about 306 mm and 1598 mm, respectively (Centre Nationale des Etudes Agricoles 2007). Soils are alluvium and the soil texture is silty to loamy-clayed. During 1998, the depth of water table (Dgw) was less than 2 m with an average EC of about 900 mSm^{-1}. Also, the average ECe at 0–1.5 m soil depth was 1020 mSm^{-1} (unpublished data). The crops are mainly forage and industrial. From 2010 to 2014, the irrigation was temporarily interrupted to increase the capacity of the wastewater treatment plant and the extension of the irrigated district.

In 2014, over the 240 ha, apparent electrical conductivity ECa was measured by EM38 in horizontal EMh and vertical EMv dipole orientations as well as the corresponding geographical coordinates UTM (x, y) which were performed in 68 plots. The ESAP software [USDA (Lesch et al. 1995a, 2000)] was used for sampling site selection, soil salinity prediction from EM readings, and for soil salinity mapping. From the selected references sites, the soil was sampled at 7 depths intervals (0–0.2, 0.2–0.4, 0.4–0.6, 0.6–0.8, 0.8–1.0, 1.0–1.2, and 1.2–1.5 m) for soil laboratory analysis (particle size, ECe, pH, water content at saturation θ sat, and gravimetric water content θ). Spatially referenced multiple linear regression model (MLR) with log-transformed signal combined with plots coordinates was used to predict soil salinity at five successive soil depths (0–0.4, 0–0.6, 0–0.8, 0–1.0, and 0–1.5 m). During our filed survey, there was almost no irrigation and the water table was below the 1.5 m soil sampling depth.

3 Results

3.1 Soil Properties

Despite that groundwater depth was below 1.5 m depth, we observed a rusty color stain at deeper soil layers (1–1.5 m) indicating a temporarily water logging. The ESAP-RSSD module allowed the selection of 12 representative sites to estimate lnECe. At these plots and for the seven soil sampling depths, the average of clay (<2 µm) and silt content (2–50 µm) was 33% and 39%, respectively. The average and the variation coefficient (CV) were 16%, 37% and 700 mSm^{-1}, 48% for θ and ECe, respectively. For EM readings, the average and the CV were 92 mSm^{-1}, 52% and 152 mSm^{-1}, 42%, for EMh and EMv, respectively. EMh and EMv were highly correlated ($R^2 = 0.96$), and all EMh/EMv ratios were inferior to 0.8. The observed soil salinity profiles were leached or heterogeneous. According to Kolmogorov–Smirnov test, only θ, θsat, and clay content had normal distribution.

3.2 Calibration of EM38 Readings

The simple linear regression between EM readings (lnEMh and lnEMv) and the observed soil properties (lnECe, θ, θsat) at the five successive soil depths was only significant (at 95% confidence level and probability value 0.05) for lnECe (average $R^2 = 0.74$ and varied from $0.55 \leq R^2 \leq 0.78$). Using ESAP software, among several proposed models (Lesch et al. 1995a), MLR was the best one to predict lnECe at the five successive soil depths intervals. The average R^2 and the root mean score error (RMSE) of this model were 0.78 ($0.63 \leq R^2 \leq 0.80$) and 0.13 mSm^{-1}($0.11\ mSm^{-1} < RMSE < 0.18\ mSm^{-1}$), respectively.

3.3 Spatial Variation of Soil Salinity

Figure 1 shows the soil salinity (ECe) maps generated by ESAP software. At the rootzone (0–0.6 m depth) about 72% of soil were saline (ECe > 400 mSm^{-1}) and 95% at soil depth layer 0–1.5 m.

4 Discussion

EM readings are affected by soil properties, mainly by soil salinity and moisture (Friedman 2005). However, in Draa-Thamar, without irrigation, the low spatial variation of θ could be one reason to explain the low R^2 (<0.2) of EM-θ relationships. EM readings were mainly affected by the spatial soil salinity variation ($0.39 \leq R^2 \leq 0.78$). Using ESAP software, the use of the plots coordinates and EM readings as input allowed better prediction of soil salinity. For large fields, the plot coordinate can be considered as an extra input that indirectly gives the statistical models input information regarding the spatial correlation of parameters that affects the EM readings and soil salinity ECe (farmers' agricultural practices, land cover, etc.). For leached soil salinity profiles, the EMh/EMv ratios were inferior to 1. This ratio could indicate the shape of the soil salinity profiles, which could help farmers to improve soil and water management. Despite the irrigation interruption and natural

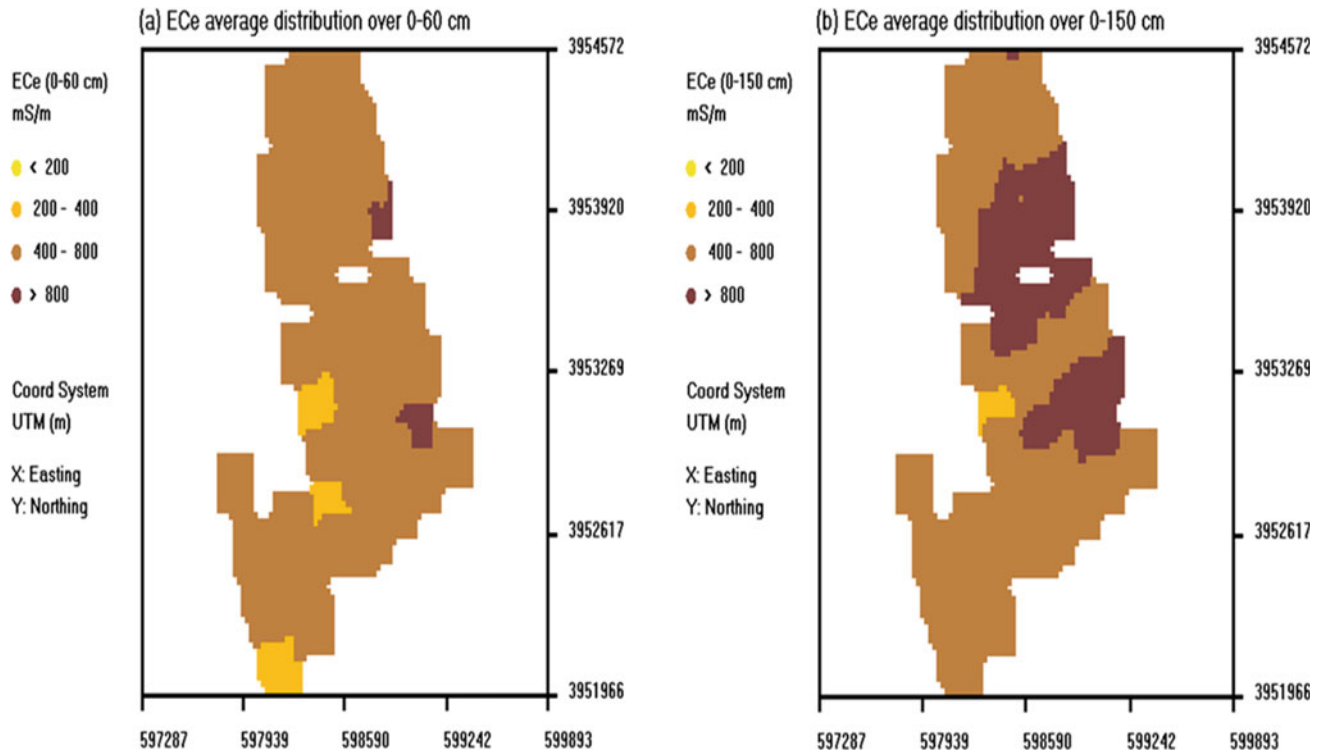

Fig. 1 Soil salinity maps ((ECe), mS/m) at soil depth interval 0–60 cm **a** and 0–150 cm **b** generated by ESAP software

leaching, the fine texture with low permeability and the shallow and saline groundwater could explain the observed saline soil in the irrigated district.

5 Conclusions

The EM38 geophysical method is fast and non-destructive for salinity assessment. EM38 readings allowed an accurate estimation of soil salinity ECe. Also, ESAP software is a helpful tool to choose the representative plots for EM readings calibration and for mapping the soil salinity. It is faster and easier to obtain soil salinity maps using EM38 and ESAP software. These maps could help decision makers, managers, and farmers for rational and sustainable management of water and soil sources. However, under irrigation with water return system, soil water content and soil temperature spatial variation could affect the accuracy to predict and map the soil salinity.

Acknowledgements This research was supported by SALTFREE project (ARIMNET2, Coordination of agricultural research in the Mediterranean).

References

Bouksila, F., Bahri, A., Berndtsson, R., Persson, M., Rozema, J., van der Zee, S.E.A.T.M.: Assessment of soil salinization risks under irrigation with brackish water in semiarid Tunisia. Environ. Exp. Botany **92**, 176–185 (2013)

Brevik, E.C., Fenton, T.E.: Influence of soil water content, clay, temperature, and carbonate minerals on electrical conductivity readings taken with the EM-38. Soil Survey Horizons **43**(1), 9–13 (2002)

Centre Nationale des Etudes Agricoles (CNEA): Rapport: Evaluation de la situation actuelle dans neuf périmètres irrigues a partir des eaux uses traitées, PPI Dhraa Tammar, Phase 2: Diagnostic de la situation actuelle et recommandations, Février 2007 (2007)

Corwin, D.L., Lesch, S.M.: Application of soil electrical conductivity to precision agriculture: theory, principles, and guidelines. Agronomy J. **95**, 455–471 (2003)

Friedman, S.P.: Soil properties influencing apparent electrical conductivity: a review. Comput. Electron. Agric. **46**, 45–70 (2005)

Lesch, S.M., Strauss, D.J., Rhoades, J.D.: Spatial prediction of soil salinity using electromagnetic induction techniques: 1. Statistical prediction models: a comparison of multiple linear regression and cokriging. Water Resour. Res. **31**, 373–386 (1995)

Lesch, S.M., Rhoades, J.D., Corwin, D.L.: ESAP-95 version 2.01R. User manual and tutorial guide. Research Report No. 146, June 2000. USDA-ARS. George E. Brown Jr Salinity Laboratory, Riverside, CA (2000)

Comparison of Organic Carbon Stock of Regosols Under Two Different Climates in Tunisia

Ahlem Znaidi, Nadhem Brahim, Hatem Ibrahim, Roland Bol, and Maher Chaouachi

Abstract

More than half of Tunisian soil is composed of Lithosols and Regosols. These soils, despite their existence in dry climates, are either steppes or farmland. The present work focuses on the state of the carbon stock in the Regosols of Tunisia. Two areas are selected for this study: a Regosol in Gafsa (S1) under arid climate, and another Regosol in Kairouan (S2) under semiarid climate. S1 and S2 are under two olive groves. The findings reveal that the granulometry, the pH, and the bulk density are very close. The difference lies in the content of organic carbon and therefore the carbon stock. The surface layer (0–20 cm) stores almost 3.01 kg/m^2 for S1 and 3.6 kg/m^2 for S2 while the depth of 0–100 cm S2 stores more than S1 with 10 and 8 kg/m^2, respectively.

Keywords

Dryland • Soil organic carbon • Carbon stock • Arid and semiarid climate • Tunisia

1 Introduction

Globally, the fertility and sustainability of soil systems are threatened by several actors like global environmental change and pollution, loss of organic matter, erosion, salinization, reduction of available water quantity and quality. However, the threats caused by these actors are not equally distributed; only a few areas in the world experience more of these simultaneous stresses upon their natural soil ecosystems environment than the semiarid and arid regions of the world. These regions cover 41% of total global land area and host 37% of the world population (Bernoux and Chevallier 2013). The soils in semiarid and arid regions are characterized by low organic matter (OM) contents, yet, they represent a significant global OM store due to their large extent.

These lands constitute a large part of Tunisia (50%) (Gallali 2004). The majority of these lands are classified as "little developed soils" or Aridisols commonly known in the FAO classification by "Lithosols" 25.64% and "Regosols" 24.51%. Aridisols make up 50.15% of the area of Tunisia (Brahim et al. 2014). In spite of their poverty in fine matter like clay and especially in organic matter, these soils are exploited under certain conditions on small farms when irrigation is possible.

Aridisols are known for their low organic matter content (<1%) (Gallali 2004). Hence, they are able to sequester even more organic carbon, which is a solution for the reduction of atmospheric greenhouse gases and, therefore, the reduction of global warming. It can also serve for the improvement of agriculture in these areas.

To this end, two study sites are selected in two different climates, one in arid climate in Gafsa, the other in semiarid climates in Kairouan, both occupied by an olive grove. This study attempts to compare the response of this soil to the storage of organic carbon under two different bioclimates.

A. Znaidi · M. Chaouachi
University of Monastir, High Institute of Biotechnology of Monastir, Avenue Taher Haddad (Bp 74), 5000 Monastir, Tunisia

N. Brahim (✉)
Faculty of Sciences of Tunis, University of Tunis El Manar, 2092 Tunis, Tunisia
e-mail: nadhem.brahim@fst.utm.tn

H. Ibrahim
Faculty of Sciences of Bizerte, University of Carthage, 7021 Jarzouna, Tunisia

R. Bol
Institute of Bio- and Geosciences, Forschungszentrum Jülich GmbH, Agrosphere (IBG-3), Jülich, Germany

A. Çiner et al. (eds.), *Recent Research on Geomorphology, Sedimentology, Marine Geosciences and Geochemistry*, Advances in Science, Technology & Innovation, https://doi.org/10.1007/978-3-030-72547-1_6

2 Materials and Methods

The first study site is located in El Guettar, 15 km south-east of the city of Gafsa in the catchment area of Orbata mountain, the climate of the area is arid (average temperature 20.9 °C and rainfall 150 mm/year). The second site is in Chebika, 15 km from the city of Kairouan to the east, the climate is lower semiarid (average temperature 18.1 °C and rainfall 300 mm/year). This semiarid climate contains the most profitable rainy agricultural soils of Tunisia. However, the arid climate still requires irrigation and is the limit of agricultural plots with the desert (Fig. 1).

In both sites, the soils come from two olive groves aged 15 years. Soil sampling was done systematically every 20 cm up to the depth of 100 cm (0–20, 20–40, 40–60, 60–80, and 80 cm). Three repeats were applied for each sample. Soil analysis included organic carbon % measured of the soil in fraction < 2 mm (Walkley–Black method), soil bulk density (D_b) g/cm^3 (cylinder method), pH measured in water (1:1), and granulometry % (Bernard calcimeter method).

Soils organic carbon stocks were estimated by the following equations (Brahim et al. 2014):

$$\mathrm{SOCstock} = \mathrm{OC} \times D_b \times D \quad (1)$$

where SOCstock represents soil organic carbon stock in ton ha^{-1}, then converted in kg m^{-2}, OC the organic carbon content (%), D_b the bulk density (g cm^{-3}), and D the sampling depth.

The estimate of carbon stock "S" in soil is the sum of all stocks in the soil's layers:

$$S = S_{\mathrm{layer1}} + S_2 + \cdots + S_{\mathrm{layer}n} \quad (2)$$

3 Results

3.1 Particle Size, Bulk Density, Organic Carbon, and pH of Both Soils

Results of particle size analysis reveal significant percentages of sands and silts compared with clays (Fig. 2). The soils have a sandy-loamy texture on the surface (0–20 cm) and in depth (>20 cm) a loamy-sandy texture. The pedogenesis is the same within the same soil type; the geographical

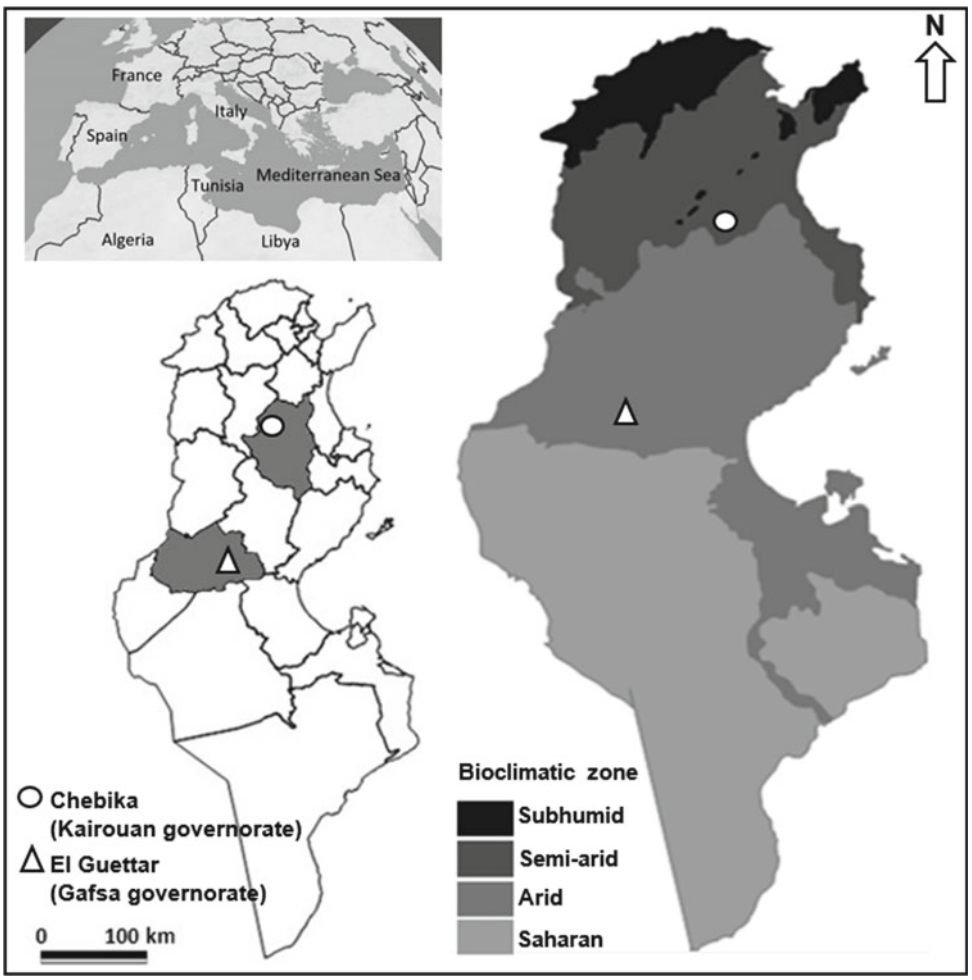

Fig. 1 Location of the two study sites on the bioclimatic map of Tunisia

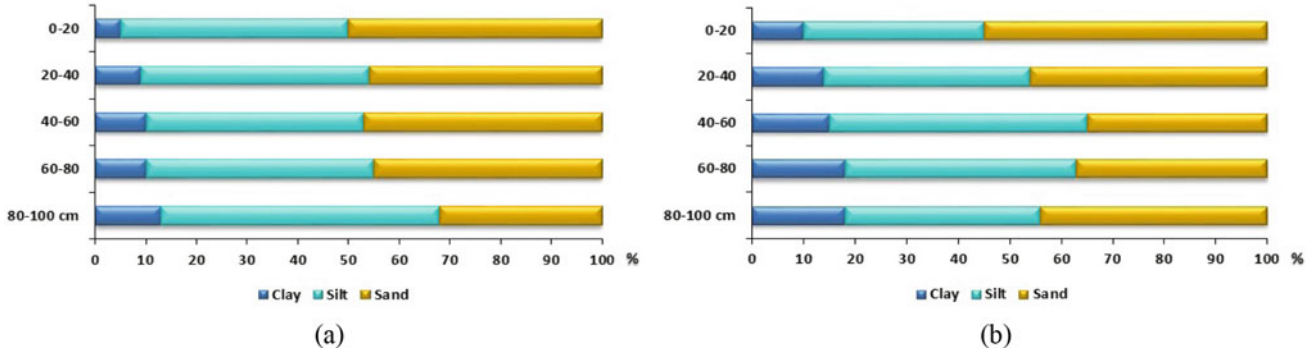

Fig. 2 Particle size (%) of the two soils: **a** S1 Gafsa soil and **b** S2 Kairouan soil

distribution does not have much significance if the topography is similar even if the climatic variable changes. Indeed, the results clearly show that the mineralogical constituents of the mineral fraction of soil remain almost invariable. The only variation is the abundance of annual organic restitution that returns to the soil. This is related to the vegetation cover, which is in turn related to the climate.

Figure 3 shows the bulk densities (D_b) of the investigated soils, their organic carbon (OC) content, and their pH. Besides the small difference in OC content, both soils have very similar values.

The D_b values range from 1.5 g/cm^3 in surface to 1.8 g/cm^3 in depth. At the level of S1, the OC content is 0.98% in the 0–20 cm surface layer and 0.12% at 1 m depth. For S2, it is relatively richer in OC where the surface layer has 1.22%. The pH of both soils is between 7.2 and 7.7 indicating that they are neutral to slightly basic.

The organic matter content of soil S2 under semiarid climate indicates a slight increase throughout the profile to a depth of one meter. This variation can be explained by the abundance of plant cover under the olive trees in spring. It could also be an effect of the temperature that is

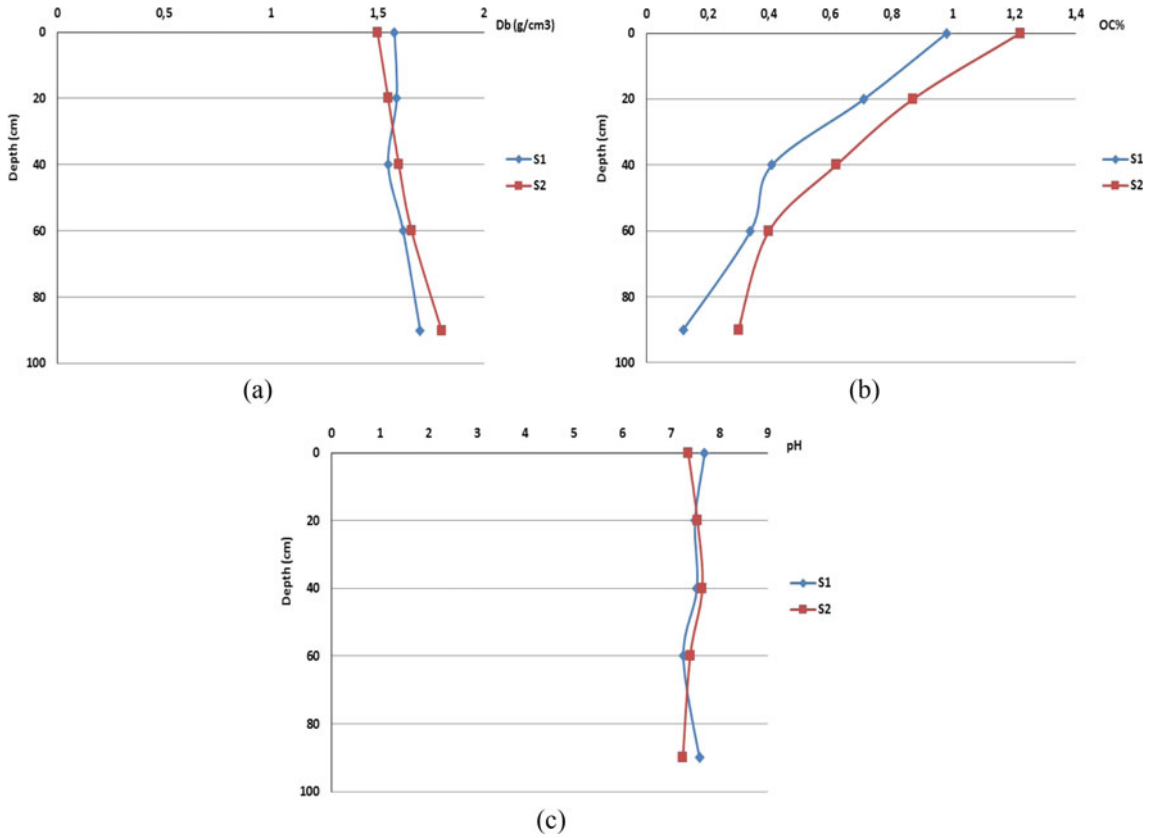

Fig. 3 Bulk density g/cm^3 (**a**); organic carbon % (**b**); and pH (**c**); S1 Gafsa soil and S2 Kairouan soil

a little lower compared to that registered the soil S1 climate.

This interpretation requires a more detailed study of the residence of organic carbon in these soils (Balesdent and Recous 1997) to determine whether there is an annual renewal or it is carbon sequestered over the years.

3.2 Soil Organic Carbon Stocks of Both Soils

Organic carbon stock determined in the two soils under the same plant occupation (olive grove) shows similar values for the surface layer (0–20 cm) where S1 and S2 are, respectively, 3.09 and 3.66 kg OC /m^2. But, at one meter deeper, 8.13 and 10.74 kg OC/m^2 are registered, respectively. This improvement is due to the enhanced climate conditions (Fig. 4).

4 Discussion

Analyzing the two Regosols confirms that soil pH increases as the soil organic matter content decreases. Furthermore, in the soil description, a test with HCl was always positive; $CaCO_3$ content increases soil pH (Gallali 2004). The means of the OC contents (%) higher values were registered in the soil surface layers. The values tended to decrease with soil depth. Overall, the range of SOC content assessed in this study confirmed with that reported in the literature, particularly for southern Tunisia region (Brahim et al. 2014; Kouki and Bouhaouach 2009). The findings of the D_b obtained state that it is low on the surface, which shows the existence of the organic matter on the surface and a low soil compaction.

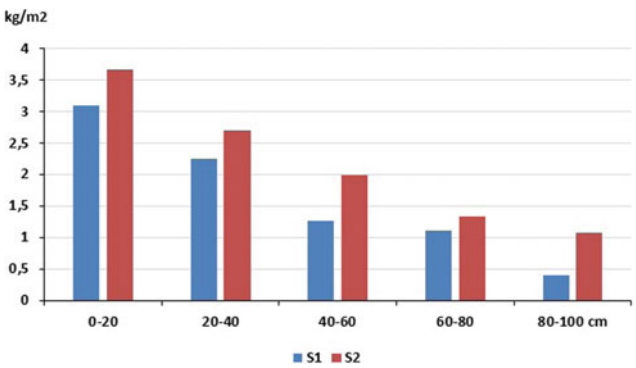

Fig. 4 Soil organic carbon stock in the two soils: S1 (Gafsa) and S2 (Kairouan)

Brahim and Ibrahim (2018) elaborate that several conditions such as drainage, slope position, texture, and organic matter abundance influence soil OC stocks. For S1, the stock values at a depth of 1 m are very close to those found in the Regosols of Tunisia by Brahim et al. (2014) which are of the order of 8.39 kg OC/m^2. But, they are higher in comparison with the other Regosols of the world which are 5 kg OC/m^2 according to Batjes (1996). As for S2, the carbon stock at a depth of 1 m is rather comparable to the fertile soils of Tunisia such as Cambisols (10.18 kg OC/m^2) or Vertisols (10.97 kg OC/m^2). These values are also close to average global Vertisols 11.1 kg OC/m^2 estimated by Batjes (1996).

5 Conclusions

Regosols, despite their poor organic matter, store carbon (8.13 to 10.74 kg OC/m^2 to 1 m depth). They have a greater storing capacity than the oasis soils due to the lack of salinity and better climate conditions compared to the desert. This work suggests that containing carbon in along with a few annual olive productions makes these soils worth investigating. More research should explore these soils in order to increase their fertility and mitigate the increase in greenhouse gases.

Faced with the current threat of global warming, these soils in dry areas or as called by the UNCCD drylands keep expanding in each year. Today, they draw particular attention to their ability to sequester carbon under good maintained, as the case of soil S2.

References

Balesdent, J., Recous, S.: Les temps de résidence du carbone et le potentiel de stockage de carbone dans quelques sols cultivés français. Can. J. Soil. Sci. **77**, 187–193 (1997)

Batjes, N.: Total carbon and nitrogen in the soils of the world. Eur. J. Soil Sci. **47**, 151–163 (1996)

Bernoux, M., Chevallier, T.: Le carbone dans les sols des zones sèches: des fonctions multiples indispensables. CSFD **10**, 44 p (2013)

Brahim, N., Ibrahim, H.: Effect of land use on organic carbon distribution in a North African Region: Tunisia case study. In: Soil Management and Climate Change, Effects on Organic Carbon, Nitrogen Dynamics, and Greenhouse Gas Emissions (Chap. 2), pp. 15–24. Elsevier edition (2018)

Brahim, N., Ibrahim, H., Hatira, A.: Tunisian soil organic carbon stock-spatial and vertical variation. Proc. Eng. **69**, 1549–1555 (2014)

Gallali, T.: Clés des sols. Edition CPU 1ère édition. 400 p (2004)

Kouki, K., Bouhaouach, H.: Etude de l'oasis traditionnelle Chenini Gabès dans le Sud Est de la Tunisie. Tropicultura **27**(2), 93–97 (2009)

Organic Carbon Stocks Evaluation After Three Years of No-Tillage Practice in a Vertisol, Northern Tunisia

Nadhem Brahim, Hatem Ibrahim, and Tahar Gallali

Abstract

This study compares the soil organic carbon stock under conventional and conservation agriculture in north Tunisia (Mateur) under sub-humid climate. After three years of no-tillage practice, a 12.6% increase of organic carbon is detected compared with conventional tillage, i.e., the total amount of carbon stored in the first 30 cm of soil is equal to 103.14 and 91.59 t/ha under no-tillage and conventional tillage, respectively. Since the study site is sloping, maximum carbon storage is obtained at the bottom of slope. The findings show that the carbon stock evolves laterally and vertically. Laterally, the stock increases according to the slope and by the carbon transfer by runoff. Vertically, the carbon is buried deep down to the depth of 30 cm.

Keywords

No-tillage • Conservation agriculture • Soil organic carbon stock • Vertisol • Tunisia

1 Introduction

Tillage is an ancient ancestral practice in agriculture. Among the primary goals of plowing is the creation of an environment conducive to seed germination and root development. The first tool for burying and covering the seeds was the Roman plow and plowing that is still considered the most common tillage technique worldwide (Lal et al. 2007).

N. Brahim (✉) · T. Gallali
Faculty of Sciences of Tunis, University of Tunis El Manar, 2092 Tunis, Tunisia
e-mail: nadhem.brahim@fst.utm.tn

H. Ibrahim
Faculty of Sciences of Bizerte, University of Carthage, 7021 Jarzouna, Tunisia

Over the last few decades, there has been a gradual transition around the world between conventional tillage and soil conservation, which is commonly referred to as direct sowing or planting under cover or with no-tillage. Soil conservation work, or the so-called conservation agriculture, includes any technique that leaves more than 30% of the previous crop residue on the surface (Labreuche et al. 2007).

In Tunisia, the practice of no-tillage is more than 15 years old, and the location of plots managed in this way is in most cases on slopes or in small watersheds (Jemai et al. 2013). The purpose of this work is to study the effect of direct seeding on organic carbon sequestration.

2 Materials and Methods

Two adjacent parcels of ≈1 ha each located in Mateur were either directly sowed or subjected to conventional tillage. Historically, the plot which was directly sowed is no longer plowed in the same way as before. It has been three years.

As the investigated plots were located in a watershed, the suitable option was to subdivide each of them into three parts:

- The upper part of the slope, i.e., "top of slope: TS";
- The middle part of the slope, i.e., "mid-slope: MS";
- And the lower part of the slope, i.e., "bottom of slope: BS."

In order to estimate stocks of organic carbon and total nitrogen, the work was on 0–30 cm, i.e., the layer concerned by the plowing. Analyses were carried out considering the following soil layers: 0–5 cm, 5–10 cm, 10–20 cm, and 20–30 cm.

Soil analysis included % organic carbon measured on <2 mm fraction (Walkley–Black method), soil bulk density (D_b) g/cm^3 (cylinder method), and granulometry % (Robenson's pipette method).

A. Çiner et al. (eds.), *Recent Research on Geomorphology, Sedimentology, Marine Geosciences and Geochemistry*, Advances in Science, Technology & Innovation, https://doi.org/10.1007/978-3-030-72547-1_7

Soil organic carbon stocks were estimated by the following equations (Brahim et al. 2014; Yigini and Panagos 2016):

$$\text{SOCstock} = \text{OC} \times D_b \times D \quad (1)$$

where SOCstock represents soil organic carbon stock in ton ha^{-1}, OC the organic carbon content (%), D_b the bulk density (g cm^{-3}), and D (cm) the sampling depth.

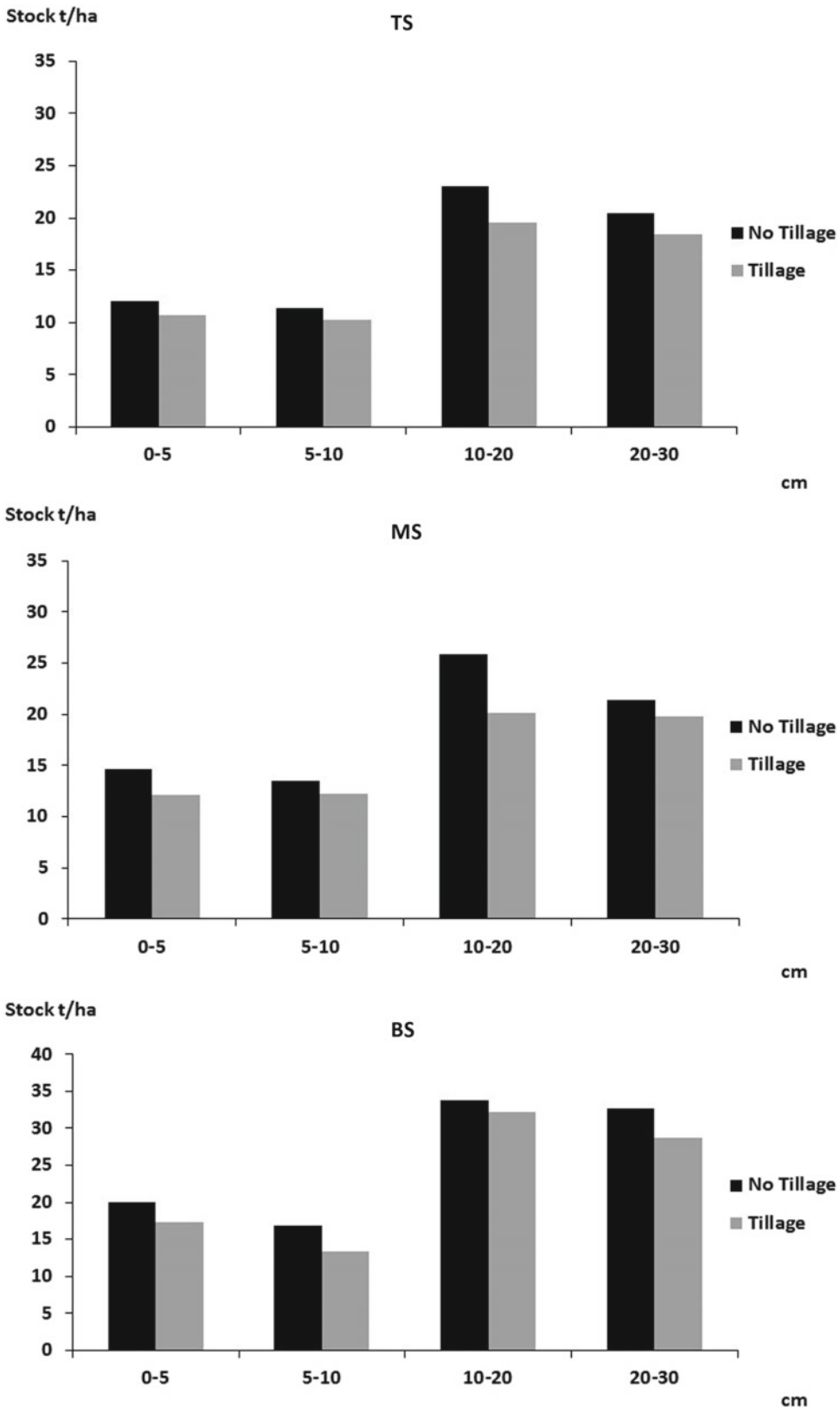

Fig. 1 Evaluation of carbon sequestration in the two plots and on the three levels (TS: top slope; MS: mid-slope; BS: bottom slope) after 3 years

3 Results

After three years, an improvement in the carbon stock was noted throughout the plot and in all layers (Fig. 1).

The total organic carbon stock after three years was as follows:

TS: the stock in t/ha under no-tillage was 66.83 against 59.01 under tillage;

MS: the stock in t/ha under no-tillage was 75.45 against 64.25 under tillage;

BS: the stock in t/ha under no-tillage was 103.14 against 91.59 under tillage.

The results revealed that the carbon stock evolved laterally and vertically. Laterally, i.e., carbon stock increased according to the slope. This could be explained by the transfer of carbon by the runoff, as well as the transfer of the fine material as the clay favorable for its sequestration. Vertically, i.e., the carbon stock was buried deep down to the deepest layers of 30 cm.

4 Discussion

According to Jemai et al. (2013), under sub-humid bioclimate, no-tillage generated a marked improvement in the surface carbon stock and a decrease in bulk density, reflecting an improvement in the porous system, in the water profile, soil moisture content and a decrease in pH. These results agree with ours in terms of increasing levels of organic carbon.

At the TS level, a gain of 7.82 t/ha in 3 years was recorded, i.e., a sequestration of 2.60 t/ha/year. For MS a gain of 11.2 t/ha was found, i.e., a sequestration of 3.73 t/ha/year. Finally, in BS the highest gain of 11.55 t/ha in 3 years was observed, a gain of 3.85 t/ha/year.

Leaving a plant cover on the soil surface throughout the year seems beneficial regardless of the topographic location as a lower or downstream of a watershed. Although, it is assumed in the literature that in slopes there is a transfer of matter (Gallali 2004; Lal et al. 2007). Now that the sequestration is validated under the effect of no-tillage, it is to check whether this sequestration is limited or not. On the environmental side, agricultural practices able to increase carbon stocks should be positively considered as they can contribute to the mitigation of global warming.

5 Conclusions

The transition to no-tillage in a sloping Vertisol resulted in carbon sequestration occurring vertically and laterally. The increase in the organic carbon stock in the first 30 cm of soil was up to 12.6% compared to the initial stock.

References

Brahim, N., Ibrahim, H., Hatira, A.: Tunisian soil organic carbon stock-spatial and vertical variation. Proc. Eng. **69**, 1549–1555 (2014)

Gallali, T.:. Clés des sols. Edition CPU 1ère édition, 400 p (2004)

Jemai, I., Ben, A.N., Ben, G.S., Ben-Hammouda, M., Gallali, T.: Impact of three and seven years of no-tillage on the soil water storage, in the plant root, under a dry Subhumid Tunisian climate. Soil Tillage Res. **126**, 26–33 (2013)

Labreuche, J., Viloingt, T., Caboulet, D., Daouze, J.P., Duval, R., Ganteil, A., Jouy, L., Quere, L., Boizard, H., Roger-Estrade, J.: Evaluation des impacts environnementaux des Techniques Culturales Sans labour (TCSL) en France. Partie I: La pratique des TCSL en France. ADEME (2007)

Lal, R., Reicosky, D.C., Hanson, J.D.: Evolution of the plow over 10,000 years and the rationale for no-till farming. Soil Tillage Res. **93**, 1–12 (2007)

Yigini, Y., Panagos, P.: Assessment of soil organic carbon stocks under future climate and land cover changes in Europe. Sci. Total Environ. **557–558**, 838–850 (2016)

Spectral Characteristics of Soil Types in Northwestern Jordan Considering Iron Oxides Effects and Colors

Wahib Sahwan, Bernhard Lucke, Tobias Sprafke, Kim André Vanselow, and Rupert Bäumler

Abstract

Remote sensing as a tool to map and monitor soil cover in Jordan is very significant for agriculture production. Nonetheless, the still poor state of information about spectral characteristics of Jordan's soils is a challenge, where the understanding of soil spectra is of essential importance. It is especially suited to demonstrate relationships between spectral reflectance data and various soil properties, which correspond to well-known relationships of color, mineral assemblages, and chemical compositions. This study explores the spectral characteristics of soil types in northern Jordan with regard to soil colors and explains the effects of iron oxides on the shape of the spectral curves. A total of 160 bulk samples were collected systematically from the soil surface at 40 locations. Based on laboratory measurements with analytical spectral devices (ASDs), a mean soil reflectance spectrum (MSRS) was calculated. Color measurements of soils were conducted with a spectrophotometer using the CIELAB color space (Commission Internationale de l'Eclairage CIE, (1978)). The results show high correlations between spectral characteristics, soil color variations, and Fe oxides. Whereas organic matter contents seem to play no detectable role. Based on these findings, we were able to distinguish six soil groups in the study area.

Keywords

Spectroscopy • Soil spectra • Iron oxides • Soil color • Jordan

1 Introduction

The need for sustainable soil management and developing the agricultural and pastoral land use in Jordan is a challenge that requires all communities to consider soils. In this context, several studies of soils were accomplished in Jordan to support soil management and land use planning at the national level. The first important work in this field started in 1950 and determined 12 great soil groups at a scale of 1:1,000,000 (Moormann 1959). A systematic nation-wide soil survey and land classification were only conducted in 1989–1993 (NSM & LUP 1993). To evaluate and corroborate these studies, there is an increased need for further research on the spectral characteristics of the soils and for establishing a spectral library of the soils in the country. This is particularly important, as studies on soil spectral reflectance features are the basis for soil remote sensing (Goetz et al. 1985; Huete 1996; Viscarra Rosselet al. 2016). In this context, spectral information has been successfully used to retrieve soil information regarding iron oxides (Stoner and Baumgardner 1981; Escadafal and Heute 1992). The purpose of this study is to determine the spectral characteristics of soil types and the effects of iron oxides on the shape of spectral curves of soils in northern Jordan.

2 Settings, Methods, and Materials

The research area covers 693.77 km^2. It is situated in northern Jordan between the major cities of Irbid and Al Mafraq. The soil types chromoxererts and calcixerollic and xerochreptic calciorthids are present in this area (NSM & LUP 1993). Soil

W. Sahwan (✉) · B. Lucke · K. A. Vanselow · R. Bäumler
Institute of Geography, FAU Erlangen-Nürnberg, Wetterkreuz 15, 91058 Erlangen, Germany
e-mail: wahib.sahwan@fau.de

T. Sprafke
Kompetenzzentrum Boden, BFH-HAFL, Länggasse 85, 3052 Zollikofen, Switzerland

A. Çiner et al. (eds.), *Recent Research on Geomorphology, Sedimentology, Marine Geosciences and Geochemistry*, Advances in Science, Technology & Innovation, https://doi.org/10.1007/978-3-030-72547-1_8

colors range from dark red and brown in the west to lighter colors (more or less yellow) towards the east (Moormann 1959; Sahwan et al. 2018). Soil sample collection sites were located along different landscape units and on transects of soil colors (40 locations covering yellow to red soil colors according to Moormann 1959; Lucke and Sprafke 2015; Sahwan et al. 2018). The samples were collected at depths of 0–10 cm. The locations are mostly on fields used as arable land and were georeferenced using a Global Positioning System (GPS). Laboratory soil reflectance spectra were obtained using an ASD (Field Spec® 3 Hi-Res). The MSRS of each location was calculated from 16 measurements (four samples of each location and four times repeated measurement). The soil colors were measured with a ColorLite sph850 spectrophotometer using the CIELAB system (CIE, 1978). The CIELAB is a three-dimensional Cartesian space with three mutually perpendicular color coordinates: L^* (brightness axis) is the parameter of lightness; a^* (red–green axis) and b^* (yellow–blue axis) are the parameters of chromaticity. Based on the L^* a^* b^* results, the $RI_{LAB\text{-}BT}$ (redness index of Barron and Torrent 1986) was calculated. The index increases with soil redness (Lucke and Sprafke 2015).

$$RI_{LAB-BT} = \frac{a* \left((a*)^2 + (b*)^2\right)^{0.5} \times 10^{10}}{b* \times L*^6} \quad (1)$$

Content of organic carbon (C_{org}), as indicator of organic matter (OM) content, and content of calcium carbonate ($CaCO_3$) were determined using an Elementar vario EL cube C/N-analyzer. Free iron oxides Fe_d (pedogenic oxides) were extracted with sodium dithionite at room temperature according to Holmgren (1967). Major element oxides were measured with an energy-dispersive SPECTRO XEPOS.

3 Results and Discussion

3.1 Soil Chemical and Color Properties

The samples represented alkaline soils, with a pH_w ranging from 7.7 to 9.4. Most of the soils showed low organic matter contents (C_{org} < 1.9%). Calcium carbonate contents varied widely between 1 and 48%. This was also the case for Fe_d (4.1–20.4 mg/g). The $RI_{LAB\text{-}BT}$ values ranged from 1.68 to 48.58. Regarding the content of Fe_d, the high $RI_{LAB\text{-}BT}$ in some cases could probably be attributed to high hematite contents (Lucke and Sprafke 2015).

3.2 Spectral and Chemical Characteristic

In the spectral ranges of major chromophores of soils, the mean soil reflectance spectra have approximately the same absorption features (Chabrillatet al. 2019). This is considerable in the region of hygroscopic water (1400, 1900 nm) and in the region of clay minerals/organic matter (>2200 nm). However, they are characterized by decreasing steep slopes in the range between 350 and 780 nm with sigmoidal form, followed by slight absorption features in the range between 780 and 980 nm. Accordingly, all MSRSs represent types of soils that are affected by Fe oxides (Stoner and Baumgardener 1981; Escadafal and Huete 1992; Sahwan et al. 2020). The effects of Fe oxides on spectra can be illustrated using four morphological distinctions: (1) reflectance intensity values (RIVs); (2) distance between concave sigmoid and Y-axis (DCS); (3) steepness of convex sigmoid (SCS); and (4) iron absorption feature (IAF) as shown in Fig. 1.

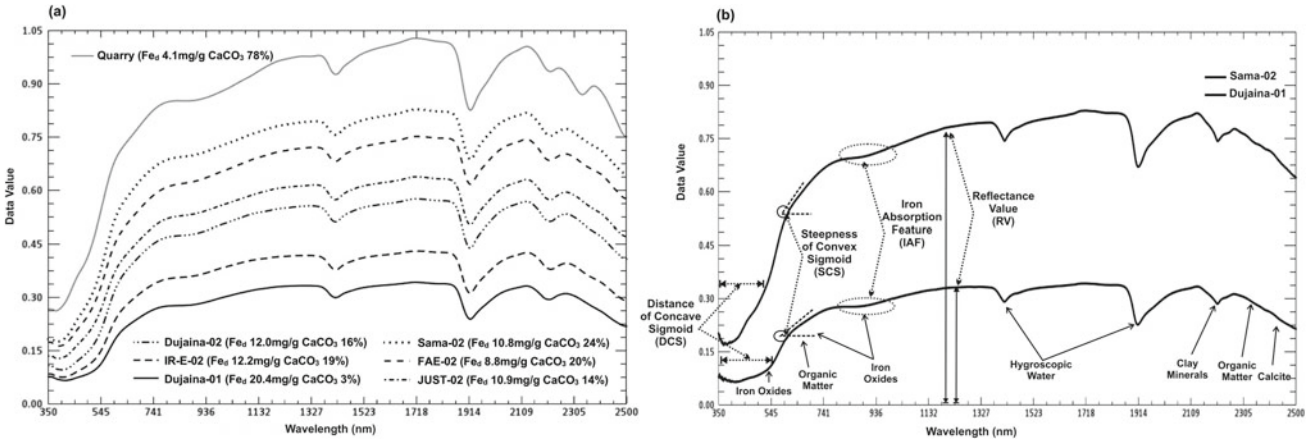

Fig. 1 **a** Representative spectra of selected soil samples and the sample from the limestone quarry and **b** illustrations of the morphological conditions of the curves

3.3 Correlation of Soil Colors with Chemical and Spectral Parameters

Considering the relatively low content of OM (C_{org}), the Fe oxides (probably hematite/goethite) are the dominant pigmenting agents. This suggests that the redness index $RI_{LAB\text{-}BT}$ can indeed be used as an indicator of hematite contents in soils (Barrón and Torrent 1986). In this context, the linear regression between $RI_{LAB\text{-}BT}$ and chemical soil components C_{org}, CaO, and Fe_d shows no ($R^2 = 0.013$, $p > 0.05$), low ($R^2 = 0.25$, $p = 0.001$), and high ($R^2 = 0.58$, $p < 0.001$) relations, respectively. This result suggests that the effect of OM on the colors of the samples is negligible. The low coefficient of determination with CaO percentage shows that calcium carbonate plays a secondary role, too. In contrast, the considerably high coefficient of determination with Fe_d highlights the effect of Fe oxides on soil colors.

$RI_{LAB\text{-}BT}$ is correlated with all spectral values of MSRSs in all spectral wavelength ranges (SWRs). The findings indicate a strong linear relationship ($R^2 = 0.82, p < 0.001$). Further, the correlation between $RI_{LAB\text{-}BT}$ and the condition SCS is evaluated indicating the proportion of hematite/goethite.

4 Conclusion

The high similarity of the spectral curve shapes in the ranges of significant soil chromophores except for the ranges of iron oxides confirms that the iron minerals are the main chromophores in the soils in northwestern Jordan. Consequently, this study used successfully morphological conditions to highlight the effects of iron oxides on spectra as well as to distinguish between these spectra. Statistically, the study demonstrated clear relationships between the spectra, chemical components, and color characteristics of the soils. It revealed that the significant contrast between the spectra is a result of Fe oxide effects, or the proportion of hematite/goethite, which dominates the soil colors, while no significant coloring effect of organic matter could be detected. Depending on the morphological conditions, the mean soil reflectance spectra were arranged qualitatively in six groups from Gr. I to Gr. VI. Figure 1 illustrates the representative curves of these groups.

References

Chabrillat, S., Ben-Dor, E., Cierniewski, J., Gomez, C., Schmid, T., van Wesemael, B.: Imaging spectroscopy for soil mapping and monitoring. Surv. Geophys. **40**(3), 361–399 (2019)

Commission Internationale de l'Eclairage CIE: Recommendations on uniform color spaces, color-difference equations, psychometric color therms (1978)

Escadafal, R., Huete, A.R.: Soil optical properties and environmental applications of remote sensing. International Society for Photogrammetry and Remote Sensing Archives **29**(B7), 709–715 (1992)

Goetz, A.F., Vane, G., Solomon, J.E., Rock, B.N.: Imaging spectrometry for earth remote sensing. Science **228**(4704), 1147–1153 (1985)

Huete, A.R.: Extension of soil spectra to the satellite: atmosphere, geometric, and sensor considerations. Photo Interpretation **34**(2), 101–118 (1996)

Lucke, B., Sprafke, T.: Correlation of soil color, redness ratings, and weathering indices of Terrae Calcis along a precipitation gradient in northern Jordan. Soils and sediments as archives of environmental change. Geoarchaeology and landscape change in the subtropics and tropics, pp. 53–68 (2015)

Moormann, F.: The soils of East Jordan: Report to the government of Jordan (Expanded Technical Assistance Program No. 1132). FAO, Rome (1959)

NSM & LUP: Hashemite Kingdom of Jordan, ministry of agriculture, hunting technical services ltd., soil survey and land research centre. National Soil Map and Land Use Project. The soils of Jordan. Level 1, Reconnaissance Soil Survey, Vol. 2, Main Report. Amman (1993)

Sahwan, W., Lucke, B., Kappas, M., Bäumler, R.: Assessing the spatial variability of soil surface colors in northern Jordan using satellite data from Landsat-8 and Sentinel-2. European Journal of Remote Sensing **51**(1), 850–862 (2018)

Sahwan, W., Lucke, B., Sprafke, T., Vanselow, K.A., Bäumler R.: Relationships between spectral features iron oxides and colours of surface soils in northern Jordan. Eur. J. Soil Sci. **72**(1), 80–97 (2020)

Stoner, E.R., Baumgardner, M.F.: Characteristic Variations in Reflectance of Surface Soils 1. Soil Sci. Soc. Am. J. **45**(6), 1161–1165 (1981)

ViscarraRossel, R. A., Behrens, T., Ben-Dor, E., Brown, D. J., Demattê, J. A. M., Shepherd, K. D., ...&Aïchi, H. (2016). A global spectral library to characterize the world's soil. Earth-Science Reviews, 155, 198-230

Examining Wind-Eroded Sediment Especially the Content of Toxic Elements, Southern Hungary

Katalin Csányi, Károly Barta, József Szatmári, and Andrea Farsang

Abstract

Intensive soil use, inadequate agricultural cultivation and agrotechnology lead to an increase in soil deflation sensitivity. Wind-eroded sediment and dust, as an environmental transport pathway of toxic elements, can result in environmental and human exposure far beyond the agricultural areas where it has been applied. Thus, it is crucial to examine the spatial and temporal variations in the harmful and pollutant content of the topsoils. These effects can be tested by in situ wind tunnel experiments. These attempts were conducted on a Chernozem soil at the summer of 2017–2018 in Southern Hungary. Before the experiments, a portion of the sample area was treated with chlorpyrifos and pendimethalin. A control area was also selected. In 2017–2018, a total of 28 wind event experiments were conducted by examining the topsoil samples (pH (H_2O)), $CaCO_3$, Arany yarn test, OM %, total salt content, humidity, pendimethalin and chlorpyrifos contents, and the toxic element contents in the rolling soil fractions. Pesticide measurements were performed by LC–MS. The enrichment ratios (ER) were then calculated. The measurements obtained in 2017 indicated that the average of the enrichment values of chlorpyrifos is 3.4. The measurements obtained in 2018 revealed that the pendimethalin ER is much higher in the rolled fraction (mean: 13.7) than chlorpyrifos (mean: 2.9). Therefore, a significant correlation between the ER of chlorpyrifos and pendimethalin can be concluded.

Keywords

Wind erosion • Pesticides • Chernozem soil • Wind tunnel

1 Introduction

Due to climate change, intensive soil use, inadequate agricultural cultivation, and agrotechniques, there has been an increase in soil deflation sensitivity. The physical degradation of nutrient-rich topsoil is not the only problem. The removal of toxic elements from the affected areas is also responsible for moving soil particles. Deflation can become a significant human health problem, especially for inhabitants of settlements where arable land under intensive cultivation is dominant. The airborne particles released by the wind have a severe impact on human and animal health. Due to their size, they can easily reach the bronchial tube by inhalation, causing severe respiratory diseases (Toy et al. 2002). At medium wind speeds, significant dust emissions have been observed in different countries of Europe (Gossens 2002; Bärring et al. 2003; Szatmári 1997).

In total, 25% of Hungary's territory is moderate, while 40% is very sensitive to deflation (Farsang et al. 2013) (Fig. 1). Deflation processes can be well modeled with in situ wind tunnels (Farsang 2016; Szabó et al. 2007). This study research aims to evaluate the potential risks of agricultural dusts using portable wind tunnel.

2 Sample Area and Methods

The study area is located near Szeged. It is composed of Chernozem soils. The wind tunnel studies were conducted in summer of 2017 and 2018 (Fig. 2). The sample area was of 20 m * 40 m and 40 * 50 m in 2017 and 2018, respectively.

Before the experiment, a part of the sample area was treated with chlorpyrifos (2 l/ha) and pendimethalin (5 l/ha). A control area was also selected. In the summer of 2017–2018, a total of 28 wind event tests were conducted. The undisturbed surface soil was measured in a portable and adjustable 12-m-long field wind tunnel in situ on the study plot. Samples were taken from the topsoil (0–5 cm) before

K. Csányi (✉) · K. Barta · J. Szatmári · A. Farsang
University of Szeged, Szeged, 6720, Hungary
e-mail: csanyi@geo.u-szeged.hu

A. Çiner et al. (eds.), *Recent Research on Geomorphology, Sedimentology, Marine Geosciences and Geochemistry*,
Advances in Science, Technology & Innovation, https://doi.org/10.1007/978-3-030-72547-1_9

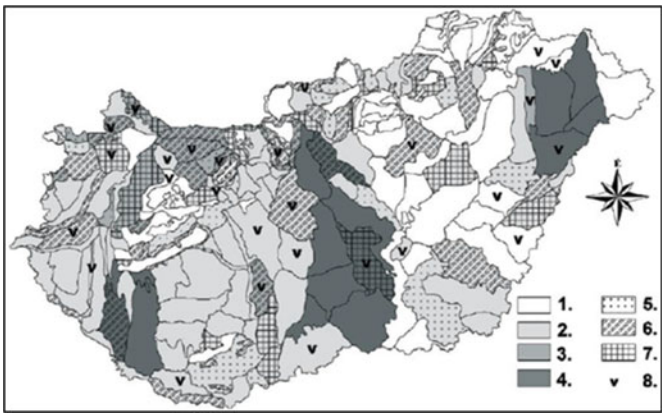

Fig. 1 Danger of wind erosion in Hungary: 1—danger of wind erosion can be neglected, 2—low, 3—medium, 4—severe, 5—25% of the small areas are threatened by lower wind erosion, 6—50%, 7—75%, 8—some parts of the small areas are threatened by high wind erosion (Csányi et al. 2019)

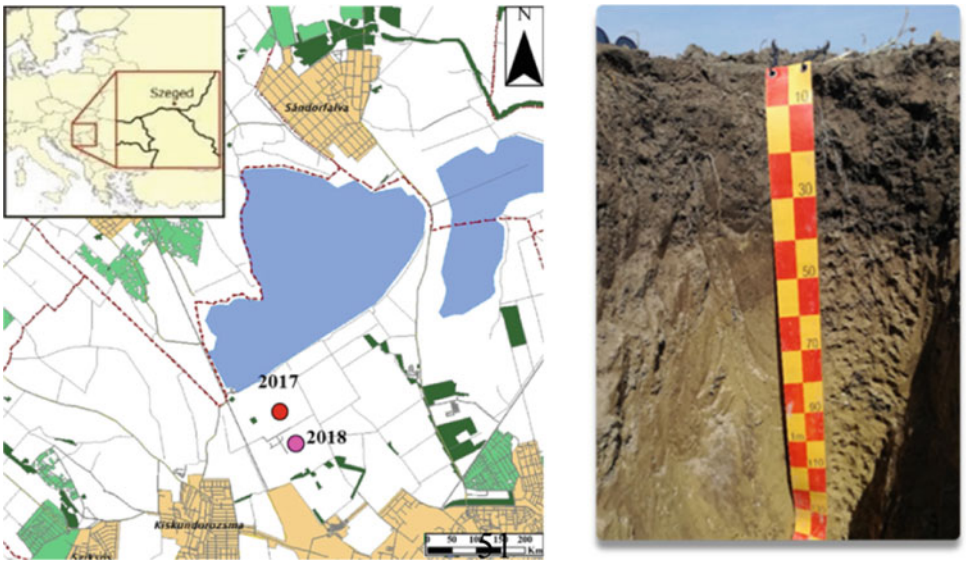

Fig. 2 Sampling points and deep soil profile in the area near Szeged

and after the wind event at three different places in the wind tunnel. The rolling soil samples (sediments) were collected at the end of the wind tunnel using a clean brush (Fig. 3) [10].

In the laboratory, the analyses of the topsoil samples (pH (H_2O)), $CaCO_3$ (%), Arany yarn test, OM %, total salt content (%), humidity (%), pesticide contents, and the collected rolling soil samples (chlorpyrifos, pendimethalin concentrations) were carried out according to standard procedures.

Furthermore, the enrichment ratios (ER) of concentrations in the rolling samples were calculated (1). The statistical tests were carried out by SPSS software (IBM SPSS Statistics, Version 24).

$$\mathrm{ER} = \text{Organic compound}_{\text{sediment}}/\text{Organic compound}_{\text{soil}} \quad (1)$$

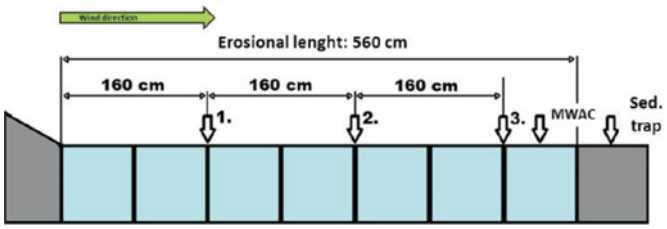

Fig. 3 Location of the soil sample points and the sediment trap (Maurer et al. 2006; Szabó et al. 2007)

Table 1 Soil properties of the Chernozem soil used in this study

$N = 28$	pH (H_2O)	OM%	$CaCO_3$ (%)	Arany yarn number	Soil texture class	Total salt content (%)
2017 (average)	8.03	3.15	0.98	35	Sandy loam	0.03
2018 (average)	7.58	2.68	7.13	39	Loam	0.02

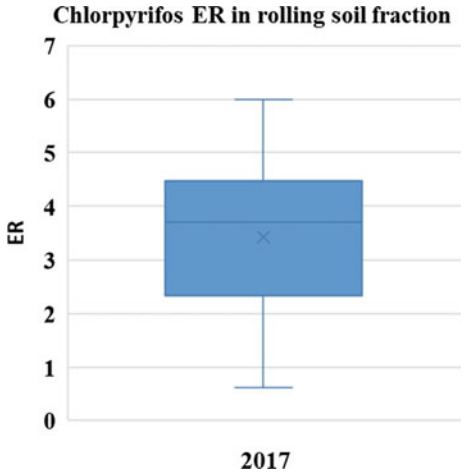

Fig. 4 Chlorpyrifos concentration and ER values based on 2017 measurements

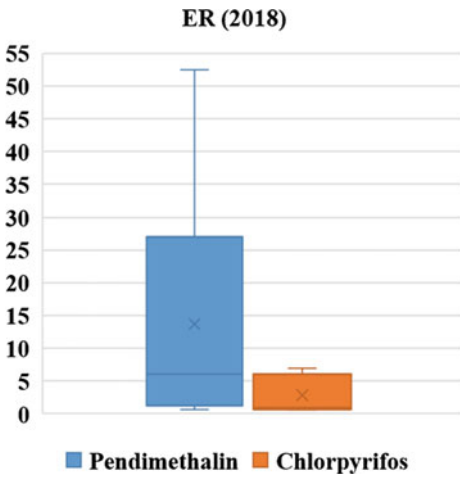

Fig. 5 Chlorpyrifos concentration and ER values based on 2018 measurements

3 Results and Discussion

The topsoil sample properties are shown in Table 1. The average humidity content was 1.44%.

Boxplot diagrams represent the evolution of enrichment factors in the scrolled sediment. The mean value of chlorpyrifos in 2017 is 3.4 (Fig. 4). In 2018, the mean value of chlorpyrifos is 2.9 and of pendimethalin is 13.7 (Fig. 5). Pendimethalin ER is much higher in the rolled fraction than chlorpyrifos.

The statistical tests revealed a strong significant relationship between the pesticide's enrichment factors and the pesticide concentration of the soil and between pendimethalin ER chlorpyrifos ER as well ($p < 0.01$) (Fig. 6).

Fig. 6 Correlation results (Made by SPSS Statistics statistic software)

Correlations					
		Chlorpyrifos in topsoil (mg/kg)	Pendimethalin in topsoil (mg/kg)	ER Chlorpyrifos	ER Pendimethalin
Chlorpyrifos in topsoil (mg/kg)	Pearson Corr	1			
	Sig. (2-tailed)				
	N	9			
Pendimethalin in topsoil (mg/kg)	Pearson Corr	,895**	1		
	Sig. (2-tailed)	,001			
	N	9	9		
ER Chlorpyrifos	Pearson Corr	-,892**	-,954**	1	
	Sig. (2-tailed)	,001	,000		
	N	9	9	9	
ER Pendimethalin	Pearson Corr	-,817**	-,822**	,828**	1
	Sig. (2-tailed)	,007	,007	,006	
	N	9	9	9	9
**. Correlation is significant at the 0.01 level (2-tailed).					

4 Conclusions

In this work, field wind tunnel measurements were performed on Chernozem soil in South Great Plain. The present study aimed to investigate the toxic element contents of wind-eroded sediment. The measurements showed that the enrichment of chlorpyrifos and pendimethalin could be detected in the rolling particles.

References

Bärring, L., Jönsson, P., Mattsson, J.O., Åhman, R.: Wind erosion on arable land in Scania, Sweden and the relation to the wind climate: a review. CATENA **52**, 173–190 (2003)

Csányi, K., Barta, K., Szatmári, J. Farsang, A.: Potential environmental impacts of powders of agricultural origin, with particular regard to the effects of pesticide, Southern Hungary. Geophys. Res. Abstracts **21**, EGU2019–16167, 1 p (2019)

Farsang, A., Duttmann, R., Bartus, M., Szatmári, J., Barta, K., Bozsó, G.: Estimation of soil material transportation by wind based on in situ wind tunnel experiments. J. Environ. Geogr. **6**(3–4), 13–20 (2013)

Farsang, A.: A víz- és szélerózió szerepe a talaj humusz- és elemtartalmának horizontális átrendeződésében. MTA doktori értekezés. Szeged, 183 p (2016)

Gossens, D.: On-site and off-site effects of wind erosion. In: A. Warren (ed.) Wind Erosion on Agricultural Land in Europe Office for Official Publications of the European Communities, pp. 29–38. EUR 20370 (2002)

Maurer, T., Herrmann, L., Gaiser, T., Mounkaila, M., Stahr, K.: A mobile wind tunnel for wind erosion field measurements. J. Arid Environ. **66**, 267–271 (2006)

Szabó, J., Lóki, J., Tóth, Cs., Szabó, G.: Természeti veszélyek Magyarországon, Földrajzi Értesítő 2007. LVI. Évf. 1–2. füzet, pp. 15–37 (2007)

Szatmári, J.: Evaluation of wind erosion risk on the SE part of Hungary. Acta Geographica Szegediensis. **XXXVI**, 121–135 (1997)

Toy, T.J., Foster, G.R., Renard, K.G.: Soil erosion: Processes, Prediction, Measurement, and Control, 338 p. Wiley, New York, (2002)

Time-Scale Variation of Organic Carbon in Paddy Soil in Sanjiang Plain, China

Wang Qiuju, Liu Feng, and Chi Fengqin

Abstract

To clarify the temporal variation of soil organic carbon in various types of paddy soil, meadow soil, black soil and planosol in the Sanjiang plain were investigated. Also, the variation in soil morphology with respect to carbon content spanning 40 years of rice cultivation was studied. The results showed that the relationships between carbon accumulation (Y) in total organic carbon, humus organic carbon, mineralizable organic carbon and carbohydrate organic carbon and rice-cultivation time (X) were consistent with the $Y = AX^B$ function model. Total organic carbon and humus organic carbon increase as rice-cultivation time increases; while there is a negative correlation between mineralizable organic carbon and carbohydrate organic carbon.

Keywords

Sanjiang plain • Paddy soil • Rice cultivation • Temporal variation • Carbon • Power function

1 Introduction

Soil organic carbon (SOC) accounts for two-thirds of the carbon pool in the entire terrestrial ecosystem () and plays an important role in global carbon circulation. Multiple factors influence the various forms of organic carbon, such as climatic conditions, topography, soil properties, vegetation types, human activities and a certain scale effect (Li et al. 2005; Tan et al. 2004; Jinfu et al. 2011). On a larger scale, climatic conditions play an important role in soil organic carbon (Xinwang 2018). At small scales, SOC distribution is closely related to soil type, vegetation type, topography and land use patterns, wherein soil type and land use patterns are the most influencing factors of spatial distribution of SOC density (Chengjun et al. 2013). Sanjiang plain is located at the northeastern border of China. It is known for soybean and wheat cultivation. Due to the low-lying terrain, the plains are highly flood-prone and have clayey soil. As a result, crop production has been low and unstable (Heilongjiang Statistic Bureau 2017). To raise crop production, Sanjiang plain has shifted toward rice cultivation since the 1990s. After shifting to rice paddy cultivation, the soil would be submerged for three months a year; thus, SOC accumulation varied significantly. However, after long-term planting of rice, under the special climatic conditions of the Sanjiang plain, the changes in SOC and different forms of organic carbon in various types of paddy soil are still undetermined. To clarify the temporal variation of SOC in various types of paddy soil, this paper conducts a comparative analysis of the variation of various forms of organic carbon in the three types of soil—meadow soil, black soil and planosol spanning 40 years.

2 Materials and Methods

2.1 Location of Sanjiang Plain

Sanjiang plain is located in the eastern part of Heilongjiang Province (129° 11′–135° 05′ E, 43° 49′–48° 27′ W). It has a temperate continental monsoon climate, with an annual average temperature of 1°–4°, annual effective accumulated growing degree units (GDU) of 2200°–2500°, average annual precipitation of 550–600 mm and a frost-free period of 110–135 days (Lian 2000). The soil texture in Sanjiang plain is sticky and vulnerable to water logging due to its low-lying terrain.

W. Qiuju (✉) · L. Feng · C. Fengqin
Institute of Soil Fertilizer and Environment Resources, Heilongjiang Academy of Agricultural Sciences, Harbin, 150086, China
e-mail: bqjwang@126.com

W. Qiuju
Key Laboratory of Heilongjiang Soil Environment and Plant Nutrient, Harbin, 150086, China

A. Çiner et al. (eds.), *Recent Research on Geomorphology, Sedimentology, Marine Geosciences and Geochemistry*, Advances in Science, Technology & Innovation, https://doi.org/10.1007/978-3-030-72547-1_10

2.2 Test Soil and Sample Collection

The soil types investigated in this study include meadow soil, black soil and planosol. A total of 45 samples were collected and tested three times. The samples were collected from Jiansanjiang Region of Sanjiang plain, adjacent to paddy soil where rice had been cultivated for 40a. Typical sectional views of each type soil are shown in Fig. 1. Meadow soil and black soil have a deep and thick black soil horizon, while planosol has a thin black soil horizon of about 20 cm. Soil samples were collected between October 10, 2015, and November 10, 2015, based on time–space inter-substitution (Liumei et al. 2011; Feng and Zhongming 2010). The sampled soil had a rice-cultivation age of 1*40a. The soil of the first year of rice cultivation was considered as the background control. For each plot, 1.5 kg of 5–15 cm soil samples was collected to avoid surface heterogeneity.

2.3 Measurement Item and Method

This paper adopts oil-bath potassium dichromate oxidation-volumetric method for total organic carbon (TOC) measurement (Xiwen et al. 2008), sodium phosphate extraction-potassium dichromate volumetric method for humus organic carbon (HOC) measurement (Bingqing et al. 2015), constant temperature culture-hydrochloric acid titration method and anthrone colorimetric method for mineralizable organic carbon (MOC) and carbohydrate organic carbon (COC) measurement (Shide et al. 2018; Wei et al. 2006).

3 Results and Discussion

3.1 Soil Carbon Variance Analysis

Table 1 shows the variance analysis of different types of organic carbon in the three types of paddy soils. It appears that the order of TOC and HOC is meadow soil > black soil > planosol. The order of COC and MOC for the three paddy soils is consistent with the order of TOC.

3.2 Soil Carbon-Level Regression Analysis

3.2.1 Relationship Between Organic Carbon of Different Soils and Rice-Cultivation Time

The results indicate that the relationships between TOC, HOC and rice-cultivation time confirm with the $Y = AX^B$ function model (Figs. 2, 3, 4 and 5). The regression equation is shown in Table 2. The B values of TOC regression equations of different soils are similar, ranging from 0.0407 to 0.0666. This indicates that TOC of different soils has similar growth rates. Moreover, in the absence of exogenous organic matter, it is difficult for planosol with low organic carbon content to reach the level of meadow soil. The initial content of HOC in meadow soil is higher than black soil and slightly higher than planosol. The HOC of planosol and black soil, which have similar initial content, is close to the same level after 25–30 years of rice cultivation. Longer rice-cultivation time indicates lower MOC and HOC.

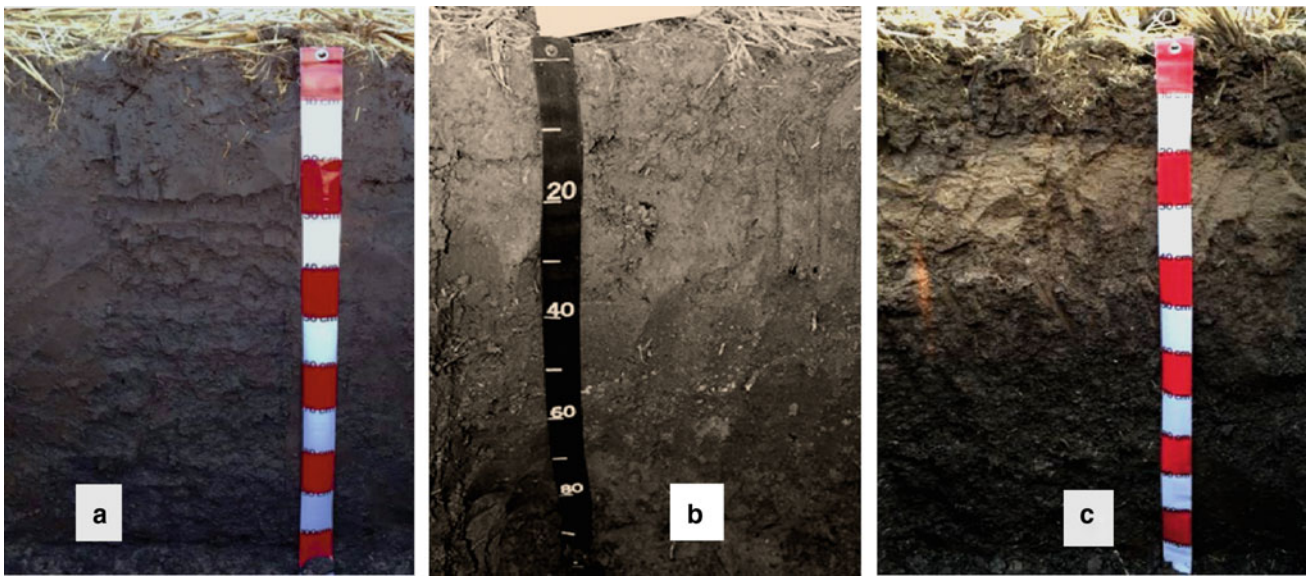

Fig. 1 Profile of typical soil (**a** meadow soil, **b** black soil and **c** planosol)

Table 1 Variance analysis of soil organic carbon

Category	Soil type		
	Meadow soil (MS) (g/kg)	Black soil (BS) (g/kg)	Planosol (PS) (g/kg)
TOC	38.03 ± 2.33aA	27.05 ± 1.67bB	20.55 ± 1.89cC
HOC	6.22 ± 0.74aA	5.29 ± 0.70abA	4.93 ± 0.78bA
COC	3.14 ± 0.73aA	2.78 ± 0.69aA	2.39 ± 0.19aA
MOC	1.40 ± 0.29aA	1.35 ± 0.42aA	1.08 ± 0.16aA

Note Lowercase letters mean significant at 0.05 level, and capital letters mean significant at 0.01 level

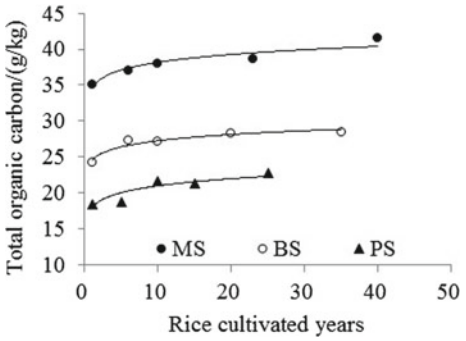

Fig. 2 Temporal variation of TOC

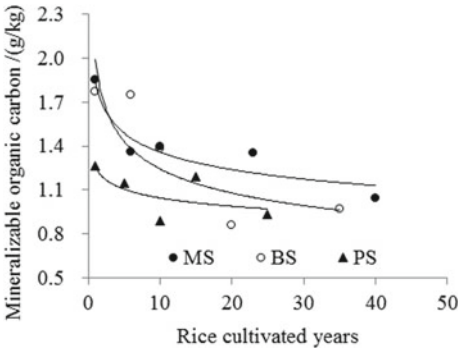

Fig. 4 Temporal variation of MOC

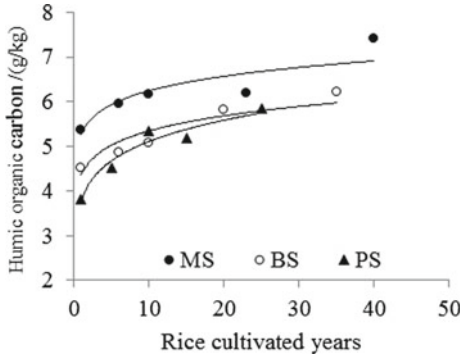

Fig. 3 Temporal variation of HOC

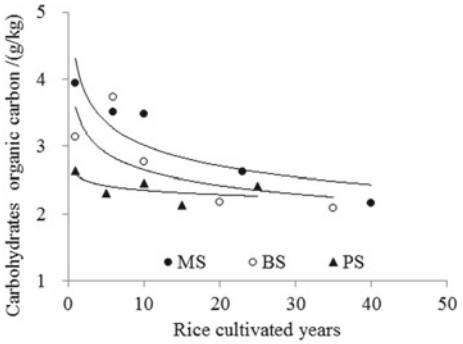

Fig. 5 Temporal variation of COC

3.2.2 Effect of Rice-Cultivation Time on Carbon Content in Different Soil Components

Measurement values of the different types of dry soil before rice cultivation are 100% standardized, respectively. Figure 6 reveals that the relationship between the accumulation of carbon content in various soil components (Y) and time (X) confirms with the $Y = AX^B$ function model: $Y_{TOC} = 99.455X^{0.0489}$; $Y_{HOC} = 98.717X^{0.0915}$; $Y_{MOC} = 104.77X^{-0.146}$; $Y_{COC} = 108.29X^{-0.117}$ respectively. In the TOC and HOC accumulation equation, $B > 0$, indicating the growth effect of power function.

4 Conclusions

(1) The relationships between TOC, HOC, MOC, COC accumulation (Y) and rice-cultivation time (X) in the tested meadow soil, black soil and planosol confirm with the $Y = AX^B$ function model.

2) In third soil type, TOC and HOC accumulation models, $B > 0$, which indicates the TOC and HOC increase as rice-cultivation time increases. Whereas in TOC and HOC model accumulation models, $B < 0$, which indicates the TOC and HOC decrease as rice-cultivation time increases.

Table 2 Fitting equations of organic carbon variation with rice-cultivation time

Organic carbon type	Regression equation $Y = AX^B$			
	Soil	A	B	R^2
TOC	MS	34.746	0.041	0.907
	BS	24.519	0.046	0.949
	PS	17.966	0.067	0.806
HOC	MS	5.265	0.074	0.807
	BS	4.342	0.089	0.867
	PS	3.785	0.129	0.954
MOC	MS	1.843	-0.133	0.859
	BS	1.995	-0.205	0.703
	PS	1.258	-0.081	0.425
COC	MS	4.309	-0.155	0.801
	BS	3.584	-0.131	0.535
	PS	2.576	-0.04	0.394

Y represents the value of the equation-dependent variable, X represents year, A represents the initial value, and B represents the cumulative coefficient

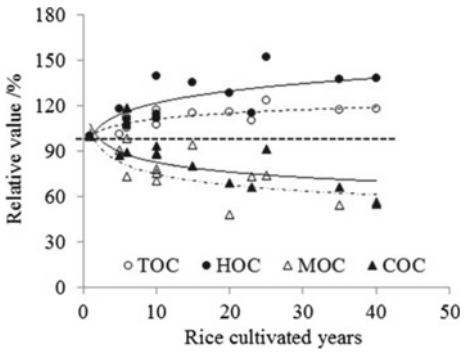

Fig. 6 Variation in relative value of different types of organic carbon

The above regression functions can be applied to estimate the cumulative variation of organic carbon in Sanjiang plain after rice cultivation.

References

Bingqing, L., Zicheng, X., Huagang, H., et al.: Composition characteristics of soil humus of light- sweet flavor style of flue- cured tobacco in Wumeng Tobacco- growing areas. Chin. J. Soil Sci. **46** (2), 382–385 (2015)

Chengjun, G.: Main factor controlling SOC spatial distribution at the province scale as affected by soil type and land use. ACTA PEDOLOGICA SINICA **50**(3), 425–432 (2013)

Feng, J., Zhongming, W.: Comprehensive evaluation of soil fertility abandoned cropland based on attribute recognition model. J. Soil Water Conserv. **24**(5), 204–208 (2010)

Jinfu, L., Songjin, S., Zhongsheng, H., et al.: Spatial distribution and influencing factors of soil organic carbon in mid-subtropical Castanopsis kawakamii natural forest. J. Mountain Sci. **29**(6), 641–648 (2011)

Li, Z., Baoguo, L., Guangsheng, Z.: Advances in controlling factors of soil organic carbon. Adv. Earth Sci. **20**(1), 90–105 (2005)

Lian, H.: Sanjiang Plain of China. Heilongjiang Science and Technology Press, Harbin (2000)

Liumei, C., Ganlin, Z.: Soil chronosequences and their signigicance in the study of pedogenesis. Acta Pedol. Sin. **48**(2), 419–428 (2011)

Shide, H., Gongfu, Y., Linjie, et al.: Effects of drying-wetting cycles on soil organic carbon mineralization along an elevation gradient in Wuyi Mountain. Chin. J. Ecol. **37**(2), 312–321 (2018)

Statistics Bureau of Heilongjiang Province: Statistical Yearbook of Heilongjiang Province. China Statistics Publishing House, Beijing (2017)

Tan, Z.X., Lal, R., Smeck, N.E., et al.: Relationships between surface soil organic carbon pool and site variables. Geoderma **121**(3–4), 187–195 (2004)

Wei, Z., Hongtu, X., Hongbo, H.: Soil carbohydrates: their determination methods and indication functions. Chin. J. Appl. Ecol. **8**(17), 1535–1538 (2006)

Xinwang, X.: Regional distribution and variation of SOC storage in agricultural soils at different scales. Nanjing agricultural university, Dissertation of doctors degree (2008)

Xiwen, Y., Dequan, M.: Technical Manual on Soil Determination Formula Fertilization. Map Press, Harbin (2008)

Geomorphology, Soil Science, Landslides, Coastal Processes, and Geoarchaeology (T9): Landslides and Debris Flows

Stability Assessment of a Cliff and Hazard Characterization Methodology of the "Landslide": Application to Korbous Cliff (Cap-Bon, Tunisia)

Nouha Brachen, Radhia Mansour, and Abdessalem El Ghali

Abstract

Areas with a high probability of a natural event occurrence such as "landslides" can be detected from a morpho-structural study of rough terrain. Indeed, morphometric and tectonic statistic analysis of a quite contrasting lithology terrain can lead to the compartments identification where discontinuities can induce slope instability. Several regions in the northeast of Tunisia are facing the "rockfall" hazard. In particular, Jebel Korbous presents a very contrasted territory, from both a morphological point of view with its mountains and its coastal exposure and a geological point of view with rugged lithological formations characterized by the diversity of their resistance (sandy limestone, sandstone, marl). The steep slopes rockfalls are quite frequent; they constitute a potential risk to infrastructure and habitats at the bottom of slopes. In this context, it is critical to understand the blocks detachment mechanism and morpho-structural conditions of their mobilization. To this end, a new multi-method approach is proposed to characterize and evaluate the potential vulnerability of an unstable ground as well as landslide risk, through morpho-tectonic, geological and morphometric analysis integrated into a geographic information system (GIS). A potential landslide risk map is proposed for the region of Korbous. The map would serve as a guide and decision-support tool for the choice of preventive measures for reducing disaster risk (RDR).

Keywords

Slope instability • Morphometric • Landslide hazard • Risk • Morpho-tectonic

1 Introduction

Despite the evolution of the recognition multitude techniques, in addition to the improvement of mitigation measures, land movements that still constitute a source of danger with negative social, economic, and environmental repercussions can sometimes have catastrophic consequences (Eberhardt et al. 2001).

Several parameters could interfere in the shaping and changing of the rocky clump morphology throughout time (Hantz and Lirigm, 1998–2000), among which, we can mention:

The geology (Fig. 6), which is expressed on the ground by the contrast of competence resulting from the alternation of an unconsolidated geological formation (laminated clays) and compact (resistant sandstone) (Ben Salem 1992).

The morpho-structures with steep slopes governed by the combination and the interaction of neo-tectonic (Fig. 2) and water erosion following a river system (Fig. 3), creating a morphometric envelope with an exhibition multi-directional surface and slopes which often exceeds 25° (Fig. 4).

This study uses GIS for the integration and examination of the database, aiming to evaluate the role of these physical parameters in the morphological change of Korbous cliff and the degree of their influence in triggering the landslide hazard. The identification and characterization of the risk associated to this sort of movement have been identified through the integration of a high-resolution digital elevation model "DEM" (Fig. 5) that provides information and derives maps such as the convexity profiles and the different sizes curves maps. The compilation of results has helped to define vulnerable landforms and detachment of the areas of the blocks and the unstable areas better (Shantanu and Debi Prasanna 2017).

The 3-dimensional representation of a digital elevation model (DEM) serves to identify the relief (slope, slope orientation, roughness of terrain) and perform geometrical treatment (identification of fault planes, study of the river

N. Brachen (✉) · R. Mansour · A. E. Ghali
Faculty of Science of Bizerte, University of Carthage, 7021 Jarzouna, Tunisia

A. Çiner et al. (eds.), *Recent Research on Geomorphology, Sedimentology, Marine Geosciences and Geochemistry*, Advances in Science, Technology & Innovation, https://doi.org/10.1007/978-3-030-72547-1_11

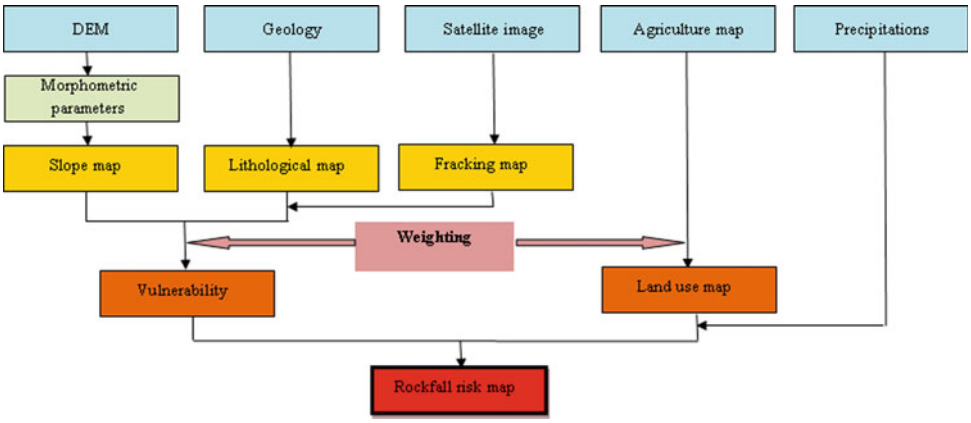

Fig. 1 Flowchart of the adopted methodology

system). Both the DEM and the derived maps processing and analysis have authorized the geo-morphological and structural characterization of the study area surface (Achu and Rajesh 2017) (Hadji et al. 2018).

2 Materials and Methods

This study aims to evaluate the landslides risk of Korbous cliff according to detailed morphometric features, hydrological studies, and meteorological analyzes. To this end, the ASTER data were used to prepare a digital elevation model (DEM), and a geographic information system (GIS) was adopted for the evaluation of linear, surface, and relief aspects, in addition to agricultural maps for the establishment of land use (Fig. 8). Precipitation values were collected from the National Institute of Meteorology (NIM) (Hammouda et al. 2014), and these thematic layers (slope, relative relief, land use, precipitation, drainage density, lithology, road proximity and curvature) were integrated into a database to elaborate the terrain movement risk map. The used data, processing as well as the analysis of the results, are presented in the flowchart in Fig. 1 (Achu and Rajesh 2017) (Hadji et al. 2018).

3 Results

3.1 Slope

The majority of landslides occurrence depends on its slope angle derived from a digital elevation model and reclassified into four different classes: flat slope (<5°), gentle slope (5–15°), moderate slope (15–25°), and very high slope (>25°) (Achu and Rajesh 2017) (Fig. 4).

This factor, in addition to the fracturing (Fig. 2) and lithological factors (Fig. 7), plays a very decisive role in the landslide occurrence (Figs. 3, 4, 5, 6, 8, 9, 10, 11, and 12).

3.2 Rainfall

With its irregularity and torrential character, rainfall is one of the critical factors triggering landslides in the unstable sectors (Achu and Rajesh 2017) (Hadji et al. 2018) (El Mekki et al. 2017). The precipitation data of 2018 were collected from the National Institute of Meteorology and analyzed for this study (see Fig. 13).

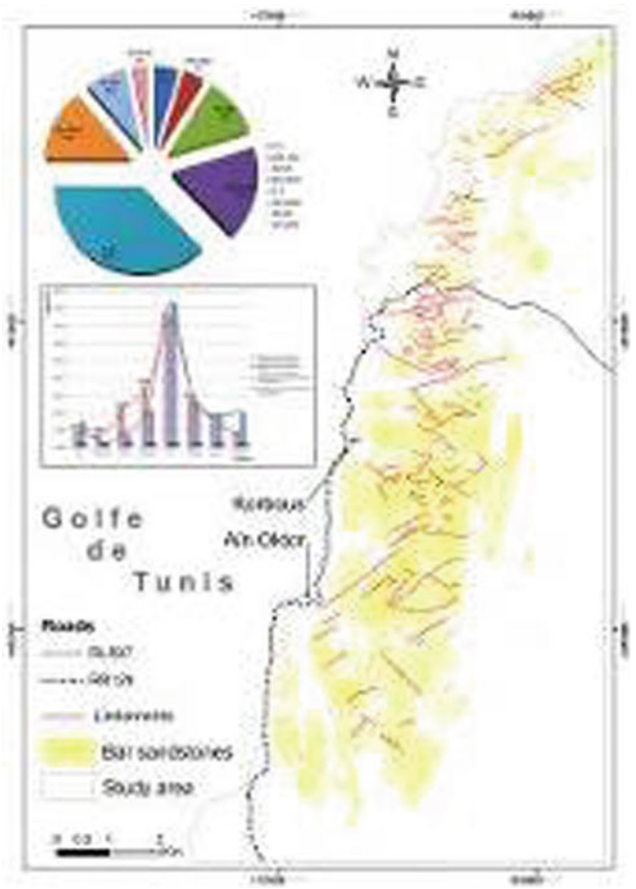

Fig. 2 Linear map

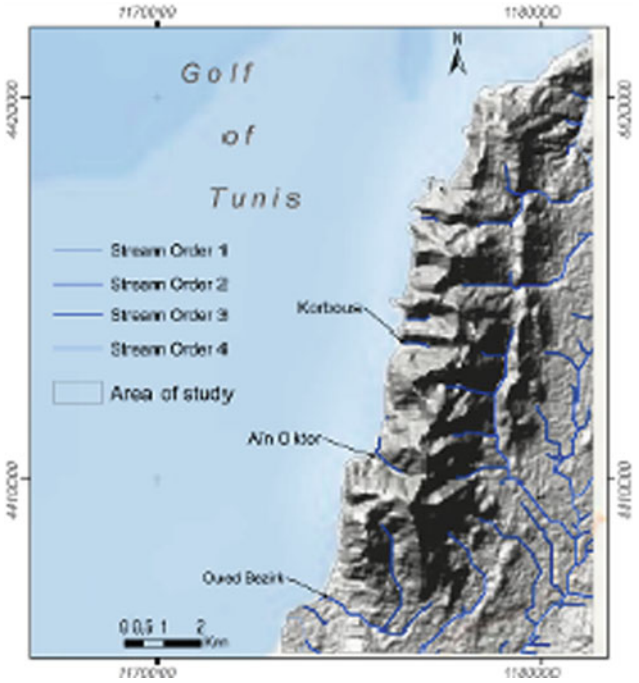

Fig. 3 Stream network

Fig. 4 Slope

4 Discussion

The findings revealed that the instability hazards of this cliff were related to the tilting and sliding dihedral manifested by block falls, in addition to landslides in sandstone caused by the erosion of soft levels. These hazards were mapped along the Korbous cliff and classified in terms of how threatening and dangerous they could be. This work was imperative to help plan and choose the necessary actions in order to stabilize the cliff and secure the road and the city.

5 Conclusions

The various combinations of the basic maps in a GIS environment allowed the establishment of the landslide risk map of our study area.

This study highlighted the importance of the interaction between the different natural parameters (topography, slope, curvature, relative relief, rainfall, drainage density, lithology, road proximity, and land use and land cover see Figs. 4, 7, 8, 9, 10, 11, and 12) and their roles in risk triggering.

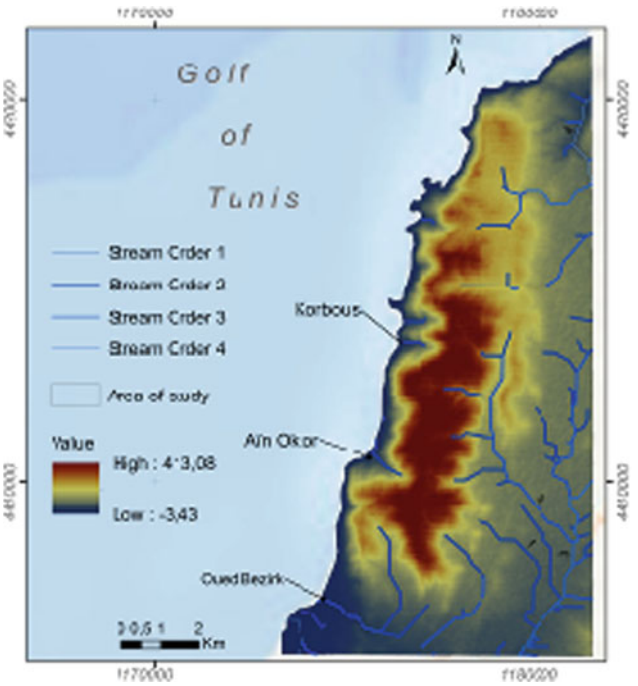

Fig. 5 Digital elevation model

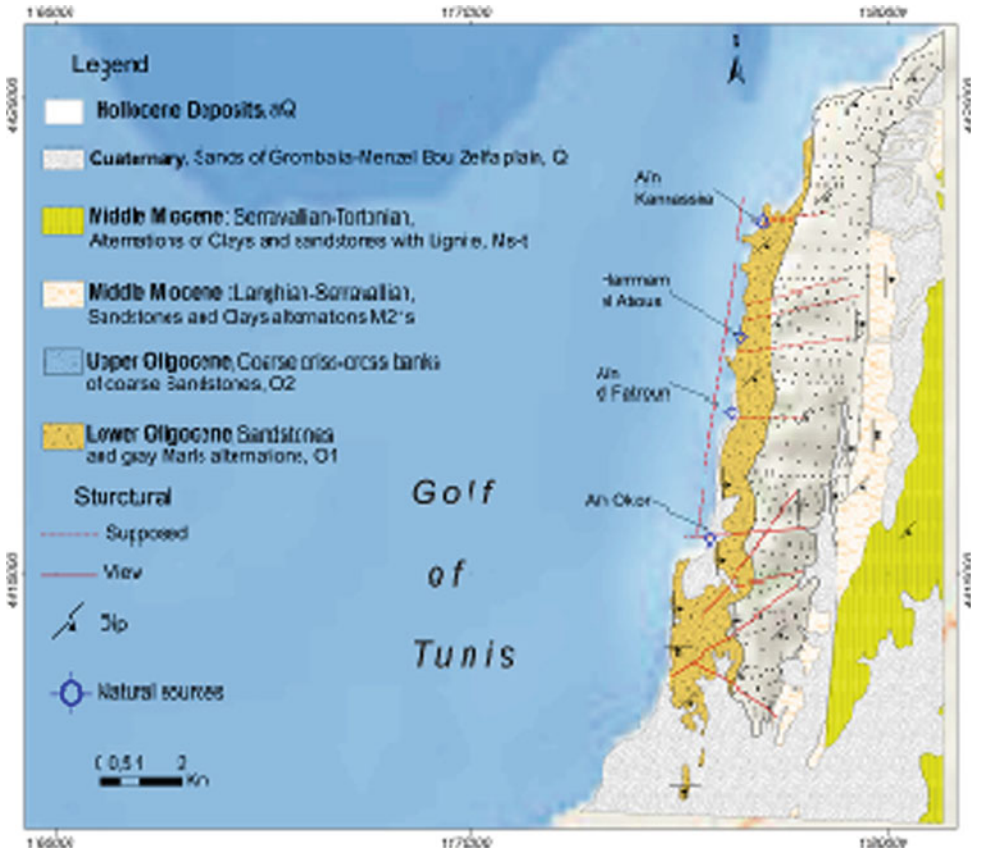

Fig. 6 Geologic map

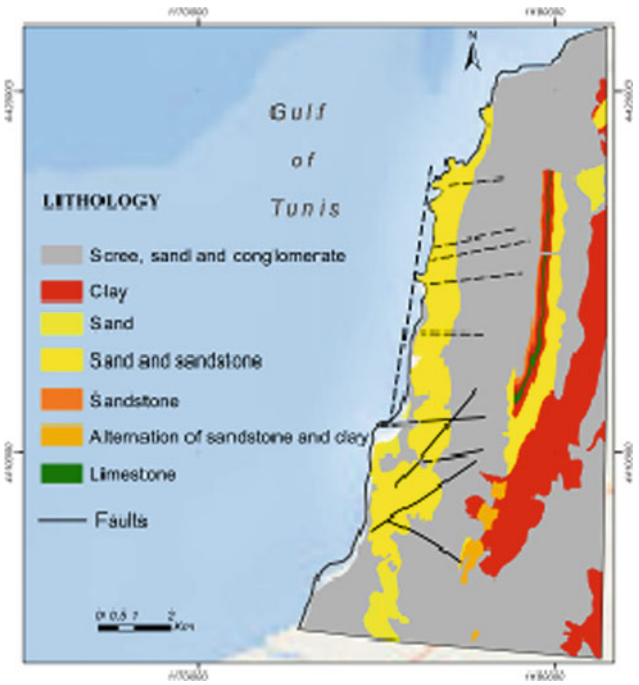

Fig. 7 Lithological map

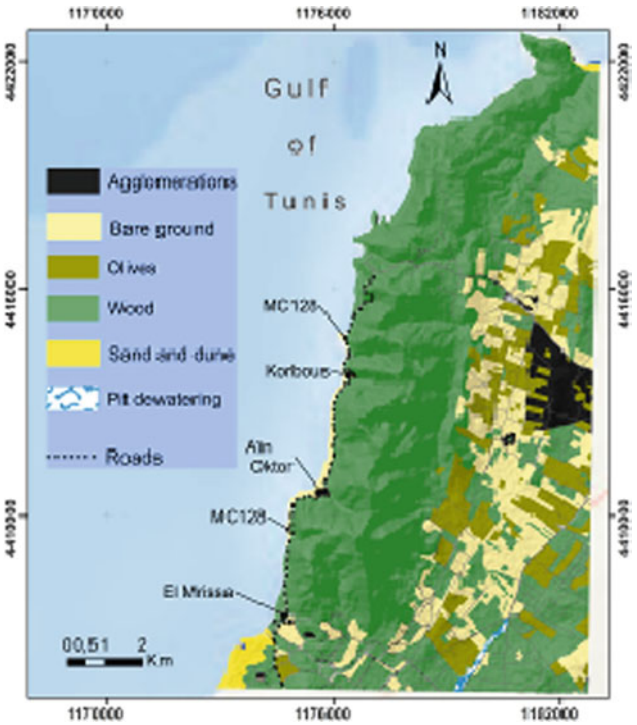

Fig. 8 Land use

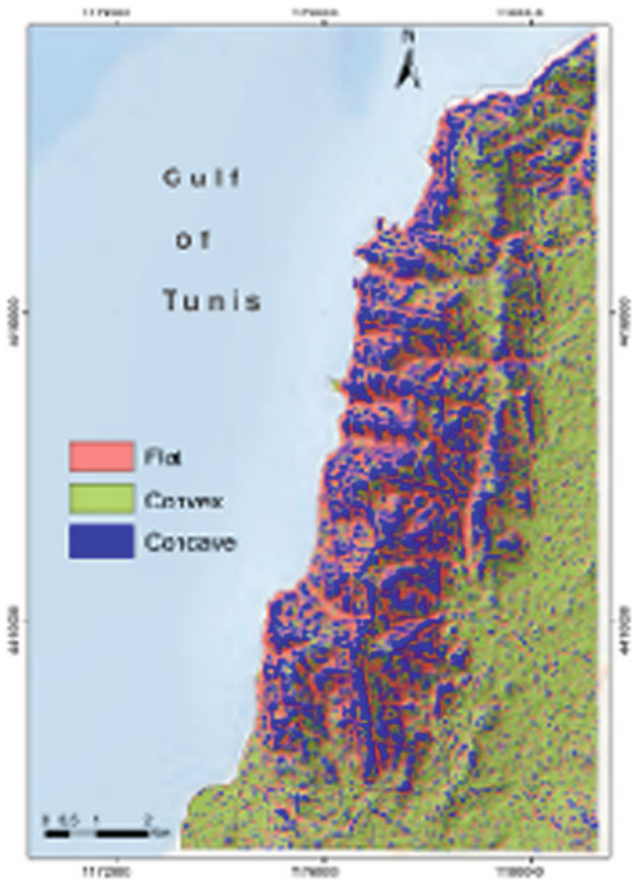

Fig. 9 Curvature

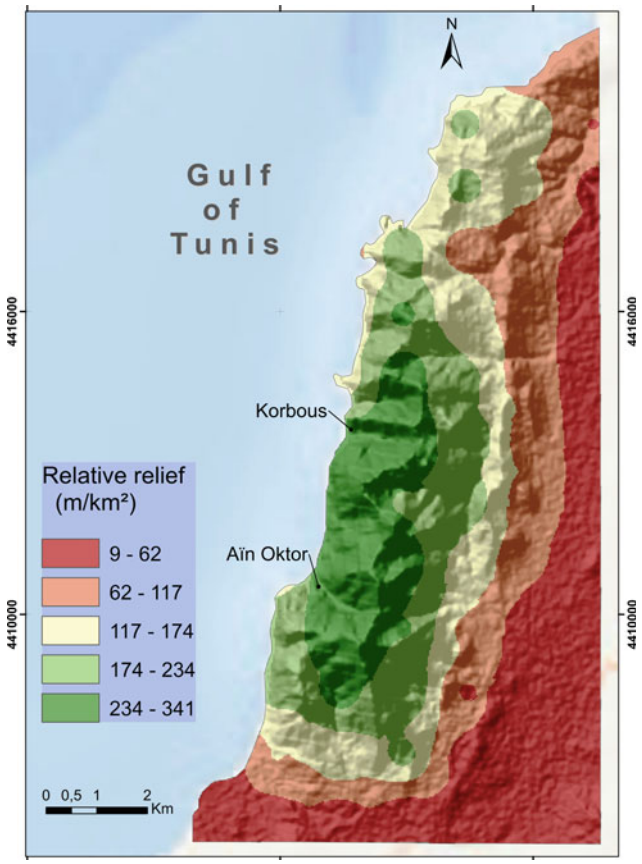

Fig. 10 Relative relief

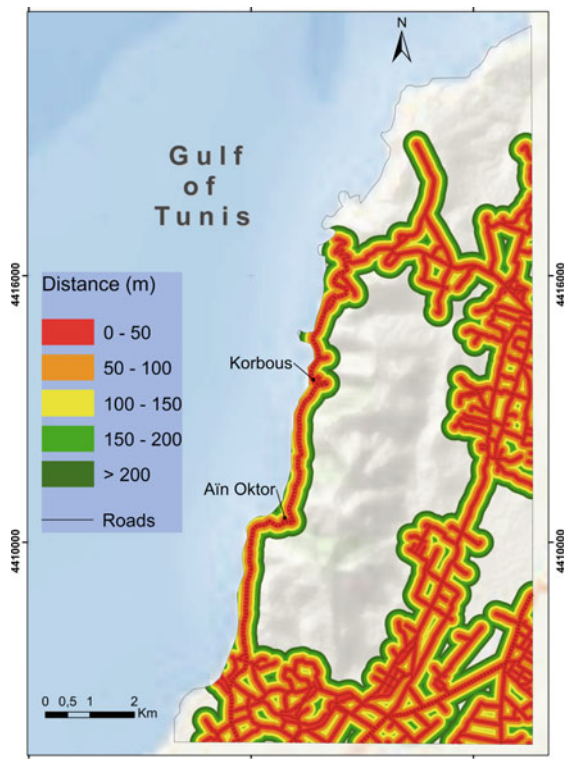

Fig. 11 Road proximity

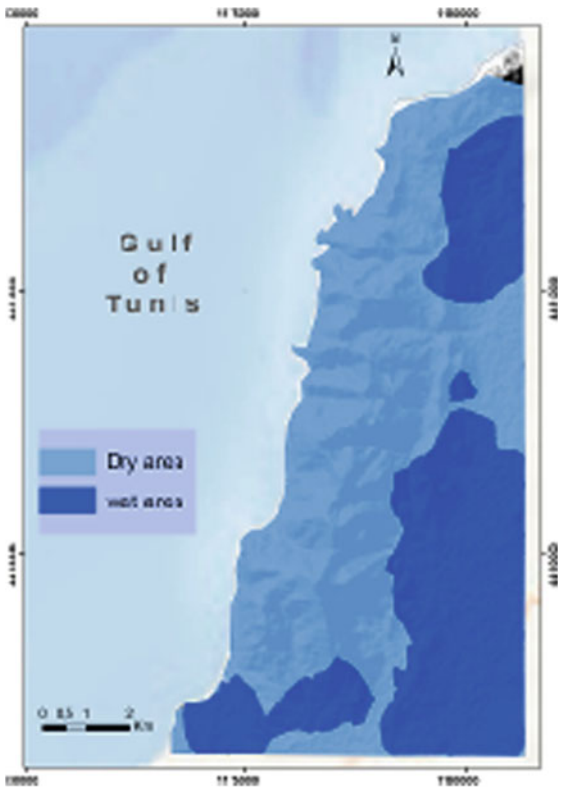

Fig. 12 Drainage density

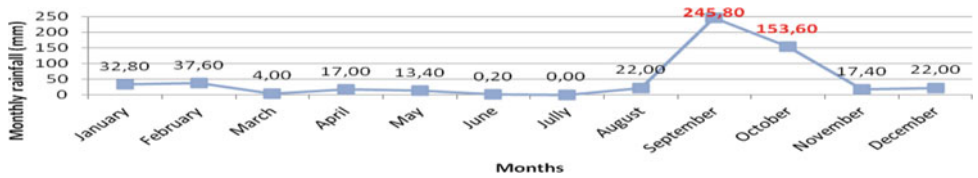

Fig.13 Monthly rainfall in Nabeul 2018

References

Achu, A.L., Rajesh, R.: Application of analytical hierarchy process (AHP) for landslide susceptibility mapping: a study from southern Western Ghats, Kerala, India (DRVC 2017).

Ben Salem, H.: Contribution a la connaissance de la geologie du Cap Bon: Stratigraphie, tectonique et sedimentologie. Thesis (1992).

Eberhardt, E., Willenberg, H., Loew, S., Maurer, H.: Active rockslides in Switzerland—understanding mechanisms and processes (2001).

El Mekki, A., et al.: Use of slope failures inventory and climatic data for landslide susceptibility, vulnerability, and risk mapping in Souk Ahras region. Min. Sci. **24**, 237–249 (2017)

Hadji et al,: Using GIS and RS for slope movement susceptibility mapping: Comparing AHP,LI and LR methods for the Oued Mellah basin, NE Algeria (Springer International Publishing AG 2018).

Hammouda, B., et al.: Mapping and analysis of the vulnerability in landslide (case study of Aïn Oktor-Korbous, Cap Bon- Northern Tunisia) (Vertical Geology Conference 2014).

Hantz, D., Lirigm.: Evaluation des risques d'éboulements rocheux: Bilan et perspectives. Project (1998–2000).

Shantanu, S., Debi Prasanna, K.: GIS application in landslide susceptibility mapping of Indian Himalayas (2017).

Landslide Susceptibility Modeling Using GIS and MAUT Combined with Artificial Neural Network Models; Case of Aghribs Watershed (Neogen Basin of Tizi-Ouzou, Algeria)

Razika Berchiche and Mohamed Saïd Guettouche

Abstract

The approach adopted in this work follows the application of the triple-coupling approaches by using the utility theory models (MAUT), the geographical information system (GIS), and artificial neural networks (ANN) to prevent and assess the landslide susceptibility in the Aghribs watershed (Algeria). To this end, selected factors and weights assigned to each one using the analytic hierarchy process (AHP) are loaded into input variables and land slide **susceptibility** (LSS) classes from the MAUT as output variables. Finally, Thiessen's polygons (LHI) is applied in the interpolation to cartography the risk. The findings from the comparison of tested values and the inventory map show that the LSS map seems more precise and significant.

Keywords

Landslide • MAUT • GIS • Artificial neural networks • AHP

1 Introduction

Landslide risks analysis can help government agencies to select suitable locations for development of schemas and plan mitigation measures in unstable areas (Gómez and Kavzoglu 2005). In this context, many studies have used probabilistic modes like multicriteria analysis (MCA) and MAUT which are common particularly in conjunction with GIS (Richard et al. 1993; Florent 2008).

In these recent decades, new methods have been adopted, such as ANN models (Arora et al., 2014; Oh and Lee 2017; Shivani et al. 2010).

Indeed, the objective of this research is to define a method that has the ability to forecast and evaluate LSS through the use of MAUT-ANN-GIS approaches. Accordingly, the chosen criteria are given high consideration using the AHP to estimate the weight of each parameter according to their preference (Rozos et al. 2011, He et al. 2019; Abella and Westen 2007; Yalcin and Bulut 2007). Also, the uses of ANN are well-considered in reason to minimize the errors and reduce the number of values in the database issue from the application of MAUT.

2 Methodology

To achieve the expected objective, an adopted methodology was organized in three steps:

- Initially, all factors classes (see Razika and Guettouche 2018) were entered into the database as "input data" and the land slide hazard (LSH) and vulnerability values issues from the application of MAUT as "target data," then the weights were also integrated as "input data" in order to reset weights;
- Secondly, the output data were exported into ArcGis.10 in order to create a random point and then interpolate theme using Thiessen polygons to obtain a LSS map.
- Finally, the achieved maps will be compared with the inventory map.

2.1 Location of the Study Area

The Aghribs watershed is part of the Neogen basin of Tizi-Ouzou. Localized between 36° 48′ 59.70″ and 36° 49′

R. Berchiche (✉)
Laboratory of natural hazards and spatial planning (LRNAT), Earth and Universe Sciences Institute, University of Batna 2, Batna, Algeria

M. S. Guettouche
Laboratory of Geomorphology and Gerisks (LG&G), USTHB, 32 El Alia, BP 16111 Bab Ezzouar, Algiers, Algeria

A. Çiner et al. (eds.), *Recent Research on Geomorphology, Sedimentology, Marine Geosciences and Geochemistry*, Advances in Science, Technology & Innovation, https://doi.org/10.1007/978-3-030-72547-1_12

04.90″ of latitude and 4° 20′ 27.54″ and 4° 20′ 55.12″ of longitude, at 45 km NE of Tizi-Ouzou (Fig. 1).

2.2 Inventory Map

Often, the Aghribs watershed area is characterized by several types of mass movements among which the most prolific is landslides and rockslides (Fig. 2).

3 Results

3.1 Land Slide Risks Map Applying MAUT

The linear combination (as in Guettouche et al. 2011) of the land slide hazard (LSH) map and potential consequences map issue from the application of MAUT (see Razika and Guettouche 2018) shows the LSS levels in Aghribs watershed (Fig. 3).

The LSS map (Fig. 3) identifies three distinct risk areas: The north where the risk is graded as moderate to very strong, the center where the risk is very strong, and the south area with negligible practically risk.

3.2 ANN Results

In this work, a feedforward ANN model called a multilayer perceptron (MLP) (as in Oh and Lee 2017) was applied. It enabled the use of the back propagation algorithm based on LogSig as a transfer function. Two parameters can guide the task through this application: performance and linear regression. To start with, the performance represents the same curving for the three curves: train, test, and validation; the best validation performance value indicated 0.00014. Linear regression was estimated perfect at 0.99.

The results obtained could be categorized into four classes according to 0.234 steps (Table 1).

3.3 Interpolation by Using Thiessen's Polygons

As a final step, the cartography of the results obtained from ANN (Fig. 4) was performed using the Thiessen polygons (THI) as an interpolation model also known as the nearest neighbor method (NNM) (Ly et al. 2013, Belgium et al. 2011).

The map of LSS shows (Fig. 4) that the area can be cut out to three distinct parts: The north with a moderate to very

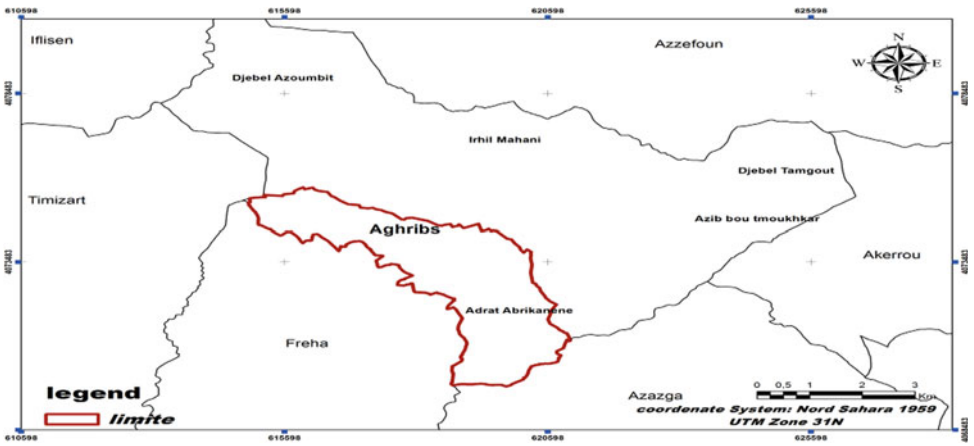

Fig. 1 Location of the study area

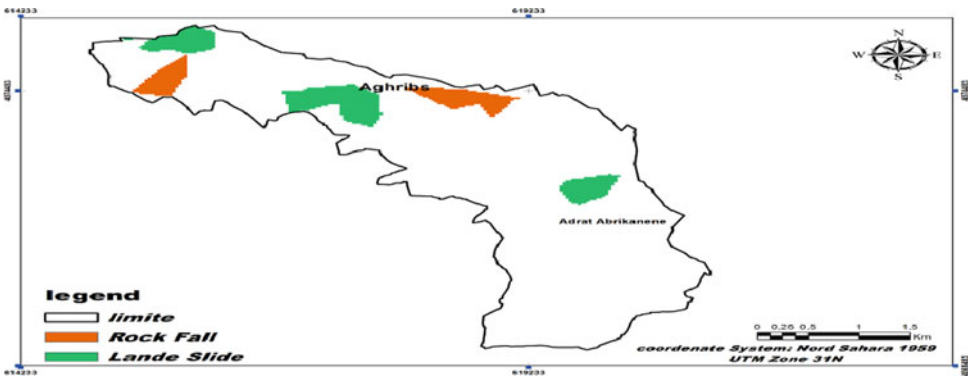

Fig. 2 Mass movement inventory map of study area

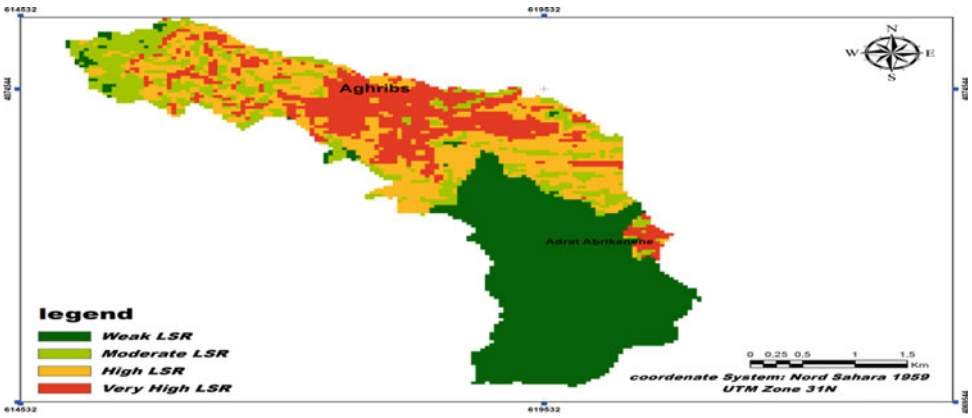

Fig. 3 LSR map in Aghribs watershed

Table 1 LSH and vulnerability (vuln) classes reached through the use of ANNs

	Weak	Moderate	High	Very high
LSH	0.115 <x> 0.346	0.355 <x> 0.576	0.593 <x> 0.826	0.829 <x> 1.053
Vuln	0.07 <x> 0.419	0.42 <x> 0.86	0.861 <x> 1.054	1.055 <x> 1.365

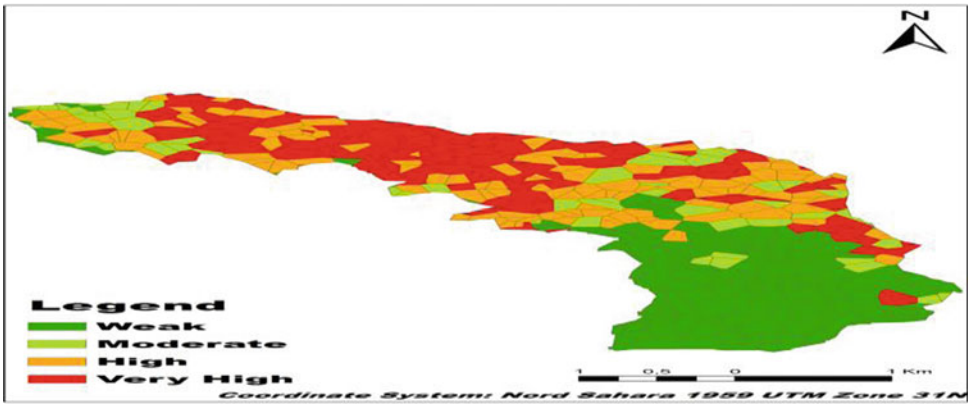

Fig. 4 LSS map in Aghribs watershed, using Thiessen polygons

high risk, the center which is present a high to very high risk, and the south that represents a negligible risk.

4 Discussion

The comparison between the mass movements inventory map (Fig. 2), the LSS degree and specialization using MAUT and ANN maps (Figs. 3 and 4) show that the positions of the very high LSS are similar; they present the same location characters in all three situations. The findings also suggest a possible occurrence of that event in the future applying MAUT and ANN especially in the north area.

Indeed, there were over 6808 imprecise, large, and blind values to manipulate in the database applying MAUT. But, by applying the ANN back propagation algorithm, this number was reduced to only 1313 values outstanding a general error of 0.0025.

5 Conclusion

The findings prove that applying the coupling approaches MAUT-ANN-GIS is more realistic than applying MAUT-GIS.

Furthermore, the reported results in this work call for the need for further research in order to shed extra light on high and very high LSS degrees, seeing as they can be expressed by the same degree around all the area.

References

Abella E.A.C., Van Westen C.J.: Generation of landslide risk index map for Cuba using spatial multi-criteria evaluation. Landslides **4**, 311–325 (2007). https://doi.org/10.1007/s10346-007-0087-y

Arora, M.K., Chauhan, S., Sharma, M.: A comparative assessment of neural network, fuzzy and neurofuzzy approaches for landslide

susceptibility zonation in Garhwal Himalayas. Blucher Mech. Eng. Proc. **1**(1), (2014). www.proceedings.blucher.com.br/evento/10wccm

Belgium, Ly, S., Charles, C., Degre, A.: Geostatistical interpolation of daily rainfall at catchment scale: the use of several variogram models in the Ourthe and Ambleve catchments, hydrol. Earth Syst. Sci. **15**, 2259–2274 (2011). www.hydrol-earth-syst-sci.net/15/2259/2011/, https://doi.org/10.5194/hess-15-2259-2011 © Author(s) 2011. CC Attribution 3.0 License

Florent, P.: Modélisation des instabilités en géomécanique, application aux glissements de terrains. Thèse pour obtenir le grade de Docteur de L'Institut Polytechnique de Grenoble (2008)

Gómez, H., Kavzoglu, T.: Assessment of shallow landslide susceptibility using artificial neural networks in Jabonosa River Basin, Venezuela. Eng. Geol. **78**(2005), 11–27 (2005). https://doi.org/10.1016/j.enggeo.2004.10.004, www.elsevier.com/locate/enggeo

Guettouche, M.S., Derias, A., Boutiba, M., Bounif, M.A., Guendouz, M., Boudella, A.: A fire risk modelling and spatialization by GIS-application on the forest of Bouzareah Clump, Algiers (Algeria). J. Geog. Inf. Syst. **3**, 254–265 (2011). https://doi.org/10.4236/jgis.2011.33022

He, H., Hu, D., Sun, Q., Zhu, L., Liu, Y.: A landslide susceptibility assessment method based on GIS technology and an AHP-weighted information content method: a case study of Southern Anhui, China. ISPRS Int. J. Geo-Inf. **8**(266), 1–23 (2019). https://doi.org/10.3390/ijgi8060266

Ly, S., Charles, C., Degré, A.: Different methods forspatial interpolation of rainfall data for operational hydrologyand hydrological modeling at watershed scale. Biotechnol. Agron. Soc. Environ. **17** (2), 392–406 (2013)

Oh, H.-J., Lee, S.: Shallow landslide susceptibility modeling using the data mining models artificial neural network and boosted tree. Appl. Sci. **7**, 25–38 (2017), 1000. https://doi.org/10.3390/app7101000, www.mdpi.com/journal/applsciBooks

Razika, B., Guettouche M.S.: Integration of an MCA-GIS approach for the modelling and assessment of mass movement risk. Case of Aïn El Hammam, basin of Tizi-Ouzou (Algeria). Analele Universităţii din Oradea, Seria Geografie, XXVIII **2**(2018), 145–155 (2018), Article no. 282101–772, ISSN 1221–1273, S-ISSN 2065–3409

Richard, G., Pascal, G., Jacques-Marie, B., Robert, B., Jean, C., Benoft, D., Jean-François, P.: Cartographie automatique de zones à aléas de mouvements de terrain sur l'île de Tahiti à partir de données digitales. Bull. Soc. géol. Frunce. **164**(4), 577–583 (1993)

Rozos, D., Bathrellos, G.D., Skilodimou, H.D.: Comparison of the implementation of Rock Engineering System (RES) and Analytic Hierarchy Process (AHP) methods, based on landslide susceptibility maps, compiled in GIS environment. A case study from the Eastern Achaia County of Peloponnesus, Greece. Environ Earth Sci. 49–63 (2011). https://doi.org/10.1007/s12665-010-0687-z

Shivani, C., Sharma, M., Arora, M.K., Gupta, N.K.: Landslide Susceptibility zonation through ratings derivedfrom artificial neural network. Int. J. of Appl. Earth Obs. Geoinf. **12**(2010), 340–350 (2010), 0303–2434/$ – see front matter © 2010 Elsevier B.V. All rights reserved. https://doi.org/10.1016/j.jag.2010.04.006, journal homepage: www.elsevier.com/locate/jag

Yalcin, A., Bulut, F.: Landslide susceptibility mapping using GIS and digital photogrammetric techniques: a case study from Ardesen (NE-Turkey). Nat. Hazards **41**, 201–226 (2007). https://doi.org/10.1007/s11069-006-9030-0

Landslide Distribution Analysis in the Foglia River Basin, Northern Apennines, Italy

Davide Baioni

Abstract

The present work is focused on the distribution of landslides in Foglia River basin (central Italy), using a heuristic approach supported by GIS tools for the construction of statistical analysis and spatial data. It aims to investigate any dependencies and/or relationships between natural factors related to the study area and landslides. In the study area, 2821 landslides were surveyed covering a total area of 155 km^2 that corresponds to 22% of the entire basin. The findings of the study highlight the importance as well as the role of individual factors, such as lithology, land use, orientation, and slopes, which led to the development of landslides analyzed.

Keywords

Landslides • Foglia River basin • Landslide events • GIS

1 Introduction

In the last decades, landslide events have been a recurring problem with increasing frequency in all areas of the Italian peninsula. In particular, the development and spreading of landslide events throughout the national territory have shown a clear increase in the costs of restoration work, protective measures, and damage caused to infrastructure and production activities by landslides and costs that have gained more weight in the national public budget. This evidence accounts for the need to develop studies of prediction and prevention of landslides and their risks. These studies can be performed by correlating information from different geographic areas with limited use of resources to run them on a large scale. Studies about landslides distribution, such as on the landslide susceptibility, are greatly influenced by the degree of detail required and by the availability of data, which is often directly proportional to the budget. The most common approaches in the literature are called heuristics. They apply the "cause and effect" instance to evaluate the intrinsic parameters, which are classified and valued on the basis of evaluations, sometimes arbitrary, to favor or not the landslides event (Atkinson and Massari 1998). Other approaches are of statistical nature. They aim to identify a set of variables based on available data. This approach is widely used, as well as that of the multivariate. For several years, the GIS was considered a reference tool for the study of landslides and more generally, as a tool for assessment of spatial relationships of landslide phenomena in a study area (Lan et al. 2004; Ayalew and Yamagishi 2005). Taking that into consideration, many factors that play a role in the development of landslides can act in different ways and combination in relation to the type of landslide and environmental conditions (Brunsden 1996). The present work is focused on the distribution of landslides in the Foglia River basin area located in the Adriatic side of the Northern Apennines, using a heuristic approach, supported by GIS tools for the construction of statistical analysis and spatial data.

The study aims to identify the possible existence of relationships between the natural factors illustrated above and landslides. To this end, the study of landslide distribution was carried out by superimposing each thematic map previously created with the landslides surveyed to recognize any possible direct relationship of cause and effect.

2 Materials and Methods

The data collected in this study represent the different parameters that can influence or can be involved in the development of landslides. The data were analyzed through available public cartographic documents and integrated by existing aerial images. In a second step, the data were

D. Baioni (✉)
Dipartimento Di Scienze Pure E Applicate, Università Di Urbino Carlo Bo, 61029 Urbino, Italy
e-mail: davide.baioni@uniurb.it

A. Çiner et al. (eds.), *Recent Research on Geomorphology, Sedimentology, Marine Geosciences and Geochemistry*, Advances in Science, Technology & Innovation, https://doi.org/10.1007/978-3-030-72547-1_13

organized and structured in GIS themes, then grouped into seven categories. All data acquisition, digitization, data entry, processing, and analysis were conducted using a GIS (ArcView 3.2 by ESRI). The topographic map provided information on the slope, altitude, and orientation (scale 1:10,000, available in vector format). It was also possible to extract contour and spot elevations. Then, a digital terrain model (DTM) was elaborated developing a triangular irregular network (TIN). Later, the DTM was resampled in a digital elevation model (DEM) with a square m network with side of 250 m. (the software was used by ThreeX Terranova). The parameters considered are summarized below:

(a) *Landslides*: The landslides recorded within the study area were surveyed using the landslide inventory prepared by the "Autorità di Bacino delle Marche," which uses data from municipality integrated with data from other projects, such as CARG (new geological map 1: 50,000) and IFFI Landslide Inventory Map (GNDCI). Data were homogenized by applying the classification by type of phenomena and processes (Hungr et al. 2014). The following step was to verify the data through field survey and analysis of aerial photographs using a tablet pc (see Fig. 1). The landslides were finally cataloged to scale 1:10,000.
(b) *Lithology*: The data used to classify the lithologies outcropping in the study area were available from the geological map scale 1:25,000 (N. 109 and 108 of the Official Italian Geological Map).
(c) *Land use*: The data related to land use within the study area were obtained using the existing maps (1:10,000 scale map of land available in vector format), suggesting that the Foglia River basin can be divided into five major classes.
(d) *Slope*: The slopes displayed by the Foglia River basin were not very steep slopes, but rather concentrated between 0 and 20°. They were found in 94% of the entire basin. Nevertheless, a detailed analysis was conducted, by grouping the frequency of landslide in classes of 2° of the slope.
(e) *Orientation of the slope*: This parameter was considered of interest because in the study area and its surrounding region, the exposure factor was always considered an important element in the morphological evolution of the landscape.

3 Results

A total of 2821 landslides were surveyed in the study area. About 1886 of these landslides were classified as debris flow (DB), 10 as rockfalls (RF), 25 as deep-seated gravitational slope deformations (DGSD), 144 as complex landslides (CL), 492 as slides (rotational and translational) landslides (SS), and 264 as solifluction flows (SF). The landslides surveyed occupied a total area of 155 km^2, corresponding to 22% areal extent of the entire basin.

3.1 Landslides and Lithology

Landslides were widely distributed mainly on deposits characterized by pelitic formations (30.5%), and marl arenaceous formations (29.7%), and to a lesser extent, on the deposits characterized by sandstone formations (9.6%).

3.2 Landslides and Land Use

The land use did not seem to provide any particular indications, given that landslides were distributed on all types of classes. In fact, the analysis of the 6 classes that comprise 97% of landslides did not seem to highlight any relations.

3.3 Landslides and Slope

In relation to the slope, the analyzed data showed: (i) 13.7% of landslides occurred on slopes of less than 6°, (ii) 70.7% of landslides occurred in the range of slope between 6° and 16°, and (iii) 15.6% of the phenomena were distributed in the classes with a slope greater than 16°. As for slopes >30°, only 0.042% of the events could be observed.

3.4 Landslides and Altitude

The distribution of landslides indicated their presence in all classes examined, highlighting an absolute maximum value of 32.58% in correspondence of the altitude 150–300 m and value of 27.89% in the class 300–450 m.

3.5 Landslides and Orientation of the Slope

The data suggested that the maximum frequency of landslide records was to NE. In fact, it was generally higher in areas exposed to the north than those exposed to south. The lower slope classes (0–5° and 5–10°) were characterized by a similar landslides' frequency between areas with north and south orientation. Whereas in the upper slope classes, landslides frequency was higher in areas exposed to north.

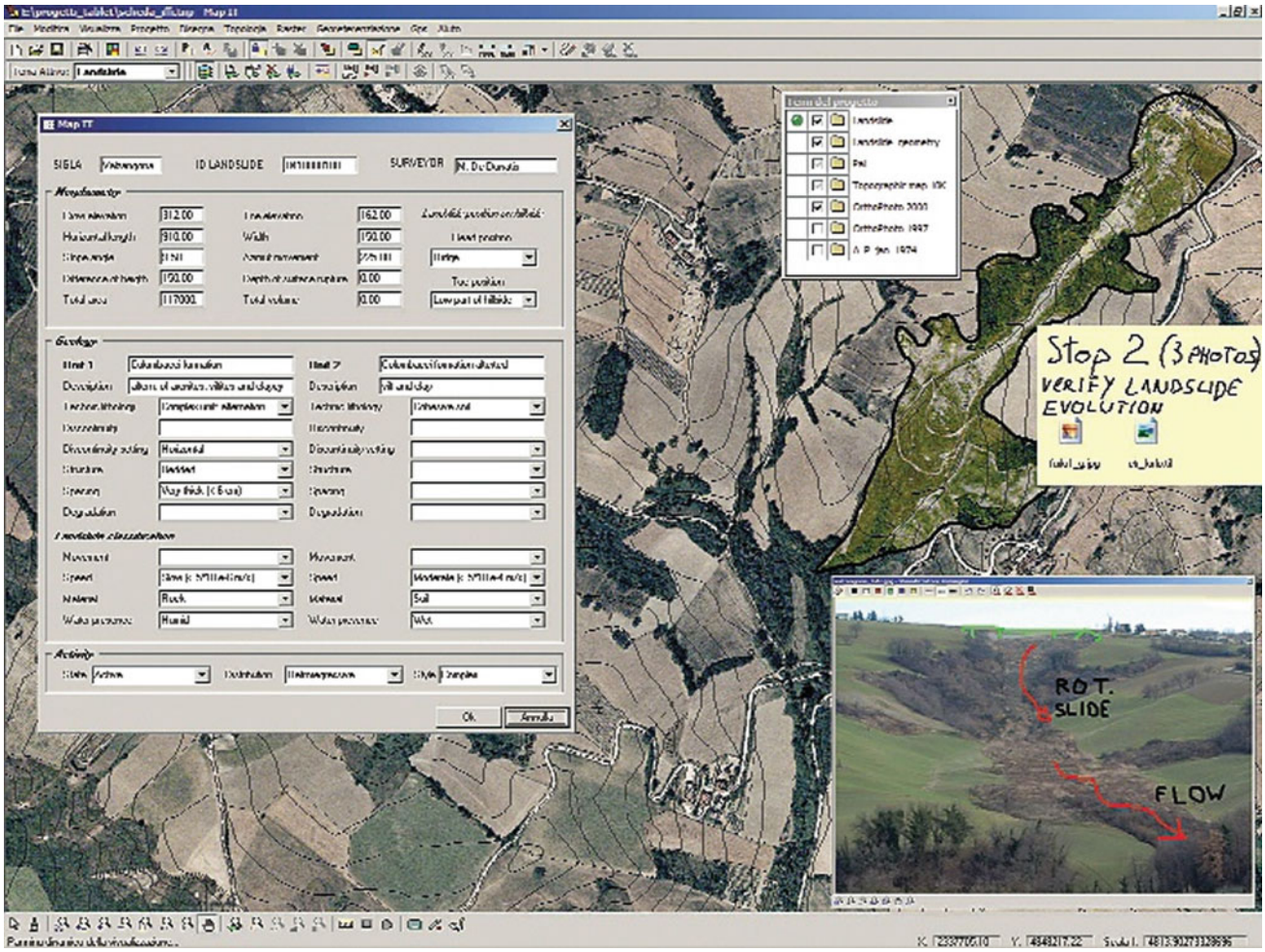

Fig. 1 Screenshot of table pc used for field survey: aerial photo with topographic base and limit of the landslide with the insertion of notes and sketches on the photo taken during the survey

4 Discussion and Concluding Remarks

Our results cast a light on the factors and their roles in contributing to the development of landslides in this area. The data analysis revealed the following insights on the study area: (a) Overall, the lithology was an important factor in controlling landslides. It was suggested that the marl and clay lithologies were very susceptible to the landslide. (b) The slope parameter showed an apparent correlation between the distribution of landslides and slope classes, highlighting the absence of direct proportionality between the increase of the slope and rise of the phenomena. (c) The exposure parameter did not influence the development of landslides, although they were generally more prevalent in the quadrants of north compared to those of south. Furthermore, this methodology could be applied to all orders of magnitude scale, needing limited resources both from an economic and a human point of view.

References

Atkinson, P.M., Massari, R.: Generalized linear modeling of susceptibility to landsliding in the central Apennines Italy. Comput. Geosci. **24**, 373–385 (1998)

Ayalew, L., Yamagishi, H.: The application of GIS-based logistic regression for landslide susceptibility mapping in the Kakuda-Yahiko mountains, Central Japan. Geomorphology **65**, 15–31 (2005)

Brunsden, D.: Mass movement, the research frontier and beyond: a geomorphological approach. Geomorphology **7**, 85–128 (1996)

Hungr, O., Leroueil, S., Picarelli, L.: The Varnes classification of landslide types, an update. Landslide **11**(2), 167–194 (2014)

Lan, H.X., Zhou, C.H., Wang, L.J., Zhang, H.Y., Li, R.H.: Landslide hazard spatial analysis and prediction using GIS in the Xiaojiang watershed, Yunnan China. Eng. Geol. **76**, 109–128 (2004)

Spatial Distribution of Debris Flow-prone Catchments in Hengduan Mountainous Area in Southwestern China

Kaiheng Hu, Li Wei, and Shuang Liu

Abstract

Hengduan mountainous area in Southwestern China is highly susceptible to debris flow hazards. In order to investigate the spatial distribution of 7181 debris flow-prone catchments, the area has been classified into six natural geographical sub-regions based on its climatic, geological, and geomorphic types. The spatial analysis reveals that their spatial distribution exhibits a significant difference in the six sub-regions. The sub-regions with East Asian monsoon climate have a higher density of the catchments than other sub-regions with Tibetan cold climate. The highest density is 286 catchments per 10,000 km^2, seven times of the lowest sub-region. The climatic factor is more important than the other factors. The histogram of the catchments with average annual rainfall shows that the regions with the annual rainfall of 800–1050 mm are more prone to debris flows.

Keywords

Debris flow-prone catchment • Hengduan Mountain • Spatial distribution • Spatial analysis • Rainfall occurrence

1 Introduction

Hengduan mountainous area is the transition belt from Tibet to Yungui Plateau and Sichuan basin in Southwestern China (Fig. 1), where the government set up fundamental infrastructures such as hydropower stations and national highways. The area is the most susceptible region to debris flow hazards in China due to its abundant rainfall, steep topography, and active tectonic movement, and the debris flows impose severe damage to the infrastructures and inhabitants in this area (Cui et al. 2017).

Rainfall is the primary triggering factor for debris flows, especially in Southwestern China; the variation in rainfall occurrence may change debris flow occurrence (Winter et al. 2010; Dowling and Santi 2014; Wei et al. 2018). To understand the spatial relationship between rainfall occurrence and debris flows, it is important to assess their risk in the region. P revious studies focused on the relations between rainfall intensity-duration and debris flow occurrence at the small catchment level or the probability of debris-flow occurrence (Hu et al. 2010; Zhou and Tang 2014). However, few studies are concerned with the spatial distribution of debris flows and rainfall occurrence at the regional scale.

In this paper, the whole Hengduan area is selected as the study area. The spatial and temporal characteristics of debris flow-prone catchments are investigated by using the spatial analysis and classification tools of ArcGIS according to the region's climatic, geological, and geomorphic types. The results show that the correlation between the number of debris flow–prone catchments and annual precipitation characteristics exhibits great regional heterogeneity in different geographical units.

2 Study Area

The Hengduan area of 600,000 km^2 is located in Southwestern China, next to Sichuan basin in the east and to Tibet Plateau in the west (Fig. 1). It has a typical alpine landscape with deeply incised valleys. The highest point is the Gongga summit with 7556 m above sea level. Many big rivers such as Jinsha (upstream Yangtze), Lancang, Nujiang, Dadu, and Yalong go through the area from north to south. The area

K. Hu · L. Wei · S. Liu
Key Laboratory of Mountain Hazards and Earth Surface Processes, Chinese Academy of Sciences, Chengdu, 610041, China

K. Hu (✉) · L. Wei · S. Liu
Institute of Mountain Hazards and Environment, Chinese Academy of Sciences, Chengdu, 610041, China
e-mail: khhu@imde.ac.cn

A. Çiner et al. (eds.), *Recent Research on Geomorphology, Sedimentology, Marine Geosciences and Geochemistry*, Advances in Science, Technology & Innovation, https://doi.org/10.1007/978-3-030-72547-1_14

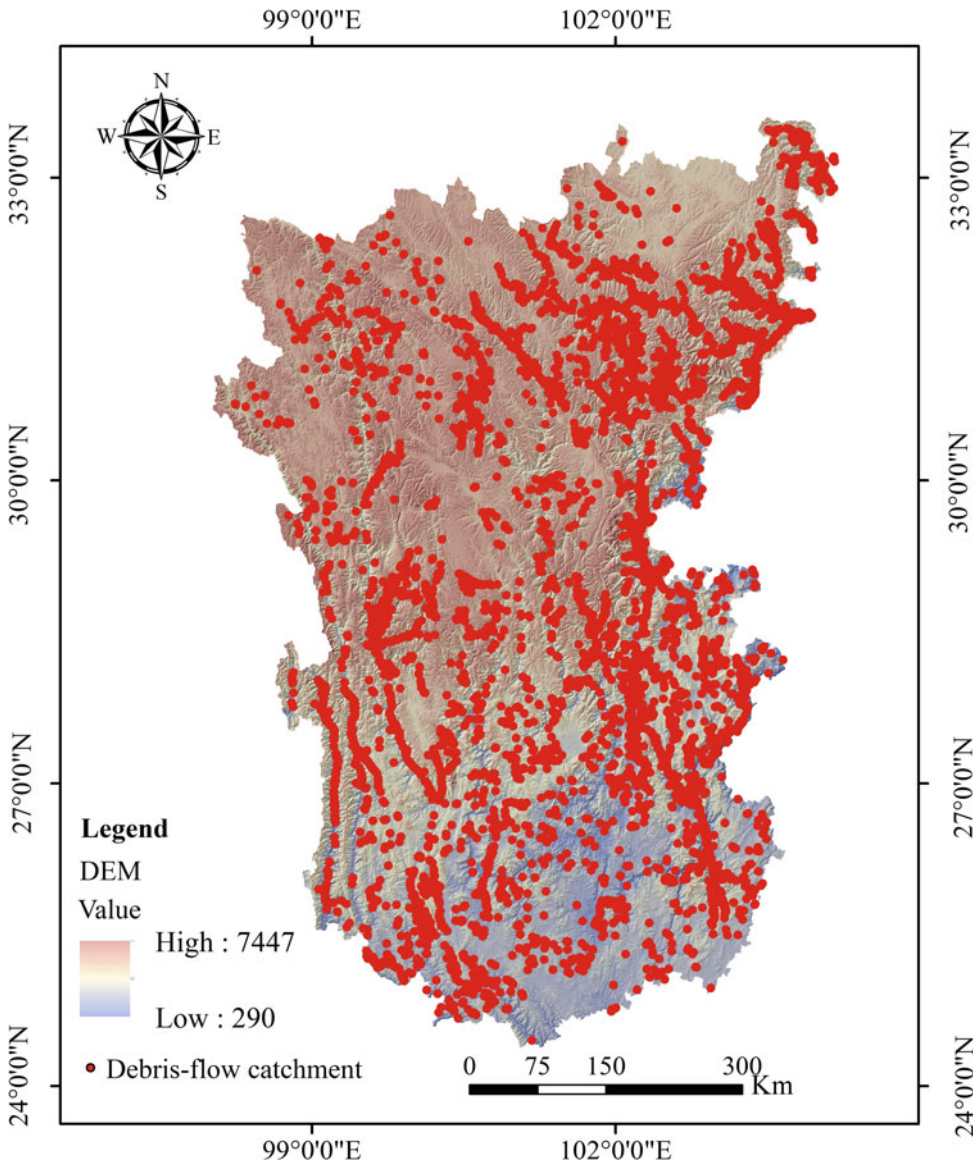

Fig. 1 Location map of Hengduan area and debris flow-prone catchments

transects sub-tropical zone and plateau temperate and cold zones and is affected by the southwest monsoon from the Indian Ocean and the southeast monsoon from the Pacific Ocean. Based on the region's climatic, tectonic, and topographic types, the whole area is divided into six sub-regions or geographical units: (I) highland and alpine landscape, Gondwana continental block, Tibetan cold climate; (II) highland and alpine landscape, Gondwana continental block, East Asian monsoon climate; (III) highland and alpine landscape, continental block of South China, and East Asian monsoon climate; (IV) highland and alpine landscape, continental block of South China, and Tibetan cold climate; (V) moderate mountain landscape, Gondwana continental block, and East Asian monsoon climate; (VI) moderate mountain landscape, continental block of South China, and East Asian monsoon climate (Fig. 2).

3 Results

3.1 Spatial Distribution of Debris-Flow Catchments in Different Units

Data from 7181 debris flow-prone catchments include catchment area, outlet's position, longitudinal gradient, and relative elevation. Figure 2 shows that the spatial distribution of the catchments has a significant difference in the six geographical units. The highest density is 286 debris flow catchments per 10,000 km^2 for Zone III. Whereas, Zone I with the cold climate has the lowest density. Hence, regions with high relief and abundant rainfall are more easily susceptible to debris flows. The results obtained by geographical detector software (Wang et al. 2016) indicate that the most

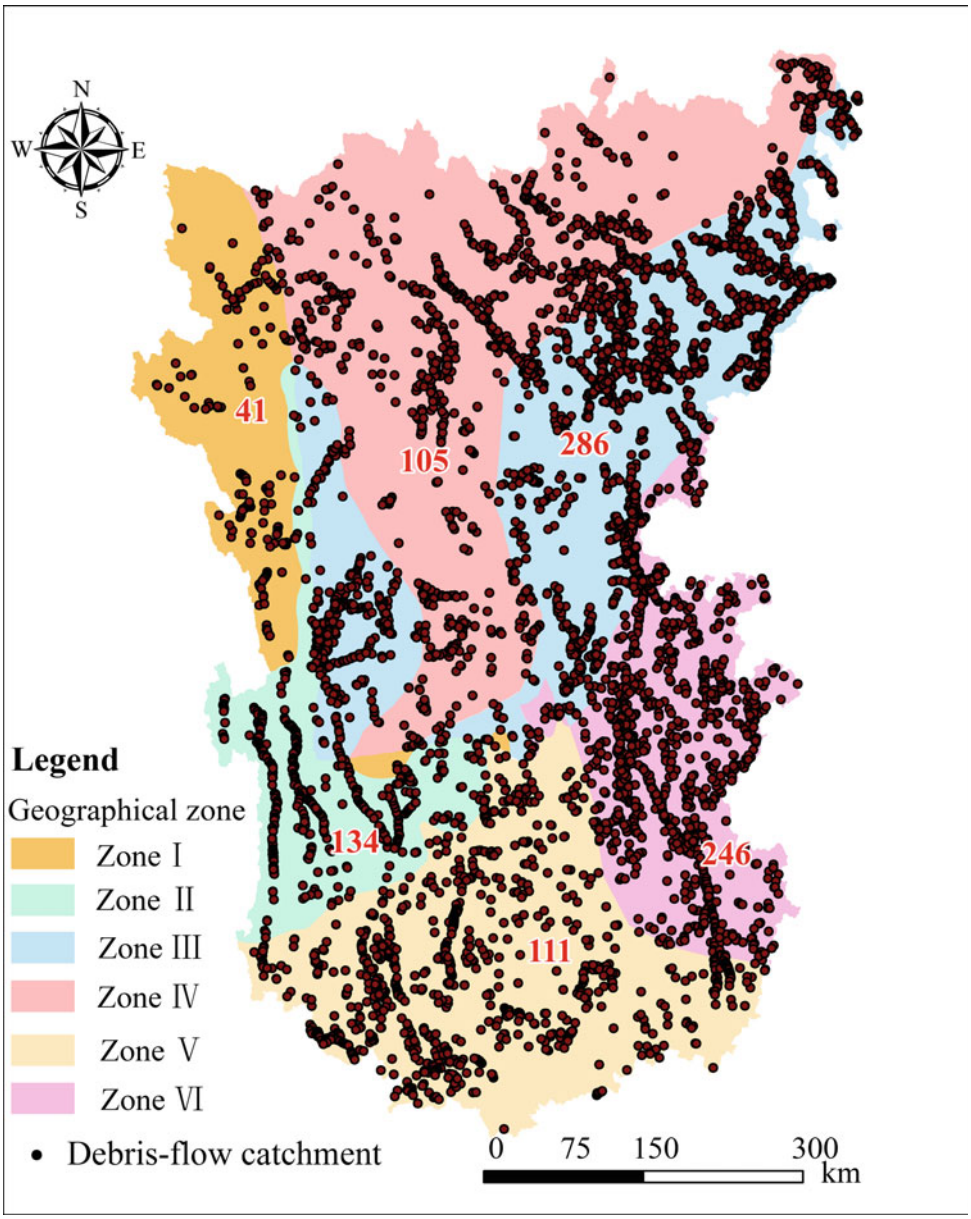

Fig. 2 Geographical zones of Hengduan area and their debris flow-prone catchments distribution (the number in each zone is the catchment density of per 10,000 km^2)

influential factor is the climatic factor, then the topographic factor (such as relative relief), while the less influential factor is the geological factor (such as tectonic structure).

3.2 Distribution of Debris Flow Catchments with Annual Rainfall Results

The average annual rainfall in Hengduan area ranges from 500 to 1650 mm. This range is classified into 16 intervals with different values (Fig. 3). Most of debris flow catchments fall in the intervals between 600 and 1150 mm. The peaks of the catchment number are in the intervals of 800–850, 850–900, 950–1000, and 1000–1050 mm. Only, nearly 5% of the debris flow-prone catchments lie in the regions where the annual rainfall exceeds 1150 mm. This indicates that more debris flows would occur in the regions with the annual rainfall of 800–1050 mm.

4 Conclusions

Hengduan mountainous area, a critical region between Tibet Plateau and Sichuan basin, where debris flows happen frequently, is chosen as the case study in this paper. The data of more than 7000 debris flow-prone catchments are collected to examine their spatial distribution at a regional scale. The findings reveal that the geographical unit with the highland and alpine landscape, continental block of South China, and East Asian monsoon climate has the highest

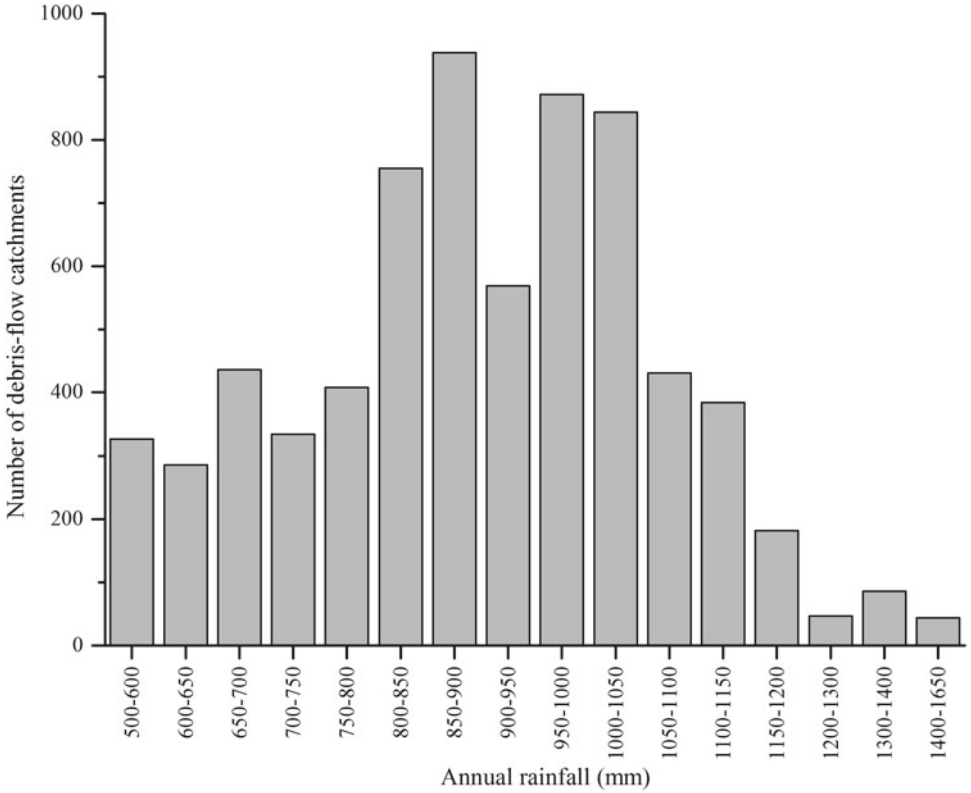

Fig. 3 Histogram of debris flow catchments versus annual rainfall in Hengduan area

density of debris flow catchment (286/10,000 km^2). The climatic factor is the most influential to the distribution of debris flow-prone catchments among the three affecting factors. The debris flow catchments concentrate highly in the regions with the annual rainfall of 800–1050 mm. When the annual rainfall exceeds 1150 mm, the number of the catchments reduces sharply.

References

Cui, P., Su, F., Ge, Y., Chen, X., Zou, Q.: Natural hazards in Tibetan plateau and key issue for feature research. Bull. Chin. Acad. Sci. **32** (9), 985–992 (2017)

Dowling, C.A., Santi, P.M.: Debris flows and their toll on human life: a global analysis of debris-flow fatalities from 1950 to 2011. Nat. Hazards **71**(1), 203–227 (2014)

Hu, K., Cui, P., Wang, C., Li, Y., Lu, X.: Characteristic rainfall for warning of debris flows. J. Mt. Sci. **7**(3), 207–214 (2010)

Wang, J.F., Zhang, T.L., Fu, B.J.: A measure of spatial stratified heterogeneity. Ecol. Ind. **67**, 250–256 (2016)

Wei, L., Hu, K., Hu, X.: Rainfall occurrence and its relation to flood damage in China from 2000 to 2015. J. Mt. Sci. **15**(11), 2492–2504 (2018)

Winter, M., Dent, J., Macgregor, F., Dempsey, P., Motion, A., Shackman, L.: Debris flow, rainfall and climate change in Scotland. Q. J. Eng. Geol. Hydrogeol. **43**(4), 429–446 (2010)

Zhou, W., Tang, C.: Rainfall thresholds for debris flow initiation in the Wenchuan earthquake-stricken area, southwestern China. Landslides **11**(5), 877–887 (2014)

Geomorphology, Soil Science, Landslides, Coastal Processes, and Geoarchaeology (T9): Coastal Processes

Evolution of Shoreline Kinematics at the Bejaia Bay (East Algeria) from 1989 to 2017

Cherif Aoudj, Mokhtar Guerfi, and Khoudir Mezouar

Abstract

The Algerian coastline stretches for 1622 km including a coastal area called Bejaia that measures 100 km in length. Bejaia is located on the east side with sandy beaches that attract tourists. This coastal fringe is subject to a remarkable decline. Several beaches are witnessing recession. In this respect, the study aims to estimate the average rates of erosion and accretion between the two coastal lineages (1989 and 2017), through a GIS on ArcGIS v 10.2 and its digital shoreline analysis system (DSAS) module. Erosion dominates most of the beaches of this coastal fringe. Measures should be urgently taken to preserve the natural heritage that is at the heart of our country.

Keywords

Coastal kinematics • DSAS • Coastline of Bejaia • Erosion • GIS

1 Introduction

Like several littorals of the globe, the Algerian coast has known for some decades. An increasing of anthropization is manifested by an important economic and urban occupation.

This is particularly reflected in sensitive coastal environments by phenomena such as coastal erosion, the risk of submersion, and saline intrusion, some of whose effects would be irreversible. The Bejaia coastline in East-central Algeria is no exception to this global reality, so we have undertaken a study of the evolution of the coastline which consists in performing two time scales (1989–2017) and finally estimate erosion and accretion rates of the study area.

2 Study Area

The Bejaia Bay is located in the central-eastern part of the Algerian coast, 265 km east of the capital Algiers. It extends on 70 km of coastline between Cape Carbon to the west and Cape Ziama Mansouria to the east (see Fig. 1). It is a fragile coastal zone that has known, recently, critical morphological changes due to both physical and anthropogenic factors. Currently, the regressive evolution of the shoreline combined with this human occupation has generated tremendous pressures on its coast.

3 Materials and Methods

The most prevalent source of historical shoreline data is derived from geometrical-corrected aerial photographs. The extraction of the historical positions of the shoreline from this data source occurs as follows: The first step consists of correcting the distortions of aerial photographs and their georeferencing. Then, the digitization of the coastline takes place. This study concerns the evolution of the shoreline along 30 km of the coastline extending from Cape Carbon in the west to Cape Aokas in the East.

The digitization of the various coastlines (1989 till 2017) was achieved using the ArcGis software. All created data were stored in a geodatabase in which an entity class set (feature dataset) was realized. It allowed to group together all feature classes (coastlines) that were established into the same projected coordinate system (WGS84_UTM) and the same type of geometry type (one line). The geodatabase, feature class set, and feature classes were gathered in ArcCatalog, with one feature class for each coastline.

C. Aoudj (✉) · M. Guerfi · K. Mezouar
Laboratoire Des Écosystèmes Marins Et Littoraux (ECOSYSMarL), Ecole Nationale Supérieure Des Sciences de La Mer Et de L'Aménagement du Littoral, Campus Universitaire de Dely Ibrahim Bois Des Cars, Dely Ibrahim, 16320 Alger, Algérie

A. Çiner et al. (eds.), *Recent Research on Geomorphology, Sedimentology, Marine Geosciences and Geochemistry*, Advances in Science, Technology & Innovation, https://doi.org/10.1007/978-3-030-72547-1_15

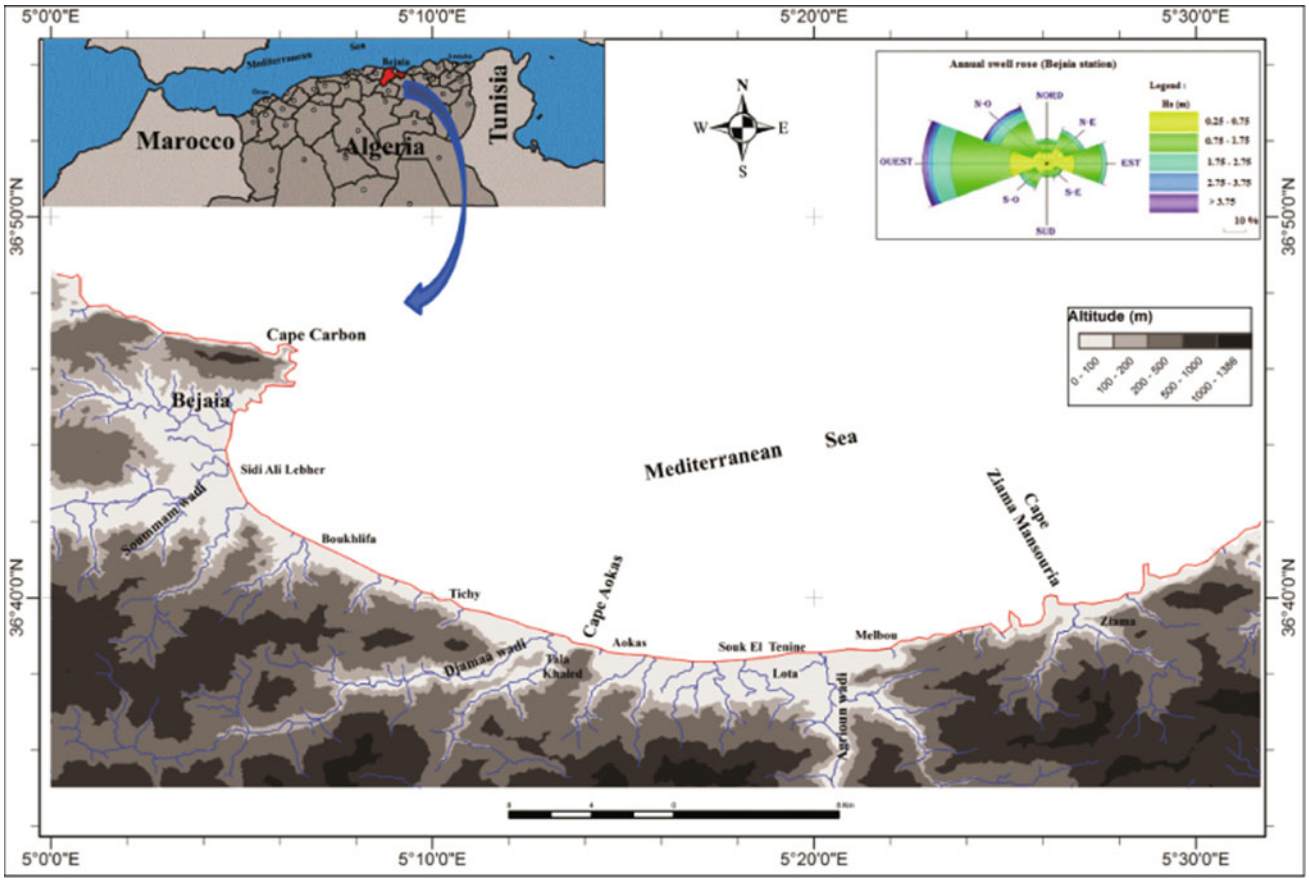

Fig. 1 Geographical location of Bejaia Bay (Djouder and Boutiba 2017 in Aoudj et al. 2017)

Besides, three other feature classes were proposed, one for the baseline (vegetation limit) and the other for transects each one length (300 m) and one measurement step (10 m), having the same geometric type (a line). The generation of perpendicular transects on the baseline was performed using the digital shoreline analysis system (DSAS) extension developed by Thieler and Danforth (1994). These transects were digitized from east to west (Fig. 2).

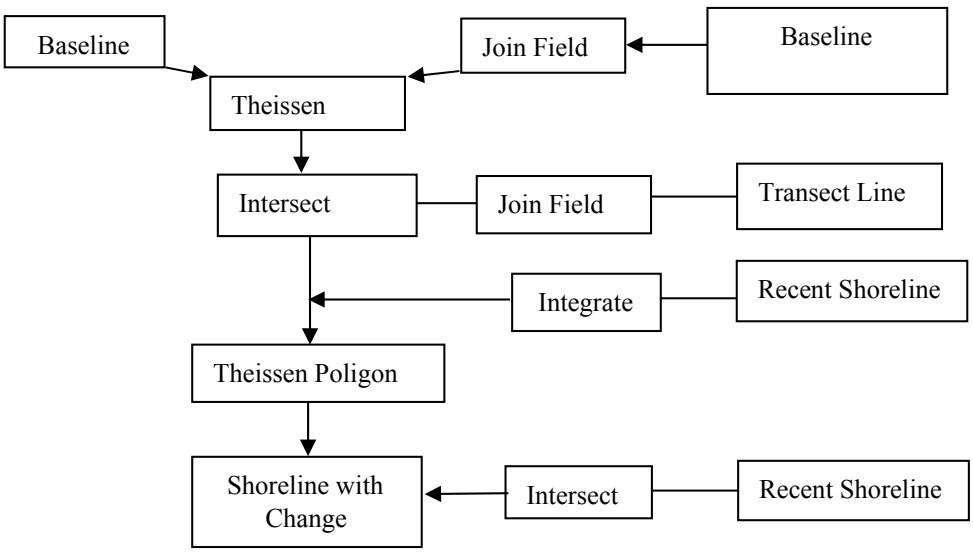

Fig. 2 Process of shoreline change calculation with reference to the end point rate (EPR) statistical method on DSAS

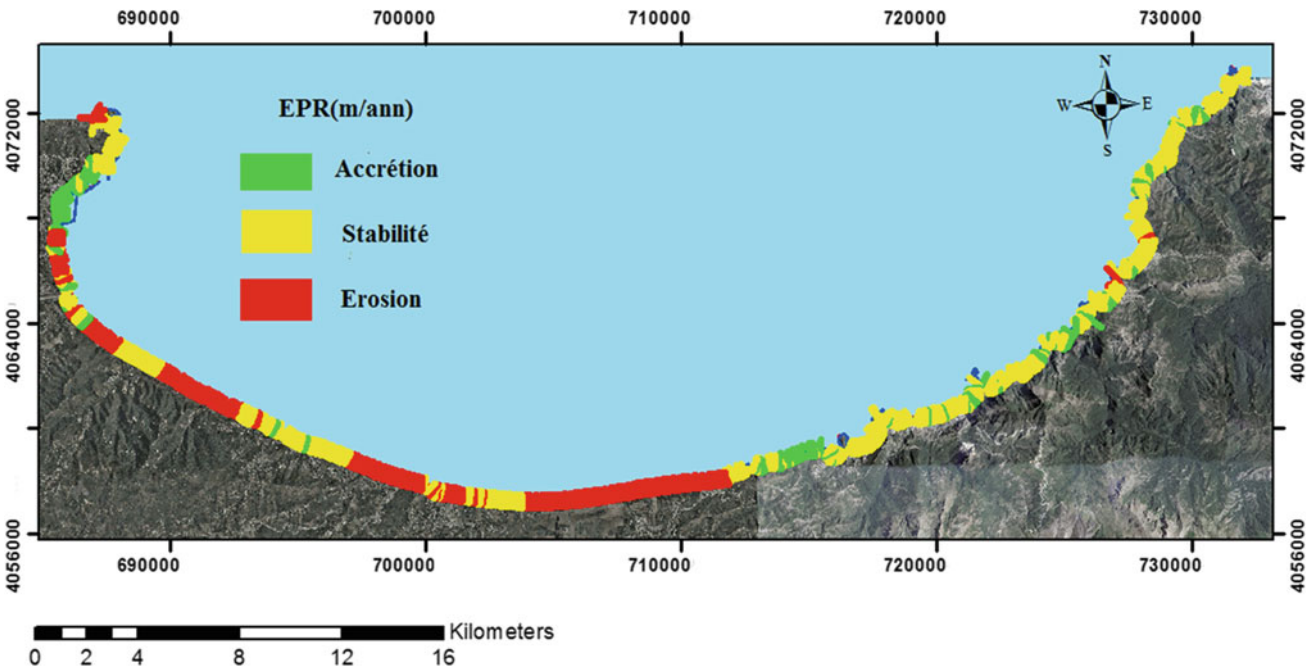

Fig. 3 Coastline evolution of Bejaia Bay between 1989 and 2017

4 Results

The evolution of the shoreline over a long period (1989–2017) was different; erosion and fattening zones followed each other (Fig. 3). The retreat of the coastline was recorded over most of the coast: east and west. However, the central part of the coast recorded a fattening of about 13.78 m as an annual average of 0.53 m/year. This could be linked to the weak lateral transits during this period against a large cross-shore transport of which a peak maximum of 86.84 m (3.34 m/year) was recorded at transect 119 (Sidi Ali Lebhar).

5 Discussion

From 1989 to 2017 (28 years), the western part of the bay (wilaya of Béjaïa) showed an eroding trend, while at the level of works, the port and the beaches of Tichy which are between Tassift and Hammadites (Tichy stade and Tichy center) showed an accretion. Stability was observed at Bejaia before the port and at Tichy and Souk El Tenine.

The stability at the level of the municipality of Tichy could be explained by the orientation of Cape Carbon (NE) which protected the beaches of this commune well from the waves of NW sectors in particular.

Coastal erosion occurred in most of the Bay of Bejaia; the eastern part of the bay was marked by deep erosion especially at Cape Aokas and the mouth of Wadi Soummam and Melbou. This could be related to the small amount of sediment that arrived in these areas and to the effects of socio-economic activities developed in the region.

6 Conclusions

This work suggests that the spatial and temporal evolution of the Béjaïa coastline is not homogeneous. The study of the coastline using the ArcGIS software and the DSAS, extension "digital shoreline analysis system," contributed to the cartography of the dynamics coastline at Béjaïa Bay and the understanding of the erosion phenomenon in this coastal zone. In the evolution of coastline erosion or accretion, phenomena are linked to natural and anthropogenic factors. In particular; coastal erosion is linked to (i) anthropogenic factors (construction of structures, sand trapping, and construction at the watershed level) and (ii) the socio-economic development of the region (tourism, industry, agriculture).

The findings drawn from Béjaïa Bay for the period between 1989 and 2017 confirm the hypothesis above. It is safe to conclude that the coastline of Béjaïa is fragile. It mainly presents unstable zones; the stable zones seem to be rare.

References

Aoudj, C., Mezhoud A., Guerfi M. Hemdane Y.: Analyse des variations spatio-temporelles du littoral sableux: Est Béjaoui (Algérie). Paralia, Croitia, 7–10 (2017). https://doi.org/10.5150/cmcm.2017.002

Djouder F., Boutiba, M.: Vulnerability assessment of coastal areas to sea level rise from the physical and socioeconomic parameters: case of the Gulf Coast of Bejaia, Algeria. Arab. J. Geosci. **10**, 299 (2017). https://doi.org/10.1007/s12517-017-3062-5

Thieler, E.R., Danforth, W.: Historical shoreline mapping (II): application of the Digital shoreline mapping and analysis systems (DSMS/DSAS) to shoreline change mapping in Puerto Rico. J. Coast. Res. **10**(3), 600–620 (1994)

Impact of Beach Surface Moisture on Aeolian Sand Transport Rate and Vertical Mass Flux Distribution, the Case of Atlantic Coast, Southern Morocco

Joanna Rotnicka and Maciej Dłużewski

Abstract

Several factors impact the aeolian sand transport rate, among which surface moisture is predominant. The current research aims to compare the simultaneous measurements of sand transport on moist and dry surfaces. The research is conducted at the Atlantic coast, 50 km south of Tarfaya, Morocco. Sand transport rate and vertical mass flux distribution are measured on three sandy surface types: (i) moist flat beach surface, (ii) dry rippled sand patch, and (iii) dry rippled sand at the dune crest. The findings show that at the same wind conditions, the total sand transport rate is greater on a dry surface than on a moist one only at lower wind velocity (up to 8–10 m/s). At higher wind speed, it is more significant on a moist surface. This can be related to the formation of a greater thickness of the saltation layer resulted from the harder rebound surface of moist sand.

Keywords

Aeolian sand transport rate • Vertical mass flux distribution • Sand moisture content • Atlantic coast • Morocco

1 Introduction

The predominant factors controlling aeolian sand transport rate in coastal areas, besides wind speed, are sand availability, grain size, density and shape, air temperature, and humidity as well as surface roughness and moisture. Therefore, every coast exhibits a very complex and unique system which, at the same wind conditions, can differ in term of sand transport rate and vertical mass flux distribution. Only a few studies have examined the impact of surface moisture on aeolian sand transport rate (e.g., Hotta et al. 1984; Borówka et al. 1990; Davidson-Arnott et al. 2008; Han et al. 2011). In coastal settings of temperate humid climate zone, there are several sources of sand moisture: (i) rainfall, (ii) tides, (iii) storm waves, and (iv) capillary rise. In the case of a tideless sand beach, its moisture varies in space and time (Davidson-Arnott et al. 2008) due to different water infiltration and drying rates, which depend not only on the amount or intensity of rainfall and frequency of storm flooding but also on different sand bulk density/porosity. Beach sand subjected to frequent flooding either by storm waves or by tides has got higher bulk density than sand in the case of a dry beach, where it is often redeposited by wind. Additionally, at coasts where rainfall is the main source of beach moisture, its content affects only the surface sand layer, whereas at coasts where tides or waves are the source of water, the moisture content is greater, and water infiltrates much deeper into the beach sand. Therefore, significant variation in surface moisture of the tideless beach is responsible for spatial and temporal variability of sand availability and sand transport rate (Rotnicka 2013). All these factors make the prediction of aeolian sand transport rate challenging. In the case of a tidal beach located in an arid zone, surface moisture results from regular tide flooding and occasional storm waves. At such coasts, there are zones of moist and dry sand, within and out of tidal range, respectively. Therefore, the moisture content in each zone is more uniform than in the case of beaches located in the temperate zone.

The present study aims to analyze the differences in sand transport rate and vertical mass flux distribution over moist and dry surfaces located on tidal coast of arid zone. To this end, field measurements were performed under conditions of full saturation, i.e., when available fetch distance was unlimited.

J. Rotnicka
Institute of Geology, Adam Mickiewicz University, Bogumiła Krygowskiego 12, 61-860 Poznań, Poland
e-mail: joanrot@amu.edu.pl

M. Dłużewski (✉)
Faculty of Geography and Regional Studies, University of Warsaw, Krakowskie Przedmieście 30, 00-927 Warsaw, Poland
e-mail: dluzewski@uw.edu.pl

A. Çiner et al. (eds.), *Recent Research on Geomorphology, Sedimentology, Marine Geosciences and Geochemistry*, Advances in Science, Technology & Innovation, https://doi.org/10.1007/978-3-030-72547-1_16

2 Settings and Methods

The research was conducted on the beach at the Atlantic coast, 50 km south of Tarfaya, Southern Morocco, in late spring (May and June 2018), i.e., in the period when unidirectional, trade wind prevailed. During field survey, dominant wind direction (north-northeast) was parallel to the coastline, and thus, the available fetch distance was unlimited. The sand transport rate and vertical mass flux distribution were measured in three experimental plots located on: (1) moist surface within intertidal zone, (2) dry rippled sand patch, and (3) dry rippled sand on the crest of a transverse dune. Sand moisture content (around 10%) in experimental plot 1 resulted from a high tide. The surface sand layer was flat and compacted during water percolation. Its bulk density measured in the field by portable densimeter was around 1.8 g/cm^3. The sand patch in experimental plot 2 developed on crusted silty surface located 50 m inland from the coastline. The sand was dry (moisture content <0.1%), and its surface was flat and covered by small ripples, its length, measured parallel to wind direction, equaled about 15 m. The experimental plot 3 was located about 40 m from the coastline, on an almost flat barchan dune crest. The windward slop was 80 m long, and the dune was 4.5 m high. The sand moisture content was also very low. The bulk density of dry sand in experimental plots 2 and 3 was around 1.65 g/cm^3.

Surface samples collected from each of experimental plots showed that the sand was on averaged 240 μm in diameter. It was moderately well-sorted (0.63 phi on average) and negatively skewed (−0.177 on average). Also, it was composed mainly of carbonate grains (mainly shell detritus) which accounted for ca. 84 wt. %. The remaining 16% was quartz, lithoclasts, and heavy minerals.

In each of the experimental plots, a set of two anemometers at 1 and 0.3 m elevations and a vane were deployed. A reference mast with six logarithmically spaced wind speed sensors and a vane was placed on a flat area near experimental plots. Wind speed and direction were recorded every second. The sand transport rate Q (kg/m/s) was measured simultaneously using six 0.5-m high passive vertical sand traps (two in each of experimental plots). Each trap was equipped with a removable catcher divided into forty compartments, each 1 cm wide and 1.27 cm high; thus, it was able to measure continuous vertical distribution of sand flux (Rotnicka 2013). Both sand transport rate and vertical mass flux profile were measured over 120 to 600 s, depending on the wind speed and transport intensity. The vertical distribution of mass flux for each measurement was developed according to the methodology recommended by Ellis et al. (2009). The mass of the sand trapped in each chamber was normalized by both the total mass of sand captured during a particular run and the chamber height. Then, it was expressed as a percentage.

The measured vertical mass flux distributions are usually best described by an exponential-decay function:

$$q(z) = \alpha \exp(\beta z).$$

where $q(z)$ is the mass flux at a height z above the bed surface, and α and β are regression coefficients (e.g., Rotnicka 2013; Namikas 2003; Liu and Dong 2004). To obtain the average value of vertical mass flux distributions for each type of sand surface, the α and β coefficients were averaged separately for the measurements taken in two wind speed classes: 8–9 m/s and 9–10 m/s.

3 Results and Discussion

A total of 32 measurements were made on the moist surface (experimental plot 1) and 24 measurements on the dry rippled surface (experimental plots 2 and 3). They were conducted during moderate winds speed (on average 8.0–10.5 m/s, guests up to 13 m/s at a height of 1 m) which generated continuous sand transport. Given the time of year and region (border of the Sahara Desert) in which the research was conducted, the air temperature was relatively low (20–23 °C), and air humidity was relatively high (60–70%).

The results showed that the highest total sand transport rate was obtained at the dune crest, regardless of wind speed (Fig. 1). It probably resulted from high sand availability on the windward slope of the barchan. When the sand was dry, the airflow at the dune crest was fully saturated, even if the wind speed slightly exceeded the critical threshold velocity. In contrast, the total mass flux over dry rippled sand patch was smaller under the same wind conditions (Fig. 1)—probably due to some limitation of sand availability. In the case of moist surface, the total sand transport rate was smaller than on dry sand patch only during low wind speed

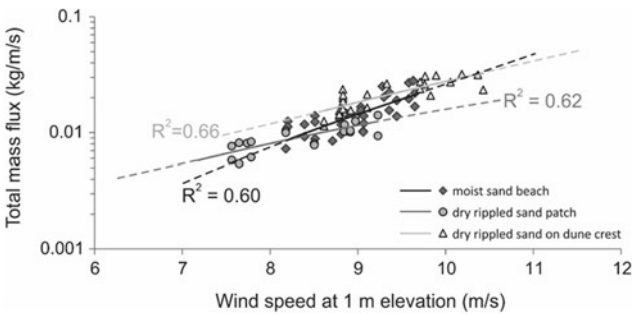

Fig. 1 Total mass flux measured on different surface types

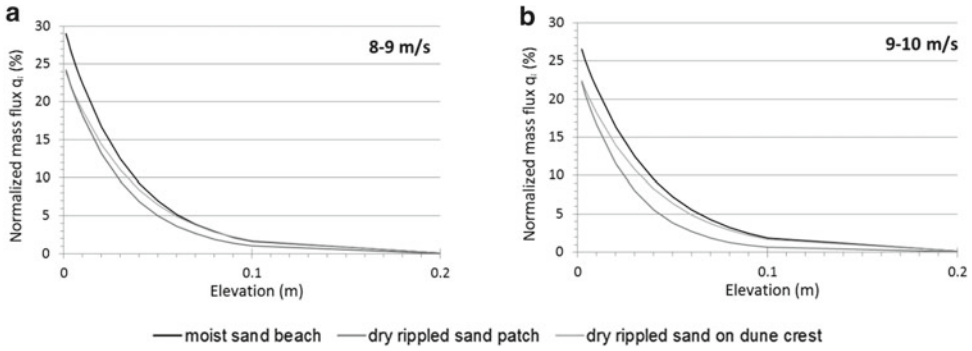

Fig. 2 Normalized mass flux measured on different surface types in wind speed classes: **a** 8–9 m/s and **b** 9–10 m/s

(up to 8 m/s) (Fig. 1). This could be linked to the increase of the critical threshold wind velocity necessary to initiate the saltation process on the moist sandy surface (e.g., McKenna-Neuman and Nickling 1989). At higher wind speed (above 8 m/s), the rate of aeolian sand transport was greater on the moist surface than on the dry sand patch. Based on the extrapolation of lines showing the relationships between the sand transport rate and wind speed on different types of sandy surfaces, it can be concluded that at wind speed above 10 m/s, the total mass flux on moist surface is greater than on dry sand at the dune crest.

The comparison of vertical averaged mass flux distributions suggested that in both analyzed wind speed ranges, much more (above 90%) sand is transported at a higher elevation on moist than on dry surface (Fig. 2). It was most likely due to the harder rebound surface of moist sand that caused grains to jump higher and further (McKenna-Neuman and Maljaars Scott 1998).

4 Conclusions

This paper presents results of sand transport rate measurements performed on dry and moist sandy surfaces. The main conclusions are: (i) At the same wind conditions, the total sand transport rate is greater on a dry surface than on a moist surface only at low wind velocity (up to 8–10 m/s). At higher wind speed, the total sand transport rate is greater on a moist surface. The difference in sand transport rate between both surfaces probably increases with the increase of wind speed, (ii) due to the differences in surface hardness, sand is transported at higher elevation on moist than on dry surface, (iii) the thicker the saltation layer, the greater the total sand transport rate, and (iv) the relatively small sand transport rate on the dry rippled sand patch is probably caused by the limitation of sand source.

The research has been supported by the grant from the National Science Center, Poland (No. 2016/23/B/ST10/01700).

References

Borówka, R.K.: The Holocene development and present morphology of the Łeba Dunes, Baltic coast of Poland. In: Nordstrom, K.F., Psuty, N.P., Carter, B. (eds.) Coastal dunes—forms and processes, pp. 289–313. Wiley, Chichester (1990)

Davidson-Arnott, R.G.D., Yang, Y., Ollerhead, J., Hesp, P.A., Walker, I.J.: The effects of surface moisture on aeolian sediment transport threshold and mass flux on a beach. Earth Surf. Proc. Land. **33**, 55–74 (2008)

Ellis, J.T., Li, B., Farrell, E.J., Sherman, D.J.: Protocols for characterizing aeolian mass-flux profiles. Aeol. Res. **1**, 19–26 (2009)

Han, O., Qu, J., Liao, K., Zhu, S., Zhang, K., Zu, R., Niu, Q.: A wind tunnel study of aeolian sand transport on wetted sand surface using sands from tropical humid coastal southern China. Environ. Earth Sci. **64**, 1375–1385 (2011)

Hotta, S., Kubota, S., Katori, S., Horikawa, K.: Sand transport by wind on a wet sand surface. In: Proceedings of the 19th coastal engineering conference. ASCE, New York, pp. 1265–1281 (1984).

Liu, X., Dong, Z.: Experimental investigation of the concentration profile of a blowing sand cloud. Geomorphology **60**, 371–381 (2004)

McKenna-Neuman, C., Maljaars Scott, M.: A wind tunnel study of the influence of pore water on aeolian sediment transport. J. Arid Environ. **39**, 403–419 (1998)

McKenna-Neuman, C., Nickling, W.G.: A theoretical and wind tunnel investigation of the effect of capillary water on the entrainment of sediment by wind. Can. J. Soil Sci. **69**, 79–96 (1989)

Namikas, S.L.: Field measurement and numerical modelling of aeolian mass flux distributions on sandy beach. Sedimentology **50**, 303–326 (2003)

Rotnicka, J.: Aeolian vertical mass flux profiles above dry and moist sandy beach surfaces. Geomorphology **187**, 27–37 (2013)

Relative Sea-Level Changes on the Southwestern Arabian Gulf since the Last Glacial Maximum

Damien Arhan, Kosmas Pavlopoulos, and Eric Fouache

Abstract

Several works have been carried out regarding Late Pleistocene–Holocene sea-level changes in the Arabian Gulf. Nevertheless, a global and regional approach is still lacking, and some critical issues remain unsolved. In this paper, a review and a reinterpretation of all published data regarding sea-level changes in the area have been completed and compared with new results obtained from fieldworks carried out in Failaka Island, Kuwait, and in Abu Dhabi Emirate, United Arab Emirates. This work relies mostly on studying geomorphological sea-level indicators, such as beach rocks and beach ridges besides combining archaeological data. Results show different trends in vertical movement within the studied area since the Last Glacial Maximum, which cannot be explained alone by the existing sea-level model, implying different, specific and local factors, such as tectonic deformations and diapirism.

Keywords

Relative sea-level changes • Arabian Gulf • Last Glacial Maximum–Holocene • Sea-level indicators • Vertical displacement

1 Introduction

During the Last Glacial Maximum (LGM), between 26.5 ka and 19 ka (Clark et al. 2009), eustatic sea level was laying between 120 and 130 m lower than present-day sea level (Clark et al. 2009; Peltier and Fairbanks 2006). During this time, the sea floor of the Arabian Gulf was therefore completely exposed to subaerial processes, until about 12 ka (Clark et al. 2009; Yokoyama et al. 2000).

After the LGM, the sea level rose quickly during a significant post-glacial transgression. Marine waters reached the Strait of Hormuz at approximately 14 ka and entered the Gulf itself by 12.5 ka; a true seaway was established (Lambeck 1996). The transgression exceeded the present-day sea level by 7100–6980 cal yr BP with a high stand of 1 m above current sea level, reached shortly after 5290–4570 cal yr BP (Lokier et al. 2015). Most coastal deposits are relicts of a Holocene sea-level high stand, dating from 7 to 3 ka. Stranded beaches at 2–4 m of elevation and up to 15 km inland are relicts of the Holocene high stand, in United Arab Emirates, Qatar, Bahrain, Kuwait and the Kingdom of Saudi Arabia.

Uplifted terraces and shorelines, and archaeological remnants indicate that the southern side of the Gulf experienced vertical displacement during late Quaternary (Uchupi 1999; Sanlaville and Dalongeville 2005). These environmental changes led to colossal landscape modifications, on very low-lying coasts, which could have affected human occupation during prehistoric and historic times. Studying these changes appears then fundamental to understand coastal human settlement in the region. Along the southern shore of the Arabian Gulf, coastal areas offered populations a broad range of resources such as food, wood and beads, while facilitating commercial and cultural relationships (Potts 2001).

2 Method and Material

In order to reconstruct sea-level history in the studied area, a database gathering all results from published studies was built, using around 250 dated geomorphological sea-level indicators, mostly beach rocks, beach ridges, algal mats and hardgrounds (see the figure below for location—one dot may

D. Arhan (✉) · E. Fouache
Sorbonne University, 75005 Paris, France

K. Pavlopoulos
Sorbonne University Abu Dhabi, Abu Dhabi, United Arab Emirates

A. Çiner et al. (eds.), *Recent Research on Geomorphology, Sedimentology, Marine Geosciences and Geochemistry*, Advances in Science, Technology & Innovation, https://doi.org/10.1007/978-3-030-72547-1_17

represent several indicators). Archaeological remains (shell middens, hearths) were not used as real sea-level indicators but as *terminus ad quem* since no sites with close relationship to sea level were excavated so far.

evidences, elevations were measured on the field with a clinometer and a metered tape (Rovere et al. 2016).

Furthermore, radiocarbon dating used in the database was (re)calibrated by means of *OxCal 4.3* online software (Bronk

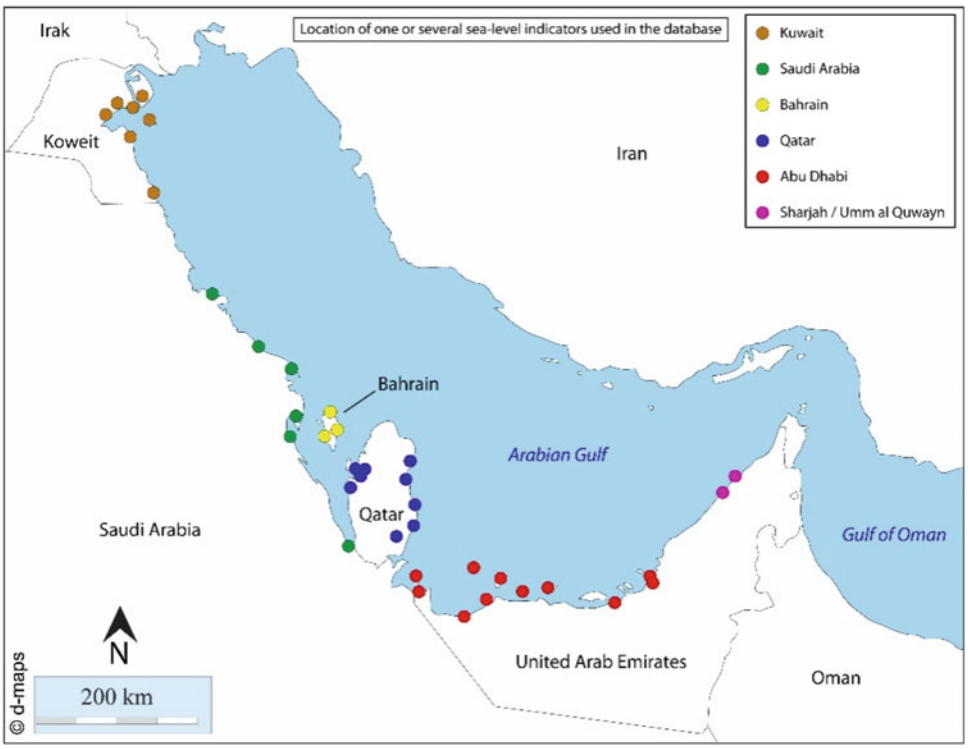

The studied area was constrained to the southern shore of the Arabian Gulf, from Kuwait to United Arab Emirates along about 2000 km. This large coastal area formed a homogeneous zone from climatic, hydrological, geological, sedimentological and geomorphological point of views.

To ensure data consistency, elevations reported from studied sea-level indicators were recalibrated regarding the same vertical datum (mean seal level), whenever it was necessary. Indeed, vertical datum often differed from one study to another which could therefore lead to significant spatial misinterpretations. Recalibration was performed thanks to published tidal data from the British Admiralty Service and from local municipalities and by considering the datum used in previous studies and the relationship between each type of indicator and the mean seal level. For instance, beach rocks were formed between the spray zone and the breaking depth while beach ridge limits were constrained between the storm wave swash height and the ordinary berm (Rovere et al. 2016). Arabian Gulf coasts were mostly micro-tidal; margins of error were applied in any case, depending on the data accuracy. Regarding the new

2009) using Marine13 curve and applying delta $\pm R$ correction from Qatar data (Southon et al. 2002). Most of the older published dating used conventional radiocarbon ages, which could represent a real issue, especially for marine environment deposits; calibration was therefore fundamental.

In addition to this published data, recent results from fieldwork and laboratory analysis carried out in Al Gharbia, Abu Dhabi western region, United Arab Emirate and Failaka Island, Kuwait, were integrated to the database and compared to the previous studies. These results relied on coastal deposits study (beach rocks and beach ridges). Also, for the dating process, the recent works applied the AMS C14 and OSL geochronological methods.

3 Results

Based on the database, local sea-level 2D diagrams, curves and chronologies have been built since LGM to recent. Oscillations observed show both similarities and specificities, highlighting the importance of local factors for uplifting and subsidence processes.

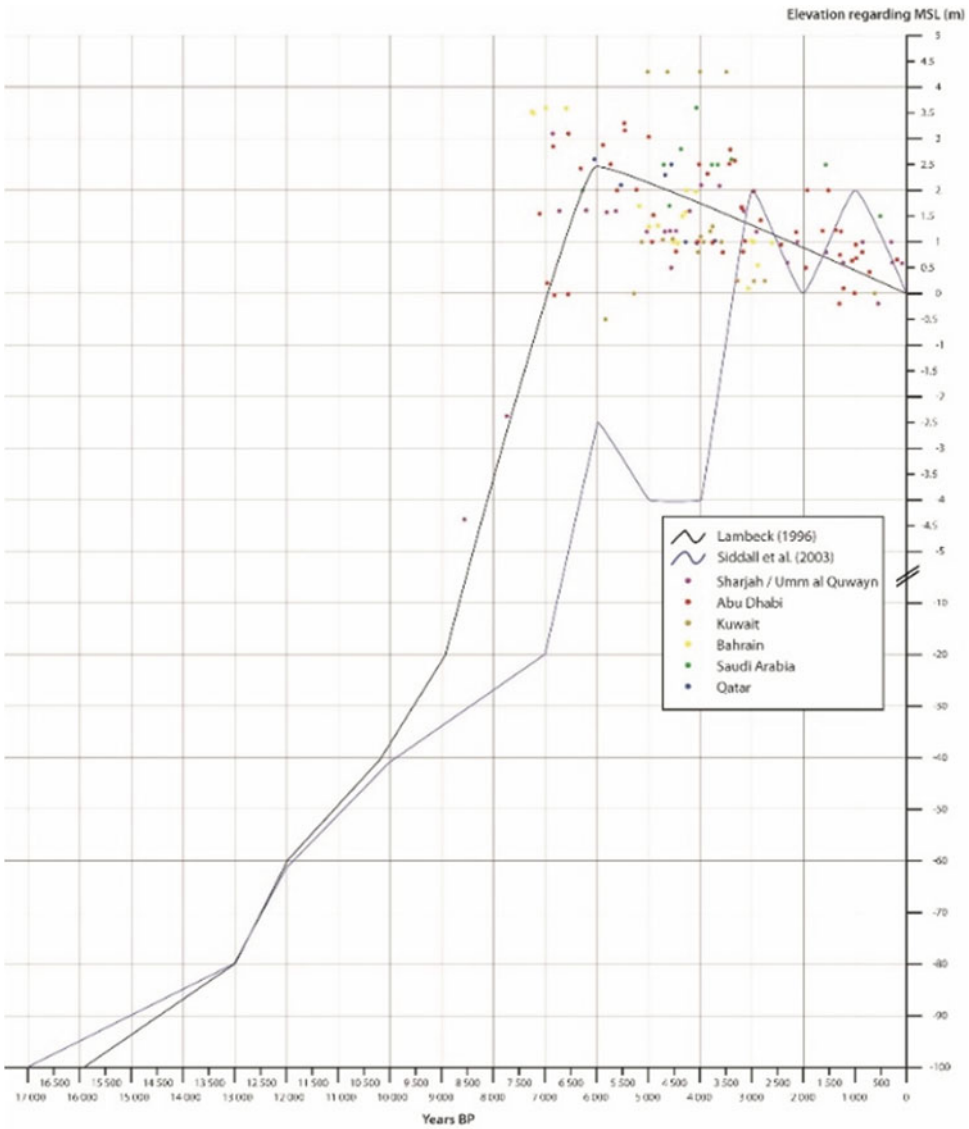

Some of the earliest and highest Holocene records in the region are found in Bahrain, showing a high stand up to +3.50 m amsl (7300–6600 cal yr BP). Relative sea level dropped down thereafter between +1.5 and +1 m amsl. A smaller high stand (< +2 m amsl) might be recorded between 4400 and 4000 cal yr BP.

In Saudi Arabia, previous studies highlight a high relative sea level (+2 m amsl) around 6500 cal yr BP, reaching +3–+3.5 m amsl between 4500 and 4000 cal yr BP. A smaller negative fluctuation (+2.5 m amsl) is recorded around 3000 cal yr BP, but the relative sea level seems to remain rather high until 1500 cal yr BP.

In Qatar, the relative sea level reached +2.6 m amsl around 6000 cal yr BP. After a small negative fluctuation (+2.00 m amsl) around 5600 cal yr BP, another high relative sea level is recorded around 4500 cal yr BP (+2.4 m amsl).

Trends in Kuwait show a low relative sea level (−0.5 m bmsl) between 6000 and 5000 cal yr BP, rising up to + 1 m amsl between 5000 and 3500 cal yr BP before falling progressively down and reaching its current position. Smaller oscillations are recorded as well: +1.2 m amsl around 4500 cal yr BP, +0.8 amsl around 4000 cal yr BP and + 1.3 around 3700 cal yr BP.

Within the United Arab Emirates, results highlight different trends. The eastern parts (Sharjah, Umm al Quwayn and east-Abu Dhabi) show some similarities, while data from the western parts (west-Abu Dhabi, Al Gharbia area) are more consistent with the trends observed in Qatar.

These curves have been compared to the global sea-level rise curves from LGM to recent (Siddall et al. 2003), and the difference highlighted corresponds to local trends in vertical displacement (i.e. uplifting and subsidence) along the studied area.

4 Discussion

So far, relative sea-level fluctuations along the Arabian Gulf have been explained by the glacio-hydro-isostatic model (Lambeck 1996), since the southern shore is considered to be tectonically stable during Holocene, without any active fault or important seismic activity observed. However, the observations and results of this study prove that the trends obtained from the data analysis cannot be supported by this sea-level model alone. Several factors could account for this hypothesis, mainly the crustal deformation, including tectonic deformations and diapirism (Cambrian salt rocks from *Hormuz Complex*), related to the ongoing convergence between Arabian and Eurasian plates, inducing a nonlinear uplift of the southern part of the Arabian Gulf.

5 Conclusions

The findings show different trends even between closed areas (e.g. eastern and western United Arab Emirates). Uplift and subsidence processes are not similar along the Arabian Gulf, characterized by specific rates and different chronologies. Moreover, they cannot be explained by the glacio-hydro-isostatic model alone. Further studies are required for the matter. However, the need for more research in this field does not eliminate the need to revise the model commonly used so far to describe Holocene relative sea-level oscillations.

References

Bronk, R.C.: Bayesian analysis of radiocarbon dates. Radiocarbon **51** (1), 337–360 (2009)

Clark, P.U., Dyke, A.S., Shakun, J.D., Carlson, A.E., Clark, J., Wohlfarth, B., Mitrovica, J.X., Hostetler, S.W., McCabe, A.M.: The last glacial maximum. Science **325**(5941), 710–714 (2009)

Lambeck, K.: Shoreline reconstructions for the Persian Gulf since the last glacial maximum. Earth Planet. Sci. Lett. **142**, 43–57 (1996)

Lokier, S.W., Bateman, M.D., Larkin, N.R., Rye, P., Stewart, J.R.: Late quaternary sea-level changes of the Persian Gulf. Quatern. Res. **84**, 69–81 (2015)

Peltier, W.R., Fairbanks, R.G.: Global glacial ice volume and last glacial maximum duration from an extended Barbados sea level record. Quatern. Sci. Rev. **25**(23–24), 3322–3337 (2006)

Potts, D.T.: Before the emirates: an archaeological and historical accounts of developments in the region c. 5000 BC to 6766 AD. In: Vine, P., Al Abde, I, (eds.) United Arab Emirates: a new perspective, pp.28–69. Trident Press (2001)

Rovere, A., Raymo, M.E., Vacchi, M., Lorscheid, T., Stocchi, P., Gómez-Pujol, Harris, D.L., Casella, E., O'Leary, M.J., Hearty, P.J.: The analysis of last interglacial (MIS 5e) relative sea-level indicators: reconstructing sea-level in a warmer world. Earth-Sci. Rev. **159**, 404–427 (2016)

Sanlaville, P., Dalongeville, R.: L'évolution des espaces littoraux du golfe Persique et du golfe d'Oman depuis la phase finale de la transgression post-glaciaire. Paléorient **31**(1), 9–26 (2005). https://doi.org/10.3406/paleo.2005.4780

Siddall, M.E., Rohling, E.J., Almogi-Labin, A., Hemleben, C., Meischner, D., Schmelzer, I., Smeed, D.A.: Sea-level fluctuations during the last glacial cycle. Nature **423**, 853–858 (2003)

Southon, J., Kashgarian, M., Fontugne, M., Metivier, B., Yim, W.W.-S.: Marine reservoir corrections for the Indian Ocean and Southeast Asia. Radiocarbon **44**, 167–180 (2002)

Uchupi, E., Swift, S.A., Ross, D.A.: Late quaternary stratigraphy, Paleoclimate and neotectonism of the Persian (Arabian) Gulf region. Mar. Geol. 1–23 (1999)

Yokoyama, Y., De Deckker, P., Johnston, P., Fifield, K.: Timing of the last glacial maximum from observed sea-level minima. Nature **406**, 713–716 (2000)

Shoreline Change Analysis Using Digital Shoreline Analysis System along Southeast Romanian Coast

Gabriel Dobrică, Constantin Cerneagă, and Carmen Maftei

Abstract

The purpose of this paper is to determine the coastal erosion in 2 May-Vama Veche sector based on historical changes in the shoreline positions. Sector 2 May is located between the breakwater dam Mangalia and the Bulgarian cross-border. The cliffs are susceptible to erosion and collapse through landslides. Changes in shoreline position are highlighted by remote sensing technique and shore surveying. The results obtained show that, compared to the orthophoto maps of 1978, 2005, 2008, 2010 and GPS measurements in 2017, there are major changes in the shoreline of 2 May sector. Image processing, geographical information system and digital shoreline analysis system methods are used in the study. The shoreline variation indicates that erosion rate varies at different timescales.

Keywords

Shoreline change • Erosion • Remote sensing • GIS • Romanian littoral

1 Introduction

Coastal erosion is a process caused by storms, floods, sea-level rise and human activities. In order to plan and manage the coastal areas, it is necessary to determine the shoreline changes and predict the future change (Alves et al. 2014). Remote sensing data, ground-based surveys and historic coastlines position integrated into a GIS-based map could offer a solution for researchers involved in coastal erosion analysis and decision-maker interested in long-term coastal management activities (Chaib et al. 2019). This study presents an analysis of the database concerning coastlines changes in order to determine the coastal erosion on Romanian Black Sea coastal zone, 2 May sector. In this sector, different studies show an erosion rate between 0 and 3 m/year (Dynamics and Studies 2011). Romanian littoral Black Sea is located in the south-eastern part of Romania having 240 km long. The geographical limits are the Musura Gulf in the north (situated on Chilia branch) and Vama Veche in the south (border with Bulgaria-Fig. 1). The study area, called 2 May Sector, is located between Port Mangalia in the north and Vama Veche in the south and characterized by high cliffs about 18–20 m (Fig. 1). Starting with 1840, there is a continuous increasing of the average level of the Black Sea, and the values range between 2.8 and 3.1 mm per year (Dan et al. 2009). The annual average wind speed is relatively high (between 4.2 and 6.95 m/s), the peaks being mainly from the north and north-west. The area is generally characterized by mild winters (when positive temperatures are mainly felt) and hot summers (when temperatures reach an average of 21–22 °C). The 2 May sector is subject of erosional processes which represent a real environmental risk, being strongly influenced by human intervention: Mangalia Port, breakwater dam and others hydraulic works. The type of soil on the coastal area is loess and clay deposits (Geological Institute of Romania 2019).

2 Materials and Methods

The data set consists in shoreline positions which was created using ArcGIS integrating topographic maps, GPS measurements and ortophoto plan acquired from geo-spatial website (Geo-spatial Homepage 2019). A Leica Viva GS08

G. Dobrică (✉) · C. Cerneagă · C. Maftei
Doctoral School of Applied Sciences, Ovidius University, Constanța, Romania

C. Maftei
Transilvania University, Brasov, Romania

G. Dobrică · C. Cerneagă
Romanian Water Agency, Dobrogea Branch, Constanta, Romania

A. Çiner et al. (eds.), *Recent Research on Geomorphology, Sedimentology, Marine Geosciences and Geochemistry*, Advances in Science, Technology & Innovation, https://doi.org/10.1007/978-3-030-72547-1_18

Fig. 1 Coastline of Dobrogea, Romania; 2 May sector (right; photo author)

Plus is used for GPS measurement. It should be noted that Black Sea has small tides (12 cm) that are not strong enough to be taken into consideration.

The erosion in the study period (1978–2017) is investigated using an ArcGIS extension (Digital Shoreline Analysis System-DSAS) originally developed in the early 1990s by US Geological Survey (USGS). This extension is freely available on USGS site; it calculates rate-of-change statistics for a shoreline time series data (Himmelstoss et al. 2018). Two of the methods offered by DSAS are chosen for this study: net shoreline movement (NSM) and end point rate (EPR). The NSM calculates the distance between two shoreline positions for each cross section (transect). If this distance is divided by the number of years between the two shoreline positions, the result is EPR.

3 Results and Discussion

The shoreline data set used for this study covered the 1978–2017 periods. In order to assess the shoreline changes, a total of 310 transects (cross section) were generated using DSAS software with a spacing of 20 m. The transects were generated along a baseline specified and overlaid on satellite

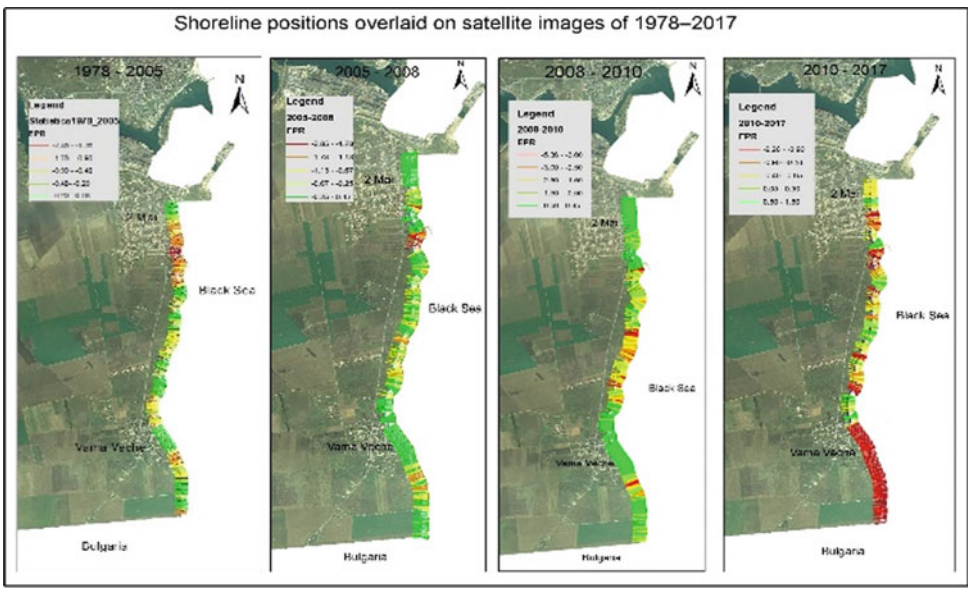

Fig. 2 Shoreline positions overlaid on satellite images of 1978–2017

Table 1 Rate of changes in shoreline positions at different time interval using EPR and NMS

Method	Period	Shoreline change mean (m/year)	Erosion		
			Max (m/year)	Min (m/year)	Mean (m/year)
(EPR) End point rate	1978–2005	−0.57	−2.36	−0.01	−0.57
	2005–2008	−0.41	−2.85	−0.01	−0.41
	2008–2010	−1.10	−5.36	−0.01	−1. 10
	2010–2017	−0.20	−2.26	−0.01	−0.20
Method	Period	Shoreline change mean (m/period)	Erosion		
			Max (m/period)	Min (m/period)	Mean (m/period)
(NMS) Net shoreline movement	1978–2005	−12.64	−63.26	−0.02	−12.64
	2005–2008	−1.35	−9.29	−0.01	−1.35
	2008–2010	−2.39	−11.62	−0.01	−2.39
	2010–2017	−1.37	−15.29	−0.02	−1.37

images (Fig. 2). The rate of changes in shoreline positions at different time interval using EPR and NMS is given in Table 1.

The shoreline investigated in this study is about 6 km length. The results displayed in Fig. 2 indicate a negative change (erosion) on the 2 May sector. The shoreline rate of changes between 1978 and 2005 indicates shoreline retreat of about 85%. Between 2005 and 2008, 63% of the shoreline was eroded. The mean EPR and NSM (Table 1) reveal that between 2008 and 2010, 76% of the shore was eroded. Respectively, between 2010 and 2017, the mean erosion rate was 0.20 m/year with the maximum rate of −2.26 m/year. The shorelines from 1978 to 2005 eroded at a faster rate compared to other study periods.

4 Conclusions

The main objective of this study was to assess changes in the shoreline positions spanning 1978–2017 period. The analysis performed in this paper indicated that erosion was a predominant phenomenon in the 2 May area and registered a net shoreline movement of −18 m in 39 years. The erosion could be explained by the regular shoreline occurrences such as waves and storm surges. Besides, the sandy nature of the soil made it susceptible to erosion. The findings suggested that the integration of shoreline positions time series data from different sources in GIS could be a solution in the monitoring and management of coastal areas.

Acknowledgements This work is supported by the project ANTREPRENORDOC, in the framework of Human Resources Development Operational Programme 2014–2020, financed from the European Social Fund under the contract number 36355/23.05.2019 HRD OP/380/6/13 – SMIS Code: 123847.

References

Alves, F.L., Sousa, L.P., Esteves, T.C., Oliveira, E.R., Antunes, I.C., Fernandes, M.D.L., Carvalho, L., Barroso, S., Pereira, M.: Trend change(s) in coastal management plans: the integration of short and medium term perspectives. The spatial planning process. In: Proceedings 13th international coastal symposium (Durban, South Africa). J. Coast. Res. Special Issue, **70**, 437–442 (2014). https://doi.org/10.2112/SI70-074.1

Chaib W., Guerfi M., Hemdane Y. (2019) Evaluation of coastal vulnerability and exposure to the risk of erosion and submersion in the coasts of Bou Ismail Bay. In: El-Askary, H., Lee, S., Heggy, E., Pradhan, B. (eds) Advances in remote sensing and geo informatics applications

Coastal dynamics and sedimentology studies: Halcrow (2011).

Dan, S., Stive, M.J.F., Walstra, D.R., Panin, N.: Wave climate, coastal sediment budget and shoreline changes for the Danube Delta. Mar. Geol. **262**(1–4), 39–49 (2009)

Geological Institute of Romania. http://www.igr.ro/. Last accessed 01 June 2019

Geo-spatial Homepage. http://www.geo-spatial.org. Last accessed 15 May 2019

Himmelstoss, E.A., Henderson, R.E., Kratzmann, M.G., Farris, A.S.: Digital shoreline analysis system (DSAS) version 5.0 user guide: U. S. Geological survey open-file report (2018). https://pubs.er.usgs.gov/publication/ofr20181179

Lithogolical and Geochemical Analysis of Mainland and Spit Sandy Beach Sediments: SE Baltic Sea (Lithuania)

Dovilė Karlonienė, Donatas Pupienis, Darius Jarmalavičius, Aira Dubikaltienė, and Gintautas Žilinskas

Abstract

The surface sediments were sampled in 2018, from a beach covering two coastal areas with different geological and geomorphological frameworks. The aim of this preliminary analysis is to (i) determine the main factors influencing the formation of the geochemical anomalies in beaches of Lithuania and (ii) evaluate the compositional differences of two beaches with different geology to understand the coastal physico-geochemical processes better. The results show different causes behind the anomalies: the coastal erosive processes, on the mainland coast and the sediments transportation from the spit's base—root, in the spit.

Keywords

Grain size • Magnetic susceptibility • Trace elements • Major elements

1 Introduction

Lithological, mineralogical and geochemical analyses of beach sands can provide valuable information about the local and regional patterns of sediment transport, distribution, provenance and condition of coasts (Hanamgond and Gawali 2017). Deeper and more complex insights on the dynamics of the beach are important as any changes in beach morphology and quality have economic and social impacts, especially in Lithuania where the coast is only 90 km long. The formation and dynamics of recent beach sediments were analyzed using lithological, morphometric and other methods in Lithuania (Jarmalavičius et al. 2017; Jarmalavičius and Satkunas 2011; Pupienis and Buynevich 2017). However, the geochemical composition of recent sediments has not been previously investigated. In this respect, the aim is to investigate the differences between two beaches with different geology for a better understanding of the coastal physico-geochemical processes.

2 Study Area and Methodology

The Lithuanian open sea coastline is divided by the 1–km-wide Klaipėda Strait, where Klaipėda Port is located, into two parts: the Curonian Spit (hereinafter—spit) sea coast (51 km) and in the mainland coast (39 km) (Fig. 1). The mainland coast and the coast of the spit differ geologically and geomorphologically (Bitinas et al. 2004). Glacial (moraine) deposits are placed at the central part of the mainland coast and mostly exposed in the cliffs. The first moraine, located at 25–27th km from Latvia border, is 2.1 km long and 5–8 m high. The second moraine, located at 30–31st km, is 950 m long and reaches 24 m at its highest point (Jarmalavičius et al. 2017). The sandy sediments (formed during 7500–4000 yrs BP) dominate in the northern and the southern parts of the mainland coastal structure. Glacial deposits in the spit are found only at depths of 25–30 m below the present sea level. The coarse sand layer is covered by a younger layer of marine sand dating to 1800 yrs BP, which is covered by a top layer of eolian sand younger than 1500 yrs BP.

For the analysis, sediment samples were collected along the entire Baltic Sea coast of Lithuania in 2018 (Fig. 1). The 43 composite surface sand (0–5 cm) samples were taken from the middle of the beach. To characterize the relative concentrations of heavy minerals (HMCs), a Bartington MS3 field scanning sensor was used for rapid and effective measurements of low-field volume magnetic susceptibility (MS) (Pupienis and Buynevich 2017). Grain size of the

D. Karlonienė (✉) · D. Pupienis · A. Dubikaltienė
Vilnius University, Universiteto St.3, 01513 Vilnius, LT, Lithuania
e-mail: dovile.karloniene@chgf.vu.lt

D. Pupienis · D. Jarmalavičius · G. Žilinskas
Nature Research Institute, Akademijos Str. 2, 08412 Vilnius, LT, Lithuania

A. Çiner et al. (eds.), *Recent Research on Geomorphology, Sedimentology, Marine Geosciences and Geochemistry*, Advances in Science, Technology & Innovation, https://doi.org/10.1007/978-3-030-72547-1_19

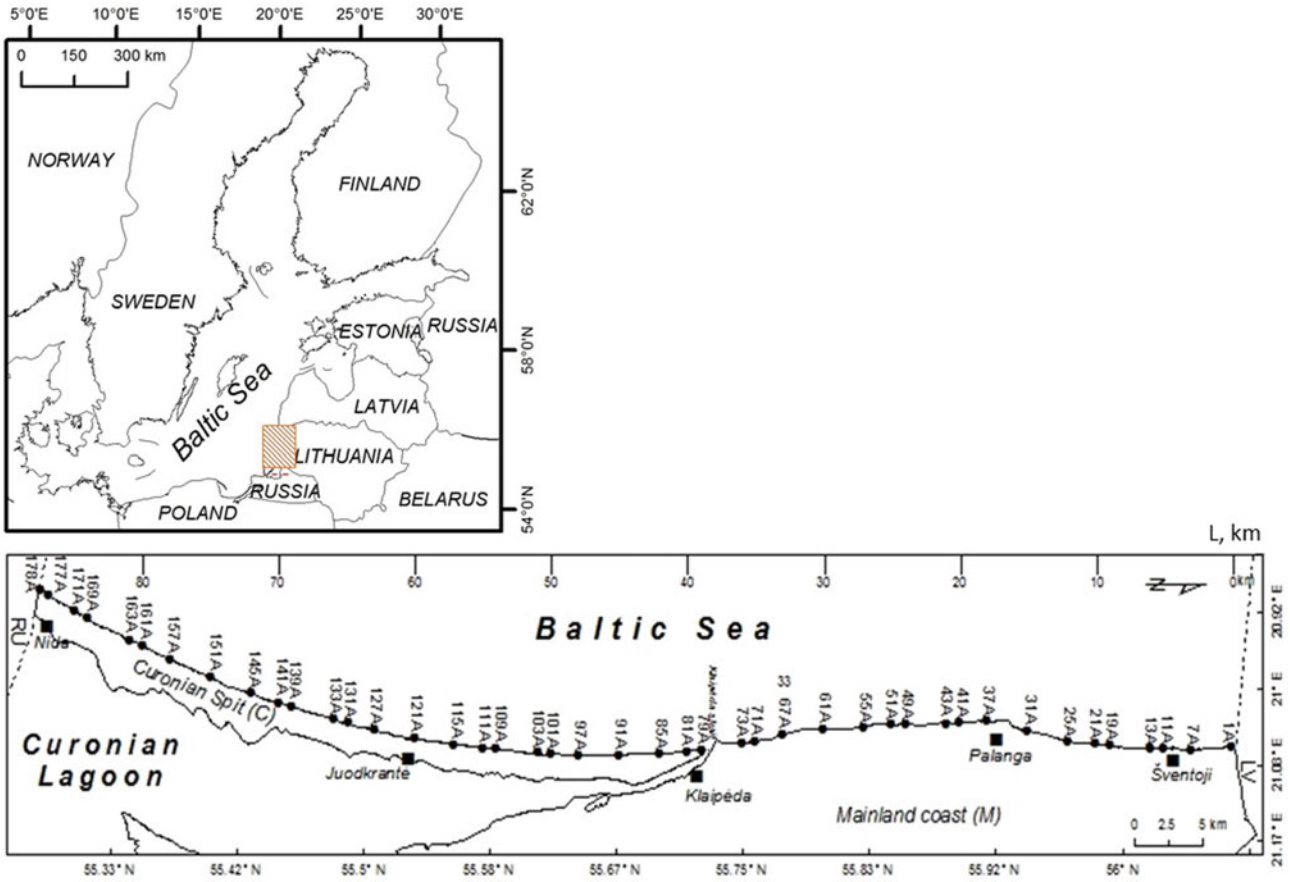

Fig. 1 Study site

samples was defined with vibratory sieve shaker "Fritsch Analysette 3 Spartan Pulverisette 0" and statistics—using the GRADISTAT 8.0 interpreter. The geochemical analyses of the samples were performed at the Bureau Veritas Commodities Canada Ltd. laboratory. The samples (no fraction was excluded) were digested in HNO_3 + HCl and analyzed with ICP-MS. Two standard reference materials (OREA-S45EA and DS11) were used. The data were standardized using formula $z = (M_i–M)/\sigma$, where M_i—measured values, M—average values and σ—standard deviation.

3 Results

The average grain size of the sediments on the beach in the mainland and spit is 0.31 mm (σ = 0.13), the smallest size is 0.18 mm (39th km) and maximum—0.77 mm (66th km). The average bulk MS values along the entire coast are 77.7 μSI (σ = 60.2), the lowest value is 7.9 (81st km) and highest—271.8 μSI (63rd km) (Fig. 2).

Our analysis of the major and trace elements distribution along the entire coast identified a few sites with exceptionally high concentrations (Fig. 2). In the mainland, the four sites distinguished: at third (high in Ti), 24th (in Zn), 25th (in Ba) and 30th km (in Ni, Mn, Ti, Al). The mentioned sites are all rich in Mg, Sr and Ca as well. In the beach sediments of the spit sea coast, the geochemical anomalies detected in the sites located at 39th (Cr, K), 42nd (Cr, K), 63rd (Cu, Pb, Ba and Al), 66th (Ni, Co, Fe, As, Al, K and Ti) and at 75th km (Cr, K).

4 Discussion

Results show that in the mainland coast, the coarser sand is observed at the sites where erosion processes are active (i.e., where significant correlation with MS is present) (Jarmalavičius and Pupienis 2014). The observed anomaly of coarse sands in the spit (57–66th km) agrees with the findings of a long-term grain size distribution analysis in this area, indicating its relict origin and stability (Jarmalavičius et al. 2017). Lithological anomalies are mostly consistent with the geochemical ones.

Besides, sediments from mainland and beaches differ in elemental composition. The sands in mainland coast are rich

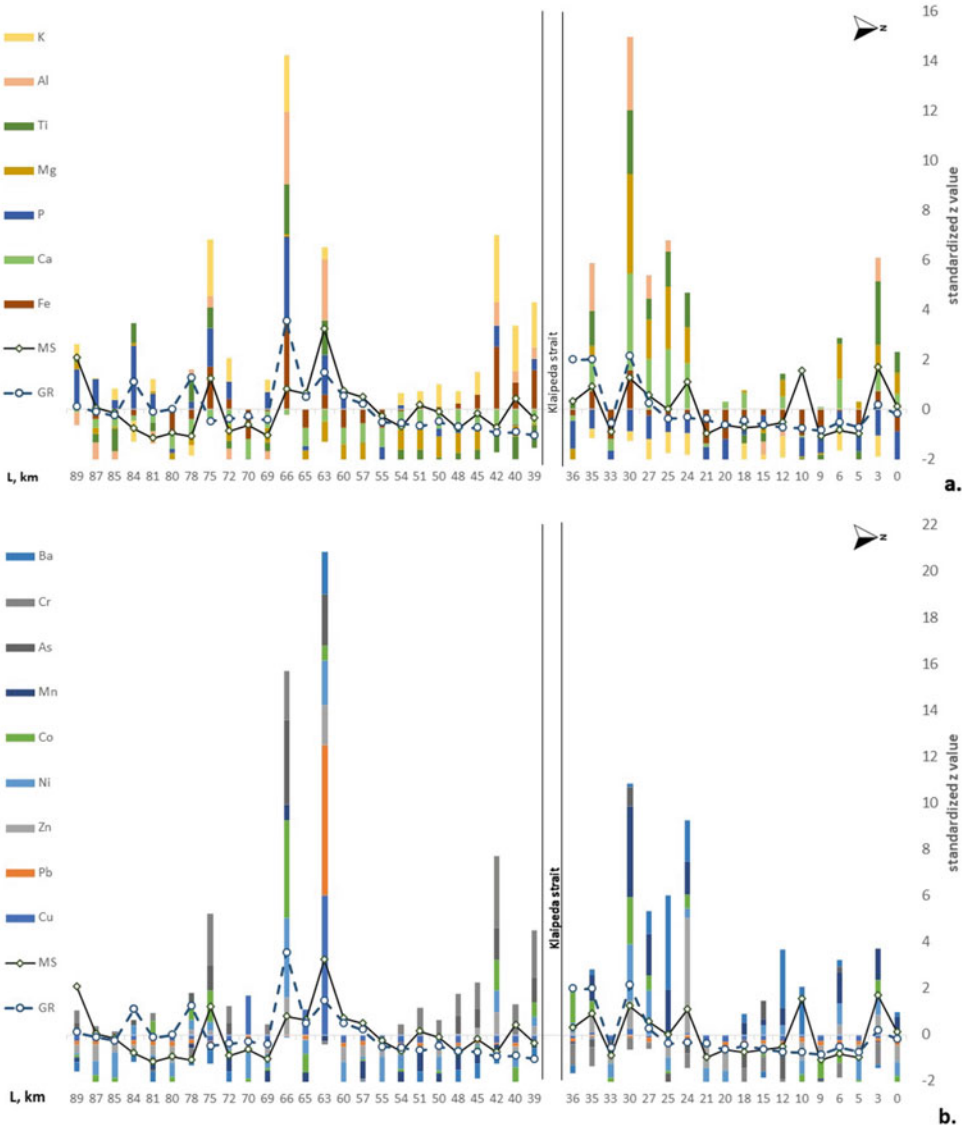

Fig. 2 Spatial trend of standardized (*z*) MS values, grain size (GR) and values of major (**a**) and trace (**b**) elements along the SE Baltic Sea coast in Lithuania (0–38 km mainland coast and 39–88 km spit)

in Ca, Mg and Sr (carbonates), which might be due to an increase in detrital dolomite and biogenic calcite (Kairyte and Stevensa 2005). Also, they have a relatively high concentration of Ba and low concentration of K which suggest that the sediments are more mature and further from the K enriched sources (Kasper-Zubillaga and Zolezzi-Ruíz 2007). The higher K content on the spit coast is likely due to higher content of glauconite, micas and orthoclase supplied from Sambia Peninsula until deposits by the northwards shoreline current. This current is strongest along the coasts of the Sambia Peninsula, but decreases considerably when reaching the distal end of the spit (Kairyte and Stevensa 2005; Parizanganeh 2008). The P and Cr are probably of the same origin. The detailed analysis of the anomalous Pb and Cu origin in the spit and Zn and Mn in the mainland coast are the topics of detailed future mineralogical analysis and research.

5 Conclusions

The geochemical anomalies defined in the mainland and spit of Lithuanian Baltic Sea coasts differ in their origin. In the mainland, they are formed where the coastal erosion processes dominate, whereas, in the Curonian Spit, the anomalies are located where the relict coarse sand dominates and where the main unloading of sediments from the alongshore current occurs. The bulk MS measurements could help to identify the geochemical anomalies, provided detailed mineralogical analysis.

References

Bitinas, A., Aleksa, P., et al.: Geological atlas of the Lithuanian coast of the Baltic Sea. Vilnius: Lithuania Geological Survey. (In Lithuanian), (2004)

Hanamgond, P.T., Gawali, P.B., et al.: Sediment texture and geochemistry of beaches between Redi-Vengurla, Sindhudurg, west coast of India. J. Coastal Res. **33**(5), 1135–1147 (2017)

Jarmalavičius, D., Satkunas, J., et al.: Dynamics of beaches of the Lithuanian coast (the Baltic Sea) for the period 1993–2008 based on morphometric indicators. Environ. Earth Sci. **65**(6), 1727–1736 (2011)

Jarmalavičius, D., Pupienis, D., et al.: Sea level fluctuation and shoreline evolution on decadal time scale, Lithuanian Baltic Sea coast. J. Coast. Res. **70**, 164–169 (2014)

Jarmalavičius, D., Pupienis, D., et al.: Geologic framework as a factor controlling coastal morphometry and dynamics. Curonian Spit, Lithuania. Int. J. Sedim. Res, **32**, 597–603 (2017)

Kairyte, F., Stevensa, R.L., et al.: Provenance of silt and clay within sandy deposits of the Lithuanian coastal zone (Baltic Sea). Mar. Geol. **2**(5), 97–112 (2005)

Kasper-Zubillaga, J.J., Zolezzi-Ruíz, H., et al.: Sedimentological, modal analysis and geochemical studies of desert and coastal dunes, Altar Desert NW Mexico. Earth Surf. Proc. Land. **32**, 489–508 (2007)

Parizanganeh, A.:Grain size effect on trace metals in contaminated sediments along the Iranian coast of the Caspian Sea. In Sengupta, M., Dalwani, R. (eds.) Proceedings of Taal2007: the 12th world lake conference, pp 329–336. (2008)

Pupienis, D., Buynevich, I., et al.: Spatial patterns in heavy-mineral concentrations along the Curonian Spit coast, south-eastern Baltic Sea. Estuarine Coast. Shelf Sci. **195**(5), 41–50 (2017)

Modeling of Lithodynamic Processes in the Area of Sea Port (Russia)

Ghinwa Hadla, Izmail Kantarzhi, and Igor Leont'yev

Abstract

This paper presents the modeling of the morphodynamical processes occurring in the coastal zone of the port terminal "Utrenny" of the Sabetta port, in Russia. The work includes calculating the local and integrated sediment flows, estimating the seabed and shoreline deformations and determining the conditions of deposition in the approach channel and the port water area. To obtain these results, the SWAN spectral wave model, version 41.10AB, is used to calculate the statistical characteristics of the wind waves. The spectral mode of the wave model ARTEMIS is also applied to calculate the wave fields in the study area.

Keywords

Lithodynamic processes • Approach channel • ARTEMIS • SWAN

1 Introduction

The study area is the coastal zone of the "Utrenny" terminal of liquefied natural gas and stable gas condensate of the Sabetta seaport, in the Ob Gulf (Fig. 1). The "Utrenny" terminal has a planned approach channel with 5.7 km length, 495 m width and 14.9 m depth.

The protected water area has a length of 4.5 km along the coast, its width from the coast to the protective structures is about 1 km, and the depths are in the range from 0 to 15 m. The entrance to the water area is open on the west side. An important feature of the design is that the fencing is not connected to the shore, and the strip of the coastal slope with 270 m width and depths of about 3 m remains open (Fig. 2). Shores in the study area are fine sandy accumulative shores, with silty precipitations deeper than 8–10 m. The wave action zone has an average coastal slope of about 0.01, characterized by the presence of a system of underwater shallow shafts, which are shifting toward the sea under the action of strong waves and moving to the coast under less wave activity. The intensive movement of sand sediments flows occurs in the coastal strip on the southern and northern directions.

An integrated methodology developed for predicting lithodynamic processes on the approach to the port allows to take into account the influence of navigation channels on waves and morphodynamics. This forecast is made for the situation with the designed facilities.

2 Materials and Methods

The SWAN model version 41. 10AB served to calculate the statistical characteristics of wind waves in the Kara Sea and the Ob Gulf. The numerical model was verified by the comparison of the calculated wave heights for three time periods 08/2012–09/2012, 17/09/2015–18/10/2015 and 10/07/2016–27/07/2016 with the measured in wave-measuring buoys and other points in the terminal water area. The wave modes in the coastal zone of the study area were calculated by the ARTEMIS model (Aelbrecht 1997). The physical model of the port in Vostok Bay was used to verify the ARTEMIS model by numerical modeling of wave fields.

The technical report (2015) revealed the characteristics of the currents in the considering area. To calculate the longshore sediment transport in the coastal zone, models from Leont'ev (2014a b) were used assuming that the average size of sand at the bottom is 0.15 mm at the zone of active sediment movement. The total displacement of the underwater shallow shafts was determined based on the models

G. Hadla (✉) · I. Kantarzhi
Moscow State University of Civil Engineering, Moscow, Russia129337

I. Leont'yev
P.P. Shirshov Oceanology Institution, Russian Academy of Sciences, Moscow, Russia

A. Çiner et al. (eds.), *Recent Research on Geomorphology, Sedimentology, Marine Geosciences and Geochemistry*, Advances in Science, Technology & Innovation, https://doi.org/10.1007/978-3-030-72547-1_20

Fig. 1 Location of the terminal "Utrenny"

(Leont'ev 2019). The deposition in the approach channel of the terminal was assumed by the method of analogy with the approach channel of Sabetta port, as published in Gladish et al. (2017).

3 Results

From the statistical processing, the west direction wave with repeatability once in 100 years and probability 1% was selected for the layout options of port structures and model presetting. This wave was of 270° azimuth, 7.03 s period and 3.57 m height. The verification of the SWAN model gave a correlation coefficient (0.87–0.90) and a standard deviation (0.21–0.25), and for the ARTEMIS, it gave a correlation coefficient (0.94). The total sediment flows on the *S* and *N* did not reveal large differences (13–15 × 10^3 m^3/year), and the resulting flow in the south direction was rather insignificant (2.3 × 10^3 m^3/year) (Fig. 3).

Thus, the total volume of deposition carried by sandy sediments was estimated at about 30 × 10^3 m^3/year. Using the calculation based on the dependence of the progressive flow on the silty bottom, it was found that the integral annual deposition amount in the channel would be 1.3 × 10^5 m^3/year. Based on the calculation for an exclusively western strong storm, the amount of incoming material would be about 35 × 10^3 m^3/year. Taking into consideration the contribution of extreme western storms, the total amount of deposition could be estimated approximately (60–70) × 10^3 m^3/year.

4 Discussion

Considering the results obtained from the hydraulic modeling of the wave mode and the obtained lithodynamical characteristics in the water area of the terminal "Utrenny," it can be found that the longshore transport of sand sediments was concentrated in a coastal striped area (to the −4 m isobath), directed only to the south; however, at depths greater than 1.5 m, it could prevail to the north and confine peaks at the underwater shallow shafts ridges. Taking into account the more intensive hydro- and lithodynamical conditions of the northern part of the Ob Gulf, the representative indicator of the deposition in the approach channel to the Sabetta seaport was estimated at 0.3 m/year, so the deposition indicators of the approach channel to the "Utrenny" terminal, located in a quieter zone, would not exceed this value. The sand cumulative bodies from the unloaded sediments would be formed as shore projections inside the water area, where waves subside (Fig. 4). Hence, it can be concluded that after a year of construction, the shore could be extended at 24–28 m with a distance of noticeable shoreline changes about 270 m.

These indicators would be more than double after five years of construction. After 10 years of construction, this

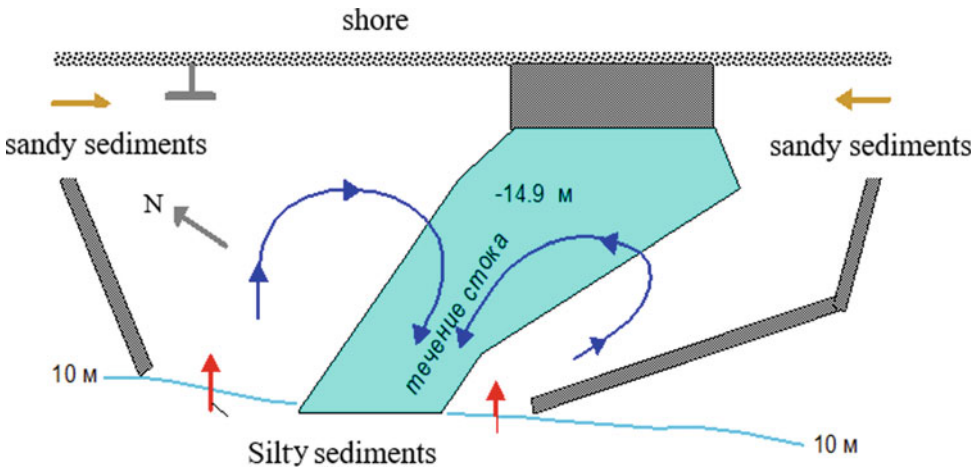

Fig. 2 Scheme of the water area of the "Utrenny" terminal

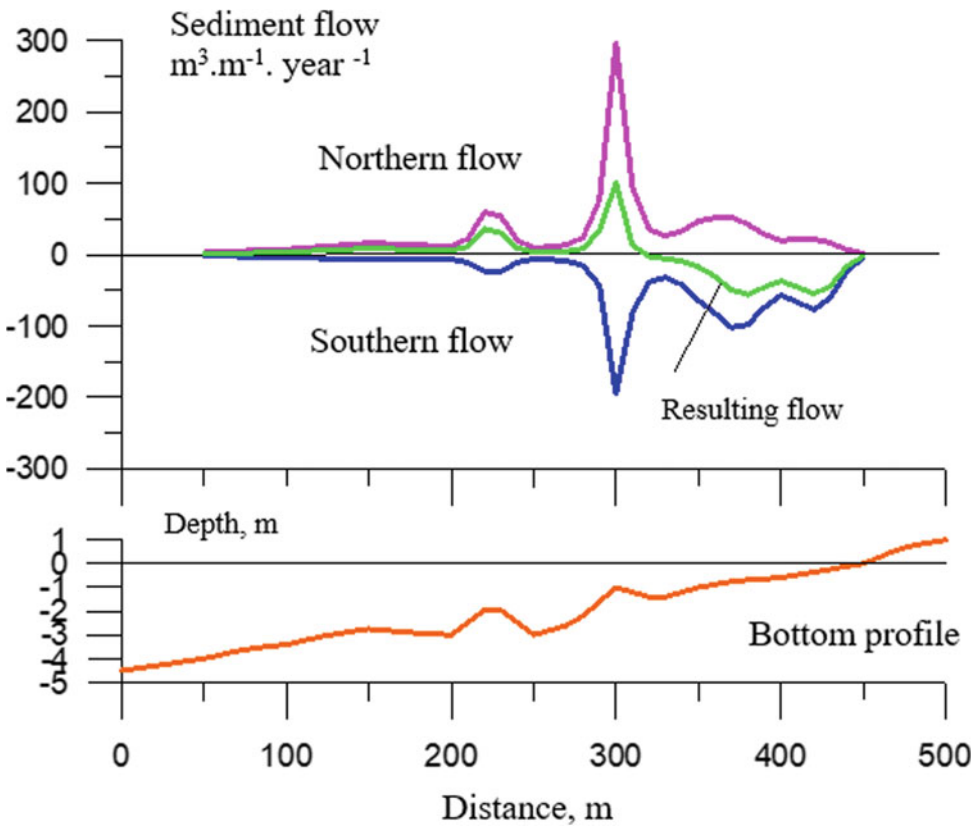

Fig. 3 Distribution of sediment flows along the shore profile

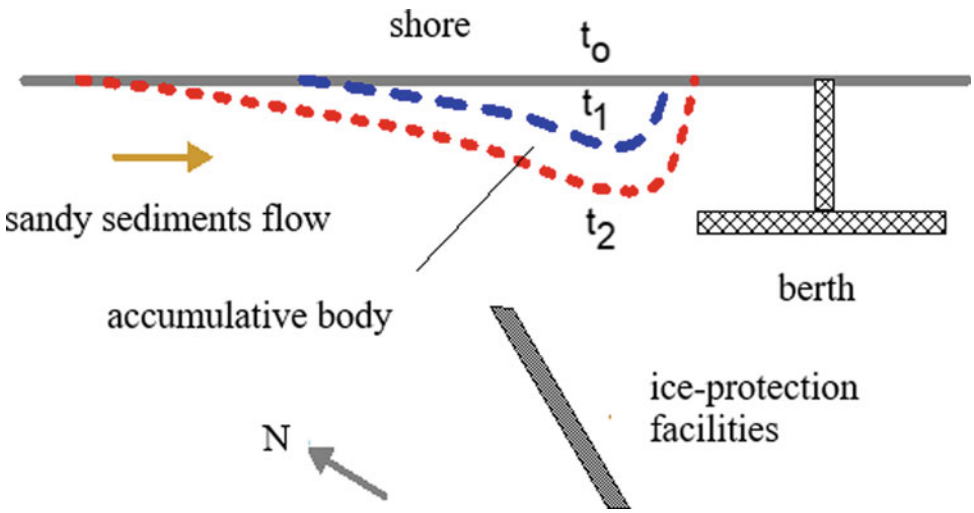

Fig. 4 Formation of the accumulative body

shore projection would be about 100 m transversely and more than 800 m longitudinally. Over time, this process of sedimentation might cause problems in the investment of the port structures, in particular, in front of the berth located in the northern part of the protected area, where a part of the incoming material might be deposited.

5 Conclusions

In this research, the task was to build a mathematical model of the water area of the port terminal "Utrenny" to forecast the waves' characteristics for each construction period of the

final layout of the protective structures and facilities of the terminal "Utrenny." The study involved calculating the total amount of deposition in the approach channel and the water area and forecasting the shoreline changes and the seabed deformation for the period after construction. The study also targeted the optimal investment of this terminal and aimed to avoid future problems.

References

Aelbrecht, D.: ARTEMIS 3.0: a finite element model for predicting wave agitation in coastal areas and harbors including dissipation. WIT Trans. Built Environ. **30** (1997)

Gladish, V.A., Logvina, E.A., Nesterov, A.V., Kubishkin, N.V.: Intensity of the lithodynamical processes in the sea navigation channel Sabetta. Eng. Stud. **4**, 36–45 (2017)

Leont'ev, I.O.: Morphodynamical processes in the sea coastal zone. LAP LAMBERT Academic Publishing, Saarbrücken, p. 251 (2014a)

Leont'ev, I.O.: On the calculation of the longshore sediment flow. Oceanology **54**(2), 226–232 (2014b)

Leont'ev, I.O.: Storm deformation of the shore slope with the underwater sharps. Oceanology **59**(1), 115–122 (2019)

Technical report on the hydrometeorological study for the "Hydraulic structures for the factory LNG-2 on the gravitational base". Saint-Petersburg, p. 270. (2015)

Geomorphology, Soil Science, Landslides, Coastal Processes, and Geoarchaeology (T9): Geoarchaeology and Geoheritage

Geophysical Investigations of the Bronze Age Archaeological Site in the Trans-Urals, Russia

Natalia Fedorova and Vladislav Noskevich

Abstract

Geophysical research is carried out on an archaeological site of the Bronze Age: the fortified multilayer settlement Andreevskoye in the Southern Ural Mountains of Russia. In this context, this paper reports the results of a detailed magnetic survey and four GPR profiles of this fortified settlement. The measurements involve two proton gradiometers and one cesium vapour gradiometer on a preliminary spaced grid of 0.5 × 0.5 m. These geophysical surveys allow researchers to determine the essential characteristics of the settlements' fortifications, layouts and chronological aspects. The research provides new insights into the inner spaces of this settlement, the parameters of dwellings and the location of some wells and household pits. The magnetic map allows the reconstruction of a more accurate scheme of settlement compared to the scheme obtained using the results of aerial photography.

Keywords

Archaeological site • Bronze Age • Geophysical investigations • Magnetic survey • GPR

1 Introduction

In the past three decades, 21 settlements with closed circular, oval or rectangular fortifications were discovered within a rather limited territory of the Southern Urals, through a wide use of aerial photography and field surveys. All settlements, ranging in size from 0.8 to 3.5 ha, were located in valleys of small steppe rivers in the Tobol and Ural basins, all within an average distance of 40–60 km apart. The settlements dated to the Bronze Age (Epimakhov et al. 2016; Noskevich et al. 2012), with some being completely destroyed due to anthropogenic activity. Most of these sites were found after decoding the aerial imagery, with the layouts of these settlements established based on the data (Zdanovich and Batanina 2007). At one fortified settlement (—Andreevskoye, 140 × 160 m) (Fig. 1), a detailed magnetic and GPR surveys were conducted to study fortifications of the settlement.

2 Survey Methodology and Initial Analysis of Measurements

For this magnetic survey, the gradiometer Scintrex SM-5 (Canada) and the magnetometer–gradiometers POS-1and MMPG (Russia) were employed. Survey sections were divided into a square grid of 40 × 40 m. Measurements were performed with an interval of 0.5 × 0.5 m between each observation point. Before conducting the magnetic survey, the sections were brushed clear of any technogenic iron remains, as the presence of such could disturb a magnetic mapping. This work was accomplished using a metal detector.

Measurements were performed in a continuous mode. The error of the survey estimate was around ±1 nT. For recording of geomagnetic field variations during observations, a magnetometer POS-1 with an interval of measuring of 3 s was used.

A ground-penetrating radar (GPR) survey was also conducted in the settlement Andreevskoye following a point data collection method. The equipment comprised a SIR-3000 (USA) with the antenna unit 5103 A tuned at a frequency of 400 MHz. The length of the four profiles ranged from 34 to 40 m, and the interval between measurement points along the profiles was 0.1 m. To determine the velocities of electromagnetic waves, two antennas 3207 (USA) were used, with a central frequency of 100 MHz according to the common middle point (CMP) scheme.

N. Fedorova (✉) · V. Noskevich
Institute of Geophysics UB RAS, Yekaterinburg, 620049, Russia

A. Çiner et al. (eds.), *Recent Research on Geomorphology, Sedimentology, Marine Geosciences and Geochemistry*,
Advances in Science, Technology & Innovation, https://doi.org/10.1007/978-3-030-72547-1_21

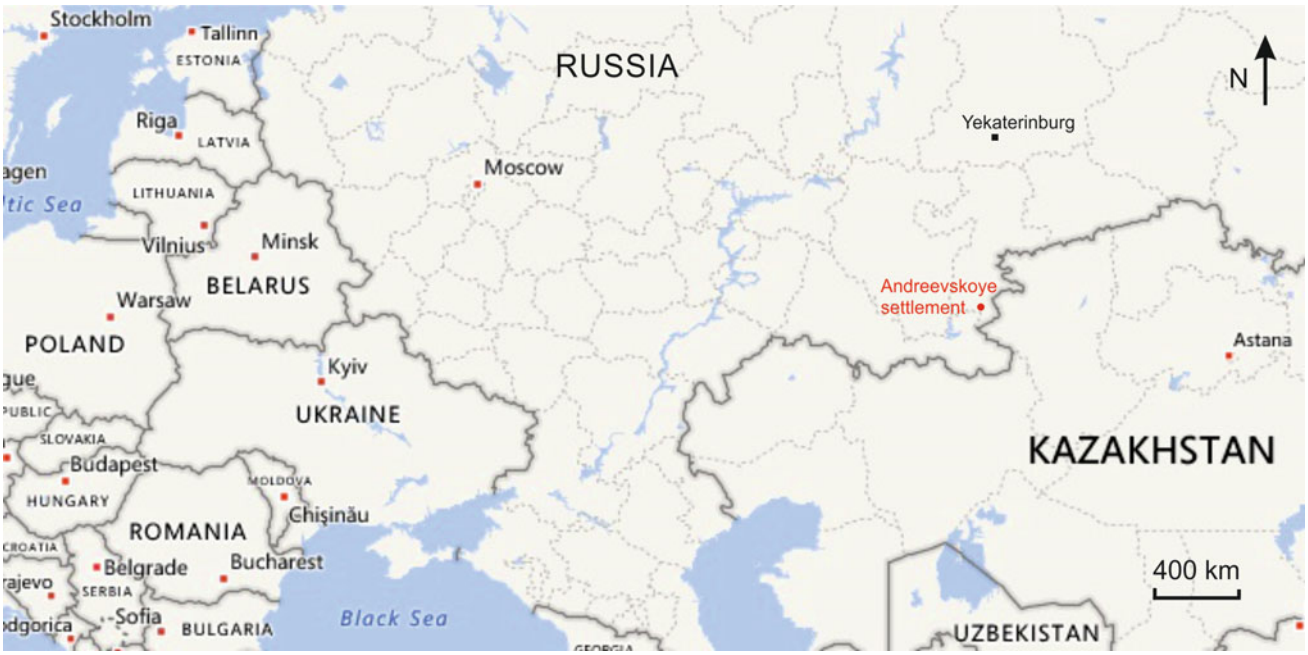

Fig. 1 Location of Andreevskoye settlement

3 Results of Geophysical Investigation

3.1 Results of Magnetic Survey

The settlement of Andreevskoye is a multilayered site (Zdanovich and Batanina 2007). According to the field measurements results, the map of magnetic anomalies was constructed illustrating the difference between measured values of modulus induction of the geomagnetic field at the heights of 0.3 and 2 m. Figure 2a shows the coloured map of anomalous magnetic field, and Fig. 2b displays the greyscale version.

Various filtering techniques were applied to the data obtained (moving average, Gaussian, first and second derivation). The findings allow better highlighting of anomalies of fortifications and interior walls that separate the space into sectors or dwellings. According to this data, a settlement scheme was built (Fig. 3a). Geophysical data does not confirm the presence of numerous passages through the defensive walls, which were revealed after decoding aerial photographs (Zdanovich and Batanina 2007) and interpreted as entrances (Fig. 3b).

Besides, the magnetic survey data does not attest the complex structure of the fortified system near the entrances to the settlements A and B. A lot of intense positive magnetic anomalies of various forms were recorded inside the dwellings in the northern part of settlement A. Usually, the most intense magnetic anomalies are observed outside of the defensive wall and the ditch. Such anomalies are caused by burnt clay, which was used for house construction. It can be assumed that the walls of dwellings were plastered with clay too. Still visible in the south-eastern part of the settlement A are a few dwellings in the third and fourth rows, the longitudinal walls of which are parallel to the eastern defensive wall. Settlement B is located in the rest of these rows. Therefore, settlement A originally consisted of four rows, with the total amount of dwellings estimated to be around 65–70. Later the northern part was abandoned, the southern part of two rows of houses was enclosed with a new fortification wall, and the settlement B was formed.

The settlement consisted of 26 dwellings. Consequently, during the second period of the settlement function, the number of inhabitants had significantly diminished. Later, it seems that the population increased, and to the south wall of the settlement B the settlement C was built, which consisted of additional ten dwellings. Thus, the geophysical data support the previous hypothesis (Zdanovich and Batanina 2007), that settlement A was built earlier, and settlement B was established later. The magnetic survey undertaken provides new information on the fortifications and the settlement structure, i.e., the locations of houses as well as the

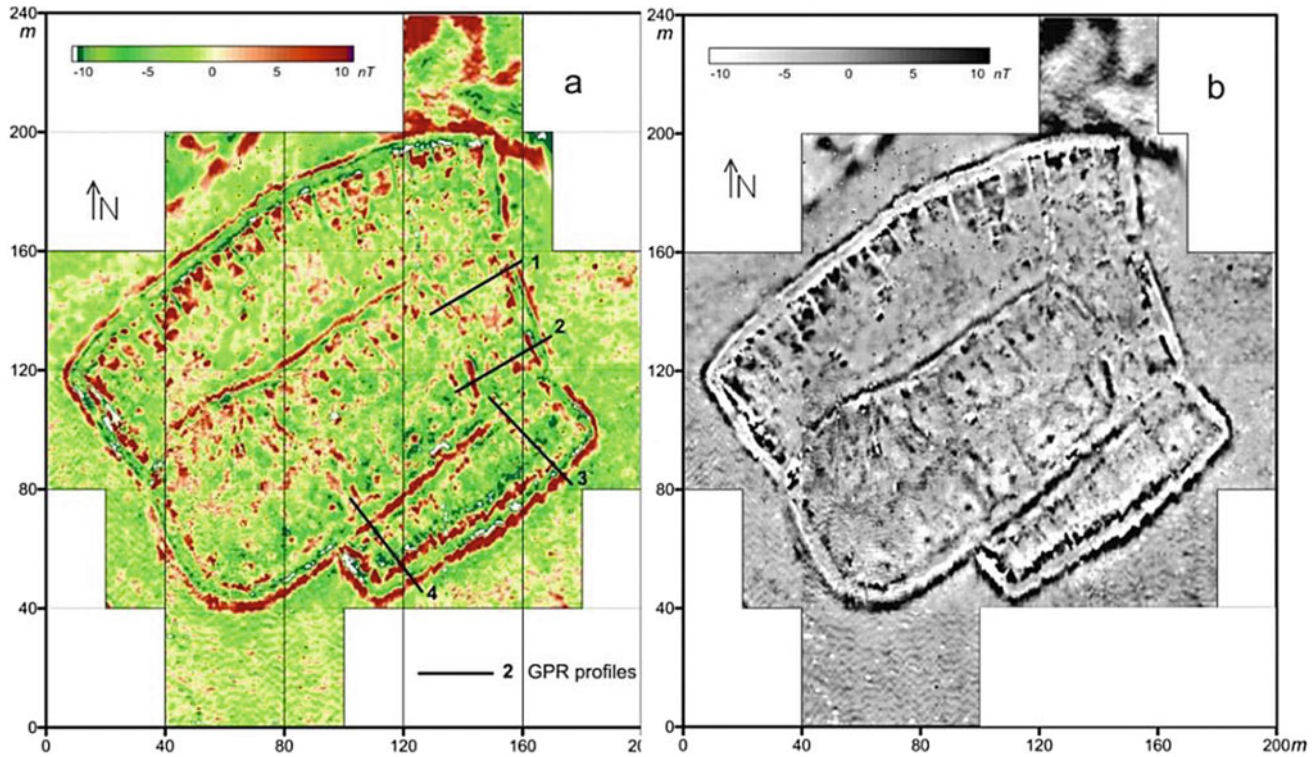

Fig. 2 Magnetic map of the Andreevskoye settlement; **a** colour-scale range −10 nT (green)/ +10 nT (dark brown); **b** greyscale range −10 nT (white)/ +10 nT (black)

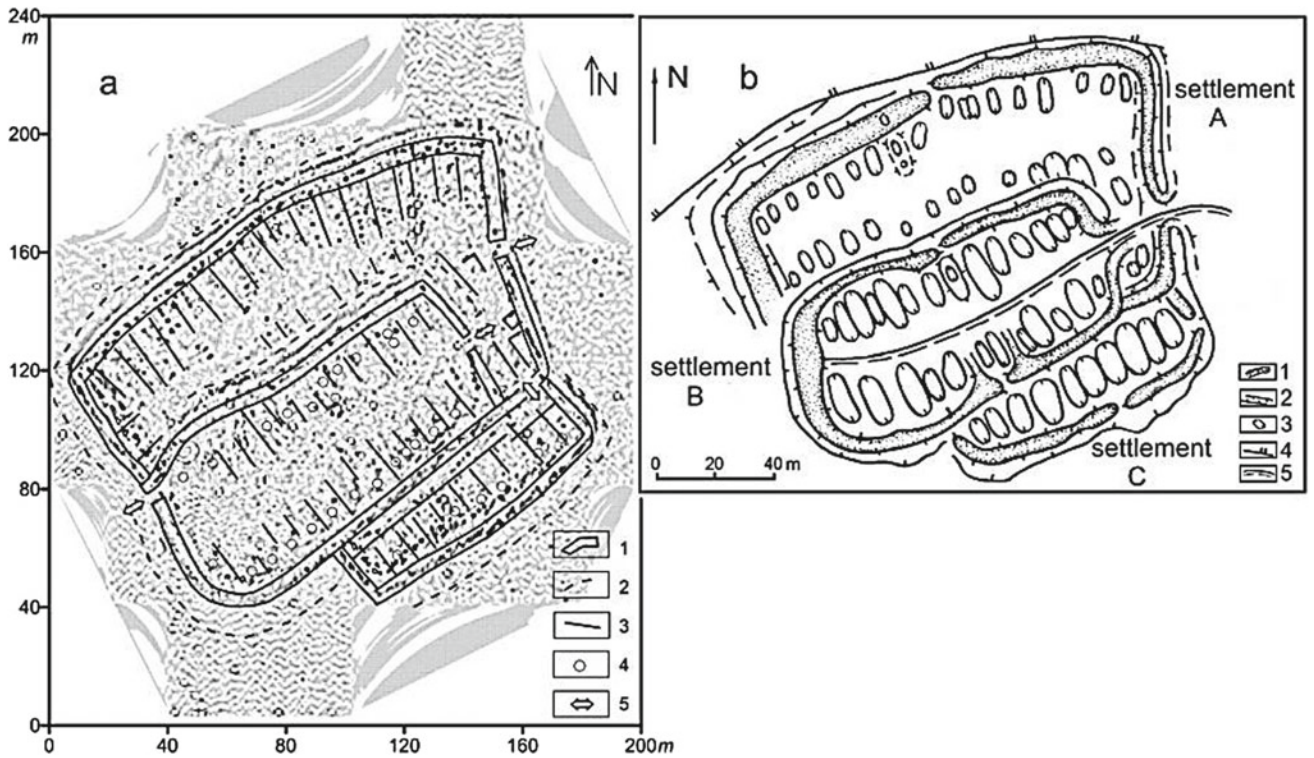

Fig. 3 Andreevskoye settlement: **a** a version of reconstruction of Andreevskoye settlement layout based on geomagnetic prospection. 1—contours of fortifications; 2—boundary ditches; 3—interior walls; 4—well or household pit; 5—entrances to the settlement; **b** a plan of the settlement based on deciphering aerial photographs (Zdanovich and Batanina 2007) 1—disintegrated defensive walls; 2—trenches; 3—depressions from houses; 4—first terrace above the floodplain; 5—an ancient road

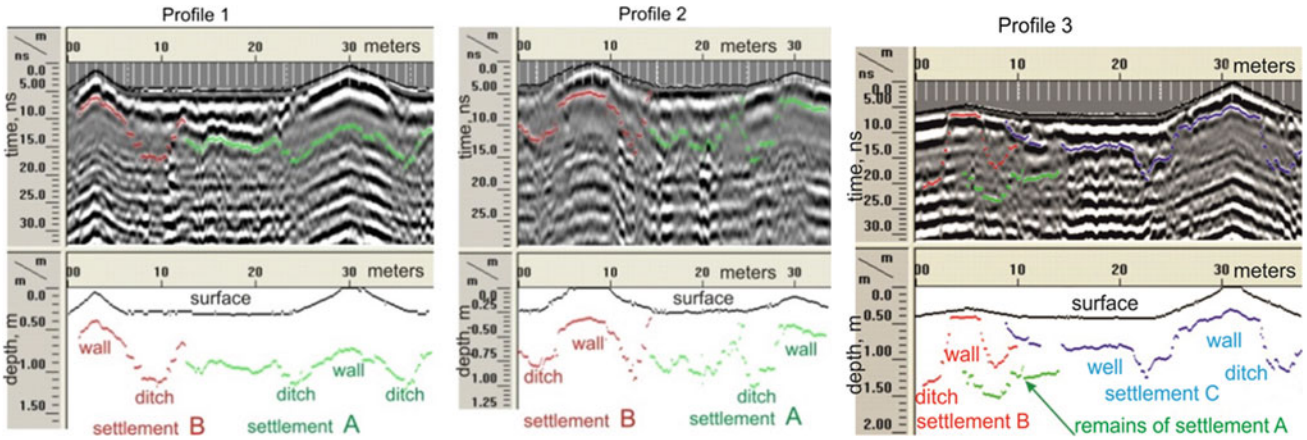

Fig. 4 Results of the measurement processing and possible interpretation profiles 1, 2 and 3

sequences of the establishment. These findings enabled the mapping of a more detailed layout of the settlement. This layout is more accurate in comparison with that obtained after decoding the aerial photographs.

3.2 Results of GPR Survey

In order to study settlement's fortifications, GPR studies (Fig. 2a) were undertaken on four profiles crossing the eastern and southern defensive fortification walls. The velocity of electromagnetic waves was estimated by the cross-correlation method when collecting paths using the RADAN 7 programme. After processing, a value of 0.135 m/ns was obtained, which corresponds to a value of the relative permittivity of soils of an approximate value of 5 at depths of 0–2 m. The obtained value does not contradict the values listed in velocity tables (0.122–0.150 m/ns) (Finkelstein et al. 1986) for dry loams, which represent the soil in the study area. Figure 4 shows the results of the measurement processing (time zero, FIR filter, background removal, stacking and surface normalization) as well as the possible interpretations of profiles 1 and 2. Profile 1 crosses the eastern walls and ditches of the settlements A and B. It is also observed inside houses of the settlement A. The obtained data indicate that settlement B was built after settlement A. Profile 2 also crosses the eastern fortification of settlements A and B, as well as houses of the settlement A. Profiles 3 and 4 are located in the area adjacent to the southern wall of settlement B and cross settlement C and its southern fortification. Profile 3 shows that the intensive magnetic anomaly is associated with a well inside the home of settlement C (Fig. 4).

4 Conclusion

The undertaken geophysical surveys allowed researchers to highlight the main characteristics of the settlement's fortifications, layouts and chronological aspects. In the course of this study, new details about inner spaces of this settlement, the parameters of dwellings and the location of some wells and household pits were defined. The magnetic map allowed the reconstruction of a more accurate layout of the settlement compared to the aerial photography. GPR profiles allowed us to estimate the depth of the cultural layer.

Acknowledgements This work was supported by the Russian Foundation for Basic Research 18-00-00030 "Geo-archaeological criteria and contexts of traditional technologies for mining and metallurgical production of the steppe Urals Bronze Age: geology and mineralogy, microgeochemical, isotopic, and geophysical."

References

Epimakhov, A.V., Berseneva, N.A., Fedorova, N.V., Noskevich, V.V.: Geophysics and archaeology of bronze age settlements—a case study from KamennyiAmbar fortified settlement (South Ural). In: Near Surface Geoscience, 22th European Meeting of Environmental and Engineering Geophysics.We22, A15, pp. 1–4 (2016)

Finkelstein, M.I., Kutev, V.A., Zolotarev, V.P.: The use GPR in engineering geology. M. Nedra. 128 (1986)

Noskevich, V.V., Fedorova, N.V., Sobolev, O.L.: Reconstruction of archaeological fortified settlements of southerns Ural mountains, of a bronze age on the magnetic data. In: Near Surface Geoscience, 18th European Meeting of Environmental and Engineering Geophysics, pp. 38, 1–4 (2012)

Zdanovich, G.B., Batanina I.M.: Arkaim—"Country of Towns". SpaceandImages. Chelabinsk, 260 p. (2007)

Reconstruction of Roman Aqueduct Route that Supplied the Ancient City of Tomis

Costin Mociu and Carmen Maftei

Abstract

The Tomis metropolis is the ancient name of the modern town of Constanta, situated on the Romanian Black Sea littoral. Tomis was founded by the Greek settlers from Miletus in the seventh century BC. Later, in the first century BC, this region, known as Scythia Minor, was annexed by the Roman Empire. Tomis achieved an important position in the region by becoming a metropolis. In the second part of the second century, Romans began to build the aqueduct-galleries system under Tomis city. This study is an early partial result of a Ph.D. research aiming to recreate the route of the ancient Roman aqueduct that supplied the Tomis metropolis by integrating different spatial and historical information including archeological topographical data. A map with the aqueduct route is presented.

Keywords

Roman aqueduct • Tomis city • GIS

1 Introduction

In recent decades, the hydraulic analysis of roman aqueducts has spiked interest among researchers (Chanson 2000). Different data are necessary in order to conduct this type of analysis: topographic, geological and geomorphological data, hydrology, surface, and groundwater resources. New technologies as GPR and GIS techniques, remote sensing data, archeological and ground survey-based data, in combination with the disciplines of Earth sciences (Scianna and Villa 2011; Ghilardi and Desruelles 2009; Bugini et al. 2019) could provide more and thorough information necessary to reconstruct the landscape (Chanson 2002) and offer a complete data set for hydraulic modeling. Following these steps supported by the new technologies, the aim is to create a map as accurate as possible outlining the most probable routes of the ancient aqueduct, the main source of water for the Tomis metropolis (known as the modern city of Constanta) located on the Romanian littoral of the Black Sea.

2 Materials and Methods.

The city of Constanta is located on the Romanian Black Sea coast, between 44°10′ N latitude and 28°38′ E longitude (Fig. 1). Historically known as Tomis, the city represented one of the most prominent settlements on the western shore of the Black Sea. Founded by the Greeks in the seventh century BC, given its strategic position, the city went through a massive evolution and expansion for centuries, managing to become the first century BC capital of Scythia Minor region during the Roman period. In this context, the city needed a well-developed infrastructure consisting of roads and aqueducts that ensured a good life for the inhabitants. Situated in the Dobrogea region, modern Constanta and its hinterlands are hiding many remains of the ancient city, especially into the area called the "Peninsula" (Fig. 1) and Siutghiol Lake.

3 Results and Discussion

To start with, the base image of the orthophotoplan (2010) was obtained from geo-spatial.org Web site. Then, different spatial data layers were overlapped over it using ArcGIS. The first layer consisted of representing all the locations of the archeological research of Scarlat mentioned in his work

C. Mociu (✉) · C. Maftei
Doctoral School of Applied Sciences, Ovidius University, Constanta, Romania

C. Maftei
Civil Engineering Faculty, Transilvania University of Brasov, Brasov, Romania

A. Çiner et al. (eds.), *Recent Research on Geomorphology, Sedimentology, Marine Geosciences and Geochemistry*, Advances in Science, Technology & Innovation, https://doi.org/10.1007/978-3-030-72547-1_22

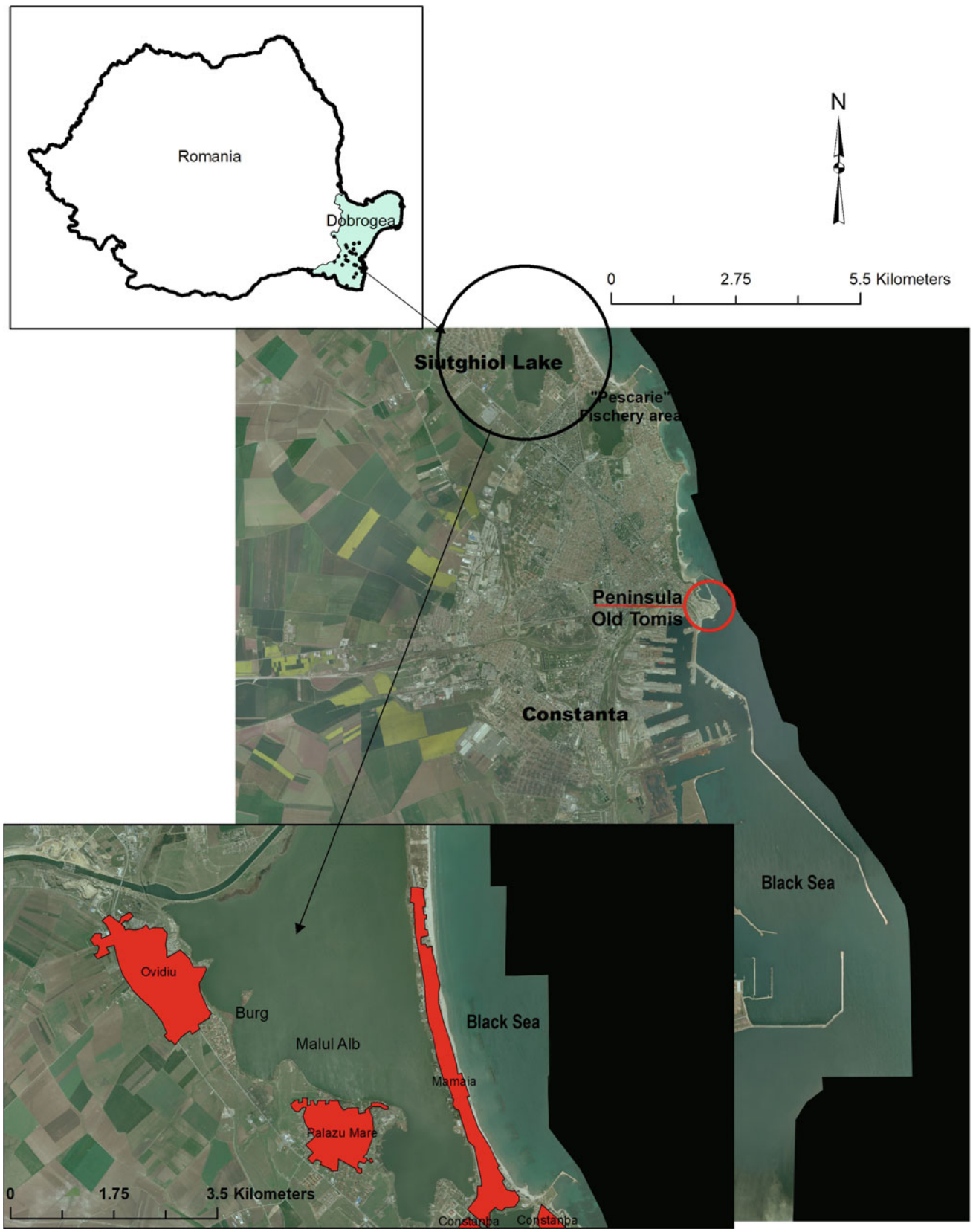

Fig. 1 Study area

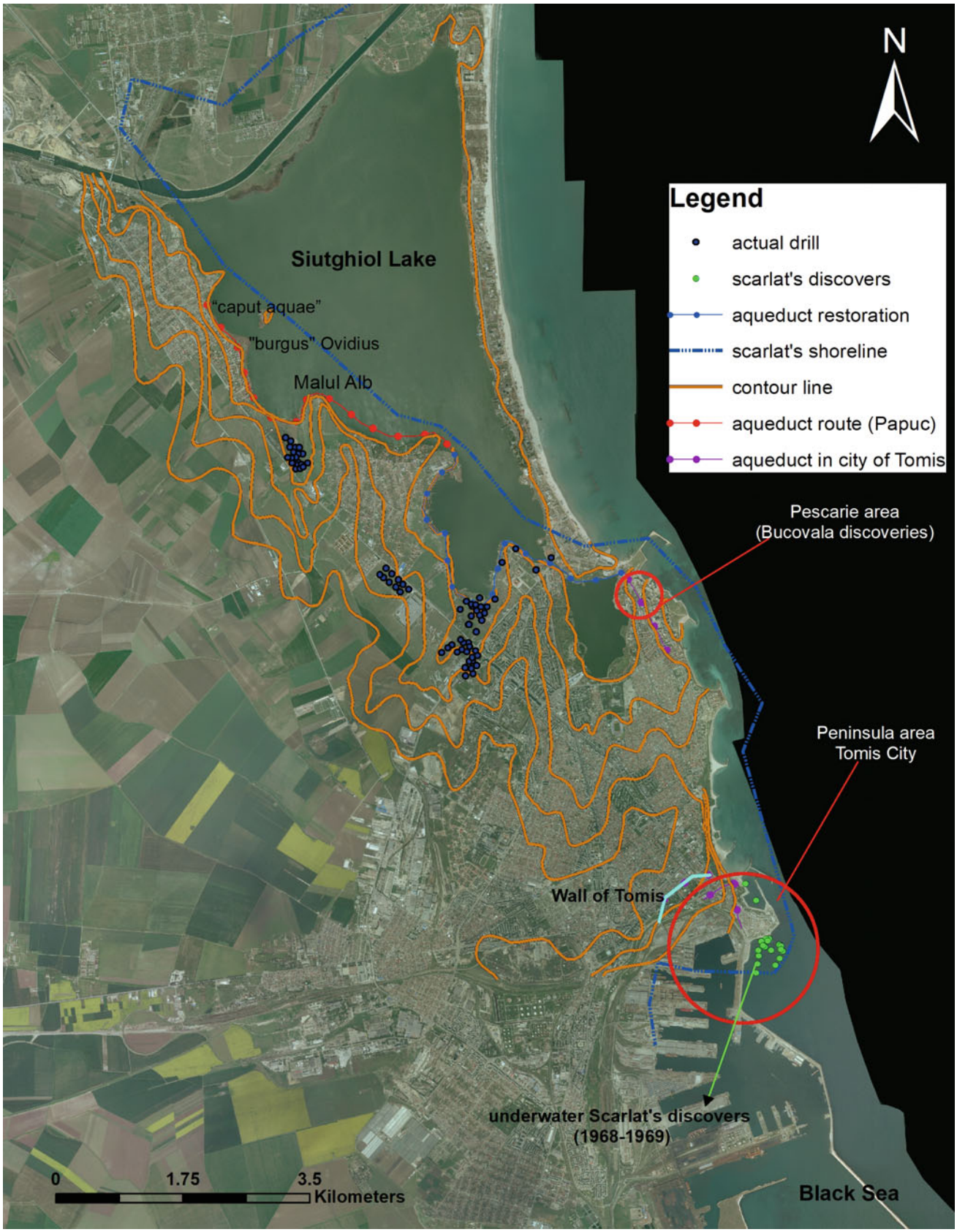

Fig. 2 Aqueduct's route restoration and Scarlat's discoveries (green dots) consisting of pieces of amphoras, ceramic furnaces, and docks

in 1975 (Scarlat 1975). Based on an old map from the Scarlat's work dating from 1976 (Scarlat 1976) showing the coastline of Pontus Euxin from antiquity (Black Sea), it was possible to reconstruct the shoreline of the Tomis metropolis (Fig. 2). Second, using archeological information from Papuc and Bucovala (Bucovala and Papuc 1980; Papuc 1982), the positions of the old city's defending walls, the route of the aqueduct were determined inside the city and outside of the walls in the peninsular zone of Constanta starting from the "Pescarie" zone, continuing along the shore to the fortress.

Also, following Papuc's writings about the aqueduct (Papuc 1982), we managed to recreate the path of the aqueduct starting from "caput aquae" situated in Ovidiu city on the Siutghiol Lake's shore, passing near the "burgus" from Ovidiu and following the shoreline, but its trace was lost near "Malul Alb" zone in the Palazu Mare neighborhood of Constanta city (Figs. 1 and 2).

With all this information placed on the map, using CAD software and following the terrain contour lines, the approximate trace of the aqueduct was recreated. Furthermore, it was possible to locate all the current wells (actual drills) used for supplying the modern Constanta city with water, wells drilled along the Caragea-Dermen Valley, and the Cismeaua water source.

4 Conclusions

Combining the historical sources, the information about the archeological discoveries and the current maps of the Black Sea coast, with the help of GIS software and CAD applications, a map of much of the aqueduct's proposed historical route was outlined, starting from Ovidiu city's source, going on to the Siutghiol Lake's shoreline until reaching the Tomis Fortress. The next phases of this research include more investigations on the features defining Tomis Fortress water supply, such as the shape of the aqueduct, its dimensions, the materials used to build it, the slope of the terrain, and the water source flow for example, in order to create a detailed hydraulic model.

Furthermore, our participation in an upcoming archeological project meant to uncover the burgus from Ovidiu that guarded the aqueduct from will allow collecting the samples of materials used in the construction. In the same respect, taking part in field research will provide great insights on the characteristics of the aqueduct needed for more accurate calculations for the next stages of this research.

References

Bucovala, M, Papuc, Gh.: Cercetarile arheologice de la Ovidiu-municipiul Constanta. Pontica **13** (1980)

Bugini, R., Folli, L., Marchisio, R.: "Giallo Antico" in Roman architecture of Lombardy: a preliminary survey. In: Chenchouni, H., Errami, E., Rocha, F., Sabato, L. (eds.), Exploring the Nexus of Geoecology, Geography, Geoarcheology and Geotourism: Advances and Applications for Sustainable Development in Environmental Sciences and Agroforestry Research. Advances in Science, Technology & Innovation. Springer, Cham, pp. 107–109 (2019)

Chanson, H.: A hydraulic study of roman aqueducts and water supply. Australian J. Water Res. **4**(2), 111–120 (2000)

Chanson, H.: Some aspects of the hydraulic design of Roman aqueducts. La Houille Blanche **6**(7), 1–16 (2002)

Ghilardi, M. and Desruelles, S.: Geoarchaeology: where human, social and earth sciences meet with technology, S.A.P.I.E.N.S., 2(2), (2009).

Papuc, Gh.: Despre apeductele Tomisului, Pontica **15** (1982).

Scarlat, C.: Portul antic Tomis si peninsula submerse Tomis, o asezare geto-dacica anterioara sosirii navigatorilor greci, Muzeul National II-41 (1975)

Scarlat, C.: Investigatii istorico-arheologice si geografico-hidrologice asupra cailor navigabile de acces in interiorul vechiului teritoriu geto-dac in Dobrogea. Muzeul National III-14 (1976)

Scianna, A., Villa, B.: GIS applications in archaeology. Archeologia e Calcolatori **22**, 337–363 (2011)

The Usefulness of Geomorphology for Finding the Landscapes Drawn by Leonardo Da Vinci in the Montefeltro Region (Central Italy)

Rosetta Borchia and Olivia Nesci

Abstract

This research follows a project on Cultural Geomorphology that led to the geographical discovery of the actual landscapes shown on the backgrounds of the works by great Renaissance artists such as Piero della Francesca, Leonardo Da Vinci, Raphael, Dürer, etc. The methodology used for the detection and reconstruction of landscapes is based on modern techniques. It enables effective geomorphological interpretation of ancient drawings. Here, we present new data relating to three drawings by Leonardo Da Vinci that have never been geographically located until now. In particular, some landscape drawings in the Arundel and Windsor Codices portrayed by Leonardo Da Vinci are in areas of central Italy, exactly in the historical region of the Montefeltro that were part of the Duchy of Urbino. These territories consist of a remarkable variety of landscapes that are fascinating for their intrinsic beauty as well as their breathtaking geomorphic diversity. These beautiful landscapes kindled the sensitivities of the artists who once traveled across this land, especially during the Renaissance.

Keywords

Cultural geomorphology • Leonardo Da Vinci codices • Montefeltro • Italy

1 Introduction

Leonardo Da Vinci devoted much of his life to the study of nature. The geological and paleontological studies carried out near his birthplace, the town of Vinci, are well known. And, the detailed geological and sedimentological structures represented in his paintings are very famous (Vai 2003 and references therein). Da Vinci is, however, less famous as a geomorphologist, which is the theme of this paper. For studying or for the needs of his clients, Da Vinci often drew maps and panoramic views of the places he visited. We remember the geographical maps of Tuscany enriched with many toponyms, and the map of the city of Imola, a true work of art for precision and detail. His work includes many drawings, classified as "unknown landscapes," which have never been located exactly (or sometimes incorrectly located) because they lack toponyms. However, these landscape drawings have unmistakable geomorphological characteristics that only those who study geomorphology can understand. In fact, in addition to the recognition of geomorphological forms and processes, knowledge of landscape modifications with respect to climatic, tectonic, and anthropic variations is essential and necessary. The present research shows that three drawings of the Arundel and Windsor Codicescan can be traced back to the landscapes of the Montefeltro, a historical region between Tuscany, Romagna, and Marche. Da Vinci frequently visited this region in 1502, when he was superintendent of fortifications by order of Duke Cesare Borgia (Fig. 1).

2 Methodology

This work, with precise comparisons and analysis on the evolution of the relief, studies and establishes the geographical locations that Da Vinci used for his drawings. The methodology used for the detection and reconstruction of

R. Borchia
Loc. Maciolla, Urbino, Italy

O. Nesci (✉)
Department of Pure and Applied Sciences, University of Urbino "Carlo Bo", Urbino (PU), Italy
e-mail: olivia.nesci@uniurb.it

A. Çiner et al. (eds.), *Recent Research on Geomorphology, Sedimentology, Marine Geosciences and Geochemistry*, Advances in Science, Technology & Innovation, https://doi.org/10.1007/978-3-030-72547-1_23

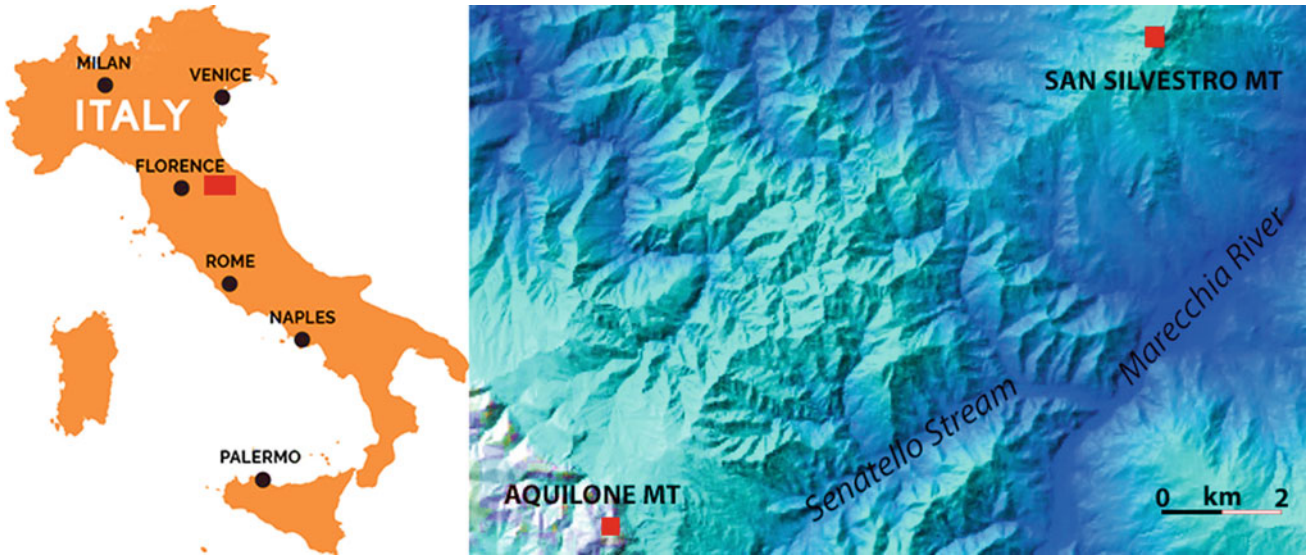

Fig. 1 Location map of the study area (red box). On the right, the digital elevation model where Leonardo's drawings are located

landscapes is image analysis both on the codex drawing and on the present landscape.

The high resolution of the drawing image made it possible to accurately investigate every aspect of the area, even the differences between the current morphology and the drawings of Leonardo. Digital elevation models and drone flights were used to visualize terrain shapes from various altitudes and angles. The geomorphological analysis was useful to understand the evolution of the landscape and explain the absence today of particular elements that were present in the drawings (e.g., lakes, landslides). Slope and river erosion processes were considered, because they may have significantly altered the landscape, particularly where extreme weather events often led to sudden changes.

This methodology, combined with artistic and historical investigations, allowed Borchia and Nesci (2017) to reconstruct the backgrounds of some immortal works by Piero della Francesca (Diptych of the Dukes of Urbino) and Da Vinci (Gioconda and Madonna Litta) and to dispel the belief that these backgrounds were imaginative creations of their painters.

3 Results

Geomorphological analyses, both of the drawings and in the Montefeltro region, have led to the recognition of some sectors belonging to the Marecchia river basin.

Figure 1 shows a drawing of the Windsor Codex representing the Fumaiolo Massif which is the watershed of the Marecchia river basin. To the right, a tiny sketch that Da Vinci drew in Arundel Codex, executed in connection with a study on the erosion of the river channel. The river basin is that of the Senatello creek, a left tributary of the Marecchia river. Despite his small drawing style, Da Vinci marked all the reliefs and valleys, with the unmistakable river confluence of "beak of an eagle." The third drawing codex found in Montefeltro (Fig. 2) is always located in the Valmarecchia and represents a sector of the Senatello basin.

4 Discussion

Recognizing the landscapes in the drawings produced by Leonardo Da Vinci indicates that the most significant geomorphological structures have been maintained for about 500 years to the present. This area, despite having undergone some variations due to the climatic conditions, has not suffered the anthropomorphic changes that characterize the nearby coastal and floodplain areas for example. This allowed the recognition of many elements of the landscape. In fact, flatirons are the typical forms of a landscape with stratified rocks, and they were perfectly reproduced by Da Vinci. Their presence in the current landscape is typical to the Marnoso-arenacea formation in a dip slope position. The peaks on the watershed instead are made up of the limestone of the allochthonous Valmarecchia Sheet and Da Vinci clearly illustrated this difference in selective erosion, specific to this formation. The comparison B of Fig. 1 shows a non-perfect coincidence with the forms due to the numerous landslides that occurred during the Little Ice Age, after the execution of the drawing. The interest of this drawing lies in the particular sign (2 in Fig. 1b) that Da Vinci highlighted indicating the risk of danger in a place subject to a hypothetical overflow of a lake area (Borchia and Nesci 2012). Finally, the third drawing (Fig. 2) perfectly reproduces the

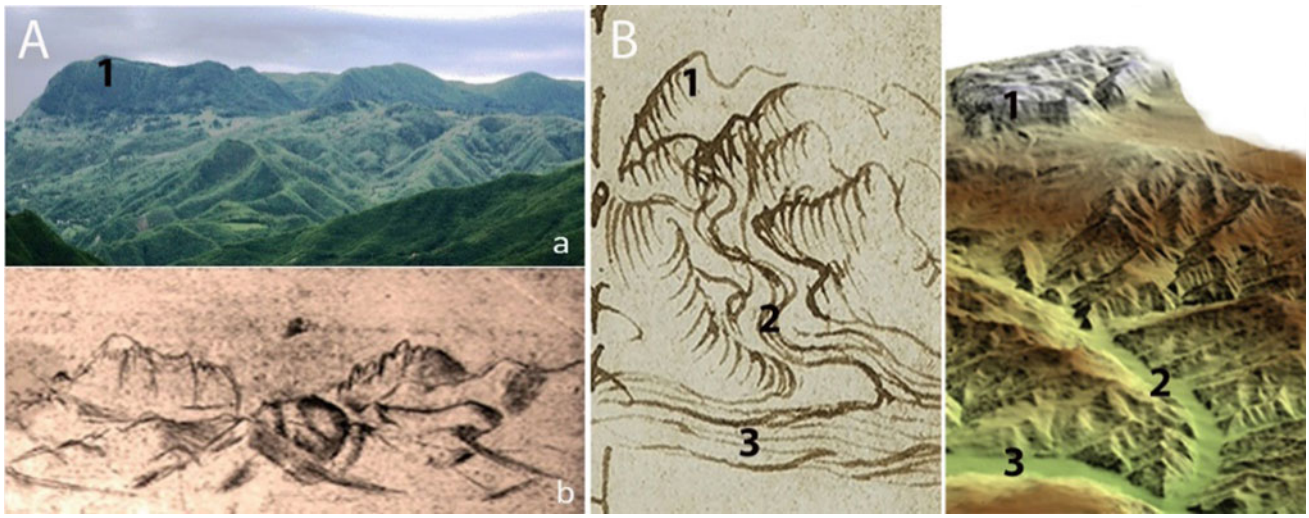

Fig. 2 **a** Mt. Aquilone present landscape (**a**) compared with Leonardo's drawing (Sheet Windsor, Royal Collection, foto Scala, Firenze) (**b**). **b** Comparison between the drawn of the Arudel Code, (ArchiviAlinari, Firenze) (left) and the DEM (right). 1. Monte Aquilone (43°47′5.84″ N, 12°6′34.38″ E), 2. Senatello stream, 3. Marecchia river

Fig. 3 Comparison with a drawing by Da Vinci belonging to the Arudel Code (ArchiviAlinari, Firenze). 1—an Silvestro Mountain, 2—Senatello stream, 3—Avezzane Creek, 4—Pozzale Hill

profiles present in the current territory, despite being very stylized. However, no exact explanation is known to why Da Vinci designed this small drawing. It is possible he was interested in river erosion, as explained in the pages written next to the drawing (Borchia and Nesci 2012). It is interesting that the hatching used to reproduce the watershed, and the little valleys follow the rules of cartography, as if they were real contour maps (Fig. 3).

5 Conclusions

The present research focuses on works of Leonardo Da Vinci. It confirms the methodology and discoveries of Borchia and Nesci (2017) that the great artists of the Renaissance portrayed the territories of the Montefeltro region. The region was part of the ancient Duchy of Urbino,

wherein the Renaissance artists, mathematicians, and architects were often guests of the court of the Dukes, known for being educated personalities and great patrons. These areas are characterized by the presence of a natural heritage that is associated with suggestive views and important historical, archeological, and architectural assets. This peculiarity makes these territories cultural landscapes and true outdoor museums.

References

Nesci, O., Borchia, R.: Landscapes and landforms of the duchy of Urbino in Italian renaissance paintings. In: Soldati, M., Marchetti, M. (eds.), Landscapes and Landforms of Italy, World Geomorphological Landscapes, Springer International Publishing AG 2017, pp. 257–269 (2017)

Vai, G.B.: I viaggi di Da Vinci lungo le valli romagnole: riflessi di geologia nei quadri, disegni e codici. In: Da Vinci Machiavelli Cesare Borgia Arte Storia e Scienza in Romagna 1500–1503. De Luca Editorid'arte. Roma, pp. 37–47 (2003)

Landscape as a Cultural Resource: Science, Poetry, and Ancient Music for the Enhancement of the Marche Region, Central Italy

Laura Valentini, Olivia Nesci, Lorenzo Carnevali, Stefano Baiocchi, Massimo Brizigotti, Sauro Teodori, and Silvia Argalia

Abstract

Born from a desire to promote the landscape by integrating its origin and physical esthetics with its cultural and artistic heritage, we develop a narrative about a place told in popular science language, and support it with visual stimulations, poetry, and ancient music. Three different disciplines focus on the same site, the combination of which results in an emotional experience where the encounter and interplay among different representations become an expression of the place. As an example, we focus on three known sites from the Marche Region, Central Italy: "The flatiron of Mount Petrano," "The Stones of Montefeltro," and "The sea-cliff of San Bartolo." For a few years, we have created a team of five researchers-artists, called "*TerreRare*" ("Rare Earth Elements"), whose mission is to promote a deeper understanding and appreciation of the gorgeous Italian landscape. This work is part of a larger project that covers 20 sites in the region through live multidisciplinary performances, and will ultimately result in the publication of a volume with scientific content on the geological-geomorphological genesis, trekking itineraries, poetry, music, video, and cultural offerings related to the place. The project is taking place thanks to an important regional announcement dedicated to the development of the Marche Region. Our purpose is to educate by creating a new perception of place, starting from its physical beauty, building on scientific study and cultural history, and reaching a knowledge of its strengths, including cultural ones, problems, and weakness.

Keywords

Landscape • Science • Poetry • Ancient music • Italy

1 Introduction

The Marche Region boasts a great variety of landscape forms, characterized by an undoubted richness in beauty and charm. This wealth is a consequence of the geological history of the Apennine chain, which produced extraordinary contrasts of physical forms in minimal space. These places have witnessed, since the dawn of history, sites of important human settlements, leaving us several testimonies of great cultural interest. The variety of landforms (mountains, hills and coasts) has also produced an enchanting floristic and faunal heritage. Besides, the Marche Region still includes a rather unspoiled area, where the landscape, nature, culture, and traditions offer an excellent opportunity for educational and touristic development (Nesci and Valentini 2016).

Unfortunately, the awareness of this cultural richness and wealth is limited by the lack of significant emotional impact due to the very limited knowledge of the territory. Our goal is to provide visitors of all ages and cultural backgrounds with the tools to understand a place in its complexity (physical, cultural, and emotional landscape).

2 Methods

Our work proceeds through two different routes. The first route analyzes the landscape from the scientific point of view, trying to understand how it evolves and responds to change. The second path examines the landscape from a

L. Valentini (✉)
Department of Biomolecular Sciences, TerreRare" Group, University of Urbino "Carlo Bo", Urbino, PU 61029, Italy
e-mail: laura.valentini@uniurb.it

O. Nesci · S. Teodori
Department of Pure and Applied Sciences, TerreRare" Group, University of Urbino "Carlo Bo", Urbino, PU 61029, Italy

L. Carnevali · S. Baiocchi · M. Brizigotti
TerreRare" Group, Urbino, Italy

S. Argalia
A.G.E. S.R.L, Via della Stazione 41, Urbino, PU 61029, Italy

A. Çiner et al. (eds.), *Recent Research on Geomorphology, Sedimentology, Marine Geosciences and Geochemistry*, Advances in Science, Technology & Innovation, https://doi.org/10.1007/978-3-030-72547-1_24

Fig. 1 Panoramic views of the chosen sites. Top left: the Simone and Simoncello Stones; top right: Mount Petrano; bottom: Mount S. Bartolo

perspective more closely related to the visual and emotional impact that a place evokes with its history, its cultural significance, and perception of its fragility. The latter is perhaps a more complicated path, more intimate, which develops fully only through the intersection of different forms of language, linked to specific arts. Three different disciplines (science, poetry, and ancient music) focused on the same site. Their combination results in an emotional experience to understand the landscape in its different aspects, in its strength but also in its fragility. Among the many amazing landscapes of Italy, we focus on three known sites from the historical region of Montefeltro, in the Marche Region, Central Italy: ``The flatiron of Petrano Mount,'' "The Stones of Montefeltro," and "The sea-cliff of San Bartolo" (Fig. 1).

3 Results and Discussion

The project consists of (i) the creation of shows dedicated to the selected places (where it is possible also outdoors, in the frames of the chosen locations) and (ii) the publication of a volume on the most beautiful and interesting sites of the region.

Starting from the geological-geomorphological description, an itinerary with some stops is recommended, from which one can enjoy the most spectacular views. Now, the main objective of *TerreRare* is to identify a key to interpretation, which can be expressed through music and poetry. Literary citations are then suggested, a poem expressly written about that place and offered as a reading, then the visitors may listen to a piece of music from the late Renaissance or Baroque period performed on the harpsichord. Altogether, these steps are able to emphasize the uniqueness and the essence of the site.

The volume will then be accompanied by USB support with video, music, and poetry dedicated to each site. The contents of the book will be posted on a Web site with links to municipalities, region, tourist companies, parks, reception, and catering facilities, for example, with the aim of promoting the area surrounding the sites and all tourism-related activities. As an example, the outline of the work carried out can be found on three geo-sites from the region.

Mount Petrano is a flat anticline mountain bordered by deep gorges. The morpho-structure has developed its peculiar arrangement by different geomorphic processes, from weathering and mass movements to slope-wash and

cryonivation. Whatever the dominant process, selective weathering and erosion have highlighted both lithologic contrasts of the Jurassic-Miocene "multilayer" and structural features. The landforms reflect the geological structure consisting mainly of carbonate rocks, intercalated with more degradable marls and clays. These structural forms promote the formation of characteristic landform named flatirons, beautifully exposed on the slopes of Mount Petrano. This landscape has inspired a poetry about the joyful game suspension, while the music, *Twelve Variations on 'Ah vous dirai-je, Maman'* K.265by W.A. Mozart, in its form of "theme with variations," reflects effectively the idea of geometric shapes in childish drawings, or a toy of building blocks.

The Simone and Simoncello Stones are two characteristic tabular landforms formed on Miocene organogenic limestone. Although the two mesas are now about 300 m apart, the considerable accumulation of detritus between them suggests they probably were once united. The two tabular features are, in fact, the remains of a landform developed more extensively during the Middle-Upper Pleistocene. The title of the poem is taken from a story by F. Kafka. It takes place in a dream in which are added the memories of bloody battles of the Second World War and the mythic memory of the enormous upheavals that have "created" the Valmarecchia. Also, "*Jupiter*" a piece by A. Forqueray (from Suite N.5 in C min), was chosen to represent the big limestone blocks of the Valmarecchia assimilated by huge divinities; Jupiter is depicted as a proud and powerful god that caught by anger toward the human race it breaks out through a series of virtuosic arpeggios, throwing thunder and lightning.

The cliff forming the coast of Mount S. Bartolo is formed on Messinian terrigenous and evaporitic rocks, ranging up to sites rich in macrofossils. The small beaches that protect the cliff base are easily eroded by waves during large storms; the least protected rocky beach ridges are directly attacked by the waves. The slope facing the sea is subject to large landslides that endanger the clifftop villages. The retreat of this stretch of coast was smooth and continuous since the Holocene. The paleo-coast is now gone even though there are unmistakable traces of its prior existence seaward of the submerged beach. Geomorphological data show that about six thousand years ago the coast was more advanced seaward than the current coastline by about two kilometers, and the relief was much more extensive and extended further toward the sea. The poetry recalls the "handle with care" written on the packaging of fragile objects. Mount San Bartolo should not exist, so much is the stress placed on it. However, it does exist and undergoes a continuous consumption by guzzling by the jaws of progress, of utility, and of profit motives, and yet remains in perfect but precarious balance just by virtue of its beauty. The selected "*Passacaille*" by G. F. Händel (from Suite N.7 in G min, HWV 432) summarizes in its structure the morphological appearance of the San Bartolo cliff. The "passacaille," in fact, is a folk dance made up of variations on a ground bass. The same melodic line proposed in a varied sequence, following accurate rules of composition, which so much resembles the repetition of layers on the cliff. In the last variations, there are several repeated arpeggios, similar to a series of sea waves on the cliff.

4 Conclusions

This project has already been presented in the context of several live shows, in which the audience's emotional participation was the best confirmation of the effectiveness of art in transmitting scientific themes. The landscape is a great wealth and to be appreciated it must be understood in its varied aspects: genetic, morphological, emotional, and cultural. However, even before that, the landscape must be understood in its fragility, so that it can be protected and preserved.

In conclusion, our purpose is to educate people to form a new perception of the place, starting from its beauty and arriving to a knowledge of its origins, uniqueness, and fragility.

Reference

Nesci, O., Valentini, L.: Landscapes of central Italy through science, poetry and music. A perspective for educating to the planet sustainability. In: Geophysical Research Abstracts, vol. 18. EGU General Assembly, Wien (2016)

Sedimentology, Stratigraphy, Paleontology, and Marine Geosciences (T14): Sedimentology—Environmental, Tectonic and Diagenetic Processses

Sedimentology and High-Frequency Cycles of the Upper Pleistocene of the Bizerte Coast (N-E Tunisia)

Widad Sahli, Jalila Saadi, and Kamel Regaya

Abstract

Quaternary deposits are well known around the Mediterranean Basin especially those exposed along the Tunisia Coast. This work focused on the Pleistocene deposits outcropping along the Bizerte Coast (Northeastern Tunisia) with special attention to coastal deposits and their evolution during the Late Pleistocene. The sedimentological analysis carried out on four cross sections exhibits a complete Quaternary series that begin with basal erosive surface and marine deposits attributed to the last interglacial period. The Pleistocene deposits represent a third-order sequence that is divided into 2 (fourth–fifth order) shallowing-upward sequences that are interpreted as a response to glacio-eustatic events. The lower sequence consists mainly of shoreface facies which evolve to the foreshore and continental facies. The upper sequence shows a dune facies with cross-stratification and continental gastropods (eolian deposit interbedded with red to gray paleosoils). Those eolian deposits and paleosoil levels are related to the high stand system track of the third-order sequence.

Keywords

Upper Pleistocene • Rejiche sequence • Chebba sequence • Eolianites • Bizerte

1 Introduction

Quaternary deposits exposed along the Tunisian Coast have been studied since the beginning of the past century and their nomenclature has evolved with the advances in dating and analysis techniques. Toward the north, the Bizerte Coast exhibits various Quaternary deposits with varied ages and lithologies providing spectacular landscapes. In this work, the Pleistocene deposits exposed along the northeastern coast of Tunisia with their various facies (littoral, continental, and eolian) and faunal content were given a special attention.

Using classical sedimentology tools (field study and sampling, granulometry, morphoscopy, and petrography), this study showed new results about these deposits leading to a better understanding of their sedimentary evolution across the fourth- and fifth-order cycles (Vail et al. 1977). Four cross sections (5–6 m thick) were investigated representing the most complete Pleistocene successions: Ras el Korane, East of Cap Blanc, Cap Bizerte, and Ras Blatt (Fig. 1).

The investigated sections crop out in the Bizerte area (northeast of Tunisia), which is characterized by a Cretaceous–Upper Eocene marine succession (Rouvier 1977; Paskoff and Sanlaville 1983) overlaid by the Numidian thrust sheet (Oligo-Miocene) (Fig. 1).

2 Results

The grain size analysis of the paleosoil levels (samples Gr7, Gr8, Gr9, and Gr11 from East of Cap Blanc section and RB3 sample from Ras Blatt section) shows that these reddish sands are well-sorted fine sand or moderately sorted medium to coarse sand (Table 1).

In addition, the petrographic analysis reveals that the analyzed levels (samples RK2, RK6, RK9, RK11, and RK13 from Ras el Korane section, samples Gr3, Gr6, and Gr10 from East of Cap Blanc section, sample CB0 from Cap Bizerte section, and sample RB1 from Ras Blatt section) have a packstone to grainstone texture hosting several marine fossils (red algae, miliolids, bivalves, planktonic foraminifera, spicules of echinoderms, and polypier) and eventually continental fossils (gastropod), reflecting especially a marine (samples RK2 and RK11 from Ras el Korane

W. Sahli (✉) · J. Saadi · K. Regaya
Department of Earth Science, Faculty of Sciences in Bizerte, University of Carthage, Bizerte, Tunisia

A. Çiner et al. (eds.), *Recent Research on Geomorphology, Sedimentology, Marine Geosciences and Geochemistry*, Advances in Science, Technology & Innovation, https://doi.org/10.1007/978-3-030-72547-1_25

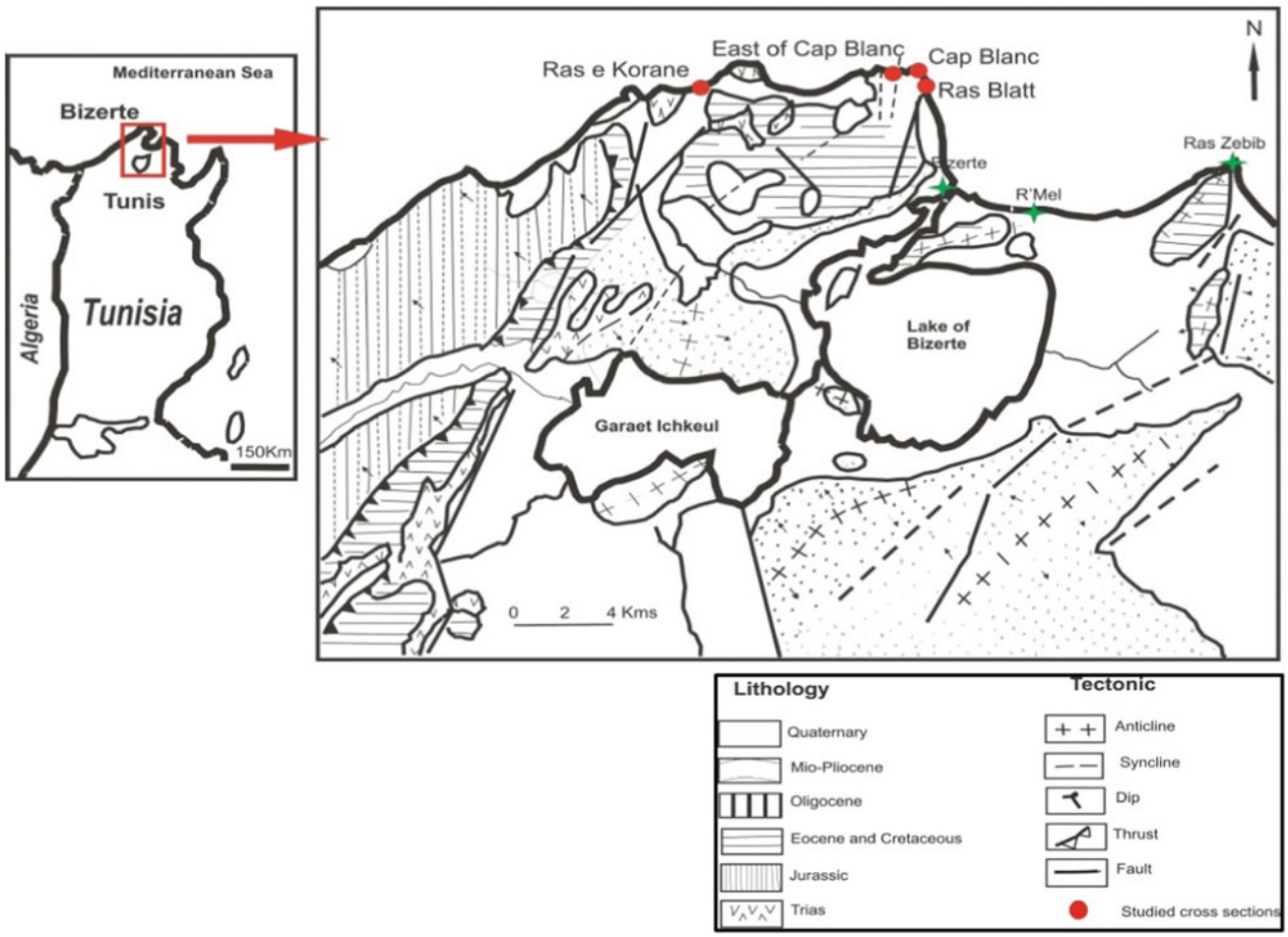

Fig. 1 Structural and tectonic map of the Bizerte area (From Rouvier 1977) and location of the studied cross sections (Ras el Korane, East of Cap Blanc, Cap Bizerte, and Ras Blatt)

Table 1 Granulometric indices of the sandy fraction of East Cap Blanc section and Ras Blatt section with Mz: mean size, SO: sorting, SK: skewness, and K: kurtosis

Section	Samples	Granulometric parameters				Description
		Mz	SO	SK	K	
East of Cap Blanc	Gr7	2.65	0.67	−0.5	0.75	Coarse sand, well to moderately sorted, negative skewed, and platykurtic distribution
	Gr8	0.2	0.65	0.033	0.5	Medium sand, well to moderately sorted, positive skewed, and platykurtic distribution
	Gr9	0.11	0.84	−0.43	1.58	Medium to coarse sand, moderately sorted, negative skewed, and mesokurtic distribution
	Gr11	1.91	0.38	−0.46	1.92	Fine sand, well-sorted, negative skewed, and leptokurtic distribution
Ras Blatt	RB3	1.91	0.29	−0.42	1.37	Fine sand, well-sorted, negative skewed, and leptokurtic distribution

section, samples Gr3 and Gr6 from East of Cap Blanc section, sample CB0 from Cap Bizerte section, and sample RB1 from Ras Blatt section), intertidal (samples RK6 and RK13 from Ras el Korane section, and sample Gr6 from East of Cap Blanc section, or continental depositional environment (sample RK9 from Ras el Korane section, and sample Gr10 from East of Cap Blanc section).

This sedimentological analysis shows sequences with marine to intertidal deposits at the base, and supratidal deposits and eolian or/and continental deposits on top, the

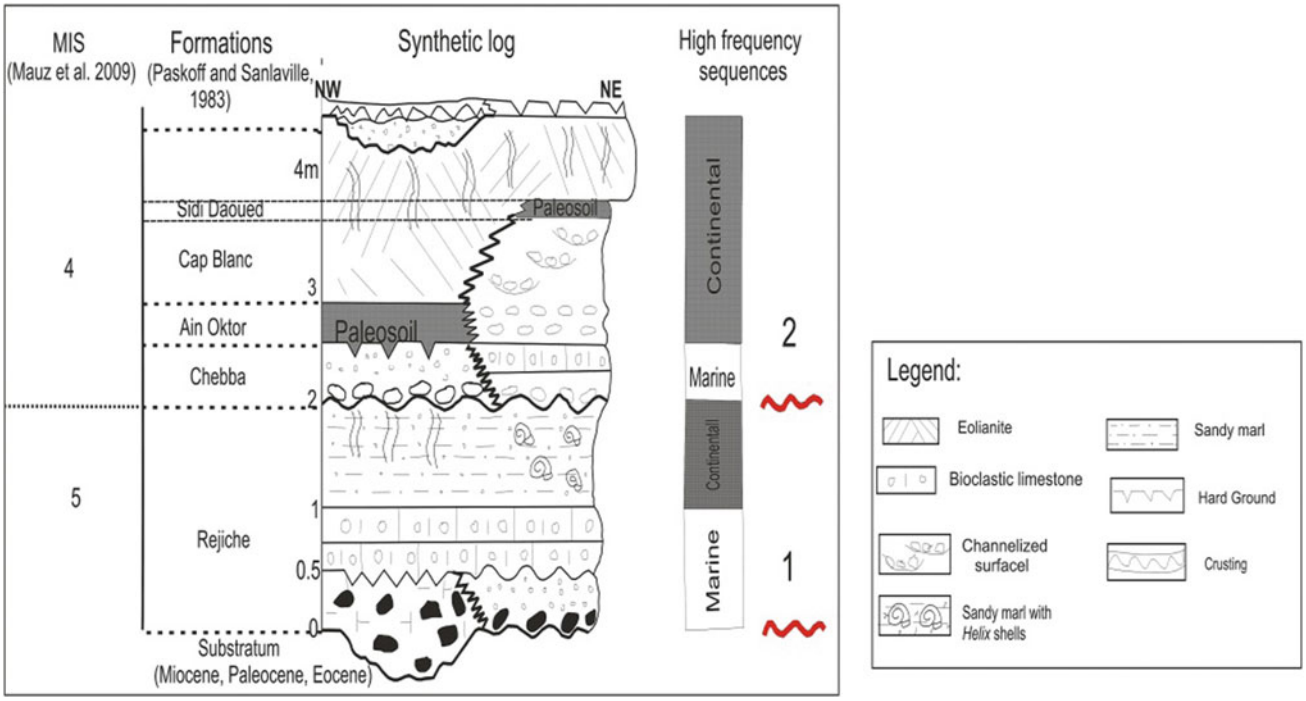

Fig. 2 Lithostratigraphic chart and high-frequency sequences of Pleistocene of the Tunisia northeastern Coast (Bizerte area)

latter attributed to the last Interglacial period MIS 5 and 4 (Paskoff and Sanlaville 1983; Mauz et al. 2009).

Based on the recognition of sedimentary trends, thicknesses (less than 5 m) and chronological terms, two high-frequency fourth−fifth-order sequences (sensu Vail et al. 1977; Catuneanu et al. 2011) can be differentiated (Fig. 2). The two sequences are separated by an unconformity identified along the Tunisian Coast (Fig. 2) (Chakroun et al. 2005, 2009; Chakroun 2006; Temani et al. 2008). The same approach was used by Le Fèvre and Raynal (2002) to describe the Plio-Pleistocene formations of Casablanca and Mejri (2012) in the Pleistocene deposits of the Tunisian East Coast.

- The first sequence (Rejiche sequence) is represented by the Rejiche Formation and is a shallowing-upward sequence, from shoreface deposits with a channelized bottom surface, with pebbles, to foreshore deposits and continental facies, with fossilized root structures and *Helix* shells.
- The second (Chebba sequence) includes the rest of the lithostratigraphic units and begins with a conglomerate facies (lag deposit) that includes pebbles and marine macrofauna, attesting a relative sea-level rise. The upper part is represented by an eolianite with fossilized root structures and *Helix* shells.

The basal discontinuity corresponds to an angular unconformity (depositional sequence boundary of a third sequence order, Vail et al. 1977). Each high-frequency sequence corresponds to a regressive cycle and is separated by a transgressive surface. The origin of these sequences corresponds to the sea-level variations in relation to Quaternary climate changes (orbital cycles of Milankovitch 1930).

3 Discussion

The sequential analysis of the Upper Pleistocene deposits exposed along the northeastern coast of Tunisia (Ras el Korane, East Cap Bizerte, Cap Bizerte, and Ras Blatt sections) and their correlation with the glacio-eustatic cycles are the basis of the definition of the sedimentary sequence (Le féver and Raynal 2002; Merzeraud 2009). In fact, after the rapid fall of the sea level during the MIS 6 (Emiliani 1955; Martinson et al. 1987), the platform was carved and an incised valley was formed that indicates the beginning of the lowstand system tract (LST) (Fig. 3a). At the MIS 5e, sea level rose and the platform was gradually flooded. During this sea-level rise, gully bedrock is marked by the occurrence of multiple-sized pebbles originating from the underlying levels. This level marks the base of the first high-frequency sequence (Rejich sequence), and it is indeed the initiation of the transgressive system tract (TST) of the third-order sequence. The maximum flooding surface (MFS) of the third-order sequence is characterized by the appearance of

Fig. 3 Field picture of Ras el Korane section with the indication of sequences limits, LST lowstand system tract, TST transgressive system tract, HST highstand system tract, MSF maximum surface flooding

numerous marine fossils (*Cerithium vulgatum, Conus ventricosus, Conus ermineus, Columbella rustica, Gibbula ardens, Patella caerulea, Phorcus richardi, Trochus sp,* and *Vermetus triquetrus*) and minor channelized surfaces with flattened pebbles at the base of shoreface deposits of the high-frequency Chebba sequence (Fig. 3c). This facies evolves to a non-marine sediment (eolianite) alternating with paleosoils, representing the last sedimentary tract (highstand system tract, HST) (Fig. 3c).

4 Conclusion

A detailed sedimentological analysis of the Pleistocene deposits exposed along the northeastern Coast of Tunisia (Bizerte Coast) allowed us to recognize an alternate succession of lower marine facies and upper continental facies. These deposits are organized into 2 high-frequency sequences (Rejiche and Chebba sequences) which are, indeed, attributed to a third-order sequence (Vail et al. 1977) with an LST corresponding to the basal discontinuity, a TST corresponding to the Rejiche sequence and a HST corresponding to the Chebba sequence. These sequences are related to the sea-level variations in relation to orbital climate changes (glacio-eustatism) of the Milankovitch frequency band.

The originality of those Pleistocene deposits outcropping along the Bizerte Coast appears through their spatial distribution which is far from homogeneous and leads us to distinguish, over very short distances, significant differences in facies as well as in their stratigraphic position.

References

Chakroun, A., Zaghbib-Turki, D., Moigne, A.M., De Lumley, H.: Discovery of a Pleistocene mammalia fauna in El Geffel Cave (Cap Bon, Tunisia). C R Paleovol **4**, 317–325 (2005)

Chakroun, A.: Etude sédimentologique et paléontologique des affleurements du Quaternaire le long de la côte Nord Orientale de la Tunisie. Ph.D. Thesis, University of Tunis and University of Perpignan (2006)

Chakroun, A., Zaghbib-Turki, D., Miskovsky, J.C., Davaub, E.: Two Tyrrhenian transgressive cycles in coastal deposits of Cap Bon Peninsula, Tunisia. Quaternary **20**, 215–226 (2009)

Catuneanu, O., Galloway, W.E., Kendall, CGStC, Miall, A.D., Posamentier, H.W., Strasser, A., Tucker, M.E.: Sequence stratigraphy: methodology and nomenclature. Newslett. Stratigr. **44**, 173-245 (2011)

Emiliani, C.: Pleistocene temperatures. J. Geol. **63**(6), 538–578 (1955)

Le févre, D., Raynal, J.P.: Les formations plioquaternaires du Casablanca et la chronostratigraphie du Quaternaire marin revisitées. Quaternaire **13**, 9–21 (2002)

Mauz, B., ElMejdoub, N., Nathan, R., Jedoui, Y.: Last interglacial coastal environments in the Mediterranean-Saharan transition zone. Paleogeogr. Paleoclimatol. Paleocol. 137–146 (2009)

Martinson, D.G., Pisias, N.G., Hays, J.D., Imbrice, J., Moore, T.C., Shackleton, N.J.: Age dating orbital theory of the ice ages : development of a high-resolution 0 to 300.000 years chronostratigraphy. Quaternary Res. **27**, 1–29 (1987)

Mejri, H.: Paléorivages marin pléistocène du littoral est tunisien: chronologie IRSL, paléoenvironnements et régime tectonique. Ph. D. Thesis, Université de Sfax, Université de Lille 1 (2012)

Merzeraud, G.: Stratigraphie séquentielle: Histoire, Principes et Applications. Société géologique de France (2009)

Milankovitch, M.: Metematische Klimalehre und astronomische theorie der klimaschwankungen. In: Koppen, W., Geiger, R. (eds.), Hanbuch der klimatologie, Gerbruder Borntraeger, pp. 1– 176 (1930)

Paskoff, R., Sanlaville, P.: Les côtes de la Tunisie: variation du niveau marin depuis le Tyrrhénien. Maison de l'Orient et de la Méditerranée, pp. 19–33 (1983)

Rouvier, H.: Géologie de l'extrême nord tunisien, tectonique et paléogéographies superposées à l'extrémité orientale de la chaine nord maghrébine. Ph.D. Thesis, Université de Paris (1977)

Temani, R., Gaaloul, N., Jedoui, Y., Razgailah, S.: Les dépôts du Pléistocène supérieur du Cap Bon (Tunisie Nord-Orientale) Caractérisation biosédimentologique et évolution spatio-temporelle. Géo. Eco. Trop. 83–90 (2008)

Vail, P.R., Mitchum, R.M., Todd, R.G., Widmier, J.M., Thompson, S. III: Seismic stratigraphy and global changes of sea level. See. Payton, 49–212 (1977)

On the Presence of Halokinetic Sequences, from Latest Aptian to Late Albian, NW Salt Province of Tunisia

Jalila Saadi, Ghassen Dhaouadi, and Mohamed Ben Youssef

Abstract

The Halokinetic sequences formations have been interpreted as a response to variations in sediment accumulation rate vs. diapir-rise rate. The phenomenon occurred during the transition from the Latest Aptian to the Late Albian at the "zone of diapir" of the NW of Tunisia. Facies analysis of the encasing rocks of the Triassic salt shows that halokinesis appears mainly in the deep facies of the Albian Fahdene Formation. The halokinetic Albian sequences above and beside the Triassic salt bodies suggest passive diapirism during this time interval. The Triassic salt flowed over the seafloor at least locally in the Early to Middle Albian times. The halokinetic sequences composites bounded by unconformities correlate to periods of slower deposition.

Keywords

Halokinetic sequences • Triassic • Albian • Diapirism • Tunisia

1 Introduction

The purpose of this paper was to report on the effects subsequent to the reactivation of structures involving Triassic evaporites during the Latest Aptian to Late Albian.

Facies and morpho-structural analysis enabled the breakdown of salt–sediment interactions at the vicinity of the NE-SW Triassic salt core associated with NE-SW elongated structures of the Kef–Tajerouine area. We demonstrated the occurrence of halokinetic sequences (Giles and Rowan 2012) deposited around these Triassic bodies.

Unconformity-bound growth strata associated with passively rising salt diapirs, defined as halokinetic sequences (Giles and Rowan 2012) have been recognized in the Debadib structure (Kef area), at the Triassic contact in Guern Halfaya and in J. Slata. These halokinetic sequences have been interpreted as forming in response to variations in sediment accumulation rate versus diapir-rise rate and roof thickness. The phenomenon was active during the transition from the Latest Aptian to the Late Albian in the salt province of the NW of Tunisia. Facies analysis of encasing Albian rocks shows that the Triassic diapirism appears mainly in the deep facies of the Fahdene Formation.

2 Materials and Methods

Stratigraphic logs of the Albian sequences were measured and dated around outcrops of the studied diapiric structures, located in NW Tunisia (in the Kef–Tajerouine area, Fig. 1) and in Central Tunisia (Jebel Chambi).

3 Results

We focus here on a small syncline, affecting the Latest Aptian–Albian sedimentary rocks that were synkinematic with the remobilization of the Triassic evaporites of Debadib at Koudiat Ennab El Azreg, (KNA—Fig. 1). The structural map (Fig. 1a) shows two major NE trending bodies of Triassic salt (Ben Gasser and Debadib), surrounded by Middle to Late Cretaceous sedimentary rocks. Because the Jurassic and Lower Cretaceous rocks are absent around Triassic bodies (Fig. 5a), the contacts between the Triassic and the younger strata are likely to be diapiric (Snoke et al. 1981; Htira et al. 2000; Chikhaoui et al. 2002; Talbot et al. 2005;

J. Saadi (✉)
Faculty of Sciences of Bizerte, University of Carthage, 7000 Bizerte, Tunisia

G. Dhaouadi
Institue of Sciences &Technologie, 2084 Borj Cedria, Tunisia

M. Ben Youssef
CERT, 2084 Borj Cedria-Tunis, Tunisia

A. Çiner et al. (eds.), *Recent Research on Geomorphology, Sedimentology, Marine Geosciences and Geochemistry*, Advances in Science, Technology & Innovation, https://doi.org/10.1007/978-3-030-72547-1_26

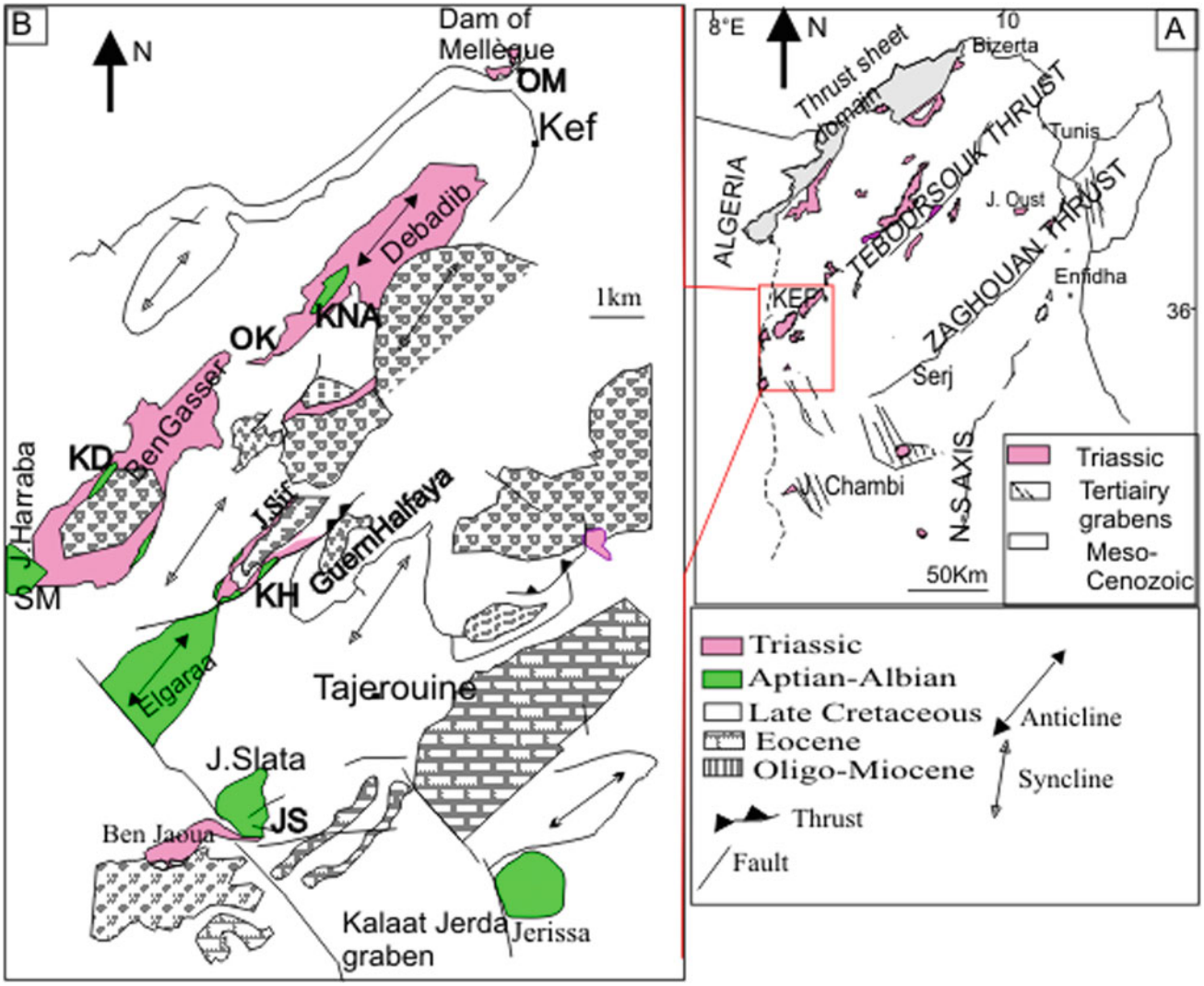

Fig. 1 **a** Location of the Kef–Tajerouine area, in the structural map of Tunisia. **b** Geological map of Kef–Tajerouine area position of studied sections. KNA, Koudiat Ennab El Azreg section. OM, Oued Mellegue section. OK, Oued el Kohol section

Jaillard et al. 2013, 2017). The contact between the Triassic and the Latest Aptian–Albian overburden is marked by an unconformity (clearly visible at Koudiat Ennab El Azreg, KNA, Fig. 5), complicated by subsequent tectonics.

The geometry of the lentils (covered by breccias followed by reefal carbonates, Fig. 2c) and the successions involved can be considered as a basal part of a hook sequence (Giles and Rowan 2012) deposited under salt rising of the Triassic Debadib structure. We may interpret the KNA structure (Fig. 2b) as a deformed overburden during downbuilding (passive diapirism, (Jackson et al. 1994)) in a relationship with drape-fold structures observed in the Northern flank of the Triassic structure of the J. Debadib.

The facies and thickness variations observed in the stratigraphic logs of the Albian successions in the Kef–Tajerouine area indicate relative lateral changes in accommodation due to downbuilding of structures into the Triassic bodies in this area. The local appearance on top of the saline structures of high-energy facies instead of distal shelf deposits is here underlined. This illustrates the influence of vertical movements of diapirs on paleobathymetry and sedimentation. The Halokinetic sequences at KNA (Fig. 2b, c), at the Albian of Guern Halfaya (KH, Fig. 1) and at the Albian, SE of JebelSlata (JS, Fig. 1), illustrate Albian stages of the halokinetic movements.

4 Conclusions

During the Aptian–Albian transition, the Albian sediments characteristic of a slope to basin setting, overlaying a previously neritic ramp of Aptian age, these sediments display a

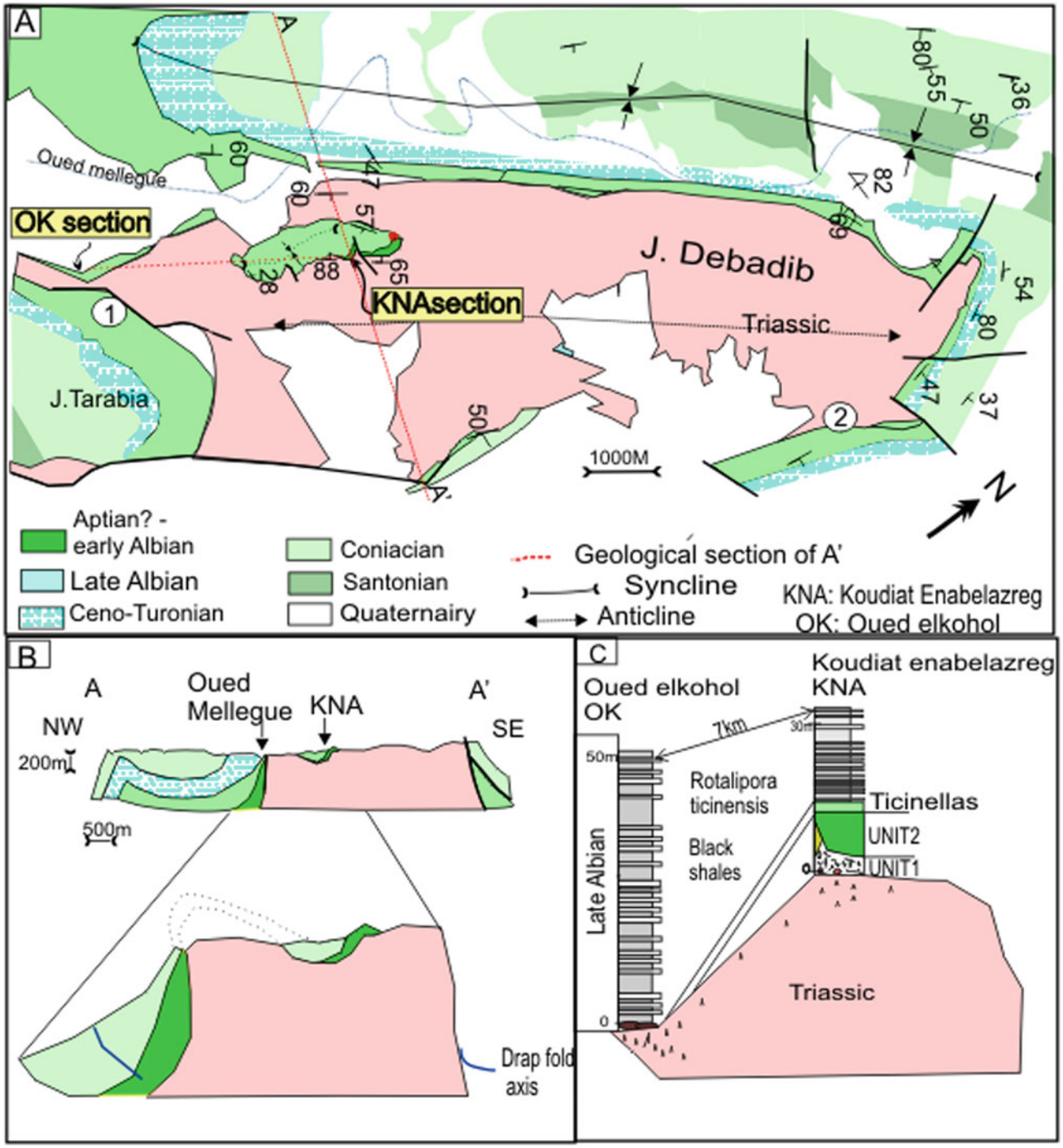

Fig. 2 **a** Geological map of the Debadib anticline with Triassic core (drawn from Snoke et al. 1981). **b** Geological section over the Triassic of the Jebel Debadib of the Kef area. **c** Correlation between the Oued El Kohol section and the KNA section showing the thinning of the overburden at the top of the structures to the northern flank

facies and thickness that indicate a platform in the South and a basin to the North, interpolated by a slope.

The facies and thickness variations shown in the stratigraphic logs of the Albian successions in the Kef–Tajerouine area indicate relative lateral changes in accommodation due to passive diapirism of the Triassic bodies in this area. The local appearance of high-energy facies related to the diapirs, instead of distal shelf deposits, was here underlined.

The morpho-structural analysis of the KNA section allows us to recognize a drape-fold halokinetic sequence

located on the Triassic of Debadib. The thinning of this series towards the Oued el Kohol section is related to the rise of Triassic salt during the Albian. The Triassic evaporites first rose as reactive diapirs along Tethyan rifts from Barremian to Aptian times. This resulted in diapiric salt canopies (Masrouhi and Koyi 2012), on the continental slope in the North of Tunisia, a columnar diapir in the Kasserine fault, and salt pillows on the platform south of the Gafsa fault (Bédir et al. 2000).

References

Bédir, M., Zitouni, L., Boukadi, N., Saadi, J., Alouani, R., Ben Timzal, F., Tlig, S., Bobier, C.: Rifting, halocinèse et structuration des bassins péri-téthysiens jurassiques et crétacé inférieur de subsurface du domaine atlasique central de la Tunisie (région de Gafsa-Sidi Ali Ben Aoun). Africa Geosci. Rev. **7**, 289–306 (2000)

Chikhaoui, M., Jallouli, C., Turki, M., Soussi, M., Braham, A., Zaghbib-Turki, D.: L'affleurement triasique du Debadib-Ben Gasseur (Nord-Ouest de la Tunisie): diapir enraciné à épanchements latéraux dans la mer albienne, replissée au cours des phases de compression tertiaires. C. r. Geosci. **334**, 1129–1133 (2002)

Giles, K.A., Rowan, M.G.: Concepts in halokinetic-sequence deformation and stratigraphy. In: Alsop, G.I., et al. (eds.), Salt Tectonics, Sediments and Prospectivity; Geological Society of London Special Publications, vol. 363, pp. 7–31 (2012)

Htira, N., Smati, A., Mansouri, A., Perthuisot, V., Rouvier, H.: Le Trias à caractère extrusif de la zone des dômes: exemple de la structure de Debadib—Ben Gasser (Tunisie Septentrinale). Bull. Soc. Geol. France **170**(3), 319–326 (2000)

Jackson, M.P.A., Talbot, C.J.: Advances in salts tectonics. In: Hanckok, P.L. (ed.) Continental deformation, pp. 159–179. The University of Bristol, Pergamon Press, U.K. (1994)

Jaillard, J.P., Dumont, T., Ouali, J., Bouillin, J.P., Chihaoui, A., Latil, J. L., Arnaud, H., Arnaud-Vanneau, A., Zghal, E.: The Albian tectonic "crisis" in Central Tunisia: nature and chronology of the deformations. J. African Earth Sci. **85**, 75–86 (2013)

Jaillard, E., Bouillin, J.P., Ouali, J., Dumont, T., Latil, J.L., Chihaoui, A.: Albian salt-tectonics in Central Tunisia: evidences for an Atlantic-type passive margin. J. African Earth Sci. **135** (2017). https://doi.org/10.1016/j.jafrearsci.2017.09.009

Masrouhi, A., Koyi H.: Submarine "saltglacier" kinematics of northern Tunisia, a case of Triassic salt mobility in the North African Cretaceous passive margin. In: Alsop, G.I., Archer, S.G., Hart-leya, Grant N.T., Hodgkinson, R. (eds.), Salt tectonics, sediments, and prospectivity. Geological Society, London, Special Publications, vol. 36, pp. 579–593 (2012)

Snoke, A., Schamel, A., Karasek: Structural evolution of DjebelDebadib anticline: a clue to the regional style of the Tunisian Atlas. Tectonics **7**(3), 497–516 (1981)

Talbot, C.J.: Evidence for triassic salt domes in the Tunisian Atlas from gravity and geological data by C. Jallouli et al. Tectonophysics **396**, 209–225 (2005)

Geological Processes Enhancing the Reservoir Quality of Aptian "Tight" Proven Reservoirs in Northwestern Tunisia

Asma Meftahi, Mohamed Hedi Negra, Mohamed Sabri Arfaoui, and Radhouane Khouni

Abstract

In Tunisia, conventional hydrocarbon production from classical petroleum systems clearly declined. Actually, great efforts are being made to explore new targets which present specific characteristics in terms of reservoir quality and types of traps. With new approaches and technological workflows combining geophysical, geological and petrophysical analyses, hydrocarbon explorers are advised to focus on non-classical petroleum system components such as "tight reservoirs" and stratigraphic traps. The Aptian M'Cherga siliciclastics and carbonates in northwestern Tunisia are such a fine-grained and hard silty carbonates "tight reservoirs". Recent wells have highlighted gas shown in certain layers of the "tight" M'Cherga reservoir. This case study of the Aptian in northwestern Tunisia shows that in addition to fracturing, some sedimentary processes and diagenetic modifications could obviously enhance the reservoir potential of these fine-grained and hard rocks. Consequently, new oil provinces that include these kinds of non-classical petroleum systems could be attractive and constitute potential hydrocarbon targets.

Keywords

Tight reservoirs • Aptian • Resedimentation processes • Fracturing

1 Introduction

The study area, located in northwestern Tunisia, is under-explored in terms of oil and gas. Despite the availability of all petroleum systems components, especially source rocks, traps and cap rocks, conventional reservoir rocks exhibiting well-connected pores networks are not well represented. However, oil seeps and hydrocarbon shows in exploration wells suggest that there remains a potential for hydrocarbon subsurface accumulations in the area.

The main purpose of the present work was to demonstrate that some geological features may suggest a process that could enhance the quality of "tight reservoirs" and offer a potential for accumulation of hydrocarbons in such "tight reservoirs".

2 Materials and Methods

Our study is based on a multidisciplinary sedimentological and petrological analysis approach using subsurface data coming from wells and outcrop studies on Aptian reservoir analogues. Data were collected from outcrops (three surveyed sections) and one well. About 100 samples were collected both from the well and outcrops. Facies types and diagenetic features were basically recognized under polarizing microscope analyses. Direct characterization of fracture network attributes such as length, spacing, aperture, orientation and intensity are the main measured parameters from outcrops.

Sedimentological and petrographical analyses were undertaken using a polarizing microscope followed by petrophysical measurements carried out on samples collected from all types of rock facies.

A. Meftahi · M. H. Negra (✉) · M. S. Arfaoui · R. Khouni
University of Tunis El Manar, 2092 Tunis, Tunisia
e-mail: hedi.negra@fst.utm.tn

M. S. Arfaoui · R. Khouni
PRIMOIL SA Campany, Emeraude building, 3rd floor, Les Berges du Lac 2, 1053 Tunis, Tunisia

A. Çiner et al. (eds.), *Recent Research on Geomorphology, Sedimentology, Marine Geosciences and Geochemistry*, Advances in Science, Technology & Innovation, https://doi.org/10.1007/978-3-030-72547-1_27

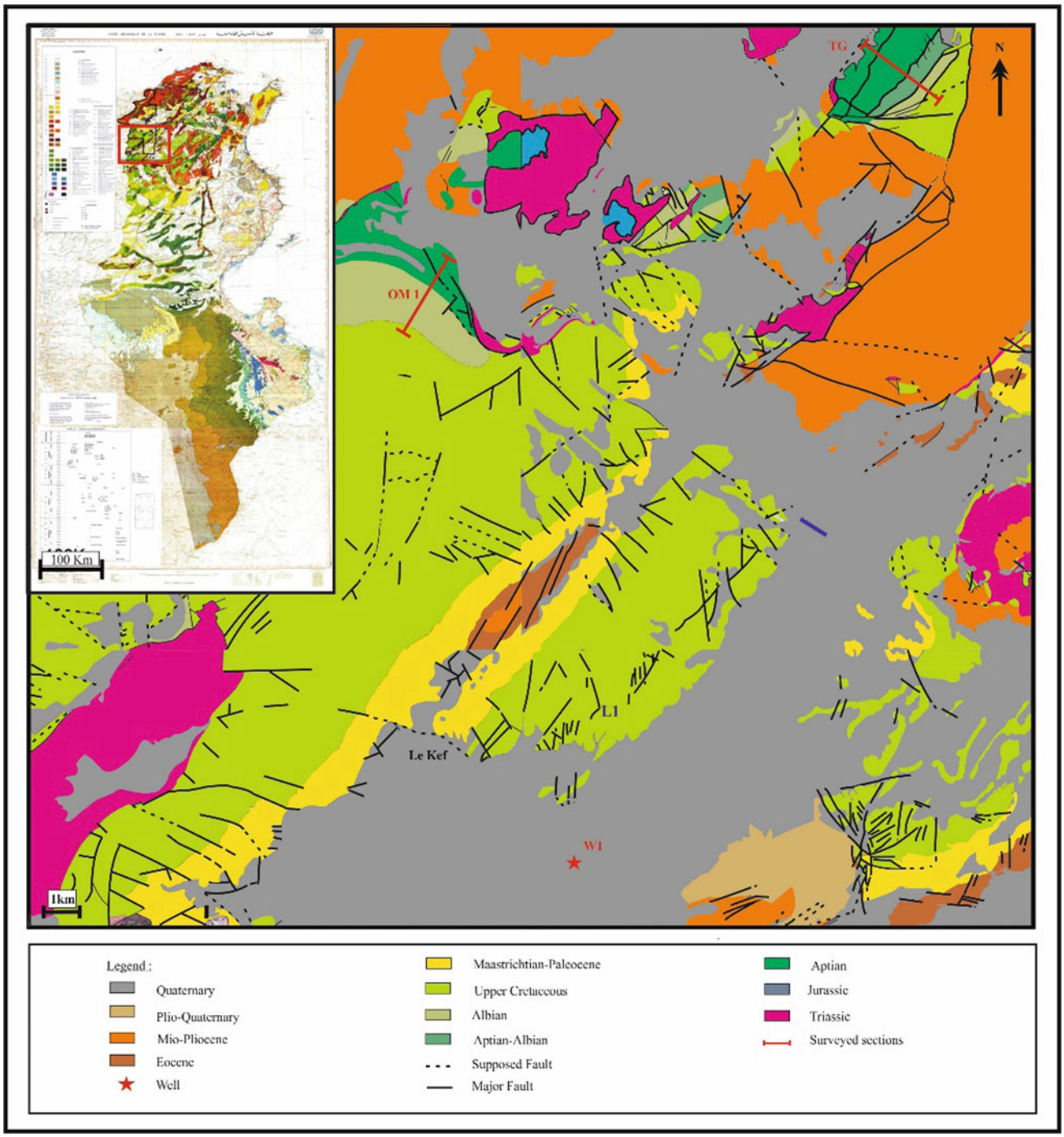

Fig. 1 Location map of the studied area on a geological map

3 Results

Detailed sedimentological studies combining field works undertaken on reservoir analogues and subsurface analyses show that despite the general "tight" character of the reservoir, some of the reservoir layers contain gas accumulations. Comparative surface/subsurface geological studies demonstrated that most gas shows are associated with bioclastic and conglomeratic layers. Bioclastic layers are relatively rich in foraminifers and echinoderm debris. Conglomeratic carbonates include non-sorted monogenetic blocks and pebbles enveloped by a matrix formed of fine-grained silty carbonates.

Micritic limestones are considered as tight reservoirs since their porosity and permeability values are very low.

However, the intercalation of "resedimented" bioclastic and conglomeratic deposits between the micritic beds offers a supplementary porosity and permeability to the Aptian reservoir. In fact, the petrophysical analyses show that porosity values measured in fine-grained carbonate layers range from 0.5 to 9% with a mean value of 2%. In conglomeratic and highly fractured layers (Fig. 2b), porosity values range up to 9%, and exceptionally 20%.

Concerning their origins and genesis, the conglomerates are interpreted as gravity deposits related to submarine erosional processes in relation to instabilities due to contemporaneous tectonic movements. The erosion product mainly corresponding to blocks and pebbles (Fig. 2c), was transported down slope and resedimented. Slump marks (Fig. 2d) which confirm transportation and sliding processes on slopes are observed in the semi-consolidated argillaceous carbonate. Similar processes were described in the Campanian Abiod chalky limestones (Bey et al. 2012; Negra and Zagrarni 2007). Subsequent tectonic movements have developed dense fracturing expressed by bidirectional fractures (Fig. 2B). The most represented fracture orientation has a N150 mean direction, crossed by orthogonal fractures with a N65 in mean direction. Most fractures are, at least partly, filled by a brownish cement (Fig. 2B) that mainly consists of oxy-hydroxides. Multidirectional fracturing, which ensures a connection between all types of pores clearly enhances the permeability of the Aptian reservoir rocks.

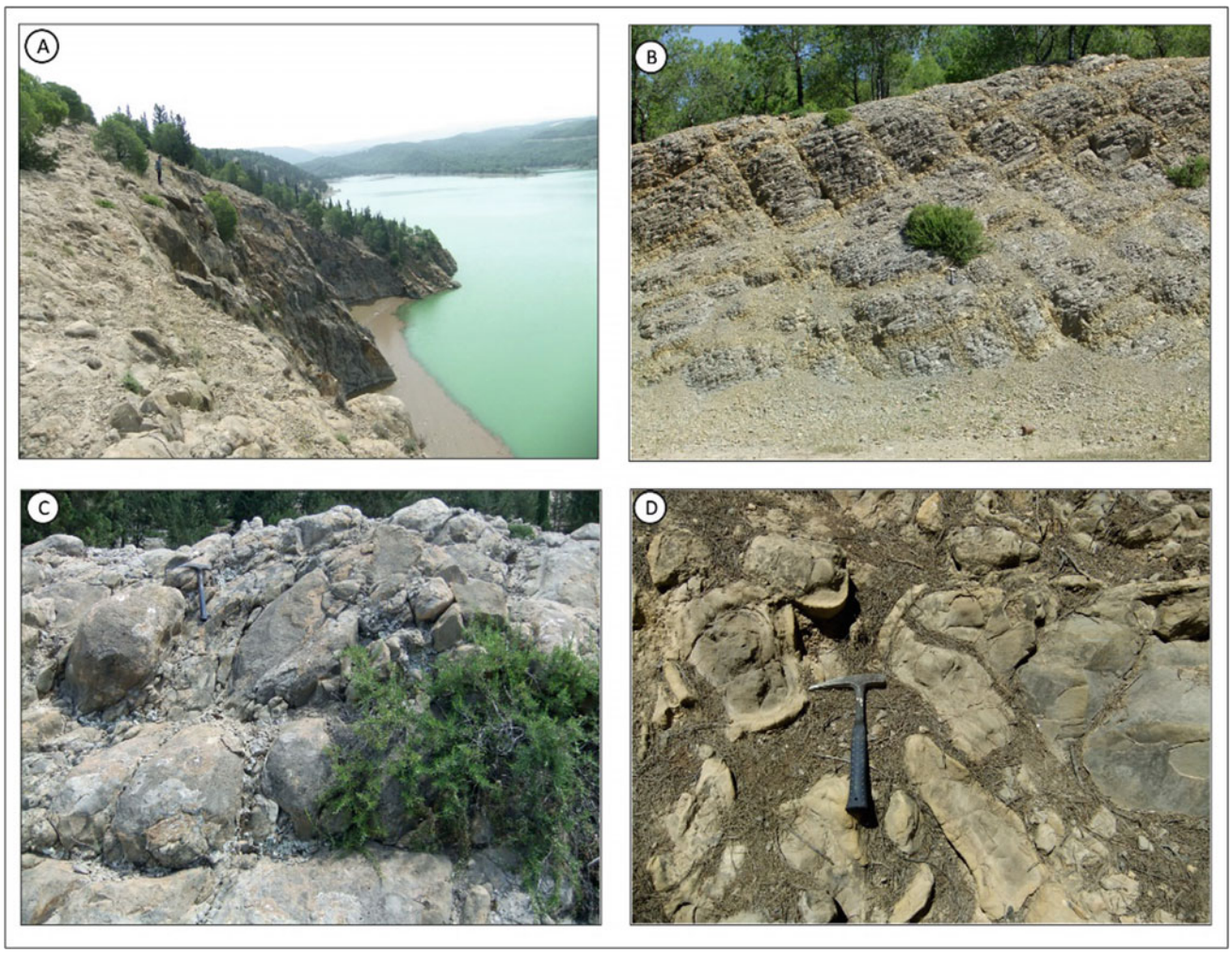

Fig. 2 Field photo showing sedimentary and tectonic features observed in the Aptian carbonates. **a** Field view showing the Aptian carbonate unit; **b** fracturing style of the Aptian carbonates; **c** syngenetic conglomeratic layers; **d** slump marks fossilized in semi-consolidated Aptian argillaceous carbonates

4 Discussion

The comparative surface/subsurface geological studies focussed on the reservoir properties of the "tight" Aptian M'Cherga deposits, show that most of porosity and permeability in the carbonates are due to fracturing. However, the latter is both generated by tectonic and sedimentary (slump) processes. Bioclastic carbonates may also correspond to tempestites redeposited during storm episodes. In both cases, the tempestites and/or gravity deposits, intercalated within the "tight" fine-grained silty carbonates constitute relatively porous and permeable layers that could be potential targets.

In terms of petroleum systems, the Aptian M'Cherga reservoirs are commonly sourced from the upper Albian Fahdene black shales. Recent studies show that older lower Cretaceous deposits could constitute supplementary source rocks. Concerning traps, folding has developed frequent, anticlines in the sector; and in addition, unconformity, tectonic and stratigraphic traps are also common. A regional unconformity which constitutes an important barrier between impermeable-sourcing upper Albian marls and porous Aptian fractured carbonates appears to be of high interest in terms of developing potential stratigraphic trapping in the area.

5 Conclusions

The study of outcrop analogues to the Aptian carbonate reservoirs of northwestern Tunisia containing gas shows in a recent drilled well provides new results that could help in the understanding of the reservoir potential of the Aptian M'Cherga Formation.

Most of the effective carbonate porosity and permeability are interpreted to be produced due to tectonic fracturing. However, contemporaneous submarine erosion and resedimentation processes can be observed, in relation to an irregular paleotopography, generating relatively porous and permeable slumped material mainly represented by gravity flow debris-flow deposits. The latter offers supplementary pores and appears more permeable than the initial material.

References

Bey, S., Kuss, J., Premoli Silva, I., Negra, M.H., Gardin, S.: Fault-controlled stratigraphy of the late cretaceous abiod formation at Ain Medheker (Northeast Tunisia). Cretac. Res. **34**, 10–25 (2012)

Negra, M.H., Zagrarni, M.F.: Upper cretaceous tempestites in rudist-rich facies, Tunisia. Cretaceous rudists and carbonate platforms: environmental feedback. In: Scott, R.W. (ed.), SEPM (Society for Sedimentary Geology) Special Publication No.87, pp. 45–50, (2007). ISBN 978-1-56576-127-8

Petrophysics and Reservoir Properties of the Turonian-Coniacian Bireno and Douleb Carbonate Members in Northern-Central Tunisia

Mabrouk Bachari, Mohamed Hédi Negra, Yves Géraud, and Danièle Grosheny

Abstract

The study of Turonian-Coniacian reservoir analogues well outcropping in Jebel Serj-Bargou in northern-central Tunisia, using a multidisplinary approach, has led to establish a detailed layering within these heterogeneous reservoir rocks. Some of the selected layers show a relatively high reservoir potential. This used approach which could be used as a guide for further studies on subsurface petroleum systems is based on sedimentological and petrophysical techniques using geophysical parameters. The conducted analyses mainly consist of measurements of the rocks density, P and S wave velocities, thermal conductivity, and porosity. All the analyses have led to encouraging results showing that the lower part of the Coniacian Douleb carbonates constitute the best layers in terms of reservoir potential. In addition to its reservoir potential, the Douleb Member locally includes organic-rich bituminous limestones that could provide supplementary source rocks and additional possibilities for the petroleum system in this area.

Keywords

Turonian-Coniacian reservoir rocks • Tunisia • Petrophysics • Geophysical parameters

1 Introduction

In Tunisia, The Bireno and Douleb Members (Turonian-Coniacian interval) are still of a great interest for oil exploration and considered as the most important reservoir rocks, which have produced oil in the region of Sfax and the Gulf of Gabes (Chaabouni 1996; Troudi 1997). These reservoirs consist of rudist-bearing carbonates in central and south-east Tunisia (Zagrarni et al. 2003) and change to fine-grained limestones, locally, rich in organic matter, in northern-central Tunisia.

The principal aims of this paper were to characterize the Turonian-Coniacian Bireno and Douleb Members in the Serj-Bargou area by means of a new multidisciplinary approach, using geophysical, petrophysical, and sedimentological analyses.

2 Materials and Methods

The present work started with detailed sedimentological studies carried out on the field (Jebel Bargou-Serj; Fig. 1) and completed by laboratory analyses. A total of 35 carbonate samples were collected (Fig. 1) from the Turonian-Coniacian series (Bireno and Douleb Members). Petrographical studies were based on macroscopic and microscopic analyses (using polarized microscope).

Thin sections of carbonates were, first, analyzed under polarized microscope. The petrophysical analyses using geophysical parameters were carried on selected samples showing visible pores, micropores, and nanopores. They consist of measurements of physical parameters, such as helium-porosity (using the "UltraPoreTM300" helium porosimeter), ultrasonic waves (using PunditLab de Proceeq®), and the measurement of bulk thermal conductivity using the optical scanning method. These analyses were performed at the "Ecole National Supérieur de Géologie" of Nancy (France).

M. Bachari (✉) · M. H. Negra
Faculty of Sciences of Tunis, Tunis El Manar University, 1060 Tunis, Tunisia

Y. Géraud · D. Grosheny
Université de Lorraine, CNRS, GeoRessources, 54000 Nancy, France

A. Çiner et al. (eds.), *Recent Research on Geomorphology, Sedimentology, Marine Geosciences and Geochemistry*, Advances in Science, Technology & Innovation, https://doi.org/10.1007/978-3-030-72547-1_28

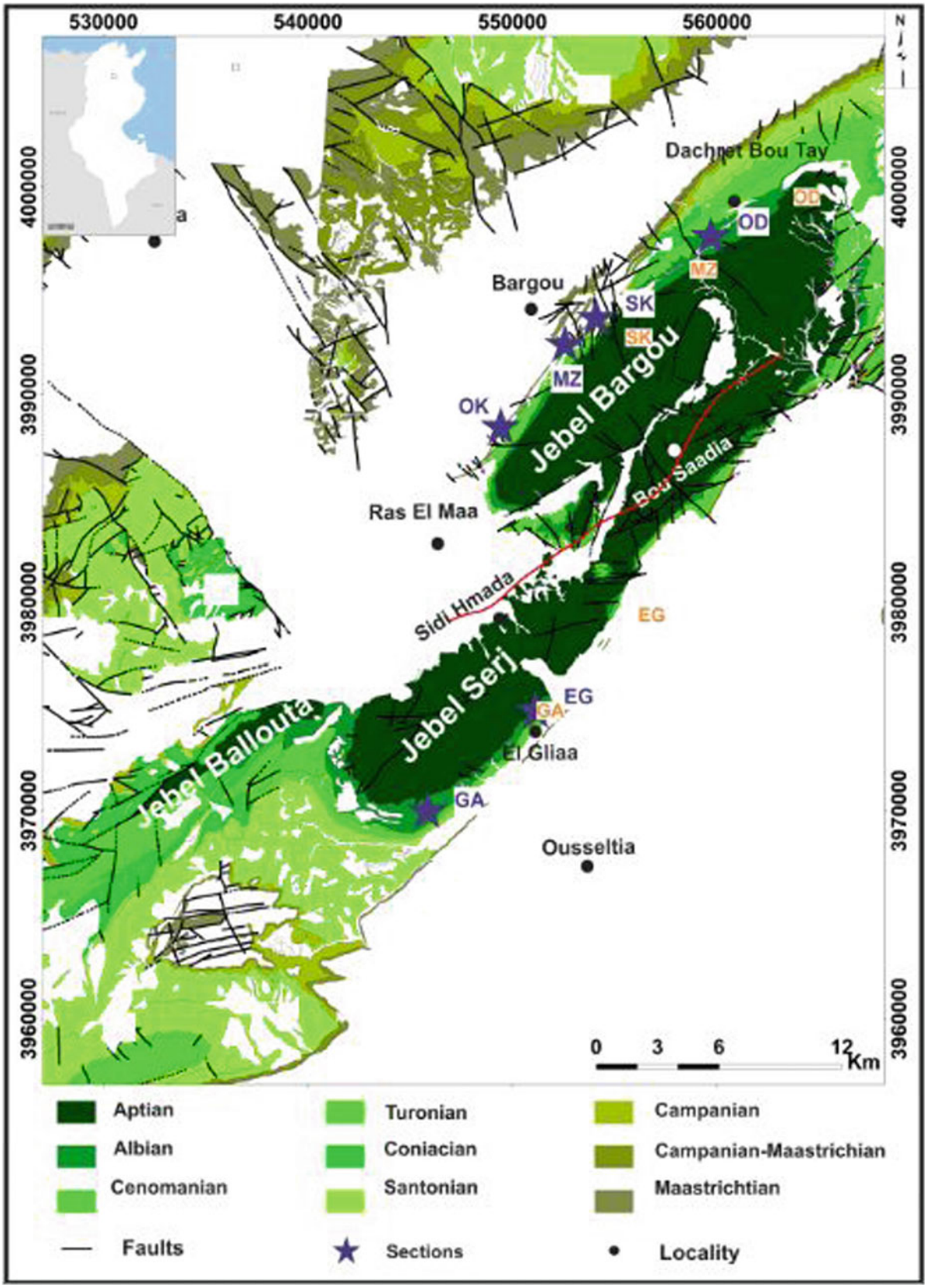

Fig. 1 Detailed geological map of the Jebel Serj-Bargou showing the location of the studied sections (Assemblage of geological maps of Tunisia 1/50.000)

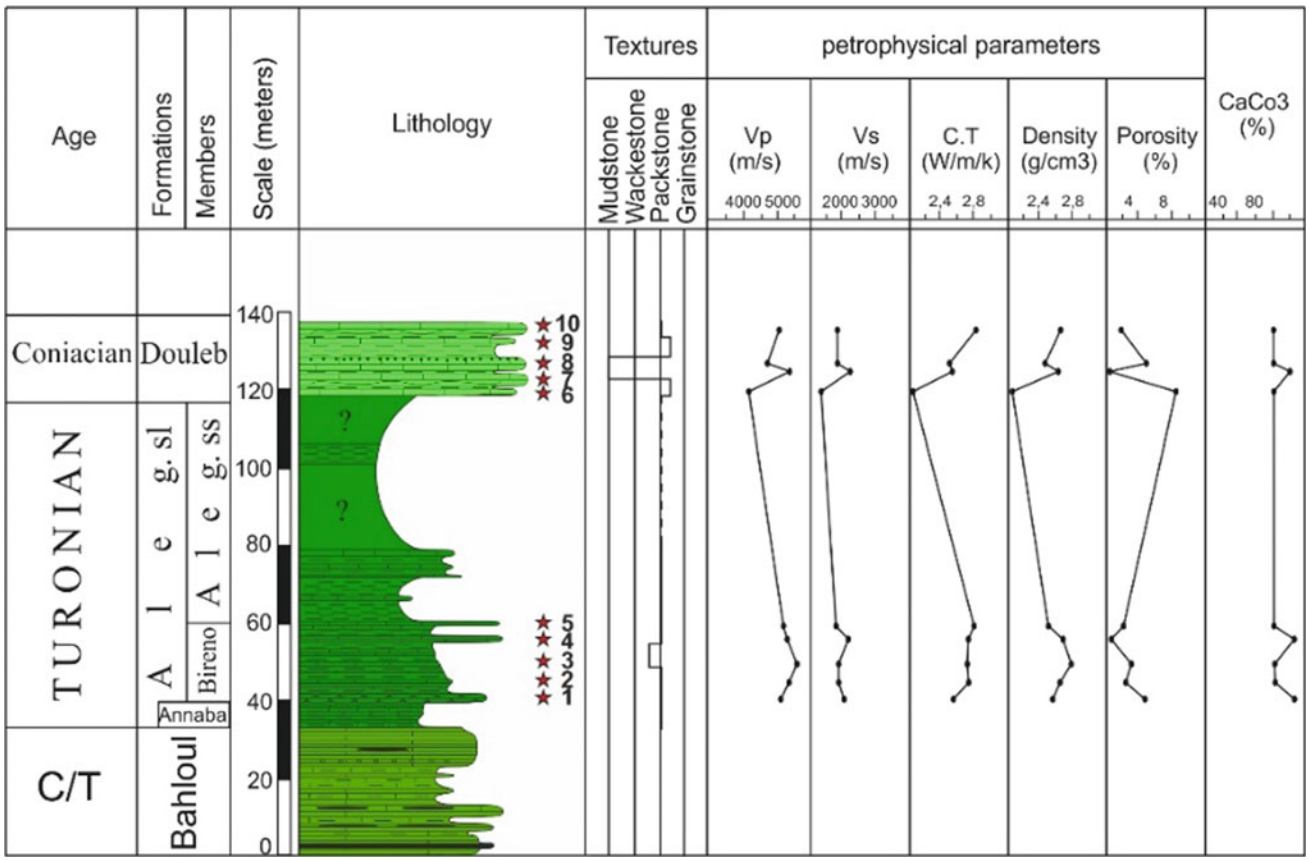

Fig. 2 Lithology, textures, and petrophysical parameters at the Mzetta section (Jebel Bargou)

3 Results and Discussion

3.1 The Turonian-Coniacian Sedimentological Characteristics

On the basis of facies changes, the Turonian-Coniacian interval is subdivided into three distinct lithologic members:

- The Bireno Carbonate Member: It started with nodular limestones**,** overlain by an alternation of dark-gray marlstones and bioclastic limestones, rich in echinoderms. At the lower part, limestones consist of wackestones-packstones rich in calcispheres, planktonic foraminifers, and pyrite crystals (Fig. 4b).
- The Aleg. ss unit: It is mainly composed of marlstones interbedded with thin-bedded limestones that consist of packstones containing echinoderms, scarce benthic, and planktonic foraminifers.
- The Douleb Carbonate Member: It consists of fine-grained and laminated packstones particulary rich in glauconite grains at its summital part.

The depositional environment mainly consists of a shallow marine platform environment. However, the Coniacian Douleb facies, which are relatively shallower, are deposited in a circalittoral environment.

Locally, at the Mzetta section, the Douleb Member is marked by the intercalation of black-colored micritic limestones apparently rich in organic matter. Further analyses could confirm the TOC content of these limestones.

3.2 Petrophysical Properties

The relationships between porosity, P-S wave's velocity, thermal conductivity, and density of the Turonian-Coniacian samples (Bireno and Douleb Members) are presented in a logarithmic graph (Fig. 3). The different distribution points show a good correlation between these physical parameters and porosity.

According to the porosity-waves velocity, porosity-thermal conductivity, and porosity-density graphics, the porosity has an inversely proportional relationship with P-S waves velocity and also with density and thermal conductivity.

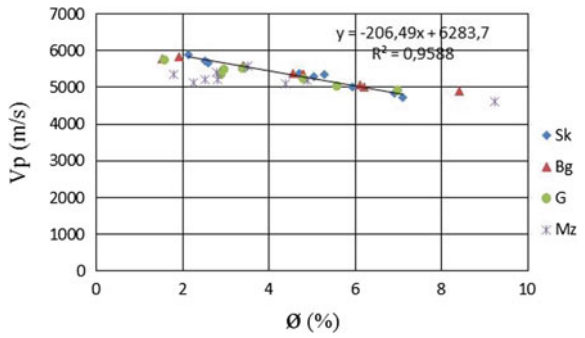

Fig. 3 Correlation between porosity and P waves velocity (Sk: Sebaa Koudiat section; Bg: Oued El Kharroub section; G: El Gliaa section; Mz: Mzetta section)

Based on petrophysical analysis, the P-S waves velocities, density, and thermal conductivity of the studied samples are controlled by the porosity, density, mineral composition, and diagenetic modifications within the rock.

3.3 Diagenesis Influence on the Porosity

Petrographical and petrophysical analyses of the studied section reveals that porosity is influenced by the facies type, fracturing (Fig. 4a), and diagenesis.

At the Serj-Bargou area, the Turonian-Coniacian series is characterized by a complex porous system that includes matrix, intercrystal, intracrystal, intergranular, and intragranular porosities (Fig. 4c, d). Microscopic studies have shown that the Douleb carbonates are mainly affected by dissolution and matrix dolomitization (Fig. 4c) that create significant secondary intercrystal and intracrystal porosities.

In contrast, the Bireno carbonates which show low porosity values are affected by a strong compaction with the development of numerous stratiform stylolites. These diagenetic processes which involve cementation of the pores tend to decrease porosity.

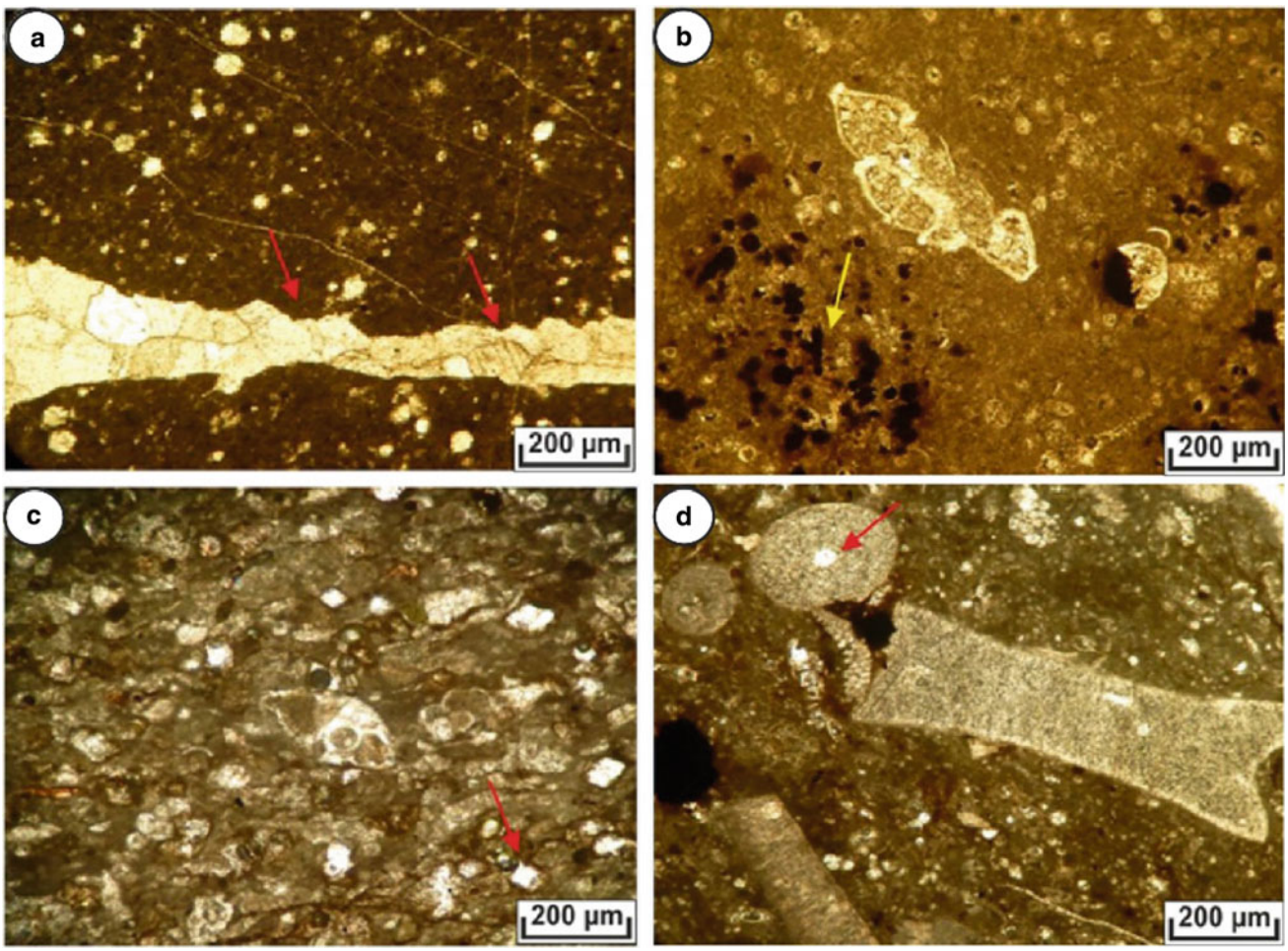

Fig. 4 Microfacies of the studied sections. **a** wackestone rich in calcispheres, showing micro-fracture (Red arrows; Bireno Member); **b** Packstone showing oxides and pyrites crystals (Yellow arrows; Bireno Member); **c** Dolomitized packstone showing an intercrystal an intracrystal porosity (Douleb Member); **d** Packstone with intergranular and intragranular porosity (Douleb Member)

4 Conclusions

Based on sedimentological and petrophysical analyses, the layering established on the Bireno–Douleb carbonates shows that the lower part of the Coniacian Douleb Member which consists of fractured fine-grained limestones is considered as a reservoir unit with porosity values ranging from 6.8 to 9.2%. In addition, in the Mzetta section, this unit locally admits the intercalation of "black shales."

Contemporaneous tectonic movements, which are mainly expressed by tilting blocks and horst-graben compartmentations, are favorable to the deposition of porous carbonates on horsts and organic-rich deposits in grabens and half grabens.

In addition to fracturing, diagenesis controls the pore system. Dolomitization and dissolution appear as the main diagenetic processes enhancing the porosity, whereas compaction and cementation are rather destructive of the reservoir potential. Considering dolomitization processes, petrophysical analysis shows that the dolomitized facies are generally more porous than the non-dolomitized ones.

References

Chaabouni. M.: The Bireno member excellent potential reservoir in central Tunisia. Mem. ETAP, No. 10 (1996)

Troudi. H.: Les réservoirs et faciès associés du Crétacé supérieur en Tunisie centrale : sédimentologie, stratigraphie séquentielle et diagenèse. Unpublished Ph.D. thesis, University Tunis II, 287 pp. (1997)

Zagrarni, M.F., Negra, M.H., Melki, S.: Turonian rudist-coral limestones in Jebel Biréno, Central Tunisia. In: Gili, E., Negra, M.H., Skelton, P. (eds.), North African Cretaceous Carbonate Platform Systems. Amsterdam, Kluwer Academic Publishers, pp. 111–128 (2003)

Effect of Volcanics on the Reservoir Quality of Coniacian Rudist-Rich Carbonates in the Gulf of Gabes, Tunisia

Senda Boughalmi, Mohamed Hédi Negra, Yves Géraud, Danièle Grosheny, and Sonia Ben Alaya

Abstract

In the Gulf of Gabes, the petrophysical properties and reservoir potential of the Coniacian Douleb rudist-rich carbonates appear directly to be influenced by sediments composition, texture, and diagenetic fabrics. Volcanic material, especially breccia, interbedded within some layers of the reservoir, initially formed of fine-grained micritic to bioclastic limestones, appears to transform the initial sediment texture and clearly enhance their reservoir potential. Similar Cretaceous features were described in China (the Songliao and the Er'Lian Basins). On the other hand, the main diagenetic processes affecting the reservoir quality are usually dolomitization, compaction, and silicification. In fact, dolomitization is the main diagenetic process which improves the porous system, whereas silicification and cementation tend to decrease it. In terms of reservoir properties, the best values of helium porosity and nitrogen permeability (reaching 16.8% and 4.2 mD, respectively) were measured in bioclastic-rich limestones (carbonates rich in rudists, peloids, echinoderms, and oncoliths) and in some volcano-sedimentary facies intercalated in the micritic facies of the Douleb Member. These beds with volcanic facies show porosity values ranging from 4 to 21.15% and negligible to low permeability values (<0.01 to 1.4 mD).

Keywords

Coniacian Douleb Member • Rudist-rich carbonates • Volcano-sedimentary facies • Diagenesis • Reservoir properties

1 Introduction

The upper Cretaceous carbonates rich in rudists, included in the Turonian-lower Campanian Aleg Formation and corresponding to the Douleb Member, are characterized by their good porosity and permeability values (Boughalmi et al. 2019). In fact, they are productive in several sectors of Tunisia, notably in the region of Sfax and the Gulf of Gabes and more specifically in several oil fields especially those of Guebiba, Gremda, El Ain, Rhemoura, and Miskar (Boughalmi et al. 2019).

The present work complements a study already carried out and published, on oil-producing carbonate reservoir rocks in the southeastern offshore of Tunisia. It dealt with another productive well of gas from a reservoir of the same age. However, a detailed layering of the reservoir shows that most facies of the impregnated layers are slightly different. In the same way, we highlighted new textures in the reservoir marked by the incorporation of a volcanic material within some layers of the reservoir. In addition, diagenetic transformations also could improve the reservoir potential.

The principal objective of this paper was to characterize the rudist-rich carbonate reservoir by sedimentological and petrophysical analyses and select, after a detailed layering, the facies having the best reservoir quality. We also proposed to show the effect of the introduction of volcanic material on the reservoir potential. Overall, it would be essential to focus on the relationship between the sedimentary characters, diagenetic transformations of the reservoir layers, and their oil–gas impregnations (oil and gas-shows).

S. Boughalmi (✉) · M. H. Negra
Faculty of Sciences of Tunis, Tunis El Manar University, U.R. Pétrologie Sédimentaire et Cristalline, Campus Universitaire, 2092 Tunis, Tunisia

Y. Géraud · D. Grosheny
Université de Lorraine, Ecole Nationale Supérieure de Géologie, GeoRessources - UMR 7359 CNRS, 2 Rue du Doyen Marcel Roubault, 54500 Vandœuvre-lès-Nancy Cedex, France

S. B. Alaya
Entreprise Tunisienne d'Activités Pétrolières (ETAP), Charguia II, 2053 Tunis, Tunisia

A. Çiner et al. (eds.), *Recent Research on Geomorphology, Sedimentology, Marine Geosciences and Geochemistry*, Advances in Science, Technology & Innovation, https://doi.org/10.1007/978-3-030-72547-1_29

2 Data and Methods

The present study is based on sedimentological and petrophysical analyses of samples taken from a Coniacian well located in the Gulf of Gabes. The used sedimentological approach is based on macroscopic studies (on cores along 203 m of series), microscopic analyses of 26 thin sections using optical microscopy, and nanoscoping analyses of 19 samples using scanning electron microscopy (SEM). In addition, the petrophysical study consisted in measurements of helium porosity and nitrogen permeability using, respectively, the "UltraPore TM300" helium porosity and the gas permeameter "UltraPerm TM400." The porosity and permeability measurements were carried out on 26 samples, 2.54 cm (1 inch) in diameter, and between 3.4 and 4.1 cm in length.

3 Results and Discussion

3.1 Lithostratigraphy of the Douleb Member in the Studied Well

The sedimentological study of cores coming from the Coniacian Douleb reservoir highlights three distinct lithological units going from the base to the top and that show the following characteristics:

- Unit 1 (**U1**): This unit which has a thickness of 27 m is essentially composed of fine-grained bioclastic facies. The base of this unit is formed of laminated clayey limestones showing packstones rich in miliolids, benthic and planktonic foraminifera, echinoderm debris, calcispheres, gastropods, scarce bivalves, and intraclasts. These facies are overlain by partly argillaceous wackestones-packstones showing fracture and stylolithes, and containing calcispheres, echinoderms, and planktonic foraminifera. The uppermost part of this unit is composed of fine-grained (Fig. 1a) oil-impregnated packstones rich in oncoliths, peloids, and lithoclasts associated with rare debris of Hippuritids (Fig. 2b).
- Unit 2 (**U2**): Oil-impregnated carbonate unit with a thickness of 55.5 m mainly formed of rudist-rich packstones (Fig. 1b) showing Hippuritids and Radiolitids (Fig. 2c). This rudist unit is intercalated by layers showing packstone-grainstone textures with rudists and peloids (small or coarse debris), and by other fine layers, microbioclastic, rich in echinoderm debris, peloids (Fig. 2a), and sometimes some miliolids.
- Unit 3 (**U3**): This unit (130.5 m thick) is formed of fine-grained micritic carbonates, partly argillaceous, nodular to laminated, composed of gastropods, echinoids, bivalves, miliolids, benthic and planktonic foraminifera, extraclasts, and scarce red algae. This unit admits the intercalation of a magmatic layer (29 m in thickness; Fig. 1c–f). The microscopic study (Fig. 2d) shows that this layer is formed of doleritic to microdoleritic rocks, gradually altered from the base to the upper part of the Coniacian Douleb limestones. These magmatic layers are marked by the presence of visible vugs and/or fractures filled with varied minerals (Fig. 1c, d).

Previous studies (Laaridhi-Wazaa 1994) highlighted contemporaneous volcanic activities during the late Cretaceous sedimentation in the Gulf of Gabes. Incorporation of volcanic material is controlled by regional tectonics. All manifestations are arranged along a trend-oriented NW-SE and also NS and EW conjugate directions, corresponding to deep faults.

3.2 Petrophysical Properties: Porosity–Permeability, Diagenesis, and Oil Shows

According to the porosity–permeability relationship (Fig. 3), four rock types are distinguished. Samples that belong to the rock types RT1, RT2, and RT3, show an evolution of the permeability parallel to that of porosity. These three distinguished groups mainly consist of oil-impregnated rudist facies containing rudist debris associated to echinoderms, peloids, oncoliths, and miliolids (F1, F3, F6, F7, and F9). Porosity values range between 12 and 16.8%, while permeability values range between 0.5 and 4.2 mD in these rock types. The reservoir quality is considered as medium to almost good.

The best petrophysical values (porosity and permeability) are observed in the RT1, RT2, and RT3. RT1 and RT3 and are composed of well-sorted and fine microbioclastic limestones formed of echinoderms, peloids and some miliolids (F3 and F9 within the Unit 2), and, of limestones rich in oncoliths, peloids, and some rudist debris (F7 of the Unit 1). RT2 (in Unit 2) consists of dolomitized packstones rich in rudists (F1) and of packstones-grainstones containing coarse rudists and peloids (F6) and show medium porosity and permeability values suggesting a medium quality of the reservoir.

In RT3, the volcanic layer facies included in the third unit (U3), especially volcano-sedimentary facies (F12; Fig. 1e and Fig. 2d), particularly volcanic breccia, that are characterized by good porosity and permeability values (respectively, 14.62% and 0.6 mD). Similar compositions and porosity values were described in China (Sun et al. 2018) (the Songliao, the Tarim, and the Bohai Bay Basins), in Canada (the Scotian Basin), in Central Mexico, and in New Zealand (the Canterbury Basin). However, pure volcanic

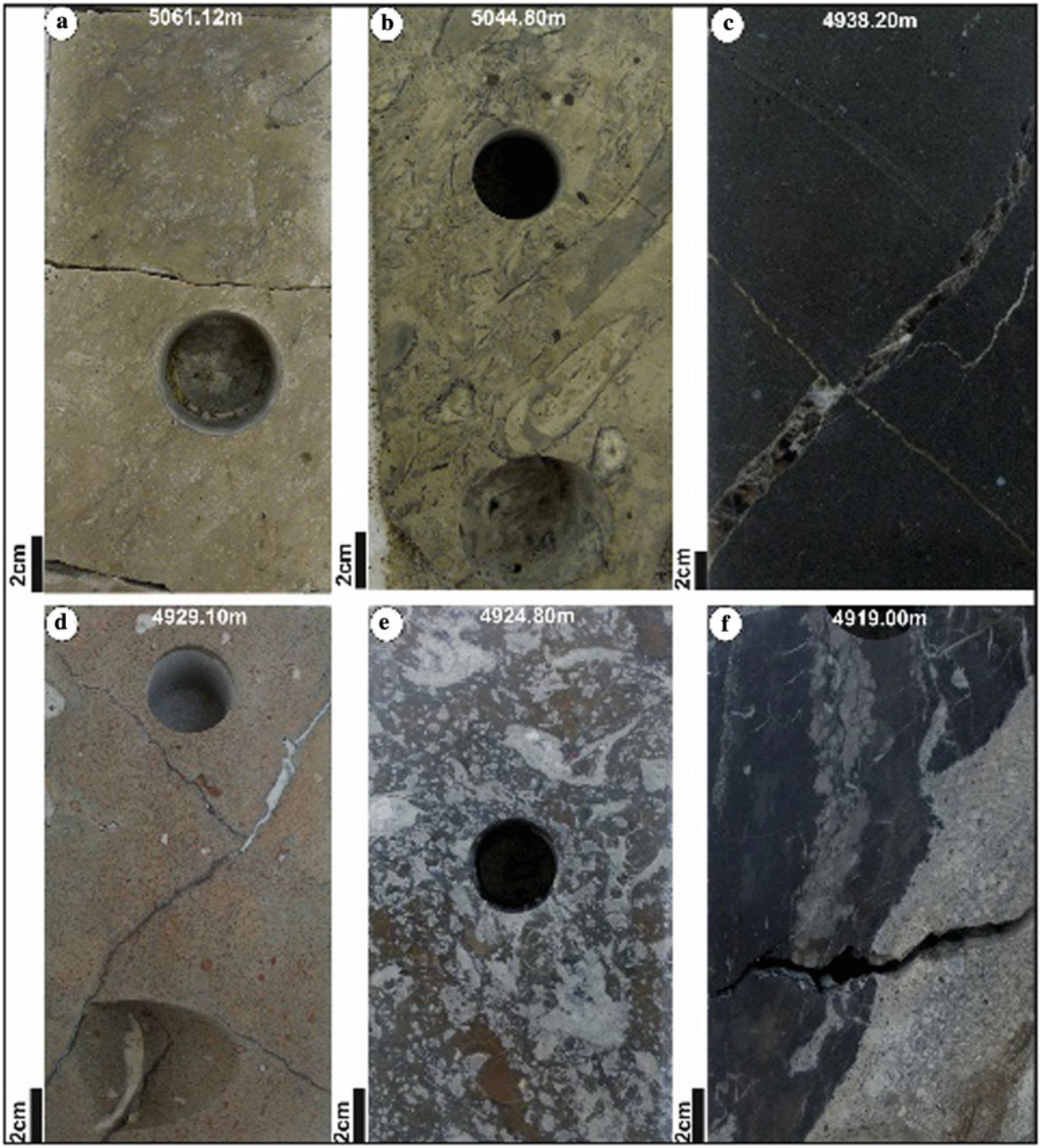

Fig. 1 Main macrofacies of the Douleb Member in the studied well. **a** Brown limestone, oil-impregnated, rich in oncoliths; **b** brown limestone, oil-impregnated, rich in rudists; **c** magmatic facies of black-gray color showing cemented fractures; **d** red magmatic facies, altered and containing nodules and mineralized fractures; **e** volcano-sedimentary facies; **f** The transition from a volcanic facies to a fine bioclastic sedimentary facies

facies (not mixed with sedimentary facies; F13) belonging to the RT4 appear highly dense; fractures are fully cemented. Porosity and permeability values are low to negligible (respectively, 1.5% on average and <0.01mD).

The rock type RT4 is formed of micritic limestones (F2, F4, F5, F8, F10, and F11) mixed with volcanic facies (F13). It shows low to negligible porosity and permeability values (porosity values range between 0.06 and 4.98% while

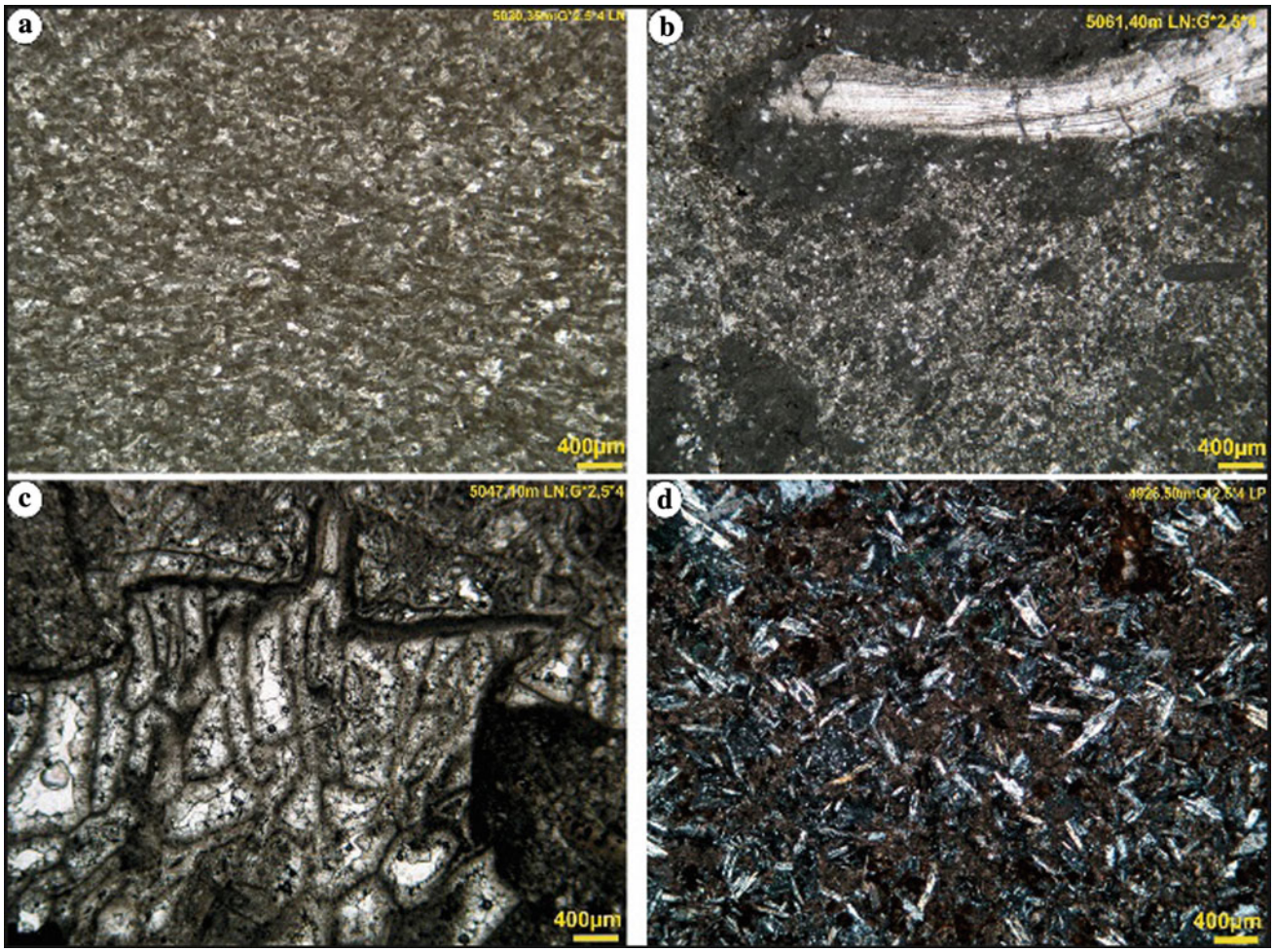

Fig. 2 Main microfacies of the Douleb Member in the studied well. **a** Fine-grained packstone-grainstone containing echinoderm debris; **b** dolomitized packstone rich in peloids, lithoclasts, and rudist debris; **c** intragranular porosity within a Radiolitidae debris; **d** volcanic microfacies: fine microdoleritic microfacies containing altered feldspars transformed into clayey material

permeability is <0.01 mD). The RT4 regrouping micritic facies and pure volcanic are *affected by a strong compaction and silicification that tends to decrease their porosity and permeability.*

As a first conclusion, porosity and permeability properties appear to be linked to the texture of the sediment and the diagenetic modifications. In fact, the best porosity values were obtained in fine-grained and well-sorted sediments rich in echinoderm debris and peloids belonging to RT1. In terms of diagenesis, dolomitization creates a secondary porosity, especially in rudist-rich packstones (RT2).

Overall, The Douleb Coniacian limestones are characterized by a complex porous system that includes matrix (Fig. 2a), intercrystal, intergranular (Fig. 2c, e), and intragranular (Fig. 2c) porosities.

4 Conclusions

The established layering based on sedimentological and petrophysical analyses shows that the oil-impregnated facies belong to RT1, RT2, and RT3. The best porosity and permeability values are measured in two types of facies: the well-sorted packstones-grainstones containing echinoderms, peloids, and some miliolids, and in the partly dolomitized packstones rich in oncoliths. Other facies types such as the dolomitized rudist-rich packstones and some volcano-sedimentary layers (mainly composed of breccia) show medium to good porosity values.

In addition to the texture type and sediment composition, certain diagenetic modifications could significantly increase

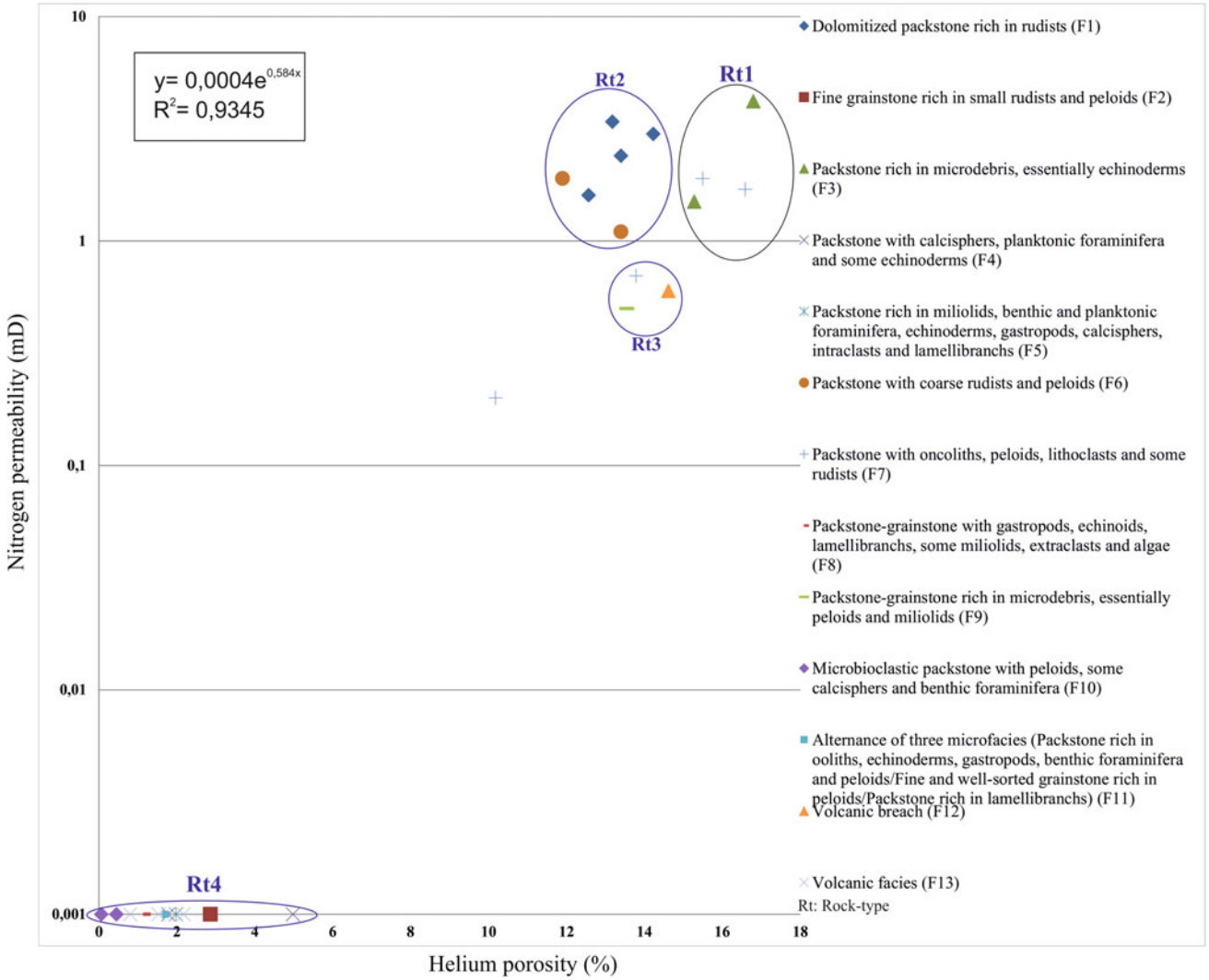

Fig. 3 Helium porosity versus nitrogen permeability

the reservoir potential. Dolomitization, for example, appears to be the main diagenetic process that improves the porous system.

References

Boughalmi, S., Negra, M.H., Géraud, Y., Ben Alaya, S., Grosheny, D.: Sedimentology and petrophysics of Turonian-Coniacian Rudist rich-reservoir rocks, offshore Tunisia. In: Boughdiri, M., Badenas, B., Selden, P., Jaillard, E., Bengston, P., Granier, B.R.C. (eds.) Paleobiodiversity and tectono-sedimentary records in the mediterranean Tethys and related eastern areas, pp. 191–194. Springer, Tunisia (2019)

Laaridhi-Wazaa, N.: Etude minéralogique et géochimique des épisodes magmatiques mésozoiques et miocènes de la Tunisie. Thèse Es-Sciences. Université de Tunis, 462 p. (1994)

Sun, H., Zhong, D., Zhan, W.: Reservoir characteristics in the Cretaceous volcanic rocks of Songliao Basin, China: a case of dynamics and evolution of the volcano-porosity and diagenesis. Energy Exploration Exploitation 1–19 (2018)

Facies and Architecture of a Tide-Dominated Estuary in the Lower Cretaceous Sidi Aich Formation of the Chotts Basin, Southern Tunisia

Kamel Boukhalfa, Mohamed Soussi, Walid Ben Ali, and Mohamed Ouaja

Abstract

The Upper Barremian amalgamated sandstone sequences of the Sidi Aich Formation cropping out throughout the Northern and southern Chotts ranges, southern Tunisia, have been used to develop and refine sedimentological models over the years. These continuous and well-exposed strata, regularly visited by geologists, serve as representative field stops for teaching siliciclastic sedimentary structures, processes, causal mechanisms, and related depositional environments. Recent work has begun to cast doubt on depositional environments interpretation of this succession; hence, the re-evaluation of these classic outcrops is warranted. Bed by bed logging of four selected lithostratigraphic sections allowed the recognition of twenty facies grouped into three facies associations characterizing tidal flat, tidal channel, and tidal bars depositional settings. The sedimentological data document an early Cretaceous transgressive tide-dominated estuarine system that developed during an important episode of relative sea-level fluctuations.

Keywords

Sedimentology • Tide-dominated estuary • Lower Cretaceous • Sidi Aich Formation • Chotts basin • Tunisia

K. Boukhalfa (✉)
Faculty of Sciences of Bizerte, University of Carthage, LR18ES07, 7021, Jarzouna, Tunis, Tunisia

M. Soussi · W. B. Ali
Faculty of Sciences of Tunis, University of Tunis El Manar, LR18ES07, 2092 Tunis, Tunisia

M. Ouaja
Faculty of Sciences of Gabes, University of Gabes, LR18ES07, 6072 Gabes, Tunisia

1 Introduction

The upper Barremian Sidi Aich Formation, as a part of the continental intercalaire, consists of thick amalgamated sandstone-dominated sequences which for the first time have also yielded diverse and rich well-preserved fauna and flora assemblages (Boukhalfa et al. 2015, 2019; Li et al. 2017; Ben Ali et al. 2018). These very useful discovered fossils allowed a direct dating of the Sidi Aich Formation as well as the characterization of good evidence for marine influence, previously described as fluvial, of its depositional environment (Ben Ali et al. 2018). Recent works (Boukhalfa et al. 2015, 2019) have shown that there was a more diverse set of depositional environments across central and southeast Tunisia than previously recognized and that marine influence is well recorded and documented (Ben Ali et al. 2018; Boukhalfa et al. 2019).

2 Geological Setting

The Sidi Aich Formation is exposed throughout the east–west trending of northern and southern Chotts ranges of southern Tunisia (Fig. 1). It is distinguished in the Zimlet El-Beidha Anticline Structure (ZBAS) and the Jebel Aziza Structure (JAS) studied areas by the widespread sandstone-dominated sequences compared to the underlying evaporitic dominated succession of the Bouhedma Formation and the overlaying carbonate-dominated deposits of the Orbata Formation. The Sidi Aïch Formation is speculated as being Late Barremian and the underlying Bouhedma Formation as Hauterivian-Early Barremian in age based on *Cratostracus tunisiaensis* (Boukhalfa et al. 2015) and *Ordosestheria chottsensis* (Li et al. 2017) conchostracan fauna, respectively. Previous works have ascribed this sandstone-dominated succession as deposited in large flat coastal setting influenced by wave and tide processes (Ouaja et al. 2011) as well as fluvial to a neritic environments with

A. Çiner et al. (eds.), *Recent Research on Geomorphology, Sedimentology, Marine Geosciences and Geochemistry*, Advances in Science, Technology & Innovation, https://doi.org/10.1007/978-3-030-72547-1_30

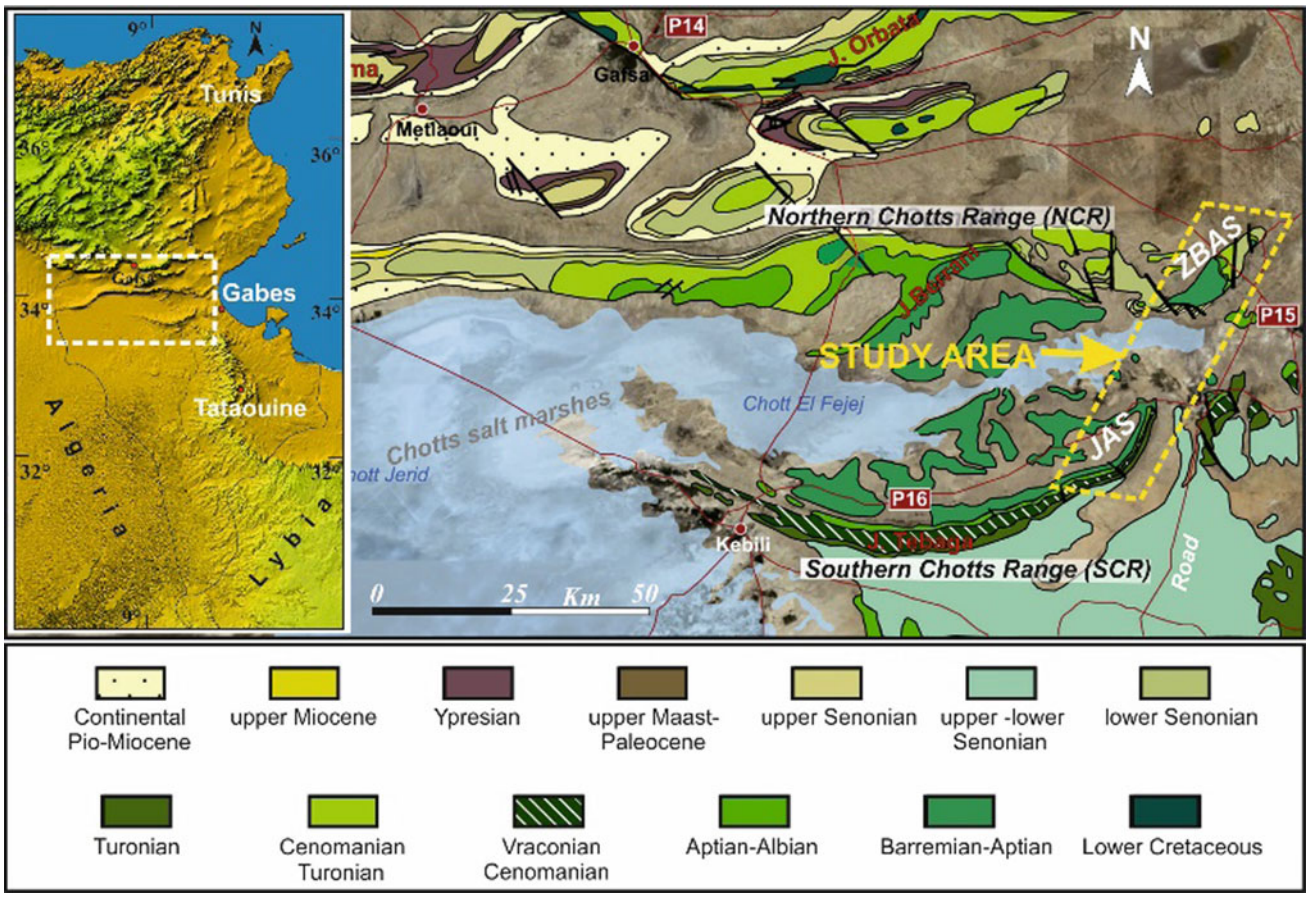

Fig. 1 Geological map of the studied area showing the Zimlet El-Beidha Anticline structure (ZBAS) and the Jebel Aziza structure (JAS) investigated outcrops throughout the Northern and Southern Chotts range, respectively

interplay of fluvial (and rarely alluvial) processes (Aloui et al. 2012). This work fits into the development of a sedimentological model for the amalgamated sandstone sequences of the Sidi Aich Formation integrating their recently published fossil contents data (Boukhalfa et al. 2015, 2019; Li et al. 2017; Ben Ali et al. 2018).

3 Facies Associations and Depositional Model

- *Facies Association A: Tidal Flat*

This facies association encompasses three amalgamated sedimentary facies including; heterolithic sandstone (A), laminated claystone (B), and red pedogenic dolocrete (C) (Fig. 2). The facies (A) (Fig. 2a) range from 1 to 5 m in thickness and consist of fine-grained heterolithic sand (Hs) containing red fine-grained dolocrete (D) and grayish-green clays (C) horizons (Fig. 2b). The facies (B) consist of a lenticular outcrop of 20 m thickness which is constituted of green-laminated claystone (Fig. 2c) hosting well-preserved faunal and floral assemblages (Boukhalfa et al. 2015, 2019). The facies (C) are about 1 m in thickness and consist of a red fine-grained dolocrete (Fig. 2d) containing root traces. Desiccation cracks (Fig. 2e), bioturbation (Fig. 2f), wavy, and flaser bedding (Fig. 2g) are the most preserved sedimentary structures. Current ripple showing trough and tabular cross-bedding is also observed (Fig. 2g). Thin (<1 m) channel-form showing erosional base with a lag deposit (Fig. 2h) is composed of fining upward succession of fine sand with cross-bedding. Abundant evidence of tidal activity is contained in the form of wavy and lenticular bedding. So the (A) facies are interpreted as tidal flat, and the channel-formed sandstone is interpreted to be tidal creeks draining the tidal flat, facies (B) as pond, and facies (C) as salt marsh settings.

- *Facies Association B: Tidal Channel*

This facies association is made up of channelized sandstone ranging from 1 to 3 m in thickness, which depends on the outcrops locality (Fig. 3). The channelized sandstone which has a sharp erosional surface (Fig. 3a–c) with flat and

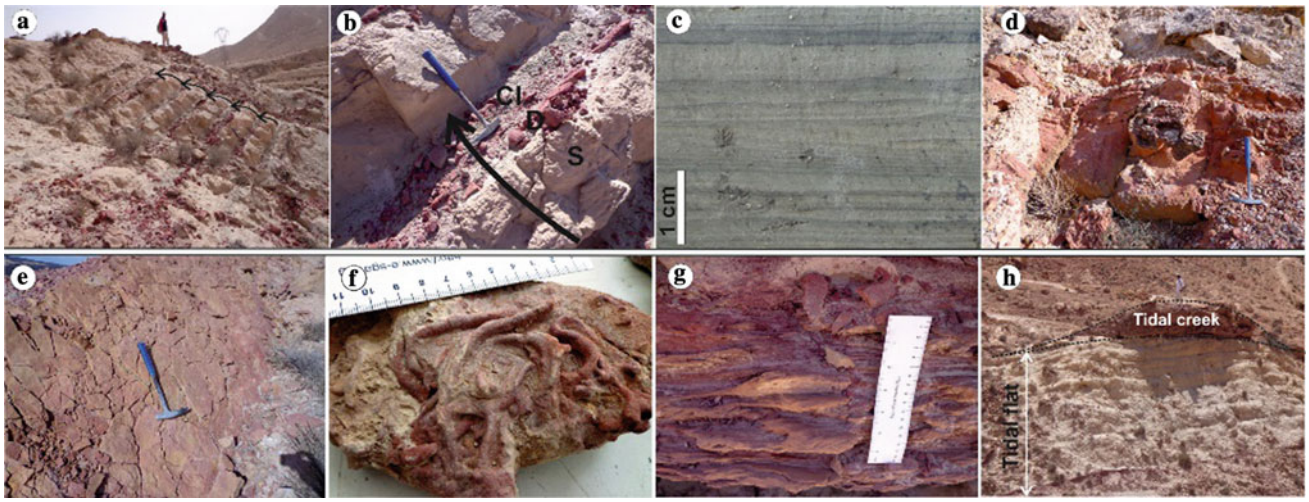

Fig. 2 Field photographs of the tidal flat facies association. **a** and **b**. Facies **a** heterolithic sand; **c** Facies; **b** laminated claystone; **d** facies; **c** pedogenic dolocrete; **e** desiccation cracks; **f** bioturbation (*Helminthopsis* sp.); **g** current ripple showing trough and tabular cross-bedding flaser and wavy beddings; **h** tidal creeks draining the tidal flat

well-rounded conglomerates (Fig. 3d), contains trough cross-bedding (Fig. 3f), low-angle cross-bedding, ripple lamination, and wavy bedding. In most cases, the cross-bedding indicates a dominating unimodal paleocurrent (Fig. 3a, e). However, a subordinate inverse paleocurrent could be observed (Fig. 3b). Rip-up clasts usually underlie the foresets (Fig. 3e). The erosional surface at the bottom of the channel body may probably result from the scouring of the underlying facies in relation to marine transgression. The rip-up clasts observed in the lag and foresets may have been eroded and transported from the muddy subtidal flats. The two reverse paleocurrent directions, in which one is dominating, reflect the characteristics of the tidal current.

- *Facies Association C: Tidal Bars*

This facies association is made up of cross-bedded sandstone with some minor siltstone and mudstone showing a coarsening-upward and thickening-upward facies succession (Fig. 4). The sandstone contains cross-bedding and

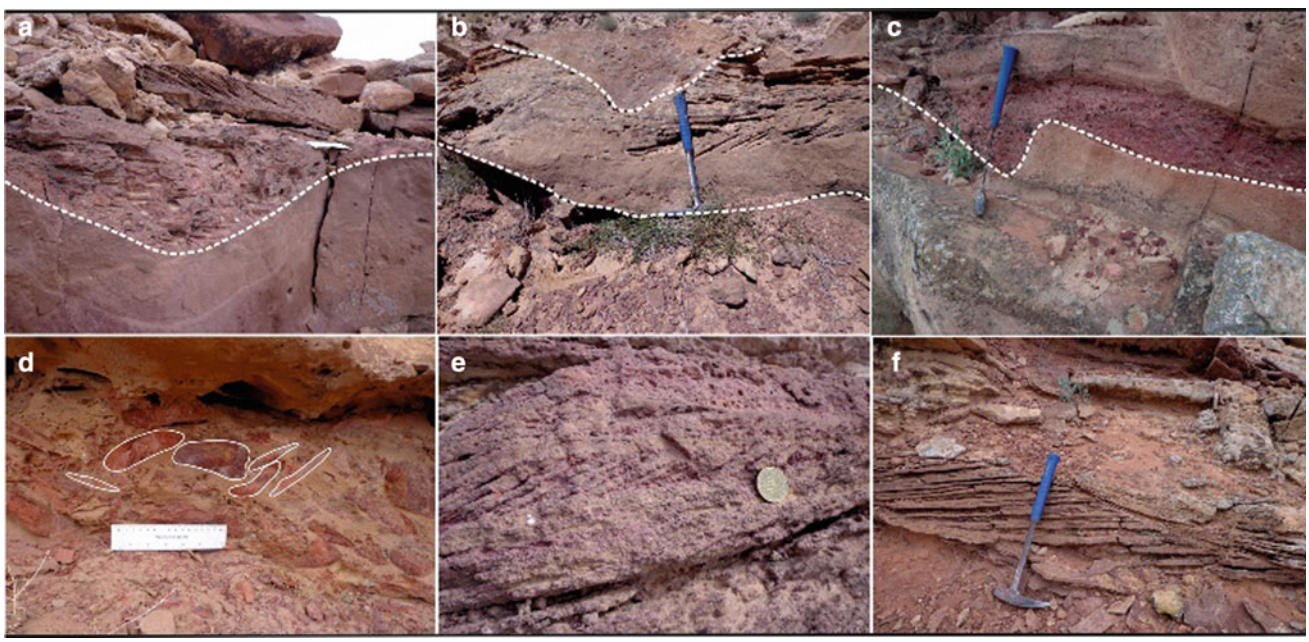

Fig. 3 Field photographs of the tidal channel facies association. **a**, **b,** and **c**. Channelized sandstone showing sharp erosional surface, conglomerate, and trough cross-bedding. **d** Close up of the flat and well-rounded conglomerate. **e** Cross-bedded conglomerate. **f** Close up of the trough cross-bedding

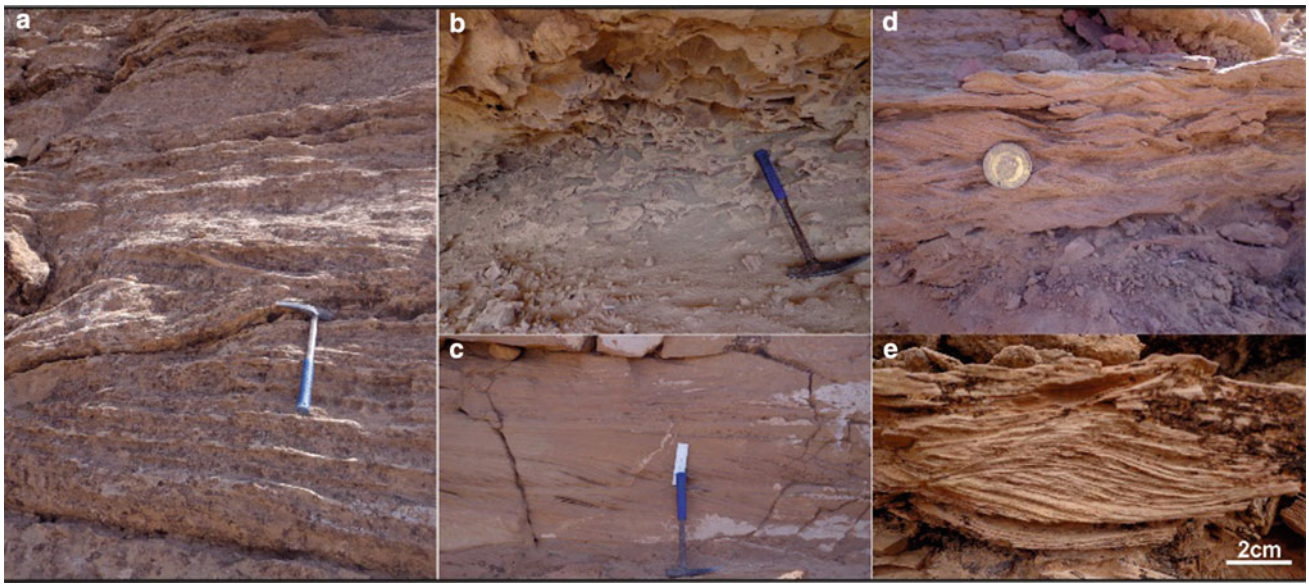

Fig. 4 Field photographs of the tidal flat facies association. **a** and **b**. Facies **a** heterolithic sand, **c** facies (**b**) laminated claystone, **d** facies (**c**) pedogenic dolocrete. **e** Desiccation cracks, **f** bioturbation (*Helminthopsis* sp.), **g** current ripple showing trough and tabular cross-bedding flaser and wavy beddings, **h** tidal creeks draining the tidal flat

reactivation surface (Fig. 4a) with well-developed drapes on the foresets (Fig. 4c) and mudclast (Fig. 4b).

Bimodal cross-bedding shows the bimodal tidal currents: both flood current and ebb current, but more commonly, cross-bedding in one specific part is unidirectional, representing the main tidal flow (Dalrymple et al. 1992). The well-developed drapes on the foresets of the cross-bedding indicate the alternating periods of low and high energy of the tidal cycles (Boyd et al. 2006). The proximity to the sea and coarsening-upward succession which is analogous to the tidal bars generated in interpreted ancient estuarine valley-fill and tide-dominated deltaic deposits (Boyd et al. 2006) suggests that facies B is a subtidal migrating tidal bar. The incoming tidal currents between the tidal bars tended to generate tempestites conditions which are very well documented by the Hummocky cross-stratification storm structures (Fig. 4d, e).

The tidal channels, tidal flat, and tidal bars facies associations, well documented in the sandstone-dominated deposits of the Sidi Aïch Formation, suggest deposition within a transgressive tide-dominated estuary (Fig. 5). This interpretation is supported by the bidirectional trends, and the backstepping character of sand body deposits. Lateral facies indicate that tidal channels were deposited further seaward, in the inner estuary. Tidal flat and ponds deposits probably accumulated on the margins of the estuary, an interpretation supported by the erosional contacts with the overlying sandstone-dominated tide-influenced channel deposits and the varved claystone. The fine-grained and well-sorted tidal bar deposits are interpreted as the seaward portions of elongate outer estuarine tidal bars (Dalrymple et al. 1992).

4 Discussion

The sedimentological investigation of the amalgamated sandstone sequences of the Sidi Aich Formation together with their faunal and floral assemblages previously published (Boukhalfa et al. 2015, 2019) indicates that the paleo-environment was characterized by the influence of mixed freshwater and marine conditions. The stacking of different facies associations which record (i) tidal flat, (ii) tidal channel, and (iii) tidal bar depositional environments deals with a tidally influenced estuarine setting that characterized the Chotts zone during the Upper Barremian and constitutes a key area for any attempt of paleogeographic reconstruction between the Sahara to the South and the Atlas domain to the North.

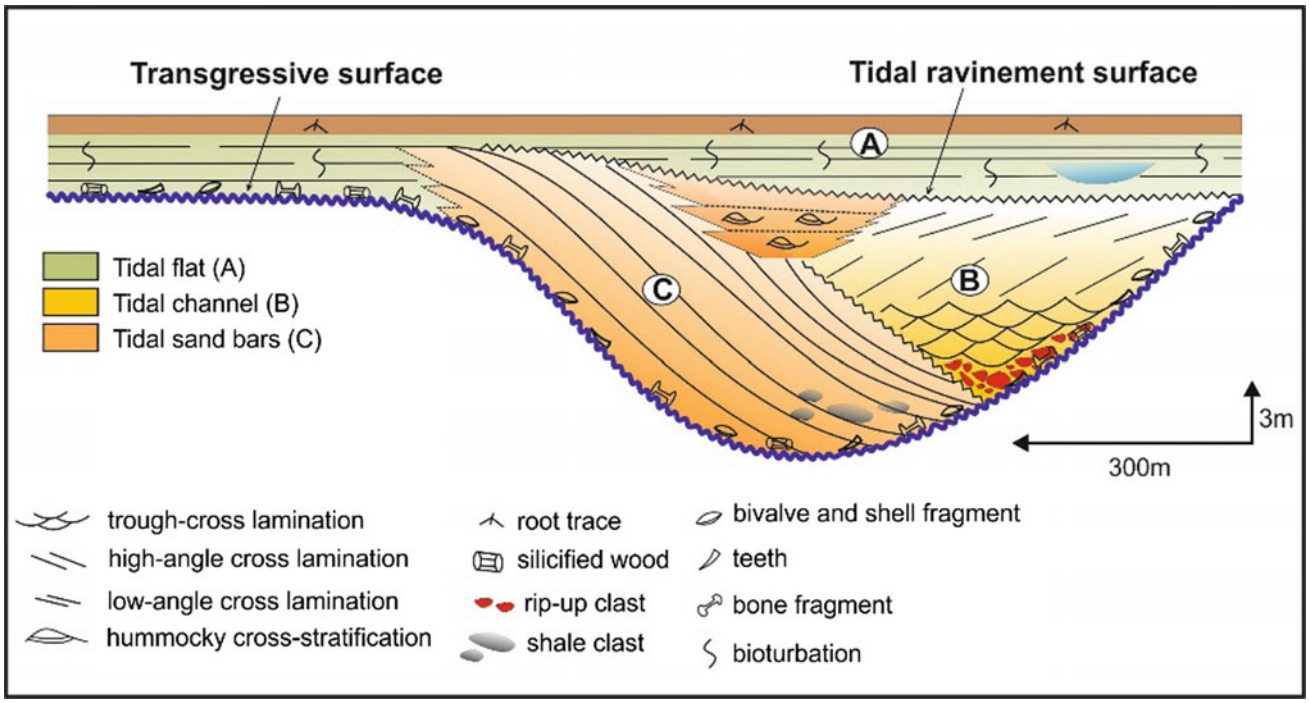

Fig. 5 Reconstruction of geometric lateral relationships between facies associations A, B, C of the sandstone-dominated interval of the lower cretaceous Sidi Aich Formation from the Chotts basin

5 Conclusions

The multidisciplinary study of the Sidi Aïch Formation of the Chotts basin including sedimentological, biostratigraphic frameworks confirms and refines the idea supporting a complex estuarine environment influenced by mixture of freshwater and marine conditions, and demonstrates the continental-marine transitional paleogeographic position of the Chotts basin during the deposition of the sandstones dominated sediment interval.

References

Aloui, T., Dasgupta, P., Chaabani, F.: Facies pattern of the Sidi Aïch formation: reconstruction of Barremian paleogeography of Central North Africa. J. African Earth Sci. **71–72**, 18–42 (2012)

Ben Ali, W., Cavin, L., Boukhalfa, K., Ouaja, M., Soussi, M.: Fish assemblage and palaeoenvironment of early Cretaceous varved neap-spring tidal rhythmites from Sidi Aïch formation of the Chotts basin (Southern Tunisia). Cretac. Res. **92**, 31–42 (2018)

Boukhalfa, K., Wu, F., Ben Ali, W., Fang, G.: A new paraclupeid fish (Clupeomorpha: Ellimmichthyiformes) from the early Cretaceous Sidi Aich formation of southern Tunisia: phylogenetic and paleobiogeographic implications. J. Vertebrate Paleontol. e1529675, 17 (2019)

Boukhalfa, K., Li, G., Ben Ali, W., Soussi, M.: Early cretaceous spinicaudatans ("Conchostracans") from lacustrine strata of the Sidi Aïch formation in the northern Chotts range, southern Tunisia: taxonomy, biostratigraphy and stratigraphic implication. Cretaceous R Search J. **56**, 482–490 (2015)

Boyd, R., Dalrymple, R.W., Zaitlin, B.A.: Estuarine and incised-valley facies models. In: Posamentier, H.W., Walker, R.G. (eds.), Facies models revisited. SEPM Spec. Publ., vol. 84 (2006), pp 171–235

Dalrymple, R.W., Zaitlin, B.A., Boyd, R.: Perspective: Estuarine Facies models: conceptual basis and stratigraphic implications. J. Sediment. Res. **62**, 1130–1146 (1992)

Li, G., Boukhalfa, K., Teng, X., Soussi, M., Ben Ali, W., Ouaja, M., Houla, Y.: New early Cretaceous clam shrimps (Spinicaudata) from uppermost Bouhedma formation of northern Chotts range, southern Tunisia: taxonomy, stratigraphy and palaeoenvironmental implications. Cretac. Res. **72**, 124–133 (2017)

Ouaja, M., Gallala, W., Assila, B., Gaied, M.E., Montacer, M., Zargouni, F.: Dynamique sédimentaire des sables barrémiens en bordure nord orientale de la Plateforme saharienne (SE de la Tunisie). In: 13ème Congrès Français de Sédimentologie, Dijon, Livre des résumés, Publ. ASF, Paris N 68, 260 (2011)

New Insights on the Marine to Non-marine Oligo-Miocene Deposits of Northern Tunisia: Sedimentary Events and Paleogeography

Kamel Boukhalfa, Mohamed Soussi, and Ercan Özcan

Abstract

The gathering of new biostratigraphic results together with those already updated and collected from previous works on the Oligo-Miocene deposits of the Bejaoua and Fortuna groups from northern Tunisia allow the establishment of an accurate regional litho-biostratigraphic framework. Furthermore, the compilation of faunal assemblages and sedimentary facies enabled the precision of the spatiotemporal relationships between the marine and non-marine sedimentary events that recorded during this time interval and also the update of three key time interval paleogeographic maps. These illustrate the major transgressive and regressive sedimentary events recorded in the southern Tethyan realm of Tunisia during the Oligo-Miocene time interval.

Keywords

Oligo-Miocene • Stratigraphy • Sedimentary events • Paleogeography • Tunisia

1 Introduction

The Oligo-Miocene siliciclastic deposits of northern Tunisia have been ranged lithologically into two distinct successions: (1) the shallow marine to non-marine sediments of the Fortuna Group with the most extensive outcrops being found in the Northern Atlas; (2) the dominantly shallow marine glauconitic series of the Bejaoua Group, occurring in the Tellian zone. The Fortuna Group (Fortuna, Messiouta, Oued Hammam, and Ain Ghrab formations) has been deeply investigated and its stratigraphic, sedimentological, and paleogeographic features were outlined (Yaich et al. 2000). However, the Bejaoua Group is still relatively poorly known regarding its chronostratigraphy, facies distribution, and paleogeographic development (Rouvier 1977; Yaich et al. 2000; Boukhalfa et al. 2009, 2015).

2 Geological Setting and Methods

Seventeen sections have been systematically logged and investigated throughout the shallow marine to non-marine Oligo-Miocene succession of the Fortuna and Bejaoua groups cropping out in northern Tunisia (Fig. 1). The Fortuna Group which frequently crops out throughout the Northern Atlas encompasses the Fortuna, Messiouta, Oued Hammam, and Ain Ghrab formations. The Fortuna formation consists of a thick Oligocene marine claystone-sandstone succession interbedded with thin limestones and glauconite-bearing horizons and Aquitanian fluvio-deltaic strata (Yaich et al. 2000). The Fortuna formation may be locally overlain by different formations including Early Burdigalian red beds made of fine-grained sandy clays (Messiouta formation) or relatively younger deposits such as the Upper Burdigalian tidal to fluvial coarse-grained sandstones of Grijima formation (Yaich et al. 2000). This siliciclastic succession overlain by Early Langhian marine clays Oued Hammam formation is regionally capped by the Middle to Upper Langhian Ain Ghrab bioclastic carbonate formation (Yaich et al. 2000). However, the Oligo-Miocene Bejaoua Group of the Tellian zone is constituted by marine glauconite-rich mud-sandstone alternations and locally continental fluvial sandstone strata (Rouvier 1977; Boukhalfa et al. 2009, 2015).

K. Boukhalfa (✉)
Faculty of Sciences of Bizerte, University of Carthage, LR18ES07, 7021 Jarzouna, Tunisia

M. Soussi
Faculty of Sciences of Tunis, University of Tunis El Manar, LR18ES07, 2092 Tunis, Tunisia

E. Özcan
Faculty of Mines, Department of Geological Engineering, Istanbul Technical University, Maslak, 34469 Istanbul, Turkey

A. Çiner et al. (eds.), *Recent Research on Geomorphology, Sedimentology, Marine Geosciences and Geochemistry*, Advances in Science, Technology & Innovation, https://doi.org/10.1007/978-3-030-72547-1_31

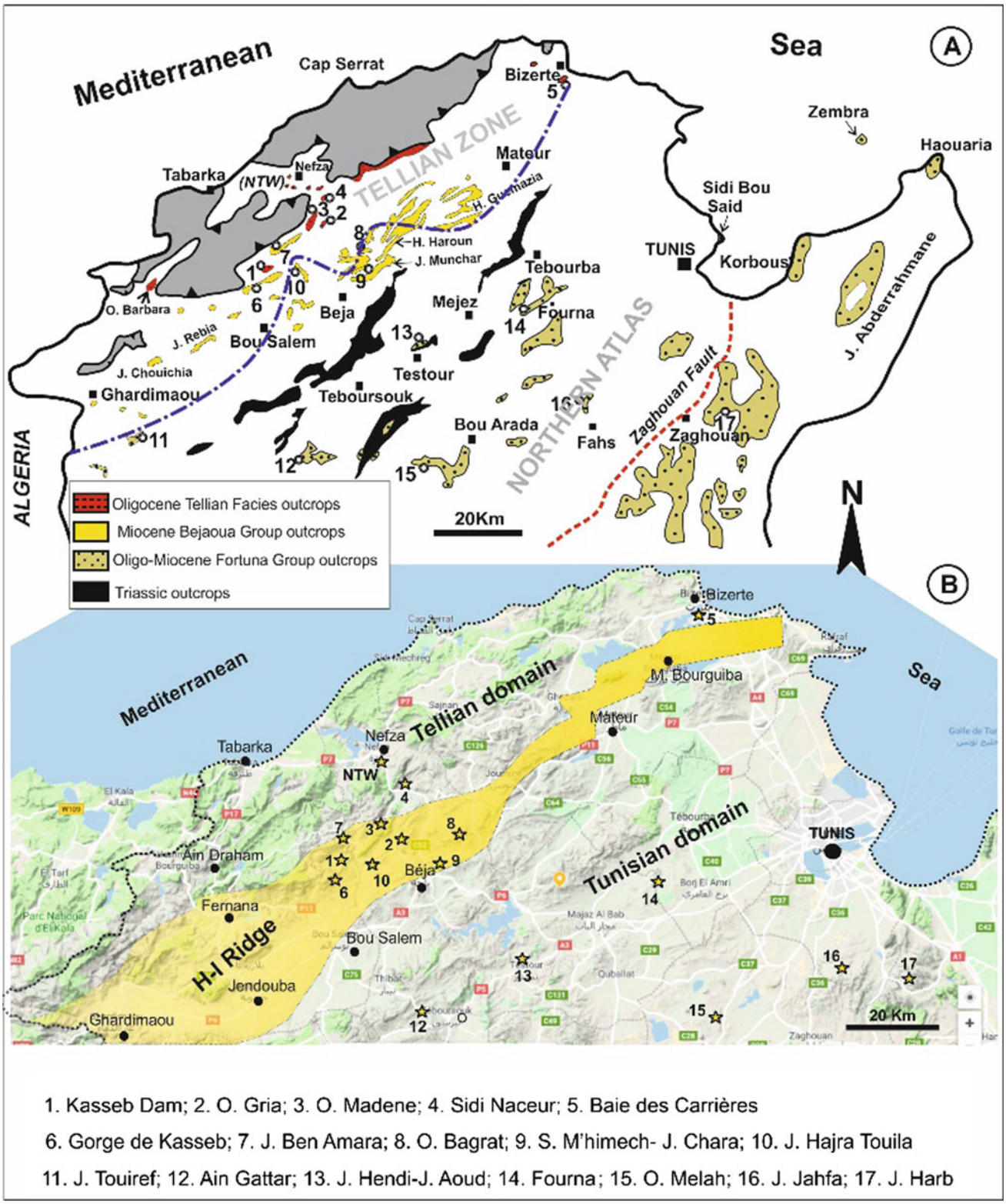

1. Kasseb Dam; 2. O. Gria; 3. O. Madene; 4. Sidi Naceur; 5. Baie des Carrières
6. Gorge de Kasseb; 7. J. Ben Amara; 8. O. Bagrat; 9. S. M'himech- J. Chara; 10. J. Hajra Touila
11. J. Touiref; 12. Ain Gattar; 13. J. Hendi-J. Aoud; 14. Fourna; 15. O. Melah; 16. J. Jahfa; 17. J. Harb

Fig. 1 **a** Oligo-Miocene outcrops of northern Tunisia showing the "Fortuna group" in the northern Atlas and the "Bejaoua group" in the Tellian zone. **b** The main paleogeographic domains of northern Tunisia at the end of the Eocene (Rouvier 1977). Tellian domain at the Northwest, Tunisian domain at the Southeast, in between, the NE-SW paleohigh lineament extended from J. Hairech (Ghardimaou) to J. Ichkeul (Bizerte) constitutes the H-I Ridge

The main purpose of this study was to provide a tool for understanding the chronology, paleo-environment, and paleogeography of the shallow marine to non-marine Oligo-Miocene stratigraphic sequences, mostly based on the new chrono-biostratigraphical constraints (planktic and large benthic foraminifera assemblages) associated with a synthesis and exhaustive review of previous data.

3 Results

3.1 Tellian Bejaoua Group: New Biostratigraphic Data

The Oligocene dominantly deep marine shales of the Tellian Kasseb unit (Rouvier 1977) revealed the presence of the P20/P21 planktic zone, whereas their mainly coastal shallow marine sandstone sequence yielded large benthic fauna represented by *Nephrolepidina praemarginata*. However, the Tellian Miocene successions, resting unconformably on the Paleocene series, yielded an Aquitanian–Burdigalian and Langhian planktic foraminifera associations (P7-P8 and P9) from the deep marine glauconitic shales, and the Aquitanian large benthic foraminifera *Miogypsinoides bantamensis* from the coastal shallow marine sandy limestone beds.

3.2 Bejaoua Group Versus Fortuna Group: Sedimentary Events and Lithostratigraphic Chart Updates

Three sedimentary events have been characterized throughout the main Oligo-Miocene stratigraphic successions of the Fortuna Group from the Tunisian domain (Fig. 2). The first sedimentary event (**SE1**), which extends from Oligocene to Aquitanian times (P18-N4), shows a thick shale interval interbedded by fine-grained sandstones and bioclastic (*Nummulites vascus*) sandy limestones horizons characterizing open marine depositional settings. The second sedimentary event (**SE2**), occurring during the Lower Burdigalian, is represented by a widespread occurrence of thick, coarse to very coarse-grained, cross-bedded fluvial sandstone. The last sedimentary event (**SE3**) consists of a shallow to open marine transgressive interval, which begins with shales and thin bioclastic limestone horizons during the Upper Burdigalian–Lower Langhian (N7/SBZ25-N8) and continues with bioclastic limestones of Upper Langhian (N9) age.

When compared to their coeval units of the Tunisian domain, the Oligo-Miocene lithostratigraphical series of the Bejaoua Group from the Tellian domain show three major particularities of considerable importance: (i) it is difficult, if not impossible, to unravel the detailed stratigraphic continuity of the Oligocene and Miocene strata, where their stratigraphic continuity is preserved, (ii) glauconite dominates throughout the Miocene deposits, and (iii) well-developed coarse-grained fluvial sandstones are lacking (Fig. 2).

4 Paleogeographic Reconstruction

At the end of the Eocene, two paleogeographic domains characterized the northern Tunisia: Tellian domain at the Northwest and Tunisian domain at the Southeast. A NE-SW elongated paleohighs (Hairech–Ichkeul Ridge (HIR)) separated these two domains (Rouvier 1977) (Fig. 1b).

During the Oligocene (30–27 Ma), the Tunisian domain recorded a clayey sedimentation with planktic and benthic

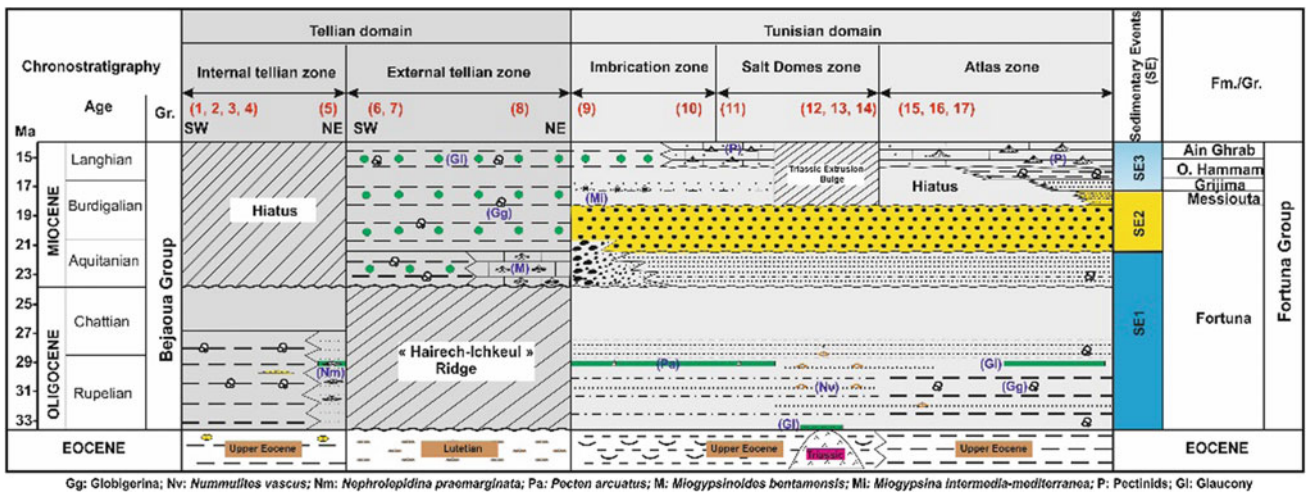

Fig. 2 Oligo-Miocene lithostratigraphic chart updates of the Bejaoua (Tellian domain) and Fortuna (Tunisian domain) groups of northern Tunisia

foraminifera assemblages that dominated the deepest parts of the basin with NE-SW and NW–SE trends. To the northwest, an elongated shallow shelfal zone extended from the western Zaghouan-NS Axis tectonic lineaments to the eastern Hairech–Ichkeul Ridge (HIR) area. Conversely, the Tellian domain that extended throughout the area located northwest of the HIR was characterized by a mainly outer shelf claystone/siltstone accumulation. During the Lower Miocene (22–20 Ma), predominantly coarse- to very coarse-grained sandstones were deposited over a wide area of the Atlas domain, while the Tellian domain received a fully marine glauconitic, mudstone/calcareous sandstone sedimentation. During the Middle Miocene (18–15 Ma), the main paleogeographic features recorded in Tunisia were the concomitant re-invasion of the sea and the establishment of marine deposition that prevailed in both Tunisian and Tellian domains.

The development of Tellian and Tunisian Oligo-Miocene basins is initiated by the inception of the horizontal tectonic movements of the Tellian units during the Late Oligocene (Rouvier 1977). Consequently, in front of this thrusted and uplifted Tellian area, a thick glauconitic-rich succession is developed instead of the HIR previously uplifted and progressively overwhelmed (Tell trough). Meanwhile, the Atlas domain is less deformed and a large carbonate platform was developed.

5 Conclusions

New biostratigraphic data coupled with the main sedimentary events recorded throughout the Oligo-Miocene Tellian and Atlas domains allow updating the lithostratigraphic chart as well as highlighting the paleogeography features of northern Tunisia during three key time intervals including the Oligocene, the Aquitanian, and the Langhian.

References

Boukhalfa, K., Amorosi, A., Soussi, M., Ben Ismail-Lattrâche, K.: Glauconitic-rich strata from Oligo-Miocene shallow-marine siliciclastic deposits of the Northern margin of Africa (Tunisia): geochemical approach for basin analysis. Arab. J. Geosci. **8**, 1731–1742 (2015)

Boukhalfa, K., Ben Ismail-Lattrâche, K., Riahi, S., Soussi, M., Khomsi, S.: Biostratigraphical and sedimentological analysis of the Eo-Oligocene and Miocene deposits of Northern Tunisia: stratigraphic and geodynamic implications. C. R. Geosci. **341**, 49–62 (2009)

Rouvier, H.: Géologie de l'Extrême nord-tunisien: tectoniques et paléogéographies superposées à l'extrémité orientale de la chaîne nord maghrébine. Thèse es Sciences, Université Paris VI, 703 p (1977)

Yaich, C., Hooyberghs, H.F., Durlet, C., Renard, M.: Corrélation stratigraphique entre les unités oligo-miocènes de Tunisie centrale et le Numidien. C. R. Acad. Sci. Paris **331**, 499–506 (2000)

Methane-Derived Carbonates Formation Triggered by the Latest Albian Anoxia in Northwestern Tunisia Basins

Moez Ben Fadhel and Njoud Gallala

Abstract

The organic-rich beds of Mouelha Member outcropping in northwestern Tunisia include authigenic carbonates typified by soft-sediment deformation (slumps) and doughnuts shaped concretions. Planktic foraminiferal biostratigraphy indicates a late Albian age (*buxtorfi* Subzone). The carbonate bodies display veins and fractures partially filled with impsonite (bitumen). Microfacies analyses of these bodies reveal multiple generations of carbonate cements, pyrite, and clotted pelmicrite. Scanning electron microscope (SEM) analysis performed on clotted micrite shows the presence of pyrite spheroids and micrometer-sized filamentous structures. Oxygen isotopes of micrite revealed slightly depleted values ranging from −3.92 to −0.6‰ PDB, similar to normal marine values. Depleted values of $\delta^{13}C$ (ranging between −36.88 and −11.63‰ PDB) for these carbonates suggested a methane-derived carbon source and its anaerobic oxidation. In addition, the ^{13}C moderate depletion suggests thermogenic methane or a petroleum source. These results provide unequivocal evidence that these carbonates are cold seeps related. The cold seep features indicate that microbial communities have used ascending methane fluids and contributed to the precipitation of authigenic carbonates. We suggest that contemporaneous volcanic intrusions into the basin may have triggered the release of thermogenic methane flux as cold seeps in the sedimentary basin. The accumulation of methane and other released gases in the water column is triggered by the presence of anoxic and sluggish waters. Therefore, they may be responsible for the upwelling of deep anoxic waters which contribute to the projection of carbonate bodies (e.g., chimney-like shape), indicating that authigenic carbonate precipitation is induced by anaerobic oxidation of methane.

Keywords

Northwestern Tunisia • Latest Albian • Cold seeps • Authigenic carbonates • Anaerobic oxidation of methane • Anoxic waters

1 Introduction

The latest Albian is a period characterized by greenhouse climate conditions, sea level rise, and high rates of organic carbon burial during short-lived interval named the Oceanic Anoxic Event OAE 1d or The Breistroffer Event (Bornemann et al. 2005; Ben Fadhel et al. 2011; Soua 2016). Time equivalent beds outcropping in northwestern Tunisia represent a black shale interval which includes peculiar isolated authigenic carbonate bodies (Layeb et al. 2012). These carbonate were interpreted as carbonate buildups derived from chemosynthetic microbial ecosystem fueled by methane seeps.

Additional field investigations performed on equivalent beds of Mouelha Member in the Kalaat Senan area would provide new insights on the formation of these authigenic carbonates and allow us to postulate relationships between them and contemporaneous black shale deposition.

2 Geological Setting

Three outcrops yielding embedded carbonate bodies have been studied (Fig. 1). Two outcrops which belong to the Dome Zone delineate Triassic extrusions (Cheid and Nebeur extrusions). The third carbonate body is located southward between the Kalaat Senan and El Khasba grabens, not far from the Tunisian-Algerian border.

M. B. Fadhel (✉)
Research Laboratory of Environmental Science and Technologies, Higher Institute of Sciences and Technology of Environment, University of Carthage, Borj Cedria, 2050 Tunis, Tunisia

N. Gallala
Civilization Department, High Institute of Theology Tunis, University of Ez Zitouna, 1008 Tunis, Tunisia

A. Çiner et al. (eds.), *Recent Research on Geomorphology, Sedimentology, Marine Geosciences and Geochemistry*, Advances in Science, Technology & Innovation, https://doi.org/10.1007/978-3-030-72547-1_32

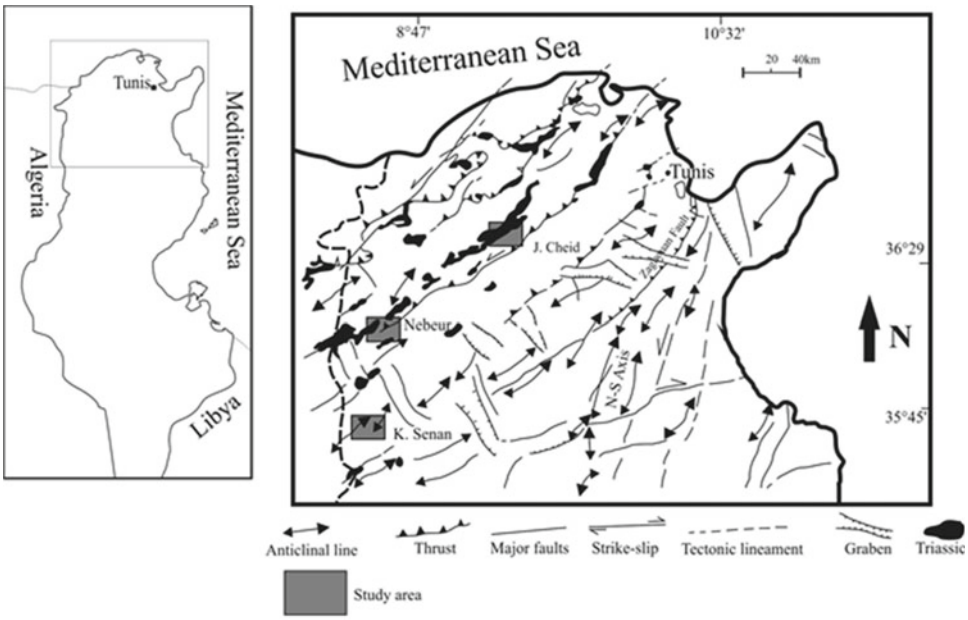

Fig. 1 Structural sketch of North Central Tunisia (Boutib et al. 2000; modified)

3 Results

The Mouelha Member consists of black whitish splintery marly limestone bed dated late Albian (base of the *buxtorfi* planktic foraminiferal Subzone). It includes cm-size and partly dolomitized carbonate mounds, flat concretions typified by soft-sediment deformation (slumps) and Chimney-like structure, and doughnuts-shaped concretions (Fig. 2).

The carbonate bodies display veins and fractures partially filled with impsonite (bitumen) and scalenohedral calcite crystals. Microfacies analyses of these bodies reveal multiple generations of fibrous and botryoidal calcite cements which morphologically resemble modern aragonites (Fig. 3b). Ankerite crystals, acicular and sparry calcite infilling cavities, in situ brecciation, framboidal pyrite, and fenestrae are also present, in addition to encrusting algae and clotted pelmicrite (Fig. 3a).

The scanning electron microscope (SEM) analysis performed on clotted micrite shows the presence of pyrite spheroids and micrometer-sized filamentous structures (Fig. 3c and d).

Fig. 2 Carbonate mud mounds embedded in the black shales of Mouelha Member. Note the doughtnut-like shape (**a**) and soft-sediment deformation (arrow, **b**), Kalaat Senan. The vein (arrows, **a**) is filled with impsonite (bitumen), Kalaat Senan, Note the chimney (**c**, Jebel Cheid area) and mound-shaped (**d**, Nebeur area) formations

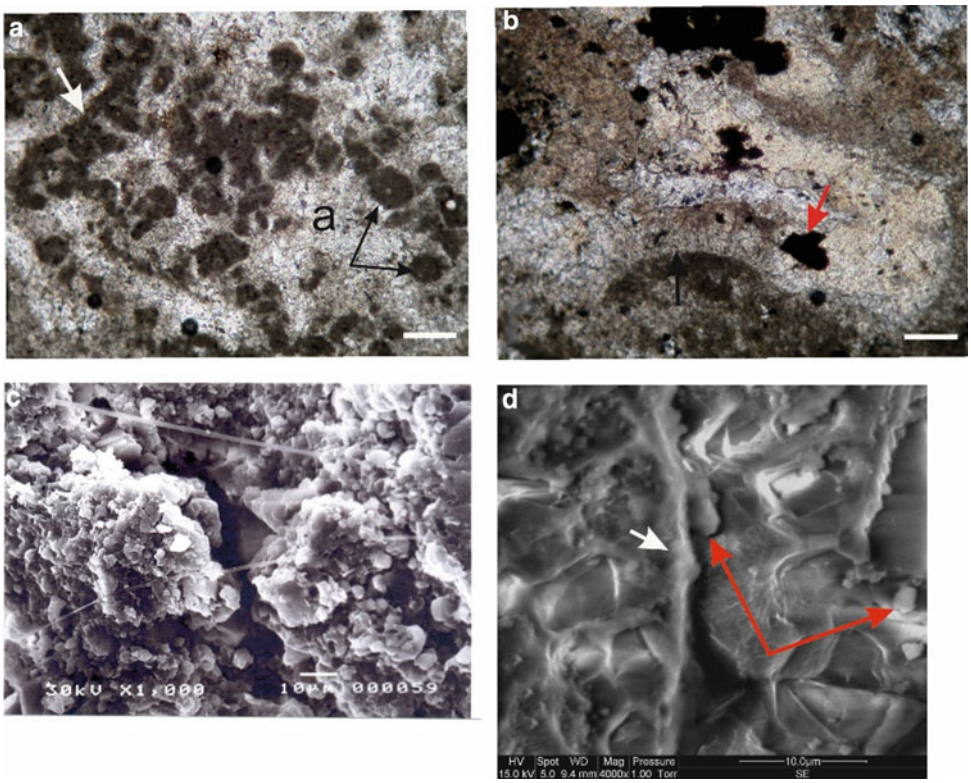

Fig. 3 Microfacies and SEM photographs of microbial structures from the carbonate bodies: **a** microfacies showing micrite clots (black arrow) and filaments-like structures (white arrows). The cavities are filled with drusy calcite cement (a) **b** microfacies showing botryoidal cement, lining cavities (black arrow). The botryoid consists of fibrous aragonite crystals. Note the pyrite crystals (red arrow) associated with the cavities. scale bar: 200 µm. **c** SEM photograph showing bacterial filaments surrounding micrite clots. (from Layeb et al. 2012). **d** SEM photograph showing filaments (white arrow) and pyrite spheroids (red arrows)

Oxygen isotopes of micrite revealed slightly depleted values ranging from −3.92 to −0.6‰ PDB, similar to normal marine values. Depleted values of δ13C range between −36.88 and −0.47‰ PDB (Fig. 4).

4 Discussion

The depleted values of $\delta^{13}C$ for these carbonates suggest a methane-derived carbon source and its anaerobic oxidation (Pekmann et al. 2001; Pierre et al. 2017). The presence of bitumen inside the veins of Kalaat Senan carbonate formations indicates that fluids contain oil in addition to methane (Peckmann et al. 2011). In addition, moderately depleted values $\delta\ ^{13}C$ (> −40 ‰ PDB) are likely to suggest thermogenic methane or a petroleum source; it can also be a mixture of methane-derived carbon with marine carbonate (Kuechler et al. 2012; Loyd et al. 2016). These results provide unequivocal evidence that these carbonates are cold seeps related, developed during the late Albian.

The cold seep features indicate that microbial communities have used ascending methane fluids and contributed to the precipitation of authigenic carbonate via methane oxidation under strictly anaerobic conditions (Smrzka et al. 2017).

The accumulation of methane and other released gases (CO_2, H_2S) in the water column is triggered by the presence of anoxic and sluggish waters (Ryskin 2003). Therefore, they may be responsible for the upwelling of deep anoxic waters which contribute to the projection of carbonate bodies (e.g., chimney-like shape), indicating that authigenic carbonate precipitation is induced by anaerobic oxidation of methane (Peckmann et al. 2001).

We suggest that contact metamorphism linked to contemporaneous volcanic intrusions in the organic-rich beds may have triggered the release of thermogenic methane flux to the sedimentary basin through cold seeps. At this point, it is debatable if the methane was mostly sequestered by the anaerobic oxidation of methane (AOM) process and authigenic carbonate formation, or if the methane was in part emitted to the atmosphere together with CO_2 (Svensen et al. 2007).

5 Conclusions

Petrographic features in addition to depleted carbon and oxygen values obviously indicate that the investigated authigenic carbonate concretions are related to methane cold seeps.

We conclude that a contemporaneous volcanic intrusion in black shales may have triggered the release of thermogenic methane, which is considered as a mechanism among others causing carbon cycle perturbation and thus the widespread of regional anoxia in deep basins of northwestern Tunisia during the latest Albian. The accumulation of released methane in the water column is enhanced by the presence of anoxic and sluggish waters. As a consequence,

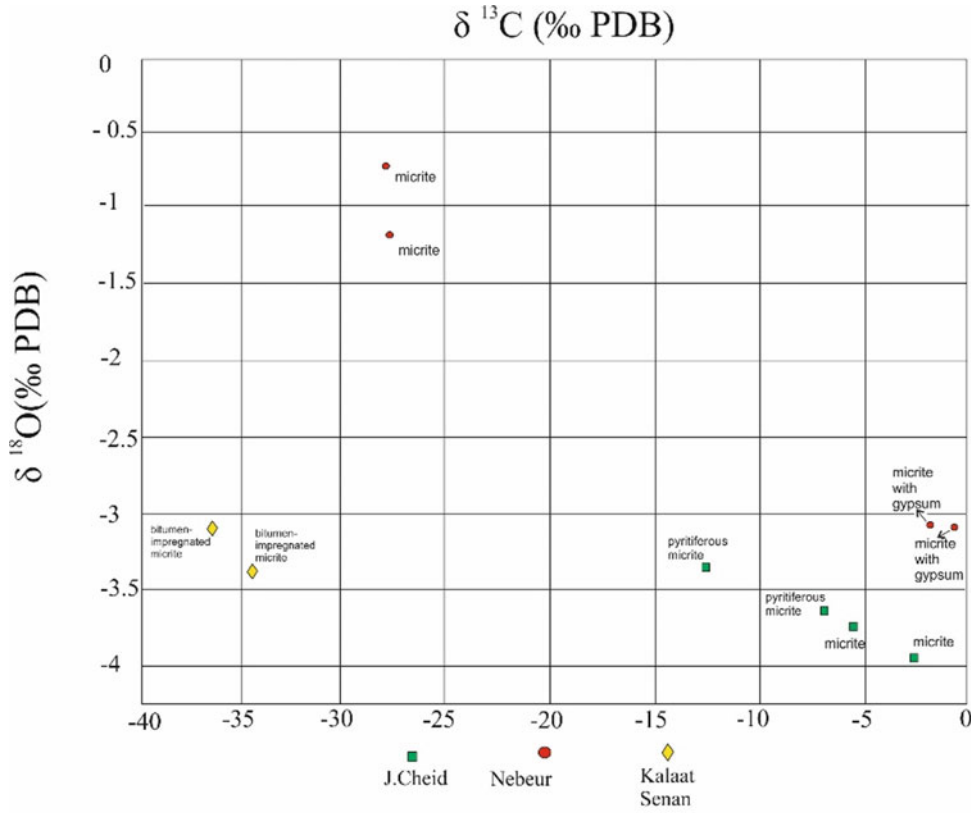

Fig. 4 Carbon and oxygen isotopes of carbonate concretions

anoxic waters tend to ascend to the surface, thereby contributing to the projection of carbonate bodies which is closely linked to anoxic environment and induced by the anaerobic oxidation of methane.

References

Ben Fadhel, M.B., Layeb, M., Hedfi, A., Youssef, M.B.: Albian oceanic anoxic events in northern Tunisia: biostratigraphic and geochemical insights. Cretac. Res. **32**(6), 685–699 (2011)

Bornemann, A., Pross, J., Reichelt, K., Herrle, J.O., Hemleben, C., Mutterlose, J.: Reconstruction of short-term palaeoceanographic changes during the formation of the Late Albian 'Niveau Breistroffer' black shales (Oceanic anoxic event 1d, SE France). J. Geol. Soc. **162**(4), 623–639 (2005)

Boutib, L., Melki, F., Zargouni, F.: Tectonique synsedimentaire d'age cretace superieur en Tunisie nord orientale; blocs bascules et reorganisation des aires de subsidence. Bulletin de la Société Géologique de France. **171**(4), 431–440 (2000)

Kuechler, R.R., Birgel, D., Kiel, S., Freiwald, A., Goedert, J.L., Thiel, V., Peckmann, J.: Miocene methane-derived carbonates from Southwestern Washington, USA and a model for silicification at seeps. Lethaia **45**(2), 259–273 (2012)

Layeb, M., Ben Fadhel, M., Ben Youssef, M.: Thrombolitic and coral buildups in the Upper Albian of the Fahdene basin (North Tunisia): stratigraphy, sedimentology and genesis. Bull. Soc. Geol. Fr. **183**(3), 217–231 (2012)

Loyd, S.J., Sample, J., Tripati, R.E., Defliese, W.F., Brooks, K., Hovland, M., Lyons, T., et al.: Methane seep carbonates yield clumped isotope signatures out of equilibrium with formation temperatures. Nature Commun. **7**, 12274 (2016)

Peckmann, J., Kiel, S., Sandy, M.R., Taylor, D.G., Goedert, J.L.: Mass occurrences of the brachiopod Halorella in Late Triassic methane-seep deposits, Eastern Oregon. J. Geol. **119**(2), 207–220 (2011)

Peckmann, J., Reimer, A., Luth, U., Luth, C., Hansen, B.T., Heinicke, C., Reitner, J., et al.: Methane-derived carbonates and authigenic pyrite from the Northwestern Black Sea. Mar. Geol. **177**(1–2), 129–150 (2001)

Pierre, C., Demange, J., Blanc-Valleron, M.M., Dupré, S.: Authigenic carbonate mounds from active methane seeps on the Southern Aquitaine Shelf (Bay of Biscay, France): evidence for anaerobic oxidation of biogenic methane and submarine groundwater discharge during formation. Cont. Shelf Res. **133**, 13–25 (2017)

Ryskin, G.: Methane-driven oceanic eruptions and mass extinctions. Geology **31**(9), 741–744 (2003)

Smrzka, D., Zwicker, J., Kolonic, S., Birgel, D., Little, C.T., Marzouk, A.M., Peckmann, J., et al.: Methane seepage in a Cretaceous greenhouse world recorded by an unusual carbonate deposit from the Tarfaya Basin, Morocco. Depositional Rec. **3**(1), 4–37 (2017)

Soua, M.: Cretaceous oceanic anoxic events (OAEs) recorded in the Northern margin of Africa as possible oil and gas shale potential in Tunisia: an overview. Int. Geol. Rev. **58**(3), 277–320 (2016)

Svensen, H., Planke, S., Chevallier, L., Malthe-Sørenssen, A., Corfu, F., Jamtveit, B.: Hydrothermal venting of greenhouse gases triggering early Jurassic global warming. Earth Planet. Sci. Lett. **256**(3–4), 554–566 (2007)

A Sedimentological, Mineralogical and Geochemical Assessment of the Upper Albian Oceanic Anoxic Event (OAE1d) of the Mouelha Member in the Fkirine Area (El Djehaf Anticline, Northern Tunisia)

Salma Soussi, Amina Mabrouk, Mabrouk Bachari, Fares Khemiri, and Anis Belhaj Mohamed

Abstract

The analysed 70 m of the uppermost Albian–Cenomanian sediments at El Djehaf outcrop, northern Tunisia, shows the occurrence of an oscillation between black to grey organic-rich pelagic limestones-black laminated limestones and organic-poor light grey limestones. The $CaCO_3$ contents range between 77 and 97% (X-ray analysis). A punctual biostratigraphic investigation based on the first occurrence (FO) of the *Rotalipora Globotruncanoides* and its associated species defines the beginning of the Cenomanian. Geochemically, the black laminated limestones (U_1 and U_3 of Mouelha Member) mark the highest TOC content reaching 9.07%. These levels are inferred as very good oil-prone (type II/III) mature source rock which was deposited in an anoxic environment. The mineralogical (XRD) and geochemical characteristics suggest a good play for conventional and unconventional resources. Furthermore, based on TOC data, facies characteristics constrained by biozonation, the section can be correlated to that of "Monte Petrano" in Italy. This study underlined the OAE1d event in the El Djehaf section and reconfirms its occurrence as a global anoxic event.

Keywords

Albian–Cenomanian boundary • El Djehaf section • OAE1d event • Sedimentology • TOC • Correlation

S. Soussi (✉) · A. Mabrouk · M. Bachari
Faculty of Sciences of Tunis, BSGP: Sedimentary Basins and Petroleum Geology Laboratory, El Manar University, 2092 Tunis, Tunisia
e-mail: amina.mabrouk@fst.utm.tn

F. Khemiri · A. B. Mohamed
Entreprise Tunisienne d'activités Pétrolière, Charguia II, CRDP: 2035 Tunis, Tunisia

1 Introduction

The studied area is situated in the Tunisian Backbone (Burollet 1981) in the Zaghouan governorate (Geological card n° 42 of «Djebal Fkirine» Office 1969). It is located in the region of El Fahs about 60 km SW of Tunis near Bled el Mahrouka village at coordinates of 36° N and 9° E.

Geologically, the El Djehaf anticline is bounded to the North by the Zaghouan accident (Turki 1980), to the South by the Nabhana graben, to the East by the Saouaf syncline and to the West by the Jurassic of Jebel Zaress and Jebel Fkirine mountains. The anticline structure of Jebel El Djehaf is around N35 in direction. It has a length of 15 km, with an average width of 5 km (Figs. 1 and 2).

2 Materials and Methods

A total of 68 samples was collected from 70 m interval of Jbel El Djehaf, and spanning the Late Albian-Early Cenomanian Lower Fahdene Formation. The average sample spacing varied between 50 cm and 1 m depending on the facies type and on outcrop conditions. The samples were collected for thin sections, X-ray diffraction (XRD) and foraminifera determination.

3 Results

3.1 Sedimentological Results

The quantitative and qualitative microscopic assessment highlights five microfacies types (Fig. 3), reoccurring throughout the vertical section without any specific order (Flügel 2004): (a) Fractured mudstone poor in planktonic foraminifera microfacies, (b) Well-bedded fine-grained, bioturbated mudstone-wackestone rich in planktonic

A. Çiner et al. (eds.), *Recent Research on Geomorphology, Sedimentology, Marine Geosciences and Geochemistry*, Advances in Science, Technology & Innovation, https://doi.org/10.1007/978-3-030-72547-1_33

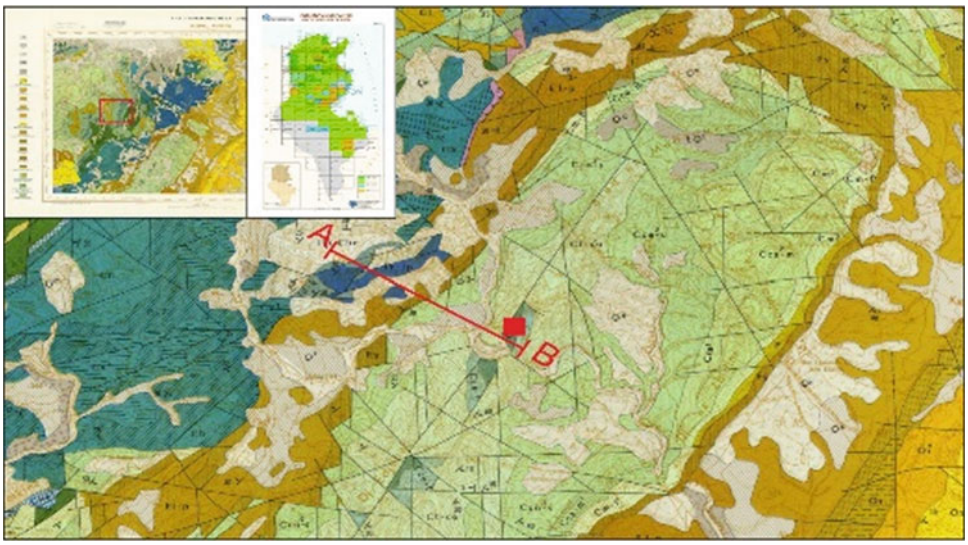

Fig. 1 Geology of fkirine structure area with "AB" as the studied section (Geological card n° 42 of «Djebal Fkirine» Office 1969)

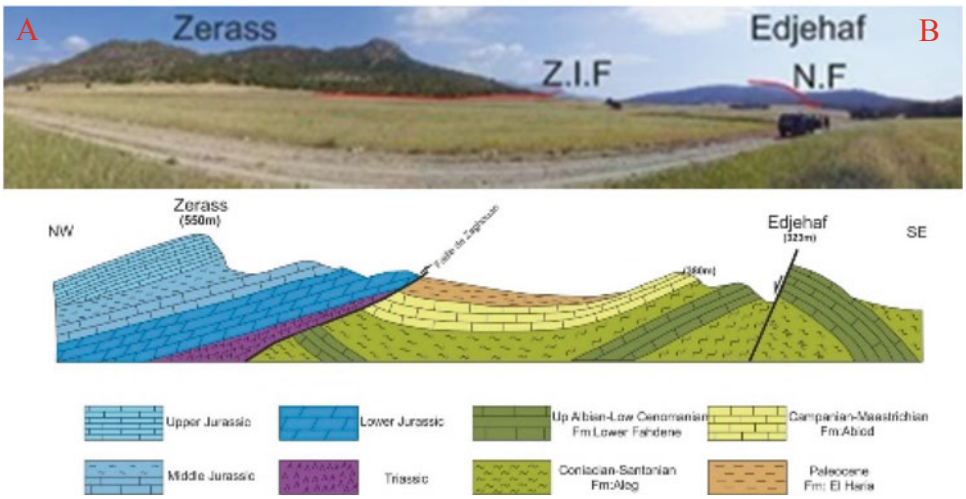

Fig. 2 The panoramic view and the geological-structural (schematic) section of the study area

foraminifera and calcispheres microfacies, (c) Fractured wackestone with planktonic foraminifera microfacies, (d) Fractured wacke-packstone rich in planktonic foraminifera microfacies, and (e) Laminated mud-packstone rich in planktonic foraminifera and filaments microfacies.

The zonal marker species (Premoli and Verga 2004) of *Rotalipora Globotruncanoides* (Fig. 4) indicating an Early Cenomanian age found at sample 53. For this reason, we believe that the Albian/Cenomanian boundary occurs around this thickness.

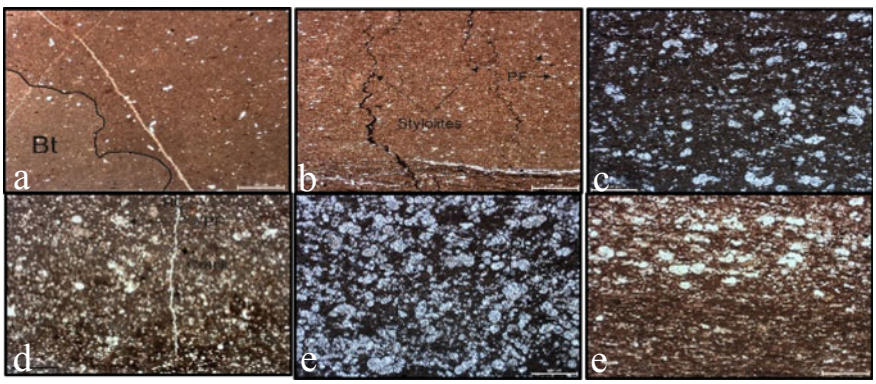

Fig. 3 Lower Fahdene formation microfacies of El Djehaf anticline

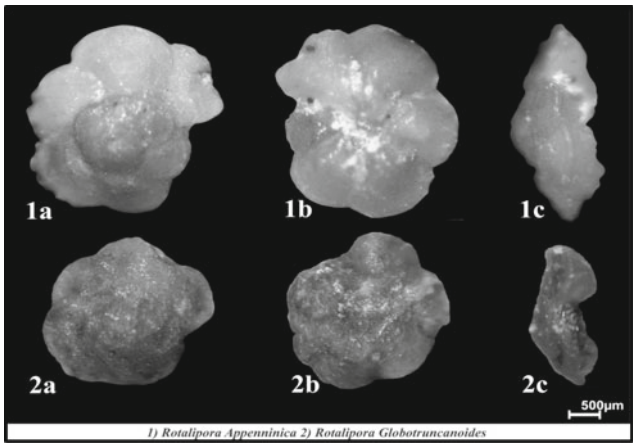

Fig. 4 The Albian/Cenomanian zonal markers identification

3.2 Mineralogical Results

Based on X-ray, the samples mainly consist of Calcite (Figs. 5 and 6) expressing Foraminiferal high productivity, accompanied with low proportions of land derived components (Quartz, Phyllosilicates) and the occurrence of hematite–pyrites affirming reduced conditions and the lack of oxygen in this bathyal environment.

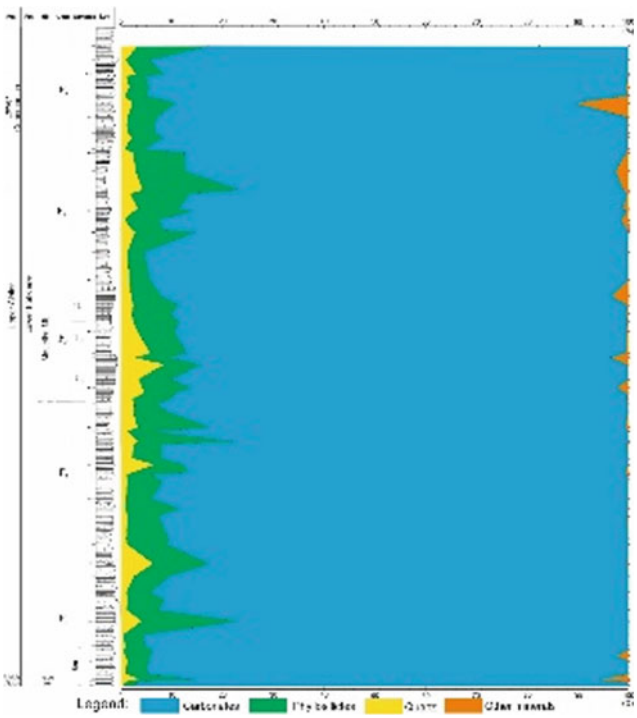

Fig. 5 The mineralogical trend curve of El Djehaf studied section

3.3 Geochemical Results

The geochemical analysis has shown that these black shale intervals are very rich in organic matter (9% TOC as the highest peak and ≃3% as a mean value of the interval) of mixed type (terrestrial and marine). The S2/S3 ratios are very high (<2 mg HC/g rock) suggesting the existence of layers that have produced liquid hydrocarbons. The rock-eval analytical results also suggests that these layers have already reached the oil window maturity. It is inferred that the El Djehaf facies has a very important organic carbon positive anomaly. Noting that high TOC values mainly correspond to high biostratigraphic occurrences and low calcite percentages (70–80%) (Khemiri 2015) (Table 1).

4 Discussion

The interpretation of the different microfacies and organisms defined in the studied Interval made it possible to elaborate a mixed terrigenous-calcareous sedimentation complex model. Within this bathyal zone, five major main sedimentary domains have been defined (Fig. 7). This subdivision is based on the relative position to the storm base limit (SWB) and the good-weather wave action limit (FWWB). Mud-wacke supported textures are typical for low-energy environment below wave base (Flügel 2004). The strong dominance of planktonic fauna and the high organic content suggest deposition in a relatively deep marine environment (Premoli and Verga 2004). The high organic production/fertility affirmed by the high calcite proportions in X-ray diffraction analysis and the water column redox conditions support these outcomes.

Based on biostratigraphic and geochemical (Khemiri 2015) ties confirming the planktonic marine origin and the maturity conditions, El Djehaf section encompasses the OAE1d event and therefore can be possibly correlated to the Monte Petrano (Giorgioni 2015) 60 m section in Italy (Fig. 8).

5 Conclusions

Herein, in the El Djehaf analysed section, an oscillation between black to grey, organic-rich pelagic fractured wacke-packstone/black laminated mud-packstone and organic-poor light grey fractured well-bedded fine-grained, bioturbated mudstone-wackestone microfacies, is sedimentologically identified. From a mineralogical point of view, the $CaCO_3$ content ranges between 77 and 97% in each

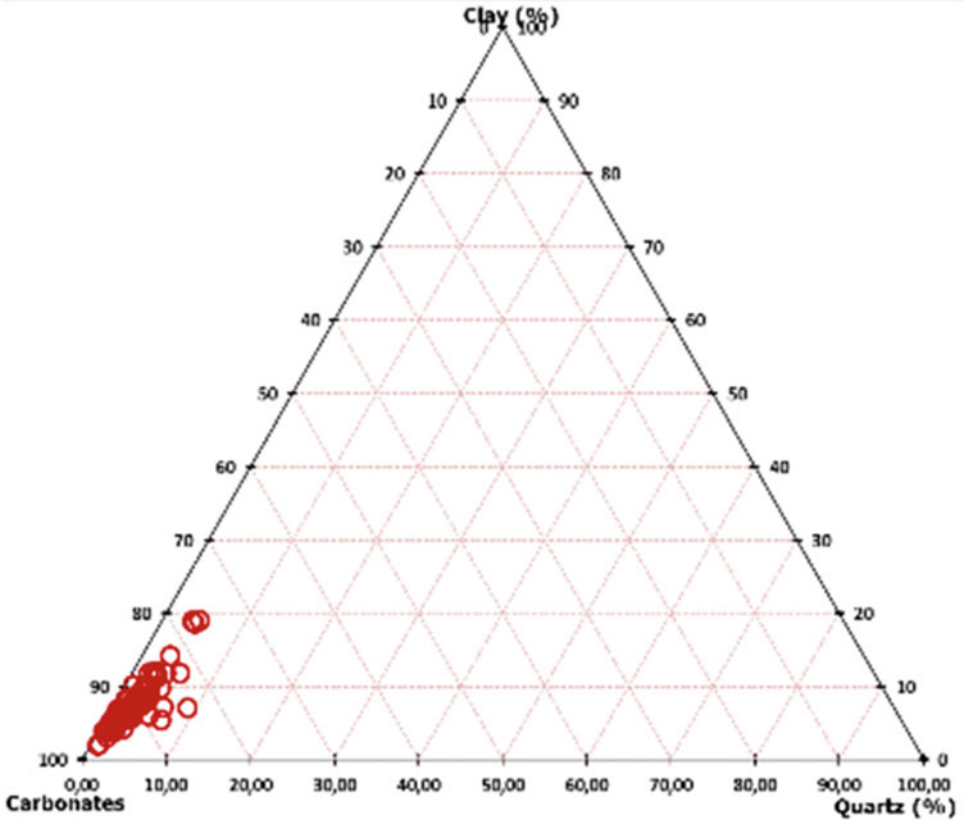

Fig. 6 Triangular diagram of the bulk rock mineral composition

Table 1 The minimum and maximum geochemical results of El Djehaf analysed samples

Parameters	TOC (%)		T_{max} (°C)		OI (mg CO_2/g TOC)		HI (mgHC/g TOC)		PP (mgHC/kg rock)		PI	
El Djehaf section	Min	Max	Min	Max	Min	Max	Min	Max	Min	Max	Min	Max
	1.23	9.07	443	447	6	24	329	557	3.77	54.67	0.03	0.26

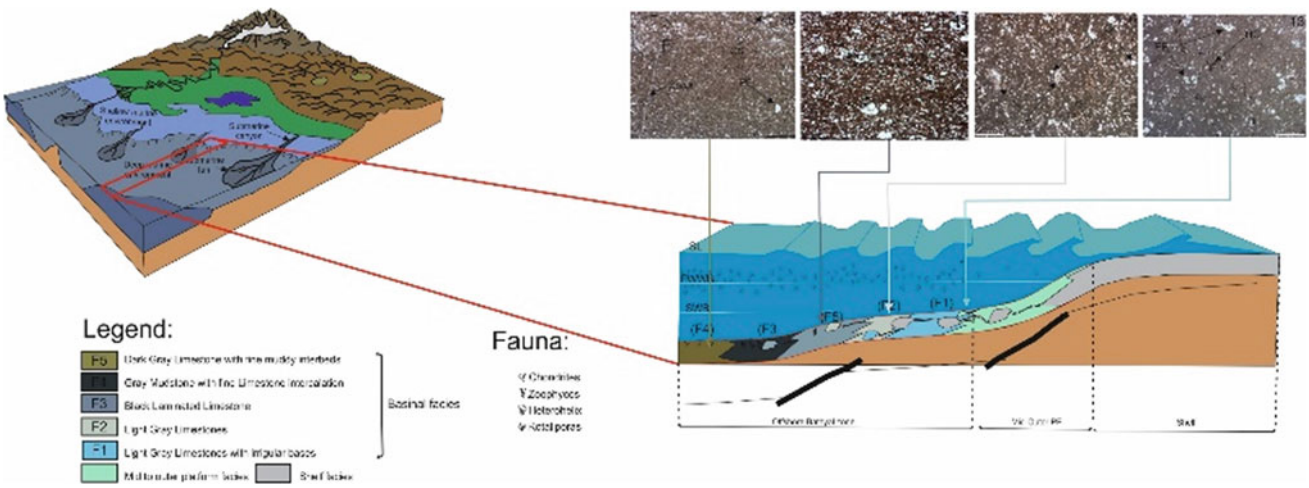

Fig. 7 The carbonate basin depositional model in the study area

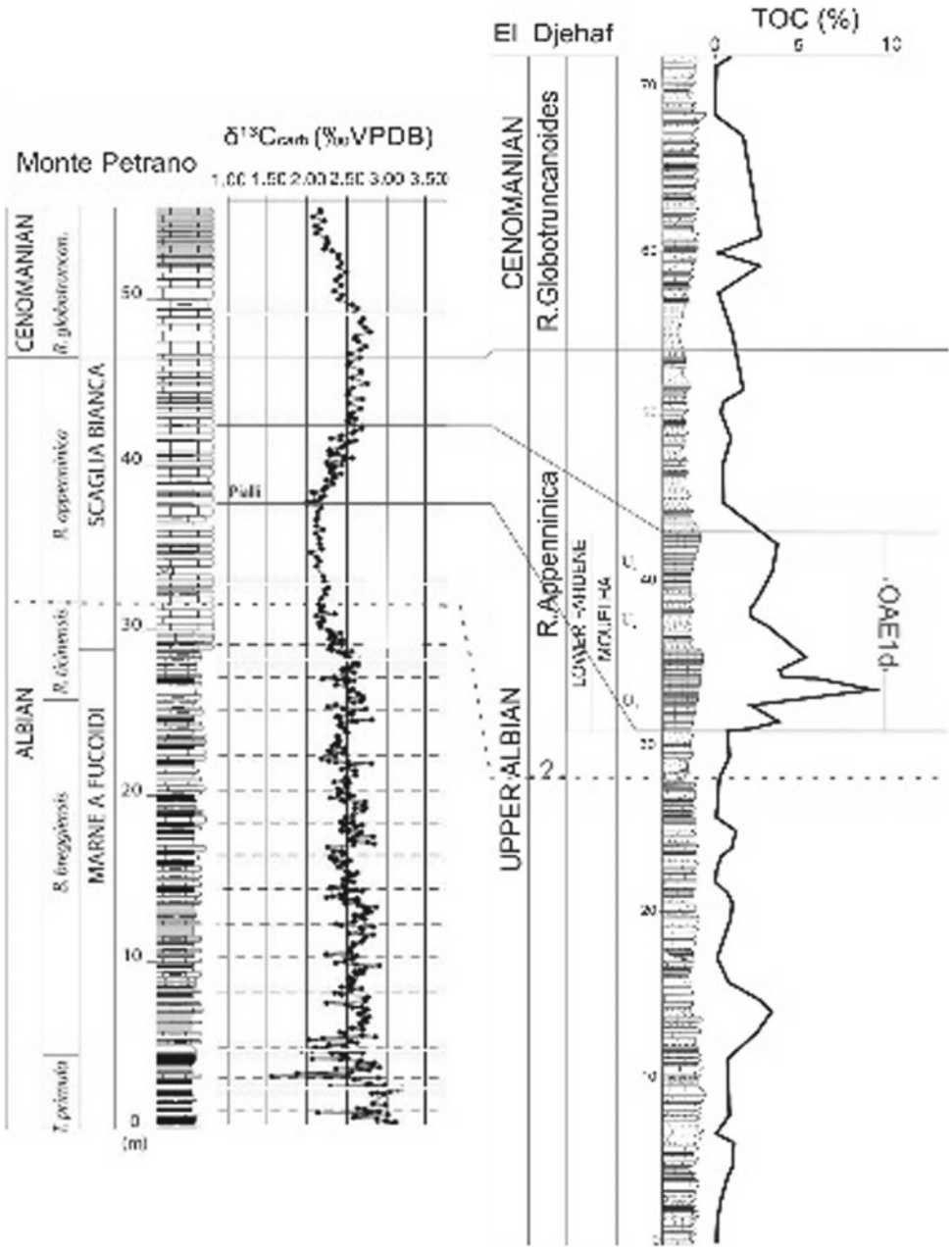

Fig. 8 The Monte Petrano δ13C and the El Djehaf TOC positive excursions (note that TOC and δ13C positive excursions are synonyms)

microfacies. The punctual biostratigraphic investigation revealed the FO of the *Rotalipora Globotruncanoides* and its associated species, signing the beginning of the Cenomanian in El Djehaf section. Geochemically, the black laminated limestones (U_1 and U_3 of Mouelha Member) mark the highest TOC content reaching 9.07%, and indicating a very good oil-prone (type II/III) source rock. The Late Albian/Early Cenomanian sediments of Mouelha Member of the Lower Fahdene Formation represents an Oceanic Anoxic Event concurred by the various used investigation methods. Furthermore, this study underlined the OAE1d event in the El Djehaf section and reconfirms its occurrence as a global anoxic event.

References

Burollet, P.F.: The Pelagian Sea east of Tunisia: bioclastic deposition under temperate climate. Mar. Geol. **44**(1–2), 157–170 (1981)

Flügel, E.: Microfacies of Carbonate Rocks, Analysis, Interpretation and Application. Springer, Germany (2004)

Geological card n° 42 of «Djebal Fkirine» Office Nationale des Mines (1969)

Giorgioni, M.: Paleoceanographic changes during the Albian-Cenomanian in the Tethys and North Atlantic and the onset of the Cretaceous chalk. Global Planet. Change **126**, 46–61 (2015)

Khemiri, F.: Characterization of Albian source rock at Jebel Djehaf, Fkirine area: correlation with oil seeps. Conference Presentation, ETAP (2015)

Premoli, S.I., Verga, D.: Practical manual of Cretaceous Planktonic foraminifera, International school on planktonic foraminifera. Third course: Cretaceous. Verga, Rettori (eds.) Universities of Perguia and Milan, Topografia Pontefelcino, Perguia (Italy) (2004)

Turki, M.: La faille de Zaghouan est la résultante de structures superposés (Atlas tunisien central). Bull. Soc. Geol. Fr. (3), 321–325 (1980)

The Diagenetic Nodules Significance in the Cretaceous Carbonate of the Akrabou Formation from Errachidia Region, Southern Morocco

Salem El Ouariti, Hicham Si Mhamdi, Zouhair Ait Taleb, Abdelmajid Benbouziane, Mouad Lyounsi, Rachid Essamoud, and Mustapha Mouflih

Abstract

This study presented the diagenetic nodules phenomenon of the Cretaceous carbonate of the Akrabou Formation. The results of the petrographic analyse revealed three types of nodules. The existence of a micritic matrix considered as the base of the exchange materials allowed the appearance of diagenetic markers as silicification and dolomitization. Geochemical analyses characterized three mineral phases: the siliceous phase, the carbonate phase (calcite and dolomite) and the clay phase. Each of these phases has variable rates; nevertheless, the carbonate phase is dominant in all the nodules. It corroborated with the calcimetric analysis where $CaCO_3$ values vary from 48 to 92% but the surrounding sediment rates show values from 32 to 54%. These variations seem to indicate a transfer of carbonate towards the nodules. The formation of the nodules occurred on the sites of accumulation of organisms, where the organic matter degraded favouring the synthesis of neogenic calcite. It would have constituted the early cement and the precursor of the early consolidation of the nodules. In addition, the intervention of the mechanical and chemical compaction causes a dissolution in the compacted zones. The nodules appear to be of diagenetic origin, formed under the combined action of organisms' destruction and diagenetic transformations production.

Keywords

Errachidia-Boudnib • Nodule • Cenomanian–Turonian • Sedimentology • Geochemistry • Organic matter • Diagenesis

1 Introduction

The Errachidia-Boudnib basin is part of the southern slope of the Moroccan Central High Atlas in the eastern part of the Pre-African Trench. It is bounded to the north by the South Atlantic Accident and to the south by the Hammada du Guir, forming an area of 70 km wide and 300 km long. This Cretaceous basin is part of the structural unit referred to as the Pre-African Trench. The study area forms a large asymmetric syncline between the High Atlas and the Anti-Atlas (Fig. 1).

The Cretaceous of Morocco's pre-African platform is subdivided into three lithological formations, including the Akrabou formation which is the subject of this work. The carbonate and clay–carbonate alternance sediments of this formation are attributed to the Cenomanian–Turonian and classified the stacking modalities into a spatial and temporal organization of five deposit sequences (SD1 to SD5). This work focused on the sedimentological, mineralogical and geochemical study of the nodules identified in the SD4 and SD5 sequences. Nodules show three main shapes: the smallest nodules are ellipsoidal, subspherical, discoidal with some nodules in the form of discs that resemble thin benches, interrupted in places and thus constituting what can be described as pseudo-beds. These two forms are present in the SD4 deposit sequence. The coalescent form shows very close nodules and touches each other. The latter form was found in the SD5 deposit sequence.

S. El Ouariti (✉) · Z. A. Taleb · A. Benbouziane · M. Lyounsi · R. Essamoud · M. Mouflih
Dynamics of Sedimentary Bassins and Geological Correlations Laboratory, Faculty of Sciences, University Hassan II of Casablanca, Ben M'Sick, Casablanca, Morocco

H. S. Mhamdi
Faculty of Sciences, Technics/University Moulay Ismail, Meknes, Morocco

A. Çiner et al. (eds.), *Recent Research on Geomorphology, Sedimentology, Marine Geosciences and Geochemistry*, Advances in Science, Technology & Innovation, https://doi.org/10.1007/978-3-030-72547-1_34

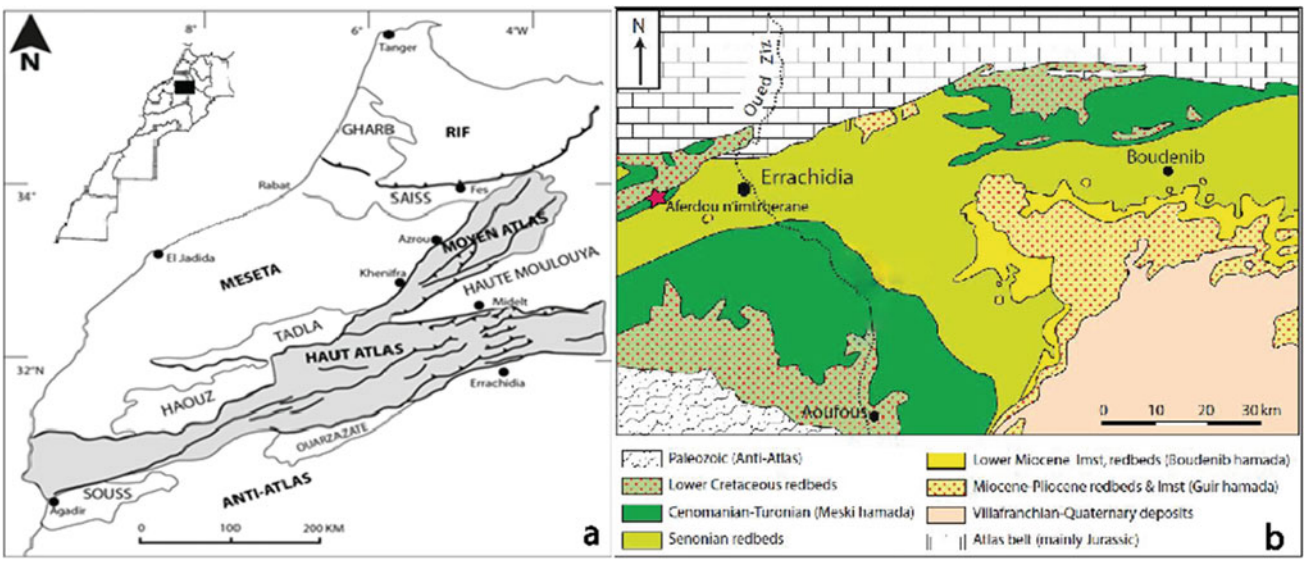

Fig. 1 **a** Structural domains of northern Morocco; **b** geological map of the Cretaceous of Errachidia basin (Zouhri et al. 2008)

2 Materials and Methods

For the microfacies study, the universal nomenclature requires the simultaneous use of the two most commonly used classifications, which are those of Dunham (1962) and (Folk 1959). They are complementary and, respectively, based on the nature of the allochems and their arrangements. For the study of the mineral phase, we used the X-ray diffractometer (type X' Pert Pro MPD from Panalytical), and finally for the geochemical study, we used the LECO RC612 which measures the total organic carbon (TOC) rate as well as the calcimeter for the determination of the $CaCO_3$ rate in the nodules.

3 Results

The petrographic study revealed three types of microfacies: Type 1 nodule is characterized by a packstone microfacies rich on lamellibrach rests and silicified debris. The type 2 nodule revealed a wackstone microfacies with pellets, ooliths and micritic cortex, and the type 3 nodule revealed mudstone microfacies rich in recrystallized bioclasts and idiotopic dolomite crystals. These three families of facies have recorded diagenetic processes such as silicification, which is quite frequent in nodule types 1 and 2 and is materialized by epigenetic organism rests. The dolomitization found mainly in type 3 nodules is expressed by the presence of idiotopic dolomite crystals. Magnesium seems to come from the degradation of organic matter and also the presence of palygorskite. The last marker is induced by ferruginization which is generally located along the cracks and stratiform lenses. Three mineral phases were identified (Fig. 2): carbonate, clay and siliceous. The carbonate phase consists of calcite and dolomite and is mainly prevalent in type 3 nodules. The clay mineral phase is mainly made up of palygorskite, chlorite, kaolinite, montmorillonite and sepiolite. Finally, the siliceous phase is well marked in types 1 and 2 nodules.

4 Discussion

The two sedimentary sequences of the nodulization phenomenon by carbonate and clay were revealed to be deposits. These deposits are arranged in elementary sequences a downshift and prograding configuration. The main diagenetic transformations were promoted by matter exchanges such as silicification, dolomitization and calcitization. The geochemistry and petrographic comparison results made it possible to define the diagenetic origin of nodulization and allowed specifying the nodules genesis.

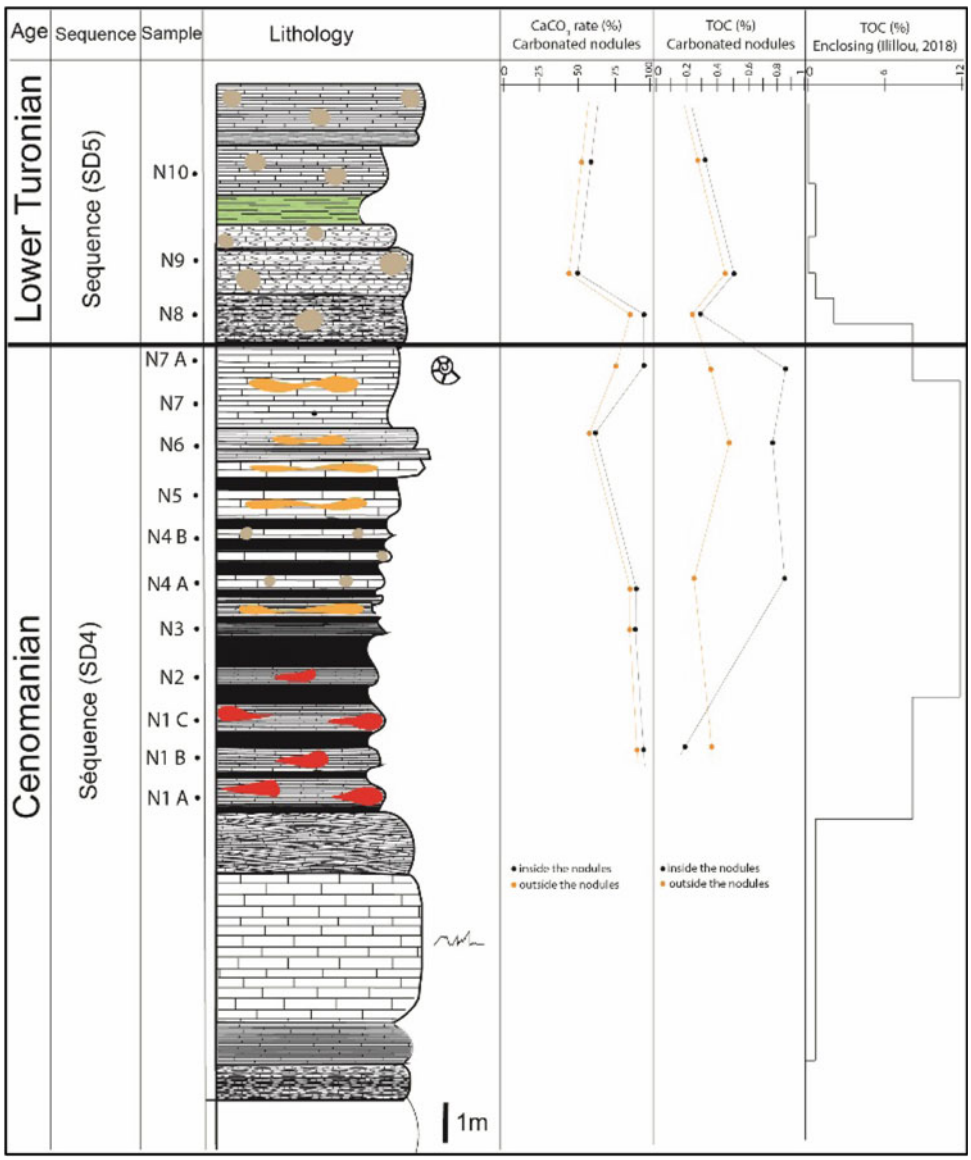

Fig. 2 Litho-geochemical column of the Jbel Tizdar (NW of the Errachidia-Boudnib basin)

5 Conclusions

The diagenetic transformations that contributed to the genesis of Jbel Tizdar's carbonate nodules were highlighted by: (i) the significant enrichment in carbonate (48–92%) in the concretions compared to the surrounding sediment (32–54%), which indicates a transfer of carbonate to the nodules. (ii) The silicification of the nodule from the centre to its periphery is mainly present in the first two types of nodules that have silicified outer crowns. (iii) The dolomitization encountered especially in type 3 nodules is showed by the presence of idiotopic dolomite crystals. The latter is closely linked to the high rate of palygorskite in the host rock and the degradation of organic matter.

References

Dunham, R.J.: Classification of carbonate rocks according to depositional texture. In: Ham, W.E. (ed.) Classification of Carbonate Rocks, vol. 1, pp. 108–121. American Association of Petroleum Geologists Memoir (1962)

Folk, R.L.: Practical petrographic classification of limestones. Am. Asso. Petrol. Geol. Bull. **43**, 1–38 (1959)

Zouhri, S., Kchikach, A., Saddiqi, O., El Haïmer, F.Z., Baidder, L., Michard, A.: The Cretaceous-Tertiary Plateaus. In: Michard, A. et al. (ed.) Continental Evolution: The Geology of Morocco. Lecture Notes 331 in Earth Sciences 116, c. Springer, Berlin, Heidelberg (2008)

Sedimentology and Paleo-environment of Phosphate Facies of the High Atlas of Marrakech (Morocco)

Salem El Ouariti, El Boukhari Hanane, Mohamed Amine Nguidi, Amine Bouwafoud, El Mostafa Benfrika, Abdelmajid Benbouziane, and Mustapha Mouflih

Abstract

The poorly studied phosphate assemblages of the eastern part of the High Atlas of Marrakech were the subject of a sedimentological, petrographic, granulometric, and mineralogical study, coupled with a description of macro- and microfacies of the geologic section surveyed in the field. Indeed, the results of the petrographic study revealed very similar compositions to those of the phosphates of central Morocco with a greater richness in detrital elements and faunal content: benthic foraminifera, ostracods, and algae. These facies testify for a marine sedimentation at the Amezmiz golf bottom, which is highly influenced by detrial inputs. The grain size analysis of phosphate facies reflects the characteristics of a very well-classified phosphate, dominated by a spherical shape to ovoid phosphate grains of different origins. There are also vertebrate bioclasts, benthic foraminifera, echinoids radioles, internal ostracods molds, and most often an abundant exogangue rich in detrital quartz. This composition suggests a closed, very shallow marine deposition environment with a strong continental influence. The first results relating to mineralogy provide valuable information on the mineral paragenesis, quality and quantity of these residual phosphate deposits. The results of these combined made it possible to assess the importance of phosphate sedimentation in this region.

Keywords

Phosphate • Sedimentology • High Atlas of Marrakech • Grain size analysis • Paleo-environment

1 Introduction

Moroccan phosphates are characterized by their importance in quantity and quality in the world. The terminal Cretaceous-Palaeogene series in Morocco is today a world reference for its phosphate richness and global geological events, particularly the crises at the Cretaceous-Tertiary (KT) and Palaeocene–Eocene (PETM) boundaries. In the vicinity of the major phosphate basins (Oulad-Abdoun, Ganntour, Meskala, and Oued Eddahab), the Moroccan subsoil contains other phosphate basins, as is the case of the Middle Atlas and the High Atlas of Marrakech. During the Senonian, the High Atlas included marine formations only in the Amezmiz Gulf (Cross et al. 1998). Away from the phosphates of central Morocco, the phosphates of the High Atlas of Marrakech are poorly documented scientifically, with very old, poorly updated studies. As part of a multidisciplinary approach, this work proposed the update of the rare and ancient works on the Cretaceous–Eocene series.

The study area is located about 80 km South of Marrakech and 15 km SW of Amezmiz (Azegour area), The Paleozoic is represented by metamorphosed and deformed sedimentary outcrops of Cambrian and Ordovician age, and magmatic outcrops represented mainly by Hercynian granite (Fig. 1).

2 Materials and Methods

The approach and methodology adopted to achieve the main objective involved two stages: a field stage and a laboratory stage. Field work consisted of surveying the geological sections, identifying the sedimentary discontinuities, figures, and sedimentary structures and detecting the fossiliferous content. The success of the laboratory work depended on the performance of a very tight systematic sampling. The laboratory work focused on sedimentology and geochemistry.

S. El Ouariti (✉) · E. B. Hanane · M. A. Nguidi · A. Bouwafoud · E. M. Benfrika · A. Benbouziane · M. Mouflih
Dynamics of Sedimentary Bassins and Geological Correlations Laboratory, Faculty of Sciences, University Hassan II of Casablanca, Ben M'Sick, Casablanca, Morocco

A. Çiner et al. (eds.), *Recent Research on Geomorphology, Sedimentology, Marine Geosciences and Geochemistry*, Advances in Science, Technology & Innovation, https://doi.org/10.1007/978-3-030-72547-1_35

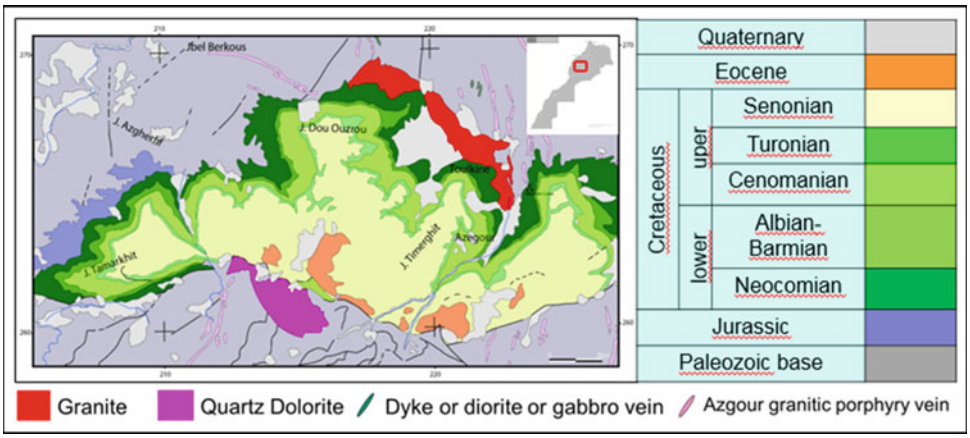

Fig. 1 Geological map of the study area compiled from the geological map of Amezmiz 1/100000 (M. Labriki et al. 1996: Carte géologique du Maroc. Notes et Mémoires du Service Géologique du Maroc N°372)

3 Results

In order to understand the sediment dynamics and the importance of phosphatogenesis in the Gulf of Amezmiz during the Senonian–Paleocene transition, a multidisciplinary approach was adopted. It enabled us to identify the following observations:

The microfacies study revealed a recurrence of high-energy barrier zone (or shoal) and low-energy intertidal zone environments. Overall, these microfacies are characterized by very diversified faunal associations (bryozoans, crinoids, lamellibranchs, gastropods, annelids, ostracods, benthic foraminifera…) and also by the richness in phosphate grains. This reveals that, from the base of the latest Cretaceous–Paleogene deposits, the sedimentation environment is a marine environment very favorable to life. It is a platform with carbonate sedimentation highly influenced by phosphate input.

The facies of the Tessilat-Médinat section are structured in seven deposition sequences. The sequences, of Senonian age, are dominated by regressive trends. These sequences reflect the continental influence of the edge of the Gulf of Amezmiz by a more or less distal alluvial cone sedimentation. The Paleocene and Eocene sequences are marked by a marine sedimentation with transgressive phosphate deposits variably sandy and marly (Fig. 2).

Figure 3 presents the results of the geochemical analysis of the Tassilat-Medinat section. This figure shows the evolution of the contents of the chemical elements over time (Fig. 3).

4 Discussion

The Tessilat-Médinat section shows seven depositional sequences. The Senonian age sequences are dominated by regressive trends that indicate the progradation of continental sedimentary systems. Paleocene deposition sequences are rather retrograde and are characterized by transgressive, sandy and marly phosphate-rich trends (Fig. 2).

The "SD1" sequence of Senonian age is relatively distant from the supply sources. This sequence occurs in a more or less distal alluvial cone domain.

Above, the coarse material (which becomes finer) alternates with sandstone and microconglomerate beds. Rivers become braided, meandering with an average grain size sorting. On the other hand, the transgressive regime is characterized by the alternation of thinner conglomeratic sandstone beds (Fig. 2a).

The "SD2" sequence is characterized by light grayish-gray phosphate-rich and microfosiliferous limestone. Under a microscope, this limestone presents a wackstone texture and a micritic binding phase with a diverse microfauna (lamelli-branch, bryozoans, echinoderms plates, gastropods, phosphatized foraminifera, and phosphatized bioclastes), phosphate grains, small coproliths of lithoclasts, and some quartz grains. These facies indicate a relatively shallow subtidal to intertidal deposition environment. They are overlain by gray phosphated sand (80 cm).

The regressive period of this sequence is characterized by phosphate-rich limestone rich in detrital elements with nodule silicification and thick greenish marls slightly phosphated. The thin sections of these limestones show a wackstones texture that shows a micritic binding phase with a faunal association (lamellibranchs, gastropods, annelids, bryozoans), some phosphate grains, and rare large detrital quartz grains. This microfacies are characterized by recrystallization and dolomitization.

The "SD3" sequence of Paleocene age is characterized by an alternation of greenish, slightly phosphatized, and calcareous marls. Under microscope, these calcareous marls show packstone to wackstone textures, bioclasts (ostracodes, small benthic foraminifera, vertebrates, echinoderms plates, bryozoans), coproliths, quartz grains in places, and silicates recrystallization.

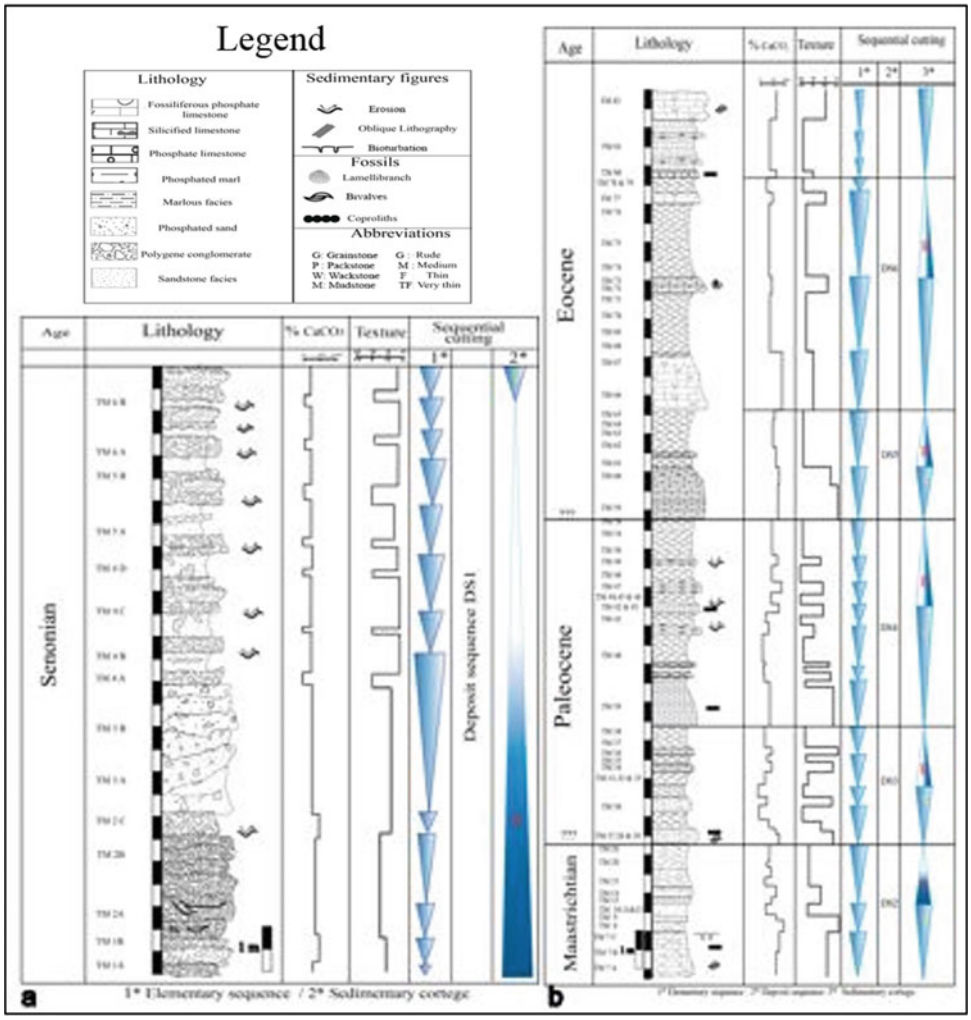

Fig. 2 Deposit sequences of the Tassilat-Medinat section (**a** lower part of the section and **b** upper part of the section)

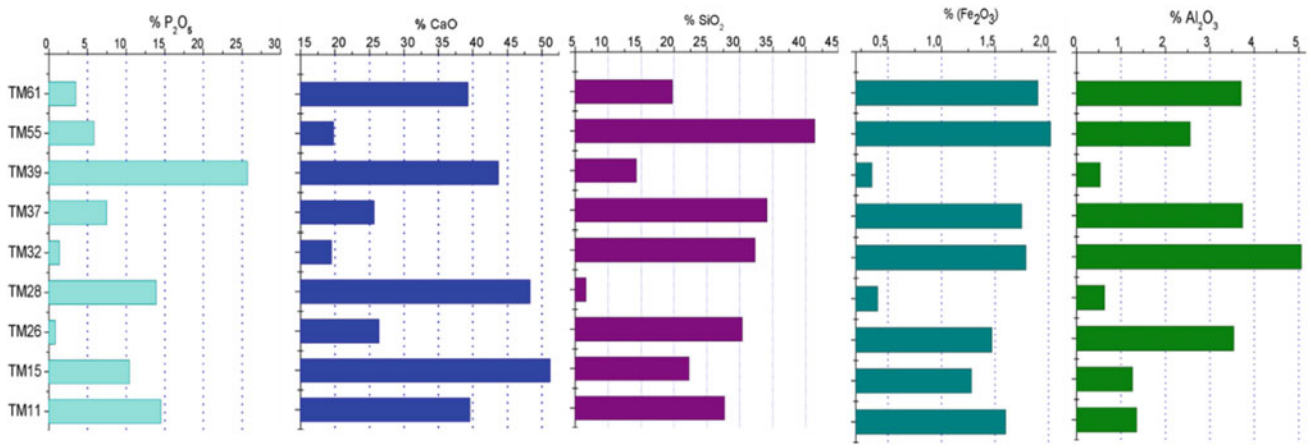

Fig. 3 Chemical composition of some samples of the Tassilat-Medinat section

The "SD4" sequence of probable Thanetian age is also defined by the alternation of slightly phosphated marls and limestone beds. This alternation is first thinning-upward and then thickening-upward. The limestone beds are sometimes capped by very coarse flint nodules with a detritic texture and polygenic aspect. Under a microscope, these limestones

present packstones to grainstones textures with bioclasts, phosphate grains, ooliths, coproliths, and carbonate grains surrounded by a cement. In addition, the lithographic pressure caused a dolomitization of the binding phase (dolomicrosparite).

The "SD5" sequence is made up of phosphate-rich limestones with silicifications on the top and slightly phosphatized marls. The limestones show a packstone/grainstone textures with bioclasts (bivalves), coprolites, phosphate grains dominated by pellets, quartz grains, small dolomite rhombohedras, and a micritic binding phase with the presence of a secondary phase such as cement dolomitization (baroque type). The regressive phase of the "SD5" sequence is characterized by phosphate-rich limestones. The latter are bioturbated and distinguished by the presence of discontinuities marked by iron oxides and marl facies.

The "SD6" sequence of Eocene age is characterized at the base by phosphatized limestones with cracked Nautile and breccia on the surface. Microfacies show packstone textures with bioclasts (bivalves, echinoderms plates) coprolites, phosphate grains, detrital grains, and a micritic binding phase whitish and greyish brown with a phosphate content. In the middle, the "SD6" sequence presents a packstone microfacies rich in fossils (bryozoans, echinoderms plates, coproliths,…) and a microsparite matrix dominated by quartz grains. The upper part of this sequence is characterized by a wackstone microfacies rich in bioclastic calcified elements (gastropods and bryozoans) and lithoclasts and a microsparite matrix.

The "SD7" sequence exhibits a transgressive trend. It is characterized by the alternation of phosphatic marls with beige limestones with flint. The microfacies present packstone textures containing coprolites, bioclasts in places (lamellibranchs plates of echinoderms), detrital grains, and a micritic to microsparitic binding phase.

The geochemical analysis of the major elements of some samples of the Tassilat-Médinat section provides a valuable clarification on the quality and quantity of phosphate deposits and reveal levels which do not exceed the 26% in P_2O_5 (Fig. 3).

5 Conclusions

Our sedimentological and stratigraphic study and a detailed sampling allowed assessing the importance of phosphate sedimentary deposits. The first results show compositions similar to those of the phosphates in Central Morocco and differ by a richness in detrital elements, benthic foraminifera, ostracods, and algae. The petrographic study of the microfacies reflects a recurrence of high-energy (barrier zone or shoal) and low-energy (internal platform or lagoon) environments. The type of stacking represents sequences specific to the environment and places them in different river environments; from the proximal alluvial plain with a conical character to the distal plain with a floodplain character. From the different studied sections, the typical sequences, which have a genetic value (Cross et al. 1998), refer to a depositional environment.

The sedimentology and geochemistry provide a valuable clarification on the quality and quantity of phosphate deposits. All these lead to the conclusion that the actual P_2O_5 content of the phosphate-rich layers results from the antagonistic effects of calcitization, on the one hand, and the weathering dissolving calcite, on the other.

References

Choubert, G., Salvan, H.: Essai sur la paléogéographie du Sénonien au Maroc. Notes Et Mémoires Du Service Géologique Du Maroc **74**, 13–50 (1949)

Cross, N.E., Purser, B.H., Bosence, D.W.J.: The tectono-sedimentary evolution of a rift margin carbonate platform: Abu Shaar, Gulf of Suez, Egypt. In: Sedimentation and Tectonics in Rift Basins Red Sea: Gulf of Aden, pp. 271–295. Springer, Netherlands (1998)

Labriki, M.: Carte géologique au 1/100 000 d'Amizmiz Notes Mém. Serv. Géol. Maroc, **372** (1996)

Evolution of Upper Triassic Fluvial Systems Across North West Africa; the Interplay of Local Versus Regional Drainage Systems

James Lovell-Kennedy, Jonathan Redfern, John Argent, and Jason Caning

Abstract

The Middle to Upper Triassic "TAG-I" sandstones were deposited in a series of intra- and pericratonic basins that developed after the Hercynian orogeny on the Saharan Platform margin. They form a broad facies belt of continental clastics that extend from Morocco to Egypt. Recent wells drilled in Eastern Morocco have proven economic gas flow rates from Late Triassic continental sandstones—sourced from Palaeozoic shales and trapped with post-Hercynian rift structures. The play bears many similarities to the prolific TAG-I play in the Berkine Basin and offers potential for extension of this petroleum system farther west into Morocco. Reservoir quality and thickness is a key uncertainty, and better understanding of the depositional systems and provenance is critical to reducing uncertainty and predicting where the sandstones offer viable exploration target.

Keywords

Triassic • TAG-I • TAG-I • Morocco • Berkine

1 Introduction

The "TAG-I" sandstones were deposited in the Middle to Upper Triassic within a series of pericratonic basins that developed on the Saharan Platform margin, resting upon the Hercynian orogeny (Guiraud 1998; Turner et al. 2001). A complex suite of Triassic facies is exposed in Morocco along the inverted Mesozoic sequences of the Atlas Mountain Chain, providing an excellent opportunity to study the sedimentology of syn-rift sequences that formed during the early break up of Pangea. Augmented by data from petroleum exploration wells, the research is investigating how the basin fill changes both temporally and spatially. Integrating the wealth of previous work undertaken on the Triassic in Morocco and Algeria provides a robust regional framework on which to build further detailed work. Our study highlights the importance of the local versus regional provenance of clastics into the basins and the intra-basinal topographic controls on drainage that influences facies variation, with significance for prediction of sandstone reservoir distribution and quality.

J. Lovell-Kennedy · J. Redfern (✉)
North Africa Research Group, School of Earth and Environmental Science, Williamson Building, Oxford Road, Manchester, M13 9PL, UK
e-mail: jonathan.redfern@manchester.ac.uk

J. Argent · J. Caning
Sound Energy PLC, 4 Pembroke Road, Sevenoaks, TN13 1XR, UK

2 Materials and Methods

This study compared the provenance and character of the Triassic section outcropping in Oukaimeden Basin (F4, F5 and F6 sandstones with the age equivalent units in the Kerrouchen Basin, Middle Atlas); to outcrops in the Oujda Mountains in the Eastern Meseta and into the subsurface, accessing data from vintage and recent exploration wells, core and seismic from the recent Tendrara gas discovery.

3 Results and Discussion

The Oukaimeden Basin, in the High Atlas, is an inverted fault bounded intra-montane basin that shows evidence of active rifting and preserves a thick succession of Triassic sediments (Benaouiss et al. 1996; Domènech et al. 2015). The Triassic clastics were deposited within an intra-montane basin, to the east of a well-documented drainage divide (the Moroccan Arch) that separates basins influenced by the Atlantic realm from those to the east, influenced by Tethys. The main coarse clastic fluvial interval, Unit F5, contains

A. Çiner et al. (eds.), *Recent Research on Geomorphology, Sedimentology, Marine Geosciences and Geochemistry*, Advances in Science, Technology & Innovation, https://doi.org/10.1007/978-3-030-72547-1_36

thick, stacked fluvial channel deposits that record the presence of a large perennial fluvial system flowing to the east (Fabuel-Perez et al. 2009). Later, more ephemeral conditions prevailed, with thinner fluvial packages and interbedded aeolian, floodplain and alluvial fans facies. Towards the end of the Triassic, a thin restricted marine to tidally influenced unit is recognised that is interpreted to mark the most westerly extent of the Tethyan transgression in the Triassic.

Farther east, the Kerrouchen Basin, in the Middle Atlas, is an inverted asymmetric half graben filled by 600 m of Triassic syn-rift continental sediments (Lorenz 1976), which was inverted during the Cenozoic Atlasic Orogeny, preserving the original geometry (Laville et al. 2004). The fluvial packages observed at outcrop are thinner than in the Oukaimeden Basin, and basin fill is dominated by alluvial fan and alluvial plain/playa deposits. Though not well exposed, thick, stacked channel sandstones are recorded in the basin. This suggests the presence of an axial fluvial system, flowing subparallel to the main structural grain, interacting with more local lateral feeder systems source from the surrounding highs.

In the Eastern Meseta, outcrops are more limited, and thus the understanding of facies distribution is more uncertain. The few good sections in the Oujda Mountains record a distal low-energy facies, composed of basal locally derived angular conglomerates, overlain predominantly by mudrocks, with only very thin laterally restricted sandstones (Ouijidi et al. 2000). The section shows an increasing marine influence, with interbedded shallow water carbonate sequences.

South of the Oujda outcrops, the Triassic plunges into the subsurface and control points are limited to widely spaced exploration wells of varying vintage. Recent exploration wells drilled by sound energy offer a valuable modern data set, which together with 3D seismic would allow an improved understanding of the depositional system. The equivalent section in the Tendrara gas discovery displays an increasing proportion of fluvial sandstones compared to the Oujda outcrops, with evidence for stacked fluvial channels interbedded with floodplain mudstone and laterally equivalent alluvial fan deposits.

A heavy mineral study is being undertaken in order to constrain the provenance of these sediments and attempt to correlate between and within the sub-basins. Previous palaeocurrent data and published provenance studies suggest a drainage divide in Morocco, with the Massif Ancien/Moroccan Arch, separating the Atlantic realm to the west from the eastern Tethyan domain (Domènech et al. 2015; Fabuel-Perez et al. 2009). Palaeocurrent data from the Kerouchen basin also support a broadly eastward direction of transport for the axial system. Correlation to the east into the Tendrara Basin and onto Algeria, ultimately entering Tethys, was speculated.

Preliminary work on the composition of samples collected during recent fieldwork in the Kerouchen Basin has identified a distinct variation in clastic composition between the fluvial and alluvial systems. In the east, alluvial plain sediments contained granitic and carbonate clasts, likely derived from the local Hercynian basement of granites and carbonates. This suggests a large alluvial plain, with deposits derived from local basement palaeohighs.

The fluvial sands found in the west contain metamorphic clasts of a schistose nature, with an absence of granitic or carbonate clasts. In this locality, a contribution from an extra-basinal metamorphic source is indicated, which based on palaeocurrent analysis, is most likely located to the south-west of the basin. This supports previous works in the region, which also indicated an extra-basinal (Anti Atlas) source for the fluvial deposits (Fig. 1). Work is ongoing, but initial investigation suggests that the Kerrouchen Basin may offer an analogue for facies distribution in the Eastern Meseta.

4 Conclusions

Understanding the controls on facies distribution and burial history is key to defining the extent of potential Triassic reservoirs and extension of the play from away from the proven Berkine basin fairway. The initial analysis of facies distribution and provenance data from the Triassic basins in Eastern Morocco suggests the interplay of long distance axial systems, sourced from the Anti Atlas or further distant terrains, running subparallel to the main structural trend. This transports more mature clastics from the distal highlands, which are subsequently interbedded with less mature sandstones from more locally derived feeder systems. The role of intra-basinal topography through time and how this affects the distribution of fluvial systems and the ability to predict the distribution of local immature sediment source from basement blocks is important to constrain reservoir prediction. The facies distributions are placed with the context of the evolution of the sedimentary fill as the basins mature. The eventual influx of marine facies allowed the deposition of thick evaporates in many of the basins, which acts as the regional seal and forms the other very important component of the play.

The recent well results in Tendrara demonstrate a working petroleum system and the potential to deliver commercial flow rates from the TAG-I equivalent sandstones in Eastern Morocco, pointing towards the extension of the play for gas in tight Triassic sandstones along the entire margin. Detailed facies analysis and the development of appropriate depositional models will allow targeting of the optimum location to encounter the best reservoirs.

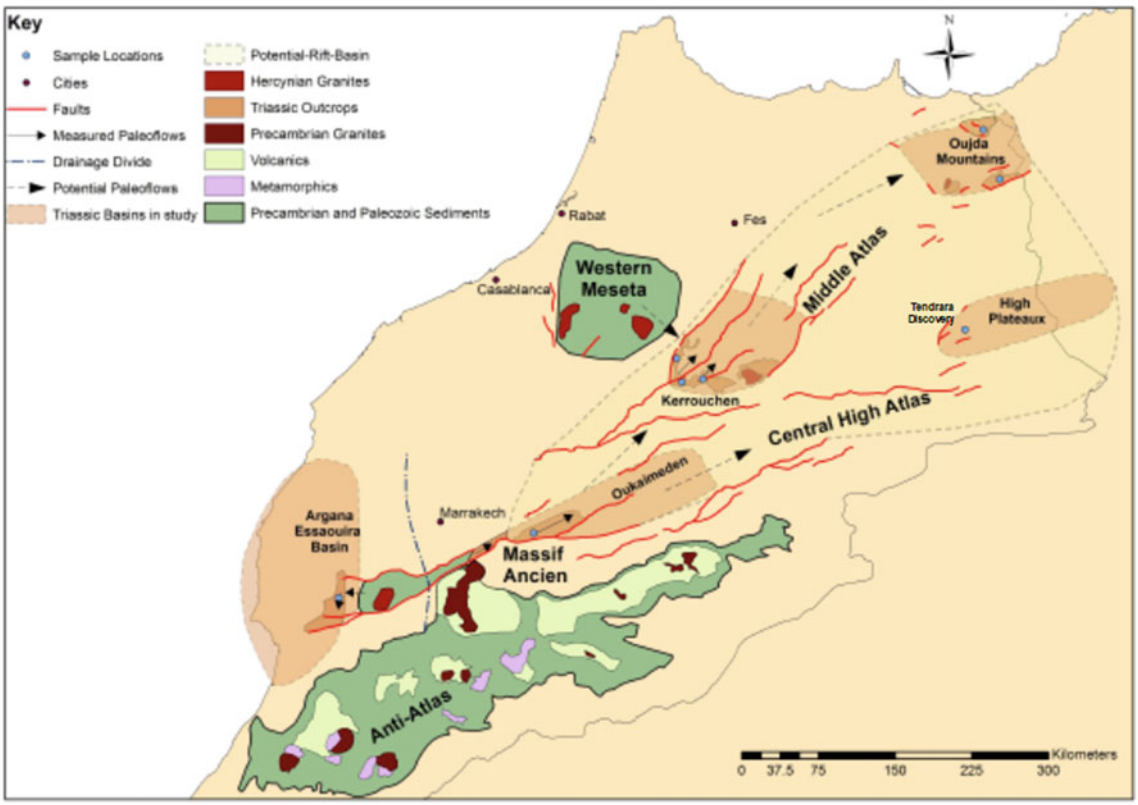

Fig. 1 Late Triassic palaeogeography and potential clastic source areas in Morocco

References

Benaouiss, N., Courel, L., Beauchamp, J.: Rift-controlled fluvial/tidal transitional series in the Oukdimeden sandstones, high atlas of Marrakesh (Morocco). Sed. Geol. **107**, 21–36 (1996)

Domènech, M., Teixell, A., Babault, J., Arboleya, M.L.: The inverted Triassic rift of the Marrakech high atlas: a reappraisal of basin geometries and faulting histories. Tectonophysics **663**, 177–191 (2015)

Fabuel-Perez, I., Redfern, J., Hodgetts, D.: Sedimentology of an intra-montane rift-controlled fluvial dominated succession: the upper Triassic Oukaimeden sandstone formation, Central High Atlas Morocco. Sediment. Geol. **220**, 103–140 (2009)

Guiraud, R.: Mesozoic rifting and basin inversion along the Northern African Tethyan margin: an overview, vol. 132, pp. 217–229. Geological Society, London, Special Publications (1998)

Laville, E., Pique, A., Amrhar, M., Charroud, M.: A restatement of the Mesozoic Atlasic rifting (Morocco). J. Afr. Earth Sci. **38**, 145–153 (2004)

Lorenz, J.: Triassic sediments and basin structure of the Kerrouchen Basin, Central Morocco **46**, 897–905 (1976)

Ouijidi, M., Courel, L., Benaouiss, N., El Mostaine, M., Ouarhache, D., Sabaoui, A., Tourani, A.-I.: Moroccan paleogeographic maps during early mesozoic times. In: Le Permian et Le Trias Du Maroc, pp. 15–24. Oujda (2000)

Turner, P., Piling, D., Walker, D., Exton, J., Binnie, J., Sabaou, N.: Sequence stratigraphy and sedimentology of the late Triassic TAG-I (blocks 401/2) Berkine basin Algeria. Mar. Pet. Geol. **18**, 959–981 (2001)

Sedimentology of Mixed Siliciclastic–Carbonate Eocene Deltaic Deposits in a Strike-Slip Basin, Eastern Oman

Iftikhar Ahmed Abbasi, Mohamed A. K. El-Ghali, and Abdulrahman Al Harthy

Abstract

Mixed siliciclastic–carbonate sedimentary deposits are challenging to interpret due to intermixing of depositional processes and changes in the basin dynamics. The Eocene Musawa Formation outcropping in the Eastern Oman Mountains provides an opportunity to study the sedimentary processes of siliciclastic deltaic sediments deposited over a regional carbonate platform. The Musawa Formation was deposited in structurally constrained Abat Basin formed due to transtensional deformation along Ja'alan and Qalhat faults. These bounding faults provided enormous amount of sediments in a laterally restricted basin undergoing strong tectonic-related subsidence and were fed by a basin axis parallel drainage system. The lithofacies assemblage represents fluvial-dominated deltaic sediments that accumulated as a local siliciclastic feature in a carbonate-dominated subtropical environment. The Musawa Formation consists of four major lithofacies associations: conglomerate, sandstone, siltstone/clay/coal, and carbonate. The coarse-grained lithofacies associations of conglomerate and sandstone were deposited by distributary channels and reworked by shoreface processes, whereas the coastal processes in delta-plain setting deposited siltstone, clay, and coal as overbank fines. The carbonate lithofacies association was deposited in open marine conditions during transgressive events.

Keywords

Musawa Formation • Oman Mountains • Ja'alan and Qalhat faults • Abat Basin • East Oman

1 Introduction

The Abat Basin in Eastern Oman Mountains is bounded by two major strike faults, the Ja'alan fault in the southwest and Qalhat fault in the northeast (Fig. 1). The Abat Basin is characterized by thick siliciclastic sediments interbedded with carbonate deposits. The Eocene Musawa Formation is over 1100 m thick and consists dominantly of sandstone, siltstone, clay, and coal interbedded with limestone and marl beds (Roger et al. 1991). The Musawa Formation is stratigraphically equivalent to the Seeb Formation carbonates in the rest of the Oman Mountains (Fig. 2) (Fournier et al. 2006). The enormous thickness of siliciclastic sediments in the Musawa Formation is due to excessive sediments supply from uplifted terrains along the active basin margin faults and tectonic-related subsidence. The Musawa Formation in Eastern Oman Mountains represents thick siliciclastic sedimentation during Eocene time while the rest of the Oman Mountains and Arabian Plate experienced large-scale carbonate deposition (Al Rajhi et al. 2021).

In the present work, we described the lithofacies associations of the Musawa Formation in Wadi Musawa, especially its lower and middle parts, to interpret the paleoenvironments of an interbedded mixed siliciclastic and carbonate sequence. This study will help in understanding the depositional mechanism of clastic interaction in a carbonate platform, which is a major challenge in the interpretation of mixed siliciclastic–carbonate system (Chiarella et al. 2017).

I. A. Abbasi (✉) · M. A. K. El-Ghali
Department of Earth Sciences, Sultan Qaboos University, Muscat, Sultanate of Oman
e-mail: iftikhar@squ.edu.om

M. A. K. El-Ghali
Earth Science Research Center, Sultan Qaboos University, Muscat, Sultanate of Oman

A. Al Harthy
Petroleum Development of Oman, Muscat, Sultanate of Oman

A. Çiner et al. (eds.), *Recent Research on Geomorphology, Sedimentology, Marine Geosciences and Geochemistry*, Advances in Science, Technology & Innovation, https://doi.org/10.1007/978-3-030-72547-1_37

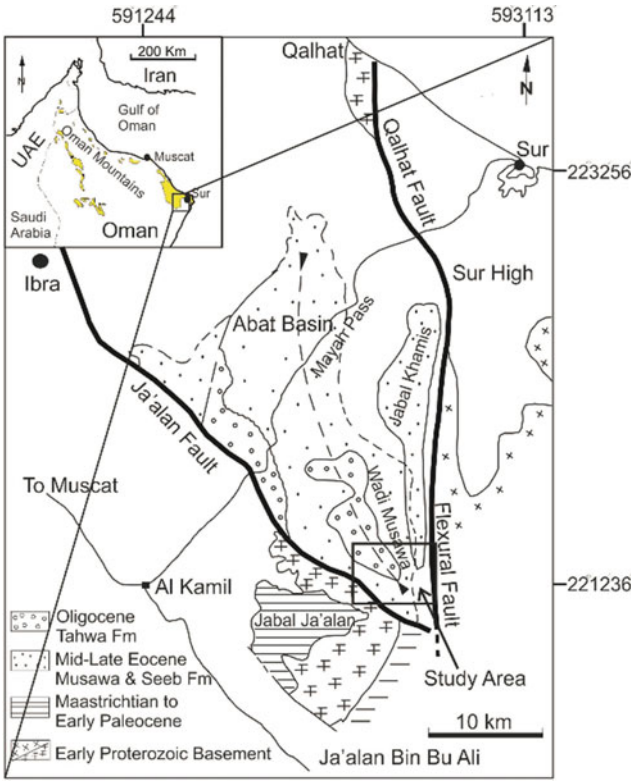

Fig. 1 Simplified geological map of Wadi Musawa and surrounding areas. Study area is marked by rectangle. Inset map shows Oman Mountains (Roger et al. 1991)

2 Stratigraphy and Methodology

The Musawa Formation is divided into three members named as the lower, middle, and upper Musawa members on the basis of their lithological characteristics (Fig. 2). The formation has conformable contacts with underlying Abat Formation and overlying Tahwah Formation (Fig. 2). Two vertical sections were measured and described in detail in Wadi Musawa to study the sedimentological details of the formation, especially through its lower and middle members. Samples were collected for compositional variations to determine the possible source of the detritus.

3 Results

Relying on its lithological characteristics, the Musawa Formation shows deposition under proximal delta-plain to a distal delta-front setting (Fig. 2). Four major lithofacies associations were identified in the formation, which are further subdivided into a number of individual lithofacies on the basis of their depositional characteristics.

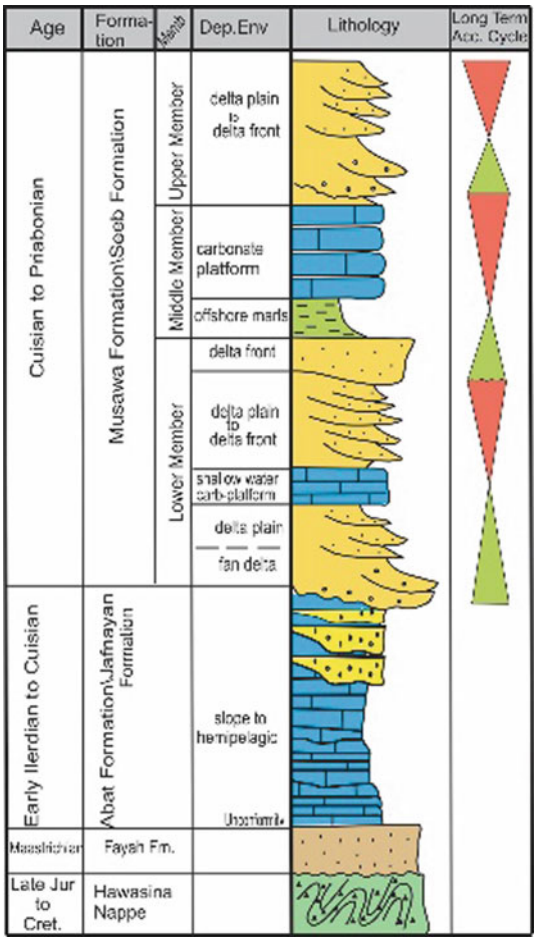

Fig. 2 Stratigraphy of the study area. The Musawa Formation and its three members along with their proposed depositional system are indicated (after Al Rajhi et al. 2021)

The Lower Musawa Member is dominated by vertically and laterally stacked tens of meters thick sandstone, which is fairly monotonous indicating high sedimentation rates (Fig. 3). Thin streaks of peat commonly interbedded with siltstone and clay beds were deposited in a delta-plain setting where swamps and marshes were common. The Middle Musawa Member consists of interbedded calcareous, planar to cross-bedded sandstone, bioturbated siltstone, shale, and fossiliferous limestone. The lithofacies assemblage represents fluvial-dominated deltaic sediments that accumulated as a local siliciclastic feature in a carbonate-dominated subtropical environment (Al Rajhi et al. 2021). The conglomerate and sandstone lithofacies associations were deposited by distributary channels and shoreface processes, whereas the fine-grain facies of siltstone and clay were deposited in interdistributary areas in delta-plain setting (Fig. 3). The carbonate lithofacies association was deposited in open marine shelf conditions during transgressive events associated with delta-lobe switching.

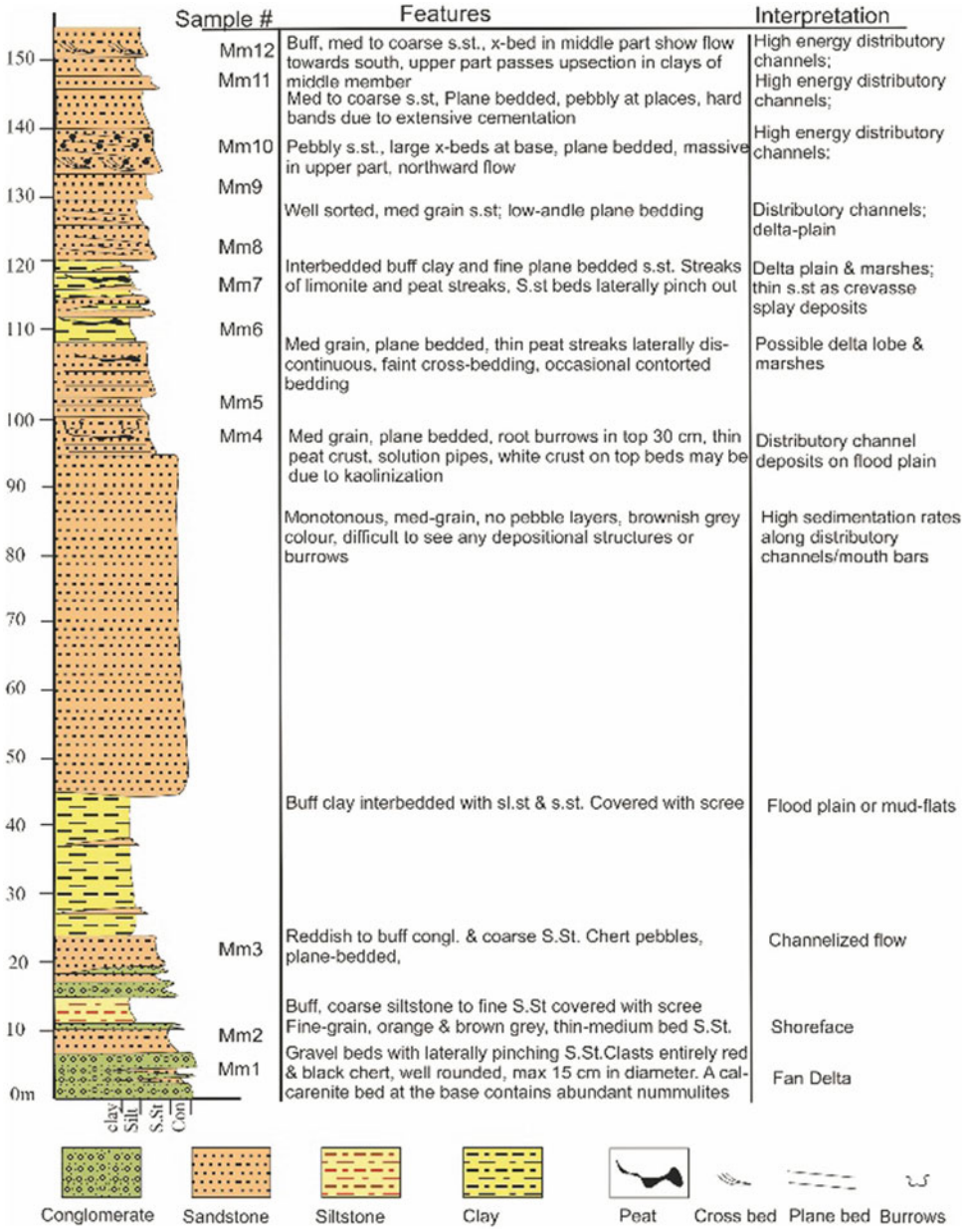

Fig. 3 Measured section of Lower Musawa sandstone in Wadi Musawa. Thick conglomerate and sandstone bodies with abundant marine fauna in the lower part of the member indicate the onset of deltaic deposits over carbonate platform of the Abat Formation. Thick sandstone bodies are multistoryed and were deposited by the distributary channels in a delta-plain setting

The lateral lithofacies heterogeneity in a N-S elongated basin is due to changes in the depositional processes and relative sea-level changes controlled by the bounding faults. The lithofacies assemblages show deposition in a fluvial-dominated delta that was rapidly prograding on a carbonate shelf.

4 Discussion and Conclusion

The mixed siliciclastic–carbonate succession of the Musawa Formation accumulated in N-S elongated Abat Basin preserving thick deltaic sequences due to the tectonic subsidence controlled by the Ja'alan and Qalhat faults (Fournier et al. 2006). A localized tectonic deformation explains the deposition of thick siliciclastic deposition in the study area during Paleogene time when most of the Arabian Plate, particularly Oman Mountain area, was dominated by the widespread carbonate sedimentation (Ume Raduma Group). The lithofacies distribution in the basin is controlled by the tectonic activity influencing both subsidence and relative sea-level changes. The siliciclastic sequences are thick in the southern part as compared to the northern part of the basin indicating deepening of the basin toward the north, which is dominated by the carbonate and fine-grain sediments. Flooding events are interpreted to be generated by the tectonic activity deposited carbonate rocks in large part of the basin, which acts as marker horizons.

References

Al Rajhi, A., Abbasi, I.A., Razin, P., AlHarthy, A.: Sedimentology of mixed siliciclastic-carbonate system in a structurally constrained Paleogene Basin: Eocene Musawa Formation in Eastern Oman Mountains. J. Afr. Earth Sci. **173**, 104020 (2021)

Chiarella, D., Longhitano, S.G., Tropeano, M.: Types of mixing and heterogeneities in siliciclastic-carbonate sediments. Mar. Pet. Geol. **88**, 617–627 (2017)

Fournier, M., Lepvrier, C., Razin, P., Jolivet, L.: Late Cretaceous to Paleogene post-obduction extension and subsequent Neogene compression in the Oman Mountains. GeoArabia **11**, 17–40 (2006)

Roger, J., Béchennec, F., Janjou, D., Le Metour, J., Wyns, R., Beurrier, M.: Geological map of Ja'alan with explanatory notes, sheet NF40-8E, scale 1:100,000. Directorate General of Minerals, Ministry of Petroleum and Minerals, Muscat, Oman (1991)

Radiochronological Studies of Modern Lake Sediments of the Kola Peninsula (Russia) Using Unsupported Pb-210 Isotope

Anna Travkina

Abstract

For the study of modern sedimentation rates (up to 100–150 years), for example, in inland, shelf seas, and lakes, Pb-210 radionuclide was used. For two columns of modern lake sediments of the Kola Peninsula, Russia (Lake Shuonijaur—N69° 15′ 03,50″ E30° 02′ 32,37″ and Lake Virtuovoshjaur N68°46′ 09,05″ E28°49′ 26,77″) radiochronological studies were carried out. The reliability of the use of unsupported Pb-210 isotope for sedimentation rates estimation was shown. It confirms the constant sedimentation in these lakes during the last 100–150 years and the absence of strong mixing during sedimentation.

Keywords

Sedimentation rate • Unsupported Pb-210 • Bottom sediments

1 Introduction

Radionuclides are widely used to determine the sedimentation rates of bottom sediments in natural reservoirs. The possibility of using certain radionuclide is determined by the features of its geochemical cycle (function of entry, the ability to bind to suspended particles, etc.). The half-life of radionuclide should be comparable with the periods of time during which a sediment is formed. Thus, in the deep part of the seas and oceans, far away from the coast, where the sedimentation process is slow, radionuclides with large half-lives (Th-230, Pa-231, Be-10) are used. For the study of modern sedimentation rates (up to 100–150 years), for example, in inland, shelf seas, and lakes, Pb-210 radionuclide was applied.

2 Methods

In the frames of this work, radiochronological studies were carried out for two columns of modern lake sediments of the Kola Peninsula (Russia)—Lake Shuonijaur—N69° 15′ 03,50″ E30° 02′ 32,37″ and Lake Virtuovoshjaur N68° 46′ 09,05″ E28° 49′ 26,77″ (Table 1). Both columns were age dated using unsupported Pb-210 isotope data (Tables 2 and 3). Bottom sediments samples were dried in layers (1–2 cm) at a temperature of 70–80 °C to a constant mass.

The determination of the Pb-210 activity in the samples was carried out using the method of non-destructive gamma-ray spectrometry using low-background gamma-spectrometer Canberra Industries with semiconductor detector made of pure germanium with an active diameter of 70 mm and a thickness of 25 mm. [The calibration for energy and efficiency was performed using preparations for inter-laboratory inter-calibration exercises MAPEP 97 S4 (Department of energy, USA) and IAEA-315 (IAEA)].

3 Results

See Tables 1, 2 and 3.

4 Discussion

Lead-210 (T1/2 = 22.3 years) is a member of the U-238 series. One of the parents of Pb-210 is Rn-222 (T1/2 = 3.8 days)—a radioactive noble gas. Radon constantly enters the atmosphere through the pores and cracks of soils and rocks, then through a chain of short-lived decay

A. Travkina (✉)
Vernadsky Institute of Geochemistry and Analytical Chemistry of Russian Academy of Sciences, Kosygina st. 19, Moscow, 119991, Russia

A. Çiner et al. (eds.), *Recent Research on Geomorphology, Sedimentology, Marine Geosciences and Geochemistry*, Advances in Science, Technology & Innovation, https://doi.org/10.1007/978-3-030-72547-1_38

Table 1 Lake location and calculated values of sedimentation rates

|Lake	Location	Lake area, km^2	Depth of selection, m	The calculated sedimentation rate, cm/year
Shuonijaur	N69° 15′ 03,50″ E30° 02′ 32,37″	11.3	8	0.07
Virtuovoshjaur	N68° 46′ 09,05″ E28° 49′ 26,77″	1.25	10	0.07

Table 2 Unsupported Pb-210 activity in the column of sediments from Shuonijaur lake

Horizon	Depth, cm	Pb-210 activity, Bq/kg	Error, Bq/kg
0–2	1	518	60
2–4	3	188	46
4–6	5	94	20
6–8	7	30	12
8–10	9	16	53

Table 3 Unsupported Pb-210 activity in the column of sediments from Virtuovoshjaur lake

Horizon	Depth, cm	Pb-210 activity, Bq/kg	Error, Bq/kg
0–2	1	1532	131
2–4	3	261	99
4–6	5	224	54
6–8	7	87	44

products**,** Pb-210 is formed, and it falls on the underlying surface with precipitation. Thus, there is a continuous atmospheric flow of Pb-210, and the activity of which is not supported by the decay of the long-lived parent—Ra-226. The average residence time of Pb-210 in surface waters is from tens of days to several years (Schell 1977). In the layers of the bottom sediments, the activity of Pb-210 gradually decreases with depth according to the radioactive decay until it reaches a value of equilibrium activity with Ra-226.

Two main models are used with Pb-210 radionuclide to calculate the absolute age date—the model of constant activity and the model of constant flow (Kuptsov 1986).

In the case of a constant sedimentation rate, both models give the same result.

Koide and co-authors (Koide et al. 1973) were among the first people to use Pb-210. They confirmed the adequacy of the lead model for the dating of annual layers of sediments taken in the vicinity of the California coast.

In this paper, Pb-210 isotope was used to estimate the sedimentation rate for two columns of modern lake sediments of the Kola Peninsula (Russia)—Shuonijaur and Virtuovoshjaur.

To evaluate the sedimentation rates, profiles of Pb-210 activity change in depth in semi-logarithmic coordinates were constructed. We obtained a good correlation of the exponential decrease in the activity of unsupported (in comparison with Pb-210 staying in equilibrium with Ra-226) Pb-210 with the depth of the column layer, which corresponds to its half-life period for both columns.

A correlation analysis was carried out in Excel. The correlation coefficient for both Pb-210 profiles was close to 1. This fact allowed us to speak about the correctness of the use of this method in general, despite the large errors in obtaining the initial data.

This confirms the constant sedimentation in these lakes over the last 100–150 years and the absence of strong mixing during sedimentation.

Besides age dating of modern sediments Pb-210 can also be used to reconstruct the chronology of anthropogenic pollution of water by radionuclides, heavy metals, and organochlorine compounds during the last century.

5 Conclusions

For two columns of modern lake sediments of the Kola Peninsula, Russia (Shuonijaur and Virtuovoshjaur), the same sedimentation rate of 0.07 cm/year was obtained.

The reliability of the use of unsupported Pb-210 isotope for age dating of these lakes is shown.

The vertical distribution of some technogenic radionuclides in the columns of sediments (Cs-137, Pu-239, 240 isotopes) can also provide additional information on the sedimentation regime. But for their use as appropriate tracers, one needs to know the function of deposition.

Acknowledgements The research results were obtained in the framework of the state assignment (topic No. 0137-2019-0010).

References

Koide, M., Bruland, K., Goldberg, E.: Th-228/Th-232 and Pb-210 geochronologies in marine and lake sediments. Geochim. Cosmochim. Acta **37**, 1171–1187 (1973)

Kuptsov, V.: Absolute Geochronology of Bottom Sediments of Oceans and Seas. Science, USSR, Moscow (1986)

Schell, W.: Concentration, physico-chemical states and mean resident times of Pb-210 and Po-210 in marine and estuarine waters. Geochim. Cosmochim. Acta **41**, 1019–1031 (1977)

Dolomitization Fluid and Genesis of Dolomite in the Devonian Guanwushan Formation in Upper Yangtze

Shuguang Huang, Mingcai Hou, Shenglin Xu, Anqing Chen, Benjian Zhang, Wen Luo, Hui Chao, Pengcheng Cai, and Yuwei Deng

Abstract

Thick-block dolomite, including microcrystalline dolomite (Type 1), fine crystalline dolomite (Type 2) and medium crystalline dolomite (Type 3), is extensively developed in the Guanwushan Formation of Devonian in the upper Yangtze region. Petrological, mineralogical and geochemical analyses indicate that the source of dolomitization fluid is contemporaneous seawater. The Type 2 and Type 3 dolomites have resulted from further dolomitization of the Type 1 dolomite. The order degree of the three types of dolomites increased in sequence, and they all show dull cathodoluminescence. The three types of dolomites have higher Sr^{2+} and lower Mn^{2+} concentrations than those of limestone. The total amount of rare earth elements of dolomites is lower than that of limestone. However, the dolomites are enriched with LREE and lack of HREE, with a consistent REE distribution pattern of the limestone. The weak negative anomalies of Ce and Eu indicate that the dolomites formed in a weak oxidizing and reducing environment with low temperature, and the dolomitization fluids inherited from the original seawater. The $\delta^{18}O_{PDB}$ values of Type 1 and Type 2 dolomites are higher than those of the limestone, indicating that the dolomitization fluid is influenced by seawater evaporation at the penecontemporaneous stage. The $\delta^{18}O_{PDB}$ value of Type 3 dolomite is lower than that of limestone, and it also shows anhedral crystal, which indicates that the dolomite has experienced more intense dolomitization stage at greater burial depth and higher temperature.

Keywords

Carbonate platform • Mineralogy • Geochemistry • Dolomitization fluid

1 Introduction

The origin of dolomite has been a hot topic in the study of sedimentary geology. Extremely rare dolomite precipitates in modern sedimentary environments. It is difficult to synthesize perfect ordered dolomite under normal temperature and pressure conditions in the laboratory, but dolomite is well developed in the strata earlier than the Mesozoic. So, most scholars believe that the large amount of dolomites developed during geological history are the product of dolomitization of limestone. As the most persuasive representative of the primary dolomite, the microbial dolomite has attracted much attention from geologists in recent years (Vasconcelos et al. 1995; Kenward 2013). Despite the discovery of microbial dolomite in modern sedimentary environments, it has no volume significance and does not address the origin of thick layer dolomite in ancient strata. At present, various dolomitization models are actually caused by the different fluid sources of the precursor limestone in different diagenetic stages. Therefore, the fundamental problem of the genesis of dolomite is the source of dolomitization fluid.

In this paper, field outcrop observation, thin slice analyses, cathodoluminescence, X-ray diffraction analysis, trace

S. Huang (✉) · M. Hou · S. Xu · A. Chen · W. Luo · H. Chao · P. Cai
State Key Laboratory of Oil and Gas Reservoir Geology and Exploitation, Chengdu University of Technology, Chengdu, 610059, China
e-mail: huangshug@163.com

M. Hou
e-mail: houmc@cdut.edu.cn

S. Huang · M. Hou · S. Xu · A. Chen · W. Luo · H. Chao · P. Cai
Institute of Sedimentary Geology, Chengdu University of Technology, Chengdu, 610059, China

B. Zhang
Chuanxibei Division of Petro China Southwest Oil and Gas Field Company, Jiangyou, 621709, China

Y. Deng
Shale Gas Evaluation and Exploitation Key Laboratory of Sichuan Province, Chengdu, 610091, China

A. Çiner et al. (eds.), *Recent Research on Geomorphology, Sedimentology, Marine Geosciences and Geochemistry*, Advances in Science, Technology & Innovation, https://doi.org/10.1007/978-3-030-72547-1_39

rare earth elements and carbon and oxygen isotope analysis were studied, in order to constrain the properties of dolomitization fluid and dolomite genesis of the Devonian Guanwushan Formation in the Upper Yangtze.

2 Geologic Setting and Analytical Methods

The northwestern Sichuan region is located in the eastern part of the Longmenshan fault belt, the eastern margin of the Qinghai-Tibet Plateau. During the sedimentary period of the Guanwushan, the Upper Yangtze is a typical continental margin carbonate platform sedimentary environment.

On the basis of microscope identification, 41 samples were selected for major elements, trace elements and REE analysis and carbon and oxygen isotope analysis, which were conducted in The MOE Key Laboratory of Orogenic Belt and Crustal Evolution. The major element analysis was tested by X-ray fluorescence spectroscopy. The sample powder was tested by Thermo ARL ADVANT`XP + sequential X-ray fluorescence spectrometer. Trace elements (including REE) were tested by plasma mass spectrometer VG Axiom. The inorganic C and O isotope analysis was carried out using MAT253. Mineral composition and order degree of dolomite were analyzed by XRD. The cathodoluminescence analysis was carried out by the CL8200 MK5 cathode luminoscope.

3 Results

3.1 Petrographic and Mineralogical Characteristics

The dolomite rock classification is based on the crystal size. The dolomites of Guanwushan Formation are identified into three types: microcrystalline dolomite (Type 1), fine crystalline dolomite (Type 2) and medium crystalline dolomite (Type 3). Their crystal sizes are, respectively, smaller than 0.1, 0.08–0.2 and 0.25–0.45 mm (Fig. 1). The average value of degree order of Type 1, 2, 3 dolomite results is 0.50, 0.64 and 0.73.

3.2 Geochemical Characteristics

The NASC treatment was carried out on REE results of the Guanwushan Formation rocks in the northwestern Sichuan Basin. The δCe values of Type 1, 2 and 3 dolomite range from 0.91 to 0.95, 0.89 to 1.0, 0.90 to 0.95, and the δEu values of Type 1, 2 and 3 dolomite range from 0.79 to 0.86, 0.68 to 0.84 and 0.74 to 0.90.

The results of $\delta^{13}C_{PDB}$ values of the Type 1, 2, 3 dolomite range from 0.96 to 3.36‰, −2.56 to 3.98‰ and 0.26 to 2.42‰, and $\delta^{18}O_{PDB}$ values of the Type 1, 2, 3 dolomite range from −5.22 to −0.59‰, −9.48 to 0.28‰ and −7.39 to −6.12‰.

4 Discussion

4.1 Dolomitization Fluid Properties

It is a good indication to determine the dolomite origin using the C and O isotopic data. According to the dull cathodoluminescence light, the $\delta^{13}C_{PDB}$ and $\delta^{18}O_{PDB}$ values of the three dolomite types fall in the value of the Middle Devonian seawater in the Upper Yangtze (Xiong et al. 2018), the content of Sr in the dolomite is lower than that of the limestone, and the weak negative anomaly Eu is not consistent with the characteristics of hydrothermal dolomite. Through the above analysis, the source of dolomitization fluid is still the ancient seawater.

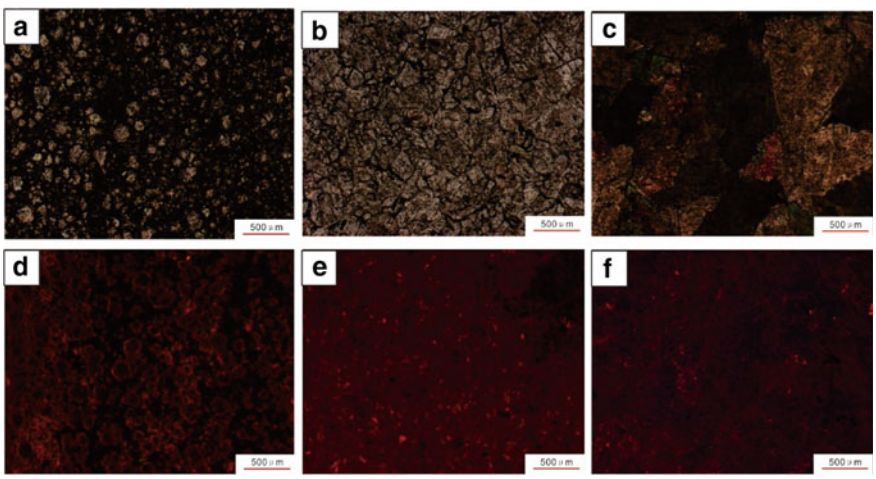

Fig. 1 Photographs showing the petrographic characteristics of the dolomites from the Hejialiang outcrop. **a**, **b**, **c** are thin microscope graph of Type 1, 2, 3 dolomite, and **d**, **e**, **f** are cathodoluminescence pictures of corresponding rocks

4.2 Origin of Dolomites

The cathodoluminescence of Type 1 dolomite is mainly dull red light. The three types of dolomites have higher Sr^{2+} and lower Mn^{2+} concentrations than those of limestone, which reflects the strong evaporation. The REE distribution curve also shows the same pattern as limestone. In general, various characteristics reflect that this dolomite was formed at the penecontemporaneous stage with strong evaporation.

The Sr content of Type 2 dolomite is lower than that of Type 1 dolomite. The REE distribution curve shows the same distribution pattern as the limestone and Type 1 dolomite, so the diagenetic system is considered to be relatively closed. Most of them are recrystallized by the Type 1 dolomite. $\delta^{18}O_{PDB}$ is low, which is more positive than the seawater. It is mainly caused by the increase of the formation depth of the stratum.

The order degree of Type 3 is higher than that of Type 2 dolomite. The content of Sr is the lowest. The REE distribution curve shows the same distribution pattern as limestone, Type 1 and 2 dolomite and the various indicators of REE are also roughly the same. The $\delta^{18}O_{PDB}$ value is more negative than that of seawater and Type 2 dolomite in the same period due to the deeper burial and higher temperature.

5 Conclusions

(1) The dolomite of the Guanwushan Formation in the northern Sichuan Basin is divided into fine-microcrystalline dolomite, fine crystalline dolomite and medium crystal dolomite.

(2) In general, it is concluded that the dolomite in the study area mainly underwent the dolomitization of penecontemporaneous stage, early shallow buried dolomitization stage and higher temperature buried dolomitization stage.

(3) Cathodoluminescence, the value of $\delta^{18}O_{PDB}$ and rare earth element analysis indicate that the diagenetic fluids of the three types of dolomites are all from the ancient seawater of Devonian Guanwushan.

References

Kenward, P.A.: Ordered low-temperature dolomite mediated by carboxyl-group density of microbial cell walls. AAPG Bull. **97** (11), 2113–2125 (2013)

Vasconcelos, C., McKenzie, J.A., Bernasconi, S., et al.: Microbial mediation as a possible mechanism for natural dolomite formation at low temperatures. Nature **377**(6546), 220–222 (1995)

Xiong, L., et al.: Origin of dolomite in the Middle Devonian Guanwushan Formation of the western Sichuan basin, Western China. Palaeogeogr. Palaeoclimatol. Palaeoecol. **495**(15), 113–126 (April 2018)

Sedimentology, Stratigraphy, Paleontology, and Marine Geosciences (T14): Stratigraphy—How to Restore the Arrow of Time

Back to the Field: The Limits of Standard Scales in High-Resolution Stratigraphy. Examples from Northwest Africa and the Middle East

Luc Bulot, Jonathan Redfern, Tim Luber, Mike Simmons, and Jason Jeremiah

Abstract

The standard references regarding the geological time-scale present charts where biostratigraphic scales and defining events are integrated and placed against the standard chronostratigraphic units (stages, periods, etc.). These charts may give the impression that these are known facts rather than an interpretation that may shift as more information becomes known. The importance here is that geologists who are not biostratigraphers assume that the purpose of biostratigraphy is to provide 'age dating' (i.e., 'these fossils indicate an Aptian age'). They are typically unaware of what a complex and uncertain process arriving at such a statement can be. These uncertainties were brought to us in the course of studies of the Cretaceous of SW Iran and Morocco. In both areas, we were able to recognize a number of ammonite, planktonic foraminifera and calcareous nannofossils key species, and hence the standard biochronozones. However, what surprised us, based on the ammonite successions, was that a completely different calibration of the planktonic foraminifera and nannofossil zones to the ammonite standard, and hence standard chronostratigraphy, was suggested than might be assumed by reference to the standard charts. This highlighted the role of endemism in biostratigraphy and the need for research into biostratigraphic/age calibration in order to provide reliable 'age dating'.

Keywords

Biostratigraphy • Carbon-isotope stratigraphy • Cretaceous • Morocco • Iran • Endemism • OAE

1 Introduction

Over the past 25 years, the senior author of the present contribution coordinated integrated biostratigraphic studies on the Late Jurassic and Cretaceous successions of the Neo-Tethys. The aim of the present contribution was to outline the need to perform extensive new investigations and define regional reference sections since fieldwork in the Arabian Plate and North African Atlantic Margin questions the validity of the standard biochronostratigraphic charts (Gradstein et al. 2012).

2 Materials and Methods

Both studies presented below are based on extensive bed by bed sampling of sections in SW Iran (Arabian plate) and SW Morocco (Essaouira-Agadir Basin—EAB). In both cases, the study performed is the establishment of a biochronostratigraphic framework based on the integration of ammonite, planktic foraminifera, calcareous nannofossils, stable isotopes and TOC. Full details that support the discussion presented below were already published (Vincent et al. 2010; Luber et al. 2019).

L. Bulot (✉)
Cerege, Aix-Marseille Université, Aix-en-Provence, France
e-mail: luc.bulot@manchester.ac.uk

L. Bulot · J. Redfern
North Africa Research Group, SEES, University of Manchester, Manchester, UK

T. Luber
Equinor, Fornebu, Norway

M. Simmons
Halliburton, Albington, UK

J. Jeremiah
Golden Spike Geosolutions, Stevenage, UK

A. Çiner et al. (eds.), *Recent Research on Geomorphology, Sedimentology, Marine Geosciences and Geochemistry*, Advances in Science, Technology & Innovation, https://doi.org/10.1007/978-3-030-72547-1_40

3 SW Iran: Chemostratigraphy as an External Control on Biostratigraphy

The Bangestan section was retained as a key section for the mid-Cretaceous Khazdumi Fm. of SW Iran (Vincent et al. 2010). The chemo- and biostratigraphic study integrates ammonites, planktonic foraminifera, carbon-stable isotope and TOC content (Fig. 1).

In order to compare the two biostratigraphic scales, the planktonic foraminifera zones were calibrated to the ammonite zones. The comparison of these schemes shows that there is a difference in the biostratigraphic interpretation of the Late Aptian. Planktonic foraminifera suggest that the latest Aptian is absent, whereas the ammonite suggest the presence of all late Aptian zones. Here, carbon-isotope chemostratigraphy is useful as an independent tool for an improved chronostratigraphic framework of both the upper part of the Aptian, as well as the barren interval that corresponds to the planktonic foraminifera crisis.

4 Aptian of the EAB: The Need of Regional Biostratigraphic Scales

A combined high-resolution litho-, bio-, chemo- and sequence stratigraphic data analysis for the Aptian of the NW African Atlantic margin was recently published (Luber et al. 2019). A reference section at Tiskatine (EAB) was proposed (Fig. 2). The study provides new information on the ranges of foraminifera and calcareous nannofossils, which have been correlated with the regional ammonoid zonation scheme previously defined for the EAB (Luber et al. 2017).

5 Discussion

The C13 curve from Bangestan was compared to the reference curve for the Alpine Neo-Tethys established in the SE France (Herrle et al. 2004). Both curves show the late early Aptian positive excursion and the subsequent decrease in $\delta^{13}C$ of the early late Aptian. In Iran, a sharp and strong negative shift to lower values was recorded in the latest Aptian. A gradual decrease is observed in the expanded northern margin across the uncertain zone of the Bangestan section, and the $\delta^{13}C$ gradually increases to heavier values with a maximum reached in the barren interval. This overall pattern of a double positive excursion is also observed in the Alpine reference curve but in a very condensed section. Two ammonite-dated C13 curves of Aptian/Albian basinal deposits (Azevedo and Rodrigues 2000; Beltramo 2004) show an expanded positive excursion around the Aptian/Albian boundary and a pronounced negative excursion in the *H. jacobi* Zone that support the biostratigraphic interpretation of Bangestan based on ammonites vs. foraminifera.

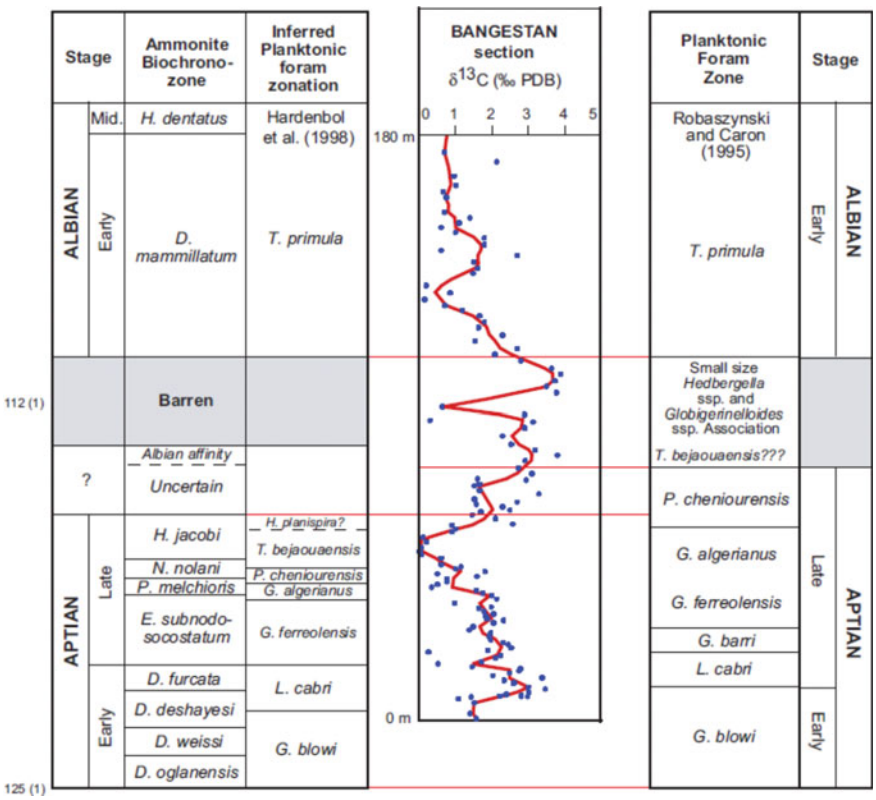

Fig. 1 Carbon-isotope curve compared to (left) the ammonite zonation established at Bangestan, and the planktonic foraminifera zones inferred from this using the standard zonation, (right) the zones based on Robaszynski and Caron (1995)

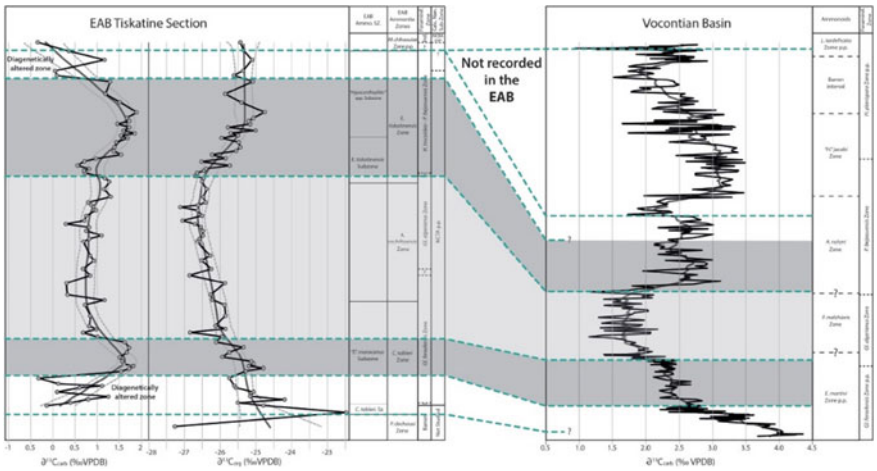

Fig. 2 Aptian to Lower Albian carbonate content, TOC, d13C_{carb} and d13C_{org} at Tiskatine correlated to the EAB ammonoid zonation and standard ammonite, planktonic foraminiferal and nannofossil zonations (Luber et al. 2019, 2017)

In Morocco, the reference section at Tiskatine extends the global biostratigraphic and chemostratigraphic database for the Aptian in the Central Atlantic Margin, providing a high-resolution well-documented reference section. The results highlight existing discrepancies between the individual disciplines, which need urgent revision.

6 Conclusions

Both studies discussed above advocate the advantage of developing multi-disciplinary local zonation schemes that would greatly enhance regional application of individual stratigraphic methodologies. These regional schemes offer improvement in the resolution of timing/ranges of global bio- and chemostratigraphic markers and industrial application, including the calibration of sequence stratigraphy boundaries.

References

Azevedo, R.L.M., Rodrigues, R.: Towards $\delta^{13}C$ and delta $\delta^{18}O$ global curves for Albian carbonate sections. In: 31st International Geological Congress, Brazil, Abstracts Volume (2000)

Beltramo, J.: Les séries carbonatées crétacées d'arc volcanique du Terrane Guerrero (Mexique). Unpublished Ph.D., Grenoble I and Université de Neuchâtel, 306 p. (2004)

Gradstein, F., Ogg, J., Schmitz, M., Ogg, G. (eds.): The Geologic Time Scale 2012. Oxford, Amsterdam, and Waltham, Elsevier, 1176 p. (2012)

Herrle, J.O., Kössler, P., Friedrich, O., Erlenkeuser, H., Hemleben, C.: Highresolution carbon isotope records of the Aptian to Lower Albian from SE France and the Mazagan Plateau (DSDP Site 545): a stratigraphic tool for paleoceanographic and paleobiologic reconstruction. Earth Planet. Sci. Lett. **218**, 149–161 (2004)

Luber, T.L., Bulot, L.G., Redfern, J., Frau, C., Arantegui, A., Masrour, M.: A revised ammonoid biostratigraphy for the Aptian of NW Africa: Essaouira-Agadir Basin Morocco. Cretac. Res. **79**, 12–34 (2017)

Luber, T.L., Bulot, L.G., Redfern, J., Nahim, M., Jeremiah, J., Simmons, M., Bodin, S., Frau, C., Bidgood, M., Masrour, N.: A revised chronostratigraphic framework for the Aptian of the Essaouira-Agadir Basin, a candidate type section for the NW African Atlantic Margin. Cretac. Res. **93**, 292–317 (2019)

Robaszynski, F., Caron, M.: Foraminifères planctoniques du Crétacé: commentaire de la zonation Europe-Méditerranée. Bull. Soc. Geol. Fr. **166**(6), 681–692 (1995)

Vincent, B., van Buchem, F.S.P., Bulot, L.G., Immenhauser, A., Caron, M., Baghbani, D., Huc, A.Y.: Carbone isotope stratigraphy, biostratigraphy and organic matter distribution in the aptian-lower Albian successions of Southwest Iran (Dariyan and Kazhdumi Formations). GeoArabia Spec. Publ. **4**(1), 167–195 (2010)

Lithofacies Analysis of Lower Acacus Reservoir and Its Impact on Reservoir Quality Utilizing Borehole Images, Ghadamis Basin—Northwest Libya

Abraheem Elmasli, Mohamed Abdelmalik, Walid Jibreel, and Ali Najem

Abstract

The Silurian Lower Acacus reservoir is known as one of the prolific hydrocarbon intervals within Ghadamis Basin. It is characterized by an alternation of siliciclastic succession represented by sandstone, siltstone and shale. These were deposited in a complex marginal depositional setting. Previous regional basin scale studies indicated a transitional pattern from fluvial channel sandstone in the south, coastal deltaic sandstone and siltstone, to offshore marine siltstone in the north. However, the study area (NC4) is located within the coastal-deltaic dominated facies. There was an attempt to understand the variations in the exploration license NC4 for further field development. From the exploratory wells drilled according to the license, it is observed that the vertical association of these rocks highly influences the reservoir quality as well as its lateral continuity. Therefore, understanding both the vertical and lateral reservoir geometries is crucial for further exploration and field development plans of the Lower Acacus play. The reservoir succession shows variations in the depositional pattern sequences from coarsening to fining upwards as per the GR log signature, paleo-flow directions and the possible depositional setting. To achieve this objective, an integration between the core, wireline logs and borehole images (full borehole MicroImager tool—FMI) data was implemented. The integration of core image and FMI analysis assisted in the recognition of four main lithofacies within the Lower Acacus reservoir, namely heterolithic bedding, cross-bedded sandstone, shaly sand and laminated shales. The association of these facies reflects a clear tidal effect on the deltaic deposition as supported by paleocurrent direction analysis. The paleocurrent measurements from the cross-bedded facies show a dominant bimodal trend toward NW and SE, with modest polymodal and few unimodal models.

Keywords

Lower Acacus • Ghadamis Basin • Lithofacies • Sedimentary structures • Reservoir quality • Borehole image • Libya

1 Introduction

This study was achieved in a detailed aspect by integrating core images and image logs to define the characterization of the Upper Silurian sequence (Lower Acacus reservoir) in northern Ghadamis Basin, NW Libya. License NC4 is one of the most profitable fields in Ghadamis Basin that has been operated by the Arabian Gulf Oil Company (AGOCO) since 2002.

The Ghadamis Basin is a large intracratonic sag basin but, in this case, developed on Pharusian basement on the passive margin of Gondwana. It covers an area of 350,000 km^2, with the basin depocentre located in Algeria. The Libyan portion represents the eastern flank of the basin, rising toward the Tripoli–Tibisti Arch (Hallett and Clark-Lowes 2016). The main aim of this study was to identify the reservoir facies and predict the rock properties with high-resolution micro-resistivity image logs. Core image will be used to support and improve the FMI analysis, as it is easier to recognize sedimentary structures on cores. Consequently, the entire facies breakdown will be based on FMI analysis as it covers the entire section of Lower Acacus reservoir.

A. Elmasli (✉)
Exploration Division, Arabian Gulf Oil Company, Benghazi, Libya
e-mail: Abraheem.Elmasli@agoco.ly

M. Abdelmalik
Earth Sciences Department, Benghazi University, Benghazi, Libya

W. Jibreel
Schlumberger, Tripoli, Libya

A. Najem
Schlumberger, Ahmadi, Kuwait

A. Çiner et al. (eds.), *Recent Research on Geomorphology, Sedimentology, Marine Geosciences and Geochemistry*, Advances in Science, Technology & Innovation, https://doi.org/10.1007/978-3-030-72547-1_41

2 Methodology

The data was processed at the Schlumberger data services center. The main objective has been to provide a continuous log of formation structure in the form of interpreted dip results and near-wellbore images. Micro-resistivity variations recorded by the tool are converted into color images after speed correction, depth alignment, electrode equalization and 'static' normalization. However, Techlog software (Schlumberger Trademark) was used for displaying and interpreting the image log (FMI), to define the main sedimentary structures in the studied wells.

3 Image Integration Using Core Data

Because of possible ambiguity such as very short lines or irregular, noisy images, some features were difficult to interpret even with the help of the other open-hole logs. Calibration against core observation was needed in this setting (Serra 1989). The fundamental benefit of core/log image integration is that it builds an understanding of the geology around the well. The identified facies in the Lower Acacus reservoir are shale facies, shaly-sand facies, heterolithic bedding facies and cross-bedding sandstone facies. These facies could reflect the depositional setting of the target reservoir, in which shale facies represent the lowest energy setting and progress through shaly-sand facies to higher energy with abundance of cross-bedding sandstone, while the heterolithic bedding is a good indicator of tidal activity supported by some bidirectional cross-bedding. Figure 1 shows a good match between core image and log image of heterolithic (associated with tidal setting), and cross-bedding facies represent the shallow marine upper shoreface setting (see Fig. 1).

4 Discussion

The FMI data of Well-1 has been fully interpreted to determine the main facies recognized within the Lower Acacus reservoir.

4.1 Well-1

The targeted interval (8020–8893 ft) revealed different lithofacies within the Lower Acacus reservoir. Normally, the Lower Acacus reservoir is split into three main units (Unit A, B and C):

- The sandstone dominated unit (Unit A) between 8600 and 8893 ft mainly characterized by blocky to coarsening upward sequence of multi-direction trend associated with fining channelized sand bodies. The cross-bedding dominates with around 41%, with a small amount of shale facies (10%) indicating that the high-energy depositional processes were dominated (shoreface setting). The unit has the cleanest, thickest and the most porous sandstone interval thorough the reservoir, but production tests revealed that this unit has a low productivity due to lack of sealing rocks.
- Unit B between 8092 and 8600 ft mainly characterized by shale-sand interbedding with a domination of both the cross-bedding facies (30%) and heterolithic bedding (29%). Furthermore, the repeating pattern of coarsening upward sequences that were mainly dipping toward NW& SE represents the tide dominated-deltaic depositional setting (see Fig. 2). The alteration of sand shale sequences has a strong contribution to hydrocarbon entrapment as confirmed by production tests.
- Unit C between 7965 and 7873 ft started with fining upward sand body followed by around three coarsening

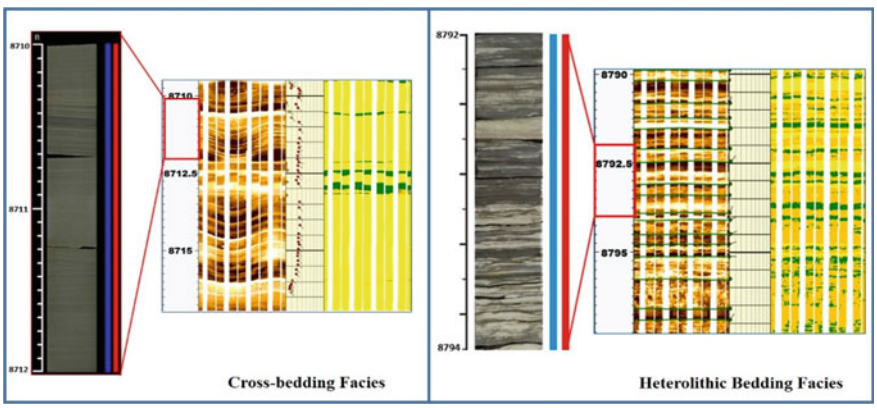

Fig. 1 Core to image calibration of heterolithic and cross-bedding facies

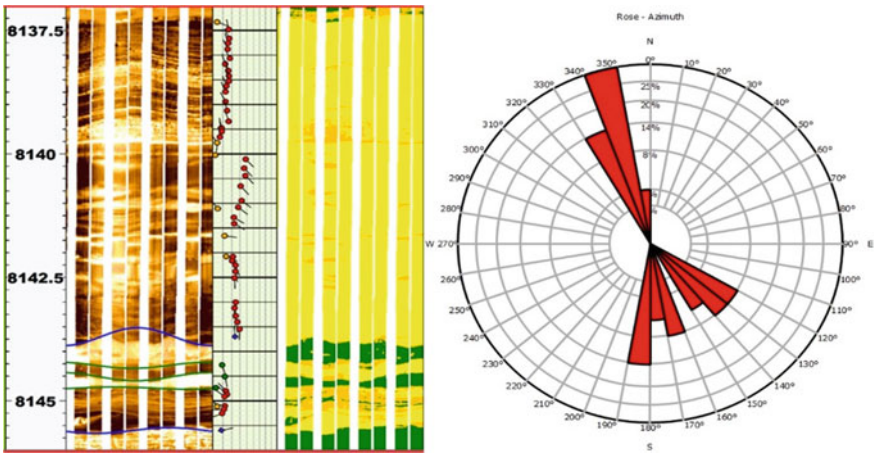

Fig. 2 Showing cross-bedding facies with bimodal trend

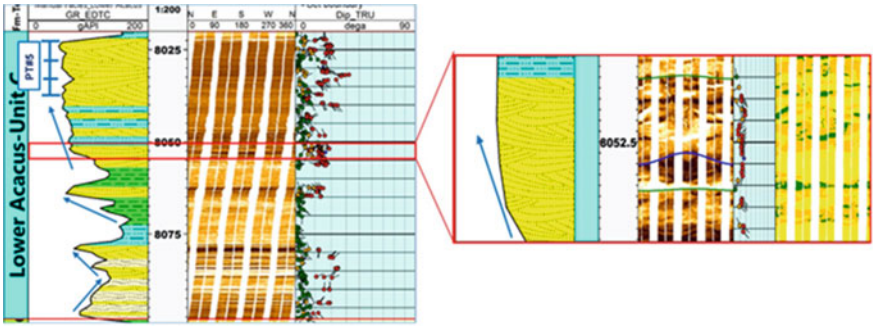

Fig. 3 Fining and coarsening upward sequences within Unit C of the Lower Acacus reservoir

upward sequences mainly composed of cross-bedding facies 44%. The paleocurrent analysis shows polymodal dip azimuth reflecting shallow marine depositional settings. The tide processes and bioturbations are present on fining sand body, which probably represents tidal channels. (see Fig. 3). This unit marks the top of the studied reservoir and is usually saturated with hydrocarbon and superimposed by the Middle Acacus marine shale.

5 Conclusion

The reservoir is divided into three main units based on log characters (A, B and C) with Unit A at the bottom followed by B and C, respectively. The integration of core images and FMI analysis assisted in the recognition of four main facies within the Lower Acacus reservoir. The associations of these facies along with the paleocurrent trend indicate a tidally influenced coastal-deltaic setting. Additionally, the paleocurrent direction measured from the existing cross-bedding shows a major trend toward NW and SE, which represents the trend of the delta geometry.

References

Hallett, D., Clark-Lowes, D.: Petroleum geology of Libya, 2nd edn, 392 p. Amsterdam, Elsevier (2016)

Serra, O.: *Formation Micro_Scanner Image Interpretation*. Schlumberger Educational Services, p. 117 (1989).

Orbital Tuning of the Berriasella Jacobi Ammonite Zone in Central Tunisia (Southern Paleotethys)

Hamdi Omar and Chokri Yaich

Abstract

Very high-resolution magnetic susceptibility record (5–10 cm sampling interval) was used to track astronomical cycles from a section belonging to the Berriasella Jacobi ammonite zone, along which 536 samples were collected. The samples were measured for magnetic susceptibility and carbonate content as paleoclimate proxies. We performed multiple spectral analyses and statistical techniques such as the evolutive harmonic analysis (EHA), multi-taper method (MTM) and average spectral misfit (ASM) to obtain the best astronomical model. The section was divided into different sub-sections assuming a stable sediment accumulation rate for each one and the previous time series analysis techniques were applied for each sub-section and showed a pervasive dominance of E_{405}-kyr and e_{100} kyr cycles. The combination of these results allowed us to review and build a new chronostratigraphic framework of the Berriasella Jacobi ammonite zone at Jebel Meloussi as follows: ~5.1 long-eccentricity cycles E_{405} were extracted which point to a duration estimate of ~2.07 Myr with an average sediment accumulation rate (SAR, dewatered and compacted) of 1.841 cm/kyr. This value of SAR goes in line with deep marine environment succession that had been deposited under a passive margin associated with the opening of the Paleotethyan Ocean around the Jurassic-Cretaceous transition.

Keywords

Berriasian • Cyclostratigraphy • Sidi Khalif formation • Orbital tuning • Spectral analysis

1 Introduction

The lower cretaceous marl-limestone alternation in central Tunisia (southern Tethyan margin) offers a scenic outcrop of strata, extremely suitable for cyclostratigraphic studies. However, some outcropping sedimentary series in central Tunisia lack accurate chronostratigraphic framework. On the opposite, the Sidi Khalif Formation at Jebel Meloussi locality (Central Tunisia) is one of the best sections. There the marl-limestone alternation has been calibrated biostratigraphically based on both ammonite and callpionellids zones (M'Rabet 1981, 1987). Hence, this study was carried out aiming to build up a reliable cyclostratigraphic framework using the Milankovitch forcing theory. These astronomical cycles are commonly used as a powerful geochronometer to refine some inaccurate geological time scales.

2 Materials and Methods

Low-frequency mass specific magnetic susceptibility (MS) χlf measurements were undertaken with a Bartington MS3 magnetometer. This is a magnetic petrophysical parameter (k) measured in SI units under an operating frequency of 0.47 kHz and a 5 s as a measurement period with the MS2B sensor. The magnetic susceptibility value indicates the ability of a material to acquire an induced magnetization when exposed to an external magnetic field. It is powerfully amenable for cyclostratigraphic studies in recent continental sediments as well as marine sedimentary environments.

We performed the spectral analysis and astronomical calibration on a MATLAB platform and under RStudio software. Prior to any analysis, the MS data were interpolated linearly at 5 cm intervals (average sample spacing). We removed long-term trends by running the "smooth" MATLAB script using a moving-average window of 150 points. Cyclicities were estimated using the multi-taper

H. Omar (✉) · C. Yaich
Laboratory of Georessources, Materials Environment and Global Change, Faculty of Sciences of Sfax, National Engineering School of Sfax, Sfax University, University of Sfax, Soukra Street km 3.5 El Habib City, 3038 Sfax, Tunisia

A. Çiner et al. (eds.), *Recent Research on Geomorphology, Sedimentology, Marine Geosciences and Geochemistry*, Advances in Science, Technology & Innovation, https://doi.org/10.1007/978-3-030-72547-1_42

method (MTM) (Thomson (1982)) upon three tapers. The MTM was coupled with a robust red noise model following the "classicconflevel.m" MATLAB script. Evolutionary spectrogram was calculated using two different methods which are the evolutionary fast fourier transform (EFFT) performed using the "evofft.m" MATLAB script of (Kodama and Hinnov 2015) script and the TF-WFFT executed using the "tfwFFT.m" MATLAB script. Orbital cycles were extracted by band-pass filtering using the Taner filter (Taner 2000) (Under R software). Magnetic susceptibility series was tuned using "depthtotime.m" script.

3 Results

We performed 2π-MTM spectral analysis on the original and the detrended (Fig. 1b) MS data. The spectrum of the entire 40 m succession of MS values shows numerous peaks with high F-test values often exceeding 0.8. Each peak corresponds to a particular wavelength on the section (Fig. 1c). To interpret these wavelengths in terms of possible orbital periods, we calculated their ratios and compared them to orbital period ratios relative to the Berriasian stage. Spectral period ratios are very close to orbital period ratios with a rather high-correlation coefficient of 0.928. The evolutive harmonic analysis (EHA) graph shows changes in the SAR along the studied section as it increases in the marly levels and decreases in the carbonate poles (Fig. 1a, d).

4 Discussion

The Sidi Khalif section is characterized by medium MS values ranging from 187 × 10^{-9} to 40 × 10^{-9} m^3/Kg (Fig. 1b), the marl by higher values and the limestone by lower values. The MS variations follow a strongly cyclic pattern. Paramagnetic clay minerals contribute to the highest values, whereas diamagnetic limestones are responsible for lower values. Magnetic hysteresis experiments indicate singular paramagnetic behavior in the clays (not shown).

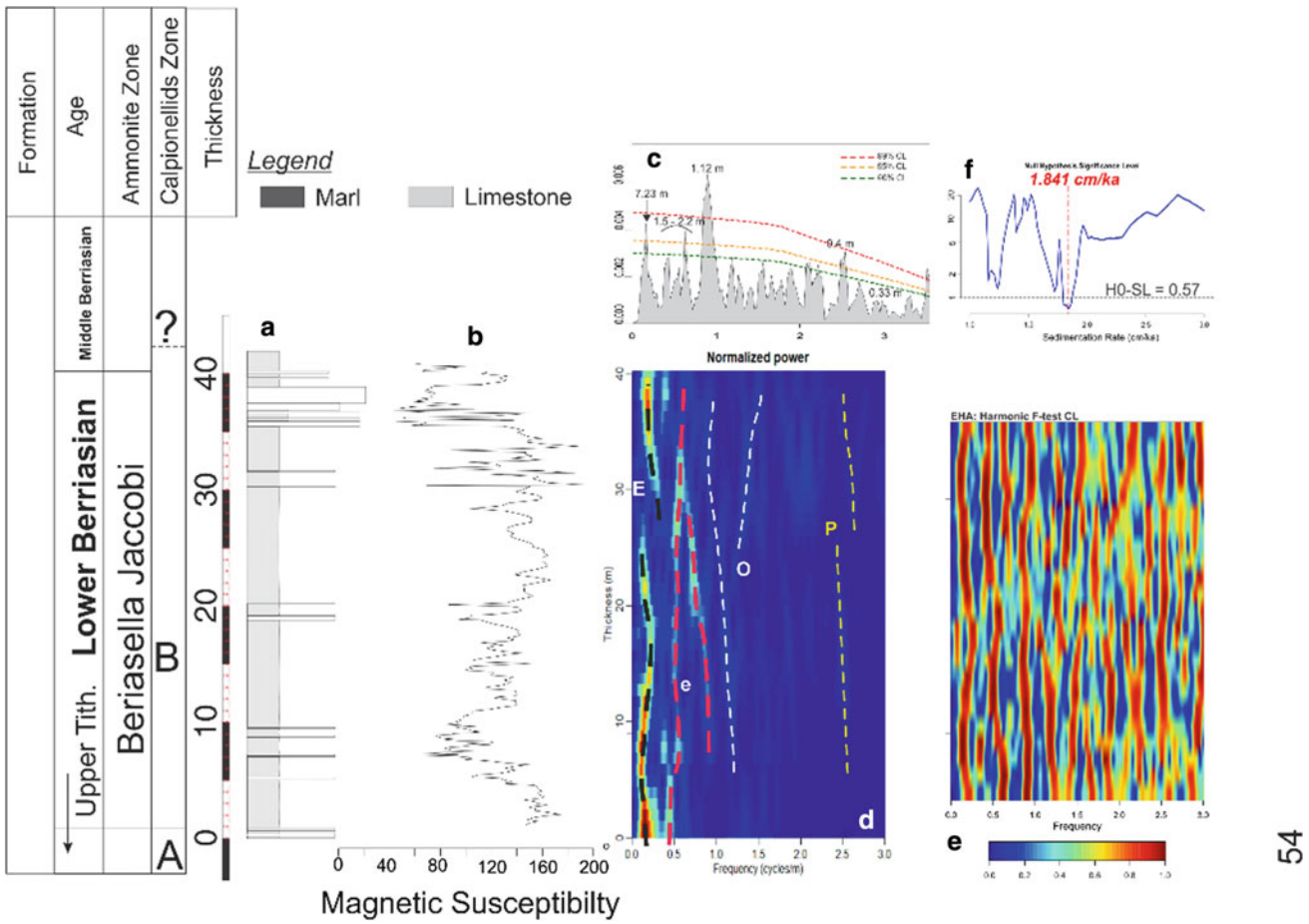

Fig. 1 Spectrogram of amplitudes of the MS data showing changes in the SAR. **a** Lithostratigraphy of the studied section (lower Sidi Khalif Formation). **b** Signal of the MS data (in 10^{-9} m^3/Kg). **c** Power spectrum density of the applied MTM. **d** Amplitude spectrogram of the MS data. **e** F-test of the corresponding detected cycles. **f** Sedimentation rate calculated using the ASM method (Meyers 2014)

Therefore, MS is most likely controlled by detrital input from clay minerals versus dilution by carbonate. Thus, an increasing trend up section (except the uppermost part of the section) is linked to a progressive enrichment of the marls with continental content.

We extracted the E405 kyr cycles from the MS signal and filtered them using the taner filter (Taner 2000). We, afterward, counted simply the number of long-eccentricity cycles along the entire analyzed section, which pointed to a number of 5 cycles. This allowed us to reconstruct a floating timescale for the Berriasella Jacobi ammonite zone in the study area. The duration estimate using the cyclostratigraphy approach has revealed a very close time interval to that estimated by the GTS 2012 (Gradstein 2012). Furthermore, the tuning of the MS signal to the astronomical solutions of Laskar et al. (2011) as well as the ASM method is an unpreceded harmony giving each the same SAR of 1.84 cm/kyr. This value of SAR goes in line with deep marine environment succession, which had been deposited under a passive margin associated with the opening of Paleotethys Ocean around the Jurassic-Cretaceous transition.

5 Conclusions

High-resolution cyclostratigraphic analysis from magnetic susceptibility (MS) was undertaken on the Berriasella Jacobi ammonite zone. Spectral analyses of MS variations in the studied section show evidences of orbital cycles (eccentricity, obliquity and precession). The 405 kyr cyclicity (long eccentricity), considered to be the dominant orbital period during the pre-Cenozoic era, was used to estimate duration of the studied ammonite zone and the average sediment accumulation rate.

References

Gradstein, F.M.: Introduction. In: The Geologic Time Scale, pp. 1–29. Elsevier (2012). https://doi.org/10.1016/B978-0-444-59425-9.00001-9

Kodama, K.P., Hinnov, L.A.: Rock Magnetic Cyclostratigraphy, p. 165. Wiley & Sons, Ltd. (2015)

Laskar, J., Gastineau, M., Delisle, J.-B., Farrés, A., Fienga, A.: Strong chaos induced by close encounters with Ceres and Vesta. Astron. Astrophys. **532**, L4 (2011). https://doi.org/10.1051/0004-6361/201117504

M'Rabet, A.: Stratigraphie, sédimentation et diagenèse carbonatée des séries du Crétacé inférieur de Tunisie centrale, 540 p. Thèse de l'Université Paris Sud, Orsay (1981)

M'Rabet, A.: Stratigraphie, sédimentation et diagenèse carbonatée des séries du Crétacé inférieur de Tunisie centrale. Annales des Mines et de la Géologie, 30, Tunis, 412 p (1987)

Meyers, S.: Astrochron: an R package for Astrochronology (2014). Available at: https://cran.r-project.org/package=astrochron

Taner, M.: Attributes Revisited. Technical Publication. Rock Solid Images Inc., Houston, Texas (2000)

Thomson, D.J.: Spectrum estimation and harmonic analysis. Proc. IEEE **70**, 1055–1096 (1982). https://doi.org/10.1109/PROC.1982.12433

New Insights About Significant Maastrichtian Chronostratigraphic Boundaries in Central-Eastern Tunisia

Ezzedine Saïdi, Radhouane Ayadi, and Dalila Zaghbib-Turki

Abstract

The Upper Cretaceous boundaries have been analyzed globally by involving several taxonomic groups (e.g., ammonites, inoceramids, belemnites, foraminifers, nanofossils) in accordance with the recommendations of the Second International Symposium on Cretaceous Stage Boundaries in Brussels in 1995. However, a few chronostratigraphic boundaries are still under debate and need further clarifications (e.g., the Campanian–Maastrichtian (C-M) boundary). In this study, we focus on the Maastrichtian boundaries, based on planktic foraminifers from subsurface successions of central-eastern Tunisia. Three boundaries are highlighted: (1) a subsurface substitute for the newly defined C-M boundary, (2) a subsurface substitute for the early-late Maastrichtian boundary, and (3) the Cretaceous-Paleogene (K-Pg) transition. The C-M boundary is indicated by the last occurrence (LO) of *Radotruncana subspinosa*, which is correlated with the first occurrences (FOs) of the planktic foraminifers *Rugoglobigerina scotti* and *Contusotruncana contusa*, and the FO of benthic foraminifer *Bolivinoides draco*. The LO of *Contusotruncana fornicata* characterizes the early-late Maastrichtian boundary, which coincides with the FO of *Abathomphalus mayaroensis*. The first downhole occurrence (FDO) of most Upper Cretaceous planktic foraminifers indicates the transition from the Cretaceous to the Paleogene. The identified boundaries are correlated with two sections from north-western Tunisia in order to delineate their lateral extent and to evaluate their chronostratigraphic value. The present study also aims at a better understanding of the biostratigraphical record of the Maastrichtian successions in the Sahel domain and at highlighting undetectable lithostratigraphic units by using either seismic and/or log data.

Keywords

Campanian–Maastrichtian boundary • *Radotruncana subspinosa* • Early-late Maastrichtian boundary • *Contusotruncana fornicata* • Central-eastern Tunisia

1 Introduction

Most biostratigraphic studies dealing with the Upper Cretaceous successions in the Tethyan realm involved foraminifers (Nederbragt 1991; Atlas of late Cretaceous globotruncanids 1984; Robaszynski et al. 2000; Saïd 1978) in order to specify the Upper Cretaceous stage boundaries. Lately, (Saïdi and Zaghbib-Turki 2016) and (Bejaoui et al. 2019) provided further accuracies about the Campanian–Maastrichtian (C-M) boundary in north-western Tunisia, in accordance with the recommendations issued from the International Commission on Stratigraphy (ICS) during the Brussels symposium of 1995. The present work aims to apply these new insights and to characterize the early-late Maastrichtian boundary and the Cretaceous-Paleogene (K-Pg) transition in three wells form central-eastern Tunisia (B1, B2 and B3) where it is challenging to identify them within the monotonous marly facies of the El Haria Formation (Burollet 1956) using only seismic and/or log data.

E. Saïdi (✉)
Petroleum Services Department, Tunisian Public Oil Company-ETAP, Petroleum Research and Development Center-CRDP, 2035 Tunis, Tunisia
e-mail: ezzedine.saidi@etap.com.tn

R. Ayadi
Faculty of Sciences of Bizerte, Earth Sciences Department, University of Carthage, Jerzouna, 7021 Tunis, Tunisia

D. Zaghbib-Turki
Faculty of Sciences, Department of Geology, University of Tunis El Manar, Campus Universitaire, El Manar, 2092 Tunis, Tunisia

A. Çiner et al. (eds.), *Recent Research on Geomorphology, Sedimentology, Marine Geosciences and Geochemistry*, Advances in Science, Technology & Innovation, https://doi.org/10.1007/978-3-030-72547-1_43

2 Materials and Methods

This study focuses on the Maastrichtian successions drilled by three wells from central-eastern Tunisia. The samples spacing varies from 2 to 10 m or more, depending on the availability of cutting samples. Sufficient amount from each sample was soaked in H_2O_2 solution, washed through a set of Afnor sieves (63–630 µm), sonically agitated, oven dried at a temperature below 50 °C, and then sorted for picking out typical foraminifers. The well preserved planktic foraminifers, which were picked out from the cutting samples were herein analyzed in order to detect the significant Maastrichtian biohorizons. The taxonomic identification was carried out using mainly the works of Nederbragt (1991) and (Atlas of late Cretaceous globotruncanids 1984).

3 Results

The studied B1, B2 and B3 wells lie in central-eastern Tunisia close to the Essouassi region (Fig. 1), which belongs to the Sahel domain (Bouaziz et al. 2002). The identified biohorizons are correlated with published results from the Kalâat Senan (Bejaoui et al. 2019; Robaszynski et al. 2000; Saïdi and Zaghbib-Turki 2016) and Ellès (Saïd 1978) regions (Fig. 2), belonging both to the Atlassic domain (Bouaziz et al. 2002).

3.1 Significant Bioevents

The Cretaceous-Paleogene (K-Pg) transition (Saïd 1978; Zaghbib-Turki et al. 2001) indicated by the first downhole occurrence (FDO) of most Upper Cretaceous planktic foraminifers (e.g. *Racemiguembelina* spp., *Guembelitria* spp.), constitutes the first identified significant boundary (in the downhole direction). Hence, we consider this boundary as the reference datum for the chronostratigraphic correlation (Fig. 2). About 50 m below the latter, the early-late Maastrichtian boundary corresponds to the FDO of *Contusotruncana fornicata* (Saïdi 2017; Saïdi and Zaghbib-Turki 2019) and constitutes the second identified biohorizon (Fig. 2). The third significant chronostratigraphic biohorizon corresponds to the C-M boundary as indicated by the FDO of *Radotruncana subspinosa* (Premoli Silva and Verga 2004; Saïdi 2017; Saïdi and Zaghbib-Turki 2019), which occurs about 50 m below in the studied B1 and B3 wells (Fig. 2).

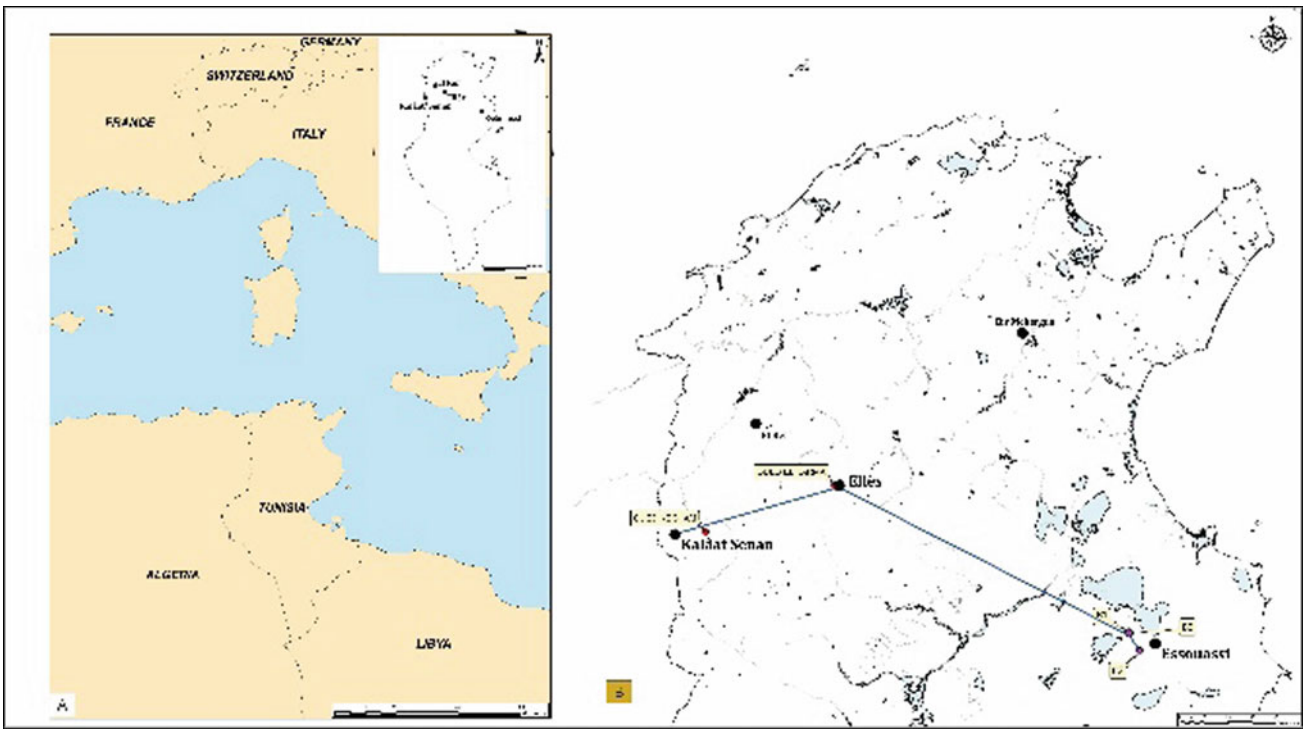

Fig. 1 Location map of the studied wells. **A** overview of the position of Tunisia in the Mediterranean Sea, **B** geographic position of the studied wells. The map shows the WNW–ESE correlation of the studied wells with selected Maastrichtian outcrops from the Kalâat Senan and Ellès regions (north-western Tunisia)

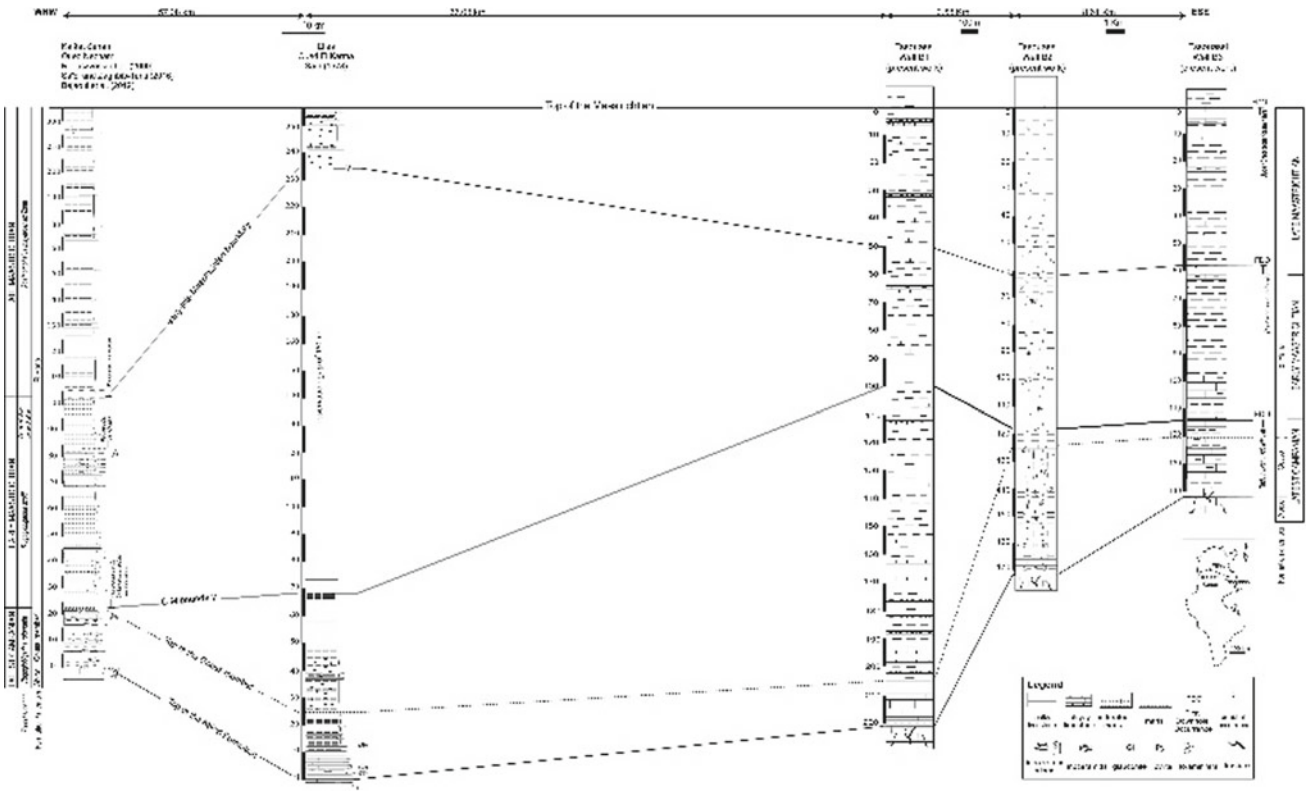

Fig. 2 Chronostratigraphic correlation between the studied wells and outcrops from north-western Tunisia (Bejaoui et al. 2019; Robaszynski et al. 2000; Saïd 1978; Saïdi and Zaghbib-Turki 2016). The lateral scales between the wells are different from the common lateral scale. Chronostratigraphic attributions in the Ellès region are exclusively proposed in this study except for the top of the Maastrichtian

3.2 Chronostratigraphic Correlation

The identified chronostratigraphic and lithostratigraphic boundaries are correlated with the published results from north-western Tunisia (Bejaoui et al. 2019; Robaszynski et al. 2000; Saïd 1978; Saïdi and Zaghbib-Turki 2016) in order to evaluate their biostratigraphic value and highlight lateral thickness changes, if any. These chronostratigraphic boundaries are discussed in the section below.

4 Discussion

The well-documented K-Pg boundary (Saïd 1978; Zaghbib-Turki et al. 2001) constitutes the most significant chronostratigraphic boundary of the present study; however, the absence of the iridium layer and the associated spinels and chocked grains of quartz (Zaghbib-Turki et al. 2001) in the studied wells evidences a probable faulting activity. Thus, we label this bioevent as the top of the Maastrichtian (Fig. 2). The LO of *Contusotruncana fornicata* is documented to occur close to the FO of *Abathomphalus mayaroensis* in the Tethyan domain (Arz and Molina 2002; Premoli Silva and Verga 2004; Atlas of late Cretaceous globotruncanids 1984; Saïd 1978), which indicates a late Maastrichtian age (Arz and Molina 2002; Atlas of late Cretaceous globotruncanids 1984; Saïdi and Zaghbib-Turki 2016). Consequently, the FDO of *Contusotruncana fornicata* characterizes the transition between the early and late Maastrichtian in the studied wells. *Radotruncana subspinosa* is documented to disappear close to the C-M boundary in the Tethyan realm (Arz and Molina 2001, 2002; Premoli Silva and Verga 2004; Saïdi and Zaghbib-Turki 2019). This species was not found in the B2 well but the C-M boundary is approximated by the occurrence of the C-M boundary index species *Rugoglobigerina scotti* in this well. *R. subspinosa* was reported in Oued El Karma 30 m above the top of the Gouss member by Robaszynski and Mzoughi (2010) close to the FO of *R. scotti* reported by Saïd (1978) (Fig. 2). Hence, we consider the LO/FDO of *R. subspinosa* as a reliable indicator of the C-M boundary, especially in the drilling [Saïdi and Zaghbib-Turki (2019), this work (B1 and B3 Wells)].

The biostratigraphic correlation between north-western and central-eastern Tunisia led to recognize: (1) a more subsiding area in north-western Tunisia, especially in the Ellès region in spite of the particularly subsiding Maastrichtian succession crosscut by the B1 well; (2) a quite

constant thickness of the early and late Maastrichtian successions in the Sahel domain, which increases towards north-western Tunisia. The increased thickness of the early Maastrichtian successions in Oued El Karma is probably related to the observation gap; and (3) the evidence of tectonic movements during the late Campanian and the Maastrichtian, which were probably more pronounced in the Essouassi region belonging to the deformed Sahel domain (Bouaziz et al. 2002). These movements can be evidenced locally by the fractures affecting the Abiod Formation limestone and the lateral change of strata thickness during the Maastrichtian (Fig. 2).

5 Conclusions

Three significant chronostratigraphic boundaries are highlighted in the Essouassi region based on planktic foraminifers; (1) the K-Pg transition; (2) the early-late Maastrichtian boundary and (3) the C-M boundary. Thus, we consider the FDOs of *Contusotruncana fornicata* and *Radotruncana subspinosa* as reliable bioevents, i.e., last occurrences (LOs) and we propose them to indicate the early-late Maastrichtian and the C-M boundaries in wells, respectively.

The chronostratigraphic correlation reveals a lateral change in thickness distribution of the Maastrichtian successions. These successions get thinner in central-eastern Tunisia in comparison with the subsiding north-western basins. This correlation highlights a tectonic activity during the Maastrichtian, which was locally more pronounced in the Essouassi region.

References

Arz, J.A., Molina, E.: Planktic foraminiferal quantitative analysis across the Campanian/Maastrichtian boundary at Tercis (Landes, France). In: Odin, G.S. (ed.) The Campanian-Maastrichtian Stage Boundary: Characterisation at Tercis les-Bains (France) and Correlation with Europe and Other Continents. Developments in Palaeontology and Stratigraphy, vol. 19, pp. 339–348. Elsevier, Amsterdam, the Netherlands (2001)

Arz, J.A., Molina, E.: Late Campanian and Maastrichtian biostratigraphy and chronostratigraphy based on planktonic foraminifera in temperate and subtropical latitudes (Spain, France and Tunisia). Neues Jahrb Für Geol P-A **224**, 161–195 (2002)

Bejaoui, A., Saïdi, E., Zaghbib-Turki, D.: Small benthic foraminiferal biostratigraphy and palaeoecology during the Campanian-Maastrichtian transition in northwestern Tunisia. Turk. J. Earth Sci. **28**, 500–530 (2019)

Bouaziz, S., Barrrier, E., Soussi, M., Turki, M.M., Zouari, H.: Tectonic evolution of the northern African margin in Tunisia from paleostress data and sedimentary record. Tectonophysics **357**, 227–253 (2002)

Burollet, P.F.: Contribution à l'étude stratigraphique de la Tunisie centrale. Ann. Mines Géologie **18**, 1–293 (1956)

Nederbragt, A.J.: Late Cretaceous biostratigraphy and development of Heterohelicidae (planktic foraminifera). Micropaleontology **37**(4), 329–372 (1991)

Premoli Silva, I., Verga, D.: Practical manual of Cretaceous planktonic foraminifera. In: Verga, D., Rettori, R. (eds.), International School on Planktonic Foraminifera, 3rd Course: Cretaceous, 283 p. Universities of Perugia and Milan, Tiporafia Pontefelcino, Perugia, Italy (2004)

Robaszynski, F., Mzoughi, M.: The Abiod Formation at Ellès (Tunisia): tripartite lithology, biohorizons based on globotruncanids and ammonites, duration, location of Campanian-Maastrichtian boundary, correlation with Kalaat Senan and the Tercis (France) stratotype. Notebooks on Geology CG2010–A04 (2010)

Robaszynski, F., Caron, M., Gonzalez Donoso, J.M., Wonders, A.A.H.: Atlas of late Cretaceous globotruncanids. Rev. Micropaléontol. **26**, 145–305 (1984)

Robaszynski, F., Gonzalez Donoso, J.M., Linares, D., Amedro, F., Caron, M., Dupuis, C., Dhont, A.V., Gartner S.: Le Crétacé supérieur de la région de Kalâat Senan, Tunisie centrale. Litho-biostratigraphie intégrée: zones d'Ammonites, de Foraminifères planctoniques et de Nannofossiles du Turonien au Maastrichtien. B Cent. Rech. Expl. **22**, 359–490 (2000)

Saïd, R.: Etude stratigraphique et micropaléontologique du passage Crétacé-Tertiaire du synclinal d'Ellès (region Siliana-Sers) Tunisie centrale. Ph.D., Université Pierre et Marie Curie, Paris, France (1978)

Saïdi, E.: Foraminifères de l'intervalle Campanien terminal-Maastrichtien inférieur en Tunisie septentrionale et centrale: Taxonomie, Biostratigraphie et Paléoécologie, pp. 1–173. Thèse Université de Tunis El Manar (2017)

Saïdi, E., Zaghbib-Turki, D.: Planktonic foraminiferal biostratigraphy and quantitative analysis during the Campanian-Maastrichtian transition at the Oued Necham section (Kalâat Senan, central Tunisia). Turk. J. Earth Sci. **25**(6), 538–572 (2016)

Saïdi, E., Zaghbib-Turki, D.: Planktonic foraminiferal evidence of upper cretaceous in the well "A" (Gulf of Hammamet Area, Northeastern Offshore Tunisia) In: Boughdiri et al. (eds.) Paleobiodiversity and Tectono-Sedimentary Records in the Mediterranean Tethys and Related Eastern Areas Advances in Science, Technology & Innovation. CAJG 2018, pp. 121–123. Springer (2019)

Zaghbib-Turki, D., Karoui-Yaakoub, N., Said-Benzarti, R., Rocchia, R., Robin, E.: Révision de la limite Crétacé-Tertiaire de la coupe d'Ellès (Tunisie): proposition d'un nouveau parastratotype. Geobios **34**(1), 25–37 (2001)

The Zone of Allochthonous "Nappes" of the North of Tunisia: A Witness of the Early Stages of the Formation of the North-Maghrebian Chain

Jalila Saadi, Narjess Karoui, and Dalila Turki

Abstract

The sedimentological study of Senonian to Eocene carbonates in the Fernana—Ain Draham area (north of Tunisia) led us to improve paleogeographic constraints in the understanding the evolution of internal domains of the Magrebian Chain. The comparison between new stratigraphic logs and the revision of previous ones measured along the autochthone, parautochthone, Ediss Unit and Ain Draham-Adissa Unit supports, in general, this structural units subdivision, and offers new results. The stratigraphic revision and the facies analysis of the Senonian—Eocene series reinforce the allochthonous structural-unit subdivisions of the nappes zone that have undergone tangential displacements during late Tertiary. The study allowed us to specify the evolution of the Tunisia Tellian domain during this span of time. The abundance of more ancient dismantled rocks, at least late Maastrichtian in age, in the allochthonous units, implies a contemporaneous beginning of shortening.

Keywords

Senonian-Eocene • Carbonate • Mélange facies • Nappes • Tellian trough

1 Introduction

The Maghrebian chain resulted from a subduction-collision of the African plate under the Iberian-European one. The chain is subdivided into internal domains (Rif and Kabylie in Marocco and Algeria) then a flysch basin and external domains (tellian basin in Algeria and Tunisia), (Fig. 1a–c). The Tunisian Tellian domain occupies the Northern part of the country and forms the Eastern part of the Maghrebian Chain (Fig. 1a). The area corresponds to a narrow NNE–SSW domain characterized by stacked thrust sheets and corresponds to the most internal portion of the foreland thrust belt of the Maghrebian Chain in Tunisia (Rouvier 1977–1985; Belayouni et al. 2012; Euchi 2006; Chabbi et al. 2019). The domain is subdivided into several allochthonous units (Rouvier 1977–1985), (Fig. 1b), in the prolongation of the Algerian Units (Euchi 2006; Chabbi et al. 2019; Charaf 2012).

The study of the Upper Cretaceous-Eocene series of the Tellian domain of the NW of Tunisia was undertaken with the aim of confirming the division into structural units (nappes) established by Rouvier (1977–1985) and supported by Belayouni et al. (2012), Euchi 2006), but argued by Charaf (2012). The work is based on stratigraphic revision and facies analysis.

The structural units considered as nappes by Rouvier (1977–1985) are superposed from SE to NW (Fig. 1b–e). The autochthonous and the paraautochthonous correspond to deformed domains, overcome by nappes with more internal provenance: Adissa, Ain Draham, Ediss and Kasseb unit. The set constitutes thin allochthonous units, recovered by tangential contact by the Oligo-Miocene of the Numidian nappe (Fig. 1d–e).

- The Ain Draham, Adissa and Ediss units (upper Cretaceous to Eocene–Oligocene) characterize the Tellian domain. These imbricates units are in tectonic contact with a major NE-SW Triassic body (Fig. 1b–d). The occurrence along the boundary of a Senonian-Eocene "microbreccias" based on marls of the Upper Eocene Tellian facies that can locally reach the lower Oligocene is a proof of the occurrence of stratigraphically abnormal recoveries of large scale in Tunisia (Rouvier 1977–1985).

J. Saadi (✉) · N. Karoui
Faculty of Sciences of Bizerte, University of Carthage, 7000 Bizerte, Tunisia

D. Turki
Faculty of Sciences Tunis El manar2, University of Tunis, 2092, El Manar 2, Tunis, Tunisia

A. Çiner et al. (eds.), *Recent Research on Geomorphology, Sedimentology, Marine Geosciences and Geochemistry*, Advances in Science, Technology & Innovation, https://doi.org/10.1007/978-3-030-72547-1_44

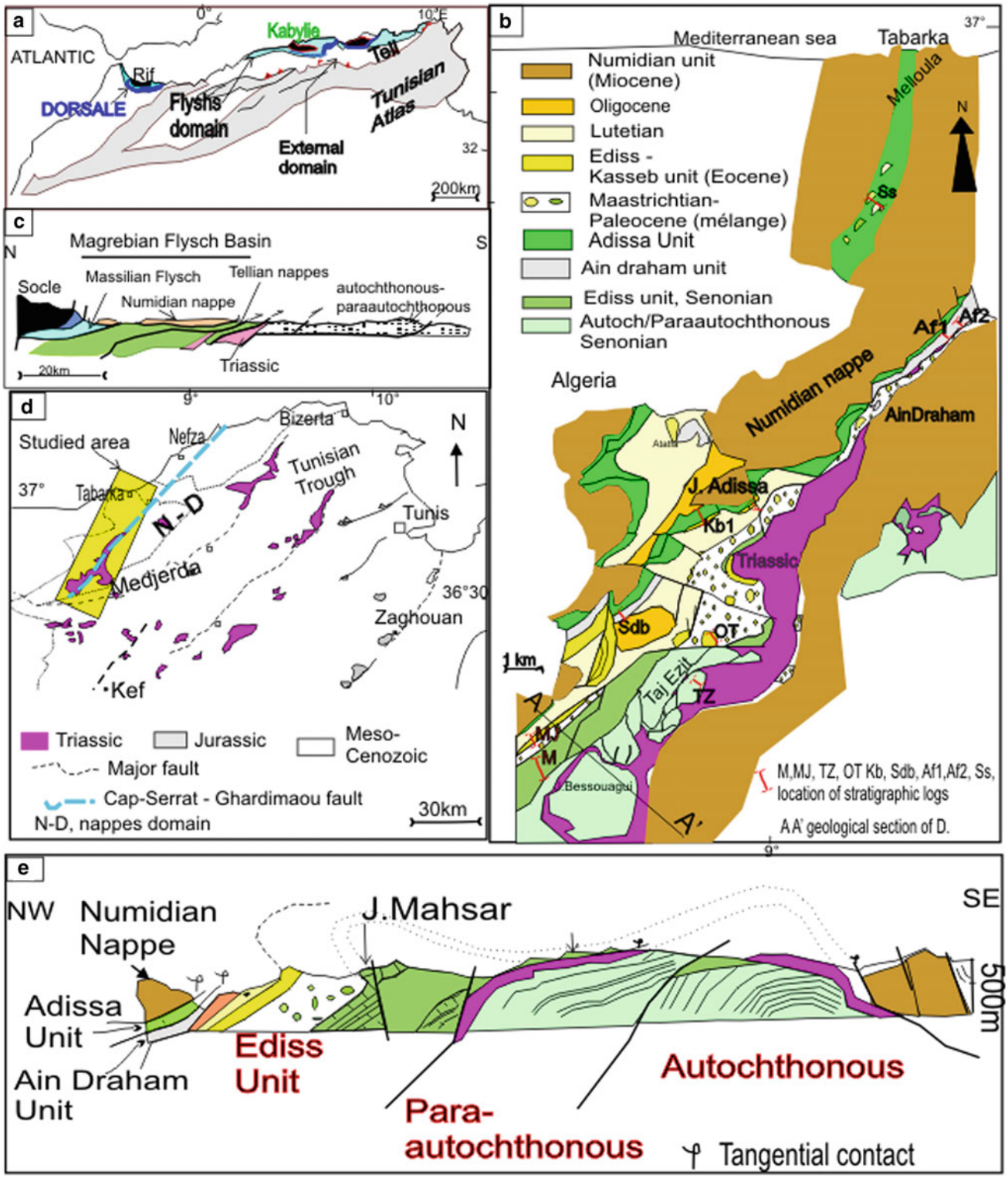

Fig. 1 **a** Location of the Maghrebian Chain in North Africa; **b** Major fault system of northern Tunisia and location of the studied area; **c** Simplified section in the eastern Algeria showing the relationship between the major domains of the north-Maghrebian Chain, from Charaf (2012). **d** Geological map of the studied area drawn from Rouvier 1977–1985; **e** Geological section showing the relationship between the structural units of the nappes domain, drawn from Rouvier (1977–1985)

- The Ediss Unit includes the same stratigraphic intervals but the facies reflect more proximal domain than the Adissa–Ain Draham series.
- The paraautochthonous and autochthonous units correspond to two structural units belonging to the most external deformed domain and constitute the substrate of the Ediss, Ain Draham and Adissa units (Rouvier 1977–1985).The two domains are separated by a major fault named "fault of Ghardimaou-Cap Serrat" (Fig. 1b) which constitute a paleogeographic major trend.
- The Kasseb unit corresponds to the most allochthonous Tellian structural unit of northern Tunisia. This deformed unit is overcome, by tectonic contact in the Medjerda Mountains, by the marine Miocene deposit.

The stratigraphic sections were studied in the different structural units to specify their depositional settings, and geodynamic evolution. Stratigraphic revisions and correlations between the different domains led to recognize the infilling of sub-basins and their evolution in the relationship with the early stage of the formation of the Maghrebian Chain.

2 Materials and Methods

Ten stratigraphic sections of the upper Cretaceous, Paleocene and Early Eocene units were measured and sampled in the Fernana–Ain Draham–Tabarka area (Fig. 1b). The sections were chosen in the different domains previously defined by Rouvier (1977–1985). Most sedimentological interpretations derive from field observations, strengthened by petrographic and microfacies observations of thin sections. Field observations include lithology, sorting, sedimentary features, faunal content and accurate thickness measurements.

3 Results

Senonian: The Adissa/Ain draham units are characterized by thin slumped limestones turbidites (late Maastrichtian) attributed to the distal domain of the basin. The autochthone/paraautochthone and Ediss unit correspond to the proximal globally hemipelagic thick carbonate slope deposits (600 m thick at the Ediss unit).

The late Maastrichtian-Paleocene is represented by a developed (over 1000 m of thickness) mélange deposit ("marnes à boules jaunes" of Rouvier 1977–1985, type 4 facies sensu (Festa et al. 2012)) characterized by marlstones with slumped metrical limestones to marlstones blocks provided by older deposits (Campanian and Maastrichtian).

Eocene (Ypresian-Lutetian): We can distinguish three major domains: Adissa/Ain Draham unit, Ediss/Kasseb unit and autochthone/paraautochthone unit corresponding, respectively, to the distal basin (thin slumped limestones turbidites), a hemipelagic slope with local turbidity currents and an isolated carbonate shelf.

The late Eocene (Lutetian) is marked by a return to a mélange facies (marlstones with boulders and gravels). The facies are deeper than the Paleocene mélange and the metrical carbonate blocks of Eocene are more anguleous.

4 Discussion

The subdivision into autochthonous/paraautochthonous/Ediss unit/Tellian units (Adissa and Ain Draham) seem to be fully justified by our data and corresponds to distinct palaeogeographical domains defined by Rouvier (1977–1985). The distinction between these structural units is consistent with the clear-cut change of the sedimentary facies, and by changes in thicknesses.

In the present state of the work, it seems that the facies of the Adissa Unit and the Ain Draham Unit come from a relatively close and much more internal domain than the Ediss/paraautochthonous/autochthonous units. (Rouvier 1977–1985; Raoult 1974) and (Vila 1971) suggested that the Adissa unit belongs to an intermediate domain between that of the Massylian Flysch (Maghrebian Flysch Basin defined in the Algerian domain (Raoult 1974; Durand-Delga 1969; Vila 1971; Guerrera et al. 2005), Fig. 1c) and the internal part of the Tellian basin.

5 Conclusions

The study of Senonian-Eocene cycle deposits of the Tellian domain of the northwestern Tunisia, led to support the idea that the Ain Draham–Fernana–Tabarka area belongs to the nappes domain on the contrary of OuldBagga et al. (2006). The paleogeographic distinction between the Adissa–Ain Draham units and the Ediss–autochthonous–paraautochthonous units is very clear. This distinction is emphasized by the Cap Serrat–Ghardimaou major fault. The Adissa–Ain Draham unit belongs to the Northern part of the Tellian basin, while the Ediss/Kasseb unit and the autochthonous/paraautochthonous belong to its Southern side.

References

Belayouni, H., Guerrera, F., Martin-Martin, M., Serrano, F.: Stratigraphic update of the Cenozoic Sub-Numidian formations of the Tunisian Tell (North Africa): Tectonic/sedimentary evolution and correlations along the Maghrebian chain. J. Afr. Earth Sci. **64**, 48–64 (2012)

Chabbi, A., Chermiti, A., Chouabbi, A., Benyoussef, M.: The external domain of Maghrebides Belt on the North–East of Algeria, Souk

Ahras Segment: Definition of Structural Units, Block Structure and Timing of Thrusts Setting. In: Rossetti, F. et al. (eds.), The Structural Geology Contribution to the Africa-Eurasia Geology: Basement and Reservoir Structure, Ore Mineralisation and Tectonic Modelling (2019)

Charaf, Ch.: La chaîne des Maghrébides. Publ. OF Univ. Université Ferhat Abbas de Sétif. Internet, pp. 1–5 (2012)

Durand-Delga: Mise au point sur la structure du Nord-Est de la Berbérie. Publ. Serv. Géol. Algérie **39**, 89–131 (1969)

El Euchi, H.: Strutural styles and tectonic habitats in northern Tunisia. In: Proceeding of the ETAP, Tunisia (2006)

Festa, A., Dilek, Y., Pini, G.A., Codegone, G., Ogata, K.: Mechanisms and processes of strata disruption and mixing in the development of mélanges and broken formations: redefining and classifying mélanges. Tectonophysics **568–569**, 7–24 (2012)

Guerrera, F., Martin-Martin, M., Perrone, V., Tramontana, M.: Tectono-sedimentary evolution of the southern branch of the western Tethys (Magrebian Flysch basin and Lucanian ocean). Terra Nova **17**, 358–367 (2005)

OuldBagga, M.A., Abdeljaouad, S., Mercier, E.: La «zone des nappes» de Tunisie: une marge méso-cénozoïque en blocs basculés modérément inversée (région de Tabarka/Jendouba; Tunisie nord-occidentale). Bull. Soc. Géol. France **177**(3), 145–154 (2006)

Raoult, J.F.: Relation entre la dorsale Kabyle et les flysch sur la transversale de J.Rhedir; phases tangentielles éocenes, paléogéographie (nord du Constantinois, Algérie). Bull. Soc. Geol. Fr **7**(11), 523–543 (1974)

Rouvier, H.: Géologie de l'Extrême Nord—Tunisien: Tectonique et paléogéographies superposées à l'extrémité orientale de la chaîne nord-maghrébine. Thèse d'Etat, Paris VI,.in Ann. Des Mines et de la Géologie, n°29. O N Mines, Tunisia, 703 p (1977–1985)

Vila, J.M.: Paléogéographie et tectonique des unitées allochtones de type tellien et de type flysch à microbrèches dans le Nord-Est du Constantinois (Algérie). C. R. Acad. Sci. Paris **272**(8), 1047–1050 (1971)

Stratigraphy of the Paleogene Tethyan Carbonate Banks and the Diachronous Arabian Plate Convergence

Basim Al-Qayim

Abstract

The shoaling sequence of the Zagros foreland basin of NE Arabia is punctuated by linear bank-ramp carbonate bodies developed over inverted intra-basinal highs. These carbonate facies are dominated by coralgal-foraminiferal associations that have been assigned to the Paleocene – Eocene age. These banks display similarities in microfacies and benthic community types with a different chronostratigraphic evolution. These carbonate bodies are shaped over a series of an intra-basinal highs arranged in a NW–SE trend parallel to the Zagros trend, and have evolved in response to the compressional tectonic and basin inversion history. The timing of the development of these banks and their facies associations reveal a diachronous basin inversion, which is consistent with the oblique convergence of the Arabian platform.

Keywords

Inversion tectonics • Carbonate banks • Iraq • Zagros • Paleogene

1 Introduction

The inversion history of the Zagros foreland basin of northeast Arabia commenced during the Paleogene time. Basin inversion is reflected by the occurrence of a series of an intra-basinal, elongated, carbonate banks developed along NW–SE trending highs during the basin shoaling stage. The banks are represented by the Sinjar Formation reefal limestone and the associated lagoonal dolostone of the Khurmala Formation in northern Iraq. The line of these carbonates banks separate a flysch trough (proximal foreland) to the northeast, and the open sea pelagic marlstone of the intra-shelf basin (distal foreland) to the southwest of these highs (Bellen et al. 1959). Three important banks are recognized in north Iraq from northwest: Sinjar, Kirkuk, and Sulaimaniyah banks (Fig. 1). Hydrocarbons accumulated in similar setting worldwide, which prompted interest in the regional study of these carbonates to reveal their origin and development as well as their association with the basin evolution and its tectonic implications.

2 Materials and Methods

The samples used in this study were collected using outcrops and subsurface sections from around 40 localities from northern Iraq. Data including field observations and stratigraphic measurements, microfacies analysis of 80 thin sections, and litho- and biostratigraphic correlation among the studied sections, and with neighboring areas. Additional sources of data were compiled from previous studies and reported for the regional coverage of the basin.

3 Results

3.1 Microfacies Analysis and Facies Associations

Petrographic studies of samples from the carbonate banks showed that all the three banks include similar microfacies types forming eight basic facies. These facies represent shallow marine coralgal carbonate banks associated with carbonate ramps on both sides of the highs (Fig. 2). The bank-ramp association was differentiated based upon benthic foraminiferal assemblages. The recognized facies include: ***inner ramp*** coralgal patch reef, algal bank, intra-bank miliolid-pelloidal pools, and the nummulitic –bryozoan fore-bank shoal. The ***middle ramp*** is dominated by flat

B. Al-Qayim (✉)
Komar University of Science and Technology, Sulaimaniyah, Kurdistan Region, Iraq
e-mail: Basim.alqayim@komar.edu.iq

A. Çiner et al. (eds.), *Recent Research on Geomorphology, Sedimentology, Marine Geosciences and Geochemistry*, Advances in Science, Technology & Innovation, https://doi.org/10.1007/978-3-030-72547-1_45

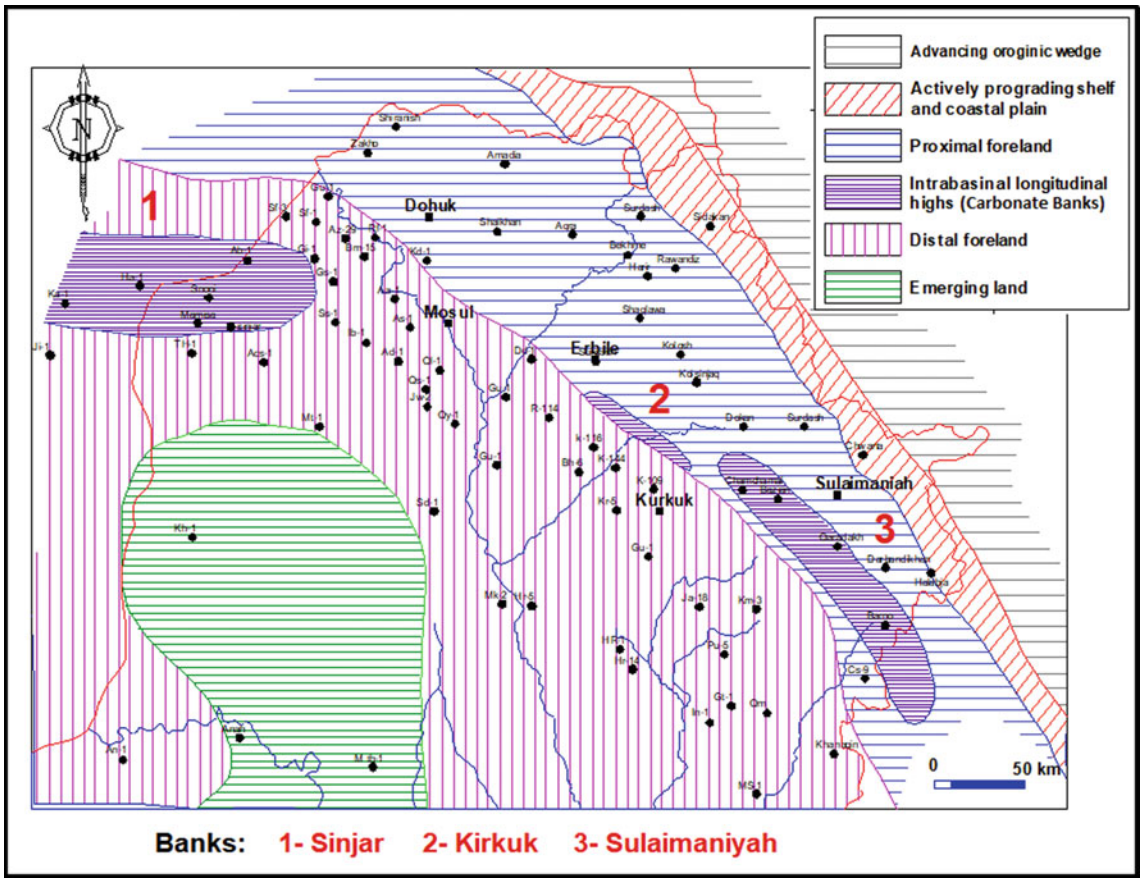

Fig. 1 Paleogeography of the Zagros foreland basin showing location of the Paleogene banks

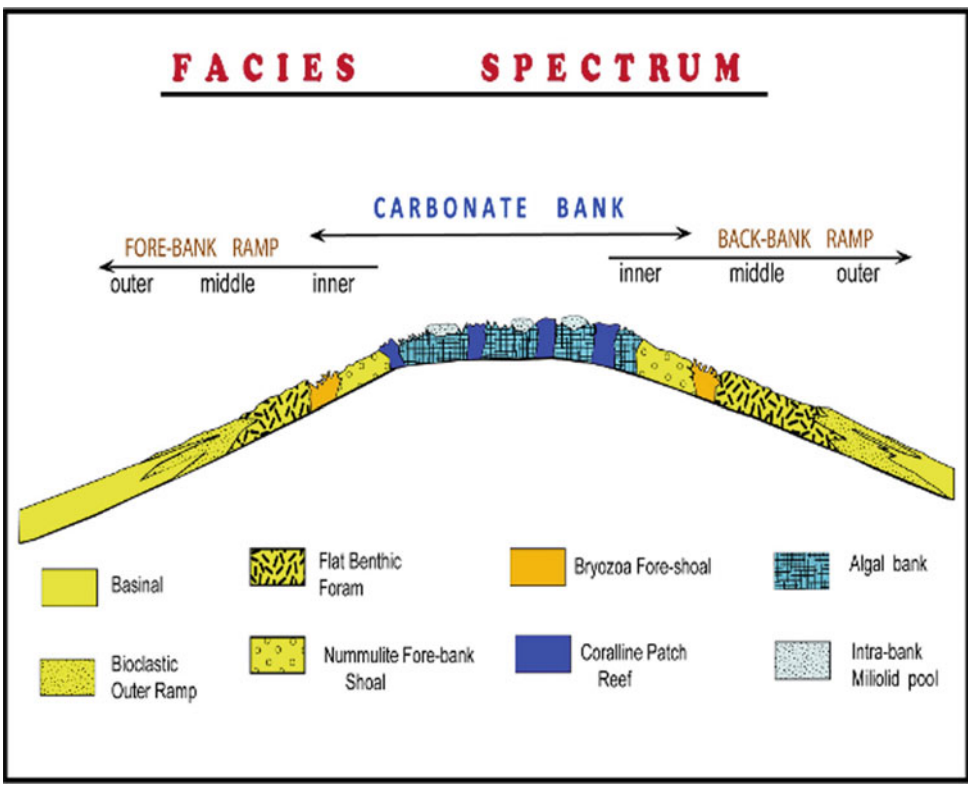

Fig. 2 Facies spectrum of the Tethyan Paleogene carbonate banks and associated ramp

benthic foraminiferal assemblages, and the ***outer ramp*** is characterized by the intercalation of bioclastic storm deposits with basinal marlstone or shale.

The distributions of these facies over each bank within the intra-basinal locations indicate that these banks developed upon structural growth that produced the intra-basinal highs during basin inversion history. The Sinjar bank is related to Sinjar trough inversion (Brew et al. 1999). The Sulaimaniya and Kirkuk banks are associated with a swelling related to a deep-seated basement fault (Berberian 1995; Ibrahim 2009).

3.2 Lithostratigraphic and Biostratigraphic Correlation

Several examined sections and localities showed that the facies evolution of these banks follows a similar pattern, with differences related to eustatic sea-level changes. However biostratigraphic correlation of the different facies at different sections of each bank shows little variation in age and history. The age of Sinjar Formation at Mamesa section from Sinjar Bank ranges from Thanetian to Ypresian (Al-Siddiki 1968). Both of the bank and the associated ramp were reported to have developed during Thanetian time (Fig. 3). The carbonates of the other two banks (Kirkuk and Sulaimaniyah) did not accumulate until early Ypresian time (Al-Siddiki 1968; Lawa 2004). At the beginning, only the bank facies were developed with no significant ramp facies. By the early Lutetian time, the Sinjar and Sulaimaniyah banks were fully developed with whole facies association, while Kirkuk bank became less effective and changed into extensive semi-restricted lagoon (The Khurmala Formation, Fig. 4). The Sulaimaniyah bank extends southeastward, that is, in the Bamo and Zhalla locations near the Iraqi-Iranian borders. The Sinjar Formation here is reported to have younger age, i.e., Lutetian (Lawa 2004). Using these chronostratigraphic data of the Sinjar Formation at these banks allows predicting that they become younger towards the southeastern part of the basin.

4 Discussion

The Zagros Paleogene carbonate banks appear to have developed in a sequence of time reflecting diachronous development. The Sinjar Bank was the first to appear (Thanetian) and grew with bank-ramp facies over a considerable area along the Sinjar anticline (Fig. 3). The other banks (Kirkuk and Sulaimaniyah) did not appear until the early Ypresian. The southeastern limit of the Sulaimaniyah Bank developed even later during the Lutetian time. Further, southeastward, the closely similar Paleogene carbonate bank of Iran (Taleh-Zang- Jahrum Formations) fully developed during the Lutetian (Taheri et al. 2008). The occurrence of

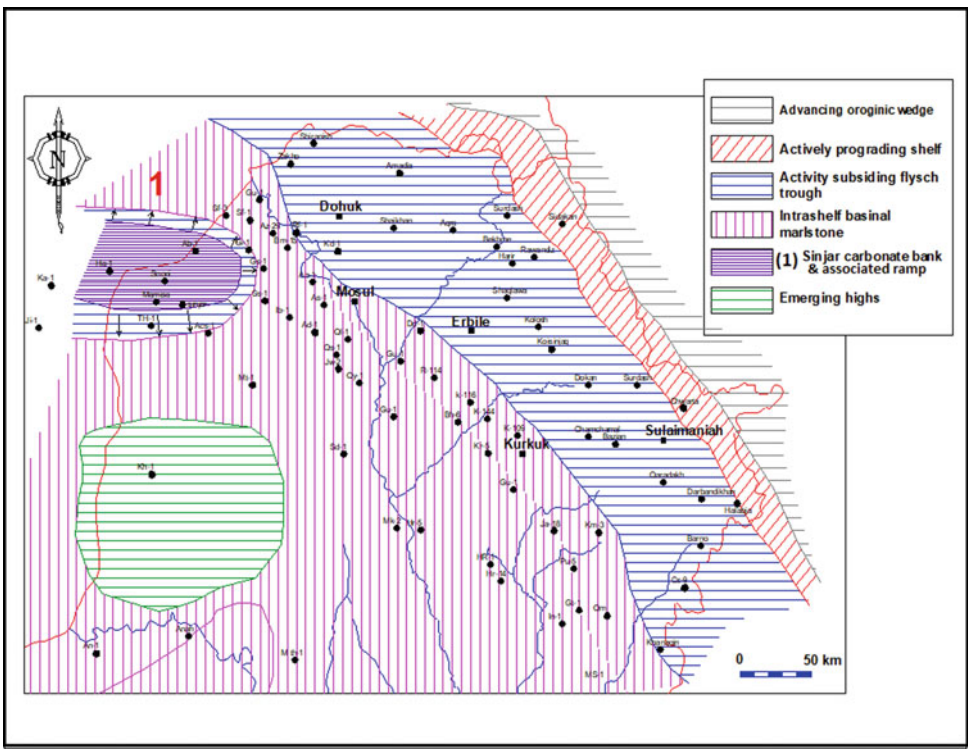

Fig. 3 Paleogeography of the Zagros foreland basin during Thanetian time

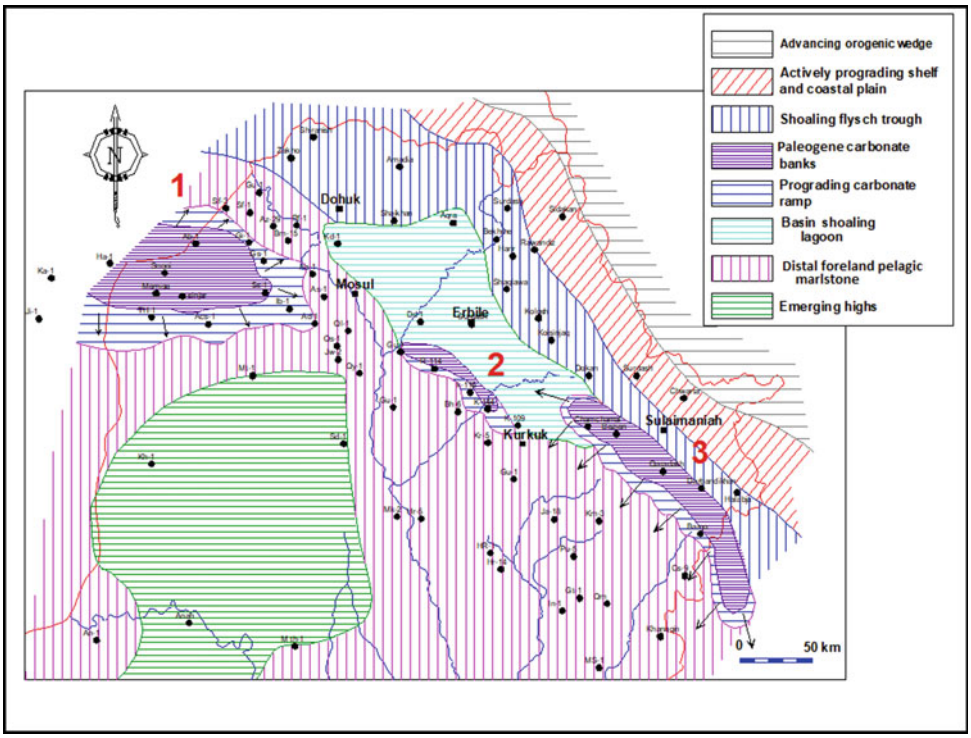

Fig. 4 Paleogeography of the Zagros foreland basin during Yepresian- Lutetian time

these banks was initiated in association with the growth of a belt of intra-basinal highs during the shoaling stage of the Zagros foreland basin (Al-Qayim 1994), and through the final convergence history of the Arabian margin. These highs are linked to a renewed movement over the basement master faults (Berberian 1995; Sherkati and Letouzey 2004) or to the shifting of the basin forebulge. Therefore, linking the age variation of these banks to the timing of tectonic developments of these basinal highs is conceivable. These highs have appeared in response to a developing basin forebulge in associattion with tectonic reactivation of basement faults during the Arabian plate convergence (Sepehr and Cosgrove 2004; Lamotte et al. 2011). The chronostratigraphic sequence of the development of the Zagros Paleogene banks appears to imply a diachronous basin evolution, and thus diachronous convergence of the Afro-Arabian margin from N- NW toward the SE.

5 Conclusions

The stratigraphic correlation of the identified facies of the Tethyan Paleogene carbonate banks, their distribution in the Zagros foreland basin, and the age of its microfossils indicate a chronostratigraphic shift from older to younger banks in NW–SE direction. The close association of these banks to the initiation to intra-basinal highs developed during the Zagros basin inversion suggests a diachronous convergence of the Afro-Arabian margin beneath the Eurasian Plate.

References

Al-Qayim, B.: Evolution of Flysch Basin along the Northeastern Margin of the Arabian Plate. In: Abed and others (eds.), Geology of Jordan and Adjacent Areas. (Geocome III), Amman, pp 347–372 (1994)

Al-Siddiki, A.: Stratigraphy and Microfacies of Sinjar Formation, 91 p. MSc. Thesis, University of Baghdad (1968)

Bellen, R.C., Dunnington,H., Wetzel, R., Morton, D.: Lexique Stratigraphique International. Asia (Iraq) **10**, 333 (1959)

Berberian, M.: Master blind thrust faults hidden under the Zagros Folds: Active basement tectonics and surface morphotectonics. Tectonophysics **241**, 193–224 (1995)

Brew, G., Litak, Barazangi, M., Sawaf, T.: Tectonic evolution of northeast Syria: regional implications and hydrocarbon prospects. GeoArabia **4**, 289–318 (1999)

Ibrahim, A.: Tectonic Style and Evolution of the NW Segment of the Zagros Fold-Thrust Belt, Sulaimani Governorate, Kurdistan Region, NE Iraq, 283 p. Ph.D. Dissertation, University of Sulaimani, Iraq (2009)

Lamotte, D., Raulin, C., Mouchot, N., Wrobel-Daveau, J., Blanpied, C., Ringenbach, J.: The southernmost margin of the Tethys realm during the Mesozoic and Cenozoic: Initial geometry and timing of the inversion processes. Tectonics **30**, 1–22 (2011)

Lawa, F.: Sequence Stratigraphic Analysis of the Middle Paleocene-Middle Eocene in the Sulaimani District (Kurdistan Region), 375 p. Ph.D. Dissertation, Sulaimani University (2004)

Sepehr, M., Cosgrove, J.: Structural framework of the Zagros Fold-Thrust Belt Iran. Marine Pet. Geol. **21**, 829–843 (2004)

Sherkati, S., Letouzey, J.: Variation of structural style and basin evolution in the central Zagros (Izeh zone and Dezful Embayment) Iran. Marine Pet Geol **21**, 535–554 (2004)

Taheri, A., Vaziri-Moghaddam, H., Seyrafian, A.: Relationships between foraminiferal assemblages and depositional sequences in Jahrum Formation, Ardal area (Zagros Basin, SW Iran). Hist. Biol. **20**, 191–201 (2008)

Sequence Stratigraphy of the Oligocene and Miocene Successions from Selected Wells in Garmian District, Kurdistan Region/Iraq

Fadhil Ahmed Ameen

Abstract

New hydrocarbon discoveries in Kurdistan region from Oligocene and early Miocene reservoirs considered as new pay zones in the middle east map. Therefore, the establishment of new chronostratigraphic framework essentially based on the integrations of well log data and biostratigraphic data of high priority in Garmian area Kurdistan region/N Iraq. The biozonations, using planktonic and large benthonic foraminifera have been integrated with different microfacies associations. Also we took in consideration gamma, density, sonic and Neutron logs that led to the reconstruction of the chronostratigraphic framework. The litho, bio and chronostratigraphic setting of each well (Ja-46, Ja-49, Qumar-1, Pulkhan-7 and Taza-2) has been identified and correlated with each other. The sequence boundaries of Type one and Two (SBT.1 or 2, Maximum flooding surfaces (MFS) of the studied interval were interlinked between the five wells. The identified sequence boundaries nature, types, causes in addition to the maximum flooding surfaces, were correlated with regional data sets from the Arabian platform. The studied lithostratigraphic successions encompass Kirkuk group, Basal Anhydrite, Serikagni, Euphrates, Dhiban and Jeribe formations. The Oligocene reefal super sequence (Back reef-reef–fore reef and open marine) differs from Miocene Lagoonal super sequence mainly on facies associations, paleogeographic setting and hydrocarbon reservoir point of view.

Keywords

Kurdistan • Iraq • Oligocene–Miocene • Sequence stratigraphy • Chronostratigraphy

1 Introduction

The studied Oligocene –Miocene interval is of a high economic and academic interest not only in Iraq and Iran, but also in Kurdistan region due to the huge oil exploration undertakings. Such importance is mainly due to the hydrocarbon potentiality and low cost of the reservoirs relatively shallow depth. The stratigraphic column is slightly obscure and needs more surface and subsurface data integration. Therefore, in this work, we tried to re-establish the chronostratigraphic framework based on multi log data and biozonations and to identify the sequence stratigraphic evolutions. The Oligocene facies deposited in Kurdistan foreland basin have a NW –SE trend in direction, characterized by deep facies in the NW part of the studied area (Fig. 1).

2 Methodology

The biozonation, using planktonic and large benthonic foraminifera, has been integrated with different microfacies associations. Also, we took into consideration gamma, density, sonic and Neutron logs that led to the reconstruction of the chronostratigraphic framework.

The litho, bio and chronostratigraphic settings of each well (Ja-46, Ja-49, Qumar-1, Pulkhan-7 and Taza-2) have been correlated with each other. The Oligocene super sequences (Represent by Kirkuk Group) have been placed at the terminal phase of the Tectonic Mega Sequence TMSAP.10, while the Miocene successions (represent by Euphrates Group) are considered as the initial part of the Tectonic Mega Sequence TMSAP.11.

F. A. Ameen (✉)
Department of Geology, College of Science, University of Sulaimani, Sulaymaniyah, Iraq
e-mail: Fadhil.ameen@univsul.edu.iq

A. Çiner et al. (eds.), *Recent Research on Geomorphology, Sedimentology, Marine Geosciences and Geochemistry*, Advances in Science, Technology & Innovation, https://doi.org/10.1007/978-3-030-72547-1_46

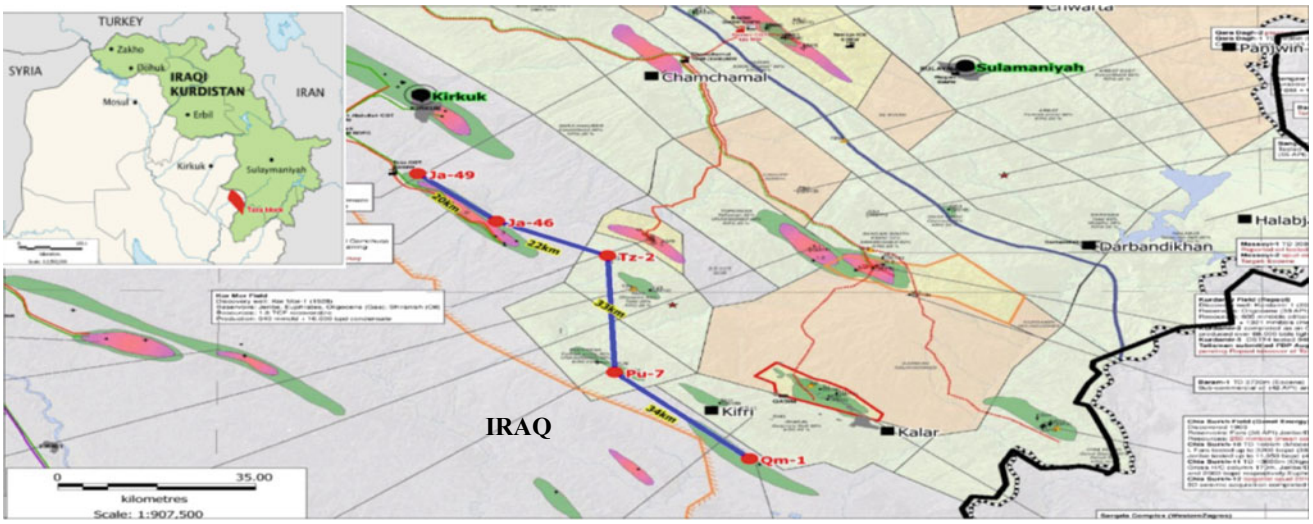

Fig.1 Location of the five studied wells, (Ja-49, Ja-46, Tz-2, Pu-7, Qm-1) at the Garmian area, Kurdistan region-Iraq. Ratified from www.westernzagros.com

3 Results

3.1 Chronostratigraphy

The complex lithostratigraphic units are subdivided into two groups Fig. 2. The Rupelian age represented by two formations of Kirkuk Group and they are Palani and Sheikh Alas formations; these are transgressive units. The Chattian age lithostratigraphic units are represented by Baba, Bajawan and Tarjili formations. The Aquitanian aged strata are represented by Anah-Azkand formations. The Burdigalian age is represented by the Serikagni-Euphrates–Dhiban and Jeribe formations.

3.2 Biostratigraphy

The shallow benthic zonation is correlated with the Iranian section Buchem et al. (2010); and the Iraqi Wells Grabowski and Liu (2010) and Lawa and Ghafour (2015). The major hiatus between the Eocene (Pila Spi fn,) and Miocene (Lower Fars fn.) shows a decrease in duration from high-folded zone toward the low folded one and the results are summarized in Table 1.

3.3 Sequence Stratigraphy

The whole studies lithostratigraphic successions are recognized as three third-order depositional system (Figs. 2 and 3).

1-First third order (Oligocene supersequences): Represent by deep basinal facial of Kirkuk Group of Oligocene age, and subdivided into fourth-order depositional system with two maximum flooding surfaces MFS pg. 30 Place in the upper parts of eth Palani formation, while MFS pg. 40 place on the middle part of Tarjili Formation. 2-s third order of Aquitanian age (Aqutanian Supersequences): Represented by last deep facies in the Neotethys basin in Kurdistan foreland basin. 3- Third order of Burdigalian age (Burdigalain Supersequences):- Represent the evaporates—Carbonate cycle deposits in restricted and semi-restricted lagoons. The sequences boundaries of Type one and Two (SBT.1 or 2, Maximum flooding surfaces (MFS) of the studied interval were interlinked between the five wells.

4 Conclusions

1. No Oligocene super sequence was detected from all the studied wells, except for Taza well-2. Such regional unconformity Known as Zagros Major Hiatuses indicates fold thrust belt of variable time durations in Zagros from 1 to 15 my.
2. The sequence boundary of type one, was estimated to be (34 Ma) age and was placed at the top Jaddala Formation (Middle to Late Eocene age), directly below the Euphrates Formation (Aquitanian) almost manifesting the boundary between Tectonomegasequence AP10 and AP11. Sequence boundary of Type one delineated the Oligocene/Eocene boundary and marks the base of Fatha formation. Sequences boundaries of type two are mostly segmented in the three above mentioned third orders and result from the interactions between tectonic and sea level changes.

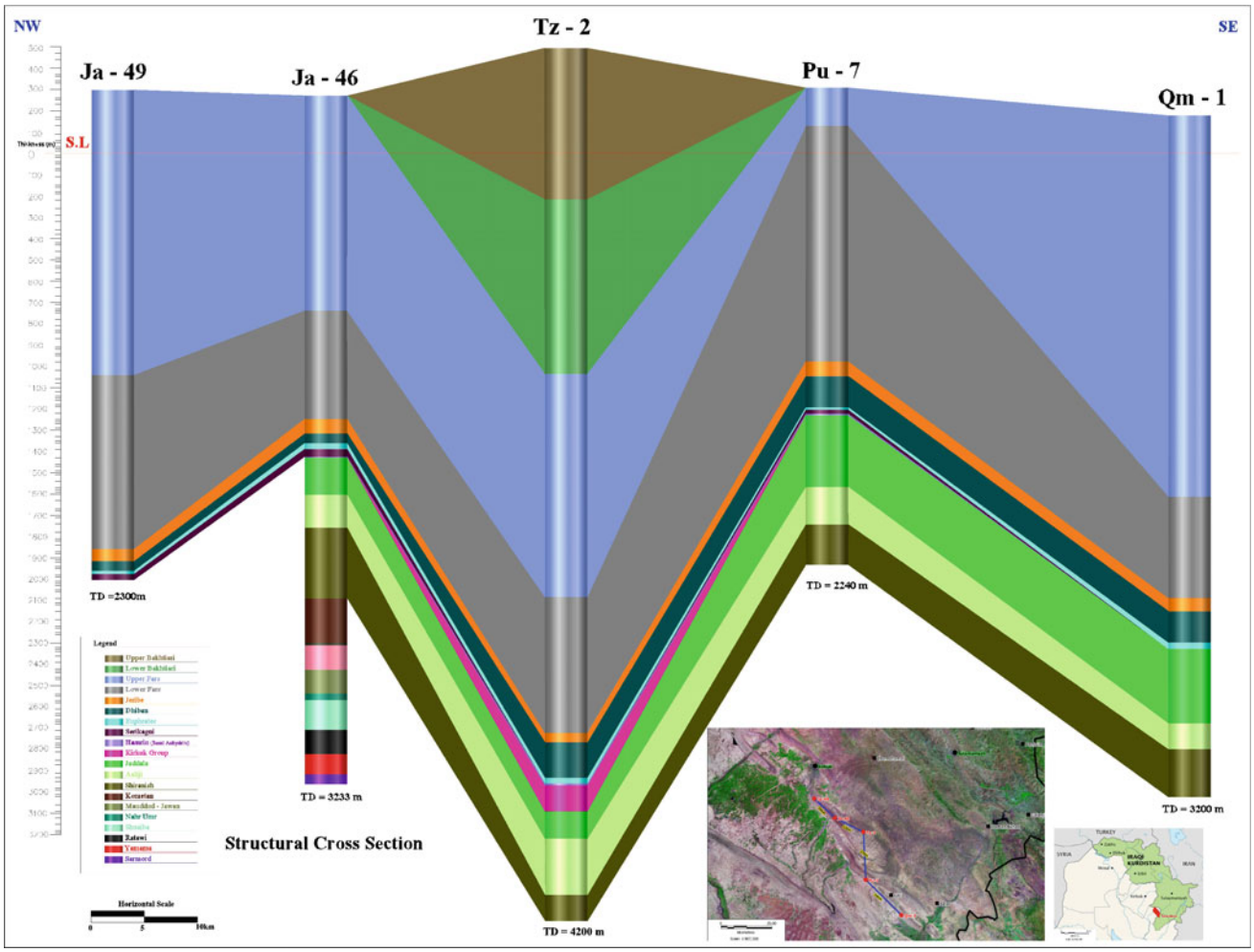

Fig. 2 Fence diagram and structural cross section of between the five wells (Ja-49, Ja-46, Tz-2, Pu-7, Qm-1), Garmian area, Kurdistan Region, N-Iraq

Table 1 Biostratigraphic zones in the studied five wells

	Epoch	Age	Formations	Foraminifera zones (SBZ)
Paleogene	Miocene	Langhian	Fatha (lower Fars)	*A. beccari (AB)* *Ostrea. marginata* (OM)
		Burdigalian Aquitanian	Jeribe-Dhiban Euphrates-Serikagni Ahnah-Azkand- (Gap)	*Borelis melo kurdica* (BMK) **(SBZ.25)** *Borelis melo melo (BMM)* *Austrotrillina howchini* (AH)(**SBZ.24**)
	Oligocene	Chattian	Tarjili Bajawan-Baba	*Praerhaypidionina delicata (PD)* ***(SBZ.23).*** *Globigerina angulisuturalis, Globorotalia opima, Globigerina ampliapertura*
		Repulian	Palani Sheikh Alas-Shurau	*Nummulites fitchteli (NF)* ***(SBZ.22 &21)*** *Globorotalia nana (GL n)*
	Late. Eocene	Pribonian	Jaddala-Pila Spi Avanah	*Discocyclina (DI),* *Alveolina (AL)*

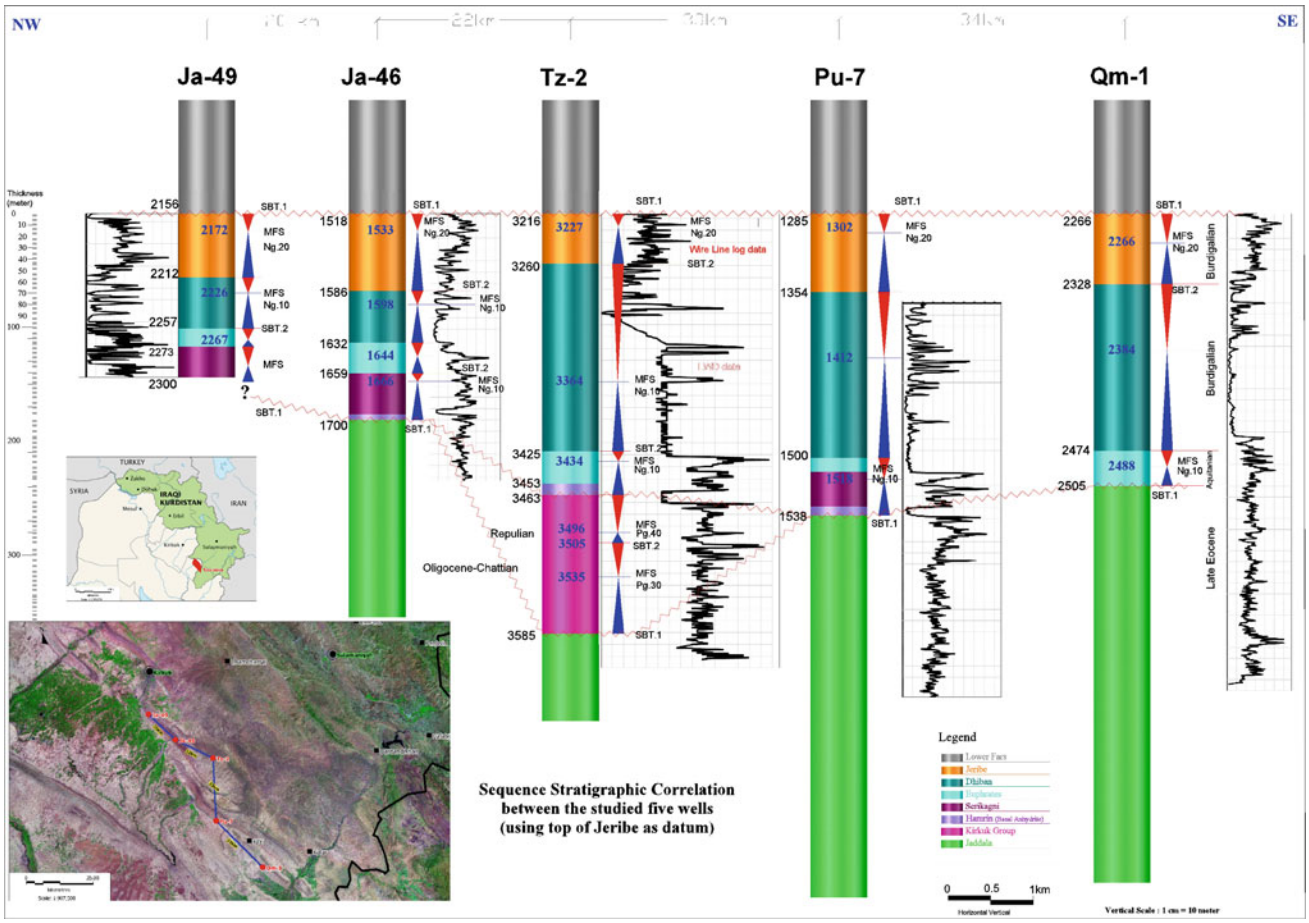

Fig. 3 Sequence stratigraphic analysis of the studied five wells using multi well log data and biostratigraphic data

3. The Paleogene reservoir is characterized by three third-order supersequences, namely (Oligocene supersequences, Aquitanian supersequences and Burdigalian supersequences). In turn, each of them are subdivided into two fourth orders. The reefal dominated carbonates might be important hydrocarbon reservoirs.

References

Buchem, F.S.P.V., Allan, T.L., Laursen, G.V., Lotfpour, M., Moallemi, A., Monibi, S., Motiei, H., Pickard, N.A.H, Tahmasbi, A.R., Vedrenne, V., Vincent, B.: Regional stratigraphic architecture and reservoir types of the Oligo-Miocene deposits in the Dezful Embayment (Asmari and Pabdeh Formations) SW Iran, Geological Society, London, Special Publications, vol. 329, pp. 219–263 (2010)

Grabowski, G., Liu, C.: Strontium-isotope age dating and correlation of Phanerozoic anhydrites and unfossiliferous limestones of Arabia. In: American Association of Petroleum Geologist, 9th Middle East Geosciences Conference, GEO 2010. GeoArabia, Abstract, vol. 16, no. 1, p. 1739 (2010)

Lawa, F.A.A., Ghafur, A.A.: Sequence stratigraphy and biostratigraphy of the prolific Late Eocene, Oligocene and Early Miocene Carbonates from Zagros fold- thrust belt in Kurdstan region. Arab. J. Geosci. **8**(10), 8143–8174 (2015)

In and Out of the Salt: How to Overcome Stratigraphic Uncertainty in Evaporitic Systems? A Case Study from the MSC in the Deep Levant Basin

Aaron Meilijson, Jie Liu, and Yizhaq Makovsky

Abstract

The Messinian Salinity Crisis (MSC) has fascinated a globally wide and multi-disciplinary array of scientists, and has been at the focus of debate ever since the first DSDP's penetrated the top of the deep-basin salt in the 1970's. Yet, after more than 50 years of research, the MSC stratigraphy is still controversial. These questions and debates are recently being answered with the availability of new deep-basin data. In the first part of this project, we conducted a multi-disciplinary study of sedimentary and geophysical data from industrial offshore wells in the Levant Basin, which recovered a continuous sedimentary record of deep-basin Mediterranean evaporites deposited during the MSC. In two recent papers, we proposed a new stratigraphic framework for the MSC, namely establishing a ~300 kyr older age for the base of the salt, and it's up section transition into clastic-anhydrite sedimentation. The parallel publication of Meilijson et al. (Geology 46:243–246, 2018) and Manzi et al. (Terra Nov 38:42–49, 2018) focused on the discussion regarding the MSC evolution in the deep Levant Basin, following the identification of a foraminifera barren interval (FBI) by the latter, not identified in our work. We hypothesized that the FBI may represent a localized short-lived depositional lobe, as opposed to a broad depositional period. Here, we used 3D seismic spectral decomposition analysis, which revealed amplitude anomalies at the base of salt reflection. These anomalies suggest the presence of thin depositional lobes, immediately underlying the base of salt, in the area reported as an FBI.

Keywords

MSC • Stratigraphy • Geophysics • Eastern Mediterranean

1 Introduction

Restriction of Atlantic connectivity during the MSC resulted in the deposition of ~2 km of evaporites within deep Mediterranean basins (Hsu and Drooger 1973). It has been suggested that deposition of the Mediterranean MSC salt-giant has greatly affected the global oceans, by sequestering 5–10% (Garcia-Castellanos and Villaseñor 2011) of their salt content into the Mediterranean Sea. One of the oldest controversies related to the MSC concerns the magnitude and timing of sea level lowering and desiccation (Hsu and Drooger 1973; Schmalz 1969; Roveri et al. 2014), where two main models for evaporite formations were suggested: a deep-basins under a deep-water environment (Schmalz 1969), or a desiccated shallow-water environment (Hsu 1983). However, the risk and vast expense of drilling through the salt in the deep-basins has resulted in a critical lack of data, rendering current ideas and scenarios as hypotheses, which could only be tested by drilling the deep Mediterranean basins (Roveri et al. 2014). It took the scientific community more than 40 years to fully access these mammoth-scaled salt deposits from the first time in which their uppermost part was penetrated (Hsu and Drooger 1973), and it is this record that is at the base of this project. We have examined industry wells recently drilled in the deep Levant basin, penetrating the thick Messinian evaporite section at depths of 2026–3616 mbsl. Here, we focused on 3D-seismic data at the base of the salt to resolve stratigraphic uncertainties.

A. Meilijson (✉) · J. Liu · Y. Makovsky
University of Haifa, Mount Carmel, 31905 Haifa, Israel
e-mail: ameilijs@campus.haifa.ac.il; aaron.meilijson@colorado.edu

A. Çiner et al. (eds.), *Recent Research on Geomorphology, Sedimentology, Marine Geosciences and Geochemistry*, Advances in Science, Technology & Innovation, https://doi.org/10.1007/978-3-030-72547-1_47

2 Salt Stratigraphy and Methodology

In our first attempt to establish the age and duration of salt deposition (Meilijson et al. 2018), we examined the 250 m underlying the salt in the deep basin. Through a combination of biostratigraphy, astronomical tuning, and geophysics, we proposed an early onset of halite in the deep basins, synchronously deposited with gypsum in the margins. However, following the work by Manzi et al. (2018) which reached a contradictive conclusion, we proceeded 'into the salt,' to try and find further evidence to resolve this debate. Through multi-proxy analysis, we reached the following conclusions (Meilijson et al. 2019; Fig. 1): (1) An early onset of halite occurred; (2) Halite was deposited in a deep-water

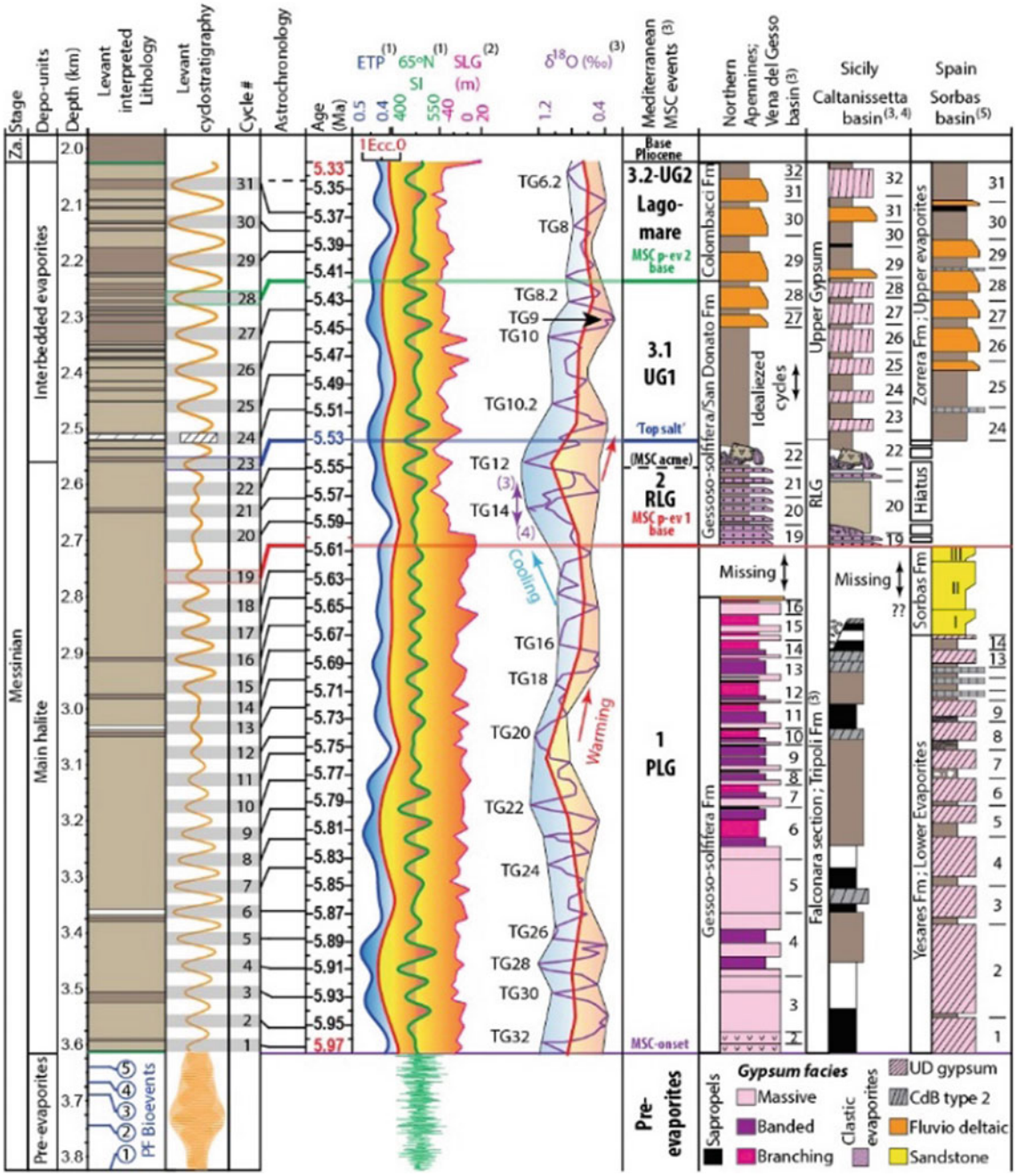

Fig. 1 Astronomical age model and regional correlation of the Levant MSC. The Levant inter-preted lithology (left), biostratigraphic refer-ence levels (PF—plank-tic foraminifera) and filtered well-log model determine a cyclostrati-graphic model, resulting in 33 cycles for the Levant MSC. This cyclostratigraphic model is tuned to astronomic target curves (center) of ETP (blue; calculated as eccentricity (Ecc; red) + obliquity − precession, and marginal MSC deposits (after Meilijson et al. 2019)

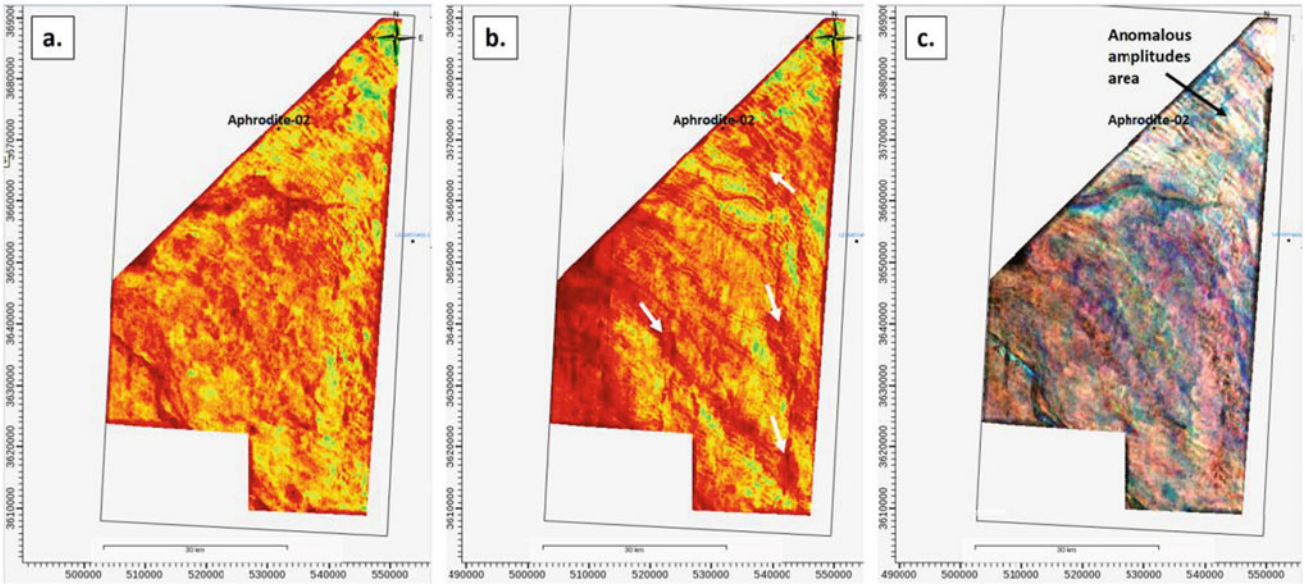

Fig. 2 Frequency dependence of reflection amplitudes of the N horizon in the Pelagic 3D seismic block. **a** The low-frequency component (5–10 Hz), representing true response of the N. **b** The high-frequency component (50–60 Hz) representing imprint of the M (particularly white arrows). **c** RGB spectral re-composition, revealing a local amplitude anomaly (whitish area) in the area of the Aphrodite-02 well

deep-basin environment; and, (3) During the MSC, high-sea level and partial connectivity with the ocean promoted the deposition of deep-basin halite, while sea-level drawdown promoted the deposition of reworked and transported material from the margins into deep Mediterranean basins. Here, we utilized time and depth migrated 2D and 3D seismic data, for a detailed investigation of the base of the salt. This investigation included regional facies analysis, as well as computation and analysis of relevant 3D advanced attributes, such as coherency cubes and spectral decomposition RGB representations. Our goal was to identify structures that might support or revoke the idea of early onset of salt.

3 Results

The parallel publication of Meilijson et al. (2018) and the contradicting (Manzi et al. 2018) focused their discussion on the identification of a foraminifera barren interval (FBI) at the base of the salt by Manzi et al. (2018) versus its absence in the Dolphin-1 well studied by Meilijson et al. (2018), just 40 km apart. We hypothesized that the FBI may represent a localized short-lived depositional lobe, as opposed to a broad depositional period as suggested by Manzi et al. (2018). The frequency-dependent seismic reflectivity, as delineated by 3D spectral decomposition, can help us detect the potential presence of a thin depositional lobe, at the limit of resolution, in the vicinity of the N horizon. However, we realized that amplitude artifacts resulting from the variability of the top evaporites M horizon overprint and biased the results of imaging at the N level (Fig. 2). We separated these effects by constraining the analysis frequencies (Fig. 2a vs. b). The resulting spectral decomposition RGB image reveals a pronounced anomaly in the area of the Aphrodite-02 well, which may represent a localized depositional lobe (Fig. 2c).

4 Conclusions

In our (Meilijson et al. 2018, 2019) publications, we presented a new stratigraphy for MSC events in the Mediterranean Sea. Uncertainty in this new model was raised by the identification of an interval barren in foraminifera below the base of the salt in the Deep Levant Basin, corresponding to the Non-Distinctive Zone (NDZ) marking the onset of the MSC (5.971 Ma) in marginal settings. In this work, we explored in high resolution the seismic attributes of the pre-evaporite interval, and raised viable assumptions as to its transported nature in the areas where the FBI was identified. A sand rich lobe might include scarce specimens of foraminifera, and in any case should not be used for interpreting in-situ depositional environments. The lack of such a lobe and the continuation in abundance of foraminifera toward the base of the salt in the Dolphin-1 well where our study was preformed, strengthens our hypothesis. We are confident in the new MSC model, where salt was deposited in deep-water environments, synchronously with gypsum deposition in the margins, ~300 kyr earlier then presumed.

References

Garcia-Castellanos, D., Villaseñor, A.: Messinian salinity crisis regulated by competing tectonics and erosion at the Gibraltar arc. Nature **480**, 359–363 (2011)

Hsu, K.J.: The desiccated deep-basin model for the Messinian events. In: Drooger, C.W. (ed.) Messinian Events in the Mediterranean, pp. 60–67. North-Holland Publ. Co., Amsterdam (1973)

Hsu, K.J.: The Mediterranean was a Desert: A Voyage of the Glomar "Challenger." Princeton University Press, Princeton, NJ (1983)

Manzi, V., Gennari, R., Lugli, S., Persico, D., Reghizzi, M., Roveri, M., Schreiber, B.C., Calvo, R., Gavrieli, I., Gvirtzman, Z.: The onset of the Messinian salinity crisis in the deep Eastern Mediterranean basin. Terra Nov. **38**, 42–49 (2018)

Meilijson, A., Steinberg, J., Hilgen, F., Bialik, O.M., Waldmann, N.D., Makovsky, Y.: Deep-basin evidence resolves a 50-year-old debate and demonstrates synchronous onset of Messinian evaporite deposition in a non-desiccated Mediterranean. Geology **46**, 243–246 (2018)

Meilijson, A., Hilgen, F., Sepúlveda, J., Steinberg, J., Fairbank, V., Flecker, R., Waldmann, N.D., Spaulding, S.A., Bialik, O.M., Boudinot, F.G., et al.: Chronology with a pinch of salt: Integrated stratigraphy of Messinian evaporites in the deep Eastern Mediterranean reveals long-lasting halite deposition during Atlantic connectivity. Earth-Science Rev. **194**, 374–398 (2019)

Roveri, M., Flecker, R., Krijgsman, W., Lofi, J., Lugli, S., Manzi, V., Sierro, F.J., Bertini, A., Camerlenghi, A., De Lange, G., et al.: The Messinian Salinity Crisis: Past and future of a great challenge for marine sciences. Mar. Geol. **352**, 25–58 (2014)

Schmalz, R.F.: Deep-water evaporite deposition: a genetic model. Am. Assoc. Pet. Geol. Bull. **53**, 798–823 (1969)

Facies Analysis, Sequence Stratigraphy and Hydrocarbon Habitat Prospectivity of the Pindiga Formation and Fika Shale, Gongola Sub-basin, Northern Benue Trough, Nigeria

Isah Goro, Muhammad Abubakar, Nuhu Waziri, Bukar Shettima, and Babangida Jibrin

Abstract

Outcrop-based sequence stratigraphic studies have been conducted on the Pindiga Formation and Fika Shale of the Gongola sub-basin, Northern Benue Trough, Nigeria. This has implications for hydrocarbon play identification in the basin especially at the intermediate temporal position where the poorly studied, recently delineated Sandy members occur. The approximately 600-m-thick interval was subjected to detailed facies, depositional environment, and depositional trend analyses as well as major bounding surfaces marking out based on 17 measured stratigraphic sections. Sequence stratigraphy analysis led to the delineation of one depositional sequence (DS), shared with the underlying formations and two complete second-order sequences using Depositional Sequence III model. Dark grey-to-black shales of the late transgressive systems tract (TST) to early highstand systems tract (HST) in the three depositional sequences constitute potential source rocks. Lowstand systems tract (LST) sandstones deposited in fluvial and tidal channels as well as bayhead delta make up potential reservoir rocks within DS2. The TST and HST of DS1 and DS2 contain potential reservoir rocks including tidal bar, estuary mouth and shoreface to nearshore sandstones. Potential intra-formational seals comprise the late TST and early HST mudstones of DS1, the early HST mudstones of DS2, and a regional top seal is provided by DS3, which consists entirely of the Fika Shale. These depositional sequences consist of varied lithologies, and their relative temporal and spatial distribution promises high potential for further exploration in the basin.

Keywords

Gongola sub-basin • Benue trough • Sequence stratigraphy • Pindiga formation • Fika Shale

1 Introduction

The mainstay of Nigerian economy is oil and gas all of which is derived from the Niger Delta basin. In order to increase the treasure base of the country, major exploration efforts are concentrated in the frontier inland basins of Nigeria with more emphasis on the Benue Trough. The drilling of only three wells led to the discovery of hydrocarbon in the Gongola sub-basin of the Northern Benue Trough. The wells include Kolmani-1-Well with reported discovery of sub-commercial oil; Nasara-1-Well and Kuzari-1-Well were reported to be dry. Controversy, however, arose after the publications of Abubakar et al. (2008) who reported the presence of migrated oil between depths of 4710–4770 ft in the Nasara-1-Well based on geochemical techniques.

It became obvious that gaps still exist in detailed understanding of the possible petroleum habitat especially at the intermediate temporal stratigraphic position where the recently delineated, understudied Sandy members (Zaborski et al. 1997) of the Pindiga Formation occur. The juxtaposition of the Sandy members between limestones and shales of Kanawa member, below and Fika Shales above makes them high-quality targets for hydrocarbon accumulation. In order

I. Goro (✉) · N. Waziri
Department of Geology, Federal University of Technology, P.M.B 65 Minna, Nigeria
e-mail: isahgoro@futminna.edu.ng

M. Abubakar
National Center for Petroleum Research and Development, Abubakar Tafawa Balewa University, P.M.B. 0248 Bauchi, Nigeria

B. Shettima
Department of Geology, University of Maiduguri, P.M.B 1069 Maiduguri, Nigeria

B. Jibrin
Department of Geology and Mining, Ibrahim Badamasi Babangida University, Lapai, Nigeria

A. Çiner et al. (eds.), *Recent Research on Geomorphology, Sedimentology, Marine Geosciences and Geochemistry*, Advances in Science, Technology & Innovation, https://doi.org/10.1007/978-3-030-72547-1_48

to effectively explore for hydrocarbon in the Gongola sub-basin, adequate understanding of the genetic evolution of the sedimentary packages of Pindiga Formation and Fika Shale using sequence stratigraphic technique is critical due to its predictive nature.

The present work provided detailed outcrop facies, facies associations, facies successions, sequence stratigraphic framework and hydrocarbon play potentials of the approximately 600-m-thick Pindiga Formation and Fika Shale.

2 Materials and Methods

Sedimentological and stratigraphic information on the outcropping sedimentary rocks in the study area were recorded through the construction of graphic logs. Seventeen sedimentological graphic logs were constructed from fairly well-exposed parts of the study area. Lithofacies were identified and analysed using the lithology, colour, texture, sedimentary structures, and geometry as well as vertical and lateral relationship of beds, bounding surfaces and trace fossil content.

The composite logs were prepared from isolated exposures that occur laterally adjacent to each other to provide more complete scenarios of their temporal relationship. The identified lithofacies were coded K, S and Fk for the Kanawa, Sandy members and Fika Shale, respectively. A two-stage approach was used for the interpretation: (1) deduction of environment of deposition and (2) identification of systems tracts and erection of sequence stratigraphic framework for the sediments using Depositional Sequence III Model (after Christie-Blick 1991).

3 Results

3.1 Facies Analysis and Environment of Deposition

A detailed outcrop facies analysis led to the identification of 21 lithofacies, 13 facies associations (Table 1) and 6 facies successions (Table 2). Lithofacies of the Kanawa Member include dark grey-black fissile mudstone (K1) and limestone (K2) facies.

The Sandy members consist of the following facies: grey mudstone (S1), ripple laminated mudstone (S2), laminated siltstone (S3), heterolithic sandstone (S4), cross-laminated sandstone (S5), planar-bedded sandstone (S6), horizontal to low angle stratified sandstone (S7), swaley cross-stratified sandstone (S8), hummocky cross-stratified sandstone (S9), herringbone cross-bedded sandstone (S10), planar cross-bedded sandstone (S11), trough cross-bedded sandstone (S12), conglomerate (S13), shell bed (S14). The fissile grey mudstone (Fk1), lime-mudstone (Fk2), graded-bedded sandstone (Fk3), heterolithic siltstone to sandstone (Fk4) and planar-bedded sandstone (Fk5) facies were recognized from the Fika Shale.

Six facies successions representing broad environments of depositions were interpreted from the juxtaposition of the 13 facies associations (Table 2).

Table 1 Facies and facies associations of the Pindiga Formation and Fika Shale

Facies association	Code	Lithofacies present
Kanawa member		
Outer ramp	FA1	K1, K2
Mid-ramp	FA2	K1, K2
Sandy members		
Wave/storm-dominated prodelta to delta front	FA3	S1, S2, S4, S6, S9, S14
Wave/storm-dominated shoreface to nearshore	FA4	S1, S7, S8, S9, S11, S12
Offshore to offshore transition	FA5	S1, S9
Tide influenced fluvial channel	FA6	S4, S10, S11, S12, S13
Tidal bar	FA7	S2, S3, S4, S11, S12, S13
Bayhead delta	FA8	S1, S4, S6, S10, S12,S13
Tidal channel	FA9	S4, S12, S13
Central bay	FA10	S1, S5
Estuary mouth	FA11	S1, S2, S4, S7, S8, S9, S12, S13
Fika Shale		
Prodelta facies association	FA12	Fk1, Fk2, Fk3
Delta front facies association	FA13	Fk1, Fk3, Fk4, Fk5

Table 2 Facies successions of the Pindiga Formation and the Fika Shale

S/N	Facies succession	Facies associations present
Kanawa member		
1	Carbonate platform	FA1, FA2
Sandy members		
2	Wave/storm-dominated prodelta to delta	FA3
3	Wave/storm-dominated offshore to nearshore	FA4, FA5
4	Wave-dominated estuary	FA6, FA7
5	Tide-dominated estuary	FA8, FA9, FA10, FA11
Fika Shale		
6	Prodelta to delta front	FA12, FA13

4 Discussion

A detailed facies analysis and delineation of major bounding surfaces that mark changes in lithofacies associations and their stacking patterns allowed the definition of three erosionally bounded packages within the Pindiga Formation and Fika Shale. These packages approximately correspond to three depositional sequences (DS, Fig. 1). The lower package is DS1 and is only partially developed within the study interval. Its lower sequence boundary is believed to occur in underlying Yolde or Bima Formations. The basal boundary of the Pindiga Formation is interpreted as a transgressive surface, and the carbonates of Kanawa Member constitute a TST due to the identification of maximum flooding zone within it. The overlying wave/storm-dominated offshore to nearshore and its adjacent wave/storm prodelta to delta front facies successions serve as the HST of the DS1. Whereas

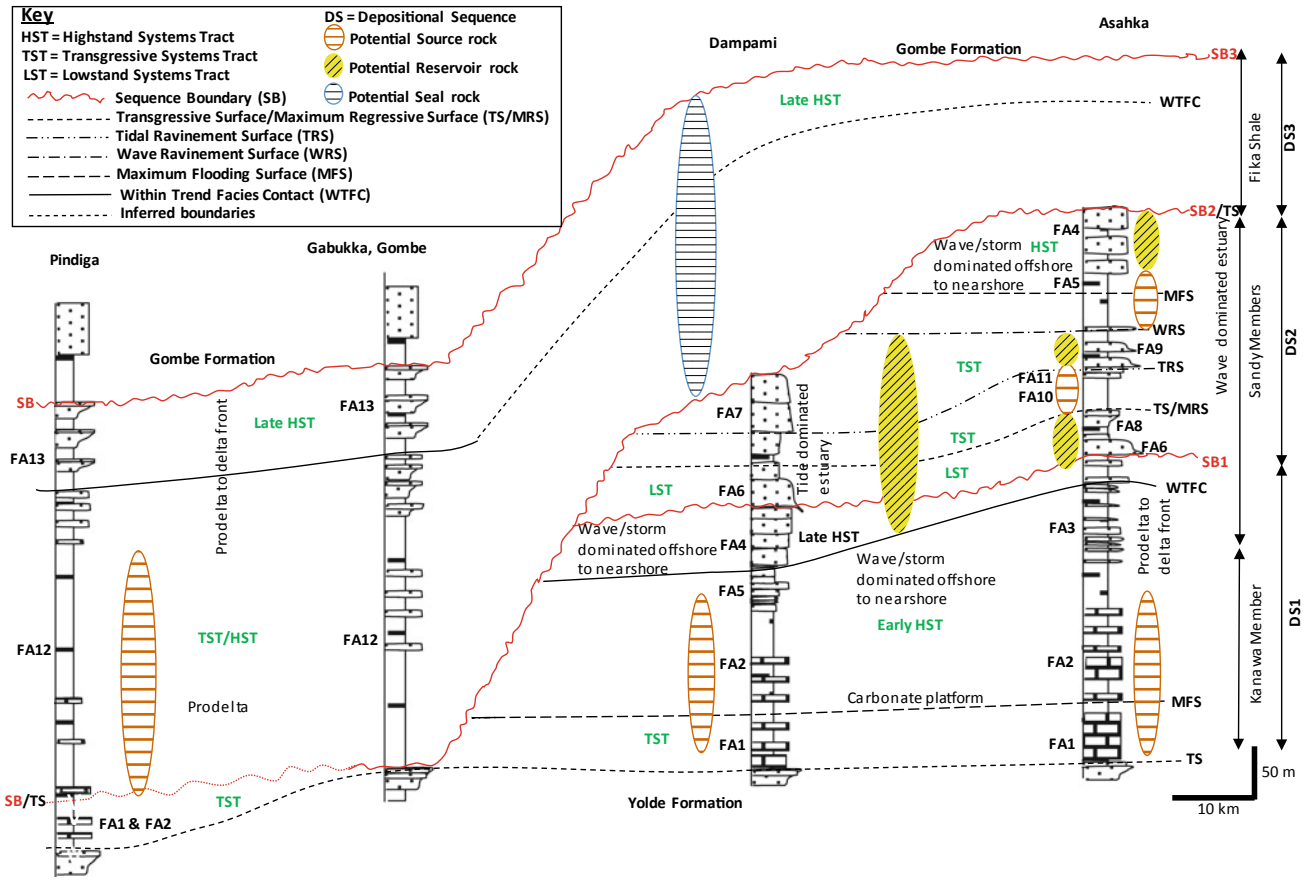

Fig. 1 Composite log illustrating the sequence stratigraphic framework of the Pindiga Formation and Fika Shale, Gongola sub-basin, Northern Benue Trough, Nigeria

the disconformity surface that temporally separates the Sandy members into two (SB1, Fig. 1) represents the upper sequence boundary of this sequence.

The DS2 is the most complete sequence in the Pindiga Formation because it contains most of the expected sequence stratigraphic surfaces and systems tracts that can be related to one complete sea level fall and rise (Fig. 1). It contains both wave- and tide-dominated estuary facies successions and is bounded at the top by angular unconformity recognized by the presence of thick paleosol unit. This gives evidence for the Santonian compressional event in the Gongola sub-basin. The DS3 is formed by the Fika Shale. The absence of LST and major facies shift across the lower sequence boundary indicates tectonic control accompanied by abrupt deepening.

Potential source rocks include hemipelagic shales of the late TST to early HST of DS1 and DS3. The former coincides with the worldwide anoxic event, which deposited organic matter-rich shales. The identified potential reservoir rocks are concentrated within DS2 and the upper part of DS1. These lithofacies associations comprise of the shoreface to nearshore sandstones of late HST of DS1 and DS2. Others include fluvial and tidal channels as well as bayhead delta sandstones of the LST and tidal bar and estuary mouth sandstones of the TST in DS2. A regional top seal is provided by the laterally extensive, approximately 200-m-thick Fika Shale constituting the DS3. Less extensive, intra-formational seal rocks may be provided by the central estuary, prodelta and offshore to offshore transition shales within DS2 and DS1.

5 Conclusions

1. Outcrop lithofacies and sequence stratigraphic analyses of the Pindiga Formation and Fika Shale reveal new insights in to the regional stratigraphy and juxtaposition of source, reservoir and seal lithofacies within the Gongola sub-basin of the Northern Benue Trough, Nigeria.
2. The interval represents one partial and two complete depositional sequences.
3. The lower depositional sequence comprises a TST and HST with potentials for source and reservoir rocks, respectively.
4. The middle depositional sequence contains LST overlain by TST and HST with great potentials for reservoir rocks provided by fluvial and tidal channels, tidal bar and shoreface to nearshore sandstones of the Sandy members.
5. Potential regional seal rock is provided by the laterally extensive, approximately 200-m-thick upper depositional sequence represented by TST and HST mudstones of the Fika Shale.

References

Abubakar, M.B., Dike, E.F.C., Obaje, N.G., Wehner, H., Jauro, A.: Petroleum prospectivity of Cretaceous formations of Gongola Basin, Upper Benue Trough, Nigeria: an organic geochemical perspective on a migrated oil controversy. J. Pet. Geol. **31**(4), 387–408 (2008)

Christie-Blick, N.: Onlap, offlap, and the origin of unconformity bounded depositional sequences. Mar. Geol. **97**, 35–56 (1991)

Zaborski, P., Ugodulunwa, F., Idornigi, A., Nnabo, P., Ibe, K.: Stratigraphy and structure of the Cretaceous Gongola basin, northeast Nigeria. Bull. Centres Recherches Explor. Prod. Elf-Aquitaine **21**(1), 153–185 (1997)

Seismic Stratigraphical Analysis of the Shelf Deposition Between Tekirdağ-Şarkoy, Turkey, Since Last Glacial Maximum

Denizhan Vardar, Hakan Alp, Sinan Demirel, Hande Aykurt Vardar, Bedri Alpar, and Ahmet Cevdet Yalçıner

Abstract

The shelf between Tekirdağ and Şarkoy, NW Marmara Sea, is controlled by a major fault system, the Ganos Fault (GF), which is claimed to be the source of the 7.3 (Ms) earthquake in 1912. The effect of GF and global sea-level changes on of the shelf between Tekirdağ and Şarkoy was discussed on the basis of seismic-stratigraphic data. Two main units (U1, U2) and three para-sequences (U1a, U1b and U1c) were determined. The para-sequences (U1b, U1c) are of fluvial origin and are mainly controlled by the sea-level fluctuations. The sea-bottom morphology and the thickness of the resulting seismic-stratigraphic units must have been controlled mainly by the GF. Moreover, the GF also controls the elevation differences between the wave-cut terraces along the Tekirdag-Şarkoy self and the others in the Marmara Sea.

Keywords

Seismic stratigraphy • Chirp seismic • Marmara Sea • Ganos Fault • Wave-cut terraces

1 Introduction

The Marmara Sea is connected to the Black Sea and the Mediterranean Sea via the Straits of İstanbul and Çanakkale (Bosphorus and Dardanelles), respectively. The water exchange between the Marmara Sea and the Mediterranean has been cut off and the shelf areas of the Marmara Sea were sub-aerially exposed during the Last Glacial Maximum (LGM), under the control of the sill depth in the Strait of Canakkale (Aksu et al. 1999; Cagatay et al. 2009). The connection was re-established with transition to warming period (Cagatay et al. 2009). The post-glacial sedimentary successions deposited on the northern shelf are generally composed of thin sediments that overly the acoustic basement (Aksu et al. 1999; Cagatay et al. 2009; Nasıf et al. 2019; Vardar et al. 2018). The coarser sediments, however, derived from erosion of tectonic highs, some terrestrial inputs and new hydrodynamic conditions. High-resolution seismic profiles concerning the sedimentary successions from the LGM to the recent at the northern shelf are scarce and a number of available profiles are not that sufficient to explain the possible formation and evolution conditions. Karakilcik and her colleagues, for example, recently used Uniboom seismic sections and outlined three units above the acoustic basement (Karakılçık et al. 2014). Later, two different research teams collected new data sets and defined additional seismic units (Nasıf et al. 2019; Vardar et al. 2018). They explained these units as isolated lakes, lacustrine deposits and deltaic successions, which implied external conditions spatially variable along the shelf. Nevertheless, there are still debates on the depositional history of the northern shelf and their relation with the sea/lake-level fluctuations in the Marmara Sea, which run in parallel with new data sets.

The shelf between Tekirdağ and Şarkoy, NW margin of this intra-continental marine basin, is mainly affected by the Ganos Fault (GF). It is a major fault system directly related with the North Anatolian Fault system.

With the help of seismic-stratigraphic analysis of a new high-resolution seismic data set gathered nearshore and offshore the GF, this study focussed on the role of the GF in the late Quaternary offshore deposition under variable water level changes.

D. Vardar (✉) · S. Demirel · B. Alpar
Institute of Marine Sciences and Management, İstanbul University, İstanbul, Turkey
e-mail: denizhan@istanbul.edu.tr

H. Alp · H. A. Vardar
Geophysical Engineering Department, Engineering Faculty, İstanbul University Cerrahpaşa, İstanbul, Turkey

A. C. Yalçıner
Civil Engineering Department, Middle East Technical University, Ankara, Turkey

A. Çiner et al. (eds.), *Recent Research on Geomorphology, Sedimentology, Marine Geosciences and Geochemistry*, Advances in Science, Technology & Innovation, https://doi.org/10.1007/978-3-030-72547-1_49

2 Materials and Methods

We have collected 450-km of high-resolution single channel CHIRP seismic data in April 2019 (Fig. 1a), and interpreted them based on the fundamental principles of sequence stratigraphy (Posamentier and Vail 1988). Bathy 2010P™ Chirp sub-bottom profiler and bathymetric echo sounder (2–8 kHz) were used to obtain much detailed sub-bottom survey capability. We used the freeware Kogeo Seismic Toolkit for basic data processing methods, such as band-pass filtering (10–15; 1750–1900 Hz) and gain adjustment. The processed profiles were transferred and interpreted with Kingdom Suite® (version 8.5; donated by "Seismic MicroTechnology"). For depth conversion, we used the velocity of 1500 m/s for the seawater.

3 Results

3.1 Seismic Stratigraphy

The seafloor bathymetry deducted from the data (Fig. 1a) indicates that the shelf is relatively wide at the offshore sectors between Tekirdağ–Kumbağ (~10 km) and Gaziköy–Şarkoy, if compared to the sector Kumbağ-Gaziköy (<500 m). We outlined two main seismic units (U1 and U2), separated by an erosional unconformity (the sequence boundary SB; Fig. 1 b, c, d). Unit U1 includes all the sediments deposited from the LGM to the present, which consist of three para-sequences; U1a, U1b and U1c. U1a is characterized by weak, continuous and parallel internal reflections while U1b is represented by roughly parallel to progradational sigmoidal reflections downlapping on the SB. As for U1c, it is characterized by aggradational clinoforms, toplapping to the overlying erosional surface (Fig. 1 b, c, d). Unit U2 is the acoustic basement, and it is characterized by high-angle internal reflections throughout the study area (Fig. 1 b, c, d). In this context, the SB, separating U1 and U2, is the sub-aerially exposed erosional surface. It is just below the thin post-last glacial deposits on the outer shelf, and nearly concordant with the recent bathymetry.

4 Discussion

The total thickness of the units U1a and U1b is nearly 20 ms at the nearshore areas, implying high rates of sediment transportation. The units become thinner towards the shelf break. The unit U1 (Fig. 1b) is rather thin above the terraces. This can be explained by the fact that the deposits might have been eroded by subaerial effects during the relative sea-level still stands or they have been transported with the longshore currents, a well-known hydrodynamic feature of the region. The units reach their maxima (~35 ms) between Gazikoy and Kumbağ. This is believed to be directly related with the activities of GF. The thickness of U1a is higher in the northern part of the GF, which may be directly related with the activities of this fault and its northward slope (Fig. 1c).

The wave-cut terraces at the northern shelf of Marmara Sea were given as −65, −87, −93 and −102 m in Cagatay et al. (2009), −95, −87 m (Posamentier and Vail 1988), − 65 m (Nasıf et al. 2019), −63 m for the shallowest terraces in Alp et al. (2018). The depth of the correspondent terraces, related with the relative still stands, are −49 m, −60 m in the study area. The difference indicates that the tectonic uplift was caused by the GF. The U1b sigmoid depositions between Tekirdağ and Kumbağ is progradational, the ascending trajectories of rollover points can be correlated with sea-level rise during the clinotheme development, and delta front is at 43 ms bsl. Therefore, the U1b unit was probably deposited during the Transgressive System Tract (TST), like U1a. The eroded top surface of the U1c implies the unit is subaerial exposed during the LGM, so the unit was deposited during the falling stage (FFST) and low stand system tracts (LST).

5 Conclusions

The distribution of the seismic units above the erosional surface SB and their stratigraphic characteristics indicate that the sedimentary units on the shelf are mainly sourced by fluvial, terrestrial and marine deposits, starting from the LGM to the present and controlled by the water level changes in the Marmara Sea. However, the thickness of the units, as well as the width of the shelf area (e.g. the sector Kumbağ-Gaziköy), have been controlled mainly by the GF. Erosion along the slopes and deepening of the E-W-trending basin were controlled by the dominant tectonic regime in the region. In addition to controlling the external shapes of the units, the tectonic regime controls the internal reflections and their terminations in the stratigraphic units in accordance with the sea-level variations. The elevated terraces in the study area, shallower than the others along the northern shelf, must have been due to the regional tectonic uplift along the GF.

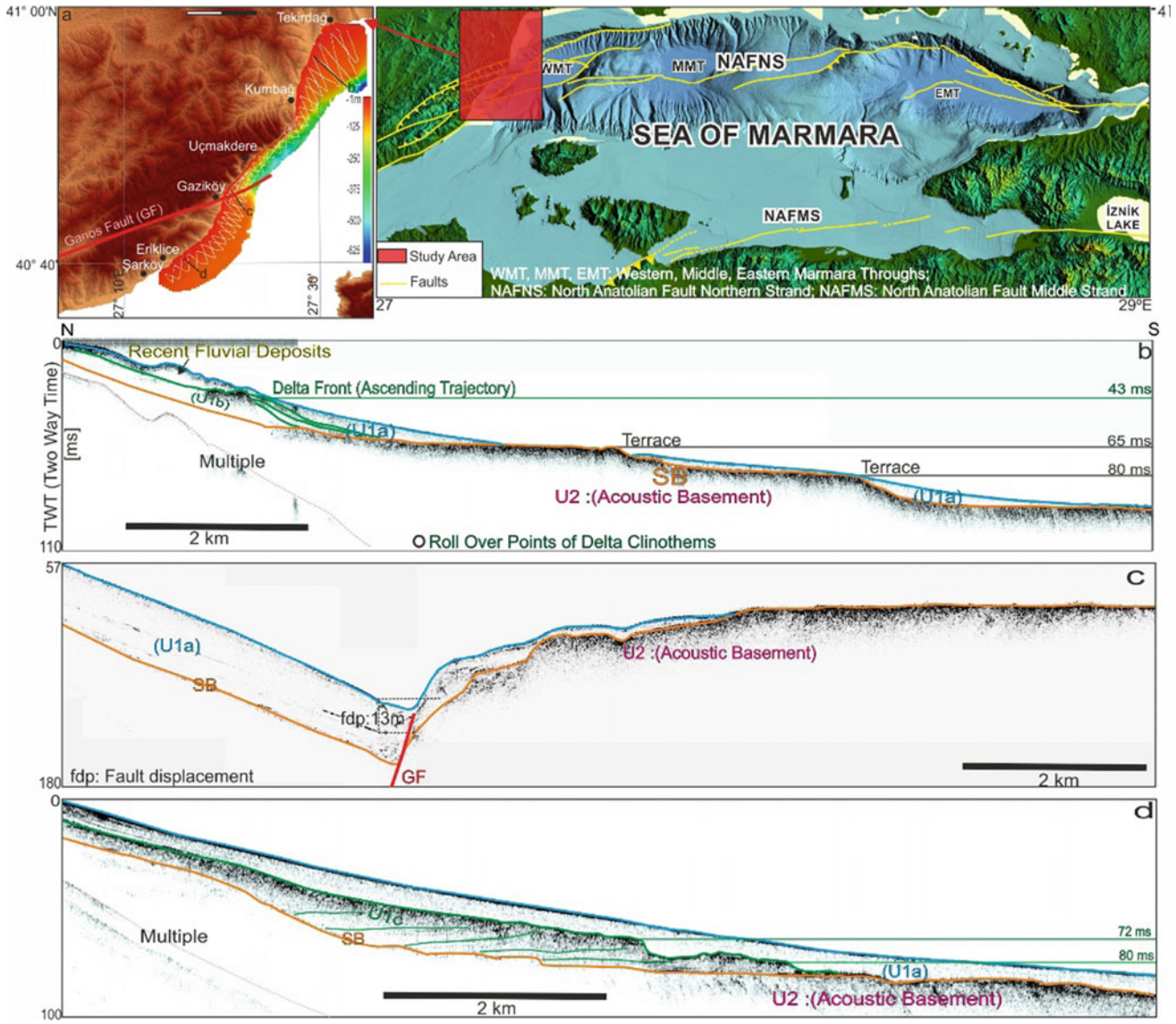

Fig. 1 **a** Location of the study area and seismic profiles; **b–d** Seismic lines evidencing stratigraphy for the study area (GF: The Ganos Fault)

Acknowledgements The authors gratefully acknowledge the financial support of the Scientific and Technological Research Council of Turkey-TUBITAK (Project 118Y079).

References

Aksu, A.E., Hiscott, R.N., Yasar, D.: Oscillating Quaternary water levels of the Marmara Sea and vigorous outflow into the Aegean Sea from the Marmara Sea-Black Sea drainage corridor. Mar. Geol. **153**, 275–302 (1999)

Alp, H., Vardar, D., Alpar, B., Ustaomer, T.: Seismic evidence for change of the tectonic regime in Messinian, northern Marmara Sea Turkey. JAES **151**, 40–53 (2018)

Cagatay, M.N., Eris, K., Ryan, W.B.F., Sancar, U., Polonia, A., Akcer, S., Biltekin, D., Gasperini, L., Gorur, N., Lericolais, G., Bard. E.: Late Pleistocene–Holocene evolution of the northern shelf of the Sea of Marmara. Mar. Geol. **265**, 87–100 (2009)

Karakılçık, H., Unlugenc, U.C., Okyar, M.: Late glacial–Holocene shelf evolution of the Sea of Marmara west of Istanbul. J. African Earth. Sci. **100**, 365–378 (2014)

Nasıf, A., Dondurur, D., Vardar, D.: Stratigraphical and morphological aspects of the northern Marmara shelf based on seismic data. J. Earth Syst. Sci. **128**, 54 (2019).

Posamentier, H.W., Vail, P.R.: Eustatic controls on clastic deposition II —Sequence and systems tract models; In: Posamentier H.W., Ross C.A., Van Wagoner, J.C. (eds.) Sea-Level Changes: An Integrated Approach. Soc. Econ. Paleontol. Mineral. Spec. Publ. **42**, 125–154 (1988).

Vardar, D., Alp, H., Alpar, B.: Seismic stratigraphy and depositional history of the Buyukcekmece Bay since Latest Pleistocene, Marmara Sea Turkey. J. Earth Syst. Sci. **127**, 13 (2018)

Sedimentology, Stratigraphy, Paleontology, and Marine Geosciences (T14): Paleontology—Evolutionary, Biostratigraphic and Paleoenvironmental Significance

Ichthyofauna from the Phosphorites of El-Kouif Locality (Algerian-Tunisian Border Area)

Salim Boulemia, Messaoud Hamimed, and Bilal Djoulah

Abstract

Paleontological content of sedimentary phosphorites in El-Kouif locality, northeastern Algeria, was analyzed. Materials were concentrated by sample washing and outcrops surface collecting of friable phosphorites facies, yielding a multitude of phosphatised fish teeth rich in species of variable morphology, representing 15 species of Elasmobranchii (Euselachii and Batoidea). The fish fauna indicates tropical to temperate paleo-environmental conditions. Most of the species represent benthic/nektonic forms of coastal areas with neritic and midwater depths. This fish fauna confirms a Thanetian age for the phosphatic formation of El Kouif, highlighting the importance of fossil fish for the formation of sedimentary phosphorites. Apparently, this Thanetian assemblage occupied a relatively narrow gulf.

Keywords

Phosphorites • El-Kouif • Elasmobranchii • Palaeoenvironment • Thanetian

1 Introduction

Phosphate deposits are widely distributed in the region of Tebessa, as elsewhere in Northern Africa. The Paleocene-Eocene period was considered privileged or of polytaxic type to the phosphatogenesis of marine sedimentary origin. The paleontological content of the phosphatic series of El-Kouif in the Algerian-Tunisian border region is still insufficiently known, despite the contributions of Flandrin (1948) and Arambourg (1952).

S. Boulemia (✉) · M. Hamimed · B. Djoulah
Department of Earth Sciences and the Universe, Larbi Tebessi University-Tebessa, Tebessa, Algeria
e-mail: salim.boulemia@univ-tebessa.dz

The fish fauna characterizing these rocks includes a multitude of species. Materials collected from outcrops of sedimentary phosphorites of El Kouif locality have been characterized to establish a general systematic overview, reconstruct the paleoenvironment and specify the age of the phosphate layers.

Teeth of sharks and rays are characterized by strong heterodontism, making the identification of fish species a very difficult task. We identified almost of isolated material at the species level. The characterization of species was mainly performed based on palaeo-ichthyology literature (e.g.: Arambourg 1952; Herman 1977; Cappetta, 1987; Smith et al. 1999; Nolf 1988; Ward and Wiest 1990). Materials were currently deposited at Tebessa University and referred with collecting number LT.

2 Overview of Geographic and Geological Settings

The study area Jebel El Kouif syncline forms part of the Saharan Atlas of eastern Algerian-Tunisian border area, extending to Tunisia. It is situated 25 km East of Tebessa city, the capital province. The main geological Paleocene-Eocene formations of Jebel El Kouif encountered at site (Fig. 1) are more precisely represented by a marly Dano-Mantian ("e^{2-3}"), a phosphatic Thanetian ("e^{4}"), Ypresian-Lutetian ("e^{5-6}") of flint limestones and Miocene ("m^{c}"), of a continental formation.

3 Materials and Methods

The research in El kouif sector was carried out during 2018. The sampling of phosphatic layers (total rock) was systematically conducted on outcrops along two sections of Djebel El kouif. The hard layers, with dolomite cement, make the collection of teeth impossible, therefore, were not sampled.

A. Çiner et al. (eds.), *Recent Research on Geomorphology, Sedimentology, Marine Geosciences and Geochemistry*, Advances in Science, Technology & Innovation, https://doi.org/10.1007/978-3-030-72547-1_50

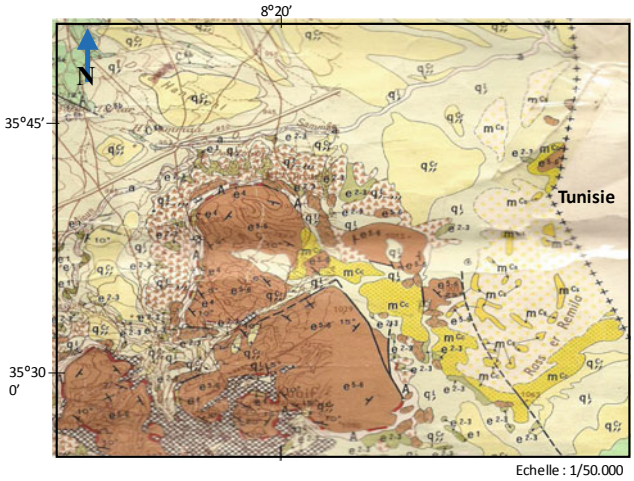

Fig. 1 Geological map for El-Kouif region (Extracted from geological map of Algeria, sheet number 151.)

Concurrently, direct investigations for teeth were carried out on field. However, the most important collection of teeth materials was completed after washing the sediment in the Laboratory of Earth Sciences at the Tebessa University (Algeria).

Clean residues were obtained from pre-dried sediment samples washed over a standard set of nested sieves (finest 100 μm mesh) after disaggregation in tap water mixed with a wetting agent (detergent). Some samples needed subsequent treatment with 5–10% hydrogen peroxide (H_2 O_2), neutralized with a few drops of ammonia. Teeth were picked from dried residues under a binocular microscope. Where appropriate, photographs and measurements were taken to aid in identification.

4 Results and Discussion

Sections carried out on the outcrops of El Kouif locality, show sub-tabular layers. A lithostratigraphic column established shows a formation revealing 08 layers of phosphorites, relatively friable of decimetric order, alternating with layers of limestone and marl-limestone (Fig. 2).

The fish assemblages of sampled phosphate of El Kouif formation include many cartilaginous fish remains. Fifteen species (Elasmobranchii, Fig. 3) were identified, twelve of which were sharks (Euselachii), and only three were rays (Batoidea). Altogether, they represented eighteen families and eight orders. Systematic specification of these fossil groups has not been published previously for the Paleogene basin of the Algerian-Tunisian border area.

The Lamniforms with 6 species and ∼35% of the total number of collected specimens were the most diverse order. Among the frequented occurring, Odontaspididaes (*Brachycarcharias* and *Carcharias*) were the most abundant, followed by Mitsukurinidaes and Otodontidaes. Next in abundance were the Carcharniforms with 5 species and ∼25% of the total number of specimens. The Myliobatiforms were represented by 2 species and were close to 10%. Among them, the rare presence of Myliobatidae was surprising. Orectolobiformes represented by four species were also, frequent with 15%. The families of the Heterodontidae and Rajidae each represented by a single species, were less frequent and together represented nearly 15% of the total number of specimens.

Table 1 displays specific climatic, environmental and bathymetric preference of the species represented in the phosphorites of El Kouif locality.

We can assert that (Table 1):

- The predominance of forms of warm water at tropical and subtropical distribution are *Brachycarcharias, Carcharias, Odontaspis*; however, stenothermic forms downright tropical as *Otodus* are rarely present;
- Another group of species preferring temperate or moderately warm water is present: *Abdounia beaugei and Archaeomanta priemi;*
- The majority of the represented fishes inhabit the neritic littoral zone, such as *Squatiscylium nigeriensis and Myliobatis sulcidens*.
- The absence of the purely pelagic and bathyal forms.
- Among the recognized species 5 are nektonic and benthic whereas 10 are benthic.
- Given the geological and paleontological data, it can be assumed that this Thanetian assemblage occupied a relatively narrow gulf between mainland and open sea, agreeing with the paleogeographical interpretation of Sassi (1974), indicating that Tebessa area was immersed between the Algerian promontory and the Kasserine island (Fig. 4).

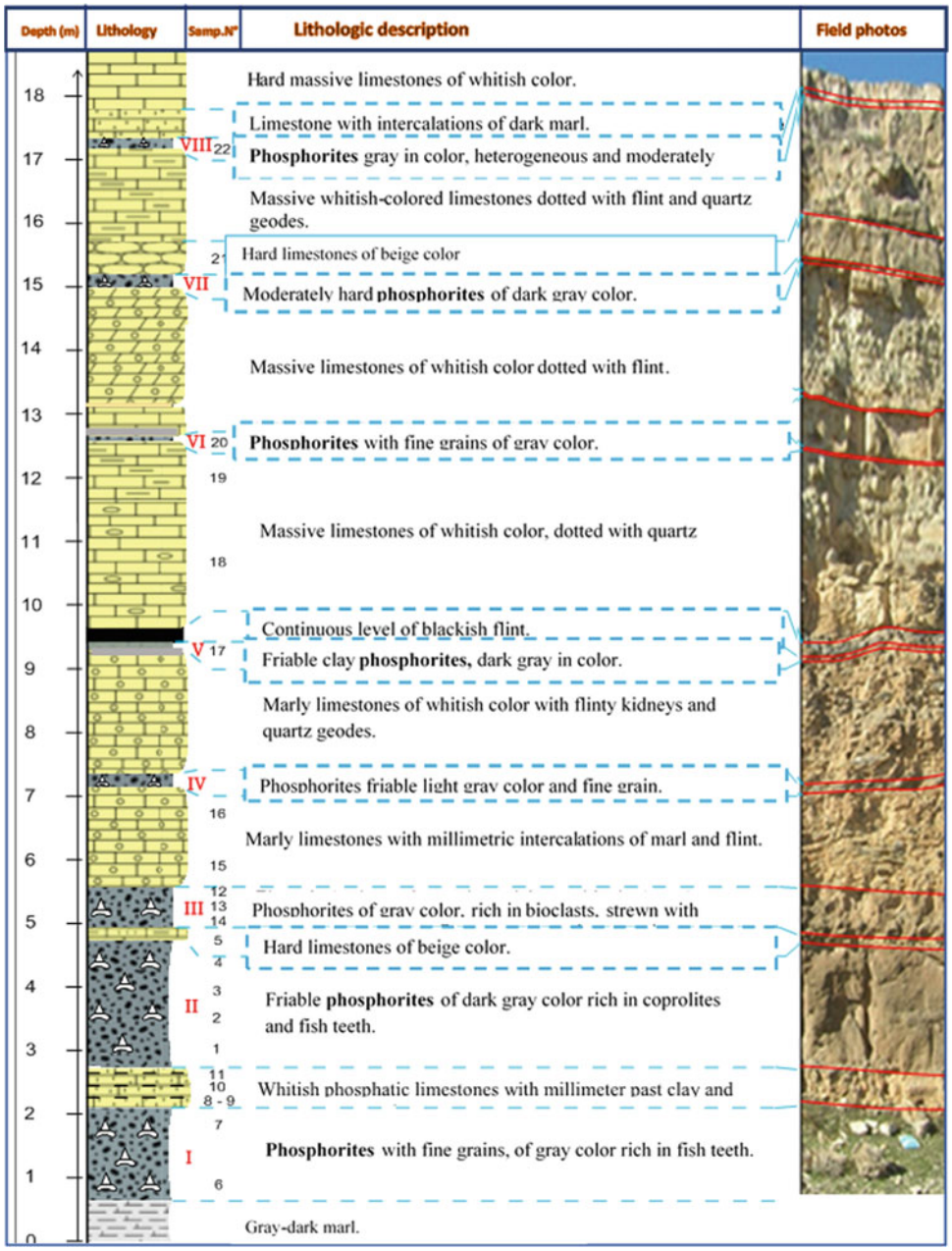

Fig. 2 Lithostratigraphy and field photographs of the studied El-kouif sections, with eight phosphorites layers

5 Conclusion

A paleontological analysis of phosphorites series from El Kouif locality showed a wealth of fish remains with many predators, represented by 15 species of Elasmobranchii (Euselachii and Batoidea).

The recognized fossils of the Elasmobranchii confirm the Thanetian age for the deposits outcropping at El Kouif locality. The fish characterize mainly, benthic and nectic forms of the neritic environment. This fish fauna indicates a marine, coastal, shallow water environment with both rocky and sandy bottom, and a temperature of subtropical climatic conditions.

Apparently, the El Kouif locality assemblage of fish occupied during Thanetian a relatively narrow golf separated from the open sea.

Fig. 3 Elasmobranchs teeth from the phosphorites series of El-Kouif locality (Algerian-Tunisian border area).

Table 1 Environmental preferences of the ichthyological assemblage recovered from phosphorites of El Kouif locality (Algerian-Tunisian border area)

Taxa	Climate			Environment			Habitat	
	Tropical/Subtropicl	Temperat	Cold	Litoral/Neritic	Semipelagic/Pela	Bathyal	Nektic	Benthic
Brachycarcharias lerichei	✪	☆		✪				✪
Odonstaspis winkleri	✪	☆		✪				✪
Carcharias hopei	✪	☆		✪				✪
Otodus obliquus	✪			✪			☆	✪
Abdounia beaugei		✪		✪	☆		✪	☆
"Scyliorhinus" gilberti	✪	☆		✪			☆	✪
Heterodontus sp	☆	✪		☆				✪
Archaeomanta priemi		✪		✪			✪	☆
Nebrius bequaerti	✪			✪				✪
Delpitoscyllium africanum	✪	☆		✪				✪
Hemiscyllium daimeriesi	✪			✪	☆			✪
Squatiscyllium nigeriensis	✪			✪				✪
Myliobatis sulcidens	✪	☆		✪				✪
Physogaleus secundus		✪		✪			✪	☆
Ginglymostoma subafricanum	✪	☆		✪	☆			✪

☆ *Less characteristic*
✪ Characteristic

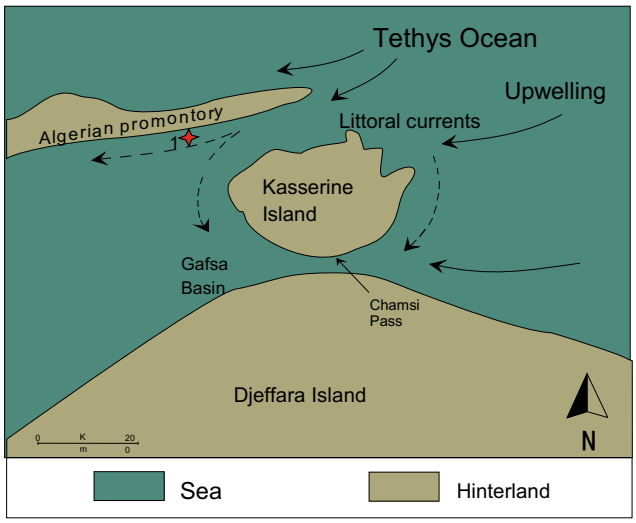

Fig. 4 Supposed Paleocene-Eocene paleogeography in Algerian-Tunisian border area. Red star indicates position of El-Kouif locality

References

Arambourg, C.: Les vertébrés fossiles des gisements de phosphates (Maroc-Algérie-Tunisie). Notes Et Mémoires Du Service Géologique Du Maroc **92**, 1–372 (1952)

Baut, J.-P., Génault, B.: Contribution à l'étude des élasmobranches du Thanétien (Paléocène) du bassin de Paris. Service Géologique de Belgique, Papier Professionnel **278**, 185–259 (1995)

Bles J.l., Fleury, J.: Notice explicative de la carte géologique du Morsot (178). Publication du Service géologique de l'Algérie, Alger (1970)

Boulemia, S., Hamimed, M.: Fossil fish teeth in phosphatic series of Jebel Dyr (Algerian-Tunisian Border Area). Open J. Geol. **8**, 1069–1083 (2018)

Boulemia, S., Hamimed, M., Bouhlel, S., Bejaoui, J.: Petro-mineralogical analysis of sedimentary phosphate of Marine Origin, Case of the Locality of El Kouif (Algerian-Tunisian Confines). Open Journal of Geology **5**, 156–173 (2015)

Cappetta, H.: Mesozoic and Cenozoic Elasmobranchii, Chondrichthyes II, vol. 3B, 193 p., 148 figs. (1987)

Cappetta, H., Nolf, D.: Revision of some Odontaspididae (Neo-selachii: Lamniformes) from the Paleocene and Eocene of the North Sea Basin). Bull. De L'institut Royal Des Sci. Naturelles De Belgique **75**, 237–266 (2005)

Cappetta, H.: Chondrichthyes: Mesozoic and Cenozoic Elasmobranchii: Teeth, pp. 1–512. In Schultze, H.-P. (ed.) Handbook of Paleoichthyology, vol. 3E. Verlag Dr. Friedrich Pfeil, Munich (2012)

Casier, E.: Faune ichthyologique du London Clay. Br. Museum Natural Hist. **496** (1966)

Compagno, L.J.V.: FAO Species Catalogue. Volume 4. Sharks of the world. An annotated and illustrated catalogue of shark species known to date. Part 1. Hexanchiformes to Lamniformes. FAO Fisheries Synopsis, pp. 125–249 (1984)

Compagno, L.J.V.: Sharks of the world. An annotated an illustrated catalogue of shark species known to date. Volume 2. Bullhead, Mackerel and Carpet sharks (Heterodontiformes, Lamniformes and Orectolobiformes). FAO Species Catalogue for Fishery Purposes, pp. 1–269 (2001)

Cyril, G., Judicael, P., Gael, P.: Le gisement de vertébrés Thanétiens (paléocène supérieur, MP6) du petit Patis prés Creil (Oise, France). Bull. Inf. Géol. Bass. Paris **46**(2), 3–11 (2009)

Dutheil, D.B.: A checklist of Neoselachii (Pisces, Chondrichthyes) from the Paleogene of the Paris Basin France. Tertiary Res **13**(1), 27–36 (1991)

Dutheil, D.B., Moreau F., De Plöeg, G.: Les ichthyofaunes du gisement à ambre de Le Quesnoy (Paléocène et Éocène du bassin de Paris, France). COSSMANNIANA **11**(1–4), 1–13 (2006)

Flandrin J.: Contribution à l'étude stratigraphique du Nummulitique algérien. Publ. Serv. Carte Géol. Alg. **19**(2) (1948)

Herman: Les Sélaciens des terrains néo crétacés & paléocènes de Belgique & des contrées limitrophes. Eléments d'une bio stratigraphie intercontinentale. Mém. Explic. Cart. Géol. Min. Belge **15**, 1–401 (1977)

Moreau, F., Mathis, S.: Les élasmobranches du Thanétien (Paléocène) du Nord de la France, des carrières de Templeuve et Leforest. Cossmanniana 7(4), 1–18 (2000)

Nolf, D.: Dents de requins et de raies du Tertiaire de la Belgique, Fossiles de Belgique. Bull. Inst. Royal. Sci. Nal. Belg, pp. 1–184 (1988)

Noubhani, A., Cappetta, H.: Évolution de la taille et de la morphologie des dents dans deux lignées de sélaciens : application biostratigraphique. Tertiary Res. **14**(1), 1–18 (1992)

Sassi, S.: La sédimentation phosphatée au Paléocène dans le sud et le centre ouest de la Tunisie. Thèse Doctrat Es-Sci. Univ. Paris Sud, Orsay, France (1974)

Smith, R., Smith, T., Steurbaut, E.: Les élasmobranches de la transition Paléocène-Eocène de Dormaal (Belgique): implications biostratigraphiques et paléobiogéographiques. Bull. Soc. Géol. France **170** (3), 327–334 (1999)

Smith, T., Smith, R.: Synthèse des données actuelles sur les vertébrés de la transition Paléocène-Éocène de Dormaal. Bull. de la Société belge de Géologie **104**(1–2), 119–131 (1995)

Ward, D.J., Wiest, R.L.: A checklist of Paleocene and Eocene sharks and rays (Chondrichthyes) from the Pamunkey Group, Maryland and Virginia, USA. Tertiary Res. **12**, 81–88 (1990)

Benthic Foraminifera from the Saïda Clays Formation (Jebel Brame, Northwestern Algeria) Biostratigraphy and Paleoecology

Khaldia Ziouit, Abbès Sebane, Abdia Touahria Sebane, and Litissia Mahroug

Abstract

Saïda clays formation "Argile de Saïda" is one of the main sedimentary series of the Upper Jurassic of Northwestern Algeria. It was first defined in the western part of the Tlemcenian domain. This domain is situated between the Tellian Atlas in the north and the high plateaux Oranaises in the south. The study area constitutes the eastern extremity of the Tlemcenian domain in the Djebel Brame section (Northwestern Algeria). It is represented by an interbedded clay and sandstone alternation of Upper Jurassic age, which is rich in foraminifera. The taxonomic study of the samples shows a population of foraminifera consisting of 28 species belonging to10 genera, 08 families and 04 suborders divided into three associations, largely dominated by the *Nodosariidae*. Paleoenvironmental interpretations based on the foraminiferal data and geochemical (calcimetry) analyses indicate a shallowing of the basin during the Upper Oxfordian.

Keywords

Saïda clays • Upper jurassic • Foraminifera • Upper oxfordian • Geochemical analyses

1 Introduction

Saida clays formation of the eastern part of the Tlemcenian domain was first described by Atger and Verdier (1965) in the area of Sidi Kadda (ex Kechrou), in the south of the city of Mascara and has been the subject of many studies in the western part of the Tlemcenian domain (Lucas 1952; Elmi 1978; Delfaud 1973; Touahria 1979; Benest et al. 1998; Cherif et al. 2015; Bendella et al. 2011). In the Djebel Brame section (Northwestern Algeria), the sediments are represented by interbedded clay-sandstone sections of Upper Jurassic age, which are rich in foraminifera. The Djebel Brame, reaching a height of 906 m, is located 21 km to the north of the Takhemaret town (Tiaret, Northern Algeria) and 8 km southeast of the village of Hadj El Arbi (Fig. 1). This section has been subdivided into three lithostratigraphic units: a lower clay-sandstone, median clay-carbonate and upper clay-sandstone. The study of the foraminifera from the Jebel Brame section has identified several species whose biostratigraphic division is consistent with that established by the Ammonites. The observations based on the nature of the test allowed us to distinguish two forms: hyaline and agglutinated. A calcimetric analysis was also undertaken on the marls to foraminiferal levels in order to formulate a palaeoenvironmental interpretation.

2 Materials and Methods

The samples, weighing approximately 2 kg each, were taken from the clay levels of the section. They were soaked in tap water for 24 h, then carefully washed in a sieve column with mesh sizes of 250, 125 and 65 µm. The collected residues were dried and sorted. The foraminifera were then picked and identified. Some of these marls were also intended for the calcimetric study in order to quantify the richness of $Caco_3$.

3 Results and Discussion

The stratigraphic distribution of foraminiferal associations is shown in Fig. 2. It identified three foraminiferal assemblages that succeeded one another during the Oxfordian. The

K. Ziouit (✉) · A. Sebane · A. T. Sebane
Faculty of Earth and Universe Sciences, Laboratory GeoBaBise, University of Oran 2, Bir El Djir, Algeria

K. Ziouit · L. Mahroug
Faculty of Hydrocarbons, Renewable Energies, Sciences of the Earth and Universe, University of Kasdi-Merbah, Ouargla, Algeria

A. Çiner et al. (eds.), *Recent Research on Geomorphology, Sedimentology, Marine Geosciences and Geochemistry*, Advances in Science, Technology & Innovation, https://doi.org/10.1007/978-3-030-72547-1_51

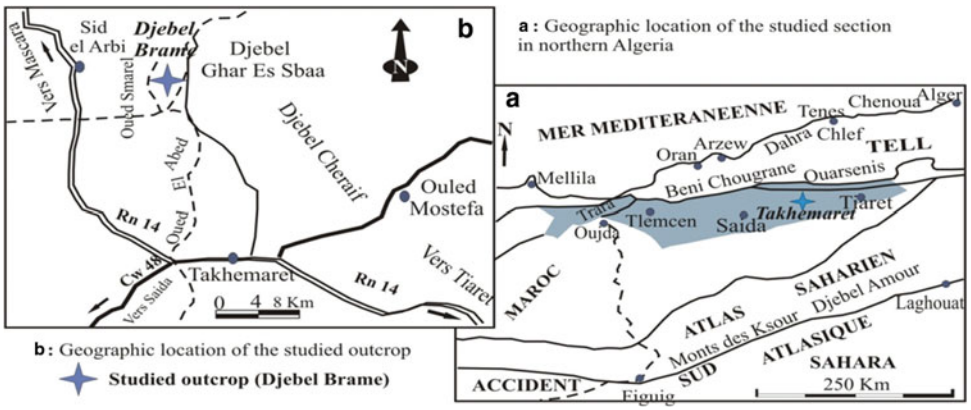

Fig. 1 Location of the study area

foraminifera are dominated by Nodosariidae and exclusively benthic in nature. Subsidary taxa belong to the suborders Textulariina, Lagenina and Rotalina.

3.1 Biostratigraphy: Study of Assemblages

Assemblage 1: It is characterized by a predominance of hyaline forms which consist mainly of *Ammodiscus* sp, *Citharina clathrata, Garentilla ampasindavensis, Lenticulina aff batrakiens* mg. *Marginulopsis, Triplasia bertensteini, Lenticulina munsteri* mg. *L Spirillina infima and Leniculina sp*. All these forms indicate an Oxfordian age.

Assemblage 2: It includes agglutinated forms, in association with the first planktonic forms. It is made up of the following forms: *Lenticulina fraasi* mg. *Astacolus, Textularia jurassica, Dentalina vetusta, Globuligerina axfordiana, Lenticulina Polymorpha* mg. *L, Spirillina elongala, Lenticulina gottimgensis.* mg. *L, Lenticulina musnsteri* mg. *L; Spirilina infima* and *Lenticulina* sp. The ammonite fauna occurring within this interval (Cherif 2017) is composed of *Subdiscosphinctes* sp., *Dichotomoceras crassus* (Enay 1966) and *Larcheria* gr. *Schilli*. It indicates a Middle Oxfordian age (Transversarium zone).

Assemblage 3: It is characterized by the predominance of *Nodosariida* and contains *Lenticulina musnsteri mg. L, Spirillina infima, Lenticulina* sp, *Lagena* sp, *Lenticulina varians* mg. *L, Marginulina jurassica* and *Ammodiscus* sp. The agglutinated forms associated quantitatively and materially are represented by *Textularia jurassica, Trochammina inflata, Ammobaculites fontinensis* and *Ammobaculites agglutinans.* This assemblage is Upper Oxfordian age (Bifurcatus zone). Ammonites harvested in this assemblage are represented by *Dichotomoceras bifurcatoides* (Enay 1966), *Dichotomoceras* aff. *Stenocycloides* (Siemiradzki 1898) and *Subdiscosphinctes* sp. This association indicates an Upper Oxfordian age (Bifurcatus zone).

3.2 Paleoecology

From the study of foraminifera, two types of test walls can be distinguished; hyaline forms and agglutinated forms (Fig. 3).Their temporal distribution is not random but seems to depend on sedimentary and eustatic variations. Their vertical distribution shows quantitative variations that are likely consistent with paleoenvironmental changes. The basal part of the section is dominated by foraminifera with hyaline tests (80%), and the calcimetry percentage is about 12%. These forms are subservient to an environment of external plate-form, well-oxygenated and favorable to the benthic life. The second assemblage is distinguished by the abundance of agglutinated forms (68%) which coincides with the increase in the argillaceous sediments, in association with a decrease in carbonate calcium $Caco_3$ (6%). These observations are in agreement with an open basin environment and are favorable for the development of benthic life.

4 Conclusions

The sedimentary, micropaleontological and geochemical data synthesis confirms the paleogeography of Oxfordian sediments. The foraminiferal distribution is controlled by the variation in sea level, as well as by the tectonics which affected the whole area. It is worth noting that calcareous hyaline forms are abundant in shallow, limestone-dominated environments, whereas, the agglutinated foraminifera taxa are present in the deeper environments and rich in terrigenous material.

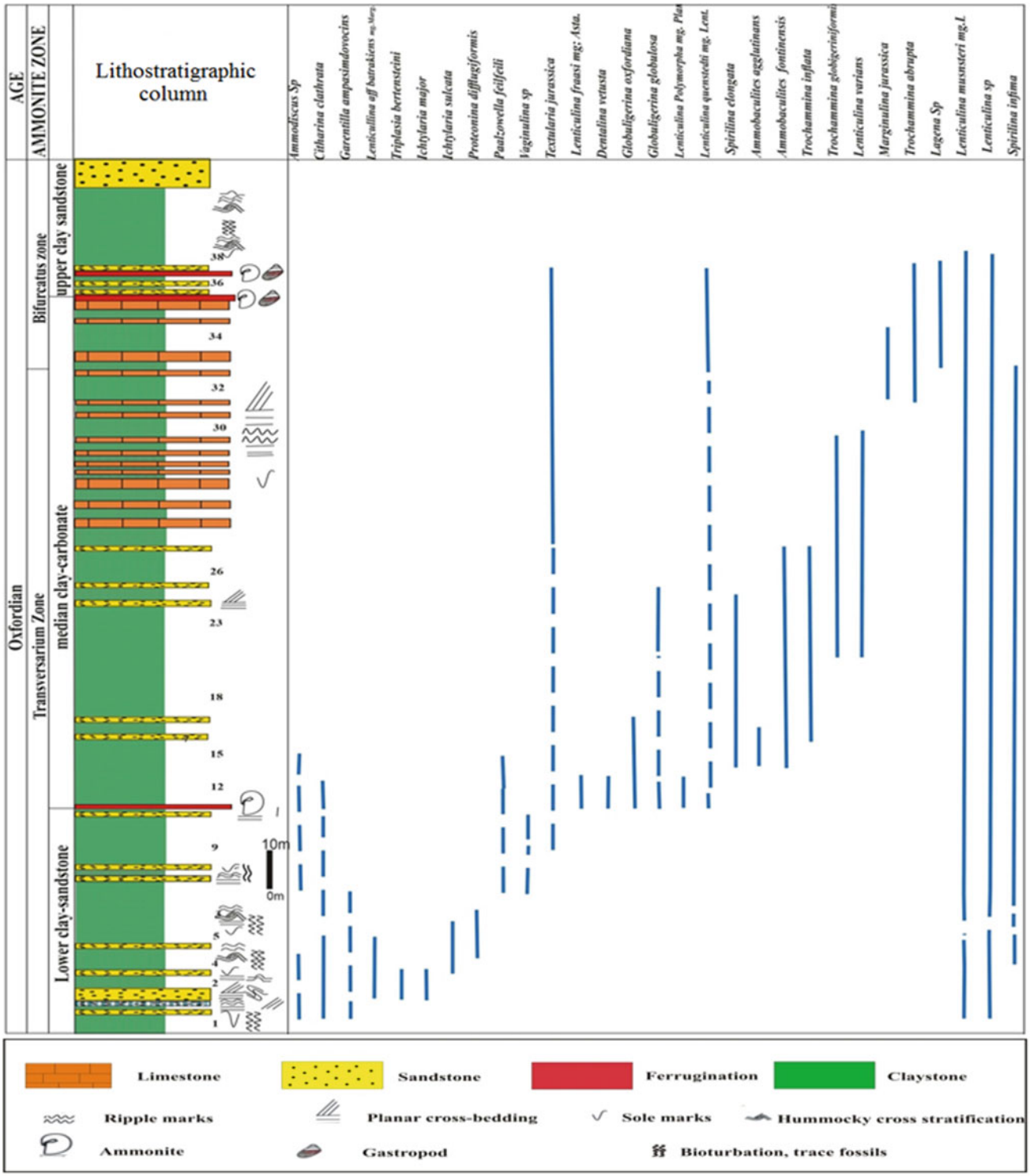

Fig. 2 Vertical distribution of foraminifera settlement

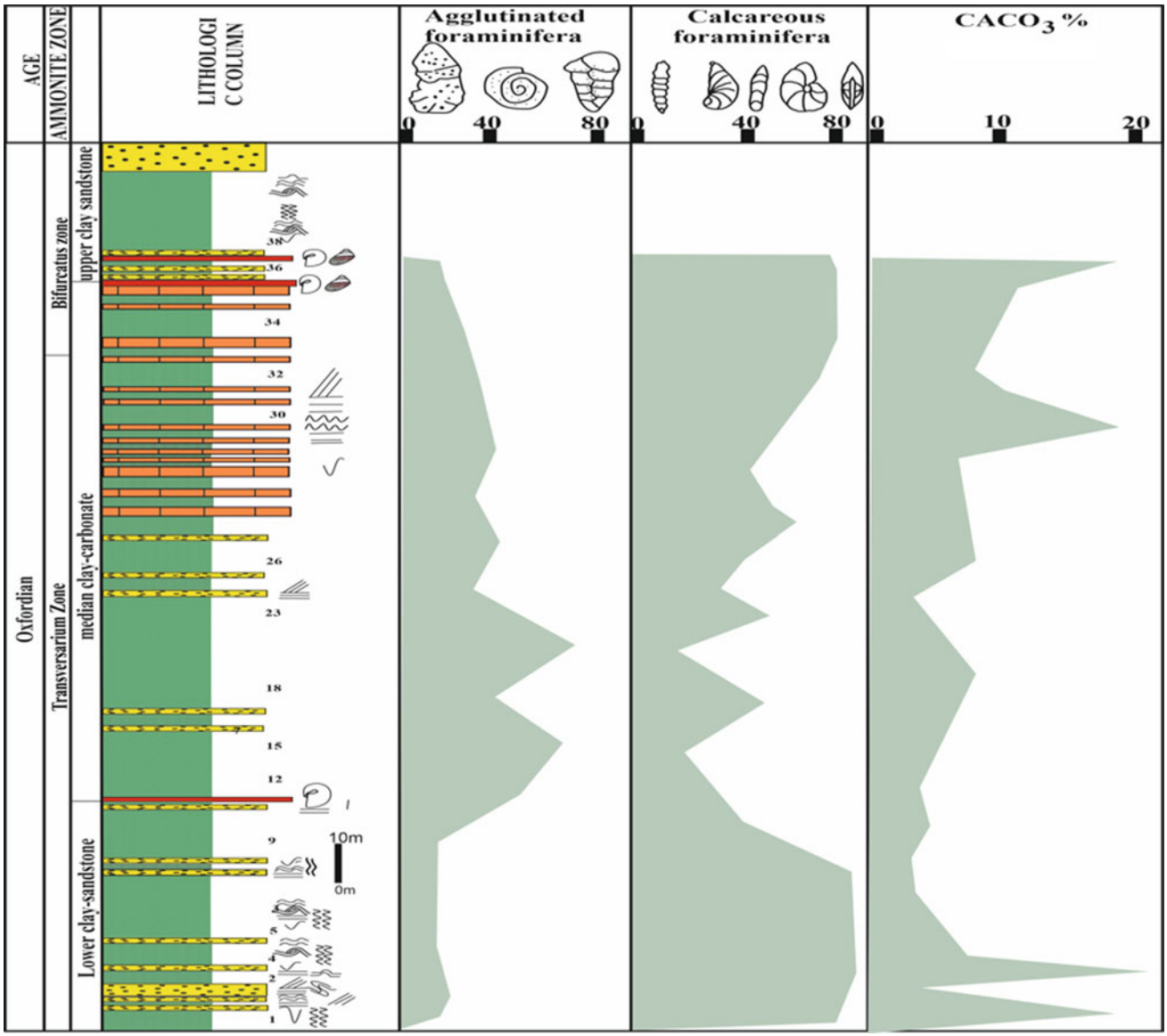

Fig. 3 Agglutinated, calcareous foraminifera variations and $CaCO_3$%

References

Atger, M., Verdier, J.: Etude géologique du plateau jurassique de Cacherou (Sidi Kada), bordure Nord des Monts de Saïda. Géosci. Soc. Nat. Res d'Exploitation Pétrol. lgérie

Bendella, M., Benyoucef, M., Cherif, A., Benhamou, M.: Ichnology and sedimentology of the Argiles de Saïdaformation (Callovo-Oxfordian) of the Djebel Brame (Tiaret, Algeria). Bull. Soc. Géol. Fr. **5**, 417–425 (2011). https://doi.org/10.2113/gssgfbull.182.5.417

Benest, M., Ouardas, T., Boullier, A.: Conditions d'installation d'un seuil corallien dans l'intervalle transgressif Oxfordien moyen et supérieur p.p. entre le bassin tellien et son avant-pays (Ouest algérien); implications paléographiques. C. R. L'académie Des Sci. Paris **326**, 399–405 (1998)

Cherif, A., Bert, D., Benhamou, M., Benyoucef, M.: La Formation des Argiles de Saïda (Jurassique supérieur) dans le domaine tlemcenien oriental (Takhemaret, Algérie) : données ichnologiques et sédimentologique **34**, 363–384 (2015)

Cherif, A.: Sédimentologie et dynamique sédimentaire de la Formation des Argiles de Saïda (Oxfordien moy-sup) de la partie orientale du

domaine tlemcenien (Algérie ouest), p. 251. Thèse Université d'Oran, Algérie (2017)

Delfaud, J.: Sur l'appartenance de certains "pseudo-flyschs" aux faciès prodeltaïques de plateforme. C. R. Del'académie Sci. Paris **277**, 1125–1128 (1973)

Elmi, S.: Polarité tectono-sédimentaire pendant l'effritement des marges septentrionales du bati africain au cours du Mésozoique (Magreb). Ann. Soc. Géol. Nord, **XCVII**, 315–323 (1978)

Enay, R.: L'Oxfordien dans la moitié Sud du Jura français. Etude stratigraphique. Publications du musée des Confluences **8**, 1–323 (1966)

Lucas, G.: Bordure nord des Hautes-Plaines dans l'Algérie occidentale. —XIXème CongrésInternationalde Géologie, Alger, (Monographie. régionale., série 1), **21**, 139 (1952)

Siemiradzki, J.: Monographic description of the ammonite group Perisphinctidae. Palaeontographia **45**, 69–296 (1898)

Touahria, A.: Biostratigraphie du Callovien des environs de Saïda (Algérie occidentale). Les Reineckeiidae (Ammonitina, Perisphinctaceae). Thèse 3ème Cycle, Univ Lyon 152 (1979)

Diatom Microflora of Ouled Djilali Section (Messinian Diatomites from Lower Chelif Basin, North-Western Algeria)

Amal Touina, Bouhameur Mansour, Safia Chernai, and Boualem Hamdi

Abstract

Quantitative and qualitative analyses of diatom assemblages of the Ouled Djilali section (lower Chelif basin, Northern Algeria) were produced for the first time. A total of 77 diatom and silicoflagelates species were determined: 43 centrics, 27 pennates, and 7 silicoflagelates. The majority of the analyzed samples essentially consists of planktic diatoms, except for a few levels where benthic pennate diatoms dominate. The diatom assemblages characterize a marine opened environment subject to oceanic waters influence. The predominance of the species *Thalassionema nitzschioides* and/or *Thalassiothrix longissima* indicates periods of strong productivity that can be associated to an upwelling system.

Keywords

Diatomite • Diatoms • Paleoenvironment • Lower-Chélif bassin • Algeria

1 Introduction

The Messinian diatomitic formation, also known as "Tripoli" in Sicily, persisted in the Mediterranean during the pre-evaporitic phase (7.1–5.97 Ma), which is considered a preconditioning interval towards the Messinian salinity crisis (Mansour 1991; Pestrea et al. 2002). It represents one of the most significant sedimentary events of the Neogene in the Mediterranean (Ouahabi et al. 2007; Mansour et al. 2008; Pestrea et al. 2002). These siliceous sedimentary rocks consist of the fossilized skeletal remains of microscopic single-celled algae called diatoms. Their susceptibility to changes in the environmental physicochemical parameters makes them excellent ecological indicators. They can therefore be used for the reconstitution of the palaeoenvironments and palaeoceanographic setting (Mansour 1991).

The object of this study was an overlooked part of the lower Chelif Basin (NW Algeria), close to the village Ouled Djilali (southwestern border of the Dahra). The aim of this study was to provide a better knowledge of the palaeoenvironment of a part of this basin during pre-evaporitic phase of the Messinian Salinity Crisis.

2 Materials and Methods

The section of Ouled Djilali consists of an alternation of marls and diatomites Fig. 1. In a total of 08 samples, 1 g of the sediment is treated simultaneously with HCl (20%) and hydrogen peroxide. After a series of washing steps using distilled water, an aliquot of the suspended material was spread out on a cover glass and mounted on a glass slide with Canada Baume resin (retraction index = 171) (Barron 2005; Van Iperen et al. 1993). The slides were observed under an optical microscope (X1000). The relative abundance of the different species was established by counting 500 individuals. An observation under scanning electron microscope was carried out at the physicochemical research and analysis center CRAPC Expertise SPA (Kolea).

3 Results

Diatoms are generally abundant, diverse, and well preserved in the diatomite. Both Centric and Pennate diatoms are well represented, but the former group is more diversified (Fig. 2a) and dominant (Fig. 2c). In the Centric class, the genera *Coscinodiscus* followed by *Actinocyclus*, and *Thalassiossira* are the characterized by the highest specific

A. Touina (✉) · S. Chernai · B. Hamdi
LCVRM ENSSMAL. BP19, 16320 Dely Ibrahim, Algeria

B. Mansour
L.P.S.P. Département de Science de la Terre, FSTU, Université d'Oran, Oran, Algeria

A. Çiner et al. (eds.), *Recent Research on Geomorphology, Sedimentology, Marine Geosciences and Geochemistry*, Advances in Science, Technology & Innovation, https://doi.org/10.1007/978-3-030-72547-1_52

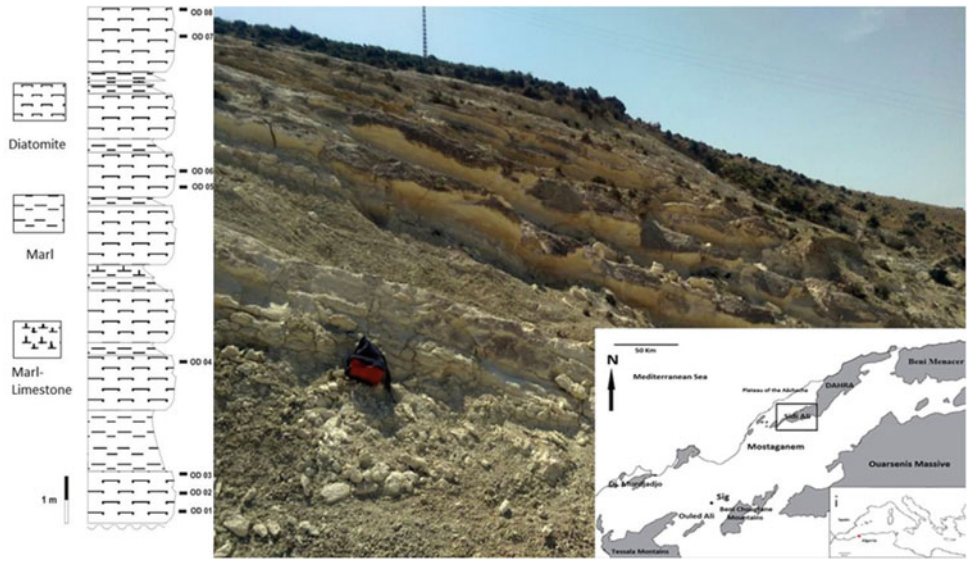

Fig.1 Ouled Djilali Diatomite deposit site

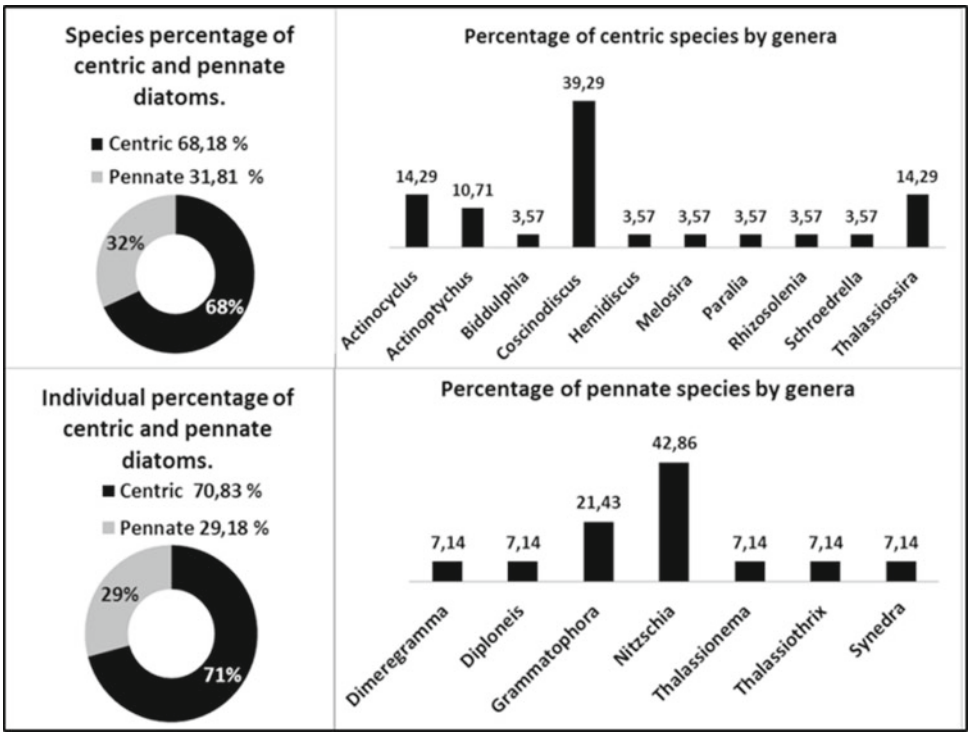

Fig. 2 Ouled Djilali diatoms biodiversity

diversity (Fig. 2b); while in the class of Pennates, the genus *Nitzschia* has the largest number of species, followed by the genus *Grammatophora* (Fig. 2d).

4 Discussion

The dominance of marine diatoms shows that the studied site is purely marine (only one brackish species: *Mélosira granulate* is present, while no freshwater species were observed). The detailed study of the assemblages generally shows alternate levels of abundance or significant frequency of species: *Coscinodiscus marginatus*, *Actinoptychus senarius*, *Thalassionema nitzschioides*, which can point for periodical rise and fall of the sea level.

Several main influences can be discerned, often superimposing and corresponding either to bathymetric variations or currents:

- A constant coastal influence on a permanent marine environment suggested by the appearance of littoral planktonic species (22,8–47,8%): *Actinocyclus cubitus*,

Actinoptychus senarius, *Hyalodiscus radiatus* and *Paralia sulcata*, warm benthic species (*Rhabdonema adriaticum*, *Grammatophora oceanica* and *Grammatophora angulosa*), and neritic-oceanic species (*Coscinodiscus asteromphalus*, *Coscinodiscus sp 1* Gardette), or by the increase of their frequencies (*Actinoptychus senarius*).

- A warm oceanic influence with the oceanic species *Thalassiosira eccentrica*, and *Hemidiscus cuneiformis*, or cold (boreal) influence with *Thalassiothrix longissima*, suggesting easy communications with the global ocean (*Coscinodiscus marginatus* and *Actinocyclus curvatulus*).
- The possible influence of upwelling system suggested by the dominance of *Thalassionema nitzschioides* and *Thalassiothrix longissima* (Gersonde 1980), also indicating high productivities, which can also probably fed by the continent (runoff).

5 Conclusions

Quantitative and qualitative analyses diatom assemblages of the Ouled Djilali section (lower Chelif basin, Northern Algeria) were carried out on 08 samples. The diatom assemblage is characterized by mainly neritic-oceanic marine forms (71.6 to 90.2%) which bear witness to a rather shallow open intermediate marine environment, in connection with the global ocean, similar to those of other Messinian basins of Western and Central Mediterranean (Pestrea and Saint Martin 2002), with the possible hypothesis of the operation of an upwelling system and/or the influence of the of coastal waters, which are probably fed by the continent (runoff).

Plate I:

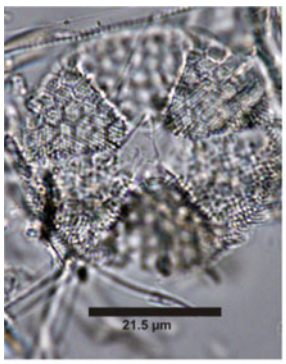

Actinoptychus senarius EHR ,1843,

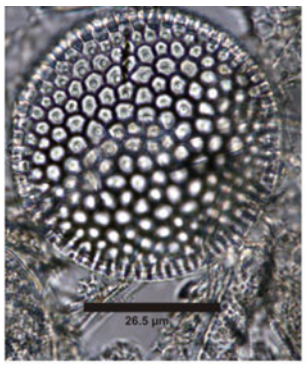

Coscinodiscus marginatus EHR 1841

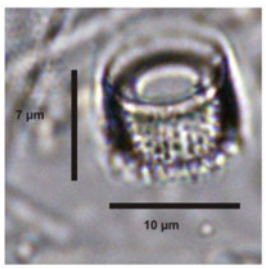

Aulacoseira granulata (Ehr) Simonsen, 1979

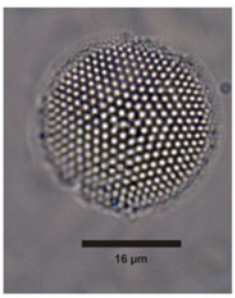

Thalassiosira eccentrica (Ehrenberg) Cleve, 1903

Thalassionema nitzschioides (Rop.) Grunow 1880

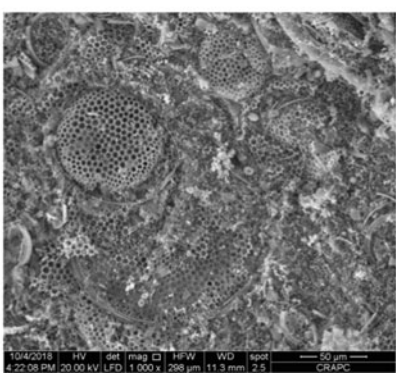

SEM image of a natural diatomite of Ouled Djilali

References

Barron, J.-A.: Diatom biochronology for the early miocene of the equatorial pacific. Stratigraphy **2**(4), 2005, 281–309 (2006), text-figures 1–4, plates 1–9, tables 1–2. https://www.researchgate.net/publication/260106000.

El Ouahabi, F.Z., et al.: Les assemblages de diatomées du bassin messinien de Boudinar (Maroc nord-oriental). Rev. Micropaléontol. **50**(2007), 149–167 (2007)

Gersonde, R.: Paläoökologische und biostratigraphische Auswertung von ditomeena assoziationen aus dem Mesinium des Caltanisseta-Beckens (Sizilien) und einiger vergleich profile in SO Spanien, NW Algerien und auf Kreta, p. 393. Thèse, université de Kiel, Allemagne, (1980)

Mansour, B.: La série diatomitique messinienne de Sig: étude systématique des diatomées et implications paleogéographiques. P. 147. Thèse de Magister, Université d'Oran (Alggrie) (1991)

Mansour, B., Bessedik, M., Saint Martin, J.-P., Belkebir, L.: Signification Paléoécologique des assemblages de diatomées du Messinien du Dahra sud-occidental (bassin du Chélif, Algérie nord-occidentale). *Geodiversitas* **30**(1), 117–139, (2008). (annexes disponibles sur: www.geodiversitas.com)

Pestrea, S., Blanc-Valleron, M.-M., Rouchy J.-M.: Les assemblages de diatomées des niveaux infra-gypseux du Messinien de Méditerranée (Espagne, Sicile, Chypre). In D. Néraudeau, E. Goubert (eds.) l'Événement Messinien: Approches Paléobiologiques et paléoécologiques. Geodiversitas, vol. 24(3), pp. 543–583 (2002)

Pestrea, S., Saint Martin, J.-P.: La microflore de diatomées du Messinien de Gibellina (Sicile occidentale, Italie). In: Néraudeau, D., Goubert E. (eds.) l'Événement Messinien: Approches Paléobiologiques et Paléoécologiques. Geodiversitas, vol. 24(3), pp. 585–610 (2002)

Van Iperen, J.M., van Bennekom, A.J., van Weering, T.C.E.: Diatoms in surface sediments of the Indonesian Archipelago and their relation to hydrography. In: Twelfth International Diatom Symposium. Hydrobiologia 269/270, pp. 113–128 © 1993 Kluwer Academic Publishers, Belgium (1993)

Micropaleontology and Biostratigraphy of the Upper Albian of Jabal Msella in Northeastern Tunisia

Abdallah Elkhazri

Abstract

In Northeastern Tunisia, the Upper Albian deposits are characterized by continuous sedimentation starting with marl-limestone alternations that include a radiolarian peak with varied morphotypes and a dominance of the species *Cryptamphorella conara*, *Dictyomitra gracilis*, *D. napaensis* and *Crucella cachensis*. The objective of this work was the biostratigraphical and micropaleontological study of the Upper Albian deposits in Jabal Msella: This analysis is based on the spatio-temporal survey coupled to a quantitative analysis of the whole microfauna. Also noted, the presence of benthic foraminifera essentially the genera: *Lenticulina*, *Dentalina*, *Nodosaria* and *Epistomina*. Toward the top, the sedimentation is essentially marly and yield of planktonic foraminifera represented by the genera *Rotalipora*, *Hedbergella* and *Ticinella*. The presence of these markers indicates the Upper Albian. The distribution of benthic foraminifera recorded vertical variations: Thus, in the basal part of the Upper Albian of hyaline, calcareous tests (Nodosaridae) are predominant, and in the middle and upper part hyaline, calcareous tests (Lagena) and agglutinated tests (Praedothia, Ammodiscus) are present. The results can be summarized as follows:

1. Lithology and biostratigraphy. The Upper Albian levels of Jebel Msella are characterized by sedimentation with calcareous clay recurrences and black platy limestones at the base and then marls and green clays at the top.
   The detailed analysis and stratigraphic distribution of planktonic and benthic foraminiferal species allowed us to specify the limits of biozones. The different biozones recognized in this section are radiolarian zones represented by *Cryptamphorella canara* zone, *Crucella cachensis* zone, *Dictyomitra gracilis* zone and *Rotalipora appenninica* zone [planktonic foraminifer].
2. Micropaleontology. In the studied material, we recognized 15 species of planktonic foraminifers grouped into 10 genera and 18 benthic species grouped into 8 genera. Radiolarians constitute a substantial component in the faunistic composition, given its dominance in this section but also because of its importance in terms of dating and characterization of the depositional environments.
3. Quantitative study. This study of the whole of the microfauna at the level of the Albian of Jabal Msella shows remarkable distribution at the level of the three units. In the first unit, we note a richness in radiolarians associated with some benthic foraminifers. The second unit shows a dominance of benthic foraminifers over the radiolarians that become less important. There is a reoccurrence of radiolarians at the third unit with a remarkable number associated with plankton foraminifers ascribed to the genera *Rotalipora*, *Hedbergella* and *Ticinella*.

Keywords

Albian • Northeastern Tunisia • Jabal Msella • Radiolaria • Benthic foraminifera • Planktonic foraminifera

1 Introduction

This work focused on the micropaleontology and biostratigraphy study of the Upper Albian of Northeastern Tunisian Jabal Msella. The aims of this paper were to study the stratigraphic distribution of planktonic and benthic foraminiferal species and to recognize the different zones. The study also involved a sedimentological analysis in order to restore the depositional environments during the Upper Albian. The results were discussed and compared with other findings of other works in the same stratigraphic interval in Tunisia.

A. Elkhazri (✉)
Department of Earth Sciences, Faculty of Sciences of Bizerte, University of Carthage, 7021 Bizerte, Zarzouna, Tunisia

A. Çiner et al. (eds.), *Recent Research on Geomorphology, Sedimentology, Marine Geosciences and Geochemistry*, Advances in Science, Technology & Innovation, https://doi.org/10.1007/978-3-030-72547-1_53

The microfossil study shows the presence of various genera of benthic and planktonic foraminifers which are divided into several species with the presence of radiolarians which are notable by their abundance and diversification through this section. The spatio-temporal distribution of the microfauna as well as their quantitative study was also carried out.

2 Materials and Methods

a. The adopted methods consist essentially of a biostratigraphy and micropaleontology studies associated with a sedimentology analysis. The results presented in this work are derived from observations and analyses carried out both on field and in laboratory. Indeed, this section consists of a detailed survey of the sequence (bed by bed), noting the sedimentology and paleontology characteristics. In addition, sampling was carried out systematically on marly levels and indurated beds. In the laboratory, the following techniques and analyses were performed: **(1)** Washed residues: steps are as follows: **(a)** Soaking the samples in the water that allows us to dissect sediments that include microfossils. **(b)** Wash the samples: The first step is to thoroughly clean the sieve column soaked in methylene blue under a stream of water until the water becomes clear; this is to avoid contaminations among samples. **(c)** Drying samples: The drying was performed in an oven preheated to a temperature of about 60 °C for a few hours. **(c)** Separation of the microfossils and observation under a binocular: Classification makes it possible to separate the microfossils residues (benthic foraminifers, planktonic, ammonites …) from those of the mineralogical ones (quartz, pyrite …). **(2)** Species determination: It is based on the use of the illustrations of specific works with a special interest in the marker species; to determine the age for the benthic foraminifers, we used the work of (Neagu 1975); for planktonic foraminifers, the work of (Bellier and Moullade 2002; Bellier et al. 2003; Ben Haj Ali 2005; Loeblich and Tappan 1984); and for radiolarians, the works of (Ben Fadhel et al. 2010; Cordey et al. 2005; Danelian 2008; Musavu-Moussavou et al. 2007; Nargess et al. 2015).

b. **Geographical framework**. Jabal Msella is located in Northeastern Tunisia near of Zaghouan state, on the geological map of Grombalia (n° 29; 1/50.0000), (Fig. 1). The section is located on the southern side of Jebel Sidi Salem precisely at Jebel Sidi Salem Garci which is bordered to the north by Jebel Ressas, to the south by Jebel Sidi Zit and to the east by Ain Safsaf.

3 Results and Discussion

Results. This section is subdivided into three units according to the lithology study and microfacies analysis coupled with a micropaleontology study. The detailed study shows a faunistic diversity consisting of planktonic and benthic foraminifers distributed over three units. From the base to the top, we note (Fig. 2):

Unit 1. It is made of a marl-limestone alternation (5.5 m). It comprises a radiolarian peak composed of various shapes and sizes. The predominant genus is *Cryptamphorella* represented by the species *Cryptamphorella conara.* We also note the occurrence of the species *Holocryptocanium barbui* in a low number. There are also less abundant species formed by the two conical and triaxial shapes represented successively by the genera *Dictyomitra* and *Crucella.*

Fig. 1 **a** Location of the area studied in Northeastern Tunisia **b** Extract from the google earth (map of Grombalia)

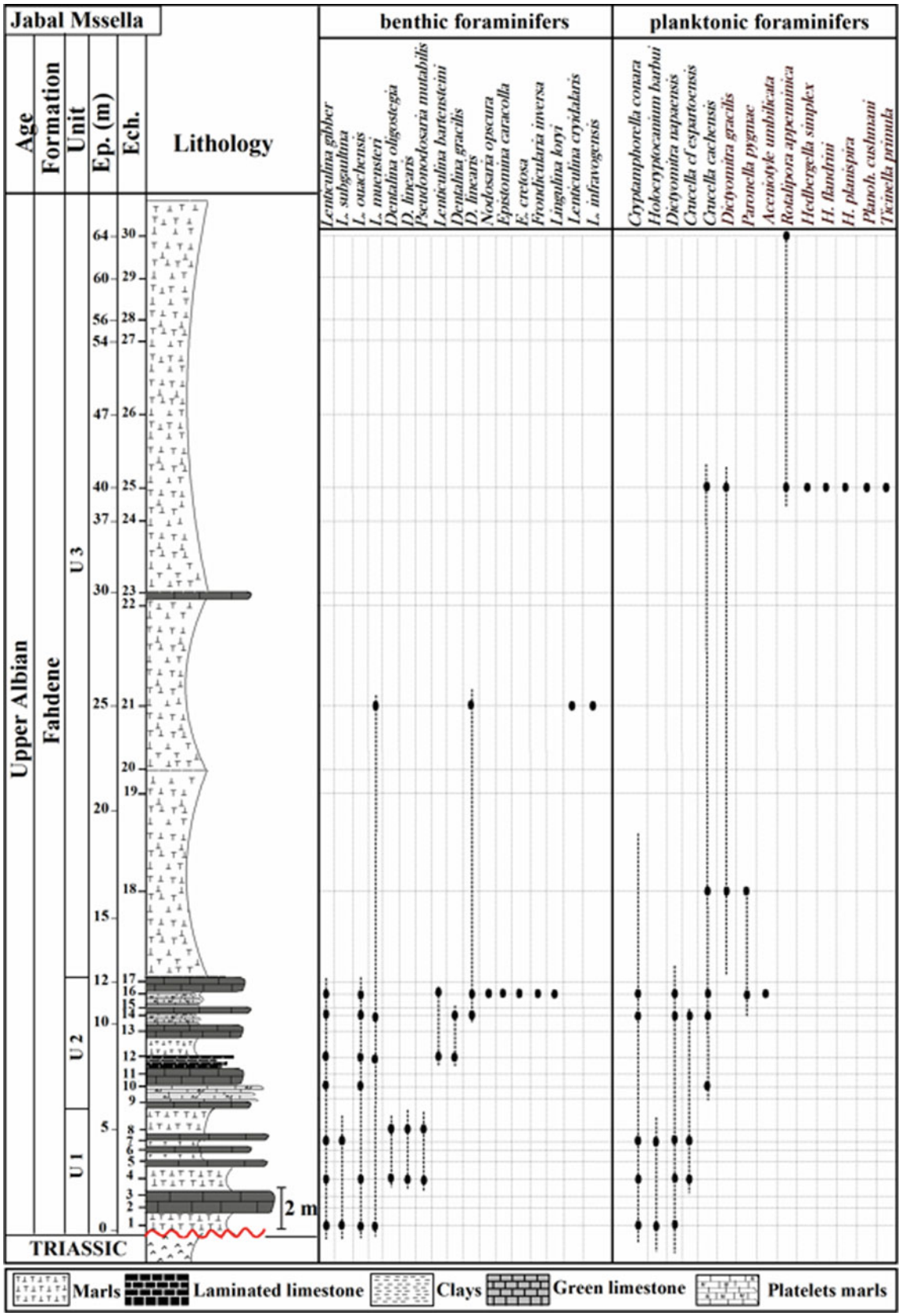

Fig. 2 Foraminifer (benthic and planktonic) distribution of the Upper Albian of J. Mssella

The characteristic species of these are *Dictyomitra napaensis* and *Crucella* cf *espartoensis*. The distribution of radiolarians is notable; in fact, it shows abundance in sample. 1; afterward, they decrease in number (Sample 4) so that they *cancel* each other in the summit part of this unit (Sample 7).

Along with this richness in radiolarians, benthic foraminifers are diversified into genera and species and are represented mainly by the species *Lenticulina gibber, L. subgaultina*, *L. ouachensis*, *L. muensteri, Dentalina Oligostegia, D. Linearis* et *Pseudonodosaria mutabilis.*

The microfacies study revealed a mudstone-wackestone texture containing sections of radiolarians of different shapes (spherical most abundant, elongated are less frequent and flattened are rare), with sometimes oxidized ledges and the presence of lamins of organic matter.

Unit 2. It is formed by alternating marls, green limestones beds, marly and limestone-laminated levels (6.5 m). At this level, the radiolarians become very rare (except for Sample 14) where the radiolarians are abundant and are represented essentially by the genera *Cryptamphorella* and *Dictyomitra* and some triaxial forms at level 16 whose species are *Cryptamorphella conara*, *Dictyomitra napaensis, Paronella pygmae, Crucella cachensis, Aceniotyle umbilicata, Praedothia* sp.. In this unit, we remark the important presence of benthic foraminifers, which take over the radiolarians. These benthos are represented by these species: *Lenticulina ouachensis, L. gibber, L. bartensteini, L. muensteri*, *Dentalina gracilis, D. linearis*, *Nodosaria opscura, Epistomina caracolla*, *E. cretosa*, *Frondicularia inversa* and *Lingulina loryi.* The microfacies study shows a predominantly mudstone texture rarely associated with spherical radiolarian sections in Sample 15 and are more frequent in Sample 17 whose edges are oxidized.

Unit 3. It is the most developed unit (55 m) essentially marly. It is formed of two valleys separated by a black carbonated level 20 cm thick. This series extends from level Ms 18 to Ms 30. The base and the top of this unit did not yield a richness in microfauna except for Sample 18 where we note some species of *Dictyomitra gracilis*. From level 21, the benthic foraminifers appear and are represented by the species *Lenticulina crepidularis, L. muensteri, L. infravolgensis*, *Dentalina linearis*. Sample 25 is remarkable for its faunistic content, in fact the radiolarians appear again with a lower frequency of species *Crucella cachensis*, associated with planktonic foraminifers formed by the species *Rotalipora appenninica*, *Hedbergella simplex*, *Hedbergella flandrini*, *H. planispira*, *Planohedbergella cushmani* and *Ticinella primula*. The microfacies at the Sample 23 reveal a mudstone texture whose figured elements are very rare and almost absent, and we can guess some organic matter indices associated with a section of *Lagena* benthic foraminifer (Plates 1 and 2).

Chronostratigraphic attribution. The spatio-temporal analysis of the benthics and planktonic foraminifera assemblages, especially the radiolarians (Ben Fadhel et al. 2010; Cordey et al. 2005; Danelian 2008; Nargess et al. 2015) and the presence of these markers: *Rotalipora appenninica*, *Hedbergella simplex*, *H. planispira* and *Ticinella primula* (Bellier and Moullade 2002; Bellier et al. 2003; Ali 2005) make it possible to attribute this series to the Upper *Albian age "Vraconian", represented by the Fahdene formation.*

Discussion. This work can be correlated with (Ben Fadhel et al. 2010) for radiolarian assemblages following the identification of the same markers but also with the works (Ben Fadhel et al. 2010; Bellier and Moullade 2002; Bellier et al. 2003; Ali 2005) for the associations of planktonic foraminifer, in particular the markers adopted for the Upper Albian. Also, the deposition environment is interpreted as a semi-enclosed basin and an intensified upwelling currents high-nutrient supply, and this is the example for several outcrops of the Upper Albian ascribed to the Tunisian trough.

Quantitative Study

Unit 1. The quantitative study of the whole fauna collected in the first unit shows a oscillation of the radiolarians, in Sample 1; there is an abundance of spherical shapes which exceed a hundred individuals, the conical shapes are less abundant (not more than 9 specimens) distributed over the two Samples 1 and 4, while the triaxial forms presented by 5 specimens (Sample 1) and 2 specimens (Sample 4).

As a result, the base of this unit is rich in radiolarians (90%) which decline toward the top (Sample 4, 9% and Sample 7, 1%). Beside this richness in radiolarians, we note the presence of benthic foraminifers which count globally 23 individuals distributed as follows: *Lenticulina* (15 individuals), *Dentalina* (5 individuals) and *Nodosaria* (3 individuals).

Unit 2. Characterized by abundance of benthics including the most representative genus *Lenticulina* (66 specimens) associated with the genus: *Praedothia* (10), *Lingulina* (7), *Dentalina* (6), *Nodosaria* (4), *Epistomina* (3), *Vaginulina* (1) and *Frondicularia* (1). This abundance is shown mainly in level 16 (60%), Sample 10 (25%) and in the top, Sample 14 (15%). The radiolarians appear again in Samples 14 with 46 individuals representing 96% of the total number of radiolarians encountered in unit 2, and the remaining 4% is in the summit part (Sample 16).

Unit 3. The quantitative study revealed the important presence of essentially benthic foraminifers represented by the genus *Lenticulina* (52 individuals, representing 50% of the total population). This genus shows an increase in its frequency from Sample 21 (8%) to Sample 26 (26%). The percentage of the remaining genera (*Frondicularia*, *Gavelinella*) represents only 30%. The level 25 is of a remarkable interest because the radiolarians reappear at this level (05

individuals which represents 5%) and the first occurrence of the genus *Rotalipora* (10 individuals which represents 10% of the totality faunistic).

4 Conclusion

The results can be summarized as follows:

Lithology and biostratigraphy. The Upper Albian levels of Jebel Msella are characterized by sedimentation with calcareous clay recurrences and black platy limestones at the base and then marls and green clays at the top. The detailed analysis and stratigraphic distribution of planktonic and benthic foraminiferal species allowed us to specify the limits of biozones. The different biozones recognized in this section are *Cryptamphorella canara* zone, *Crucella cachensis* zone, *Dictyomitra gracilis* zone and *Rotalipora appenninica* zone.

Micropaleontology. In the studied material, we recognized 15 species of planktonic foraminifers grouped into 10 genera and 18 benthic species grouped into 8 genera.

As part of this work, we also discussed the generic attribution of certain genus. The radiolarian group is a substantial component in the faunistic composition, given its dominance in this section but also because of its importance in terms of dating and characterization of the depositional environments (Plates 3 and 4).

Quantitative study. The study of the whole of the microfauna at the level of the Albian of Jabal Msella shows a remarkable distribution at the level of the three units:

- In the first unit, we note a richness in radiolarians associated with some benthic foraminifers.
- The second unit shows a dominance of benthics foraminifers compared to the radiolarians which become less important in their frequency.

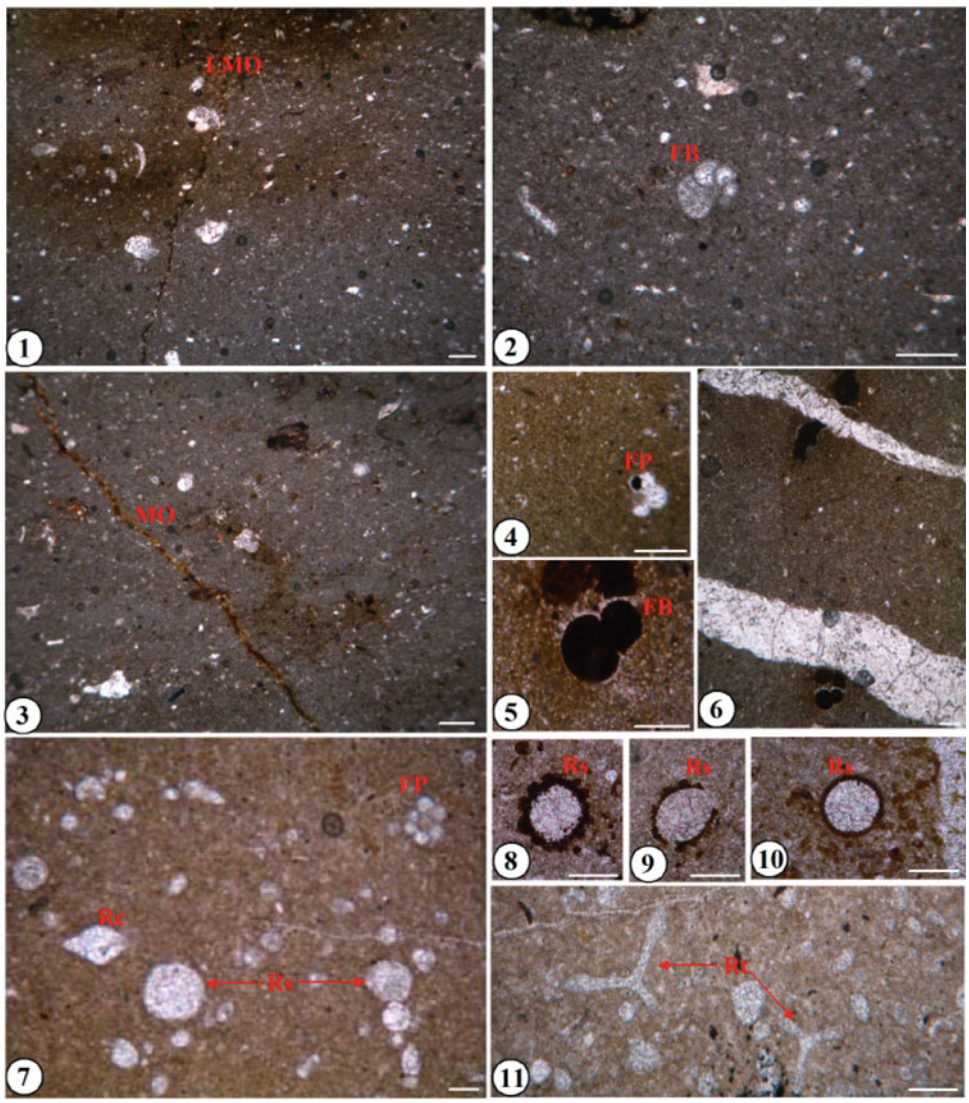

Plate 1 Upper Albian microfacies. **1–3**. Mud-wackestone texture showing laminated facies in which some laminae are organic-rich (LMO) with benthics foraminifera section (FB) and radiolarian. Fig. 3 shows organic matter (MO) concentrated at the level of cracks; (1–2, Sample 5; 3, Sample 7). **4–6**. Benthic foraminifera section totally oxidized (FB) in a mudstone texture associated with rare plankton (FP); (Sample 9). **7**. Wackestone texture containing rare plankton (FP) with 6 globular chambers associated with radiolarian sections: spherical (Rs) and conical (Rc) shaped; (Sample 11). **8–10**. Detail of the radiolarian sections of spherical shaped but in their borders are oxidized following a dissolution of their siliceous tests; (Sample. 17). **11**. Radiolarian section of triaxial shaped belonging to the genera *Crucella*; (Sample 17). Scale bar represents 50 µm

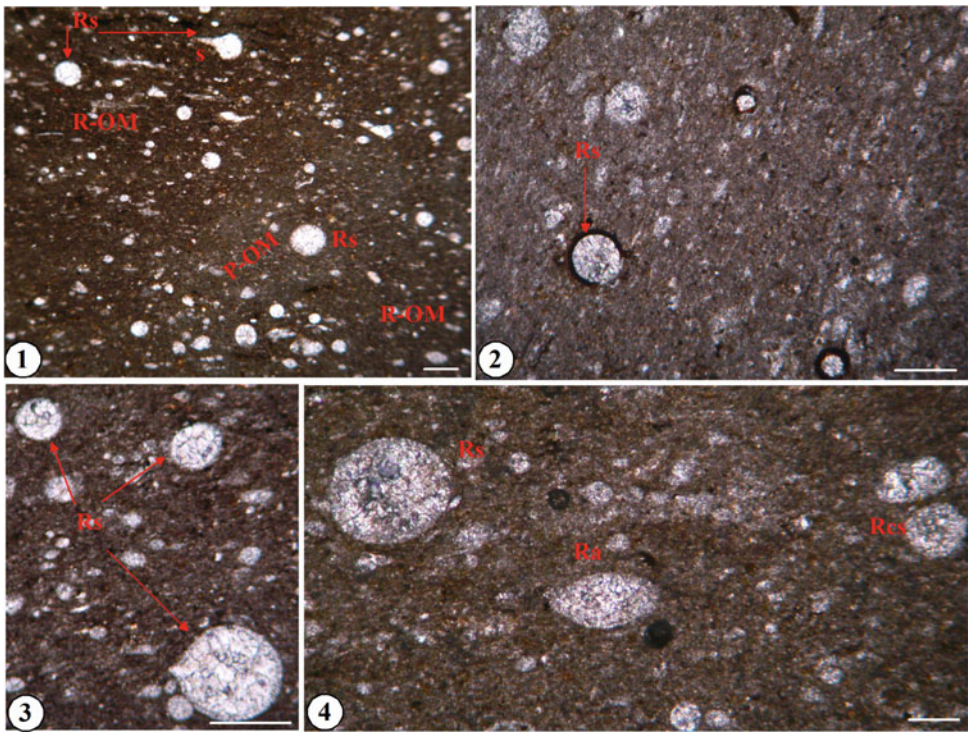

Plate 2 Upper Albian microfacies. **1**. Mud-wackestone texture with radiolarian sections of spherical shape (Rs) that predominate and different sizes, sometimes with preserved spicules (s) texture showing three laminae of which two (R-OM) are richer in organic matter (MO) than the central one (P-OM); (Sample 2). **2**. Spherical radiolarian (Rs) with locally oxidized pyrite following the dissolution of its siliceous test; (Sample 2). **3–4**. Detail of the radiolarian section: Spherical radiolarian (Rs), elongated radiolarian (Ra) and radiolarian with sinuous contour (Rcs); (Sample 2). Scale bar represents 50 µm

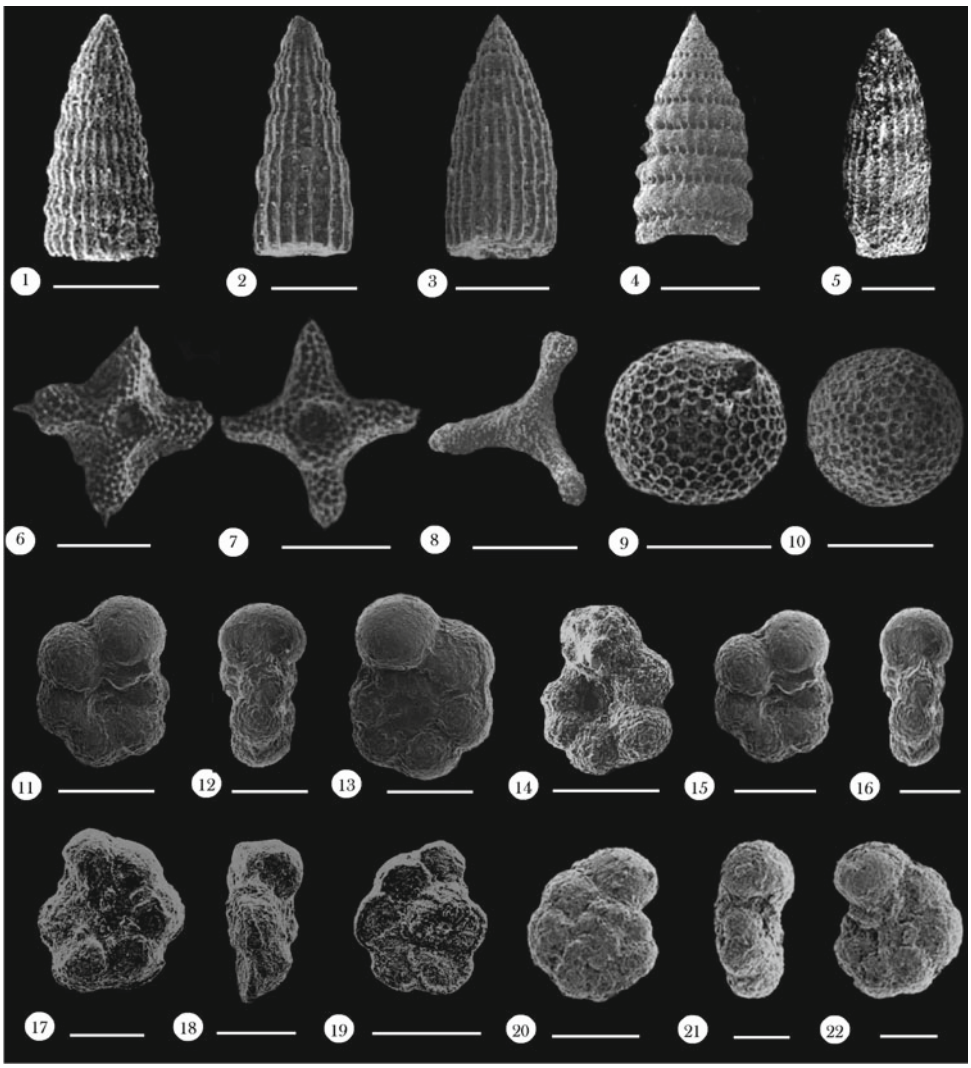

Plate 3 SEM micrographs of planktonic foraminifera of the Upper Albian in Jabal Msella. **1**. *Dictyomitra* sp. cf. *D. densicostata* (Sample 15). **2**. *Dictyomitra formosa* (Sample 18). **3, 4**. *Dictyomitra* (Sample 8). **5**. *Archaeodictyomitra montisserei* (Sample 16). **6**. *Crucella espartoensis* (Sample 7). **7**. *Crucella cachensis* (Sample 18). **8**. *Paronella pygmae* (Sample 16). **9–10**. *Cryptamphorella conara* (Sample 4, 8). **11–13**. *Hedbergella planispira* (Sample 25). **14–16**. *Hedbergella simplex* (Sample 25). **17–19**. *Rotalipora appenninica* (Sample 30). **20–22**. *Ticinella primula* (Sample 25). Scale bar represents 100 µm

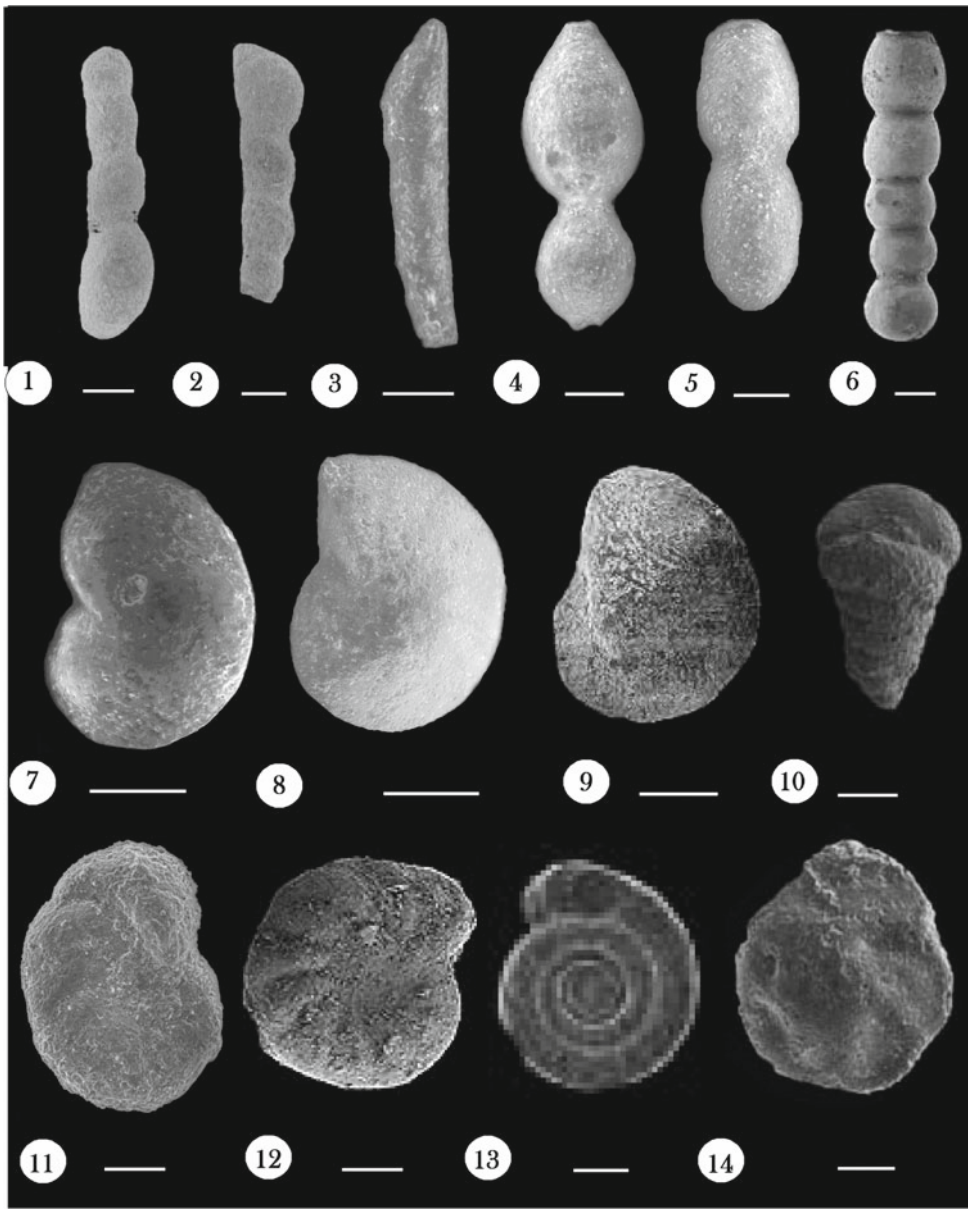

Plate 4 SEM micrographs of benthic foraminifera of the upper Albian in Jabal Msella. **1–3**. *Dentalina.* **1**. *D. gracilis* (Sample 14). **2**. *D. linearis* (Sample 16). **3**. *D oligostegia* (Sample 4). **4–6**. *Nodosaria*. **4**. *N. opscura* (Sample 16). **5**. *N. Pseudonodosaria mutabilis* (Sample 8). **6**. *N. sp*. (Sample 4). **7–9**. *Lenticulina*. **7**. *L. gibber* (Sample 12). **8**. *L. subgaultina* (Sample 1). **9**. *L. muensteri* (Sample 12). **10**. *Praedothia hechti (?) trochus* (Sample 8). **11–12**. *Gavelinella barremiana* (Sample 8). **13**. *Ammodiscus sp.* (Sample 4). **14**. *Epistomina caracolla* (Sample 16). Scale bar represents 100 µm

- There is a reoccurrence of radiolarians in the third unit with a remarkable number associated with plankton ascribed to the genera *Rotalipora*, *Hedbergella* and *Ticinella* .

References

Ben Fadhel, M., Layeb, M., Ben Youssef, M.: Upper Albian planktic foraminifera and radiolarian biostrarigraphy (Nebeur—northern Tunisia). C. R. Palevol (9), 73–81 (2010)

Bellier, J.P., Moullade, M.: Lower cretaceous planktonic foraminiferal biostratigraphy of the western north Atlantic (ODP LEG 171B), and taxonomic clarification of key index species. Rev. Micropaléontol. (45), 9–26 (2002)

Bellier, J.P., Moullade, M., Tronchetti, G.: Les Schackoïnes (foraminifères planctoniques) de l'Albien supérieur du Blake Nose (marge atlantique de la Floride, Leg ODP 171B). Rev. Micropaléontol. **46**, 131–141 (2003)

Ben Haj Ali, N.: Les foraminifères planctoniques du Crétacé (Hauterivien à Turonien inférieur) de Tunisie : systématique, biozonation et précisions stratigraphiques. Thèse, Doctorat d'Etat, Faculté des Sciences de Tunis, 348 p. [inédit]. (2005)

Cordey, F., Boughdiri, M., Sallouhi, H.: First direct age determination from the Jurassic radiolarian-bearing siliceous series (Jedidi Formation) of north-western Tunisia. C.R. Geosci. **337**, 777–785 (2005)

Danelian, T.: Diversity and biotic changes of Archaeodictyomitrid Radiolaria from the Aptian/Albian transition (OAE1b) of southern Albania. Micropaleontology **54**, 3–12 (2008)

Loeblich, A.R., Tappan, H.: Suprageneric classification of the Foraminiferida (Protozoa). Micropaleontology **30**, 1–70 (1984)

Musavu-Moussavou, B., Danelian, T., Baudin, F., Coccioni, R., Frohlich, F.: The radiolarian biotic response during OAE2. A high-resolution study across the Bonarelli level at Bottaccione (Gubbio, Italy). Rev. Micropaléontologie (50), 253–287 (2007)

Nargess, S., Sarah, K., Jonathan, C.A., Ramin, S.: Mid-Cretaceous radiolarian faunas from the Ashin Ophiolite (western Central-East Iranian Microcontinent). Cretac. Res. **56**, 110–118 (2015)

Neagu, T.: Monographie de la faune des foraminifères éocrétacés du couloir de Dimbovicioara, de Codlea et des Monts Persani (couches de Carhaga). Institut Géol Géophysique, Mémoires, Bucarest (25), 141 (1975)

Biostratigraphy and Microfacies of Azkand Formation in Qarah Chaugh- Dagh Section, Kirkuk Area (Northeastern Iraq)

Imad M. Ghafor

Abstract

Twenty-six rock samples were collected from Qarah Chaugh-Dagh section, 50 km northwest of Kirkuk city. Succession, ca. 61 m thick, belongs to the Azkand Formation. It is dominantly composed of fossiliferous foraminiferal limestones, which can be divided in two superposed units. Unit I is composed of fine- to coarse-grained bioclastic packstone-type deposits, while Unit II comprises fine- to very coarse-grained bioclastic packstone- to boundstone-type deposits. In this study, fifteen genera and with twenty-eight species of larger foraminifera were described and figured, associated with two species of corals and algae. Based on the distribution of the larger foraminifera, two assemblage biozones have been recognized in the Azkand formation. These assemblages of larger foraminifera indicate the age of the section is the Latest Oligocene (Assemblage zone I) (Chattian) to Early Miocene (Assemblage zone II) (Aquitanian).

Keywords

Larger foraminifera • Azkand Formation • Late Oligocene • Early Miocene • Kirkuk • Northeast Iraq

1 Introduction

The type section of Azkand limestone formation, defined by (Bellen 1956), is situated northeast face of the Azkand cirque, at about three miles N-65°-E of the village of Azkand on the southern dome of the Qarah Chauqh-Dagh. It consists of massive, dolomitic and recrystallized limestone, generally with high porosity (Bellen et al. 1959). The thickness of the Azkand formation is variable, usually around 100 m (Buday 1980), 104 m thick at the type section (Bellen 1956). Several researchers investigated the biostratigraphical and stratigraphical properties of these deposits (Al-Hashimi and Amer 1985; Al-Eisa 1992; Abid 1997; Ghafor 2004; Ghafur 2012). The exposure investigated within this study lies in Qara Chaugh-Dagh structure, 50 km northwest of Kirkuk city, Northeastern Iraq. (Fig. 1).The aim of this study was biostratigraphic and microfacies analyses of carbonate succession of the Azkand formation.

2 Methodology

In this study, 26 samples were collected from a 61 m thick outcrop of the Azkand formation in the Qara Chaugh-Dagh section. (Fig. 2). Thin sections were made and later examined by using polarized microscope to identify different types of larger foraminifera and other microfossils. This research focused on the biostratigraphic analysis of benthic foraminifera using (Laursen et al. 2009) and microfacies analysis after Dunham (1962).

3 Results

3.1 Microfacies

Azkand formation of the studied area can be subdivided into two superposed microfacies units (Fig. 2).

3.2 Unit I: Fine to Coarse-Grained Larger Foraminiferal Bioclastics Packstone.

This unit with a thickness about 34 m (Samples 1–17) consists of bedded fine to very coarse-grained bioclastics packstone with larger benthic foraminifera. The coarse

I. M. Ghafor (✉)
Department of Geology, College of Science, University of Sulaimani, Sulaimaniyah, Kurdistan Region, Iraq
e-mail: imad.gafor@univsul.edu.iq

A. Çiner et al. (eds.), *Recent Research on Geomorphology, Sedimentology, Marine Geosciences and Geochemistry*, Advances in Science, Technology & Innovation, https://doi.org/10.1007/978-3-030-72547-1_54

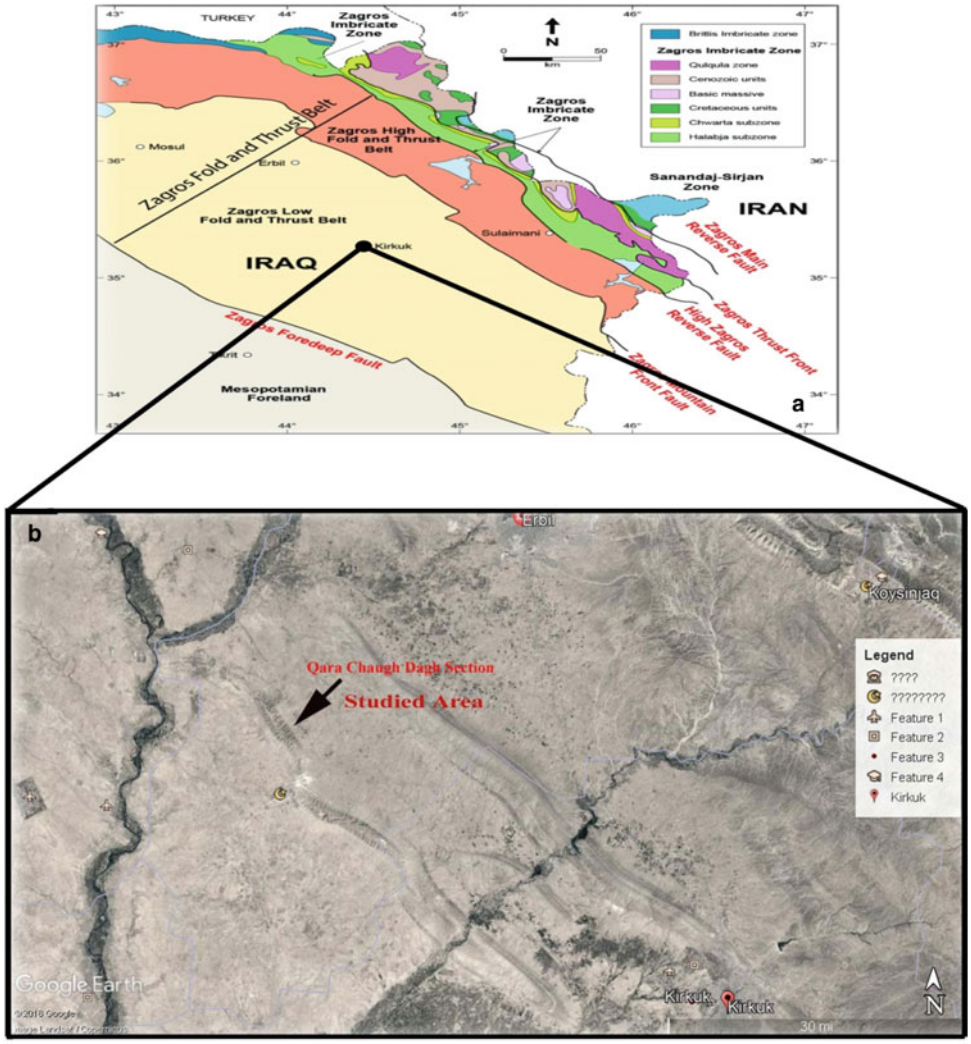

Fig. 1 Location map of the studied area. **a** Tectonic map of Iraq after (Al-Kadhimi et al. 1996). **b** Satellite map of the study area taken from Google Earth (2018)

portion of the packstone is dominated by larger foraminifera (varying from poor to moderately well-preserved). Genera: *Miogypsinoides, Amphistegina*, *Heterostegina*, *Spiroclypus*, *Operculina*, *Eulepidina*, *Nephrolepidina* and *Nummulites* are in this unit.

3.3 Unit II: Fine to Very Coarse Larger Foraminiferal Bioclastics Packstone to Boundstone

This unit with a thickness about 27 m (Samples 18–24) consists of vaguely bedded fine to medium-grained packstone. Numerous small- and large-scale burrows are present, bioclasts consisting of large foraminiferal genera *Lepidocyclina, Miogypsinoides* and *Miogypsina*, encrusting foraminifera, algae and coral patches.

4 Biostratigraphic Analysis

The benthic foraminiferal assemblages, including a total of 15 genera and 28 species, were analyzed to establish the biostratigraphic framework of the Azkand formation in the studied section from base to top. Two assemblage zones were recognized (Figs. 3 and 4), pointing to the Late Oligocene to the Early Miocene age.

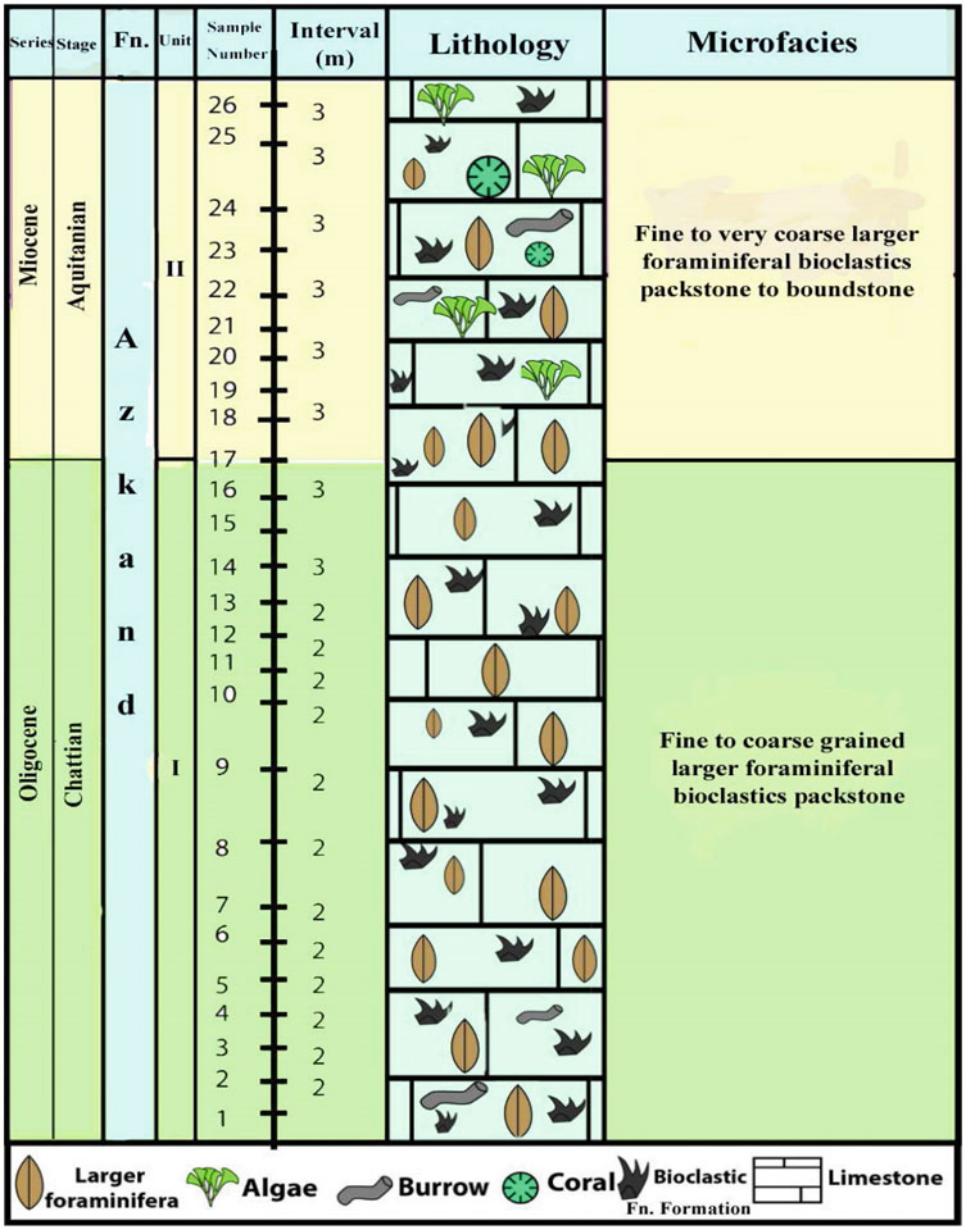

Fig. 2 Stratigraphic column and microfacies of the studied section of the Azkand Formation

4.1 Assemblage Zone I

This assemblage is recorded in the lower part of the section, from the Samples 1–17 (thickness 34 m). The most diagnosed species include: *Spiroclypeus blankenhorni, S. ranjani, S. morgratus Operculina complanata, O.* sp., *Elphidium* sp, *Eulepidina elephantina*, *E. dilata, E.* sp., *Miogypsinoides complanatus, M.. deharti, M.* sp. *Nephrolepidina morgani, N.. verdeki, N.* sp.,*Heterostegina involutea, H.* sp., *Neorotalia viennoti, N.* sp., *Dendritina rangi, D.* sp., *Amphistegina* sp., *Triloculina trigonula, T.* sp., *Lepidocyclina* sp., *Nummulites* sp., and *Quinqueloculina* sp. *The* microfauna corresponds to the *Archaias asmricus–Archaias hensoni–Miogypsinoides complanatus* assemblage zone of (Laursen et al. 2009) and Van Buchem et al. (2010), and according to (Taheri et al. 2017), this assemblage zone is restricted to the Late Oligocene (Late Chattian).

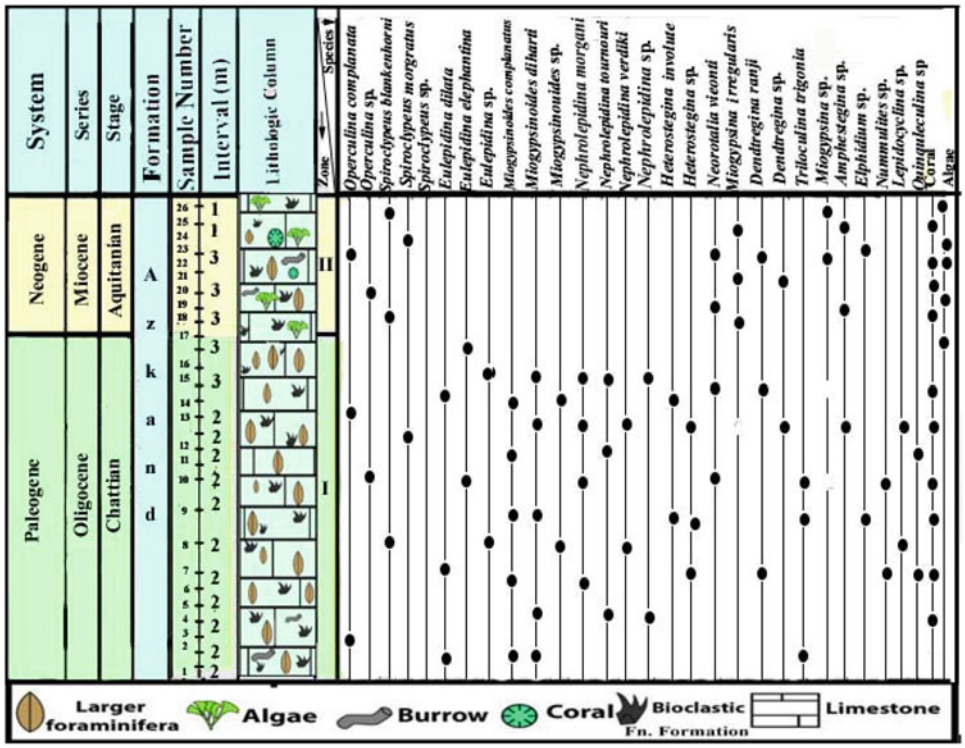

Fig. 3 Distribution of the identified foraminifer's of the Azkand Formation in the studied section

4.2 Assemblage Zone II

This assemblage is recorded in the upper part of the section, from Samples 18–28 (thickness 27 m). The most diagnosed species include: *Spiroclypeus blankenhorni, S. ranjani, Operculina complanata, O.* sp., *Elphidium* sp, *Miogypsinoides complanatus*, *Neorotalia viennoti, N.* sp., *Dendritina rangi, D.* sp., *Amphistegina* sp., *Miogypsina irregularis, Miogypsina* sp., *M.* sp., corals and algae. The determined microfauna corresponds to the *Archaias asmricus–Archaias hensoni–Miogypsinoides complanatus* assemblage zone of (Laursen et al. 2009) and Van Buchem et al. (2010). According to (Taheri et al. 2017), this zone is restricted to the Early Miocene (Early Aquitanian).

5 Conclusions

This study led us to deduce the following conclusions:

1. Twenty-eight species of larger foraminifera, with calcareous algae and coral, were identified in the Azkand formation of the studied area.
2. The section is subdivided in two microfacies units (Unit I —Fine- to coarse-grained bioclastics larger foraminiferal packstone (lower part of the section) and Unit II—Fine- to very coarse-grained bioclastics larger foraminiferal packstone to boundstone) (upper part of the section).

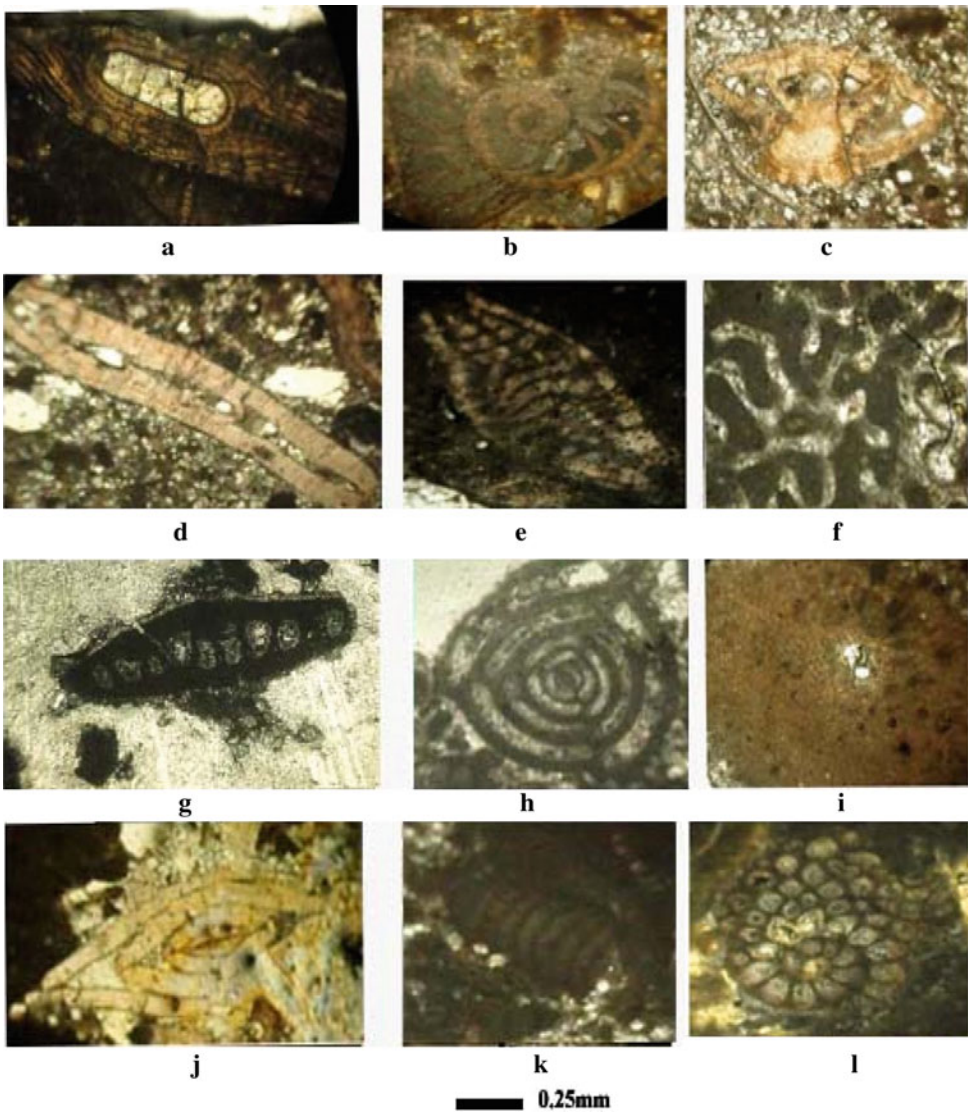

Fig. 4 **a** *Eulepidina elephantina* (Lemoine and Douville 1904) sample no.10. **b** *Spiroclypeus blankenhorni* (Henson 1937), sample no.26. **c** *Neorotalia viennoti,* (Greig 1935), sample no.18. **d** *Operculina complanata* (Defrance 1882) sample no.13. **e** *Heterosteginas* sp. sample no.9. **f** Coral sample no.18. **g** *Miogypsina irregularis* (Michelotti 1841), sample no.24. **h** *Triloculina trigonia* (Lamarch 1804), sample no.9. **i** *Nephrolepidina tournouri* (Lemoine and Douville 1904) sample no.15. **j** *Nummulites* sp. sample no.10. **k** Algae sample no.22. **l** *Miogypsinoides complanatus* (Schlumberger 1900), sample no.14

3. Based on the stratigraphic range of the identified larger foraminifera, the section comprises two superposed assemblage biozones (I and II).
4. The identified microfossils from the Azkand formation extend in age from the Late Oligocene (Chattian) to the Early Miocene (Aquitanian).

References

Abid, A.A.: Biostratigraphy and Microfacies of the late Oligocene-Miocene Formations center and North Iraq (unpublished Ph.D. Thesis, Arabic). pp. 1–258. College of Science, Baghdad University (1997)

Al-Eisa, M: The two depositional sub cycles of Early Miocene, around Kirkuk field, North Iraq. Iraqi Geol. J. **25**(1), 41–58(in Arabic) (1992)

Al-Hashimi, H., Amer, R.: Tertiary microfacies of Iraq. p. 56. Published and printed by D. G. S. M. I. Baghdad. 159 Plates, (1985)

Al-Kadhimi, J.M.A., Sissakian, V., Fattah, A.S., Deikran, D.B.: Tectonic map of Iraq, scale1: 1000 000, 2nd edit., GEOSURV, Baghdad, Iraq (1996)

Bellen, R.C. Van, Dunnington, H, Wetzel, R, Morton D.: Lexique stratigraphique, interntional. Asie, Iraq **333** (1959)

Buday, T.: "Regional *geology of Iraq"* Vol. 1. In: Kassab, I.I.M., Jassim S.Z. (eds.), Stratigraphy, D.J. Geology Survy, p. 445. Mul. Invast. Public., (1980)

Dunham, R.: Classification of carbonate rocks according to depositional texture. In Ham, W.E., (ed.), Classification of carbonate rocks: AAPG Memoir (1), Tulsa, 108–121 (1962)

Ghafor, M.I.: Biometric analysis of *Lepidocyclina (Nephrolepidina)* and Miogypsinoids from Baba and Azkand formations (Oligocene—Miocene) in Kirkuk area, Iraq. Unpub. Ph.D. Thesis., College of Science. University of Sulaimani, Iraq, 1–170 (2004)

Ghafur, A.A.: Sedimentology and reservoir characteristics of the Oligocene-early Miocene carbonates (Kirkuk Group) of Southern Kurdistan. Ph.D. thesis, Cardiff University, 1–304 (2012)

Greig, D.A.: Rotalia viennotti, an important foraminiferal species from Asia Minor and Western Asia. J. Paleontol. **9**, 523–526 (1935)

Henson, F.R.S.: Larger foraminifera from Aintab, Turkish Syria. Eclogae Geologicae Helvetiae **30**, 45–57 (1937)

Lamarch, P.: Suite Des Memories, Sur les fossils des environs de paris, Annales du Meseum (1804)

Laursen, G., Monibi, S., Allan, T., Pickard, N., Hosseiney, A., Vincent, B., Hamon, Y., van- Buchem, V., Moallemi, A., Druillion, G: The asmari formation revisited, changed stratigraphic allocation and new biozonation. In: First international petroleum conference and exhibition, Shiraz, vol. 11(5) (2009)

Lemoine, P., Douvillé, R.: Sur le genre Lepidocyclina Gümbel: Mémoires de laSociété Géologique de France, sér. **12**(32), 1–41 (1904)

Michelotti, G.: Saggio storico dei rizopodi caratteristici dei terreni supra-cretacei: Memorie della Societa Italiana delle Scienze **22**, 253–302 (1841)

Taheri, M.R., Mogaddam V.H.V., Taheri, A., Ghabeishavi, A.: Biostratigraphy and paleoecology of the Oligo-Miocene Asmari Formation in the Izeh zone (Zagros Basin, SW Iran Boletín dela Socie dad Geológica Mexicana (2017).

Van Bellen, R.C.: The stratigraphy of the Main Limestone of the Kirkuk, Bai Hassan and Qara Chauq -Dagh structures in Northern Iraq. J. Inst. Pet. **42**, 233–263 (1956)

Van Buchem, F.S.P., Allan, T.L., Laursen, G.V., Lotfpour, M., Moallemi, A., Monibi, S., Motiei, H., Pickard, N.A.H., Tahmasbi, A.R., Vedrenne, V., Vincent, B.: Regional stratigraphic architecture and reservoir types of the Oligo-Miocene deposits in the Dezful Embayment (Asmari and Pabdeh Formations) SW Iran: geological society, Londom. Special Publ. **329**(1), 219–263 (2010)

Sedimentology, Stratigraphy, Paleontology, and Marine Geosciences (T14): Marine Geosciences—Form Molecular Proxies to Geophysical Surveys

A Brief Overview of Some Molecular Proxies Commonly Used to Unravel Part of the Earth's Climate History

Johan Etourneau

Abstract

Molecular proxies, also named organic biomarkers, have increasingly been used over the last decades in both marine and continental environments to track past climate variability at several timescales. Marine and terrestrial living organisms synthetize organic compounds, in particular some lipids that are exported to lake and deep ocean sediments where they remain preserved for million years. Based on their distribution, abundances, and isotopic signatures, they can reveal crucial information on changes in ocean and atmosphere temperatures, marine phytoplankton productivity, sea ice extent, type of vegetation, or precipitations for instance. Here is presented a brief review of some marine and terrestrial organic proxies that have been commonly used to reconstruct past climate changes in both low, mid, and high latitudes regions during different periods of time.

Keywords

Biomarkers • Specific compounds • Paleoclimate • Marine • Terrestrial environments

1 Introduction

In paleoclimatology, a molecular proxy could be defined as a specific biologically sourced molecule extractable by organic solvents. More than 30 biomarkers have been identified in marine and lake sediments to infer past climate and environmental changes in the ocean and on land (Briggs and Summons 2014), even though less than 10 are routinely applied. However, new proxies are regularly discovered, thereby increasing the number of potential candidates within the next decades. In comparison to other traditional proxies, their advantages lie in their ease of analysis, specific origin, good resistance to biodegradation, chemical inertness, and capability to provide high-resolution records in a relatively short time (Eglinton and Eglinton 2008).

After being produced in the ocean and on land by living organisms, these compounds are exported by wind, rivers, ocean currents, aggregated to marine snow, or several types of particles and debris that reach the sediment where they can be preserved for million years (Fig. 1). The common approach to establish molecular proxy-based records is to extract first the lipids from the sediment using an organic solvent, followed by several steps of separation and purification. Afterward, they are identified and quantified by gas or liquid chromatography coupled to a mass spectrometer (GC-MS and LC-MS, respectively) or an ion flame detector (GC-FID). More recently isotopic analyses on these compounds have been conducted thanks to new technological developments, especially on the improvement of the sensitivity of the isotope mass spectrometer (IRMS). This methodology allows to robustly and accurately constrain hydrological and atmospheric parameters in any environment, including the most extreme ones like desert areas. However, not all these organic proxies can be applied in the same area. Some of them are strictly produced under specific conditions depending on the living zone of the organisms producing them. Therefore, before tracking molecular proxies in sediments, it is important to fully consider the targeted zone and the focused parameters.

2 Marine Biomarkers

2.1 The Alkenones

One of the first biomarkers extensively applied in marine sediments is the alkenone proxy (Brassell et al. 1986). The long chain ($C_{37:2}$ and $C_{37:3}$) ketones (Brassell et al. 1986;

J. Etourneau (✉)
Instituto Andaluz de Ciencias de la Tierra, CSIC-Universidad Granada, Granada, Spain
e-mail: johan.etourneau@iact.ugr-csic.es

A. Çiner et al. (eds.), *Recent Research on Geomorphology, Sedimentology, Marine Geosciences and Geochemistry*, Advances in Science, Technology & Innovation, https://doi.org/10.1007/978-3-030-72547-1_55

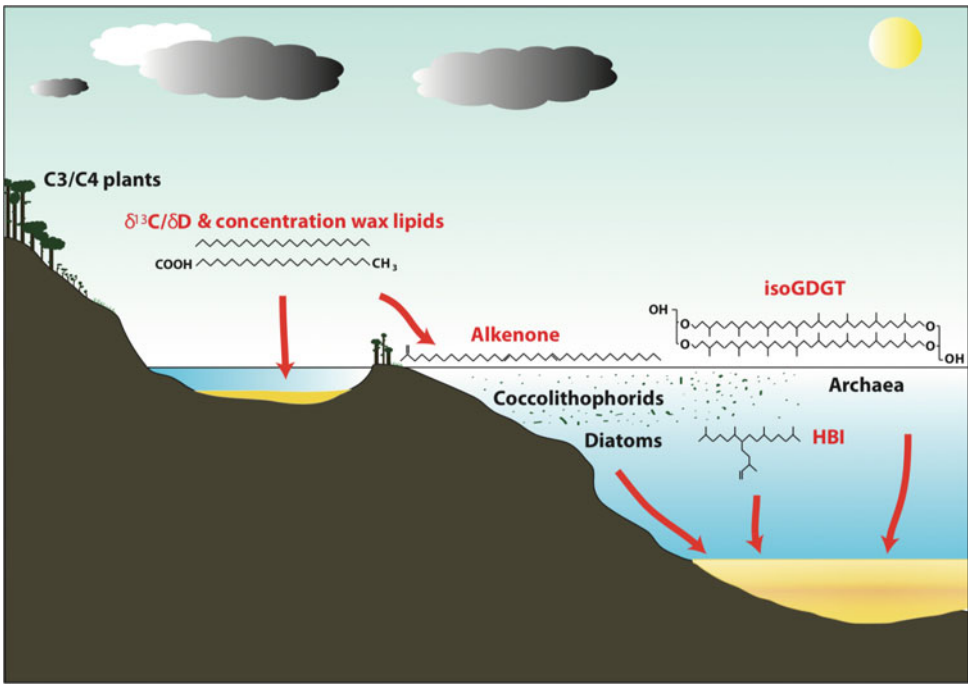

Fig. 1 Schematic view of the transfer of some biomarkers from their producers (i.e., plants, archaea, or phytoplankton species) to marine and lake sediments

Prahl and Wakeham 1987) are synthesized by some specific coccolithophorid species, mainly living in the surface layer (0–50 m) of the photic zone (Conte et al. 2001; Prahl et al. 2005). Two unicellular haptophytes, i.e., *Emiliana huxleyi* (*E. huxleyi*) and *Gephyrocapsa oceanica* (*G. oceanica*) (Marlowe et al. 1990; Conte et al. 1995; Volkman et al. 1995), mostly produce alkenones in the modern ocean. Although these two species have appeared relatively recently at the geological timescale, at about 0.27 Ma and 1.7 Ma respectively, their ancestral families are suggested to produce these lipids in the same manner as today, i.e., regulator of membrane fluidity (Brassell et al. 1986), metabolic storage lipids (Epstein et al. 2001) and buyoancy controllers (Sawada and Shiraiwa 2004). The alkenones have been found in Cretaceous sediments (de Bar et al. 2019), thus implying a strong resistance to biodegradation. They have been widely used for reconstructing past sea surface temperature (SST). Indeed, the $U^{k'}_{37}$ index, based on the $C_{37:2}$ and $C_{37:3}$ ratio, has shown a strong correlation with annual average SST in the modern ocean (Conte and Eglinton 1993) and has been extensively calibrated from surface sediments throughout the world ocean (Conte et al. 2006; Müller et al. 1998). Depending on the studied area, it is worth mentioning that some calibrations are more relevant than others, especially given the estimated SST range. For instance, the Müller et al. (1998) calibration is considered as the one of the most suitable for the Benguela upwelling or Eastern Equatorial Pacific regions to reconstruct SST over the last 3.5 Ma (Etourneau et al. 2009, 2010) (Fig. 2). It is also assumed that alkenone-derived SST estimation is not significantly altered by nutrient availability, production depth, seasonality changes, or by coccolithophorid extinction or speciation events. In addition, high productive regions where the abundance of alkenones in the sediment are relatively high, significantly reduce the bias tied to the microbial alteration through diagenetic processes in the water column and deep sediments. For instance, this proxy has been successfully applied in Arabian (Huguet et al. 2006c) and Mediterranean (Castañeda et al. 2010) sea sediments. When analyzing the $U^{k'}_{37}$, it is possible to also determine the alkenone concentration at the same time. When computed into Mass Accumulation Rate (MAR), this proxy can be used as a reliable proxy for past marine paleoproductivity (Etourneau et al. 2009). Once these two proxies ($U^{k'}_{37}$ and alkenone concentration) are combined, it can tell us for instance how a coastal upwelling system might have evolved through time and responded to regional and global climate processes (e.g., Etourneau et al. 2009) (Fig. 2). In addition to the two aforementioned proxies, the alkenones could also be very useful to investigate past regional salinity and pCO_2 changes as demonstrated by the hydrogen (δD) and carbon ($\delta^{13}C$) isotopes measured on these compounds (Pagani et al. 2002; Leduc et al. 2013).

2.2 The GDGTs

The alkenone-derived SST cannot be applied for example in polar regions due to the limited growing conditions of the two coccolitophorid species synthesizing them. In comparison, the TEX_{86} (TetraEther Index of tetraethers with 86 carbons) (Schouten et al. 2007) could be a good alternative

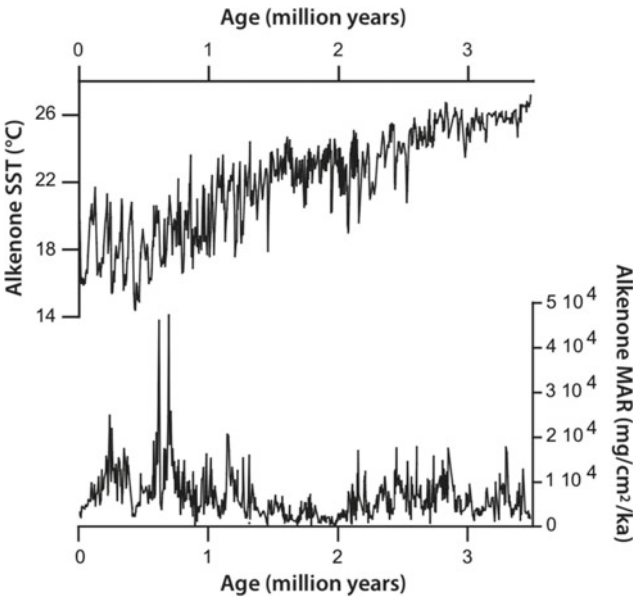

Fig. 2 Alkenone-derived SST and alkenone MAR spanning the last 3.5 million years at the IODP (Integrated Ocean Drilling Program) Site 1082, located within the modern Benguela Upwelling System, of Namibia (Etourneau et al. 2009). Both records document two periods of upwelling intensification (from 3 to 2 and from 1 to 0.5 million years) in line with the Pliocene–Pleistocene and Mid-Pleistocene global climate transitions

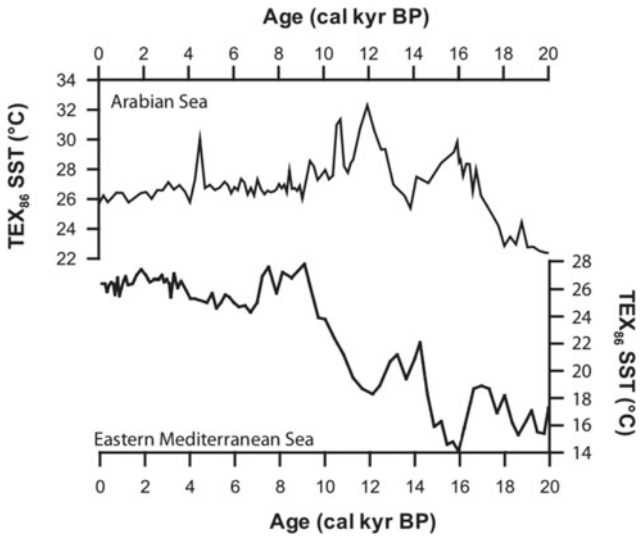

Fig. 3 TEX_{86}-derived SST records from the eastern Mediterranean and Arabian seas (Castañeda et al. 2010; Huguet et al. 2006c) since the last glacial period (i.e., the last 20 ka) showing a similar warming trend during the deglaciation and opposite variations at shorter timescale in response to different atmospheric and ocean forcing

in such marine environments. Indeed, this proxy is based on the relative distribution of isoprenoid glycerol dibiphytanyl glycerol tetraethers (isoGDGTs) containing up to cyclopentane rings mainly produced by Thaumarchaeota, a marine phylum of archaea. These species are living in diverse ocean environments and might represent the most dominant pelagic picoplankton. However, it remains unclear where the main production zone of the GDGTs used for paleotemperature predominantly is. While some suggest that in most of the oceanic regions, they are mainly synthesized in the photic zone and correlate well with the mean annual SSTs (Kim et al. 2008, 2010), it seems that their main locus of production is slightly different in coastal Antarctic zones where it appears to be more produced at the subsurface (Etourneau et al. 2019). Caution must be therefore taken before applying this proxy in marine sediments. Similar to the alkenones, several calibrations exist to convert the TEX_{86} into SST or sea subsurface temperature in all latitudes and the most reliable one depends on the considered area (Kim et al. 2008, 2010). It has been shown that the GDGTs can be preserved as long as the alkenones as revealed for instance by their application in Cretaceous sediments (O'Brien et al. 2012). The TEX_{86} (or TEX_{86}-L and TEX_{86}-H for low and high temperature areas, respectively) could thus be a reliable proxy to reconstruct past ocean temperature changes at least over the last 140 million years. This proxy has been successfully applied to numerous regions, including Antarctica (Etourneau et al. 2013) (Fig. 4), or the Mediterranean (Castañeda et al. 2010) and Arabian (Huguet et al. 2006c) (Fig. 3) seas to scrutinize the past SST variability since the last glacial period.

2.3 The Highly Branched Isoprenoids (HBIs)

Relatively new source-specific organic compounds have been developed over the last 10 years to investigate past sea ice extent in both Arctic and Antarctic regions: the C_{25}-highly branched isoprenoid (HBI) alkenes (Belt 2018; Massé et al. 2011; Smik et al. 2016a). These lipid biomarkers contain 25 carbon atoms and exhibit several structures (Belt et al. 2017), such as the mono-unsaturated C_{25}-HBI with a single bond, also referred to as monoene or IP25 (Belt et al. 2007), the di-unsaturated C_{25}-HBI with a double bond, also named diene, HBI II, or more recently $IPSO_{25}$ (Belt et al. 2016), and the tri-unsaturated C_{25}-HBIs with three double bonds, also named triene or HBI III. These lipids are mostly sourced by sympagic or pelagic diatom species (Belt et al. 2016, 2017) growing either under sea ice, at the sea ice edge, or in open ocean waters (Riaux-Gobin and Poulin 2013); the IP_{25} and $IPSO_{25}$ being mostly synthesized by sea ice diatom species, while the triene is produced by open water ones. In a similar way as the alkenones or the marine isoGDGTs, the HBIs are transferred downward through the water column to the surface sediment probably attached to particles produced from the melting of sea ice or ice shelf (Belt and Müller 2013). During the vertical transport, the effect of the visible light induced photo-degradation was invoked (Belt and

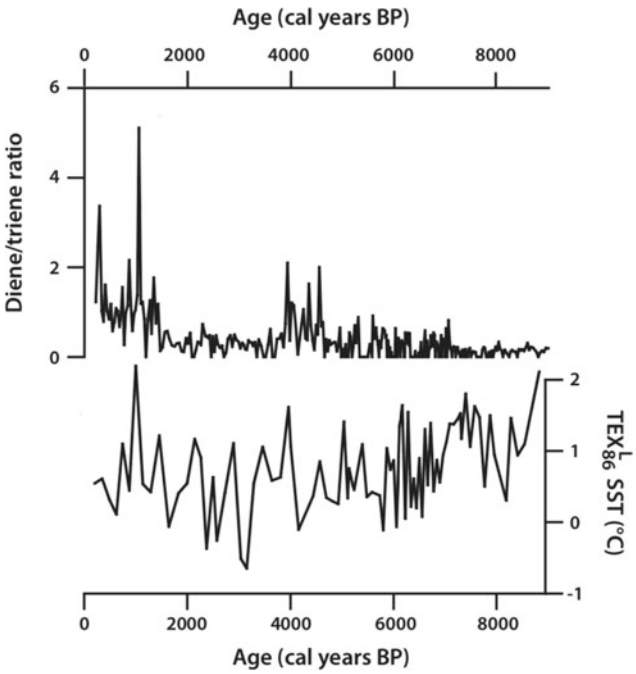

Fig. 4 Comparison between the diene/triene ratio and the TEX_{86}-L at the JPC-10 core site, western Antarctic Peninsula (Etourneau et al. 2013). These records show that sea ice was gradually increasing throughout the Holocene, while the estimated temperature was first cooling before warming over the late Holocene

Müller 2013); however, it seems to have a little impact, especially for the IP_{25} and $IPSO_{25}$ (Rontani et al. 2011). The HBI distribution in surface Arctic and Antarctic sediments is overall well consistent with modern sea ice or open water conditions (Massé et al. 2011; Smik et al. 2016a), making the IP_{25}, $IPSO_{25}$ or the diene/triene ratio reliable enough to reflect past sea ice changes as demonstrated for the Holocene (Etourneau et al. 2013) (Fig. 4) and beyond (Collins et al. 2013).

3 Terrestrial Biomarkers

Changes in marine conditions (e.g., temperature, evaporation, humidity transport, position of the high pressure atmospheric cells) can have a strong impact on continental climate variability and vegetation change, and reciprocally. To compare both ocean and terrestrial conditions, it is important to generate records from the same area and at the same resolution if possible. The molecular proxies can provide such information as numerous organic compounds preserved in marine or lake sediments are also sourced by terrestrial plants. In particular, C3 (grasses, trees and shrubs) and C4 (tropical grasses, and sedges) plants are a strong contributors of lipids to the organic matter stored in sediments. These lipids are abundant components of terrestrial higher plant epicuticular waxes (Eglinton and Hamilton 1963) that coat the leaf surfaces and stems. Three groups of molecules constitute the wax lipids: the *n*-alkane, the *n*-alkanol and the *n*-alkanoic acid. These long normal straight chains contain between 24 and 36 carbon atoms. Their distribution and isotopes in sedimentary deposit mostly rely on the type of dominant land vegetation (e.g., Bush and McInerney 2013) responding to atmospheric temperature, precipitation, and CO_2 variations. They can be transported to the marine and lake sediment by rivers or wind by aerosols. These plant-wax proxies are refractory to biodegradation as they can persist for million years in sediments as detected within Triassic sediments (Whiteside et al. 2010), making them probably the most resistant biomarkers. To determine their origin and reconstruct past vegetation changes, their abundance, their distribution, and the related indices based on long chain ratios (e.g., the CPI (Carbon Preference Index), the ACL (Average Chain Length), the $C_{31}/C_{31} + C_{29}$)) (e.g., Diefendorf et al. 2015) can be calculated. The carbon and hydrogen isotopic composition (i.e., the $\delta^{13}C$ and δD, respectively) can also be measured on the same compounds, thus providing independent information on the type of vegetation and the evaporation/precipitation balance (e.g., Schefuß et al 2005). When compared to additional records, especially the pollen ones, this could provide accurate information on continental conditions. These proxies have been widely used in several environments such as in tropical areas (Utida et al. 2019) (Fig. 5) or around the African continent (Schefuß et al 2005).

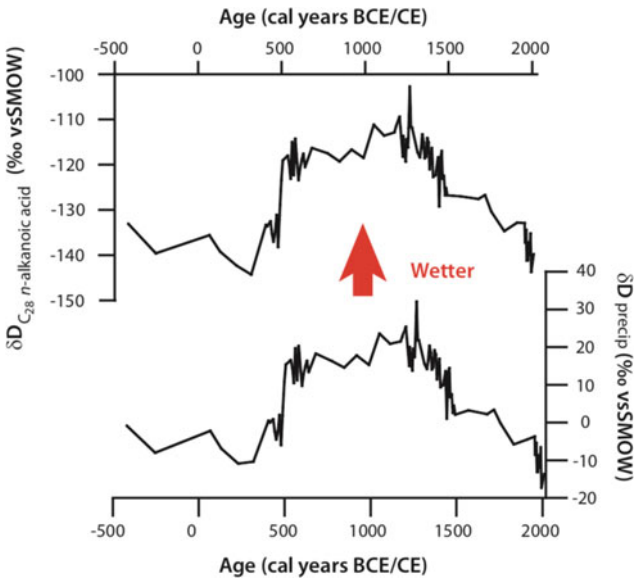

Fig. 5 δD of the C_{28} *n*-alkanoic acid (D_{wax}) and the calculated δD of the precipitation (δD_{precip}) considering the C3/C4 plant fractions at the Bocqueiro lake core (Boqc0901) in Nordeste, Brazil. These records show that this semi arid area experienced prolonged wetter periods between 500 and 1500 years BCE (Before Common Era) than nowadays (Utida et al. 2019).

4 Conclusions

The application of biomarkers (concentrations, indices, and isotopes) has proven its strong potential in investigating past climate and environmental variability in many environments. Along with new technological developments, we could expect an increasing number of organic proxies coming in the near future. It would not only concern lakes and marine sediments but also include caves, soils, and peatlands sediments for instance. Although improvement regarding the regional calibration is still needed, the molecular proxies, when combined with complementary records, especially terrestrial, marine micropaleontological, and inorganic data, could provide a detailed picture of past climate fluctuations in several areas for different periods of time and hence unravel part of the Earth's climate history.

References

Belt, S.T., Massé, G., Rowland, S.J., Poulin, M., Michel, C., LeBlanc, B.: A novel chemical fossil of palaeo sea ice: IP25. Org. Geochem. **38**, 16–27 (2007)

Belt, S.T., Müller, J.: The Arctic sea ice biomarker IP_{25}: a review of current understanding, recommendations for future research and applications in palaeo sea ice reconstructions. Quat. Sci. Rev. **79**, 9–25 (2013)

Belt, S.T., Smik, L., Brown, T.A., Kim, J.H., Rowland, S.J., Allen, C. S., Gal, J.K., Shin, K.H., Lee, J.I., Taylor, K.W.R.: Source identification and distribution reveals the potential of the geochemical antarctic sea ice proxy $IPSO_{25}$. Nat. Comm. **7**, 12655 (2016)

Belt, S.T., Brown, T.A., Smik, L., Tatarek, A., Wiktor, J., Stowasser, G., Assmy, P., Allen, C.S., Husum, K.: Identification of C_{25} highly branched isoprenoid (HBI) alkenes in diatoms of the genus *Rhizosolenia* in polar and sub-polar marine phytoplankton. Org. Geochem. **110**, 65–72 (2017)

Belt, S.T.: Source-specific biomarkers as proxies for arctic and antarctic sea ice. Org. Geochem. **125**, 277–298 (2018)

Brassell, S.C., Eglinton, G., Marlowe, I.T., Pflaumann, U., Sarnthein, M.: Molecular stratigraphy: a new tool or climatic assessment. Nature **320**, 129–133 (1986)

Briggs, D.E.G., Summons, R.E.: Ancient molecules: their origins, fossilization, and role in revealing the history of life. BioEssays **36**, 482–490 (2014)

Bush, R.T., McInerney, F.A.: Leaf wax *n*-alkane distributions in and across modern plants: Implications for paleoecology and chemotaxonomy. Geochim. Cosmochim. Acta **117**, 161–179 (2013)

Castañeda, I.S., Schefuß, E., Pätzold, J., Sinninghe Damsté, J.S., Weldeab, S., Schouten, S.: Millennial-scale sea surface temperature changes in the eastern Mediterranean (Nile River Delta region) over the last 27,000 years. Paleoceanography **25**, 1208 (2010)

Collins, L.G., Allen, C.S., Pike, J., Hodgson, D.A., Weckström, K., Massé, G.: Evaluating highly branched isoprenoid (HBI) biomarkers as a novel Antarctic sea-ice proxy in deep ocean glacial age sediments. Quat. Sci. Rev. **79**, 87–98 (2013)

Conte, M.H., Thompson, A., Eglinton, G.: Lipid biomarker diversity in the coccolithophorid Emiliania huxleyi (Prymnesiophyceae) and the related species Gephyrocapsa oceanica. J. Phyco. **31**, 272–282 (1995)

Conte, M.H., Weber, J.C., King, L.L., Wakeham, S.G.: The alkenone temperature signal in western North Atlantic surface waters. Geochim. Cosmochim. Acta **65**, 4275–4287 (2001)

Conte, M.H., Sicre, M-A., Rülhemann, C., Weber, J.C., Schulte, S., Schulz-Bull, D., Blanz, T.: Global temperatura calibration of the alkenone unsaturation index ($U^{k'}_{37}$) in surface waters and comparison with surface sediments. Geochem. Geophys. Geosys. 7. https://doi.org/10.1029/2005GC001054 (2006).

Conte, M.H., Eglinton, G.: Alkenone and alkenoate distributions within the euphotic zone of the eastern North Atlantic: correlation with production temperature. Deep-Sea Res. **I**(40), 1935–1961 (1993)

de Bar, M.W., Rampen, S.W., Hopmans, E.C., Sinninghe Damsté, J.S., Schouten, S.: Constraining the applicability of organic paleotemperature proxies for the last 90 Myrs. Org. Geochem. **128**, 122–136 (2019)

Diefendorf, A.F., Leslie, A.B., Wing, S.L.: Leaf wax composition and carbon isotopes vary among major conifer groups. Geochimi. Cosmochimi. Acta **170**, 145–156 (2015)

Eglinton, G., Hamilton, R.J.: The distribution of alkanes. In: Swain T (eds.) Chemical Plant Taxonomy. Academic Press, London (1963)

Eglinton, T.I., Eglinton, G.: Molecular proxies for paleoclimatology. Earth Planet. Sci. Lett. **275**, 1–16 (2008)

Epstein, B.L., D´Hondt, S., Hargraves, P.E.: The possible metabolic role of C_{37} alkenones in *Emiliania huxleyi*. Org. Geochem. **32**, 867–875 (2001)

Etourneau, J., Martinez, P., Blanz, T., Schneider, R.: Pliocene-pleistocene variability of upwelling activity, productivity, and nutrient cycling in the Benguela region. Geology **37**, 871–874 (2009)

Etourneau, J., Schneider, R., Blanz, T., Martinez, P.: Intensification of the walker and hadley atmospheric circulations during the pliocene-pleistocene climate transition. Earth Planet. Sci. Lett. **297**, 103–110 (2010)

Etourneau, J., Collins, L.G., Willmott, V., Kim, J.H., Barbara, L., Leventer, A., Schouten, S., Sinninghe Damsté, J.S., Bianchini, A., Klein, V., Crosta, X., Massé, G.: Holocene climate variations in the western Antarctic Peninsula: evidence for sea ice extent predominantly controlled by changes in insolation and ENSO variability. Clim. Past 9, 1431–1446 (2013)

Etourneau, J., Sgubin, G., Crosta, X., Swingedouw, D., Willmott, V., Barbara, L., Houssais, M.-N., Schouten, S., Sinninghe Damst-e, J. S., Goosse, H., Escutia, C., Crespin, J., Massé, G., Kim, J.-H.: Ocean temperature impact on ice shelf extent in the eastern Antarctic Peninsula. Nature Comm. **10**, 304 (2019)

Huguet, C., Kim, J.-H., Sinninghe Damsté, J.S., Schouten, S.: Reconstruction of sea surface temperature variations in the Arabian Sea over the last 23 kyr using organic proxies (TEX_{86} and $U^{k'}_{37}$). Paleocean. Paleoclim. 21. https://doi.org/10.1029/2005PA001215 (2006c)

Kim, J.-H., Schouten, S., Hopmans, E., Donner, B., Sinninghe Damsté, J.S.: Global sediment core-top calibration of the TEX_{86} paleothermometer in the ocean, Geochim. Cosmochim. Acta **72**, 1154–1173 (2008)

Kim, J.-H., Meer, J.V.D., Schouten, S., Helmke, P., Wilmott, V., Sangiorgi, F., Koç, N., Hopmans, E.C., Sinninghe Damsté, J.S.: New indices and calibrations derived from the distribution of creanarchaeal isoprenoid tetraether lipids: Implications for past sea surface temperature reconstructions. Geochim. Cosmochim. Acta **74**, 4639–4654 (2010)

Leduc, G., Sachs, J.P., Kawka, O.E., Schneider, R.R.: Holocene changes in eastern equatorial Atlantic salinity as estimated by water isotopologues. Earth Planet. Sci. Lett. **362**, 151–162 (2013)

Massé, G., Belt, S.T., Crosta, X., Schmidt, S., Snape, I., Thomas, D.N., Rowland, S.J.: Highly branched isoprenoids as proxies for variable

sea ice conditions in the Southern Ocean. Antarctic Sci. **23**, 487–498 (2011)

Marlowe, I.T., Brassell, S.C., Eglinton, G., Green, J.C.: Long-chain alkenones and alkyl alkenoates and the fossil coccolith record of marine sediments. Chem. Geo. **88**, 349–375 (1990)

Müller, P.J., Kirst, G., Ruhland, G., von Storch, I., Rosell-Melé, A.: Calibration of the alkenone paleotemperature index $U^{k'}_{37}$ based on core-tops from the eastern South Atlantic and the global ocean (60° N-60°S). Geochim. Cosmochim. Acta **62**, 1757–1772 (1998)

O'Brien, C.L., Robinson, S.A., Pancost, R.D., Sinninghe Dmasté, J.S., Schouten, S., Lunt, D.J., Alsenz, H., Bornemann, A., Bottini, C., Brassell, S.C., Farnsworth, A., Forster, A., Huber, B.T., Inglis, G. N., Jenkyns, H.C., Linnert, C., Littler, K., Markwick, P., McAnena, A., Mutterlose, J., Naafs, D.A., Pütmann, W., Sluijs, A., van Helmond, N.A.G.M., Vellekoop, J., Wagner, T., Wrobel, N.E.: Cretaceous sea-surface temperature evolution: Constraints from TEX86 and planktonic foraminiferal oxgen isotopes. Earth Sci. Rev. **172**, 224–247 (2012)

Pagani, M., Freeman, K.H., Ohkouchi, N., Caldeira, K.: Comparison of water column [CO_{2aq}] with sedimentary alkenone-based estimates: A test of the alkenone-CO_2 proxy. Paleoceanography **17**, 1069 (2002)

Prahl, F.G., Wakehahm, S.G.: Calibration of unsaturation patterns in long-chain ketone compositions for paleotemperature assessment. Nature **330**, 367–369 (1987)

Prahl, F.G., Popp, B.N., Karl, D.M., Sparrow, M.A.: Ecology and biogeochemistry of alkenone production at Station ALOHA. Deep-Sea Res. **I**(52), 699–719 (2005)

Riaux-Gobin, C., Poulin, M.: Possible symbiosis of Berkeleya adeliensis Medlin, Synedropsis fragilis (Manguin) Hasle et al. and Nitzschia lecointei van Heurck (bacillariophyta) associated with land-fast ice in Adélie Land, Antarctica. Diatom Res. **19**, 265–274 (2013)

Rontani, J.-F., Belt, S.T., Vaultier, F., Brown, T.A.: Visible light induced photooxidation of highly branched isoprenoid (HBI) alkenes: Significant dependence on the number and nature of double bonds. Org. Geochem. **42**, 812–822 (2011)

Sawada, K., Shiraiwa, Y.: Alkenone and alkenoic acid compositions of the membrane fractions of *Emiliana huxleyi*. Phytochem. **65**, 1299–1307 (2004)

Schefuß, E., Schouten, S., Schneider, R.: Climatic controls on central African hydrology during the past 20,000 years. Nature **437**, 1003–1006 (2005)

Schouten, S., Forster, A., Panoto, F.E., Sinninghe Damsté, J.S.: Towards calibration of the TEX86 palaeothermometer for tropical sea surface temperatures in ancient greenhouse worlds. Org. Geochem. **38**, 1537–1546 (2007)

Smik, L., Belt, S.T., Lieser, J.L., Armand, L.K., Leventer, A.: Distributions of highly branched isoprenoid alkenes and other algal lipids in surface waters from East Antarctica: further insights for biomarker-based paleo sea-ice reconstruction. Org. Geochem. **95**, 71–80 (2016a)

Utida, G., da Cruz Junior, F.W., Etourneau, J., Bouloubassi, I., Schefuß, E., Vuille, M., Novello, V.F., Figueiredo, L., Sifeddine, A., Klein, V., Zular, A., Viana, J.C.C., Turcq, B.J.: Tropical South Atlantic influence on Northeastern Brazil precipitation and ITCZ displacement during the past 2300 years. Sci. Rep. 9, 1698 (2019)

Volkman, J.K., Barrett, S.M., Blackburn, S.I., Sikes, E.L.: Alkenones in *Gephyrocapsa oceanica*: Implications for studies of paleoclimate. Geochim. Cosmochim. Acta **59**, 513–520 (1995)

Whiteside, J., Olsen, P.E., Eglinton, T., Brookfield, M.E., Sambrotto, R.: Compound-specific carbon isotopes from Earth's largest flood basalt eruptions directly linked to the end-Triassic mass extinction. Proc. Natl. Acad. USA **107**, 6721–6725 (2010)

Multidisciplinary Study of Marine Archives: Reconstruction of Sea-Level, Sediment Yields, Sediment Sources, Paleoclimate, Paleoceanography and Vertical Movement on Margins: Examples from the Western Mediterranean Sea

Marina Rabineau, Romain Pellen, Virgil Pasquier, Massimo Bellucci, Shray Badhani, Stéphane Molliex, Marta Garcia-Garcia, Estelle Leroux, Mohamed Arab, Damien Do Couto, Gwenael Jouet, François Bache, Matthieu Gaudin, Manfred Lafosse, Elda Miramontes, Johanna Lofi, Tadeu dos Reis, Maryline Moulin, Philippe Schnurle, Jeffrey Poort, Bernard Dennielou, Alexandra Afilhado, Speranta-Maria Popescu, Maria-Angela Bassetti, Samuel Toucanne, Sidonie Révillon, Antonio Cattaneo, Pascal Le Roy, Elia d'Acremont, Didier Granjeon, Christian Gorini, Jean-Pierre Suc, Sierd Cloetingh, Philippe Joseph, François Guillocheau, Serge Berné, Laurence Droz, Jean-Loup Rubino, and Daniel Aslanian

M. Rabineau (✉) · R. Pellen · V. Pasquier · M. Bellucci · S. Badhani · S. Molliex · S. Révillon · P. Le Roy · L. Droz
CNRS, Univ Brest, Univ. Bretagne-Sud, Laboratoire Géosciences Océan (LGO), UMR6538, IUEM, rue Dumontd'Urville, F-29280 Plouzané, France
e-mail: marina.rabineau@univ-brest.fr

R. Pellen · S. Badhani · M. Garcia-Garcia · E. Leroux · G. Jouet · E. Miramontes · M. Moulin · P. Schnurle · B. Dennielou · S. Toucanne · A. Cattaneo · D. Aslanian
IFREMER, GM, LGS, Centre de Brest, 29280 Plouzané, France

M. Arab
Sonatrach, Alger, Algeria

D. Do Couto · M. Lafosse · J. Poort · E. d'Acremont · C. Gorini · J.-P. Suc
Sorbonne Université, ISTeP, Paris, France

F. Bache
Santos Ltd., Adelaide, Australia

M. Gaudin
Aker Energy AS, Fornebu, Norway

J. Lofi
University Montpellier, Montpellier, France

T. dos Reis
Faculdade de Oceanografia (FAOC), University Estadual do Rio de Janeiro (UERJ), Rio de Janeiro, Brazil

A. Afilhado
ISEL, Instituto Dom Luiz, FCUL, Lisboa, Portugal

S.-M. Popescu
GeoBioStratData.Consulting, Rillieux la Pape, France

M.-A. Bassetti · S. Berné
University Perpignan, Perpignan, France

D. Granjeon · P. Joseph
IFPEN, Rueil-Malmaison, France

S. Cloetingh
University Utrecht, Utrecht, Netherlands

F. Guillocheau
University Rennes, Rennes, France

J.-L. Rubino
TOTAL, Pau, France

A. Çiner et al. (eds.), *Recent Research on Geomorphology, Sedimentology, Marine Geosciences and Geochemistry*, Advances in Science, Technology & Innovation, https://doi.org/10.1007/978-3-030-72547-1_56

Abstract

The numerous processes (superficial and deep) occurring on margins, their origins, consequences, interactions and quantifications are only very partially described and understood. The identification of the relative role of factors is sometimes completely contradictory between authors. Here, we showed the results of a long-term multidecadal and multidisciplinary study (using geophysical, geological, stratigraphic, paleontological, geomorphologic, geochemical, microbiological and numerical models) in the Western Mediterranean Sea that acts as a natural laboratory at many different scales. We showed how sediments efficiently recorded at the same time: variations of glacio-eustatic sea-level changes, variations of sediments yield and sources, and also enabled quantifying vertical movements and geodynamic worldwide events but also detailed regional mass transport, turbidites and contourites deposits. They are also an archive of paleoclimatic, palaeoceanographic and diagenetic processes.

Keywords

Sea-level • Subsidence • Sediment yields • Erosion • Isostasy • Messinian • Pliocene • Quaternary • Mass-transport • Contourites

1 Introduction

The study of margins is stimulated by several economic challenges like that of the oil industry, on the one hand, that of mineral exploitation (extraction of sand, gravel, diamonds,), on the other, and finally that of coastal activities (coastal management, fishing activities, renewable marine energy and human settlement), all in relation to global changes, in particular, the consideration of past, present and future climate change.

However, the mechanisms active on the so-called passive margins are numerous, and their interactions remain poorly understood, especially the link between deep structural processes (rifting, extension, subsidence) and surficial processes (erosion, transfer, deposition processes from the continent to the deep basin, impact of climate, currents, diagenetic processes).

The study of sediments on margins is fundamental for a better understanding of the organization and mechanisms of deposition in four dimensions (in space and time) and their link to deeper processes. It is, in fact, the geological history that needs to be reconstructed while determining, prioritizing and quantifying the relative importance of the various parameters (tectonic, climatic, eustatic and hydrodynamic) that have controlled sedimentation and sediment preservation. These fundamental questions are recurrent at all scales of time and space.

2 Settings and Materials

Here, we showed a long-term multidecadal study in the Western Mediterranean Sea that has been undertaken at different scales. Due to its geographical and political situation, the Western Mediterranean represents a key area whose exploration allows crucial progress on the study of margins. The Mediterranean represents what can be called a natural laboratory, i.e., a small site where hypotheses and models of fundamental interest for Earth Sciences can be tested in a more global way: on the formation and evolution of margins, on sedimentary records, sea-level variations, sediment fluxes, on paleoclimate influence and on the influence of tectonic heritage on vertical movements.

This long-term study took advantage of a large academic and industrial database and effective collaborations during the GDR Marges Gulf of Lions (2000–2007), then the Action Marges Programs (2008–2016) and the Labex Mer (2010–2018) and ISblue (2019–2029) ANR Programs, all with numerous cruises using the French Oceanographic vessels and facilities (http://campagnes.flotteoceanographique.fr). In addition, the EC-funded Eurostrataform, TOPO-EUROPE and PROMESS 1 projects gave access to in situ-monitoring of present-day, deeply rooted processes, and long (100-300 m long) boreholes, respectively.

3 Results and Discussion

3.1 Sediments: An Archive of Glacio-Eustatic Variations and Their Impacts

We showed for the first time through a combination of seismic stratigraphic interpretation, cores and stratigraphic modelling that the sequences preserved on the outer shelf corresponded to 100,000-year climate cycles (Rabineau et al. 2005) resolving a controversy dating back to the 1990s. We then proposed a re-evaluation of sea-level amplitudes at the last five glacial maxima based on direct observation of paleo-shorelines by correcting their present-day depths from post-depositional subsidence (Rabineau et al. 2006, 2014) (Fig. 1).

A higher-frequency eustatism is also imprinted in sediments at 20 to 40 ka but also at the scale of bond cycles (7 ka) (Bassetti et al. 2006; Jouet et al. 2006; Jouet 2007; Mauffrey et al. 2015). Those glacio-eustatic sea-level changes have a strong impact on canyons functioning

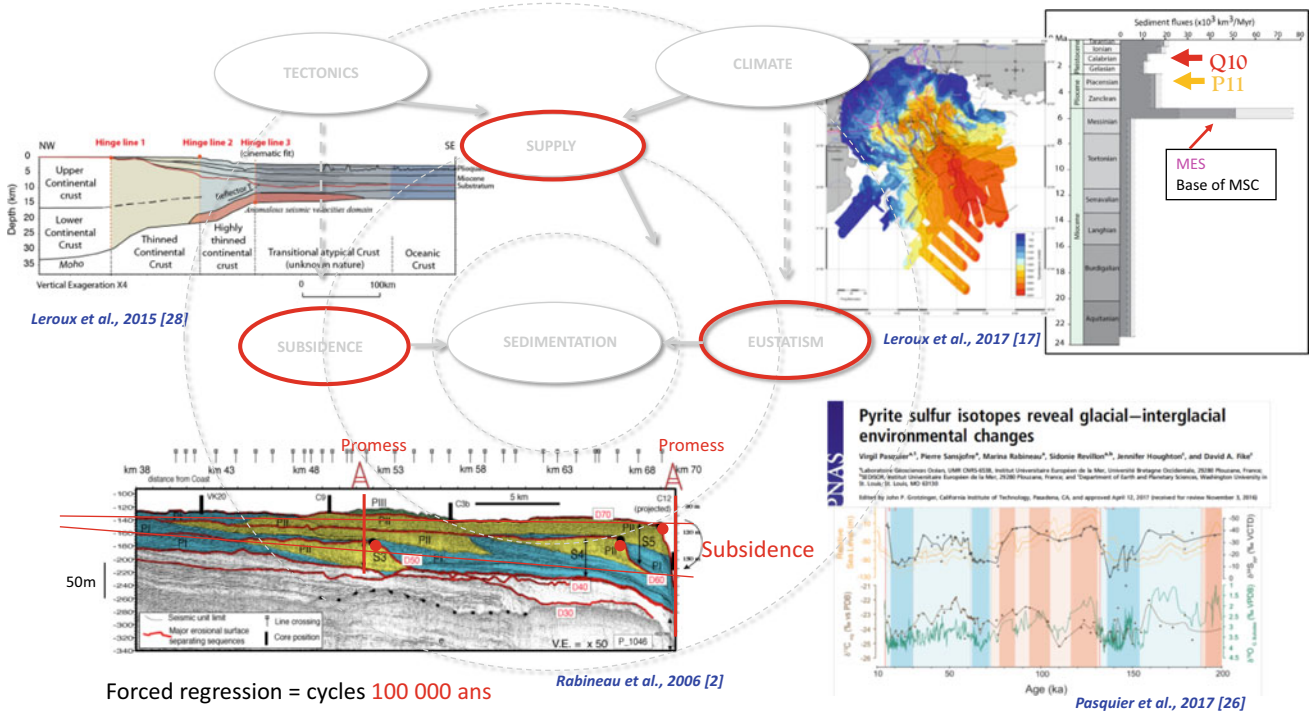

Fig. 1 Quantification of different factors influencing sediment transfer and sediment record (modified from Rabineau et al. (2006), Leroux et al. (2017); Pasquier et al. (2017), Leroux et al. (2015a)

(Baztan et al. 2005; Gaudin et al. 2006) and sediment delivery to the deep-sea through turbidites, mass-transport deposits and contourites (Droz et al. 2006; Lombo Tombo et al. 2015; Miramontes et al. 2016, 2019; Dennielou et al. 2019; Badhani et al. 2019).

On larger scale, two erosional surfaces D1 and D0 have been interpreted as corresponding to two major paleoclimatic stages over the entire Plio-Quaternary period: the establishment of 100,000-year cyclicities around 0.9 Ma and the establishment of glaciations in the Northern Hemisphere around 2.6 Ma (Leroux et al. 2014).

3.2 Sediments: An Archive of Sediment Fluxes

Leroux established for the first time and with an unprecedented resolution on a global scale, the sedimentary volumes and erosion/deposit balances over the last 6 Ma in the Liguro-Provencal Basin (Leroux et al. 2017, 2018) (Fig. 1). This study describes a very strong increase (×2) in detrital flows around 1 Ma in relation to the climate changes of the Mid-Pleistocene Revolution. The global acceleration (×3) of terrigenous flows over the last 5 Ma, defended by many authors and correlated with an uplift of the great orogens (here in connection with the Alps), is also observed in the Liguro-Provencal basin, even if the famous Messinian Salinity Crisis tends to disturb the signal (Leroux et al. 2017). These results are confirmed by onshore multi-approach quantification of denudation rates using cosmologic and geomorphologic methods (Molliex et al. 2016). A similar study has been performed in the Valencia Basin (Pellen et al. 2016). Pellen et al. (Pellen et al. 2019) also addressed the apparent paradox concerning the Ebro and Rhône basins, i.e., the fact that the current drainage areas of the two rivers are equivalent (85,835 km^2 and 98,800 km^2, respectively) while the Messinian river networks identified so far were very different (<100 km for the Ebro and >400 km for the Rhône). Pellen et al. (2019) solve this paradox by showing an incision length of the Ebro that extends well beyond the edge of the Miocene platform into the Valencia Basin and actually reaches 270 km-long. Pellen et al. (2019), also show that at the outlet of this river network, the product of Messinian erosion is preserved in the form of a forced regression prism identified in the Minorca Sub-basin.

3.3 Sediments: An Archive of Onshore Sources

Can we read in the offshore sediments the relative impact of the differentially eroded zones and therefore quantify the relative influence of onshore sources of sediments? This topic was studied using radiogenic isotopes Nd and Sr. This work has revealed unexpected variations in isotopic

compositions of Gulf of Lion sediments between periods of low sea levels and periods of high sea levels. Thus, during the glacial periods, sediments from the catchment basins draining the Languedoc-Roussillon, Lower Rhône and the Pyrenees dominate. Conversely, during interglacial periods, sediments from the Rhône catchment area (especially the upper Rhône) are predominant in the sediment mixture (Révillon et al. 2011).

Finally, the question of the relative part of terrigenous inputs compared to that of biogenic (in situ) inputs is critical for sediment flux studies and difficult to understand; it is therefore a strong uncertainty factor for quantification. This question is particularly true with regard to carbonate inputs, which occurs in different forms (terrigenous, biogenic, dissolved). In the "classical" studies, the authors focus mainly on the terrigenous fraction, i.e., the sedimentary fraction resulting from continental erosion transported to the sea by the action of rivers, winds, etc., as opposed to the carbonate fraction of biogenic origin, resulting mainly from biological production (organisms synthesizing carbonate exoskeletons such as foraminifera, nannofossils, bivalve shells, etc.). As a result, the authors equate the non-carbonated flux with the terrigenous flux.

The original use of elemental and isotopic geochemistry (87Sr/86Sr) on the carbonate fraction alone demonstrated that the sediments of the Aude-Hérault interfluvial (Promess drilling) correspond to a mixture between current and recent biogenic carbonates but also to much older carbonates (Jurassic, Cretaceous, Miocene) directly exported from the onshore watersheds (Pasquier et al. 2019a).

3.4 Sediments: An Archive of Paleoclimate and Microbial Activities

Can we use isotopic studies to decipher the relative role of sea-level and climate (hydrologic) changes? The variations in isotopic carbon (∂13C) and nitrogen (∂15 N) compositions of organic matter preserved in Gulf of Lion sediments shows a correlation of variations with sea level for the last G/IG cycle (MIS4 to MIS2). At the lowest sea level, the borehole is in a prodeltaic position with more negative (lighter) isotopic values. On the other hand, for the previous glacial (MIS6) and last interglacial (MIS5) it is the climate that predominates with strong periods of river discharges. We proposed that the latter results from the intensification of North Atlantic disturbances and precipitation in the Mediterranean (Pasquier et al. 2019b). On a smaller time-scale (Holocene), the influence of both melt-water pulses and hydrological changes were also found (Bassetti et al. 2016).

In addition to the analyses of organic carbon and nitrogen, a characterization of sulfur isotopes preserved in sedimentary pyrite was also carried out (Pasquier et al. 2017). Pasquier shows that the sediments deposited in the Gulf of Lions over the past 500,000 years have one of the highest isotopic variations reported to date (Fig. 1). In addition, the cyclicity observed suggests that strong climate control is at play, which calls into question the overall aspect of this geochemical tool. Two important mechanisms are proposed to explain this isotopic fractionation: (i) a modulation of bacterial activity by climate, and/or (ii) a local modulation related to the nature of the sediments involved in the formation of pyrite in relation to eustatic variations (Pasquier et al. 2017).

3.5 Sediments: An Archive of Vertical Movements and Geodynamic

The precise and detailed reading of sediment markers makes it possible to quantify vertical movements over the entire margin (Rabineau et al., 2006, 2014) and to show that sediments reflect, until very recent periods, the crustal structure of the margin and thus represent a window into the Earth's deep processes (Bache et al. 2010; Leroux et al. 2015a; Afilhado et al. 2015; Moulin et al. 2015; Arab et al. 2016; Do Couto et al. 2016) (Fig. 1).

Using a 3D-grid of seismic and wide-angle data, drillings and numerical stratigraphic modelling, a quantification of the post-rift vertical movements of the Provence Basin can be described with three domains of subsidence: seaward tilting on the platform and slope and purely vertical in the deep basin. These domains fit with the deeper crustal domains highlighted by wide-angle seismic data. The post-break-up sedimentary markers may therefore be used to identify the initial hinge lines of the rifting phase and the subsidence laws (Leroux et al. 2015b; Rabineau et al. 2015) (Fig. 1).

Using markers related to the Messinian salinity crisis (MSC, e.g., Clauzon et al. 2015), we were also able to propose a novel estimate of the isostatic rebound associated with this erosional and salinity crisis which reached 1.3 km of uplift at the edge of the platform in less than 700,000 years (maximum duration estimated for the crisis) (Rabineau et al. 2014).

Do Couto et al. (2016) also used stratigraphic markers on high-resolution 2D seismic profiles located in the Alboran Sea to propose that the pull of the dipping subducting lithosphere controlled the subsidence of the thickest depocenter during the Miocene.

Very recently, new heatflow measurments have been undertaken in the Western Mediterranéean Sea (Poort et al. 2020), Leroux and co-authors also showed that the MSC event was, in fact, linked to a world-wide geodynamic revolution (Leroux et al. 2018).

4 Conclusions

Our results obtained on the continental margins from oceanographic campaigns, deep boreholes or land-based studies, do shed new light on the understanding of the dynamics of the mantle, the lithosphere and their interactions with the hydrosphere and the biosphere and challenge certain concepts considered as established, thus demonstrating the importance of deeply holistic and integrated studies.

However, further studies are needed to better understand and quantify (1) the sediment origin and explanation of the variability of initial (upstream) erosion and the transfer time of those sediments to the deep-sea (2) the origin, importance and consequences of major oceanographic currents and their influence on the sediment record.

References

Afilhado, A., Moulin, M., Klingelhoefer, F., Aslanian, D., Schnurle, P., Nouzé, H., Rabineau, M., Beslier, M.O.: Deep crustal structure across a young passive margin from wide- angle and reflection seismic data (The SARDINIA Experiment)—II. Sardinia's Margin, bSGF, ILP Spec. **186**(4–5), 331–351 (2015)

Arab, M., Rabineau, M., Bracene, R., Déverchère, J., Belhai, D., Roure, F., Marok, A., Bouyahiaoui, B., Granjeon, D., Andriessen, P., Sage, F.: Origin and tectono-sedimentary evolution of the Eastern Algerian Basin (offshore) from Upper Oligocene to Present-Day. Mar. Petrol. Geol. **77**, 1355–1375 (2016)

Bache, F., Olivet, J.-L., Gorini, C., Aslanian, D., Labails, C., Rabineau, M.: Evolution of rifted continental margins: the case of the Gulf of Lions (Western Mediterranean Basin). Earth Planet. Sci. Lett. **292** (3–4), 345–356 (2010)

Badhani, S., Cattaneo, A., Dennielou, B., Leroux, E., Colin, F., Thomas, Y., Jouet, G., Rabineau, M., Droz, L.: Morphology of retrogressive failures in the Eastern Rhone Interfluve 1 during the Last Glacial Maximum (Gulf of Lions, Western Mediterranean). Geomorphology **351**. https://doi.org/10.1016/j.geomorph.2019.106894 (2020) *s*.

Bassetti, M.A., Jouet, G., Dufois, F., Berné, S. Rabineau, M., Taviani, M.: Sand bodies at the shelf edge in the Gulf of Lions: De-glacial history processes and deposits in the outer continental shelf of the Gulf of Lions (western Mediterranean). Mar. Geol. **234**(1–4), 93–109) (2006)

Bassetti, M.A., Berne, S., Sicre, M.A., Dennielou, B., Alonso, Y., Buscail, R., Jalali, B., Hebert, B. and Menniti, C.: Holocene hydrological changes in the Rhone River (NW Mediterranean) as recorded in the marine mud belt. Clim. Past **12**(7):1539–1553, (2016). https://doi.org/10.5194/cp-12-1539-2016

Baztan, J., Berné, S., Olivet, J.-L., Rabineau, M., Aslanian, D., Gaudin, M., Réhault, J.-P., Canals, M.: Axial incision: the key to understand canyon evolution. Mar. Petrol. Geol. **22**, 805–826 (2005)

Clauzon, G., Suc, J.-P.., Do Couto, D. et al.: New insights on the Sorbas Basin (SE Spain): the onshore reference of the Messinian Salinity Crisis. Mar. Petrol. Geol. **66**, 71–100 Part: 1, *Special Volume, Messinian events and hydrocarbon exploration in the Mediterranean* (2015)

Dennielou, B., Jegou, I., Droz, L., Jouet, G., Cattaneo, A., Aslanian, D., Berné, S., Loubrieu, B., Rabineau, M., Sultan, N.: Sylvain Bermell: major modification of sediment routing by a giant mass transport deposit in the gulf of lions (Western Mediterranean). Mar. Geol. **411**, 1–20 (2019)

Do Couto, D., Gorini, C., Jolivet, L., Lebret, N., Augier, R., Gumiaux, C., d'Acremont, E., Ammar, A., Jabour, H., Auxietre, J.-L.: Tectonic and stratigraphic evolution of the Western Alboran Sea Basin in the last 25 Myrs (2016)

Droz, L., Dos Reis, T., Rabineau, M., Berné, S., Bellaiche, G. (2006) Quaternary turbidite systems on the northern margin of the Balearic Basin (Gulf of Lions, Western Mediterranean): a synthesis. Geo-Mar. Lett. **26**(6), 347–359 (2006)

Gaudin, M., Berné, S., Jouanneau, J.M., Palanques, A., Puig, P., Mulder, T., Cirac, P., Rabineau, M., Imbert, P. (2006) Recent sedimentary activity in the Bourcart canyon head, Gulf of Lion, northwestern Mediterranean Sea). Mar. Geol. **234**(1–4), 111–128 (2006)

Jouet, G., Berné, S., Rabineau, M., Bassetti, M.A., Bernier, P., Dennielou, B., Sierro, F., Flores, J.A., Taviani, M.: Shoreface migrations at the shelf edge and sea level changes around the last Glacial Maximum (Gulf of Lions, NW Mediterranean). Mar. Geol. **234**(1–4), 21–42 (2006)

Jouet: Enregistrements stratigraphiques des cycles climatiques et glacio-eustatiques du Quaternaire terminal : modélisations de la marge continentale du Golfe du Lion, Ph.D. thesis, Université de Brest (2007)

Leroux, E., Rabineau, M., Aslanian, D., Granjeon, D., Gorini, C., Droz, L., et al.: Stratigraphic simulation on the shelf of the Gulf of Lion: testing subsidence rates and sea-level curves during Pliocene and Quaternary. Terra Nova **26**, 230–238 (2014)

Leroux, E., Aslanian, D., Rabineau, M., Moulin, M., Granjeon, D., Gorini, C., Droz, L.: Sedimentary markers in the Provencal Basin (western Mediterranean): a window into deep geodynamic processes. Terra Nova **27**, 122–129 (2015a)

Leroux, E., Rabineau, M., Aslanian, D., Gorini, C., Bache, F., Moulin, M., Pellen, R., Granjeon, D., Rubino, J.-L.: Post-rift evolution of the Gulf of Lion margin tested by stratigraphic modelling, *bSGF*. ILP Spec. **186**(4–5), 291–308 (2015b)

Leroux, E., Rabineau, M., Aslanian, D., Molliex, S., Bache, F., Robin, C., Granjeon, D., Gorini, C., Droz, L., Moulin, M., Suc, J.-P., Rubino, J.-L.: High resolution evolution of terrigenous sediment yields in the Provence Basin during the last 6 Ma: relation with climate and tectonics. Basin Res. **29**(3), 305–339 (2017)

Leroux, E., Aslanian, D., Rabineau, M., Pellen, R., Moulin, M.: The late messinian event 6 Ma ago: a worldwide revolution. Terra Nova **30**(2–3), 207–214, (2018). https://doi.org/10.1111/ter.12327

Lombo Tombo, S., Dennielou, B., Berné, S., Bassetti, M.A., Toucanne, S., Jorry, S.J., Jouet, G., Fontanier, C.: Sea-level control on turbidite activity in the Rhone canyon and the upper fan during the Last Glacial Maximum and Early deglacial. Sed. Geol. **323**(0), 148–166 (2015)

Mauffrey, M.A., Berne, S., Jouet, G., Giresse, P., Gaudin, M.: Sea-level control on the connection between shelf-edge deltas and the Bourcart canyon head (western Mediterranean) during the last glacial/interglacial cycle. Mar. Geol. **370**, 1–19 (2015)

Miramontes, E., Cattaneo, A., Jouet, G. et al.: The pianosa contourite depositional system (Northern Tyrrhenian Sea): Drift morphology and Plio-Quaternary stratigraphic evolution. Mar. Geol. **378**(SI Pages), 20–42 (2016)

Miramontes, E., Garreau, P., Caillaud, M., Jouet, G., Pellen, R., Hernández-Molina, F.J., Clare, M.A., Cattaneo, A.: Contourite distribution and bottom currents in the NW Mediterranean Sea: Coupling seafloor geomorphology and hydrodynamic modelling. Geomorphology **333**, 43–60 (2019)

Molliex, S., Rabineau, M., Leroux, E., Bourlès, D.L., Authemayou, C., Daniel, A., Chauvet, F., Civet, F., Gwenael, J.: Multi-approach quantification of denudation rates in the Gulf of Lion source-to-sink system (SE France). Earth Planet. Sci. Lett. **444**, 101–115 (2016)

Moulin, M., Klingelhoefer, F., Afilhado, A., Feld, A., Aslanian, D., Schnurle, P., Nouzé, H., Rabineau, M., Beslier, M.O.: Deep crustal structure across a young passive margin from wide-angle and reflection seismic date (The SARDINIA Experiment)—I- Gulf of Lion's Margin *bSGF*. ILP Spec. **186**(4–5), 309–330 (2015)

Pasquier, V., SansJofre, P., Rabineau, M., Revillon, S., Houghton, J., Fike, D.: Pyrite sulphur isotopes: a new proxy for glacial-interglacial environmental changes. PNAS **114**(23), 5941–5945 (2017)

Pasquier, V., Révillon, S., Leroux, E., Molliex, S., Mocochain, L., Rabineau, M.: Quantifying biogenic versus detrital carbonates on marine shelf: an isotopic approach, Front. Earth Sci. Section Sedimentology, Stratig Diagenesis. **7**, (Ed. Brian Romans) (2019a). https://doi.org/10.3389/feart.2019.00164

Pasquier, V., Toucanne, S., SansJofre, P., Dixit, Y., Revillon, Mokeddem, Z., Rabineau, M.: Organic matter isotopes reveal enhanced rainfall activity in Northwestern Mediterranean borderland during warm substages of the last 200kyr. Quat. Sci. Rev. **205**, 182–192 (2019b). https://doi.org/10.1016/j.quascirev.2018.12.007

Pellen, R., Aslanian, D., Rabineau, M., Leroux, E., Gorini, C., Silenzario, C., Blanpied, C., Rubino, J.-L.: The minorca basin: a buffer zone between Valencia and Provençal Basins. Terra Nova **28** (4), 245–256 (2016). https://doi.org/10.1111/ter.12215(2016)

Pellen, R. Aslanian, D., Rabineau, M., Suc, J.-P., Gorini, C., Leroux, E., Blanpied, C., Silenziario, C., Popescu S.-M., Rubino, J.-L.: The Messinian Ebro River incision. Glob. Planet. Changes. **181** (2019). https://doi.org/10.1016/j.gloplacha.2019.102988

Rabineau, M., Berné, S., Aslanian, D., Olivet J-L., Joseph, P, Guillocheau, F, Bourillet, J-F., Ledrezen, E., Granjeon, D.: Sedimentary sequences in the Gulf of Lions : a record of 100,000 years climatic cycles. Mar. Petrol. Geol. 22, 775–804 (2005)

Rabineau, M., Berné, S., Olivet, J.-L., Aslanian, D., Joseph, P., Guillocheau, F.: Paleosea levels reconsidered from direct observation of paleoshoreline position during Glacial Maxima (for the last 500,000 yr). Earth Planet. Sci. Lett. 252(1–2), 119–137. https://doi.org/10.1016/j.epsl.2006.09.033 Published: NOV 30 (2006)

Rabineau, M., Leroux, E., Aslanian, D., Bache, F., Gorini, C., Moulin, M., Molliex, S., Droz, L., Dos Reis, T., Rubino, J.-L., Olivet, J.-L.: Quantifying Subsidence and Isostasy using paleobathymetric markers : example from the Gulf of Lion. EPSL **388**, 353–366 (2014)

Rabineau, M., Cloetingh, S., Kuroda, J., Aslanian, D., Droxler, A., Gorini, C., Garcia-Castellanos, D., Moscariello, A., Hello, Y., Burov, E., Sierro, F., Lirer, F., Roure, F., Pezard, P.A., Matenco, L., Mart, Y., Camerlenghi, A., Tripati and the GOLD and DREAM Working Groups: Probing connections between deep earth and surface processes in a land-locked ocean basin transformed into a giant saline basin: the Mediterranean GOLD project. Mar. Petrol. Geol. **66**, 6–17 Part: 1 (2015)

Révillon, S., Jouet, G., Bayon, G., Rabineau, M., Dennielou, B., Hémond, C., Berné, S.: The provenance of sediments in the Gulf of Lions, Western Mediterranean Sea. Geochem. Geophys. Geosyst. **12** Article Number: Q08006 (2011). https://doi.org/10.1029/2011GC003523

Some Features of Hydrological Processes in the Ponto-Caspian Seas During the Late Pliocene—Early Pleistocene

Nikolay Esin, Nikolay Igorevich Esin, and Igor Podymov

Abstract

The present theory of the transgression mechanism of the Caspian Sea in the Akchagylian time is based on the hypothesis that the water for transgression came from the ocean. But, this hypothesis is unacceptable because the sea level was supposed to have risen above the ocean level. In addition, if the salty ocean water had flowed into the closed Caspian Sea for a long time, the salinity of the sea water would have increased to the brine concentration, the wildlife of the sea would have died, and a layer of evaporites would have been formed at the bottom. The calculation of the sea water salinity with salty ocean water showed that the salinity of the sea water would have increased annually by 0.12‰. Consequently, after 1000 years, sea salinity would have been 120, which would lead to an ecological catastrophe with the formation of evaporites. The comparison of the calculation results with the geological studies results showed that in the period of Akchagyl tangression, there was not a single sign of prolonged influx of salt water into the sea and could not be. Consequently, the Akchagylian transgression of the Caspian Sea, like all other transgressions, was created by the fresh water resulting from the melting glaciers. Theoretically, there is evidence of melting glaciers (Svitoch Svitoch, A.A.: Large Caspian, structure and evolution history. Pub. MSU (2014)).

Keywords

Continental glaciation • Transgressive seas and ocean level • Akchagylian transgression • The evolution of salinity in the Akchagylian Sea

1 Introduction

Recently, researchers have shown interest in the processes of mutual influence of the Ponto-Caspian seas and the Mediterranean Sea. This influence appears as in the hydrophysical processes (e.g., Marzocchi et al. 2016) and in the processes occurring in the earth's mantle (e.g., Esin and Esin 2018).

During the last 10 million years, very complex hydrological processes have taken place in the northern hemisphere of the earth, changing the relief of the earth's surface, the water level in the oceans, the salinity of the water, and the flora and fauna in the water bodies. The most significant role in these processes was played by the climate, which itself was determined by the action of endogenous and cosmic factors—the position of the center of gravity in the body of the earth and the position in space of the axis of rotation of the earth. It should be borne in mind that the formation of a glacier changes the position of the earth's center of gravity. As a result, the tilt of the earth's axis of rotation changes in space, and accordingly, the amount of solar energy that enters to the northern hemisphere changes. Thus, the evolution of the planet's climate essentially depends on the processes occurring on it.

Over the last 10 million years, the following hydrodynamic processes have taken place on the globe: The enormous sea-lake Paratethys was formed, and then it disappeared at the end of the Miocene; the Bosphorus and Dardanelles straits were created; there was a desiccation of the Mediterranean Sea to the depth of −1500 m. At its bottom, a thick layer of evaporites is formed. This changed the eustatic pressure on the seabed and, accordingly, the tectonic movements of the coasts. In particular, due to the action of gravity, the Strait of Gibraltar and the sea arose again filled with water of the Atlantic Ocean (Yesin and Dmitriyev 1987; Yesin et al. 1986; Garcia-Castellanos et al. 2009). We (Esin et al. 2016) also showed that the Messinian Salinity Crisis affected to the evolution of a number of seas

N. Esin (✉) · N. I. Esin · I. Podymov
Shirshov Institute of Oceanology, Russian Academy of Sciences, Moscow, Russia

A. Çiner et al. (eds.), *Recent Research on Geomorphology, Sedimentology, Marine Geosciences and Geochemistry*, Advances in Science, Technology & Innovation, https://doi.org/10.1007/978-3-030-72547-1_57

associated with the Mediterranean Sea. Thus, we see that all the seas of the region are developing, interacting with each other. Therefore, they need to be studied, taking into account the mutual effects, as well as the environmental ones.

2 The Mechanism of Formation of the Transgressive Caspian Seas in the Pliocene–Pleistocene

After the formation of the Bosphorus Strait and the disappearance of the Paratethys seas, the glacier formation regime was preserved. Consequently, periodically, during the melting of glaciers, the water flow in rivers flowing into the Black and Caspian Seas sharply increased, and the territories were flooded, and a large number of reservoirs were formed. But, the nature of the flood has changed significantly. During this period, the water of the glaciers entering the Black Sea did not raise its level upward significantly, since it freely passed through the strait into the Mediterranean Sea. And in the Caspian Sea, which was a closed depression, the level rose to the elevation where the volume of evaporated water was equal to the volume of incoming water. Another option is to fill the depression with water, when the sea level rose to the bottom level of the Manych strait. After that, part of the water evaporated and the remaining water went through the strait into the Azov Sea. In this case, the water level in the sea was determined by the mark of the Manych strait plus the water depth in the strait. The important point is that in the conditions of the existence of the Bosphorus, the course of the Black Sea level did not correlate with the course of the Caspian Sea level. The impression that was made was that the indicated seas receive water from various sources (Svitoch 2014).

3 Results

The evolution mechanism of one of the first Caspian transgressive seas—Akchagylian— is based on the hypothesis that the water for creating this transgressive sea, and the level of which is elevated according to geological studies to the level of +100 m or even +180 m (Svitoch 2014) came from one of the three oceans: the Arctic, the Indian, or the Atlantic (across the Mediterranean Sea). A river with salty ocean water flowed from an unknown ocean into the Akchagylian Sea. And, it was assumed that the ocean level was zero (present elevation). Arguments of experts that water cannot flow upstream against the action of gravity are not taken into account. Another hypothesis of geologists that the ocean level in Akchagylian time was at the level of +100 m does not solve the problem, because in such a case, there would be a global ocean transgression against which Akchagylian transgression would be hardly noticeable.

In order to evaluate the hypothesis of the creation of the Akchagylian Sea with water flowing from the ocean, we performed calculations that showed the dynamics of the salinization process of water in the Caspian Sea in such a situation. The calculations showed the following. If water had flowed from the ocean, its salinity would have been 35‰ (35 kg of salt per 1 m^3 of water) and the volume of evaporated saline water about 480 km^3/year, and in this situation, the salinity of sea water would have increased annually by 0.12‰. Therefore, for 100 years, salinity would have increase by 12‰, for 250 years by 30‰ and for 1000 years by 120‰. Thus, in the first thousand years of transgression, water in the Caspian Sea would have turned into brine and the sea into a lifeless reservoir. Then, as new portions of salt arrived, the deposition to the bottom of evaporites would have begun, as it did in the Mediterranean Sea during the Messinian Salinity Crisis.

Now, compare the theoretical studies results with those of geological studies. In the monograph, Svitoch (2014) collected the results of studies of various authors. According to their data, the maximum salinization of sea water for the whole Akchagylian time was only 20–25‰. The tragic loss of biota during an ecological catastrophe has not been fixed; the process of evaporite formation is also not established. Thus, the geological materials about the Akchagylian transgression do not even contain a hint of a long flow of ocean salt water into the sea. It can be assumed that the short-term relationship between the sea and the ocean occurred previously, before the transgression. During the transgression, the sea level rose and the flow of ocean water stopped. Until transgression, the elevation of sea level probably would have been below the ocean level because of the significant evaporation in the sea. Thus, it can be concluded that the water from the ocean could not have flowed upward in accordance with physical laws, and it did not do that. Consequently, the Akchagylian Sea was created by water from melting glaciers, as were the seas of Paratethys and the next transgression of the Caspian Sea. Such a conclusion does not contradict either physical laws or common sense.

It should be borne in mind that if salty ocean water had entered the Caspian Sea, part of it would have flowed into the Sea of Azov and the Black Sea, increasing the salinity of the water in these seas. For the Azov Sea, this would have ended as an environmental disaster, whose result would have been the disappearance of the freshwater fauna.

As can be seen, the assumption that ocean water flowed into the Caspian Sea in the Akchagylian period leads to the following contradictions: On the one hand, this would have led to catastrophically quick salinization of water in the Caspian and Azov Seas and an ecological disaster, but it was established by geological methods, that there was neither a catastrophic salinization of water nor any ecological disaster. P.V. Fedorov (1978) made a very reasonable assumption

that insignificant salinization of the Caspian waters from 5–9‰ to 20–25‰ is caused by salt that came from Kara-Bogaz-Gol Bay and from salt domes of the northern Caspian Sea. Compared to the river of the ocean water, these salt sources are weaker and temporary, which is more consistent with the weak and slow salinization of the Caspian waters, which is established by geological methods.

In addition to the theoretical results regarding the Akchagylian transgression, there is also material evidence of the Akchagylian glaciation. These are the discovered moraine residues belonging to the Akchagylian period and band clay clays-satellites of glacial moraines (Moskvitin 1962). The evidence of glaciation is also the numerous conclusions of various researchers (e.g., Kovalenko 1971; Kovalskii 1944) about the cooling of the climate in the Akchagylian period. The analysis of pollen in the range from 3.6 to 3.4 million years ago showed a cooling of the climate and change in the structure of dendroflora, and warming began 3.2 million years ago. The second cold snap began 2.5 million years ago (Naidina and Richards 2018).

4 Conclusions

The analysis of all transgressive Caspian Seas showed that their level was not determined by the discharge of inflowing water, but by the elevation of the Manych strait bottom. It follows that during each transgression, a significant amount of water flowed through the strait into the Azov Sea and then into the Mediterranean Sea. Chepalyga (2005) estimates the additional volume of water that came from the glacier at 1600 km^3/year. According to our calculations, in order to raise the level of the first seas of Paratethys to the level of +120 m, 2200 km^3/year of water are required to flow into them. This correlates with the assessment of Chepalyga (2005). If we add the natural runoff of rivers flowing into the Black and Azov seas to 1600 km^3/year, we get a figure close to 2200 km^3/year. Since the level of the bottom of the strait decreased in time (at present, it is equal to 27 m), an ever-increasing amount of water flowed into the Mediterranean Sea. Roughly, it could reach a value of 850 km^3/year. This is much more than the volume of fresh water that entered the Mediterranean Sea during the optimum climatic period. It follows that a significant desalination of water in the Mediterranean occurred during the melting of glaciers.

References

Chepalyga, A.L.: Prototip Vsemirnogo potopa. (The prototype of the flood). Znanie-Sila (Knowledge is Power), pp. 85–91. Moscow (2005)

Esin, N.V., Esin, N.I.: The formation of deep sea features during conditions of Mediterranean Sea desiccation and appearance of negative pressure in the Earth's mantle. In: IGCP 610 "From the Caspian to Mediterranean: Environmental Change and Human Response during the Quaternary", pp. 50–52. Turkey (2018)

Esin, N.V., Yanko-Hombach, V.V., Esin, N.I.: Evolutionary mechanisms of the Paratethys sea and its separation into the Black sea and Caspian sea. Quatern. Int. **465**, 46–53 (2016)

Fedorov, P.V.: Pleistotsen Ponto-Kaspiya (The Pleistocene of the Ponto-Caspian). Trudy Geologicheskogo Institute Akademii Nauk SSSR (Proceedings of the Geological Institute of Sciences of the USSR Academy of Sciences), V.310, p. 163 (1978)

Garcia-Castellanos, D., Estrada, F., Jiménez-Munt, I., Gorini, C., Fernàndez, M., Vergés, J., DeVicente, R.: Catastrophic flood of the Mediterranean after the Messinian salinity crisis. Nature **462**, 778–781 (2009)

Kovalenko, N.D.: Palinologicheskaia kharakteristika verkhnepliotcenovykh otlozhenii Severnogo Prikaspiia (Palynological characteristics of the Upper Pliocene deposits of the Northern Caspian). Stratigrafiia neogena vostoka Evropeiskoi chasti SSSR (Neogene stratigraphy of the east European part of the USSR), pp. 99–106. Moscow, Nedra (Subsoil), (1971)

Kovalskii, C.A.: Velikaia akchagylskaia transgressiia i ee uchastie v formirovanii produktivnoi tolshchi (Great Akchagylian transgression and its participation in the formation of the productive stratum). News of the USSR Academy of Sciences, №5 (1944)

Marzocchi, A., Flecker, R., Van Baak, C.G.C., Lunt, D.J., Krijgsman, W.: Mediterranean outflow pump: An alternative mechanism for the Lago-mare and the end of the Messinian Salinity Crisis. Geology **44** (7), 523–526 (2016)

Moskvitin, A.I.: Pleistocen Nizhnego Povolzh'ya (The Pleistocene of the Lower Volga). In: Trudy Geologicheskogo Instituta Akademii Nauk SSSR (Proceedings of the Geological Institute of the USSR Academy of Sciences), Moscow, V.64 (1962)

Naidina, O.D., Richards, K.: The Akchagylian stage (late Pliocene-early Pleistocene) in the North Caspian region: Pollen evidence for vegetation and climate change in the Urals-Emba region. Quatern. Int. (2018). https://doi.org/10.1016/j.quaint.2018.12.012

Svitoch, A.A.: Large Caspian, structure and evolution history. Pub. MSU (2014)

Yesin (Esin), N.V., Dmitriyev, V.A., Shimkus, K.M., Ovchinnikov, I. M.: A model for the messinian events in the Mediterranean sea. Int. Geol. Rev. 28:1, 10–14 (1986)

Yesin (Esin), N.V., Dmitriyev, V.A.: On the possible mechanism of formation of the Messinian evaporites in the Mediterranean Sea. Int. Geol. Rev. **29**(3), 258–263 (1987)

Acquisition of Geophysical Data in Shallow Water Environments Using Autonomous Vehicles: A Tool for Marine Geology, Archeology and Environmental Studies

Luca Gasperini, Giuseppe Stanghellini, Fabrizio Del Bianco, and Alina Polonia

Abstract

The fast ongoing progress in the field of the "open content" technologies, i.e., those hardware and software resources designed and offered to a wide community by people belonging to the open-source culture movement, strengthened and fostered by the availability of low cost, highly performing electronic devices, is creating a "revolution" in the world of applied sciences. This is particularly true for waterborne geological-geophysical data acquisition in shallow water environments, such as marine coasts, lagoons, lakes and rivers, sites that preserve, in general, relatively continuous recent geological records. We presented some examples of geophysical data acquisition in different shallow water environments carried out by means of an unmanned surface vehicle (USV) equipped with different sensors providing high-resolution images of the sediment–water interface and some tens of meters within the sediments. The tests indicate that these technologies can be employed to collect densely spaced grids of high-resolution data, quickly, efficiently and at a very low cost, allowing for execution of repeated surveys even in those areas not accessible through conventional systems. The intensive use of "open" technologies and software for data acquisition and processing has the potential of widening the application of these methods to an increasing audience of earth scientists studying geological processes in rapidly evolving environments.

Keywords

Unmanned surface vehicles • Open technologies • Marine geology • Shallow water • Archeology • Coastal geology • Geophysical techniques

1 Introduction

A number of underwater natural or artificial environments, including harbors, coastal areas, river streams, natural and artificial lakes and coastal lagoons, are particularly affected by anthropic pressures. For this reason, they would require periodical monitoring. To date, geo-environmental studies of shallow water areas are not a consolidated practice, because they require a multidisciplinary knowledge and special instruments. As a result, such "transitional" zones between underwater and the onshore, also interesting for archeological studies, are poorly investigated through geophysical techniques. The ongoing research and developments in the field of robotics could represent an opportunity to fill this gap. In fact, the relatively recent availability of miniaturized yet accurate sensors, such as accelerometers, GPS receivers, compass and motion sensors, as well as innovative "open" hardware architectures (Arduino©, Raspberry™, etc.) facilitate the development of unmanned surface vehicles (USV) that could eventually operate in extremely shallow, difficult to access environments. This is the case of shallow water prospector (SWAP) developed by *ISMAR-CNR* and *Consorzio Proambiente* (*Tecnopoli dell'Emilia Romagna*), a small, flexible vehicle that could be employed in a variety of subaqueous environments. Because it was developed by a pool of scientists and technicians employed in public institutions, the algorithms and the technological solutions developed for SWAP are disclosed and will be soon published technical reports and scientific articles. This is probably the real strength of the project, which is still a "work in progress."

L. Gasperini (✉) · G. Stanghellini · A. Polonia
Istituto di Scienze Marine, CNR, Bologna, Italy
e-mail: luca.gasperini@ismar.cnr.it

F. Del Bianco
Consorzio Proambiente, Bologna, Italy

A. Çiner et al. (eds.), *Recent Research on Geomorphology, Sedimentology, Marine Geosciences and Geochemistry*, Advances in Science, Technology & Innovation, https://doi.org/10.1007/978-3-030-72547-1_58

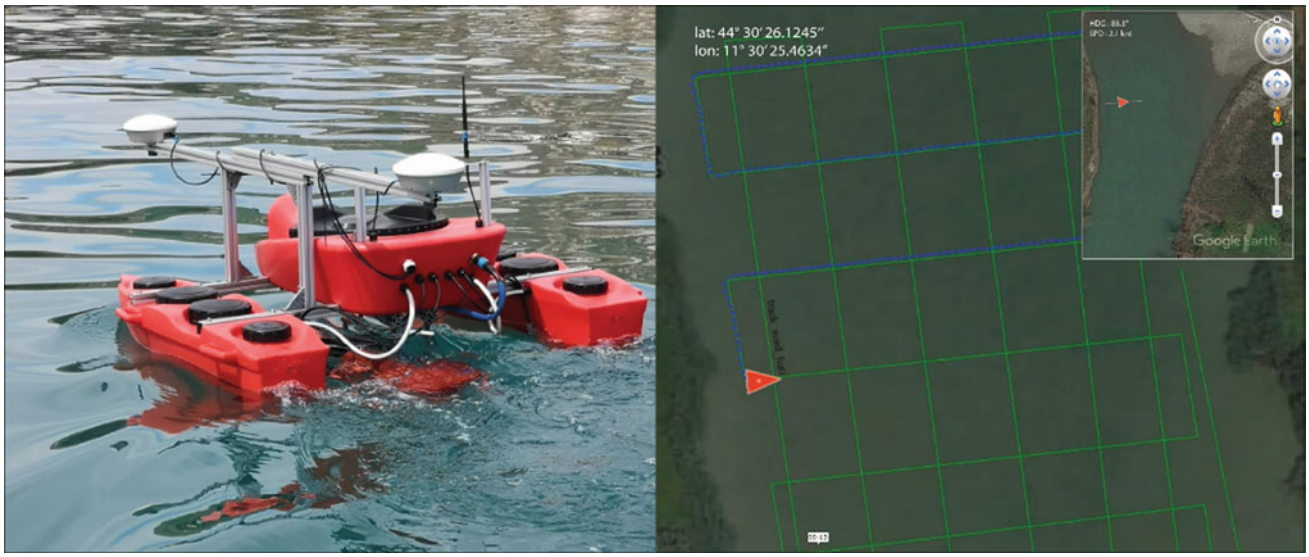

Fig. 1 **Left** Unmanned surface vehicle shallow water prospector (SWAP) collecting multibeam data. **Right** Screenshot taken during data acquisition; the error between planned and executed acquisition lines (green and blue lines, respectively) is within 30 cm along straight routes, opening the possibility for repeated (4D surveys).

2 Methods

SWAP (Fig. 1) is an USV based on a catamaran hull specifically designed to gather information with the least possible noise and turbulence in the area where geophysical sensors are deployed. Although the architecture of the system is modular and could be easily expanded to other USB-based digital sensors, three basic devices are installed on each prototypes: (1) a DGPS receiver; (2) a high-resolution single beam echosounder; and (3) a chirp-sonar subbottom profiler.

The vehicle is equipped with a differential RTK GPS system that provides an accuracy of <0.1 m in the *x*–*y* positioning. A HMC5883L magnetometer, an ADXL345 accelerometer and a ITG3200 gyroscope interfaced in an Arduino board which constitute the basic system for inertial navigation and correction of gophysical data positioning for pitch, roll, heave and heading. All data, including echograms, seismic lines and side-scan sonar records were processed and interpreted using the open-source package SeisPrho (Gasperini and Stanghellini 2009). The integration of software and hardware resources allowed for obtaining an accuracy within 30 cm of error in the execution of planned navigation lines, opening the possibility of repeated (4D) surveys.

3 Results

3.1 The *Valli di Comacchio* Coastal Lagoon

The Valli di Comacchio coastal lagoons are shallow water brackish environments connected to the Adriatic Sea located south of the Po River between Comacchio and the Reno River (northern Italy). These lagoons (*Valli*) were formed around the tenth century as a consequence of subsidence and were originally fresh water basins supplied by river floods (Bondesan et al. 1995). The hydrodynamics of the Valli di Comacchio is controlled by the inflow of freshwater from several sources, but the tidal cycle is a major controlling factor on water circulation, causing water-depth excursions of over 1 m. Because the average depth is <2 m, most areas in the lagoon system are not accessible by boats equipped with geophysical instruments. For this reason, we carried out a combined high-resolution seismic reflection and mopho-bathymetric survey of the lagoon using a chirp-sonar and a 200 kHz echosounder mounted onboard of SWAP. The acquisition of the entire echosounder sweeps at each sounding point rather than the simple depth value and gave us the opportunity to calculate the bottom reflectivity and use it to estimate the mean grain size of the lagoon–floor sediments (Gasperini 2005). The data collected using SWAP in the Valli di Comacchio lagoons were used to take actions toward their use in a more sustainable way and to prevent episodes of eutrophication. We note how relatively basic and inexpensive (because carried out with USV) geophysical surveys could give important insights for understanding complex geological processes regulating the equilibrium of such sensitive environments.

3.2 The Lake Trasimeno (Central Italy)

Lake Trasimeno, located in the Umbria Region (Central Italy), is the broadest lake of Central Italy and an interesting

geological and archeological site (Gasperini et al. 2010). It has been a natural crossroad since proto-historical times, and important events took place around its shores and in the vicinity of the lake, such as the famous Trasimeno battle (217 B.C.), when the Romans were defeated by Hannibal's army during the Second Punic War. For these reasons, the lake was surveyed using different geophysical techniques including a close spaced grid of high-resolution seismic reflection lines (Gasperini et al. 2010). However, some sectors of the lake close to the N shore, too shallow to be accessible using a boat, were surveyed using SWAP, equipped with an echosounder, a side-scan sonar and a subbottom chirp, which penetrated the first tens of meters below the lake floor. It was then possible to reconstruct the coastline position during roman times and imaging objects buried below the lake's sediments close to the 217 B.C battle site (Brizzi et al. 2018).

4 Discussion

The geophysical instruments presently installed onboard of SWAP is not exhaustive of the variety of studies that could be carried out in shallow water areas. In fact, the possibility of installing other instruments, such as multibeam echosounders or electromagnetic sensors (ground-penetrating radars, magnetometers, resistivity meters, etc.), represents a dramatic improvement in the data collection potential. The peculiar design of the hull is suitable for installing ADCP currentmeters, useful for a wide range of applications in hydraulic and physical oceanography. Furthermore, some basic chemical sensors, such as oxygen, nitrates and pH, now available in small and light vessels, could represent interesting payloads to carry out rapid assessment of the water quality. The key point of SWAP is, however, the intensive use of open technologies that disclose the use of these instruments to a wider community of scientists and students. The "open" and modular architecture of SWAP led possible interfacing to its control unit, virtually all instruments that fit within the vehicle.

5 Conclusions

We presented some case studies of geophysical surveys carried out in different shallow water environments using an unmanned surface vehicle (USV). The possibility of carrying out such kind of surveys quickly, and at a fraction of the cost of conventional surveys, allows the use of these techniques to a wide range of users. Moreover, having an accuracy of <0.3 m in following a survey trackline, it could be used to perform repeated surveys, which would enable a time-variant approach to the study of natural processes in rapidly evolving environments.

References

Bondesan, M., Favero, V., Vignals, M.J.: New evidence on the evolution of the Po-delta coastal plain during the Holocene. Quatern. Int. **29**(30), 105–110 (1995)

Brizzi, G., Gambini, E., Gasperini, L.: Annibale al Trasimeno, Indagine su una Battaglia, 1st edn. Lombardi Editore (2018)

Gasperini, L.: Extremely Shallow-water morphobathymetric surveys: the valle fattibello (Comacchio, Italy) test case. Mar. Geophys. Res. **26**, 97–107 (2005)

Gasperini, L., Stanghellini, G.: SeisPrho: an interactive computer program for processing and interpretation of high-resolution seismic reflection profiles. Comput. Geosci. **35**, 1497–1504 (2009)

Gasperini, L., Barchi, M.R., Bellucci, L.G., et al.: Tectonostratigraphy of lake trasimeno (Italy) and the geological evolution of the Northern Apennines. Tectonophysics **492**, 164–174 (2010)

Geochemistry and Metallogenesis: Processes and Products (T7): Sedimentary Geochemistry and Mineralogical Characterization

Mineralogy and Geochemistry of Clay Minerals from the Ouled Bou-Sbaa Phosphate Deposit (Meskala Basin, Morocco)

Hanane El Boukhari, Hicham Si Mhamdi, Mustapha Mouflih, Abdelmajid Benbouziane, Essaid Jourani, Salem El Ouariti, and Mohammed Amine Nguidi

Abstract

The Meskala basin is one of Morocco phosphate basins. It is the first of the vast phosphate complexes from the Atlas border going to the north. This Basin is characterized by a phosphate series of late Cretaceous-Paleogene age and three deposits: Ouled Bou-Sbaa, Imin-Tanout and Khemiss Meskala. Besides this mineralization, we also have other natural materials that are as important in quantity as quality. It is about clay and marl sediments intercalary and associated with phosphatic deposits. This work aims at characterizing and studying the spatial and temporal distribution of the clay processions of the Ouled Bou-Sbaa deposit located in the northern part of the basin. Several techniques and methods were adopted, namely X-ray diffraction (XRD), infrared spectroscopy (IR) and X-ray fluorescence (FX). The mineralogical study shows that the clays of the Ouled Bou-Sbaa deposit display a relatively normal slow drift from montmorillonite to palygorskite and sepiolite. We note the dominance of montmorillonite clays from Maastrichtian to Ypresian and magnesian sepiolite clays. Palygorskite-type clays are frequent at the upper end of the phosphate series. The results found by infrared spectroscopy confirm the results of X-ray diffraction by the presence of the characteristic bands of montmorillonites and palygorskite. The geochemical study by fluorescence of X-rays shows the dominance of oxides of silicon, aluminum and magnesium. These elements are the major constituents of clay minerals such as montmorillonite, palygorskite and sepiolite. This clay cortege reflects more humid climatic conditions that evolve into warmer and arid climatic conditions at the top of the Ouled Bou-Sbaa phosphate series.

Keywords

Phosphate • Montmorillonite • Palygorskite • Sepiolite • Ouled Bou-Sbaa • Meskala

1 Introduction

The series of Moroccan phosphates reveal the highest phosphate concentrations in terms of quality and quantity. This wealth makes Morocco the world leader in the production and exploitation of phosphates in all its forms. In addition to this richness, the country also has other natural materials that are equally significant, quantitatively and qualitatively. These are clayey and marly sediments that are interposed and/or associated with phosphate deposits. This study aims to evaluate the potential of the clays of the phosphate series of the Meskala Basin by studying their mineralogical, chemical, thermal and texture properties.

The study area is in the north of Ouled Bou-Sbaa deposit about 70 km west of the city of Marrakech and is part of the Essaouira Basin (Fig. 1).

2 Materials and Methods

2.1 Field Work

A field mission was carried out in the Ouled Bou-Sbaa deposit (Meskala basin) in which a lithostratigraphic section (Sidi Mokhtar section) and a systematic sampling of the

H. E. Boukhari (✉) · M. Mouflih · A. Benbouziane · S. E. Ouariti · M. A. Nguidi
Dynamics of Sedimentary Basins and Geological Correlations Laboratory, Faculty of Sciences Ben M'Sick, University Hassan II of Casablanca, Casablanca, Morocco

H. S. Mhamdi
Faculty of Sciences and Technics, University Moulay Ismail, Meknes, Morocco

E. Jourani
Geology Division, Industrial Development Department, (OCP S. A), Casablanca, Morocco

A. Çiner et al. (eds.), *Recent Research on Geomorphology, Sedimentology, Marine Geosciences and Geochemistry*, Advances in Science, Technology & Innovation, https://doi.org/10.1007/978-3-030-72547-1_59

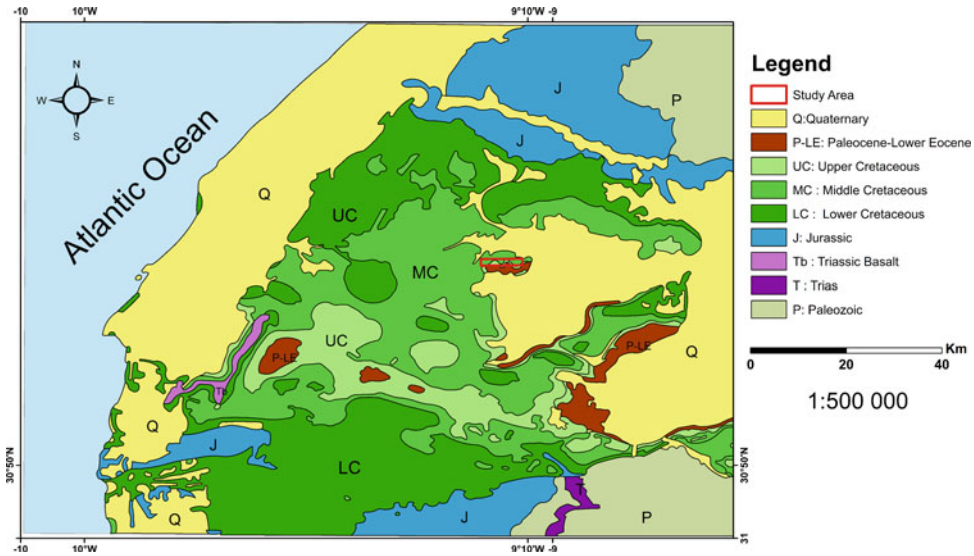

Fig. 1 Geological map of the Ouled Bou-Sbaa deposit

interleaved clays and those associated with phosphate deposits were carried out (Ten samples).

2.2 Laboratory work

Determination of water pH and pH KCl: The pH was measured according to the (Mc Lean 1982) method in a Clay/H_2O and clay/KCl suspension in a report from 1/2 at room temperature. The clay solution obtained is homogenized by a magnetic stirrer for 20 min. The reading is done directly on a pH meter.

Electrical conductivity: The electrical conductivity makes it possible to obtain an estimate of the overall dissolved salt content by extraction with demineralized water. 10 g of clay is placed in a beaker, rinsed with 50 ml of distilled water. The clay solution obtained is homogenized by a magnetic stirrer for 20 min. The reading is done directly on a Conductivity meter.

Humidity level (%): The humidity measurement allows determining the mass of water eliminated by drying wet clay until a constant mass is obtained at a temperature of 105 °C for 24 h (Chossat 2005).

$$\text{Humidity level}(\%) = (\text{water mass}/\text{particulate mass}) * 100$$

X-ray Diffraction: X-ray diffraction provides valuable information on clay mineralogy. The XRD spectra were recorded in position 2 Theta (0–30°) at the National Center for Scientific and Technical Research in Rabat on a type Philips PANalytical XRD equipment.

Infrared Vibration Spectroscopy: Infrared spectroscopy is considered as another means of studying clays and therefore as a means of identifying clay minerals. The analysis of the various clay samples by infrared spectroscopy was carried out using a Perkin Elmer spectrometer equipped with an ATR-FTIR module "The clays analyzed are in the form of pellets containing 1 mg of clays mixed with 100 mg of potassium bromide (KBr). The mixture is well homogenized born and compressed to 10 T cm-2.

X-ray fluorescence: fluorescence spectrometry is a chemical analysis method that determines the elemental composition of clays and therefore the mass concentrations of elements. The analysis of the major elements (SiO_2, Al_2O_3, MgO, CaO, Fe_2O_3, P_2O_5, TiO_2, K_2O) of the clays in the deposit was carried out by Epsilon 3XL X-ray fluorescence spectrometry.

3 Results

3.1 Physical–chemical Parameters

The results of the water pH, pH Kcl, electrical conductivity and humidity of the clays of the Ouled Bou-Sbaa deposit (Meskala basin) are presented in Table 1.

Noticeably, the pH of the water in the Ouled Bou-Sbaa deposit varies from 3.8 to 8.48. It is slightly to moderately basic in the lower levels and acidic in the upper levels of the series. The pH KCl values are always lower than the pH of the water. The difference between pH water and pH KCl is less than 1, so the studied clays have an average reserve acidity. The obtained conductivity results show that the Ouled Bou-Sbaa deposit clays have values ranging from 1.8 to 23.4mS/cm. The clays of the Ouled Bou-Sbaa deposit are slightly to moderately humid.

Table 1 Physico-chemical parameters of the clays of the Ouled Bou-Sbaa phosphate series

Samples	pH water	pH KCl	Electrical conductivity	Humidity levels
CHSM 1	7.23	6.95	7.51	18
CHSM 2	8.48	8.10	2.47	1
CHSM 3	7.32	7.26	1.81	7
CHSM 4	5.81	5.72	5.06	11
CHSM 5	7.82	7.72	2.11	7
CHSM 6	5.02	6.47	23.4	17.76
CHSM 7	6.02	6.15	4.68	7.28
CHSM 8	3.8	5.51	10.9	18.24
CHSM 9	4.4	4.2	4.3	12.92
CHSM 10	3.36	3.8	3.21	6.5

3.2 X-Ray Diffraction

The analysis of the diffractogram of the clays of the Ouled Bou-Sbaa deposit (Meskala Basin) using disoriented powders shows the presence of Quartz at d = 3.34 Å (26.63 in 2 ö) and d = 4.24 Å (20.93 in 2 ö). Characteristic peaks of clay minerals are observed at two ö = 8.43 and 5.83 corresponding, respectively, to the reticular distances 10.47 Å and 15 Å in the majority of the samples analyzed. The distance 10.47 Å is typical of Attapulgite clay (Palygorskite), while the distance 15 Å is typical of montmorillonite clay (smectite) (Viani et al. 2002). The peak at 12.47 Å (7.07 in 2 ö) is a low-intensity corresponding to sepiolites. The presence of illites is noted at about 4.48 (19.81 in 2 ö) (Fig. 2).

3.3 Infrared Spectroscopy

Examination of the IR spectra of the clays of the Ouled Bou-Sbaa deposit (Meskala Basin) reveals several absorption bands. The bands between 3410 cm-1 and 3480 correspond to the vibrations of the OH water groups absorbed between the clay sheets. These bands are characteristic of hydrophilic materials and are specific to smectites (Montmorillonites) (Bouras 2003). 1631, 1637 and 1645 cm-1 strips also originate from the OH vibrations of the water absorbed between the sheets of montmorillonite. The characteristic bands of impurities appear at 1034 and 798 cm-1, corresponding to the valence vibrations of the Si–O bond. They are manifested by shoulders that we attribute to the presence of quartz (Fig. 3).

3.4 X-ray Fluorescence

The results of the quantitative chemical analysis of the clays studied are shown in Table 2: The results indicate that the predominant constituents in our clay are silicon oxides and aluminum oxides. This is due to the dominance of palygorskite-type clays of the chemical formula Si8O20 Al2 Mg2 (OH)2 (H2O)4. These minerals are clay minerals very rich in silicon and aluminum.

4 Discussion and Conclusion

The Ouled Bou-Sbaa deposit is one of Meskala phosphate basins. The main objective of this work is to characterize the clay of the Ouled Bou-Sbaa deposit. The experimental

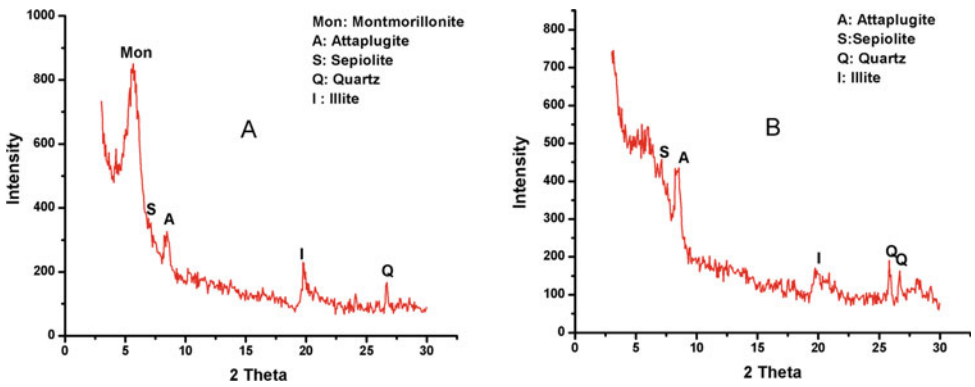

Fig. 2 Clay X-ray diffractogram of the Ouled Bou-Sbaa deposit. **a** The base **b** The summit

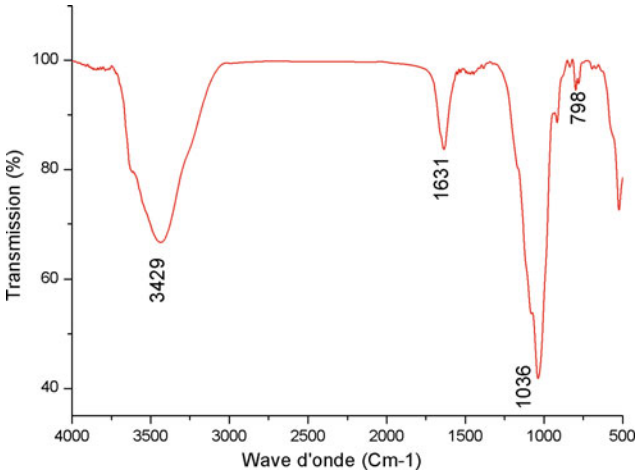

Fig. 3 Infrared spectrum of the Ouled Bou-Sbaa deposit clay

Table 2 Elementary chemical composition of the clays of the Ouled Bou-Sbaa deposit

	SiO_2 (%)	Al_2O_3 (%)	MgO (%)	CaO (%)	Fe_2O (%)$_3$	P_2O_5 (%)	TiO_2 (%)	K_2O (%)	Perte au feu (%)
CHSM 1	31.35	7.34	4.372	5.95	9.01	0.91	0.92	0.90	35.13
CHSM 3	34.13	7.62	6.33	5.99	7.34	2.99	0.77	1.34	32.84
CHSM 4	40.93	8.79	3.30	3.83	9.33	4.77	1.07	2.37	25
CHSM 6	35.32	6.701	5.569	9.531	6.791	3.104	0.809	1.682	35.13

techniques (X-ray diffraction (XRD), infrared spectroscopy (IR) and X-ray fluorescence (FX)) used allowed us to identify the different types of clay existing in the Ouled Bou-Sbaa deposit and their chemical composition. The clay of the Ouled Bou-Sbaa deposit is essentially composed of montmorillonite in the lower section of the series and clays of the palygorskite and sepiolite type in the upper section. The clay cortege of the Ouled Bou-Sbaa (montmorillonite, palygorskite and sepiolite) reflects more humid climatic conditions that evolve into warmer and arid climatic conditions at the top of the Ouled Bou-Sbaa phosphate series.

References

Bouras, O.: Propriétés Adsorbantes des Argiles Organiques Pontées : Synthèse et Caractérisation. Thèse de doc-torate. Université de Limoges, France (2003)

Chossat J.C.: Mesure de la Conductivité Hydraulique Dans les Sols - Choix des Méthodes, p. 720. Lavoisier, USA (2005)

Mc Lean, E.O.: pH and lime requirements. In: Page, A.L. et al. (eds.), Methods of Soil Analusis, Part 2, second ed., Agronomy, vol. 9, pp. 199–244.Soil Society of America, Madison, WI (1982)

Viani, A., Gualtieri, A., Artioli, G.: The nature of disorder in montmorillonite by simulation of X-ray powder patterns Note: Structural simulation model. Am. Mineral. **87**, 966–975) (15 de 001) (2002)

Preliminary Geochemical Results from Sediments of Pantelleria, Linosa, and Malta Basins (Sicily Channel)

Elisa Droghini, Enrico Dinelli, Federico Spagnoli, Mario Tramontana, Giuseppe Baldelli, and Giulio Pappafico

Abstract

The Sicily Channel is an NW–SE trending area characterized by three primary tectonic depressions (i.e., Pantelleria, Linosa, and Malta basins). Five gravity cores collected in these basins were studied. Through geochemical analyses, the main elements characterizing the sampled sediments were recognized. The normalized values of Ti and K allowed identifying some changes in sediment composition and potential source areas controlling the more recent sedimentation. These source areas were identified as the Pantelleria soil and rocks, Linosa rocks, Sicily stream sediments, Libyan soil and Saharan dust, which differently occur as control factors of the sedimentation in different sectors.

Keywords

Sediments • Geochemistry • Marine basins • Sicily channel

1 Introduction

The Sicily Channel is an NW–SE trending area (see Fig. 1) characterized by three primary tectonic depressions (Pantelleria, Linosa, and Malta Basins; Argnani 1990; Winnock and Wezel 1981), containing more than 1000 m thick Pliocene–Quaternary succession consisting of turbidites, pelagic/hemipelagic deposits, and "volcano-derived materials". The Sicily Channel belongs to the African Plate and represents the foreland of the Sicilian Sector of the Apennine-Maghrebian fold-thrust belt. The Pantelleria, Linosa, and Malta basins represent deep basins (Boccaletti et al. 1987) where fine-grained deposits prevail. Frequent failures on slope deposits acted as the primary source for turbidite deposition (Colantoni et al. 1993). This paper aims to present preliminary data on geochemical features of upper Pleistocene *p.p.*-Holocene. Sediments of Pantelleria, Linosa, and Malta basins were analyzed also in order to identify different sedimentary source areas.

2 Materials and Methods

Fifty-five samples from gravity cores (see Fig. 1) collected during the BS 80, and BS 81 cruises, carried out by the Urbino University in the Sicily Channel were studied. We applied X-ray fluorescence analysis (XRF) to obtain qualitative and quantitative information on the sediment's chemical composition, identifying major and trace elements. Major and trace element analyses were performed by X-ray fluorescence (XRF) spectrometry using an AXIOS 4000 PANalytical spectrometer. Major elements were determined on fused glass disks. While for trace elements pressed powder pellets have been used (Spagnoli et al. 2014).

E. Droghini (✉) · M. Tramontana · G. Baldelli · G. Pappafico
Department of Pure and Applied Sciences (DiSPeA), University of Urbino Carlo Bo, Campus Scientifico E. Mattei, 61029 Urbino, Italy
e-mail: e.droghini@campus.uniurb.it

E. Dinelli
Department of Biological, Geological, and Environmental Sciences, University of Bologna, Sant'Alberto, 163, 48100 Ravenna, Italy

F. Spagnoli
Institute of Biological Resources and Marine Biotechnology (IRBIM), National Research Council (CNR), Largo Fiera della Pesca, 2, 60125 Ancona, Italy

M. Tramontana
CoNISMa, Consorzio Nazionale Interuniversitario Per le Scienze del Mare, Piazzale fv, 9, 00196 Roma, Italy

A. Çiner et al. (eds.), *Recent Research on Geomorphology, Sedimentology, Marine Geosciences and Geochemistry*, Advances in Science, Technology & Innovation, https://doi.org/10.1007/978-3-030-72547-1_60

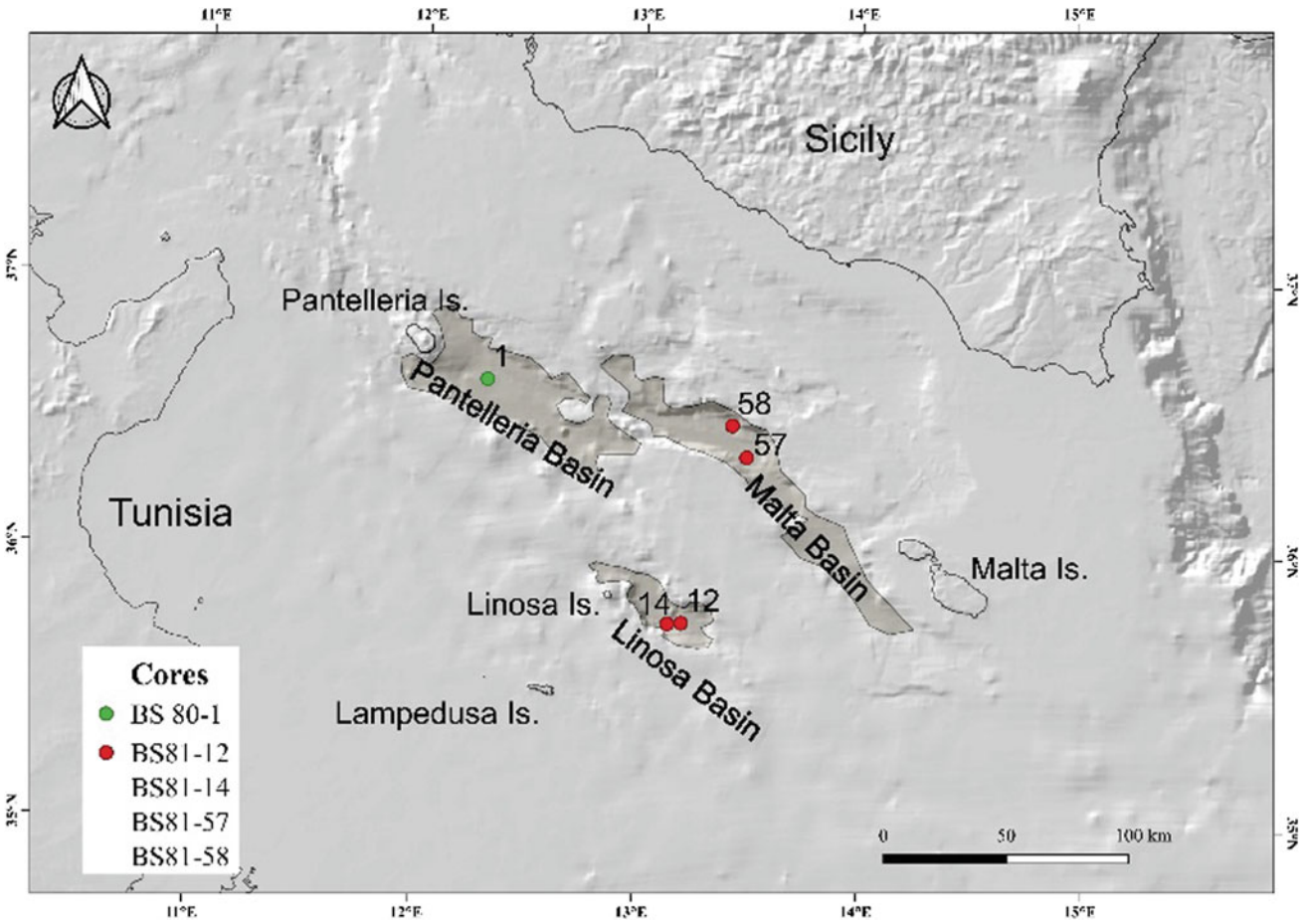

Fig. 1 Map of the Sicily Channel showing the location of studied sediment cores

3 Results

The cores are mainly composed of muds (clay and silty-clay) with subordinate thin sandy and silty beds. The coarser fractions are represented by sediments of volcanic and/or biogenic origin. The relatively highest sandy content was found in the two cores collected in the Linosa Basin. The sampled sediments display a variety of sedimentary structures related to turbidite sedimentation. In some cases, dm-thick horizons of slump deposits were recognized. The geochemistry shows a generally homogeneous composition with the presence of localized mutual proportions of elements linked to carbonate or silicate minerals. Levels with high amounts of Ti, Ba, and Sr or Ca and Mg were recognized in the different basins.

4 Discussion

The use of Ti/Al and K/Al is typical in geochemical studies in the Mediterranean area as they could be representative of differences in source areas. Besides, some authors (Wu et al. 2016; Figlia et al. 2007) identified possible source areas in the studied sector. The application of Ti/Al and K/Al ratios to our cores (see Fig. 2) points out some differences related to distinct types of sediments and their possible origin areas. At present, no data about the distribution between turbidite and non-turbidite facies are available, but some differences in turbidites can be unquestionably related to their provenance from different margins of the basins. The core BS80-1 (Pantelleria Basin) shows a tendency toward higher K/Al and lower Ti/Al,

Fig. 2 Plot of Ti/Al versus K/Al. Potential source areas are shown. Libyan Soil data deduced from Wu et al. (2016); Pantelleria rocks and soils from Figlia et al. (2007); Linosa rocks data from Peccerillo (2005); data of Saharan dust from Krom et al. (1999)

comparable to the mean values of Sicily stream sediments (see Fig. 2) and Pantelleria soils suggesting their origin from these areas. A different geochemical composition characterizes the cores BS81-57 and 58 (Malta Basin) (see Fig. 2). The core BS 81–57 shows a tendency toward lower values of Ti/Al and higher values of K/Al. Instead, the core BS 81–58 shows low values of K/Al and higher values of Ti/Al. This difference is ascribed to diversified sediment source areas. The sediments of the core BS81-57 are supplied mainly by Pantelleria soil, Libyan soil and Sicily stream sediments, while the sediments of the core BS81-58 are related only to Sicily stream sediments.

The K/AL and Ti/Al relationships for cores BS81-12 and 14 (Linosa Basin) show an evident influence of the Linosa rocks. This is more marked for the coarser beds. Instead, the sediments of the core BS81-12 are also from Saharian dust and Linosa rocks other than another source that has not still identified. Finally, the sediments of the core BS81-14 show values very close to the Linosa rocks.

5 Conclusions

The preliminary data obtained from the sediment cores collected in the Pantelleria, Linosa, and Malta basins highlight the importance of geochemical investigations to infer different sediment source regions that feed separate basins and depositional zones. Future more detailed investigations will allow to better identify the relative importance of different source areas and sedimentological processes controlling the deposition in the Pantelleria, Linosa, and Malta Basins.

References

Argnani, A.: The Strait of Sicily rift-zone, foreland deformation related to the evolution of a back-arc basin. In: Danobeitia, J.J., Pinet B. (eds.), Geophysics of the Mediterranean Basin. Journal of Geodynamics, vol. 12, pp. 311–331 (1990)

Boccaletti, M., Cello, G., Tortorici, L.: Transtensional tectonics in the sicily channel. J. Struct. Geol. **9**, 869–876 (1987)

Colantoni, P., Tramontana, M., Alberini, C.: Some notes on recent turbiditic sedimentation in the Pantelleria Basin (Sicily Channel). UNESCO Rep. Mar. Sci. **58**, 147–152 (1993)

Di Figlia, M.G., Bellanca, A., Neri, R., Stefansson, A.: Chemical weathering of volcanic rocks at the island of Pantelleria, Italy: Information from soil profile and soil solution investigations. Chem. Geol. **246**(1–2), 1–18 (2007)

Krom, M.D., Cliff, R.A., Eijsink, L.M., Herut, B., Chester, R.: The characterisation of Saharan dusts and Nile particulate matter in surface sediments from the Levantine basin using Sr isotopes. Mar. Geol. **155**, 319–330 (1999)

Peccerillo, A.: Plio-Quaternary Volcanism in Italy. Petrology, Geochemistry, Geodynamics (2005).

Spagnoli, F., Dinelli, E., Giordano, P., Marcaccio, M., Zaffagnini, F., Frascari, F.: Sedimentological, biogeochemical and mineralogical facies of Northern and Central Western Adriatic Sea. J. Mar. Syst. **139**, 183–203 (2014). https://doi.org/10.1016/j.jmarsys.2014.05.021

http://weppi.gtk.fi/publ/foregsatlas/ForegsData.php

Winnock, E.: Structure du bloc palagien. In: Wezel, F.C. (ed.) Sedimentary basins of Mediterranean Margins, pp. 445–464. C.N.R. Project of Oceanography, Bologna (1981)

Wu, J., Böning, P., Pahnke, K., Tachikawa, K., de Lange, G.J.: Unraveling north-African riverine and aeolian contributions to central Mediterranean sediments during Holocene sapropel S1 formation. Quat. Sci. Rev. **152**, 31–48 (2016)

Can the High Subcritical Water Contribute to Explain the Neoproterozoic BIFs?

Marie-Paule Bassez

Abstract

The banded iron formations of the Precambrian rocks located in the Arabian-Nubian shield (ANS) yield Neoproterozoic ages. Their origin is still questionable. The present study attempts to consider the interaction of anoxic alkaline water in the high subcritical domain with ferrous silicate rocks, at the origin of the Neoproterozoic BIFs. The model is based on the same kind of interaction that was proposed to explain the minerals observed in the BIFs of the Archean to very early Proterozoic eras, in Western Australia and South Africa. The anoxic water arises from the dehydrated rocks located along a subducted zone and leads to BIFs in a forearc basin.

Keywords

Banded iron formations • Arabian-Nubian shield • Anoxic oxidation of ferrous iron

1 Introduction: Formation of Ferric Iron in Archean BIFs

In Bassez (2013), it was shown for the first time that the domain of liquid water called high subcritical, hsubc, can induce the anoxic alkaline oxidation of ferrous iron and the oxidation of ferrous silicates into ferric minerals. The properties of hsubc water are ~300–350 °C for the temperature, ~10–25 MPa (and higher) for the pressure, and ~700–600 kg/m^3 for the density (ρ). Results in Bassez (2013–2019b) show that in these conditions of T, P and ρ, ferrous silicates dissolve and lead to the formation of the ferric minerals observed in the Archean BIFs in the absence of UV light, oxygen and microorganisms, as illustrated in Fig. 1. The chemical Eq. (1) are proposed for the reduction of H^+ and the oxidation of Fe^{2+} in anoxic alkaline hsubc water.

$$\begin{aligned} &Fe^{II}(OH)_{3\ diss}^{-} + H_2O_{hsubc} \rightarrow Fe^{III}(OH)_{4\ diss}^{-} + 1/2H_{2\,diss}\ \ pH\,9.5-14 \\ &Fe^{2+} + H_2O_{hsubc} \rightarrow Fe^{3+} + 1/2H_{2\,diss} + OH^- \end{aligned} \quad (1)$$

2 Methods

The method is a composition, first, of thermodynamic calculations on hydrolyses and carbonations conducted on 13 elementary reactions of the serpentinization reaction, second, of theoretical studies of E-pH and solubility published diagrams, third, of Raman spectroscopic studies of Archean rocks drilled in banded iron formations, BIFs, and fourth, of published data on minerals observed in the Neoproterozoic iron formations, NIFs.

3 Preliminary Results on NIFs of the Arabian-Nubian Shield

Thirteen Neoproterozoic iron formations are observed in the Central Eastern Desert, CED, of Egypt (El Shazly and Khalil 2016 and refs herein) and one in the geological equivalent terrain of Northern Western Saoudi Arabia (Stern et al. 2013). Their geological environments are widely studied and presented in a very recent compilation (Hamimi et al. 2020). Discrepancies can be noticed in the ages of the NIFs. However, authors seem to consider 750 Ma as average. The iron formations are interbedded with metavolcanic and ophiolite rocks both also dated around 750 Ma. This age does not coincide with the Sturtian glaciation occurring from 717 to 660 Ma (Rooney et al. 2015). The NIFs include quartz, hematite, magnetite, goethite, lepidocrocite,

M.-P. Bassez (✉)
University of Strasbourg, Frontier Research in Chemistry, 67000 Strasbourg, France
e-mail: marie-paule.bassez@unistra.fr

A. Çiner et al. (eds.), *Recent Research on Geomorphology, Sedimentology, Marine Geosciences and Geochemistry*, Advances in Science, Technology & Innovation, https://doi.org/10.1007/978-3-030-72547-1_62

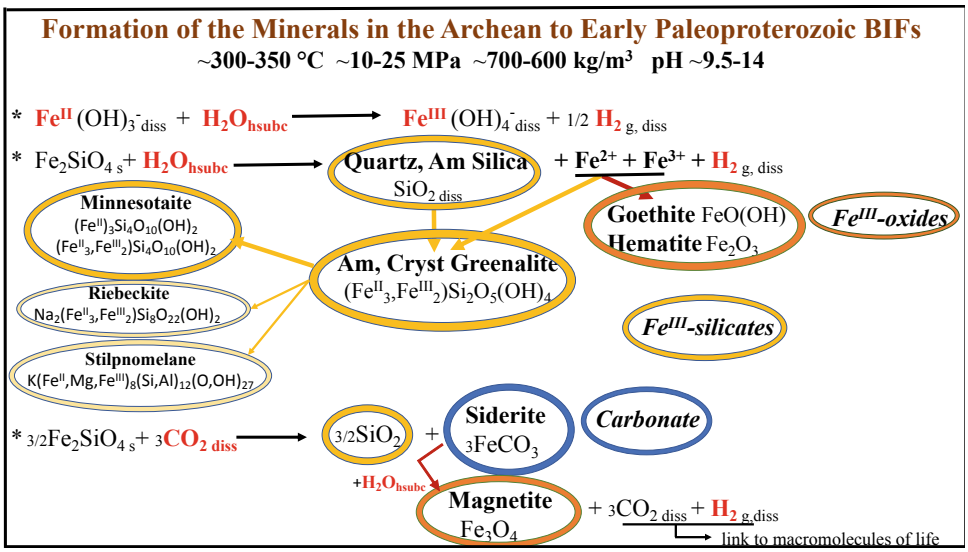

Fig. 1 A possible formation of ferric minerals in the absence of UV light, oxygen and microorganisms. Colours are as follows: brown: silicates; rusty red: ferric oxides; blue: carbonate. This figure is published in Bassez (2019b) and is an extended version of Fig. 1 in Bassez (2018)

greenalite and stilpnomelane. The CED is proposed to form above a subduction zone. Paleogeographic maps for the deconstruction of Rodinia by a superplume and the related construction of Gwondana were described between 825 and 540 Ma (Li et al. 2013, 2008 herein). Both versions show maps at 750 Ma with Arabia and Nubia which are separated and located near an active margin and above a superplume.

From the above assembly of data, I conclude that the oceanic crust may subduct underneath the continental crusts of Arabia and Nubia as shown in Fig. 2. Along the subducted zone, at various levels of depth, minerals dehydrate and let water escape and contribute to the formation of magmas and magmatic chambers leading to volcanic eruptions and hydrothermal venting. This water, which is anoxic, can reach temperature and pressure of the high subcritical domain within approximately 1–5 km depth, as calculated in Bassez (2019b), depending on the hydrostatic pressure of the oceanic column, the porosity of the upper crust and the glaciation period. Interaction with a block of alkaline fayalite Fe_2SiO_4 and/or ferrosilite $FeSiO_3$ may occur inside pores, cavities and channels. A kind of magmatic-hydrothermal reaction chamber can be created.

The hydrothermal chambers fill and discharge, allowing the low-density water to escape through conduits with the synthesized amorphous and crystallized ferrous-ferric oxides and silicates and also with ferrous carbonates if CO_2 is present. Products deposit by gravity on the bottom of the ocean and form the BIFs. Layers of minerals are the consequence of the size of the reaction chambers which require filling before the next discharge, thus creating a rhythm in the deposit.

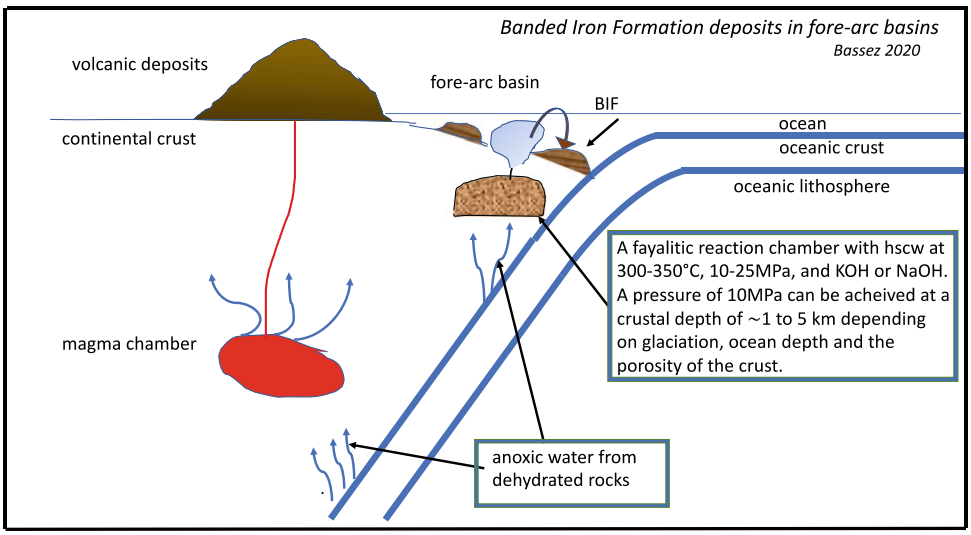

Fig. 2 Anoxic water from rocks in the process of dehydration along a subduction zone, at the origin of the formation of NIFs and volcanic rocks

4 Conclusions

The interaction of anoxic alkaline water in the high subcritical domain, with rocks containing Fe^{II}-silicates, allows the formation of ferric minerals in the absence of UV light, oxygen and microorganisms, and may explain the presence of the ferric minerals which are observed in the Archean to Paleoproterozoic rocks of the banded iron formations such as those of the Pilbara craton in Western Australia and the Kaapvaal craton in South Africa (Bassez 2018, 2019b). This interaction seems also an appropriate hypothesis for the explanation of the Neoproterozoic banded iron formations, such as those observed in the Arabian-Nubian Shield, considering that the rocks which dehydrate along a subduction zone, produce anoxic water.

Acknowledgements Dr. Jonathan Naden, British Geological Survey, Keyworth, UK, is warmly acknowledged for discussions on the crustal porosity of the Earth.

References

Bassez, M.-P.: Geochemical origin of biological molecules. In: Geophysical Research Abstracts 2013, vol. 15, EGU2013-22. EGU'2013, PS8.1, Oral 9 Ap.2013, Vienna, Austr (2013)

Bassez, M.-P.: Water, air, earth and cosmic radiation. Orig. Life Evol. Biosph. **45**(1), 5–13 (2015). https://doi.org/10.1007/s11084-015-9402-0

Bassez, M.-P.: Geobiotropy. In: Proceedings of 47th Lunar Planetary Science Conference 2016, Abstract #1853. Session 804, The Woodlands, TX, USA, 21–25 March 2016

Bassez, M.-P.: Anoxic and oxic oxidation of rocks containing Fe(II) Mg-silicates and Fe(II)-monosulfides as source of Fe(III)-minerals and hydrogen. Geobiotropy. Orig. Life Evol. Biosph. **47**(4), 453–480 (2017a). https://doi.org/10.1007/s11084-017-9534-5

Bassez, M.-P.: Ferromagnesian silicate and ferrosulfide rocks as a source of magnetite and hydrogen. Proc. Earth Planet. Sci. WRI-15 2017, **17**, 492–495 (2017b). https://doi.org/10.1016/j.proeps.2016.12.124

Bassez, M.-P.: Water near its supercritical point and at alkaline pH for the production of ferric oxides and silicates in anoxic conditions. A new hypothesis for the synthesis of minerals observed in banded iron formations and for the related geobiotropic chemistry inside fluid inclusions. Orig. Life Evol. Biosph. **48**(3), 289–320 (2018). https://doi.org/10.1007/s11084-018-9560-y

Bassez, M.-P.: High subcritical water–rock interaction for the formation of ferric minerals, in the absence of oxygen, UV light and microorganisms. In: Proceedings of the EDP-Science, E3S Web of Conference, WRI-16 2019, Tomsk, Russia, 21–26 July 2019a

Bassez, M.-P.: Follow the high subcritical water. Geosciences **9**(6), 249, (2019b). https://doi.org/10.3390/geosciences9060249

El Shazly, K.A., Khalil, I.K.: Metamorphic and geochronologic constraints on the tectonic evolution of the Central Eastern Desert of Egypt. Precambr. Res. **283**, 144–168 (2016). https://doi.org/10.1016/j.precamres.2016.07.016

Hamimi, Z., et al. (eds.): The Geology of Egypt. Springer (2020). https://doi.org/10.1007/978-3-030-15265-9

Li, Z.X., Evans, A.D.D., Halverson, P.G.: Neoproterozoic glaciations in a revised global paleogeography from the breakup of Rodinia to the assembly of Gondwanaland. Sed. Geol. **294**, 219–232 (2013). https://doi.org/10.1016/j.sedgeo.2013.05.016

Rooney, D.A., Strauss, V.J., Brandon, D.A., Macdonald, A.F.: A Cryogenian chronology: two long-lasting synchronous Neoproterozoic glaciations. Geology **43**(5), 459–462 (2015). https://doi.org/10.1130/G36511.1

Stern, J.R., Mukherjee, K.S., Miller, R.N., Ali, K., Johnson, R.P.: ~750Ma banded iron formation from the Arabian-Nubian Shield. Precambr. Res. **239**, 79–94 (2013). https://doi.org/10.1016/j.precamres.2013.07.015

Mineralogy and Petrography of Palaeocene Limestones of the Ewekoro Formation, Dahomey (Benin) Basin, Nigeria

Taiwo Bolaji, Ajibola Oyebamiji, Otobong Ndukwe, and Racheal Akinpelu

Abstract

Palaeocene limestone strata freshly exposed by quarry activities at the Dangote Cement Ibese, Nigeria, were examined and sampled. The recovered samples were subjected to qualitative lithologic description, X-ray diffraction (XRD) analyses and thin-section petrography in order to determine the mineralogical characteristics and carbonate microfacies. Results show that calcite dominates the mineralogy. Three (3) carbonate microfacies identified from petrographic observations are wackestone, packstone and mudstone. Various diagenetic processes such as cementation, neomorphism, micritization and compaction have affected the limestone unit. The results obtained suggest that the studied limestones are deposited in a shallow marine environment and are considered suitable for cement production.

Keywords

Limestone • Palaeocene • Microfacies • Mineralogy • Dahomey basin

1 Introduction

The limestones of the Ewekoro formation are an essential resource, which has contributed significantly to the Nigerian economy. It has been mined for cement production years, but most of the previous studies were carried out on core samples which rarely consider the aspects of limestone diagenesis. Paleocene carbonate strata of the Ewekoro formation exposed by quarry activities at the Ibese area of the Dahomey basin were studied. This study aims to determine the mineralogical characteristics of the limestones and microfacies features to understand the associated diagenetic processes to which the rocks were subjected. The combination of limestone mineralogy, geochemistry and petrography is useful to infer the depositional environment of a sedimentary basin (Armstrong-Altrin et al. 2003, 2011).

2 Geology and Stratigraphy of Dahomey Basin

Dahomey (Benin) basin is one of the many marginal basins formed along the coasts of Africa and Brazil following the opening of the South Atlantic. The basin was described as a marginal sag or pull-apart basin, which developed in the Mesozoic as a result of the drifting of the African and South American plate (Whiteman 1982). The Nigerian sector of the basin extends from the boundary between the Benin Republic and Nigeria to Benin hinge line consisting of an arcuate belt roughly parallel to the coastline (Fig. 1) (Billman 1992; Whiteman 1982). It is a great wedge of Cretaceous to recent sediments lying unconformably on the crystalline basement complex.

The Cretaceous Abeokuta group is sub-divided into three formations: Ise, Afowo and Araromi formations (Omatsola and Adegoke 1981), while the Palaeogene-Neogene sediments (Oluwajana et al. 2018; Bolaji et al. 2020) conformably overlie the Abeokuta group which consists of the Ewekoro, Akinbo, Oshosun, Ilaro and Benin formations. Ewekoro formation is made up of thick fossiliferous limestone, while Akinbo and Oshosun formations are made up of flaggy grey and black shales, with glauconitic bands and phosphatic beds, which define the boundary between the Ewekoro and Akinbo formations (Bolaji et al. 2020).

T. Bolaji (✉) · A. Oyebamiji · O. Ndukwe · R. Akinpelu
Department of Geology, Federal University Oye Ekiti, Oye, Nigeria
e-mail: taiwo.bolaji@fuoye.edu.ng

A. Çiner et al. (eds.), *Recent Research on Geomorphology, Sedimentology, Marine Geosciences and Geochemistry*, Advances in Science, Technology & Innovation, https://doi.org/10.1007/978-3-030-72547-1_63

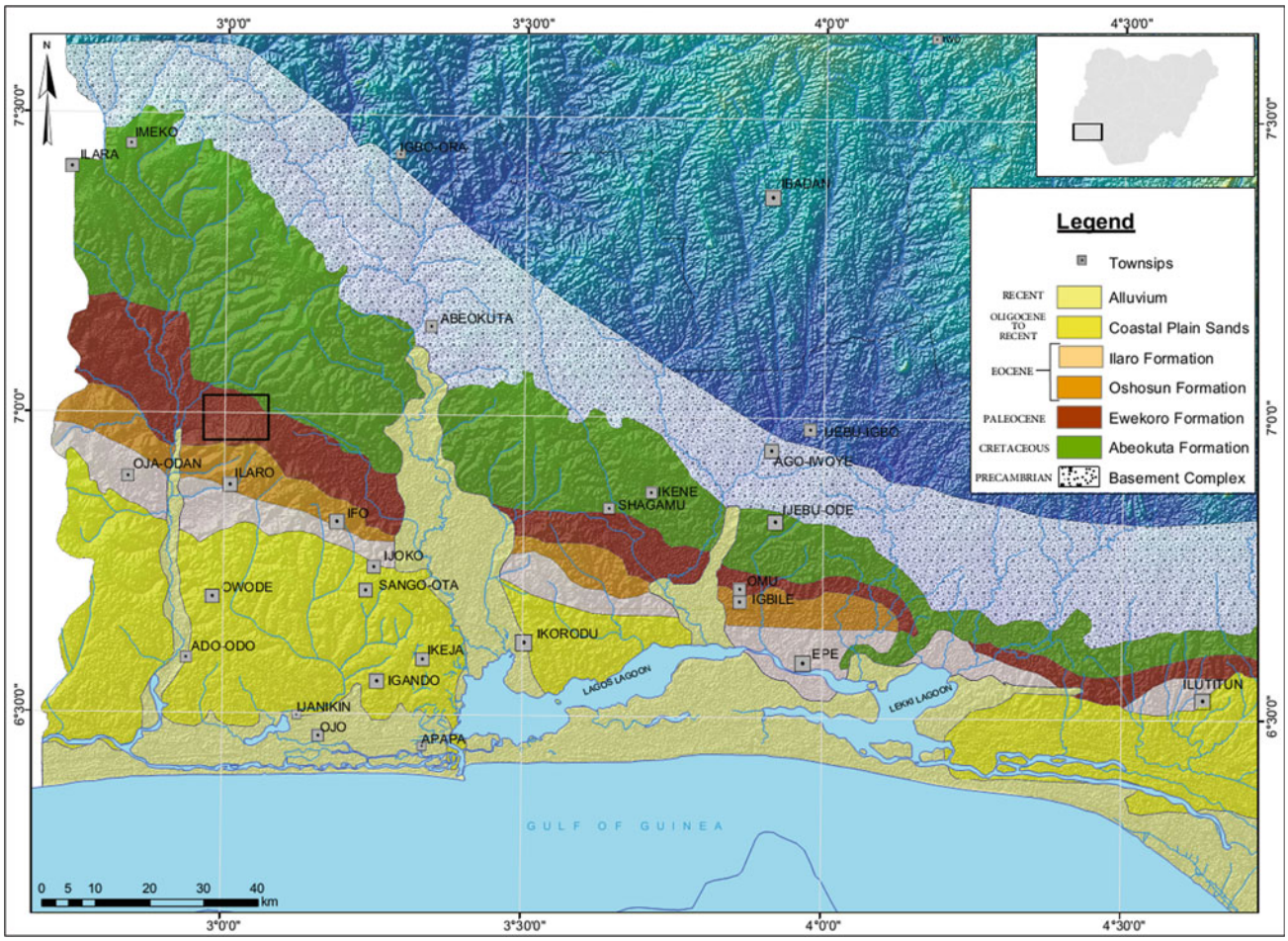

Fig. 1 Study area shown on the geological map of the Eastern Benin (Dahomey) Basin (Bolaji et al. 2020)

3 Materials and Methods

In the area, field mapping was carried out within the Ibese quarry. The rocks were examined in their respective locations with geologically significant observations of their features recorded. Eight samples recovered from the freshly exposed section of the Ewekoro formation were examined by X-ray diffraction (XRD) and thin section petrography. Modal estimates were made under the polarizing microscope.

4 Results

4.1 Geochemistry and Mineralogy

X-ray diffraction (XRD) analyses on selected samples revealed that the mineralogical composition is predominantly calcitic (calcite >97%), with minor phases of quartz, dolomite, and lizardite (Fig. 2). Calcite ranges from 97.39 to 99.57%, while quartz and dolomite range between 0.37–0.43% and 0–1.56%, respectively. Lizardite (0.63%) was reported in one of the samples.

4.2 Petrography

A megascopic examination of the limestone sections reveals that they are whitish to greyish in colour and fossiliferous. The limestone framework was evaluated using petrological studies of thin sections, which revealed the relative abundance of allochems, micrites, and sparry cement. The allochems constitute the dominant rock fabric. Sparry calcite cement is next in abundance, followed by micrite and thinly present ferruginous fragments. In most of the thin sections studied, the allochems are generally elongated and poorly sorted. Some of the limestones contain detrital quartz grains. The fossils are mostly shell fragments of molluscs (gastropods and bivalves), some of which have recrystallized to

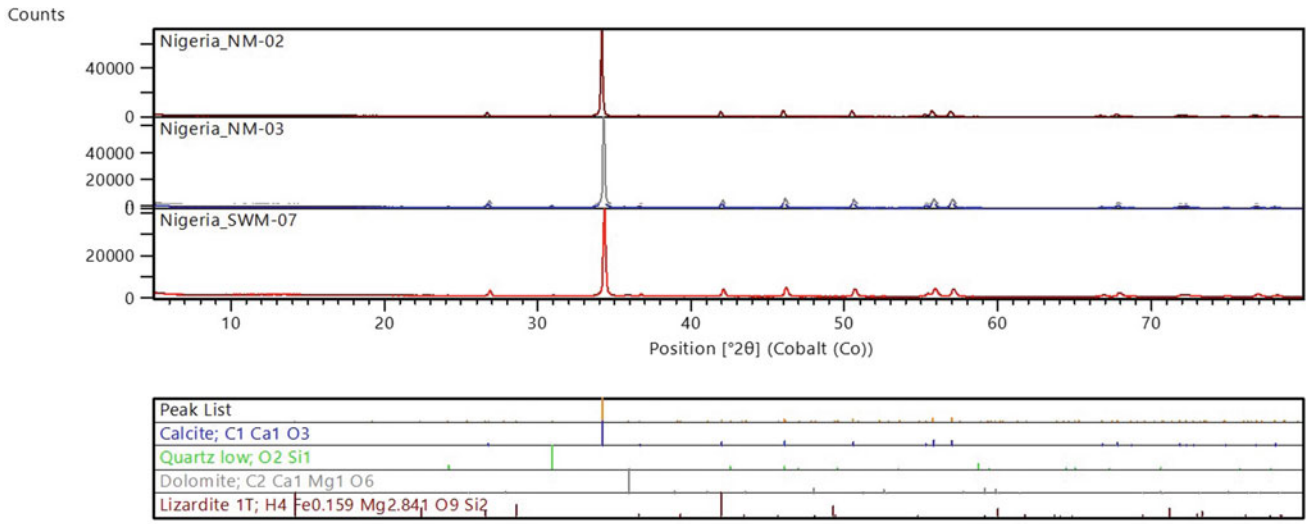

Fig. 2 Representative XRD patterns of the studied limestone samples

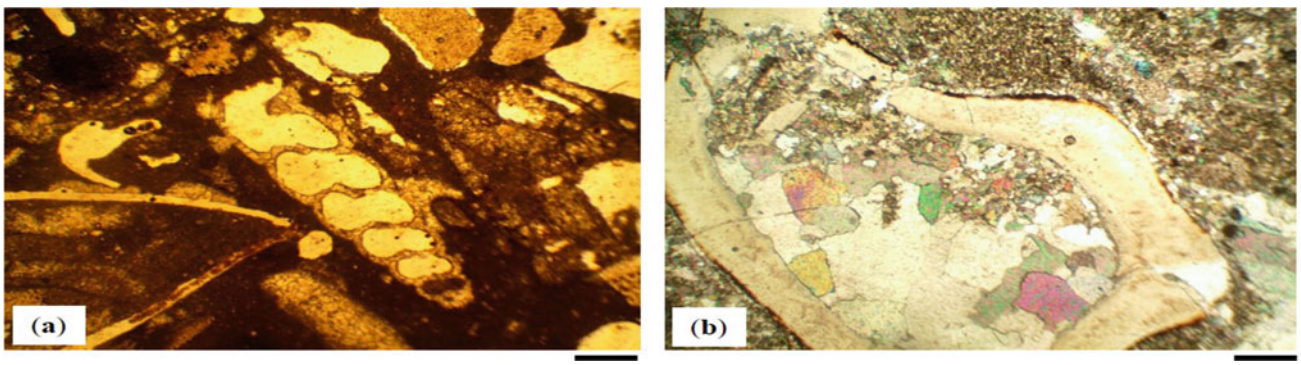

Fig. 3 Photomicrograph showing **a** Packstone, grain-supported. Gastropod, ostracod bioclast, bivalve and fossil fragments **b** Wackestone. Bioclast filled with neomorphic spar. Micritic envelope observed around the bioclast, showing evidence of compaction

calcite. The majority of the limestone samples studied are mud-supported, but grain-supported texture is also present. Microfacies of the former type are classified as wackestone, whereas those of the latter are known as packstone due to the presence micrite mud matrix (Fig. 3).

5 Discussion

The mineralogical composition reveals that the limestones in the study area are of dominantly calcite limestones. Based on field and laboratory evidence, wackestone, packstone and mudstone were the dominant microfacies observed. The fossils contain some nucleus of calcitic replacement or recrystallization of fossils shells (Fig. 3), which is known as neomorphism (Oluwajana et al. 2018), which is the formation of new crystal forms on top of the initial limestones deposited. In some thin sections, bivalve fragments were observed to consist of equant calcite spars.

6 Conclusions

Petrographic studies reveal that these limestone samples are highly fossiliferous with the identified fossils indicating deposition in a shallow marine environment. From the abovementioned textural characteristics, three distinct microfacies were recognized in limestones based on allochem constituents and depositional textures. These microfacies are wackestone, packstone and mudstone. The diagenetic influences on the limestones include cementation, micritization, neomorphism and compaction.

References

Armstrong-Altrin, J.S., Madhavaraju, J., Lee, Y.I., Ramasamy, S.: Geochemistry of upper Miocene Kudankulam Limestones, Southern India. Int. Geol. Rev. **45**, 16–26 (2003)

Armstrong-Altrin, J.S., Madhavaraju, J., Sial, A.N., Kasper-Zubillaga, J.J., Nagarajan, R., Flores-Castro, K., Rodriguez, J.L.: Petrography and stable isotope geochemistry of the Cretaceous El Abra Limestones (Actopan), Mexico: implication on diagenesis. J. Geol. Soc. India **77**, 349–359 (2011)

Billman, H.G.: Offshore stratigraphy and paleontology of Dahomey embayment, West Africa. NAPE Bull. **7**(21), 121–130 (1992)

Bolaji, T.A., Ndukwe, O.S., Oyebamiji, A.R., Ikegwuonu, O.N.: Palynological age control and paleoenvironments of the Paleogene strata in Eastern Dahomey Basin Southwestern Nigeria. Sci. Rep. **10**(1), (2020). https://doi.org/10.1038/s41598-020-65462-7

Oluwajana O.A., Ehinola, O.A., Ofiwe, C.U., Akhayere, E., Egunjobi, K.J., Asanbe, J., Akinjo, O.: Microfacies analysis and geochemical evaluation of Campanian-Maastrichtian limestone along the benin flank, Southwestern Nigeria. In: Doronzo, D., Schingaro, E., Armstrong-Altrin, J., Zoheir, B. (eds.) Petrogenesis and Exploration of the Earth's Interior. Advances in Science, Technology & Innovation (IEREK Interdisciplinary Series for Sustainable Development). Chapter 20, pp. 85–87. Springer, Cham (2018)

Omatsola, M.E., Adegoke, O.S.: Tectonic evolution and Cretaceous stratigraphy of the Dahomey Basin. J. Mining Geol. **18**, 130–137 (1981)

Whiteman, A.J.: Nigeria, Its Petroleum Geology, Resources and Potential. Graham and Trottan, London (1982)

Geochemical Analysis for Evaluating the Climatic Controls on the Depositional Environment of the Siliciclastic Miocene–Pliocene Sequence at Al-Rehaili Area, Northern Jeddah, Saudi Arabia

Faisal Alqahtani and Mohammed Khalil

Abstract

Geochemical data and their various approaches are useful to evaluate the climatic controls on the depositional environments. The sandstone layers of the siliciclastics are intercalated within the Miocene–Pliocene siliciclastic sequence and are overlain by Harrat Rahat Basalt et al. Rehaili area, north of Jeddah. These sandstone samples were geochemically and petrographically examined to determine (1) the chemical and mineralogical changes, (2) paleo-weathering, and (3) climate and the depositional environments using major oxides and trace elements chemical analysis. The results of this analysis were plotted on binary and ternary diagrams to achieve the goal of this study. This study reveals that the examined sandstones were deposited on areas close to the coastal plain of the Red Sea and suffered from weak to intermediate chemical weathering and intense physical induration under semi-arid to semi-humid climatic conditions in a non-marine (fluvial/alluvial-lacustrine) environment.

Keywords

Geochemistry • Paleo-weathering • Climate control • Fluvial deposits • Al-Rehaili area

F. Alqahtani (✉) · M. Khalil
Faculty of Earth Sciences, King Abdulaziz University, Jeddah, Saudi Arabia
e-mail: falqahtani@kau.edu.sa

M. Khalil
University of Asyut, Asyut, Egypt

1 Introduction

The Miocene–Pliocene siliciclastic successions exposed in numerous scattered regions alongside the coastline plain of the Red Sea, especially in the northeastern part of Jeddah et al. Rehaili area. However, very few studies have been conducted to study the lithology and depositional environments of these deposits (e.g., Ghandour and AL-Washmi 2013; Alqahtani and Khalil 2015, 2019). Besides, no studies completed on evaluating the factors that control the formation and deposition of these deposits using geochemical analysis. The present study aims to evaluate the main controlling factors such as climate, tectonic on the depositional environments of Miocene–Pliocene succession (Bathan formation) exposed et al. Rehaili area using geochemical data.

2 Geologic Setting, Data, and Methodology

The study area is located in the northeastern part of Jeddah et al. Rehaili area, a few kilometers (ca. 35 km) from the Red Sea. It lies between latitudes 21° 15′ 00″ N and 21° 45′ 00″ and longitude 39° 45′ 00″ E and 40° 15′ 00″ (Fig. 1). The Red Sea is a rift basin, and the successions within this rift were divided into two main subdivisions. (1) pre-rift deposits which are characterized by inland/fluvial siliciclastic beds, where the oldest strata are found close to Jeddah (40 km in the north) at Salman Gulf, and (2) syn-rift deposits, which are characterized by thick evaporite-siliciclastic units (Schmidt and Hadley 1984). Fifteen columnar sections were created, described, measured, and sampled covering the four exposures et al. Rehaili area (Fig. 2). These columnar sections were correlated throughout the study area by lateral tracing, soil horizons, and the pronounced erosional surfaces. Besides, several sedimentary facies were identified and described based on their lithology and petrography (Fig. 3). Furthermore, seventeen samples

A. Çiner et al. (eds.), *Recent Research on Geomorphology, Sedimentology, Marine Geosciences and Geochemistry*, Advances in Science, Technology & Innovation, https://doi.org/10.1007/978-3-030-72547-1_64

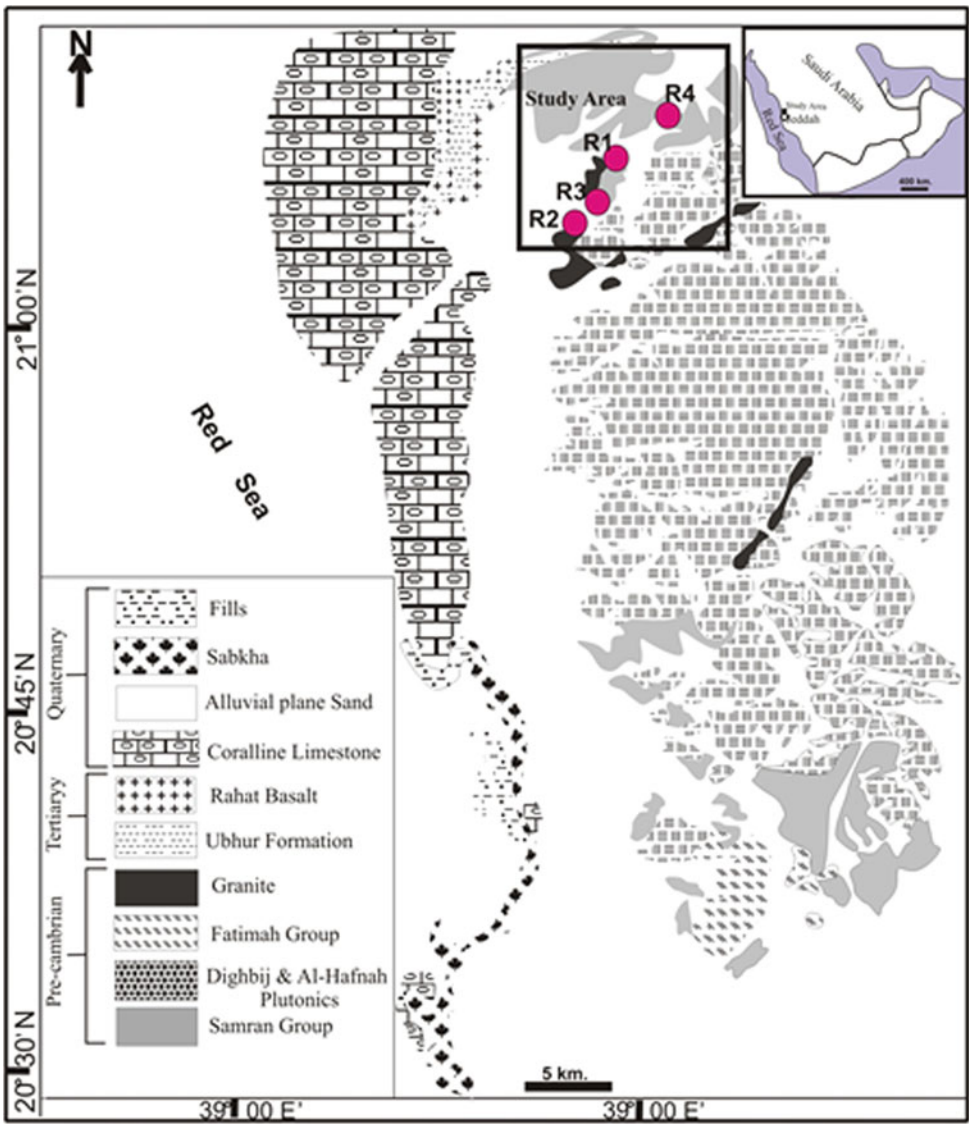

Fig. 1 A geological map of Al-Rehaili area, north of Jeddah

from different sandstone layers and units were selected to carry out the geochemical analysis as this study is focusing only on the sandstone samples taken from the siliciclastic sequence (Fig. 2). Several significant elements were determined using X-ray fluorescence spectrometry (XRF) and trace element analysis of inductively coupled plasma-mass spectrometry (ICP-MS). Eleven principal oxides elements, including SiO_2, Al_2O_3, CaO, Fe_2O_3, K_2O, MgO, MnO, Na_2O, P_2O_5, TiO_2, and SO_3, were evaluated. Twenty-nine trace elements including Ag, As, Ba, Be, Bi, Cd, Ce, Co, Cr, Cu, Ga, Ge, Hf, La, Li, Mo, Nb, and Ni. XRF identified pb, Rb, Sb, Sn, Sr, Ta, Th, U, V, W, Y, Zn, and Zr on ICP-MS. Primary elements data were in normalized proportions, and trace elements data were testified in parts per million (ppm).

3 Results

In the study area, some paleosol horizons were developed (Fig. 2). Thin section analysis for these paleosols at the base of the studied units were carried out. Figure 3 shows that paleosol consisted of fine-grained sandstone/siltstone facies. In addition, the quartz grains are well-sorted and sub-angular to sub-rounded (Fig. 3). Several researchers developed and used ternary diagram of Al_2O_3–(CaO + Na_2O)–K_2O to deduce degree of weathering (Bibi et al. 2019a, b; Iqbal et al. 2019; Jacobson et al. 2003). Figure 4 shows the ternary plot of the degree of weathering of the studied sandstones which ranges from weak to intermediate chemical weathering. The

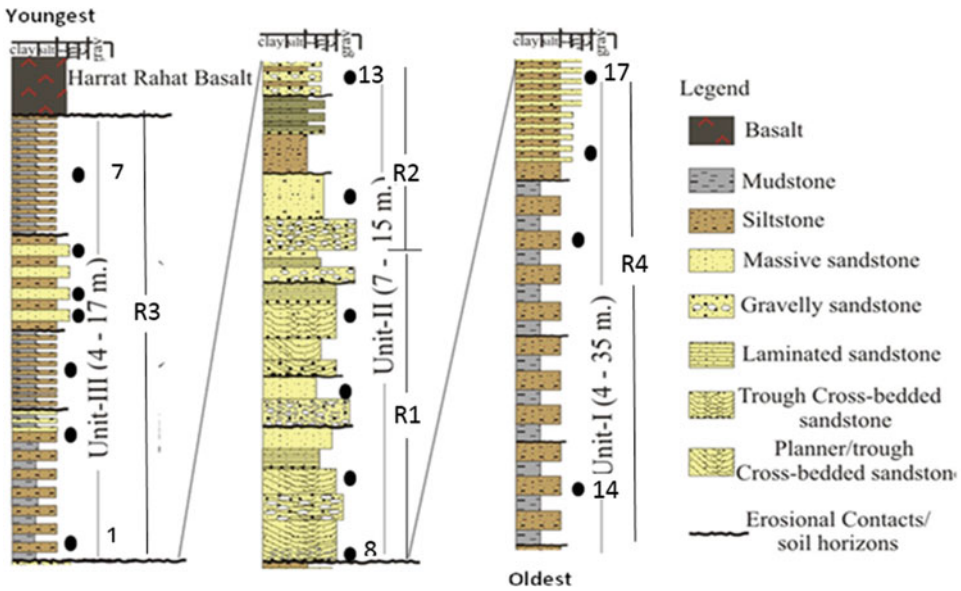

Fig. 2 A measured composite stratigraphic columnar section taken from R1, R2, R3, and R4 (in Fig. 1) showing the sandstone samples (black dots) taken for geochemical analysis (adopted from Alqahtani and Khalil 2015)

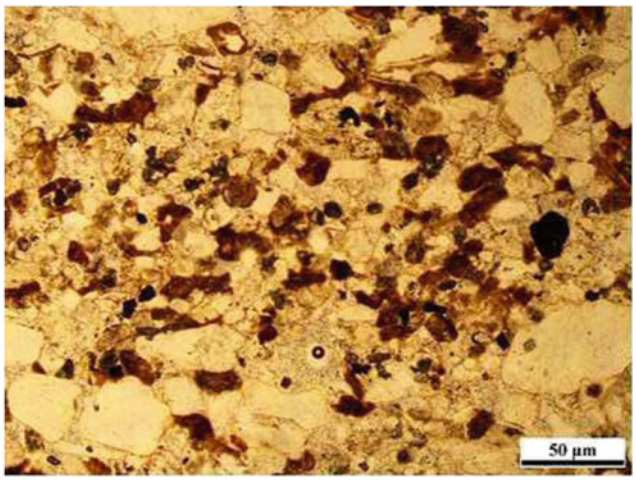

Fig. 3 Shows paleosol which consisted of fine-grained sandstone/siltstone facies. The quartz grains are well-sorted and sub-angular to sub-rounded

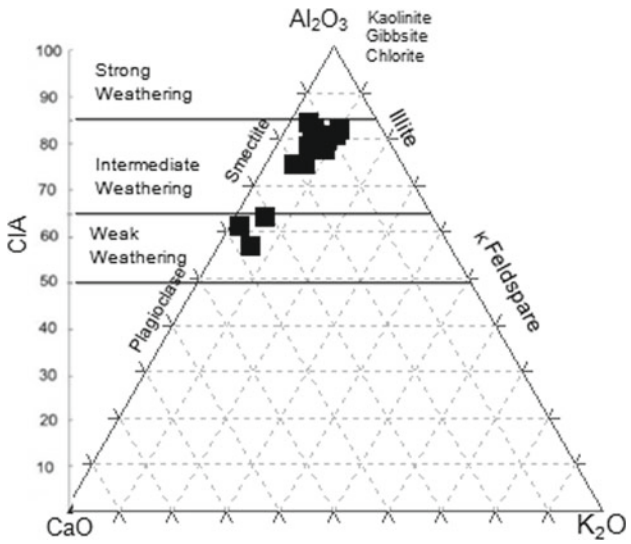

Fig. 4 Shows ternary diagram mineral composition and weathering

applicability of the ratios of $SiO_2/(Al_2O_3 + K_2O + Na_2O)$ for paleo-climatic condition during deposition of the sediments is well-recognized by many workers such as Jacobson et al. (2003). The binary diagram of SiO_2 against $(Al_2O_3 + K_2O + Na_2O)$ displays reasonable semi-arid to semi-humid climatic circumstances in the study area during the Miocene–Pliocene times (Madukwe et al. 2016; Fig. 5). In addition, the ternary diagram of $MgO–Fe_2O_3–(SiO_2/Al_2O_3)$ categorizes and separates the marine from non-marine and deltaic sandstones. This plot shows that all examined samples are plotted in the field of non-marine and deltaic sandstones (Fig. 6). Moreover, Ni/Co versus V/Cr binary plot shows that the examined sandstones deposited in a depositional environment that has oxic conditions (Fig. 7).

4 Discussion

Sedimentary rocks formed under different climatic conditions have variable geochemical characteristics. Many minerals from source rocks are usually destroyed during weathering, while chemically resistant minerals released from the decaying and disintegrating rock and accumulate as

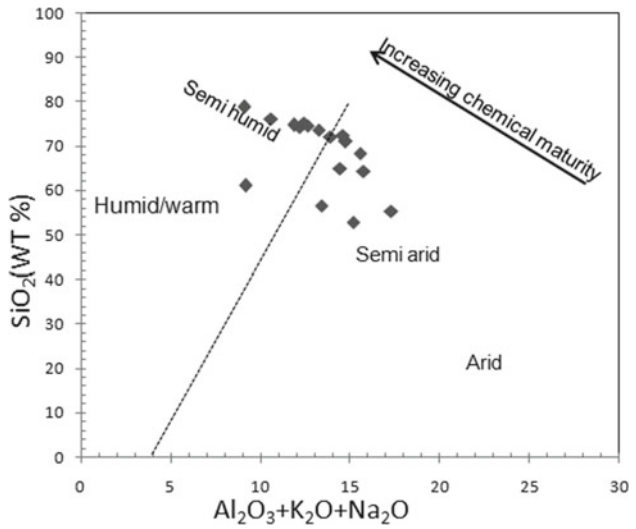

Fig. 5 Shows binary diagram of climatic variations

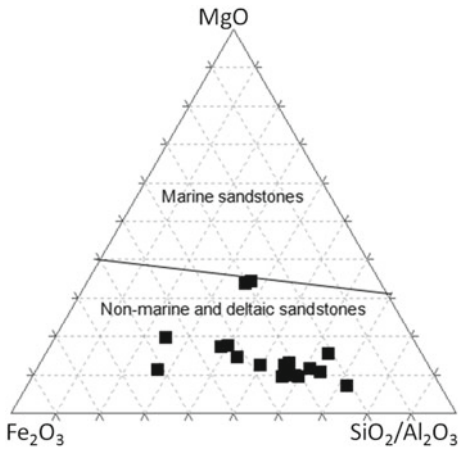

Fig. 6 Shows ternary discrimination diagram of depositional environments

residues. Throughout this process, new minerals such as ferric oxides and clay minerals may form in situ in the soils. Continental successions with multistory paleosols can also provide a continuous record of ancient climatic conditions and climatic changes through time (Taylor and McLennan 1989). The examined soils provide a continuous record of climatic fluctuations from semi-arid to semi-humid. Accordingly, soil composition controlled not only by the parent-rock composition but also by the nature, strength, and duration of weathering and soil-forming processes. Al_2O_3–(CaO)–K_2O plot indicates that the degree of weathering ranges from an intermediate to weak. Furthermore, SiO_2 against (Al_2O_3 + K_2O + Na_2O) plot displays reasonable semi-arid to semi-humid climatic circumstances in the study area during the Miocene–Pliocene times.

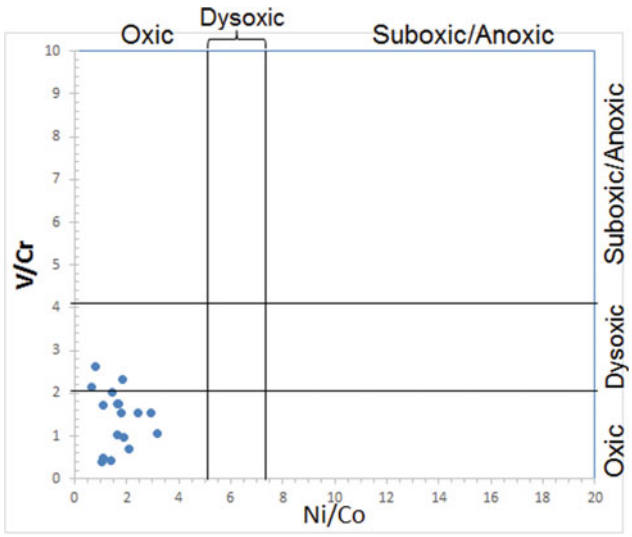

Fig. 7 Shows binary discrimination diagram of depositional environments

5 Conclusions

The siliciclastic succession of Miocene–Pliocene sequences et al. Rehaili area is interpreted to be deposited in a non-marine (fluvial/alluvial-lacustrine) environments. The climatic condition during the deposition of this sandstone is interpreted to be semi-arid to semi-humid.

References

Alqahtani, F.A., Khalil, M.: Depositional environments of the Miocene-Pliocene siliciclastic succession, Al Rehaili Area, North of Jeddah, Saudi Arabia. J. Geol. Soc. India **86**, 706–716 (2015)

Alqahtani, F.A., Khalil, M.: Geochemical analysis and tectonic evaluation of the Miocene–Pliocene sequenceat Al Rehaili area, Northern Jeddah, Saudi Arabia. Arab. J. Geosci. **12**, 323 (2019)

Bibi, M., Wagreich, M., Iqbal, S.: Regional sediment sources versus the Indus River system: The Plio-Pleistocene of the Peshawar basin (NW-Pakistan). Sed. Geol.https://doi.org/10.1016/j.sedgeo.2019.05.010)

Bibi, M., Wagreich, M., Iqbal, S., Gier, S., Jan, U.I.: Sedimentation and glaciations during the Pleistocene: Palaeoclimate reconstruction in the Peshawar basin, Pakistan. Geol. J. (2019b). https://doi.org/10.1002/gj.3445Iqbal

Ghandour, M., AL-Washmi, A.: Stratigraphic architecture of the fluvio-lacustrine deposits Bathan Formation, Al-Rehaili area, North Jeddah, Saudi Arabia. Arab. J. Geosci. **6** (2013)

Iqbal, S., Wagreich, M., Jan, I.U., Kuerschner, W.M., Gier, S.: Hot-house climate during the Triassic/Jurassic transition: the evidence of climate change from the southern hemisphere (Salt Range, Pakistan). Global Planet. Change **172**, 15–32 (2019)

Jacobson, A.D., Blum, J.D., Chamberlian, C.P., Craw, D., Koons, P.O.: Climate and tectonic controls on chemical weathering in the New Zealand Southern Alps. Geochim. Cosmochim Acta **37**, 29–46 (2003)

Madukwe, H.Y., Ayodele, S.O., Akinyemi, S.A., Adebayo, O.F.: Classification, maturity, provenance, tectonic setting, and source-area weathering of Ipole and Erin Ijesa stream sediments, South West Nigeria. Int. J. Adv. Sci. Tech. Res. **1**(6), 232–255 (2016)

Schmidt, D., Hadley, D.: Middle tertiary continental rift and evolution of the red sea in Southwestern Saudi Arabia. Saudi Arabian Deputy Ministry Mineral Resour. **56**, 3–6 (1984)

Taylor, S.R, McLennan, S.M.: The Continental Crust: Its Composition and Evolution. Geoscience Texts, Blackwell, Oxford, p. 312 (1989); Wrafter', J.P., Graham, J.R.: Short Paper: Ophiolitic detritus in the Ordovician sediments of South Mayo, Ireland. J. Geol. Soc. **146**, 213–215 (1985)

Short-Term Maturation of Clays in a Chlorinated Sodic Mineral Water (Ain Echfa, Tunisia)

Samir Mefteh and Mounir Medhioub

Abstract

This study aims to test the potential of some clay as a thermal mud by mineralogical and physicochemical characterization of clays matured for a short time in the laboratory using thermal waters of Ain Echfa of Korbous (north of Tunisia, Cap Bon). The results evidenced the interactions between the solid and the liquid phases. The mineralogical and physicochemical transformations were more pronounced for smectite than for illite-kaolinite samples. Additionally, an improvement in the cooling kinetics and a decrease in pH value were observed after the maturation process.

Keywords

Clays • Thermal muds • Maturation • Mineralogy • Interaction

1 Introduction

Thermal mud or peloid, from the Greek TTAOS (=mud), is defined by the International Society of Medical Hydrology as 'natural products constituted by a mix of mineral water and/or sea or salt lake water with organic or inorganic materials, resulting from geological actions and/or biological actions, used in therapy as local applications or baths'. Peloids should be considered as medicinal and/or cosmetic products and, therefore, must comply with several requirements (Gomes et al. 2013). In particular, as regards to safety attributes of these health care products, both the single components and final product (clay mineral—medicinal water suspension) must be conveniently controlled.

This study aims to understand the behaviour and the physical and chemical changes that affect clays during the maturation process. To this end, clays are brought in contact with thermal water during a short period of 7 days, and we used X-ray diffraction (XRD), chemical analysis (X-ray fluorescence) and physicochemical determinations (pH and kinetic cooling rate) for the characterization of these muds.

2 Materials and Methods

We set up a suitable experimental protocol at the laboratory, which consists in putting some clay in contact with the thermal water of Ain Echfa, Korbous, using a water bath designed and manufactured via separate compartments (Fig. 1).

The mineralogical composition was determined by X-ray powder diffraction (XRPD) using a Philips® X-Pert diffractometer with Cu Kα radiation. The chemical composition of major and trace element was determined using a spectrometer of the type BRUKER S4 Pioneer X-ray Fluorescence, equipped with an anode with X-rays Rh (60 kV, 150 my).

Five samples (R3, AYD3, CBLL4, JAD12 and GHM) were selected for a short-term maturation trial in the laboratory. The choice of these samples was based primarily on the nature of the raw materials with a large clay fraction (Table 1).

The maturation of these clays was carried out for a short time. In fact, the sampling was performed after 2 days and then after 7 days of contact with thermal waters.

S. Mefteh (✉) · M. Medhioub
Department of Geology, Faculty of Sciences of Sfax, 3018 Sfax, Tunisia

A. Çiner et al. (eds.), *Recent Research on Geomorphology, Sedimentology, Marine Geosciences and Geochemistry*, Advances in Science, Technology & Innovation, https://doi.org/10.1007/978-3-030-72547-1_65

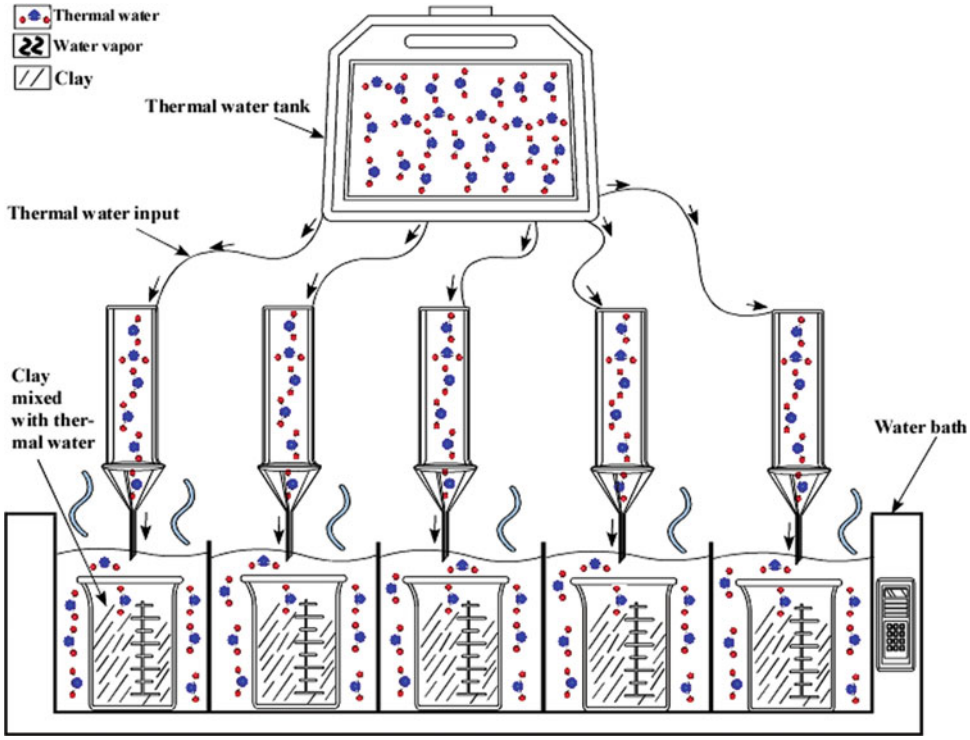

Fig. 1 Experimental protocol adopted for the maturation of clays in the laboratory

Table 1 Origin of matured clays and maturation period

Sample	Origin	Maturation period (days)
$R3_{(0,\ 1,\ 2)}$	Jebel Romana (South of Tunisia)	0*, 2, 7
$AYD3_{(0,\ 1,\ 2)}$	Jebel Aidoudi (South of Tunisia)	
$JAD12_{(0,\ 1,\ 2)}$	Jebel Ayat (South of Tunisia)	
$CBLL4_{(0,\ 1,\ 2)}$	Menzel Témime (North of Tunisia)	
$GHM_{(0,\ 1,\ 2)}$	Jebel Ghassoul (Morocco)	

*('0' indicates the non-matured clay)

3 Results

3.1 Evolution of the Mineralogical Composition During Maturation

The mineralogical composition of the various types of peloids and the clay samples studied are primarily similar. It is made up of a significant fraction of phyllosilicates generally associated with quartz, feldspars, dolomite, calcite, gypsum and halite.

The mineralogical evolution observed during maturation exhibited a slight fluctuation of to the amounts of phyllosilicates, quartz, feldspars and calcite. This evolution varies gradually according to the type of clay used and according to the time of contact between clay and thermal water (Table 2).

The most remarkable phenomenon during the maturation process is the deposition of gypsum and halite associated with the decrease of the crystallinity of the smectites. As an example, it was observed in the diffractograms of the total rock of the sample ($AYD3_0$) during maturation that the peak (d_{001}) of the smectite moves from (12.78 Å) to (11.36 Å) associated with the decrease in crystallinity.

3.2 Evolution of the Chemical Composition During Maturation

The monitoring of the major elements of the different matured clays during the different maturation periods shows (Table 3): (i) a decrease in the SiO_2 and Al_2O_3 contents accompanied by a decrease in the phyllosilicate and quartz content in the total rock, (ii) an increase in CaO and Na_2O levels towards the end of the maturation period (after 7 days), consistent with the increase in the calcite and halite rate observed by XRD, (iii) MgO contents display a slight decrease for most samples, (iv) the K_2O contents remain

Table 2 Mineralogical composition (%) of the starting and matured clay samples as a function of the maturation period

Sample	Phyllosilicates content in the total rock	Mineralogy of the total rock								
		Sm	I	K	Qz	Fd	Ca	D	G	H
$R3_0$	88	76	5	7	9	0	2	0	1	0
$R3_1$	85	74	5	6	8	0	2	0	3	2
$R3_2$	82	72	5	5	7	0	4	0	4	3
$AYD3_0$	92	62	10	20	8	0	0	0	0	0
$AYD3_1$	89	61	10	18	7	1	1	0	1	1
$AYD3_2$	87	60	9	18	7	1	1	0	2	2
$CBLL4_0$	87	26	40	21	10	0	2	0	1	0
$CBLL4_1$	86	26	40	20	9	0	2	0	2	1
$CBLL4_2$	84	25	40	19	9	0	3	0	3	1
$JAD12_0$	77	0	54	23	8	4	0	3	1	7
$JAD12_1$	76	0	53	23	8	4	0	3	1	8
$JAD12_2$	76	0	53	23	7	4	0	3	2	8
GHM_0	94	94	0	0	6	0	0	0	0	0
GHM_1	93	91	0	0	5	0	1	0	2	1
GHM_2	90	90	0	0	4	0	1	0	3	2

With: Sm: smectite; I: illite; K: kaolinite; Qz: quartz; Fd: feldspar; Ca: calcite; D: dolomite; H: halite; G: gypsum

practically constant; this is reflected by the quasi-constant percentages in illite (XRD results) and (v) a significant increase in loss of ignition during the maturation period. This increase can be explained either by the dehydroxylation of clay minerals and the decomposition of carbonates or by the presence of the newly formed organic matter during the ripening process.

In general, the variation of the trace elements for the maturated samples (Table 4) reveals that their Cr, Cu, Y, Zn, V, Ga and Ba contents decrease after seven days of maturation. On the other hand, S, Cl, St, Br and Zr contents increase throughout the maturation period.

The high level of Cl and S detected in some matured samples (e.g. R31 and R32) is explained by the presence of gypsum and halite. Indeed, the nature of the thermal water of Ain Echfa (Na–Cl) favoured the concentration of these elements (S and Cl) in the liquid phase, which favoured the neoformation of these two minerals.

Table 3 Major element (wt%) analyses of the maturated clays

Sample	SiO_2	Al_2O_3	Fe_2O_3	MnO	MgO	CaO	Na_2O	K_2O	TiO_2	P_2O_5	LOI
$R3_0$	47.00	18.56	8.63	0.02	2.03	1.62	1.78	1.44	0.90	0.27	16.90
$R3_1$	45.16	17. 94	8.86	0.02	1.89	1.66	2.20	1.48	0.93	0.28	17.20
$R3_2$	42.53	17. 84	8.45	0.03	1.87	2.82	3.57	1.46	0.88	0.28	17.40
$AYD3_0$	48.88	19.79	7.10	0.02	1.71	0.36	2.18	1.92	0.99	0.16	15.70
$AYD3_1$	47.32	18.78	8.42	0.02	1.65	0.98	2.98	1.90	0.99	0.13	15.60
$AYD3_2$	46.57	18.47	8.41	0.02	1.64	1.10	3.38	1.91	0.98	0.14	15.50
$CBLL4_0$	47.85	20.51	7.74	0.03	2.18	1.67	0.23	2.84	0.88	0.14	13.90
$CBLL4_1$	46.13	19.79	7.64	0.03	2.03	1.79	1.72	2.83	0.93	0.14	14.20
$CBLL4_2$	44.65	18.84	7.32	0.03	1.96	2.97	3.20	2.85	0.90	0.14	14.90
$JAD12_0$	37.44	14.67	6.05	0.03	3.73	1.28	6.69	4.24	0.80	0.12	18.90
$JAD12_1$	36.42	14.55	6.23	0.03	3.75	1.13	6.57	4.27	1.01	0.13	18.80
$JAD12_2$	33.93	14.17	6.35	0.03	3.79	1.03	6.55	4.29	1.03	0.14	18.10
GHM_0	53.49	1.62	0.65	0.00	22.23	0.97	0.62	0.41	0.09	0.12	17.60
GHM_1	51.32	2.38	0.95	0.00	20.23	1.65	1.09	0.43	0.14	0.09	18.90
GHM_2	50.55	2.70	1.32	0.01	19.44	2.18	3.73	0.42	0.18	0.07	19.40

Table 4 Trace element (ppm) analyses of the maturated clays

	As	Cr	Cu	Ni	V	Zn	Ga	Br	Rb	Sr	Y	Zr	I	Ba	Nb	S	Cl	F
R_{30}	0	197	50	57	249	118	23	21	59	102	17	128	0	72	0	2286	2202	0
R_{31}	0	163	47	61	240	121	13	38	41	260	3	124	0	22	0	6217	5758	0
R_{32}	0	147	39	68	239	110	14	60	61	338	0	131	0	20	0	7340	26926	0
AYD_{30}	0	237	47	39	0	99	26	14	75	150	12	149	0	125	19	1050	10408	0
AYD_{31}	0	226	46	55	192	119	24	38	76	202	13	143	0	0	0	1391	24257	0
AYD_{32}	0	223	51	62	230	113	30	56	77	195	15	145	35	0	0	2454	27210	0
$CBLL_{40}$	0	145	49	47	200	138	30	0	128	161	21	167	0	197	19	7281	84	0
$CBLL_{41}$	0	124	55	54	210	144	31	26	131	229	22	170	0	172	6	7740	14100	0
$CBLL_{42}$	0	118	54	57	276	139	23	33	138	237	24	163	0	165	3	8695	21942	0
JAD_{120}	0	134	97	58	0	65	22	17	134	78	19	152	0	254	18	10115	43468	0
JAD_{121}	0	170	94	71	0	82	21	44	169	187	19	167	0	324	18	10287	43860	0
JAD_{122}	0	167	91	76	0	86	22	49	147	170	18	187	48	359	20	20507	44746	0
GHM_0	0	0	57	37	0	50	3	34	20	147	6	42	0	59	0	1461	2437	27957
GHM_1	0	74	53	47	21	54	4	44	26	184	11	47	0	58	0	2074	7597	26872
GHM_2	76	84	49	61	31	54	4	92	39	220	10	75	42	68	0	2764	33174	23299

Toxic elements Impurity Others elements

Particular attention must be attributed to the variations of trace elements of the GHM sample. The analyses revealed the presence of arsenic after seven days of maturation. Indeed, this sample was able to adsorb 76 ppm of arsenic during a short period of contact with thermal waters of Ain Echfa. The high levels of As, observed in sample GHM2, are unusual (the content of 'As' exceeds the limits of the pharmacopoeia which is 15 ppm) and cannot be justified only with the mineralogical nature of GHM (94% smectite with a high adsorption capacity); in fact, smectite can exchange cations in the interlayer, but it is implausible that As is present in cationic form in the thermal water. It could be present, instead, as arseniate (AsO_4^{3-}) or arsenite (AsO_3^{3-}).

3.3 Variation in the Cooling Kinetics and pH During Maturation

The curves obtained from the cooling kinetics of the different clay samples studied were fitted using an exponential curve by a regression analysis following a function of type: A + Be-Kt (Table 5). Overall, it can be noticed that the maturation was found to prolong the cooling time of the different samples so that they maintain heat for a longer period.

Table 5 shows a pH variation of different matured samples. All these samples have an initial pH greater than 8 (except for the Menzel Témime and Morocco samples, which have a neutral pH). The pH decreases slightly with the maturation time and becomes neutral for the most samples.

4 Discussion

Previous work by Veniale et al. (2004), Carretero et al. (2007), Gámiz et al. (2009), Casás et al. (2013) and Díaz Rizo et al. (2017) shows that three main parameters have a crucial role during the maturation process. The first parameter is the solid phase of the sample (quantitative mineralogical composition). The second parameter is the type of thermal waters and its contents of chemical elements capable of carrying out cationic exchanges with the solid phase. The third parameter is the contact time between the two stable and liquid phases; this parameter also has significant importance (Tateo et al. 2009). These findings are confirmed in the present work.

From a physicochemical point of view, there have been fluctuations in the content of major and trace elements which are generally correlated with the mineralogical compositions of the mature samples. Many studies (Wang et al. 2000; Koning and Comans 2004; Anaya-Gregorio et al. 2018) have demonstrated the ability of clays to adsorb trace element; however, they have also demonstrated their ability to desorption and, therefore, the reversibility of adsorption/desorption reactions.

An improvement of the cooling kinetics was recorded after the maturation process, with a slow cooling rate allowing excellent heat retention and, therefore, a better transfer of calories, especially for the GHM sample.

The pH decreases slightly with the maturation time. Several factors related to the properties of the thermal muds can be at the origin of the slight variation of the pH, as an

Table 5 Variation of the adjustment parameters, the time to reach 35 °C and the pH of the maturated samples

	A (°C)	B (°C)	K	Time (mn)	pH
$R3_0$	36.26	33.73	0.17	43.5	9.98
$R3_1$	36.16	32.84	0.16	44.5	8.39
$R3_2$	36. 01	31.11	0.14	47	7.23
$AYD3_0$	36.47	27.59	0.19	39.5	8.09
$AYD3_1$	36.47	26.62	0.16	41	7.87
$AYD3_2$	36.22	23.35	0.14	48	7.22
$CBLL4_0$	36.52	32.04	0.21	36.5	7.50
$CBLL4_1$	35.84	30.97	0.19	38.5	7.10
$CBLL4_2$	35.72	29.55	0.18	40.5	7.07
$JAD12_0$	36.21	31.62	0.25	31	8.14
$JAD12_1$	35.85	31.33	0.23	33.5	8.12
$JAD12_2$	35.46	30.05	0.21	36	7.92
GHM_0	36.72	30.98	0.12	49	7.28
GHM_1	36.06	28.68	0.12	57.5	7.22
GHM_2	35.60	30.75	0.10	59.5	6.93

example, the initial pH, the temperature of the thermal waters used for the maturation, the appearance of new mineral phases such as gypsum and halite and the increase in the rate of calcite (Veniale et al. 2004; Gámiz et al. 2009; Rebelo et al. 2011).

5 Conclusions

The study of different types of clays which matured with Ain Echfa thermal water of Korbous for a short time showed a chemical and mineralogical evolution.

From a mineralogical point of view, the observed transformations are more pronounced for smectite than for illite–kaolinite samples.

For physicochemical parameters, we detected fluctuations in the content of major and trace elements, which are generally correlated with the mineralogical compositions of the maturated samples. Besides, the cooling kinetics improved, and the pH decreased slightly after the maturation process.

References

Anaya-Gregorio, A., Armstrong-Altrin, J.S., Machain-Castillo, M.L., Montiel-García, P.C., Ramos-Vázquez, M.A.: Textural and geochemical characteristics of late Pleistocene to Holocene fine-grained deep-sea sediment cores (GM6 and GM7), recovered from southwestern Gulf of Mexico. J. Palaeogeogr. **7**(1), 3 (2018)

Carretero, M.I., Pozo, M., Sánchez, C., García, F.J., Medina, J.A., Bernabé, J.M.: Comparison of saponite and montmorillonite behaviour during static and stirring maturation with seawater for pelotherapy. J. Appl. Clay Sci. **36**(1–3), 161–173 (2007)

Casás, L.M., Pozo, M., Gómez, C.P., Pozo, E., Bessières, L.D., Plantier, F., Legido, J.L.: Thermal behavior of mixtures of bentonitic clay and saline solutions. J. Appl. Clay Sci. **72**, 18–25 (2013)

Díaz Rizo, O., Suárez Muñoz, M., González Hernández, P., Gelen Rudnikas, A., D'Alessandro Rodríguez, K., Melián Rodríguez, C. M., Martínez-Villegas, N.V.: Assessment of heavy metal content in peloids from some Cuban spas using X-ray fluorescence. Nucleus 61 (2017)

Gámiz, E., Martín-García, J.M., Fernández-González, M.V., Delgado, G., Delgado, R.: Influence of water type and maturation time on the properties of kaolinite–saponite peloids. J. Appl. Clay Sci. **46**, 117–123 (2009)

Gomes, C., Carretero, M.I., Pozo, M., Maraver, F., Cantista, P., Armijo, F., Legido, J.L., Teixeira, F., Rautureau, M., Delgado, R.: Peloids and pelotherapy: historical evolution, classification and glossary. J. Appl. Clay Sci **75**, 28–38 (2013)

Koning, A., Comans, R.N.: Reversibility of radiocaesium sorption on illite. Geochim. Cosmochim. Acta **68**(13), 2815–2823 (2004)

Rebelo, M., Viseras, C., López-Galindo, A., Rocha, F., Ferreira da Silva, E.: Rheological and thermal characterization of peloids made of selected Portuguese geological materials. J. Appl. Clay Sci. **52**, 219–227 (2011)

Tateo, F., Ravaglioli, A., Andreoli, C., Bonina, F., Coiro, V., Degetto, S., Giaretta, A., Menconi Orsini, A., Puglia, C., Summa, V.: The in-vitro percutaneous migration of chemical elements from a thermal mud for healing use. J. Appl. Clay Sci. **44**, 83–94 (2009)

Veniale, F., Barberis, E., Carcangiu, G., Morandi, N., Setti, M., Tamanini, M., Tessier, D.: Formulation of muds for pelotherapy: effects of "maturation" by different mineral waters. J. Appl. Clay Sci. **25**, 135–148 (2004)

Wang, X.K., Dong, W.M., Dai, X.X., Wang, A.X., Du, J.Z., Tao, Z.Y.: Sorption and desorption of Eu and Yb on alumina: mechanisms and effect of fulvic acid. Appl. Radiat. Isot. **52**, 165–173 (2000)

DNA Detection After Interaction with Clay Minerals and Soils: An Analytical Approach

Amira Lajmi, Isabelle Bourven, Emmanuel Joussein, Stéphane Simon, Marilyne Soubrand, and Mounir Medhioub

Abstract

Isotherms adsorptions were generated using calf thymus DNA (10–300 µg/mL), two types of clay minerals, namely kaolinite KGa-2 and montmorillonite STx-1b and two soil (Cambisols and Andosols with clearly different mineralogical features and organic matter contents). The adsorption of calf thymus DNA with or without humic acid (C = 60 µg/mL) by clay mineral was studied using a new detection method: the colorimetric method at 600 nm and is compared to the traditional method (absorption at 260 nm). The adsorption isotherms of calf thymus DNA on the clays minerals using the colorimetric method conform to the Langmuir equation. The results show that the colorimetric method is independent of organic matter contents or the type of soils. It allows a better understanding of the interactions between DNA and clay minerals. To sum up, this method is straightforward, insensitive and sufficient with a limit of detection to plot isotherms of DNA on minerals in complex matrices.

Keywords

DNA • Adsorption • Detection methodology • Soils • Clay minerals

1 Introduction

There are different ways to measure DNA: liquid chromatography (LC-MC) (Chowdhury and Guengerich 2011), mass spectrometry (MC) and thin-layer chromatography (TLC) (Kriaucionis et al. 2009). These methods require time and costly material. In order to study the adsorption of DNA on minerals, the literature uses a direct and straightforward method: the measurements of absorbance by spectrophotometry at 260 nm (Cai et al. 2006; Gardner and Gunsch 2017). Indeed, the adsorption of DNA on adsorbents is one of the most critical processes affecting persistence and availability. It is an essential phenomenon for gene transfer between nonspecific bacteria: genetic transformation (Meyer et al. 2004). It has been well established that nucleic acids can persist for a long time in soils, containing high clay content (Pietramellara et al. 2009). Nevertheless, DNA adsorptions which include the interaction between organic molecules and clay minerals have not yet been studied, and neither was sorption of DNA on a mineral in a complex matrix as well as soils. To our knowledge, studies about interaction DNA-clay minerals used "simple models" to model the mineral sorption capabilities of DNA. This study aims to develop a method for assaying DNA in a complex medium or a mixture of organic molecules. This method relies on spectrophotometric colorimetric assays, and the DNA adsorption protocol by clay minerals described by Cai et al. (2006) will be the basis of our work.

2 Materials and Methods

DNA: The calf thymus DNA was purchased from Sigma Aldrich with an approximate GC content of 41.9%. It is a double-stranded DNA with ten base pair (bp) and a negative charge at pH = 7.0. Calf Thymus DNA was used for kaolinite and montmorillonite adsorption isotherms. Because this DNA has been used historically as a DNA source in

A. Lajmi (✉) · I. Bourven · E. Joussein (✉) · S. Simon · M. Soubrand
University of Limoges, PEINENE-EAU EA 7500, 87060 Limoges, France
e-mail: Myralajmi@outlook.fr
e-mail:

A. Lajmi · M. Medhioub
University of Sfax, 3029 Sfax, Tunisia

A. Çiner et al. (eds.), *Recent Research on Geomorphology, Sedimentology, Marine Geosciences and Geochemistry*, Advances in Science, Technology & Innovation, https://doi.org/10.1007/978-3-030-72547-1_66

adsorption experiments (Courtney et al. 2017), it will allow straight comparisons between the clay adsorption findings in this study and those of earlier studies.

Clay minerals and soils: The two clays are always found in the soil and correspond to raw commercial samples and Source Clays Repository (CMS): Montmorillonite STx-1B and Kaolinite KGa-2 from size fraction <2 μm.

Soil samples have been chosen in the way to have different organic matter content and mineralogical features. Each soil was air-dried and sieved through a 2 mm mesh sieve after sampling. The first soil is classified as Andosol with a silky texture, and the second is a Cambisol with loamy texture.

DNA Detection:

Direct Method

The assay is performed spectrophotometrically in the ultraviolet at 260 nm. The DNA is quantified by absorbance measurement at 260 nm (Cai et al. 2006) corresponding to the maximum absorption band of nucleic acids around 260 nm (π π* transitions in purines and pyrimidines) with a value of ε 260 nm ≈ 1 × 104 M-1 cm-1 in water.

Absorption is defined as the unit of optical density measured at 260 nm. It is a direct measurement of solutions at λ = 260 nm. A quantification limit is of 2–3 μg/mL in the water.

Colorimetric method for DNA detection, the diphenylamine method—Burton, 1956: The colorimetric method relies on the specific reaction of diphenylamine with deoxyribose residues resulting in an absorbent complex at 600 nm. The limit of quantification is five times higher than the classical method: 10 μg/mL. The DNA calibration range is 0.1–1 μg/mL (Burton 1956).

3 Results

3.1 Validation of Colorimetric Method for DNA Essay

In order to validate the colorimetric method, we conducted two experiments at pH = 7.00 ± 0.01. The first consists in detecting the DNA directly at 260 nm (direct method) in solutions containing HA (from 0 to 300 μg/mL) mixed with a fixed concentration of DNA [150 μg DNA/2.5 mL Tris (Fig. 1)]. The second manipulation is the same, but we used the colorimetric method (detection at 600 nm with diphenylamine as a reagent) (Fig. 1).

The results are reported in Fig. 1. When we take measurements using the "direct method" at 260 nm, there is an increase of the absorbance with HA content, whereas the concentration of DNA remained constant. Therefore, HA clearly interfere the DNA quantification, inducing over-evaluation of the DNA concentration. Indeed, HA have a maximum absorbency close to 260 nm (λmax HA = 254 nm) (Uyguner and Bekbolet 2004, 2005). This method is not efficient when DNA is measured in a complex matrix that contains HA. In the case of the "Colorimetric method," there is no influence of HA onto DNA quantification: the absorbance remains constant for all tested HA concentrations.

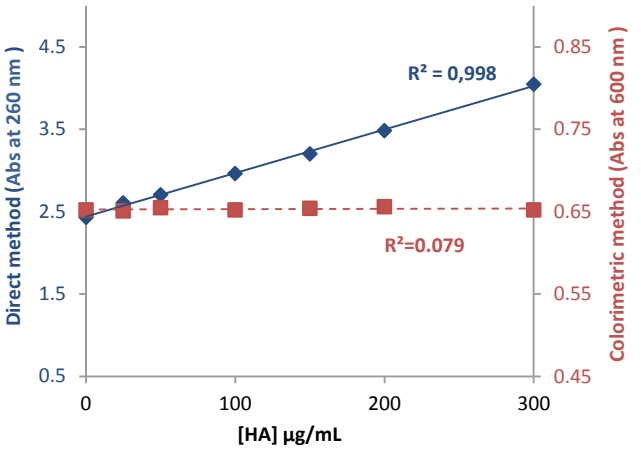

Fig. 1 Absorbance of DNA from calf thymus ([150 μg]) mixed with humic acid (HA) (25–300 μg/mL) with two detection methods. (n = 2) (STD DEV = 0.002)

3.2 Equilibrium Adsorption of DNA with or Without Humic Acid HA on Clay Mineral

The adsorption trends of calf thymus DNA at different concentrations with or without HA at a constant concentration of C = 60 μg/mL were tested using two types of clay minerals (Kaolinite KGa-2 and Montmorillonite STx-1b) (Fig. 2). We use humic acid to compare the adsorption of DNA in a simple matrix and another complex one.

The colorimetric method is the means to detect the DNA. Table 1 displays the parameters calculated from the Langmuir equation for two types of clay minerals.

4 Discussion

Figure 1 which analyzed mainly the correlation between the DNA absorbance at 600 nm and the humic acid concentration shows that there is no correlation between the DNA and humic acids (r^2 very low = 0.079) (Fig. 1). Therefore, the DNA contents are not correlated with the humic acid contents. In the direct method (260 nm), there is an increase of the absorbance while the concentration of DNA is constant

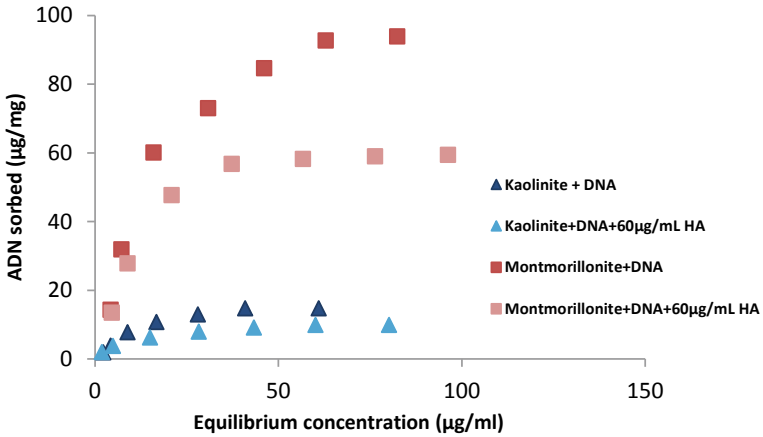

Fig. 2 Isotherm adsorption of DNA from calf thymus (25–350 µg) with or without humic acid (HA) (60 µg/mL) on 1 mg of montmorillonite and 10 mg of kaolinite

Table 1 Isotherm parameters for hybrid clay/DNA and hybrid clay/DNA + humic acid

Clay	DNA alone		DNA with HA = 60 µg/mL
Montmorillonite	KL (ml/µg)	0.05 ± 0.01	0.08 ± 0.02
	Qm (µg/mg)	124 ± 7	72 ± 3
	r^2	0.987	0.982
Kaolinite	KL (ml/µg)	0.06 ± 0.03	0.09 ± 0.02
	Qm (µg/mg)	17 ± 4	12 ± 0.6
	r^2	0.878	0.984

with a significant correlation ($r^2 > 0.99$) (Fig. 1). For the colorimetric method (600 nm) using diphenylamine as a reagent, the absorbance seems constant, which is following a constant concentration of DNA. Values of absorbance are the same as the one from DNA alone (0 µg/mL SH). Therefore, there is interference between humic acids and DNA. Subsequently, the direct method is less robust than colorimetric method.

The DNA adsorption isotherms on clay minerals are illustrated in Fig. 2. The DNA adsorbed by these minerals could correspond to the Langmuir equation (Table 1). The amount of DNA adsorption on montmorillonite was much higher than that of kaolinite. A significant difference also was detected between the adsorption capacities of montmorillonite and kaolinite for calf thymus DNA. This variation is directly attributable to differences in CEC, SSA and particle size. The amount of DNA adsorbed by the mineral in the presence of HA is less than the amount adsorbed in the presence of DNA alone (Ratio Qm ≈ 1.7) (Table 1). This phenomenon could be due to humic acid and has more affinity than DNA for clay minerals. So the colorimetric method allows showing the competition between humic acid and DNA. Surprisingly KL is more significant in the case of the adsorption of the DNA within the presence of HA (60 µg/mL) than DNA alone.

To better confirm the reliability of the diphenylamine method, we tested two methods in the presence of DNA with a soil (Cambisol and Andosol) that has a very complex matrix and contains several organic molecules and measurements of DNA alone and DNA in the presence of soils. For the colorimetric method, a triplicate of tests has been done. With the colorimetric method, the same absorbance ABS DNA alone and ABS DNA + soil are statistically equal (≈0.65). Whereas factor 2 is present with the direct method. The DNA may interact with soil molecules, and this modifies the functional groups responsible for the absorbance at 260 nm. With the direct method, the concentration of DNA in the soils alone is equal to 0.183 g DNA/g soil, which is very high. The direct method detects other organic molecules present in the soil with DNA (HA, tannin, protein).

In contrast with colorimetric method, the content of soil DNA is 0.008 ± 0.002 g DNA/g soil. This direct method is less robust than colorimetric method. Thus, when there is a complex matrix, we have to work with the colorimetric method being the most reliable and accurate method and conforming to the results of the literature review.

5 Conclusions

A new DNA detection method has been developed using diphenylamine as a reagent and validated for a complex matrix. This method is less sensitive (lower limit of detection) (10 µg/mL) than the direct method (2–3 µg/mL) but isotherms DNA-clay (Montmorillonite and Kaolinite) give parameters following literature data (Cai et al. 2006).

Nevertheless, the colorimetric method is more specific and therefore more robust, which open substantial application possibility (behavior of DNA-clay in the mix, in a complex matrix as soil). Lastly, this colorimetric method is not expensive and more convenient to set up.

References

Burton, K.: A study of the conditions and mechanism of the diphenylamine reaction for the colorimetric estimation of desoxyribonucleic acid. Biochem. J. **62**, 315–323 (1956)

Cai, P., Huang, Q., Zhang, X., Chen, H.: Adsorption of DNA on clay minerals and various colloidal particles from an Alfisol. Soil Biol. Biochem. **38**, 471–476 (2006)

Chowdhury, G., Guengerich, F.P.: Liquid chromatography-mass spectrometry analysis of DNA polymerase reaction products. Curr. Protoc. Nucleic Acid Chem. **47**(1), 7–16 (2011)

Courtney, M.G., Gunsch, C.K.: Adsorption capacity of multiple DNA sources to clay minerals and environmental soil matrices less than previously estimated. Chemosphere **175**, 45–51 (2017)

Gardner, C.M., Gunsch, C.K.: Adsorption capacity of multiple DNA sources to clay minerals and environmental soil matrices less than previously estimated. Chemosphere **175**, 45–51 (2017)

Kriaucionis, S., Heintz, N.: The nuclear DNA base 5-hydroxymethylcytosine is present in Purkinje neurons and the brain. Sci. **324**, 929–930 (2009)

Meyer, A., Deiana, J., Bernard, A.: Cours de microbiologie générale avec problèmes et exercices. Biosciences et Techniques **2**, 437 (2004)

Pietramellara, G., Ascher, J., Borgogni, F., Ceccherini, M.T., Guerii, G., Nannipieri, P.: Extracellular DNA in soil and sediment: fate and ecological relevance. Biol. Fertil. Soils **45**, 219–235 (2009)

Uyguner, C.S., Bekbolet, M.: Evaluation of humic acid, chromium (VI) and TiO_2 ternary system in relation to adsorptive interactions. Appl. Catal. B Environ. **49**, 267–275 (2004)

Uyguner, C.S., Bekbolet, M.: Evaluation of humic acid photocatalytic degradation by UV-VIS and fluorescences pectroscopy. Catal. Today **101**, 267–274 (2005)

Geochemistry and Metallogenesis: Processes and Products (T7): Magmatic and Metamorphic Processes and Products

Early Ediacaran Volcanism of Taourirte Area (Western High Atlas, Morocco): Evidence for the Onset of a Post Pan-African Extension Event

Youssef Taib, Ahmed Touil, Mohamed Aissa, Mohamed Hibti, Brahim Ouargaga, Mohamed Zouhair, and Abdelmalek Ouadjou

Abstract

Recently, early Ediacaran volcanic activity has been recorded in Tighardine area from the Moroccan High Atlas. The field investigation in Taourirte area allows the distinction of three volcanic and volcano-sedimentary units quite similar to those already described on Tighardine area. Volcanic rocks of Tighardine show high affinities to continental tholeiites typical of an extensional tectonic environment. This tholeiitic geochemical affinity contrasts with that of calc-alkaline types described from volcanic rocks belonging to the Lower Ediacaran Ouarzazate Supergroup in the Anti-Atlas. Whole-rock geochemical characteristics: high TiO_2 contents ranging from 1.2 to 2.81 wt%, high Zr/Y (5.43–12.08), Zr/Nb (23.81–10.50) and Zr/P_2O_5 (0.03–0.2) ratios suggest an intracontinental tholeiitic affinity for these volcanic. They have Ti/Y ratio varying from 240 to 1200 and Th/Ta ranging from 0.68 to 5.2 supporting their derivation from an enriched mantle source, akin to that of E-MORB, during an extensional regime. They were deposited in an extensive basin evolved during a post-collisional regime. Their geochemical signature is a result of complex interaction processes between parental asthenospheric mantle melt and the surrounding crust.

Keywords

Western High Atlas • Taourirte • Intracontinental tholeiites • Extension • Post-collision

Y. Taib (✉) · A. Touil · M. Hibti · B. Ouargaga
Laboratoire Géoressources (Unité Associée au CNRST, URAC42), Faculté Des Sciences et Technique Gueliz, B.P. 549, 40010 Marrakech, Morocco

M. Aissa
Laboratoire d'Etudes Des Ressources Minérales et Energétiques, Faculté des sciences, Université Moulay Ismail, Meknès, Morocco

M. Zouhair · A. Ouadjou
Goupe Managem, Twin Center, Tour A, Angle Boulevard Zerktouni et Massira Khadra, BP 5199, Casablanca, Morocco

1 Introduction

The Moroccan Western High Atlas is a mountainous region that includes numerous volcanic and volcano-sedimentary formations. These volcanic rocks were previously attributed to the Cambrian. However, recently obtained U-Pb zircon geochronological data of tholeiitic volcanic rocks in the Tighardine area yielded an early Ediacaran age of about 600 ± 3 Ma (Boukerrou et al. 2018), and this volcanism shows a tholeiitic geochemical affinity. Ediacaran magmatism was earlier recognised in areas to the south, in the Ouarzazate Supergroup of the Anti-Atlas belt (Fig. 1a). However, the volcanic rocks of the Ouarzazate Supergroup show a high K-calc-alkaline affinity. Therefore, this high K-calc-alkaline signature confirms that the volcanism took place in a thick crust consistent with a post-collisional event during the final stages of the Pan-African orogeny. This study aims to characterise the nature and affinity of the Taourirte magmatism and discuss its age and geodynamic context and to compare it with equivalent rocks in the Anti-Atlas at the NW margin of the West African Craton (WAC).

2 Geological Setting

The Western High Atlas Massif belongs to the Atlas fold-thrust intracontinental belts raised by the Alpine tectonic event (Piqué et al. 2002; Teixell et al. 2003). Two NE-SW major dextral shear zones border it; (1) Imi-N-Tanout fault zone in the north and (2) Tizi-N-Test shear zone to the south (Fig. 1b). It is comprised mainly of Precambrian and Paleozoic formations folded, metamorphosed and granitised by the Variscan orogeny and unconformably overlain by Mesozoic to Cenozoic cover. The stratigraphic series of the basement consists of a succession of about 600–1000 m of Ediacaran to Ordovician metasedimentary and volcanoclastic sequences (Piqué et al. 2002; Ezzouhairi et al. 2008 *and references therein*). The oldest

A. Çiner et al. (eds.), *Recent Research on Geomorphology, Sedimentology, Marine Geosciences and Geochemistry*, Advances in Science, Technology & Innovation, https://doi.org/10.1007/978-3-030-72547-1_67

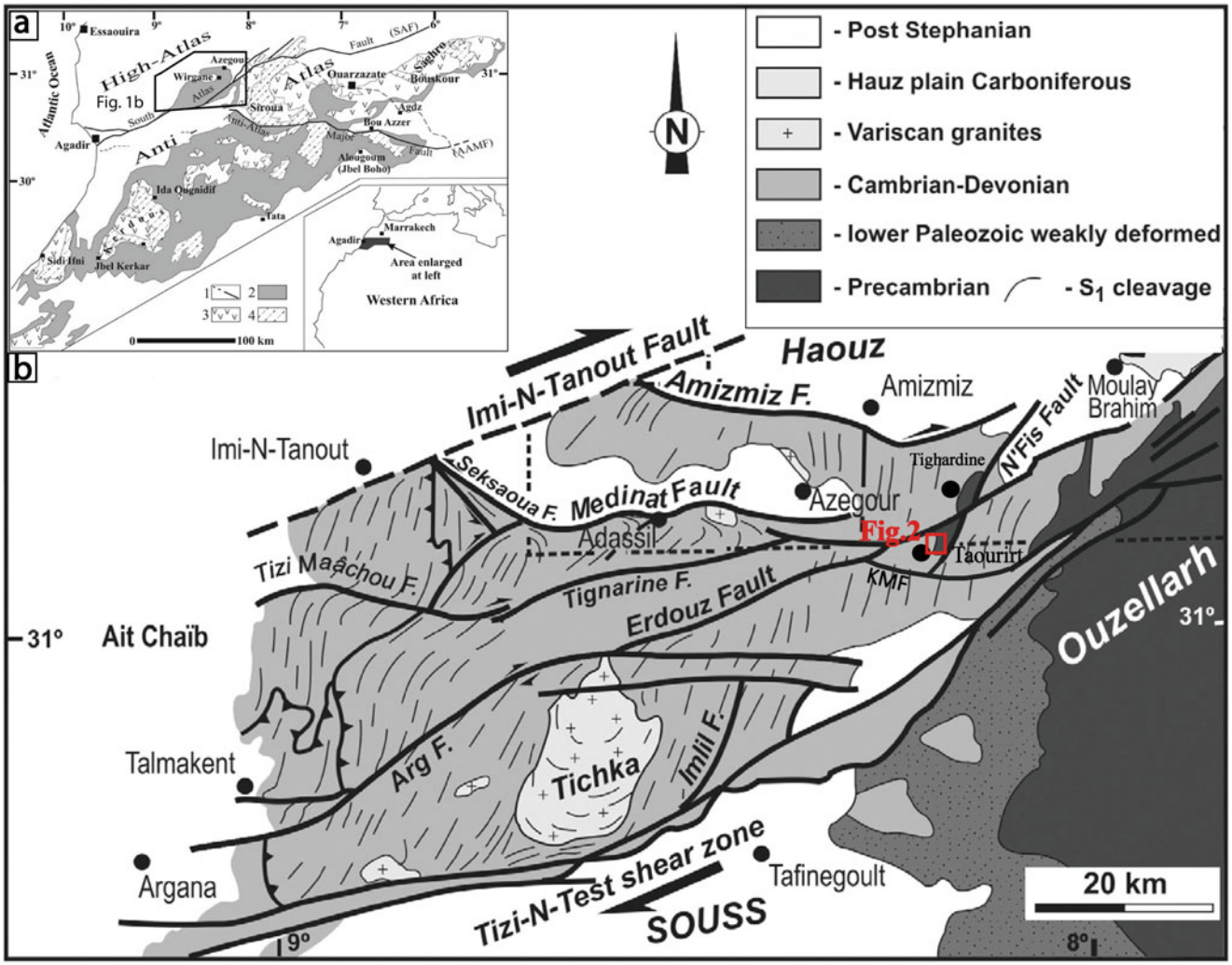

Fig. 1 (a) Simplified geological map showing the Proterozoic to the Early Cambrian formations in the High Atlas and Anti-Atlas domains (1, Fault; 2, Lower Cambrian; 3, Late Neoproterozoic; 4, Palaeoproterozoic and Early Neoproterozoic) (Ezzouhairi et al. 2008), and (b) Structural outline of Western High Atlas (Dias et al. 2011; modified)

terrains in this area are the Wirgane granodioritic intrusion and The Tighardine volcanic complex (including basalt, andesite and dacites) dated at about 625 ± 5 by Eddif et al. (2007) and c. 596–603 Ma by Boukerrou et al. (2018).The age of this volcanism is synchronous with the rhyolites age from the lower part of the Ouarzazate Supergroup in the Anti-Atlas belt at the northern WAC margin (Blein et al. 2014; Walsh et al. 2012).

3 Results

3.1 Taourirte Area: Mapping, Units and Field Relations

Detailed field observations, in the scope of this work, on the Taourirte area (Fig. 2) allowed to establish a new lithostratigraphic synthesis. The investigated area includes three volcanic and volcano-sedimentary units deposited on the early Ediacaran Takoucht-Wirgane granodiorites (625 ± 5 Ma; (Eddif et al. 2007)) and covered in discordance by a mudstone and siltstone formation assumed to be Cambrian in age.

The lower volcanic unit (LVU) is formed by basalt to the andesite lava flow, unconformably deposited on the Ediacaran granodiorite. The middle unit (MVU) is mainly volcano-sedimentary. It is formed by shale and tuffaceous siltstone including dolomitic and pyroclastic breccia layers and lenses. The lava flows are less abundant in this unit and are reduced to small lenses of basalt–andesite with few differentiated rocks. The upper volcanic (UVU) unit is formed mainly by a substantial basaltic to andesitic lava flow. The correlation with the stratigraphic column of Tighardine shows that the two areas have the same

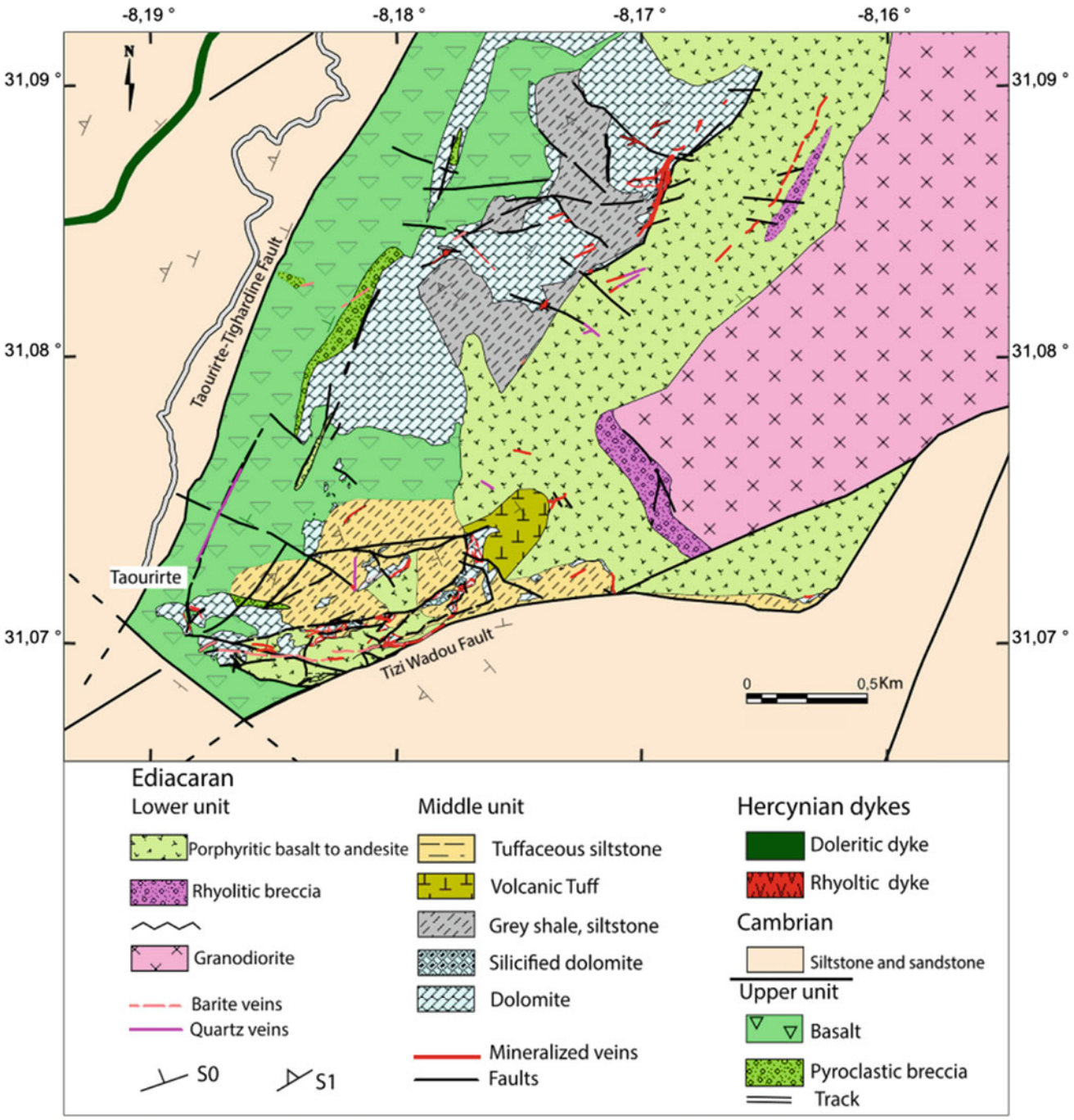

Fig. 2 Geological map of the Taourirte area

stratigraphic succession with significant variations in thickness. Indeed, the Taourirte area exhibits relatively thick volcanic and volcano-sedimentary formations. However, dolomitic beds and lenses are less developed. According to Froitzheim et al. (1988), the formation thickness is controlled by the inherited substrate morphology and syngenetic faults occurring in late Precambrian time.

3.2 Petrography

The Taourirte volcanic rocks have a quite similar mineral composition. They are microlitic to hyalo-microlitic, more or less porphyritic phenocrysts. Primary minerals have been partially to severely transformed into secondary minerals owing to low-grade metamorphic processes. The basal unit

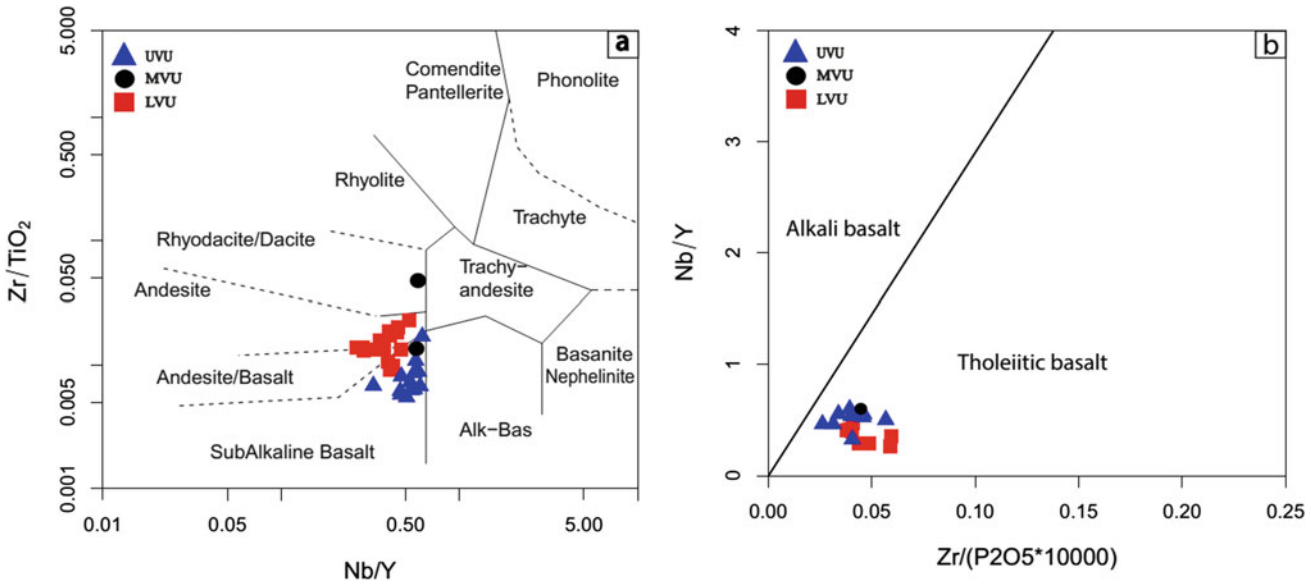

Fig. 3 **a** Classification of Taourirte volcanic rock on the Zr/TiO_2 vs Nb/Y diagram of Winchester and Floyd (1977); **b** (Winchester and Floyd 1977) diagram's Nb/Y vs. $Zr/P_2O_5*10^4$ discrimination diagram of Taourirte mafic volcanic rocks (*LVU: lower volcanic unit; MVU: middle volcanic unit; UVU: upper volcanic unit*)

is formed mainly by lava flow composed by Plagioclase phenocryst-bearing andesites, locally containing aphanitic basalt lenses. The middle unit is formed by andesites, basalt–andesites, basalts, tuffs and pyroclastic breccias with pelitic and carbonates intercalations. The summit unit is essentially a huge basaltic to andesitic lava flow.

3.3 Geochemistry

The studied metabasites cover a wide compositional range from basalt to rhyolite. Silica content ranges from 47.32–58.37 wt%, 52.43–72.05 wt% and 46.24–59.31 wt% from lower to upper units. Such silica variations allow the classification of the LVU into basalts to andesites, and the MVU as basalts with minor rhyolites and the UVU is ranging from basalts to andesites. Based on Nb/Y versus Zr/TiO_2 classification by Winchester and Floyd (1977), confirming the petrographic conclusions, the Taourirte metabasites are basalts to rhyodacites with a subalkaline signature (Fig. 3a, b).

Examining only metabasites with SiO_2 lower than 55 wt % and MgO higher than 4.5 wt%, in which most HFSE, Th and REE are incompatible, the Zr/Th, Nb/Ce and $TiO_2/P2O_5$ ratios are higher in the UVU and allow distinguishing these rocks from the other metabasites.

4 Discussion

In the commonly used Zr/Y versus Zr diagram of Pearce and Norry (1979) (Fig. 4a), Th/Ta versus Yb of Schandl and Gorton (2002) (Fig. 4b) and Zr-Nb-Y triangular diagram of Meschede (1986) (Fig. 4c), most of the Taourirte metabasites plot in the within plate basalt field suggesting an enriched mantle-derived source. It is noteworthy that the Ti/Y ratio is higher in the within-plate basalts than other basalts (Rollinson 1996). In the metabasites studied, the Ti/Y ratio varies from 240 to 1200 and the Zr/Y ratio from 5.43 to 12.08, supporting their derivation from an enriched mantle source.

Crustal contamination may occur during the mantle source melting or throughout melt ascension (Hawkesworth and Calsteren 1983). Chondrite- and primitive mantle-normalised plots are commonly used in an attempt to quantify this effect. The Nb-anomaly observed in such diagrams is indicative of the tectonic setting and reflects the effects of subducted slab or crustal contamination during magmatic processes (Gower and Swinden 1991). Plots of the average of Taourirte mafic rocks ($SiO_2 < 52$ wt% and $MgO > 5$ wt%) on a primitive mantle-normalised multi-element diagram (Sun and Mc Donough 1989) show a high enrichment of Ba, Rb, La and Ce with depletion of Sr in all

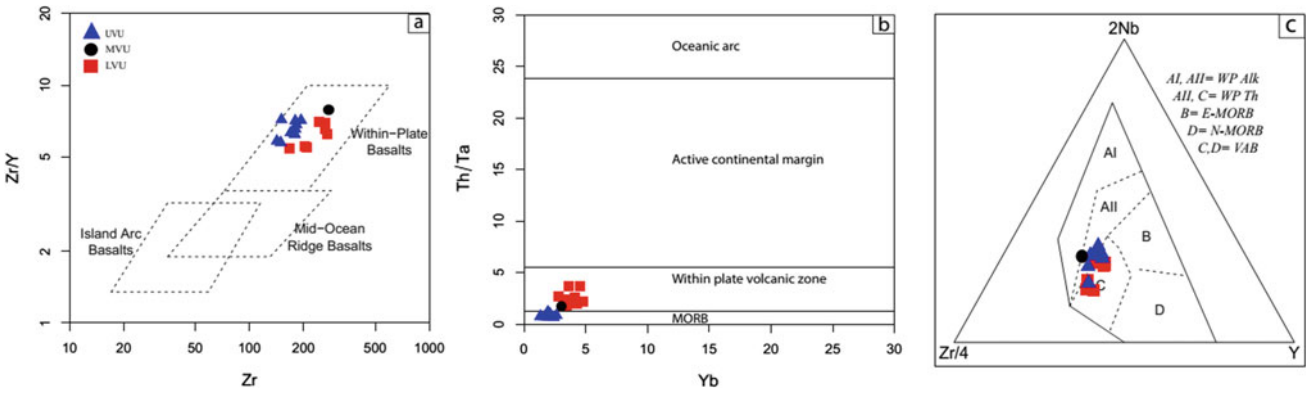

Fig. 4 Tectonic setting discrimination diagrams for Taourirte mafic volcanic rocks. **a** Zr vs Zr/Y (Pearce and Norry 1979); **b** Yb vs Th/Ta (Schandl and Gorton 2002); **c** Zr–Nb-Y triangular diagram (Meschede 1986); (*E-MORB: Enriched Mid-Ocean Ridge Basalt, N-MORB: Normal Mid-Ocean Ridge Basalt, VAB: Volcanic Arc Basalt, WP Alk: Within-Plate Alkaline, WP Th: Within-Plate Tholeiite*)

of the rocks studied. The metabasites from the lower and middle units are distinguished by their Nb negative anomaly and a flat slope between Ti and Yb (Fig. 5). Spectra of these metabasites are very similar to those of continental tholeiites of the Siroua Inlier (Fig. 5). The metabasites from the upper unit have no Nb-anomaly, exhibit enrichment in Nb compared to Th and depletion in Nb relative to La. This implies increased crustal contamination in lower and middle metabasites. Such variation in within plate environment supposes a setting up of lower and middle volcanic unit in a continental break-up region. With intensified extension, the upper volcanic unit took place in a relatively thinning crust.

Magmatic activity of the Early Ediacaran age has also been reported from the base of the Ouarzazate Supergroup (e.g. Tadmant and Tamriwine rhyolites, 606 ± 6 Ma and 605 ± 9 Ma (Thomas et al. 2002), Oued Alqantrat rhyolite, 588 ± 4 Ma (Walsh et al. 2012); Amlouggui tonalite, 586 ± 8 Ma (Thomas et al. 2002).

The Taourirte formation would be, therefore, a lateral equivalent of the Ouarzazate Supergroup, particularly the Bou Salda formation in Siroua inlier, which displays numerous similarities with the Taourirte sequence. According to Thomas et al. (2002), the Bou Salda formation was deposited in narrow fault-bound grabens. The Ediacaran Ouarzazate Supergroup remains a debate. All authors agree that volcanic and plutonic activities from its base display a high K-calc-alkaline affinity (Thomas et al. 2002; Gasquet et al. 2005); Ennih and Liégeois 2008; Walsh et al. 2012; Blein et al. 2014) and took place during a post-collisional stage.

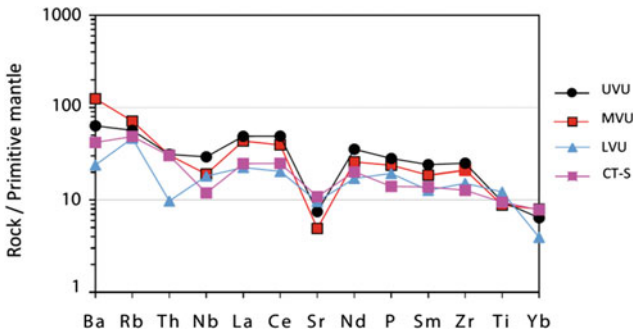

Fig. 5 Spider diagrams normalised to primitive mantle (Sun and Mc Donough 1989) for the average of Taourirte mafic volcanic rocks. Comparison with Siroua continental tholeiit (*CT-S*) (Touil et al. 2008)

5 Conclusion

The study of the early Ediacaran volcanic event in Taourirte area in Moroccan High Atlas allows us to distinguish three units dominated by volcanic and volcano-sedimentary rocks with interlayered dolomite beds and lenses. Geochemical and petrological studies performed on volcanic rocks of the Taourirte formation show that they are basalts, basalt–andesites and andesites with a few acidic derivatives. These rocks have geochemical signatures of intracontinental tholeiites, whose parental magmas should have been derived from an enriched mantle source, consistently with an extensional continental setting. The age of this volcanic activity is synchronous with the post-collisional stage of the Pan-African orogeny in the northern border of the West African Craton.

References

Blein, O., Baudin, T., Soulaimani, A., Cocherie, A., Chèvremont, P., Admou, H., Ouanaimi, H., Hafid, A., Razin, P., Bouabdelli, M., Roger, J.: New geochemical, geochronological and structural constraints on the Ediacaran evolution of the south Sirwa, Agadir-Melloul and Iguerda inliers, Anti-Atlas, Morocco. J. Afr. Earth Sc. **98**, 47–71 (2014)

Boukerrou, S., Nalini, H., Moreira, H., Maacha, L., Zouhair, M., Outhounjite, M., Ouirouane, S., Hibti, M., Touil, A.: Geochronology and geochemistry of Ediacaran volcanic rocks of the Tighardine ore deposit formation (western High Atlas, Morocco). Arab. J. Geosci. **11**(2), (2018)

Dias, R., Hadani, M., Leal Machado, I., Adnane, N., Hendaq, Y., Madih, K., Matos, C.: Variscan structural evolution of the western High Atlas and the Haouz plain (Morocco). J. Afr. Earth Sc. **61**(4), 331–342 (2011)

Eddif, A., Gasquet, D., Hoepffner, C., Levresse, G.: Age of the Wirgane granodiorite intrusions (Western High-Atlas, Morocco): New U-Pb constraints. J. Afr. Earth Sc. **47**(4–5), 227–231 (2007)

Ennih, N., Liégeois, J.P. (2008). The boundaries of the West African craton, with special reference to the basement of the Moroccan metacratonic Anti-Atlas belt. Geological Society, London

Ezzouhairi, H., Ribeiro, M.L., Ait Ayad, N., Moreira, M.E., Charif, A., Ramos, J.M.F., de Oliveira, D.P.S., Coke, C.: The magmatic evolution at the Moroccan outboard of the West African craton between the Late Neoproterozoic and the Early Palaeozoic. Geological Society, London, Special Publications, 297, 329-343 (2008)

Froitzheim, N., Stets, J., Wurster, P.: Aspects of Western high atlas tectonics. In: The Atlas System of Morocco, pp. 219–244. (1988)

Gasquet, D., Levresse, G., Cheilletz, A., Azizi-Samir, M.R., Mouttaqi, A.: Contribution to a geodynamic reconstruction of the Anti-Atlas (Morocco) during Pan-African times with the emphasis on inversion tectonics and metallogenic activity at the Precambrian-Cambrian transition. Precambr. Res. **140**(3–4), 157–182 (2005)

Gower, C., Swinden, H.: Pillow lavas in the Dead Islands area, Grenville province, southeast Labrador. Research, New Found Land Department of Mines and Energy, Geological Survey Branch, Report 91, 205–215 (1991)

Hawkesworth, C.J., Van Calsteren, P.W.C.: Radiogenic isotopes—some geological applications. In: Henderson, P (ed.) Rare Earth Elements, pp. 375–421. (1983)

Meschede, M.: A method of discriminating between different types of mid-ocean ridge basalts and continental tholeiites with the Nb-Zr-Y diagram. Chem. Geol. **56**(3–4), 207–218 (1986)

Pearce, J.A., Norry, M.J.: Petrogenetic implications of Ti, Zr, Y, and Nb variations in volcanic rocks. Contrib. Miner. Petrol. **69**(1), 33–47 (1979)

Piqué, A., Tricart, P., Guiraud, R., Laville, E., Bouaziz, S., Amrhar, M., Ouali, R.A.: The Mesozoic-Cenozoic Atlas belt (North Africa): an overview. Geodin. Acta **15**(3), 185–208 (2002)

Rollinson, H.R.: Tonalite-trondhjemite-granodiorite magmatism and the genesis of Lewisian crust during the Archaean. Geological Society, London, Special Publications **112**(1), 25–42 (1996)

Schandl, E.S., Gorton, M.P.: Application of high field strength elements to discriminate tectonic settings in vms environments. Econ. Geol. **97**(3), 629–642 (2002)

Sun, S., Mc Donough, W.F.: Chemical and isotopic systematics of oceanic basalts: implications for mantle composition and processes. Geological Society, London, Special Publications **42**(1), 313–345 (1989)

Teixell, A., Arboleya, M.L., Julivert, M., Charroud, M.: Tectonic shortening and topography in the central High Atlas (Morocco). Tectonics **22**(5), (2003)

Thomas, R.J., Chevallier, L.P., Gresse, P.G., Harmer, R.E., Eglington, B.M., Armstrong, R.A., de Beer, C.H., Martini, J.E.J., de Kock, G. S., Macey, P.H., Ingram, B.A.: Precambrian evolution of the Sirwa Window, Anti-Atlas Orogen Morocco. Precambr. Res. **118**(1–2), 1–57 (2002)

Touil, A., Hafid, A., Moutte, J., Boukhari, A.E.: Petrology and geochemistry of the Neoproterozoic Siroua granitoids (central Anti-Atlas, Morocco): evolution from subduction-related to within-plate magmatism. Geological Society, London, Special Publications **297**(1), 265–283 (2008)

Walsh, G.J., Benziane, F., Aleinikoff, J.N., Harrison, R.W., Yazidi, A., Burton, W.C., Quick, J.E., Saadane, A.: Neoproterozoic tectonic evolution of the Jebel Saghro and Bou Azzer—El Graara inliers, eastern and central Anti-Atlas, Morocco. Precambr. Res. **216–219**, 23–62 (2012)

Winchester, J.A., Floyd, P.A.: Geochemical discrimination of different magma series and their differentiation products using immobile elements. Chem. Geol. **20**, 325–343 (1977)

A New Clue on Neoproterozoic Underplating-Related Magmatism and Origin of Adakites in Zaranda (North-Central Nigeria)

Hafizullah Abba Ahmed, Lian-Xun Wang, Musa Bala Girei, and Victor Ikechukwu Vincent

Abstract

Granitic rocks were emplaced in Zaranda complex in north-central Nigeria during the Neoproterozoic Pan-African orogeny. These rock suites are characterized by elevated concentrations of Na_2O, Al_2O_3 and Sr as well as low contents of Y, Yb and MgO. The dominant samples except one are characterized by elevated Sr/Y (107–128) and La/Yb (36–40) ratios in addition to positive Eu anomaly (Eu/Eu* = 2.2–2.58). These geochemical characteristics allow us to consider them as adakitic rocks. Based on their high SiO_2 (73.44–73.97 wt. %) contents, they can be defined as high silica adakites (HSA). Besides, their low MgO contents (0.21–0.25 wt. %) and Mg# (24.10–27.13) are lower than those of typical slab derived melts (Mg# 58–72). Hence, in this working hypothesis, we interpret them as adakitic rocks formed from partial melting of the thickened lower crust triggered by underplating of mafic melts. Such mafic melts rose from the asthenospheric mantle to heat up the base of thickened continental crust. The heat prompted the partial melting that resulted in the formation of Zaranda adakitic rocks. Subsequent fractional crystallization of the adakitic melts yielded the associated biotite granite in the study area. However, further studies involving a larger number of samples are recommended to confirm this model.

Keywords

Adakites • Zaranda • North-central Nigeria • High silica adakites • Pan-African granite

1 Introduction

The geodynamic development of Pan-African granitoids of Nigeria (PAGN) is associated to the continent–continent collision ca. 630–600 Ma (Dada et al. 1995, Goodenough et al. 2014) and post-collision (590–450 Ma). They belong to an orogenic belt cut by numerous NNE–SSW-trending ductile shear zones that are comparable with similar shear zones in the Borborema Province of Brazil (Goodenough et al. 2014).

Current knowledge of the (PAGN) is limited to some petrological and whole-rock geochemical studies carried out in the last few decades (e.g., Dada et al. 1995). In this contribution, therefore, we present for the first time the zircon U-Pb geochronology in addition to new geological, geochemical and Sr-Nd isotopic data for the (PAGN) from Zaranda complex in north-central Nigeria. The new data are used to discuss the origin of these granitoids.

2 Geological Background, Sampling and Analysis

North-central Nigeria basement consists of Precambrian gneisses and migmatite, which were later intruded by Pan-African granitoids.

Accordingly, four samples of the (PAGN) were collected in this study (Fig. 1a) for whole-rock geochemistry, U/Pb zircon dating and Sr-Nd isotopes. Besides, other published data are used for comparison. The U-Pb dating of zircons was performed at Samples Solution Co. Ltd., Wuhan, China, using a 193 nm GeoLasPro and an Agilent 7700e ICP-MS.

H. A. Ahmed · L.-X. Wang (✉) · M. B. Girei · V. I. Vincent
Faculty of Earth Sciences, China University of Geosciences, Wuhan, 430074, China
e-mail: lianxunwang@cug.edu.cn

H. A. Ahmed · V. I. Vincent
Department of Geology, Modibbo Adama University of Technology, Yola, Nigeria

M. B. Girei
Department of Geology, Bayero University, Kano, Nigeria

A. Çiner et al. (eds.), *Recent Research on Geomorphology, Sedimentology, Marine Geosciences and Geochemistry*, Advances in Science, Technology & Innovation, https://doi.org/10.1007/978-3-030-72547-1_68

Whole-rock major and trace elements were prepared and analyzed at Australia Laboratory Services Guangzhou and Samples Solution Co. Ltd., Wuhan, China, respectively. A Neptune MC-ICP-MS was used to measure the 87/86Sr and 143/144Nd isotope ratios at Sibada Co. Ltd. (Qingdao, China).

3 Results

3.1 Petrography

The rocks range from fine to coarse grained in texture and composed of biotite 5%, K-feldspars ~40–45%, quartz ~30–35% and plagioclase ~5% as the major minerals and apatite and zircon ~2% as accessory minerals (Fig. 1b).

3.2 Geochronology

The analytical result of LA–ICP–MS zircon U-Pb dating of adakite sample yielded a $^{206}Pb/^{238}U$ weighted mean age of 633 ± 3 Ma as the emplacement age of the rock (Fig. 1c).

3.3 Geochemistry

The Zaranda intrusive rocks are characterized by high SiO_2 (73.44–75.87 wt. %), Na_2O (3.24–4.48 wt. %), K_2O (3.99–5.04 wt. %) contents but low MgO (0.02–0.09 wt. %), Y (2.8–15 ppm) and Yb (0.28–1.34 ppm) contents with high Sr/Y (107–128), La/Yb (36–40) ratios. These geochemical features indicate that the rock belongs to the peraluminous and adakite series (Figs. 2a and 3b).

3.4 Sr-Nd Isotopes

The Sr-Nd isotope analysis of one sample yielded $^{87}Sr/^{86}Sr$ of 0.717588, while Nd isotope analysis of three samples yielded the εNd (t) values ranging from −3.48 to −5.00 (Fig. 3a).

4 Discussion

Studies regarding the origin of adkites have received much attention since Defant and Drummond (1990) first coined this term. However, the genesis of adakite is still a subject of debate (Castillo 2012). Different models have been postulated to account for their origin, and they include (1) Fractional crystallization and contamination of basaltic melts (Castillo 2012), (2) Melting of young subducted oceanic slab (Zhao and Zhou 2008) and (3) Partial melting of thickened lower crust (Castillo 2012).

Typically, rocks that are classified as adakites show significant variation in major and trace element contents, and hence, several classification schemes have been proposed for adakites: foremost of which is the use of Si_2O content as a discriminant. In this scheme, adakitic rock with high Si_2O is interpreted as derivatives of pristine melts from melting of subducted slab, while those with low Si_2O content are considered to have been generated through melting of mantle wedge peridotite altered by intermingling with felsic melts (Zhao and Zhou 2008).

The Zaranda rocks exhibit high Sr/Y and La/Yb ratios (Fig. 3b) except (ZR7-01), which is a geochemical feature that is typical of adakitic rocks. Their high silica content placed them in the clan of high SiO_2 adakites. Such high SiO_2 content coupled with their negative εNd (t) values and high $^{87}Sr/^{86}Sr$ rule out the possibility that the Zaranda ada-

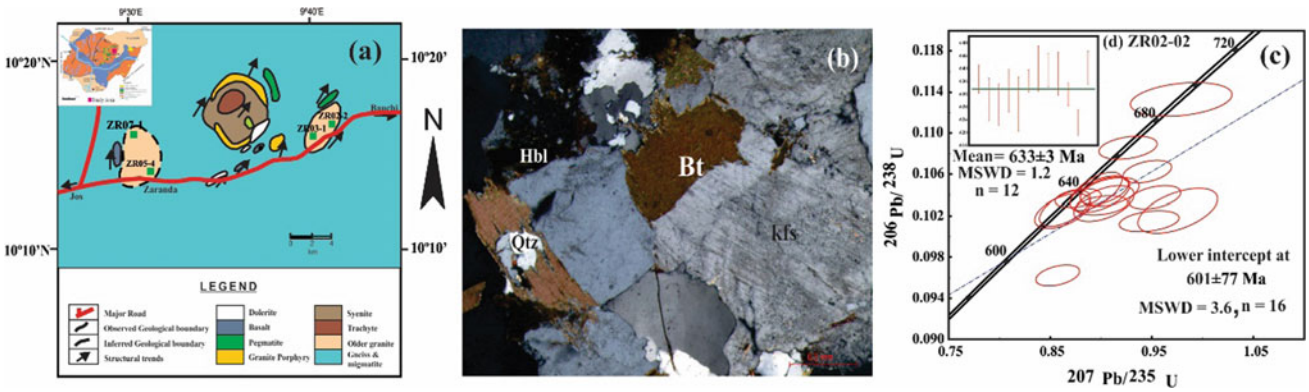

Fig. 1 **a** Geological map of Zaranda (Modified after Ahmed et al. 2019), **b** Photomicrograph of adakitic sample from Zaranda. **c** LA-ICP-MS zircon U-Pb concordia plot of Zaranda

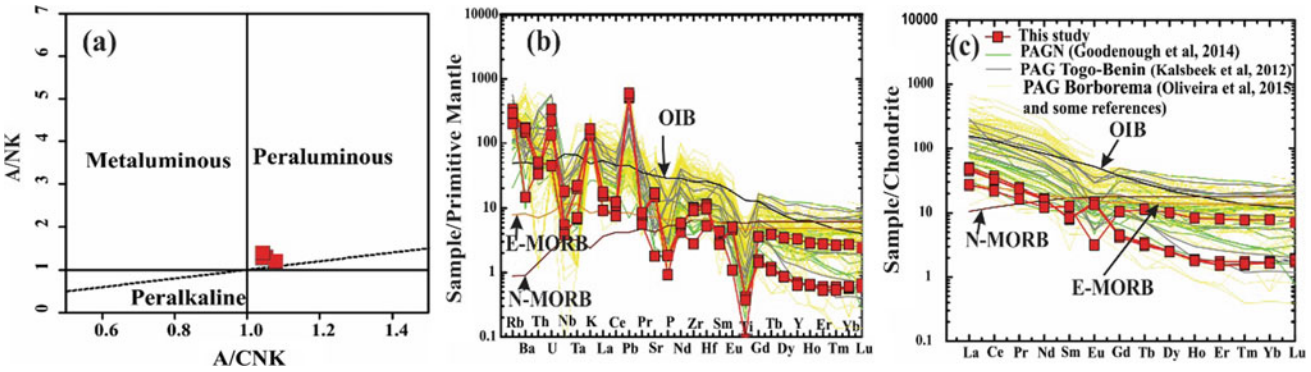

Fig. 2 **a** ASI diagram (Shand 1943), **b** primitive-mantle normalized trace element spidergram **c**. Chondrite-normalized REE patterns. Normalization factors were taken from Sun and McDonough (1989)

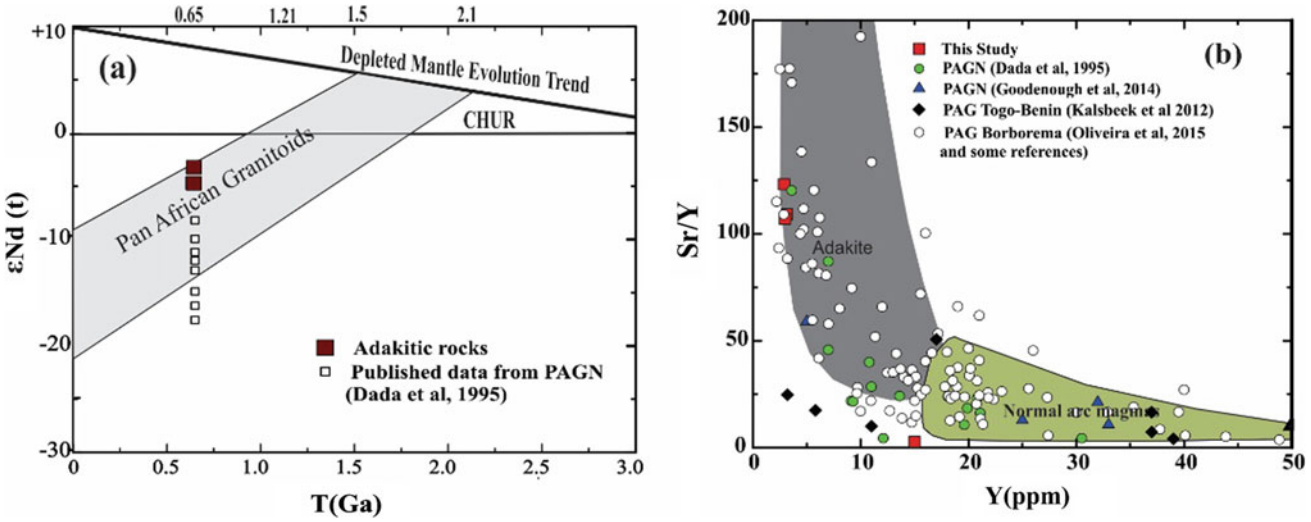

Fig. 3 **a** εNd (t) vs, Age plot **b** Sr/Y versus Y plot

kites originated from fractional crystallization of basaltic magmas. Besides, their low MgO and Mg# are inconsistent with the formation through melting of the subducted oceanic slab because melt generated from subducted oceanic slap melting usually has high MgO and Mg# (Zhao and Zhou 2008). Instead, it is more likely that the Zaranda adakites formed from melting of a thickened lower crust as evidenced by their low MgO, Rb/Ba (~0.1), Nb/U (0.4–2.9) and Ce/Pb (0.3–0.5) (Ma et al. 2015).

Furthermore, the Zaranda adakites are characterized by significant depletion in Nb, Ti and Ta as well as positive Eu anomaly (Fig. 2b, c). These geochemical characteristics suggest that rutile and garnet were the main residual mineral phases in the course of their formation (Zhao and Zhou 2008), whereas the absence of plagioclase as a residual phase during partial melting led to an increase in Eu and Sr in the adakitic magma (Zhao and Zhou 2008). On the other hand, the sample with low Sr/Y and La/Yb ratios and pronounced negative Eu anomaly (ZR7-01) probably evolved from the adakitic magma through fractional crystallization involving plagioclase at a relatively shallow crustal level. Comparison of Zaranda rocks data with published data of Pan-African granitoids from some parts of Nigeria, Togo-Benin (West Africa) and Borborema (South America) indicate that all the rocks exhibit similar geochemical features (Figs. 2b, c and 3b).

5 Conclusions

1. A combined LA-ICP-MS U-Pb zircon age, Sr-Nd isotope and whole-rock geochemical data yielded valuable clues on the origin and age of the Pan-African granite in Zaranda, north-central Nigeria.
2. The LA-ICP-MS U–Pb geochronology result indicates that the adakitic and biotite granite in Zaranda were emplaced during the Neoproterozoic period at 633 ± 3 Ma.

3. Geochemical and isotopic data indicate that the Zaranda adakitic rocks were formed from the melting of the thickened lower crust. The low Nd(t) and high $^{87}Sr/^{86}Sr$ isotopic signatures of the rock further suggest that they might have formed from the partial melting of the Paleoproterozoic lower crust. Partial melting probably took place at high P-T in a thickened crust leaving garnet and rutile as residuals phases which gave rise to adakitic signature in the Zaranda granitoids. The heat for such melting was sourced through underplating of the lower crust by hot mafic magmas from the asthenospheric mantle.
4. However, given the limited data presented in this study, our interpretations at this stage are mere working hypotheses that require further investigation to confirm.

Acknowledgements We acknowledge the NNSF of China (Grant: 41530211, 41502046) and the Fundamental Research Funds for the Central Universities, China University of Geosciences (Wuhan), (CUGCJ1711) for their financial support. The Society of Economic Geologists Inc., USA, is sincerely acknowledged for fully funding the fieldwork for this study.

References

Ahmed, H.A., Wang, L.X., Ma, C.Q., Garba, I., Girei, M.B., Vincent, V. I.: Geochronology, Petrogenesis and Tectonic Implication of A-Type Granite from Zaranda (North-Central Nigeria). In: Doronzo D., Schingaro E., Armstrong-Altrin J., Zoheir B. (eds) Petrogenesis and Exploration of the Earth's Interior. Advances in Science, Technology & Innovation (IEREK Interdisciplinary Series for Sustainable Development). Proceedings of the 1st Springer Conferenceof the Arabian Journal of Geosciences (CAJG-1) 17–21, Tunisia Springer, Cham (2019)

Castillo, P.R.: Adakite petrogenesis. Lithos **134–135**, 304–316 (2012)

Dada, S.S., Briqueu, L., Harms, U., Lancelot, J.R., Matheis, G.: Charnockitic and monzonitic Pan-African series from north-central Nigeria: trace-element and Nd, Sr, Pb isotope constraints on their petrogenesis. Chem. Geol. **124**, 233–252 (1995)

Defant, M.J., Drummond, M.S.: Derivation of some modern arc magmas by melting of young subducted lithosphere. Nature **374**, 662–665 (1990)

Goodenough, K.M., Lusty, P.A.J., Roberts, N.M.W., Key, R.M., Garba, A.: Post-collisional Pan-African granitoids and rare metal pegmatites in western Nigeria: age, petrogenesis, and the 'pegmatite conundrum.' Lithos **200–201**, 22–34 (2014)

Ma, Q., Zheng, J.P., Xu, Y.G., Griffin, W.L., Zhang, R.S.: Are continental "adakites" derived from thickened or foundered lower crust? Earth Planet. Sci. Lett. **419**, 125–133 (2015)

Shand, S.J.: Eruptive rocks. Their Genesis, Composition, Classification, and Their Relation to Ore-Deposits with a Chapter on Meteorite. John Wiley & Sons, New York, pp. 1–350. (1943)

Sun, S.S., McDonough, W.F.: Chemical and isotopic systematic of oceanic basalts: implications for mantle composition and processes. In: Saunders, A.D., Norry, M.J. (eds.) Magmatism in the Ocean Basins: Geological Society, vol. 42, pp. 313–345. London, Special Publications (1989)

Zhao, J.H., Zhou, M.F.: Neoproterozoic adakitic plutons in the northern margin of the Yangtze Block, China: partial melting of a thickened lower crust and implications for secular crustal evolution. Lithos **104**, 231–248 (2008)

Eruptive History and Petrologic Evolution of the Lechmine N'Aït El Haj Maar (Middle Atlas, Morocco)

Sara Mountaj, Toufik Remmal, Samira Makhoukhi, Iz-Eddine El Hassani El Amrani, Kawtar Lakroud, Pierre Boivin, and Benjamin Van Wyk De Vries

Abstract

The maar of Lechmine N'Aït El Haj (LNH) is a monogenetic Plio-Quaternary volcano, located in the volcanic province of the Middle Atlas (Morocco). It is represented by a 110 m deep crater hosted in Liasic limestones. The tephra deposits surrounding the crater are mainly made up of pyroclastic beds interpreted as deposits of phreatomagmatic origin. They are overlain by a small unit of massive breccia tuff that reflects the transition of the eruptive style to the Strombolian. A supply of karstic water caused another transition of the eruptive style from the Strombolian to the phreatomagmatic dynamism. At the end of the volcanic activity, a significant karst collapse of the LNH maar occurred, leading to its current morphology. Petrographic data shows that the volcanic rocks are nephelintes. They are composed essentially of pyroxene and subsidiary olivine. They are silica-undersaturated and belong to sodic magma series. The distinctive geochemical characteristics indicate that the magma has a high MgO (11.4–14.2 wt%) concentration, a low silica content (38.5–40.8 wt%), and a high Ni and Cr concentrations (220–318 ppm and 330–451 ppm, respectively).

Keywords

Lechmine n'Aït el Haj • Maar • Karst • Monogenetic • Middle Atlas

1 Introduction

Monogenetic volcanoes are the most common type of subaerial volcanoes (Tchamabé et al. 2016). They result from a single volcanic eruption or several volcanic eruptions that have occurred in a short period of time, not exceeding a few days. The eruptions are usually provoked by the intrusion of small amounts of magma (Németh 2010; Walker et al. 2000).

Among monogenetic volcanoes, those of phreatomagmatic type, emerging from the interaction between the ascending magma and superficial water, lead to energetic volcanic eruptions and create a volcanic structure of «maar» type. These volcanoes consist of large depressions usually surrounded by a tephra wall composed of pulverized volcanic materials (pyroclastics), lava flows, and fragments of the bedrock that has been intruded during the volcanic eruption (White and Ross 2011; Lorenz 2003). The Lechmine n'Aït el Haj maar located in the Middle Atlas, Morocco (33° 22′ 50″ N, 5° 04′ 15″ O) (Fig. 1a), is 900 m of width and 112 m deep (Fig. 1b). It is an excellent example of this type of monogenetic volcano.

This work aims to investigate the volcanic mechanism of the Lechmine n'Aït el Haj maar based on tephrostratigraphy, in order to improve the knowledge about the evolution of tephra ring around LNH. The geochemical, mineralogical, and petrographic features constrain the origin and type of magma.

2 Material and Methods

Seventy representative rock samples have been collected from the LNH. Thin sections were studied under polarizing microscope. Fourteen samples were crushed and powdered using techniques suitable for geochemistry. Major elements were analyzed by inductively coupled plasma mass spectrometry (ICP-MS) at the Laboratory Magmas et Volcans

S. Mountaj (✉) · T. Remmal · S. Makhoukhi · K. Lakroud
Faculty of Sciences Aïn Chock, University Hassan II, Casablanca, Morocco

I.-E.E. H. E. Amrani
Institute of Scientific Research, Rabat, Morocco

P. Boivin · B. V. W. De Vries
Université Blaise Pascal - Clermont-Ferrand II, Clermont-Ferrand, France

A. Çiner et al. (eds.), *Recent Research on Geomorphology, Sedimentology, Marine Geosciences and Geochemistry*, Advances in Science, Technology & Innovation, https://doi.org/10.1007/978-3-030-72547-1_69

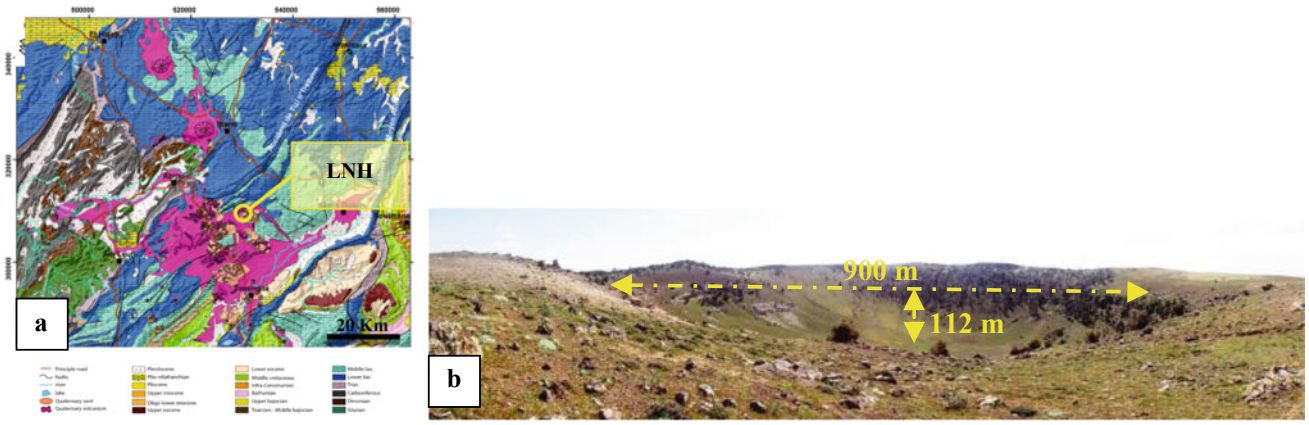

Fig. 1 **a** Geological map of the volcanic area of the Middle Atlas chain (Martin 1981); **b** Photo of the crater of Lechmine n'Aït el Haj taken from the W

(LMV), University of Clermont-Ferrand, France. The trace elements were analyzed by inductively coupled plasma atomic emission spectrometry (ICP-AES) at the Centre de Recherches Pétrographiques et Géochimiques (CRPG) of Nancy.

3 Results

3.1 Tephrostratigraphy

The LNH environment is characterized by outcrops of the Liasic limestone substrate mostly in the NW. The latter records intense fracturing. Locally, in the northwestern flank, 1.5 m of lacustrine deposits is at the base of the pyroclastic deposits (Mountaj and Remmal 2014). Based on stratification criteria and deposition, transport, and fragmentation mechanisms, five main units were distinguished (Fig. 2). The first three units, U1, U2, and U3, consist of beds of lapilli tuff, composed of juvenile clasts and accidental lithics and a small proportion of xenoliths. These elements are cemented by fine volcanic ash. The distinction between the three units is based on the observation of the distribution, the size, the shape, and the proportion of accidental lithics and juvenile clasts.

This variation depends on the intensity of the explosion, the water/magma ratio, and the location of the eruptive vent. The passage toward the fourth unit (U4) is branded with a figure of mud cracks. U4 consists of massive breccia tuffs. It contains scoria, lava blocks, and volcanic bombs, forming a kind of lava breccia rich in peridotites and pyroxenites xenoliths. This unit is devoid of accidental lithics. The upper and last unit (U5) is represented by thin level of lapilli tuff, located mostly in the SE flank, with few outcrops in the NW. The southern side of the crater is covered by massive lava flow.

3.2 Petrography, Mineralogy and Geochemistry

The LNH mafic lavas show a fluidal microlitic texture. The phenocrysts are mostly composed of clinopyroxene and olivine (Fig. 3). Mineralogical analysis allows classifying the clinopyroxenes using the ternary diagram enstatite/wollastonite/ferrosilite (Morimoto 1989); they plot generally in the augite–diopside field. Olivines show a resorbed texture due to their destabilization or rapid crystallization. Olivine ($Fo_{74–87}$) also shows a forsterite composition. Major elements data was obtained on 14 samples (Fig. 4). The LNH rocks are very similar in composition and have comparable ranges of major and trace element concentrations. The chemical analyses show that the mafic samples display low silica content 38.5–40.8 wt% and very high concentrations of Ni and Cr (220–318 ppm and 330–451 ppm, respectively). The TiO_2 varies from 2.87 to 3.12%, MgO from 11.45 to 11.16%, and Mg# from 40.62 to 45.42. Those values reflect the primitive character of the magma.

4 Discussion

The pyroclastic deposits are influenced by the conditions of the eruption, namely the water/magma ratio (Fisher and Schmincke 1984). In LNH, the first burst was caused by the arrival of ascending magma into water from a preexisting lake highlighted by the lacustrine deposits; this generated a strong phreatomagmatic first explosion and consequently the birth of the LNH maar (White and Ross 2011; Lorenz 2003; Wohletz and Sheridan 1983). The tephrostratigraphic study allowed defining five units of pyroclastic deposits. U1, U2, and U3 are composed of lapilli tuff and were inherent of phreatomagmatic activity (presence of lake water). The intensity of every explosion depends on the water/magma

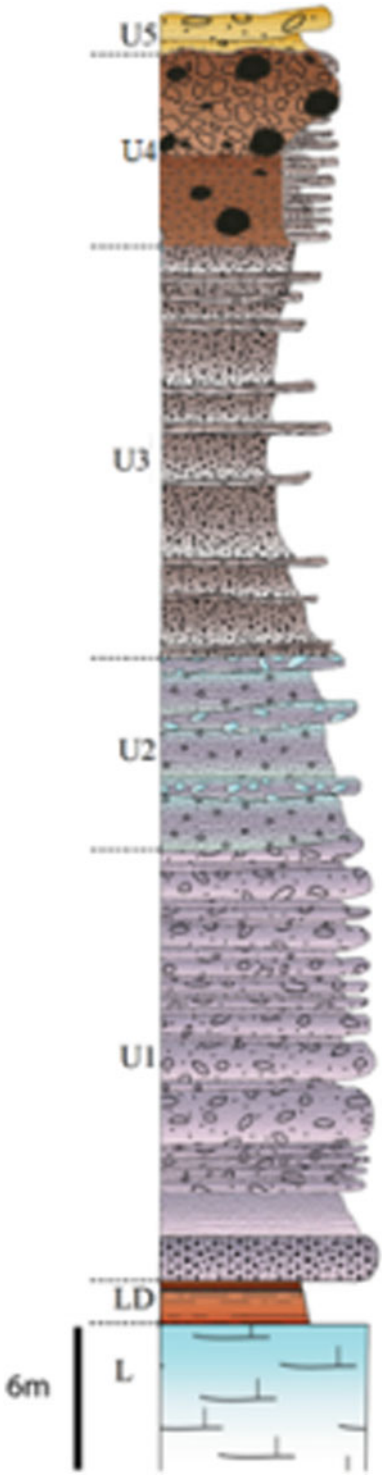

Fig. 2 Global stratigraphic log of LNH pyroclastic deposits (L: limestone; LD: lacustrine deposits)

ratio. Toward the summit of the third unit (U3), the proportion of accidental lithics decreased inversely to the juvenile clasts, which became very abundant, meaning that the volume of water also decreased until it dried. This is attested by the structures of mud cracks at the top of U3. At this stage, the dynamic of eruption changed from a phreatomagmatic to a Strombolian one and the formation of the fourth unit of breccia tuff. Meanwhile, a lava flow came from the plateau of the Middle Atlas and poured into the LNH crater from the south. A second transition of the eruptive occurs at the fifth unit (U5), which consisted of lapilli tuff; the ascending magma met water again and provoked the final phreatomagmatic explosion.

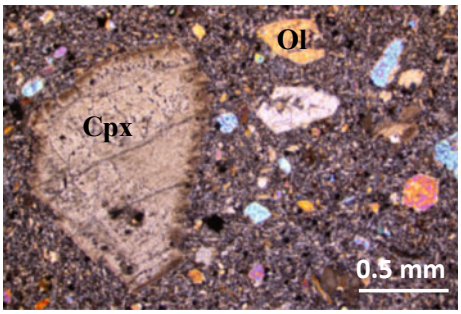

Fig. 3 Thin section of LNH nephelinite (Cpx: clinopyroxene, Ol: olivine)

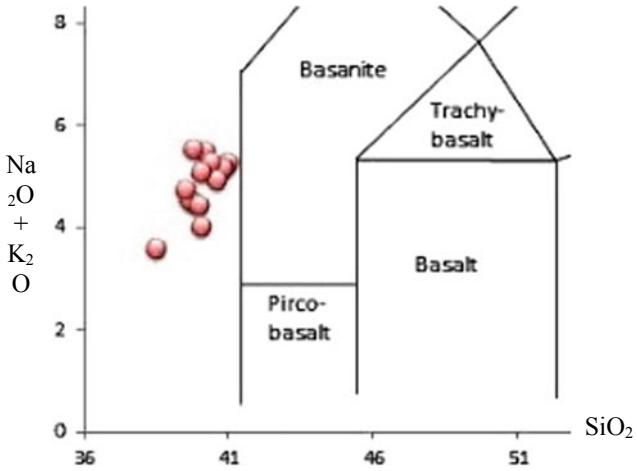

Fig. 4 TAS plot for the LNH lavas (Bas et al. 1986)

The mafic lavas of LNH are nephelinites. They derived from a primary magma that is near primary. The phenocrysts of LNH lavas consisted of olivine and diopside. The enrichment of incompatible element (Ni, Cr) suggested a low degree of partial melting (2%) of a mantle source located at 65 km deep (2 GPa) (Bosch et al. 2014). This depth corresponds to the lithosphere–asthenosphere boundary under the Middle Atlas (60–80 km) (Bosch et al. 2014).

5 Conclusions

This study presents the first detailed volcanological stratigraphy of tephra composing the maar of Lechmine n'Aït el Haj. From an old lake to an exceptional and didactic maar,

the LNH is characterized by a double transition of eruptive style, starting by a phreatomagmatic to a strombolian dynamic, then from a strombolian to a final phreatomagmatic explosion. The petrological, mineralogical, and geochemical analyses show that the LNH nephelinites were not fractioned with formation via a low degree of partial melting degree (2%). The origin of this magma is the lithosphere–asthenosphere boundary. The LNH is an educational site for maars. It is deemed a model of geosite in the volcanic province of the Middle Atlas.

References

Bas, M.J.L., Maitre, R.W.L., Streckeisen, A., Zanettin, B.A.: Chemical classification of volcanic rocks based on the total alkali-silica diagram. J. Petrol. **27**(3), 745–50 (1 June 1986)

Bosch, D., Maury, R.C., Bollinger, C., Bellon, H., Verdoux, P.: Lithospheric origin for neogene-quaternary Middle Atlas lavas (Morocco): clues from trace elements and Sr–Nd–Pb–Hf isotopes. Lithos **205**, 247–265 (2014)

Fisher, R.V., Schmincke, H.-U.: Pyroclastic Rocks [Internet]. Springer, Berlin, Heidelberg (1984)

Lorenz, V.: Maar-diatreme volcanoes, their formation, and their setting in hard-rock or soft-rock environments. Geolines **15**, 72–83 (2003)

Martin, J.: Le Moyen Atlas central étude géomorphologique, vol. 258. Editions du Service géologique du Maroc (1981)

Morimoto, N.: Nomenclature of pyroxenes. Mineral. J. **14**(5), 198–221 (1989)

Mountaj, S., Remmal, T., El Amrani, El Hassani, I.-E., Van wyk de vries, B.: Reconstruction of the morphological evolution and the eruptive dynamics of the lachmine n'Ait el Haj Maar in the Middle Atlas. Karstic province of Morocco. In: Proceeding 5th International Maar Conference Quéretaro Mexico, pp. 4–5, 22 Nov 2014

Németh, K.: Monogenetic volcanic fields: origin, sedimentary record, and relationship with polygenetic volcanism. In: Geological Society of America Special Papers [Internet]. Geological Society of America (2010)

Tchamabé, B.C., Kereszturi, G., Németh, K., Carrasco-Núñez, G.: How polygenetic are monogenetic volcanoes: case studies of some complex maar-diatreme volcanoes. In: Nemeth, K. (ed.) Updates in Volcanology—From Volcano Modelling to Volcano Geology [Internet]. InTech (2016)

Walker, G.P.L., Sigurdsson, H., Houghton, B., Rymer, H., Stix, J., McNutt, S.: Basaltic volcanoes and volcanic systems. In: Encyclopedia of Volcanoes, pp. 283–289. Academic Press (2000)

White, J.D.L., Ross, P.-S.: Maar-diatreme volcanoes: a review. J. Volcanol. Geotherm. Res. **201**(1), 1–29 (2011)

Wohletz, K.H., Sheridan, M.F.: Hydrovolcanic explosions; II, evolution of basaltic tuff rings and tuff cones. Am. J. Sci. **283**(5), 385–413 (1 May 1983)

Mineralogical and Geochemical Characteristics of Weathered Products of Basaltic Volcanites of Trias in the Débadib Structure (El Kef, Tunisia)

Randa Ben Abdallah, Abir Chihaoui, Hana Galai, and Mounir Medhioub

Abstract

This work explores the mineralogical, petrographic and geochemical aspects of the basaltic volcanic rocks as persistent in the Débadib structure (Northern Tunisia) and their alteration outcomes. The outcrops, as studied in the area, are those belonging to diapiric zone. These rocks appear to display argilization associated with weathering and significant hydrothermal circulation. The clay fractions consist mainly of chlorite, kaolinite, mica and talc associated with significant amounts of plagioclase, olivine and minor amounts of calcite, talc and analcime. The chemical composition of the Jebel Débadib samples revealing high levels of TiO_2, Fe_2O_3, and MgO.

Keywords

Basaltic volcanites • Diapiric Trias • Chlorite • Talc • Alteration processes

1 Introduction

Clay minerals in volcanic environments are widely distributed over the Earth's surface as products of different processes such as chemical weathering and hydrothermal alteration of volcanic rocks. According to Roberson et al. (1999), alteration of associated basalts with hydrothermal fluids provides an excellent natural laboratory for the study of transformation products with fine-grained phyllosilicates that are the most characteristic products of this process. This paper aims to use the mineralogical and geochemical characterization of clay minerals which result from the alteration of basaltic rocks from Jebel Débadib in order to (1) determine and specify the mineral paragenesis of the materials studied, to (2) establish the structural relationships between the different minerals, their chemical compositions and to (3) study their state of deterioration and the products that flow.

2 Geological Setting

In northern Tunisia, outcrops of the Triassic are under the form of diapiric masses and are distributed an NE-SW alignment. These diapiric formations of chaotic aspects present a relatively varied lithology composed of gypsum, marls, sandstones, dolomitic limestones and dolomite. The presence of magmatic bodies in this Triassic has been mentioned by several authors Bajanik (1971), Bolze et al. (1952), Castany (1953), Crampon (1971), Moïsseef (1959) and Solignac (1927). The Débadib structure situated between El Kef and the Algero-Tunisian border belongs to one of the main diapiric alignments of the oriental Maghreb (Fig. 1). It constitutes an elliptic form oriented NE-SW. The heart is occupied by Triassic residual evaporites containing basaltic volcanites which seem to indicate extensional setting during the Triassic period (Hatira 2000).

3 Methodology

The petrographic analysis was carried out with an optical microscope type Zeiss equipped with Olympus digital Camera (3,3 mega pixel).

R. B. Abdallah (✉) · H. Galai
Faculty of Sciences of Bizerte, University of Carthage, Tunis, Tunisia

R. B. Abdallah · M. Medhioub
Laboratory of Spectroscopic Characterization and Optics of of Materials (LaScom), Sfax, Tunisia

A. Chihaoui
Faculty of Sciences of Gabès, University of Gabès, Gabès, Tunisia

M. Medhioub
Faculty of Sciences of Sfax, University of Sfax, Sfax, Tunisie

A. Çiner et al. (eds.), *Recent Research on Geomorphology, Sedimentology, Marine Geosciences and Geochemistry*, Advances in Science, Technology & Innovation, https://doi.org/10.1007/978-3-030-72547-1_70

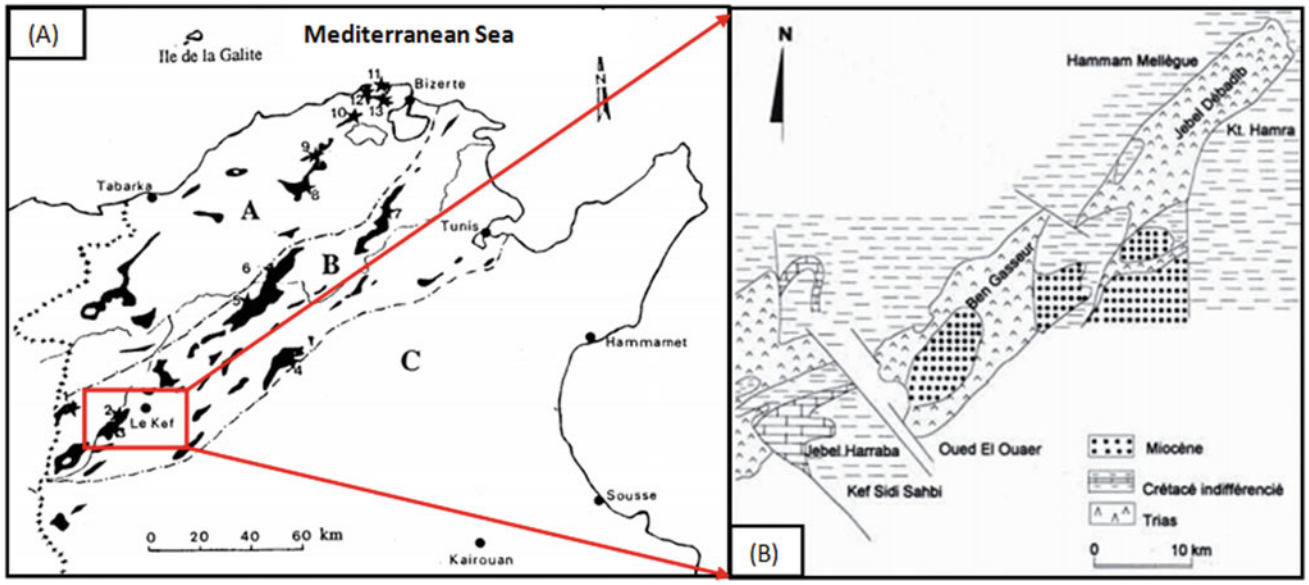

Fig. 1 Geological map of the studied area (Hatira 2000; Laridhi and Dali 1991)

The mineralogical compositions of the bulk and clay fractions were determined using a Siemens Cristalloflex 810 (radiation Cu Kα, 40 kV, 30 mA). For each sample, a quantity is dried in an oven at 30 °C. Then this amount is milled for 10 min. The sample is prepared either as a flattened powder in a cup or as a flat solid wafer (glass slide). Chemical analysis was carried out by X-ray fluorescence (XRF) using a Philips PW XRF spectrometer. Loss on ignition was estimated by measuring the difference in weight between dried 10 g of a sample and calcined at 1000 °C. The chemical analyses were carried out at the mineralogy laboratory of the faculty of Sciences of Sfax (Tunisia).

4 Results and Discussion

4.1 Mineralogy, Petrography and Paragenesis

Using the polarizing optical microscope, we found that the rock is composed of minerals rich in iron and magnesium such as olivine and plagioclase. In the matrix, iron oxide occurs in a sporadic form. These iron oxides have an elongated brownish-black spot shape that can reach 1 mm in length.

Alterations are represented through two types: meteoric (surface) and hydrothermal (post-magmatic). Weathering is easily observed in volcanic rocks. It is represented by the oxidation of olivine (Fig. 2a). The latter, which presents in the form of automorphic crystals, is often iddingsitized and chloritized. Hydrothermal alteration is also evident in the Jebel Débadib rocks. It is represented by the presence of chlorite (Fig. 2b) and Talc (Fig. 3). Illite is also an alteration mineral in which it partly invades the mesostasis (Fig. 2a, c) of basalts as well as the phenocrysts of plagioclase (Fig. 2c). Plagioclase alteration occurs from the centre to the periphery. There is also calcite filling the vesicles (Fig. 2d).

The X-ray diffraction (XRD) patterns of whole rocks show that the Jebel Débadib samples are rich in clay minerals associated with significant amounts of plagioclase, olivine and minor amounts of calcite, talc and analcime (Fig. 3). The presence of the latter tends to make us think that his formation is secondary and is likely related to postvolcanic hydrothermal phenomena at the origin of the mineralization in this region.

4.2 Chemical Composition

The chemical composition of the Jebel Débadib samples reveals high levels of TiO_2, Fe_2O_3, and MgO ranging from 1.54% to 2.06%; 5.87% to 9.26% and 5.11% to 11.81, respectively. The relatively low levels of SiO_2 (46–50%) are comparable with basalt compositions. For the diapiric Triassic volcanics, it is noted that the Na_2O and CaO contents are abnormally low. In contrast, those of K_2O can be sometimes high (Table 1).

5 Conclusions

The mineralogical study by XRD and the petrographic analysis reveal that they are rocks made of plagioclase, automorphic crystals of iddingsitized olivine, chloritized, calcite which fills vesicles, accessory minerals such as

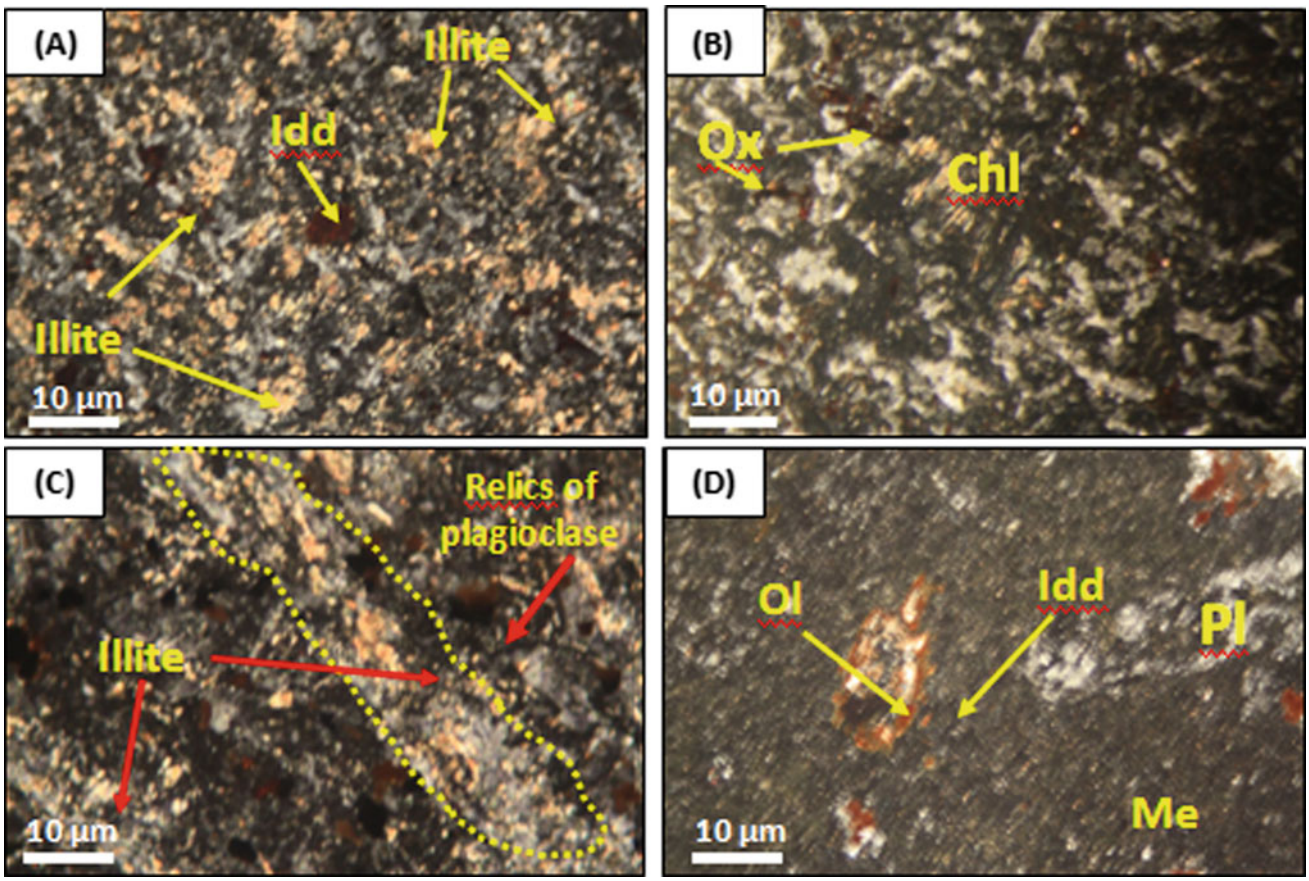

Fig. 2 Photomicrographs showing, **a** microlitic structure that contains olivine (Ol) iddingsitized and greyish colour illite; **b** chlorite and oxide; **c** phenocrystas of plagioclase at heart completely altered by illite; **d** olivine with a calcitized core and iddingsitized border

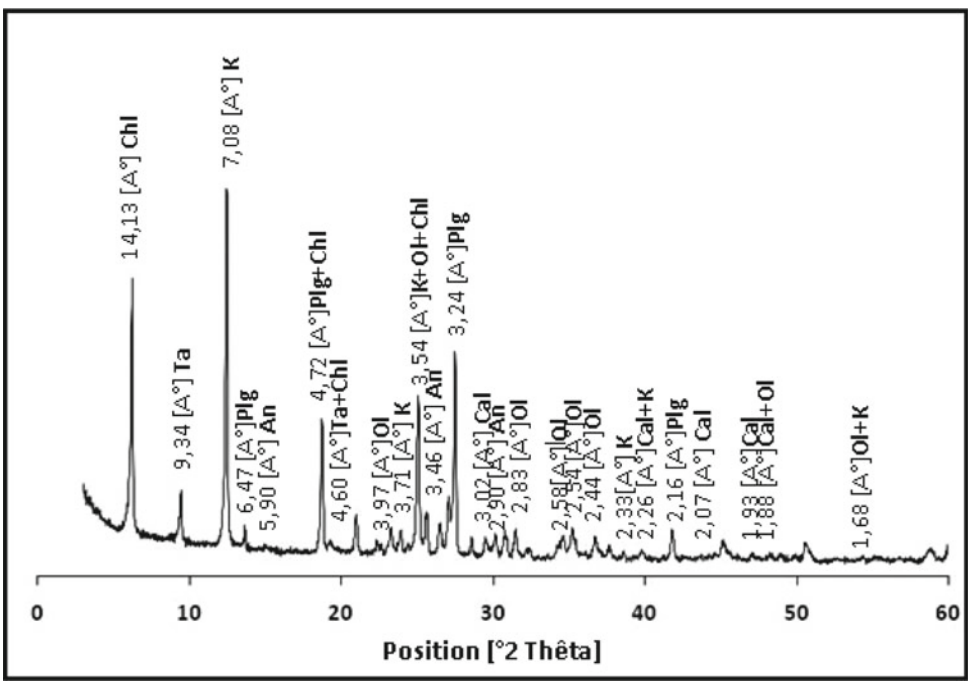

Fig. 3 X-ray diffraction patterns of C1 sample of Débadib structure. Chl: Chlorite; K: kaolinite; Ol: Olivine; Cal: Calcite; Plg: Plagioclase; An: Analcime; Ta: Talc

Table 1 Chemical analyses (oxide wt %) of Jebel Débadib samples

Oxide	C1	C2	C4	C5	C6	C7	C9	C10	Ce
SiO_2	49.27	50.77	50.57	49.24	48.84	48.66	49.06	46.23	47.99
Al_2O_3	14.94	16.1	15.08	17.98	15.83	14.54	15.96	14.66	17.99
MgO	7.78	6.93	7.86	7.78	6.28	11.81	5.11	7.24	9.26
K_2O	7.54	8.02	7.91	7.54	4.82	3.74	4.3	7.28	7.43
CaO	0.84	2.47	2.82	1.16	7.17	4.85	7.06	2.79	1.96
Fe_2O_3	5.87	8.12	6.59	7.45	9.01	8.3	8.6	9.26	6.89
MnO	0.038	0.09	0.11	0.08	0.12	0.036	0.12	0.1	0.05
TiO_2	1.9	1.69	1.84	2.06	1.62	1.54	1.69	1.88	1.88
Na_2O	3.46	3.83	2.86	3.51	3.56	3.32	2.85	3.47	0.79
LOI	7.55	1.3	3.5	2.36	0.96	2.96	5.32	6.23	5.99
Total	99.188	99.32	99.14	99.16	98.21	99.756	100.07	99.14	100.23

analcime, opaque minerals and sometimes alteration products represented by clay minerals such as illite, kaolinite, talc and chlorite (detected from the microscopic study and XRD). All these minerals are embedded in a microlithic matrix. In the studied rocks, clay minerals are the results of interactions between basaltic volcanite and meteoric or hydrothermal fluid.

References

Bajanik, S.: Volcanisme en Tunisie Ann. Min. Géol. Tun., n° 25, p (1971)

Bolze, J., Burrollet. P.F., Castany, G: Le sillon Tunisien. XIXe congr. Geol. Intern. Alger. Monog. Région, 2ème Sér., Tunisie, n°5, 112 p (1952)

Castany, G.: Notice explicative. Carte géologique de la Tunisie aux 1/500.000 2ème édition Serv. Min., Industrie et Energie Tunis, vol. in 8, 143 p (1953)

Crampon, N.: Etude géologique de la bordure des Mogods, du pays de Bizerte et du Nord des Hédils (Tunisie septentrionale). Thèse Doct., Es-Sciences Naturelles (1971)

Hatira, N.: Le Trias à caractère extrusive de la zone des dômes: exemple de la structure de Débadib-Ben Gasseur (Tunisie septentrionale). Bull. Soc. Geol. Fr. T. **171**(3), 319–326 (2000)

Laridhi, N., Dali, T.: Etude minéralogique des roches volcaniques métamorphisées du Trias diapirique de la Tunisie septentrionale. Notes Serv. Géol. de Tunisie. n°58, pp. 101–110 (1991)

Moïsseef, A.: Etude géologique et métallogénique de district minier El Gréfa-Bazina. Le Semene (Tunisie). Thèse, Univ., Paris, 152p (1959)

Roberson, H.E., Reynolds, R.C., Jenkins, D.M.: Hydrothermal synthesis of corrensite: a study of the transformation of saponite to corrensite. Clays Clay Miner. **47**, 212–218 (1999)

Solignac, M.: Etude géologique de la Tunisie septentrionale. Thèse Lyon, 756p (1927)

Geochemistry and Mineral Chemistry of Amphibolites in Parts of the Proterozoic Ilesa Schist Belt, Southwestern Nigeria

Jerry Olajide-Kayode, Olugbenga Okunlola, and Akinade Olatunji

Abstract

We conducted a study of the amphibolites of Itagunmodi-Igun area within the Ilesa Schist Belt to determine their petrochemical affinities and pressure–temperature conditions of formation. The amphibolites of the area are massive and comprise magnesio-hornblende, actinolite, labradorite, albite, and accessory titanite. The major and trace element characteristics revealed that they are ortho-amphibolites with tholeiitic and calc-alkaline affinities, plotting in Within-Plate Basalt field of the Zr versus Zr/Y diagram. Plagioclase-hornblende thermobarometry constrained the temperature of formation of the amphibolites to 450-6870C and pressure of 0.5–4.3 kbar. Further, the average pressure of the formation corresponds to approximately 6.6–7.4 km depth of emplacement for the amphibolite.

Keywords

Itagunmodi-Igun • Ortho-amphibolite • Within-Plate Basalt • Magnesio-hornblende • Plagioclase-hornblende thermobarometry

1 Introduction

Itagunmodi and Igun areas occur within the Ilesa Schist Belt; a prominent feature of the basement geology of southwestern Nigeria believed to have been formed in a back-arc basin setting which developed after the beginning of subduction at the margin of the West African Craton ca. 1000 Ma ago. Pelitic and semi-pelitic schists, quartzites, marbles, gneisses, phyllites, banded iron formation (BIF), and amphibolites make up the geology of the Nigerian Schist Belts. The amphibolites are best exposed and most extensive in the Ilesa area (Elueze 1988); experiencing multiple deformations and metamorphism episodes. Petrographic, structural and geochemical studies have been conducted on the am-phibolites in parts of the Ilesa area. However, their petrochemical affinity and pressure–temperature (PT) conditions of formation of amphibolites of Itagunmodi-Igun area (7°30″–7°35″ N and 4°37″–4°42″ E) have not been determined. Petrographic and whole-rock chemical studies, as well as studies on the chemistry of amphibole and plagioclase in the amphibolites of Itagunmodi-Igun area, have been carried out in order to determine the origin, tectonic setting, and P–T conditions during metamorphism.

2 Methodology

Nineteen rock samples were collected and studied by petrographic methods under a transmitted light polarizing microscope at the Department of Earth Sciences, University of the Western Cape, South Africa. Seven samples mounted in polished 1″ epoxy discs at the University of Free State, South Africa, were analyzed for amphibole and plagioclase chemistry using the scanning electron microscopy-energy dispersive/wavelength dispersive X-ray (SEM-EDX/WDX) technique on a Zeiss EVO MA 15 spectrometer housed at the Central Analytical Facility of Stellenbosch University, South Africa. Whole-rock geochemical analysis of pulverized rock samples was done at Bureau Veritas Pty Ltd., Vancouver, using Lithium Metaborate digestion.

J. Olajide-Kayode (✉)
Pan African University Life and Earth Sciences Institute, University of Ibadan, Ibadan, Nigeria

O. Okunlola · A. Olatunji
University of Ibadan, Ibadan, Nigeria

A. Çiner et al. (eds.), *Recent Research on Geomorphology, Sedimentology, Marine Geosciences and Geochemistry*, Advances in Science, Technology & Innovation, https://doi.org/10.1007/978-3-030-72547-1_71

3 Results

3.1 Geologic Setting and Petrography

The Itagunmodi-Igun area consists of amphibolite, talc-chlorite schist, quartzite, and quartz-biotite schist. Hand specimens of the amphibolites are green to greyish-green and fine-grained with plagioclase seen as aggregates in some of the outcrops.

In thin sections, rocks consist of hornblende as it is the most abundant mineral, with subordinate actinolite, plagioclase, and epidote. They also contained accessory titanite with minor opaques. The alteration was evident in some samples with amphibole and plagioclase replaced by epidote. The amphibolites contain 63–72% amphibole (hornblende plus actinolite), 11–20% plagioclase, 8–15% epidote, with quartz and opaque minerals averaging 3.45% and 3.75%, respectively.

3.2 Geochemistry

The CaO-MgO-Fe_2O_3 diagram reveals the amphibolite is an ortho-amphibolite, and all samples plotted in the field of basalt on the Cr versus Ni plot. Cr/Ni ratios range from 2.07 to 2.80; with an average of 2.30; characteristic of basaltic rocks. CaO + MgO values for the rocks range from 12.12 to 17.71; within the 12% < CaO + MgO < 20% range of Pearce rocks commonly classified as basalts (Table 1).sss

The Itagunmodi-Igun amphibolites produce a more tholeiitic than alkaline basalt trend on the Zr/P_2O_5 versus Nb/Y plot (Fig. 1). The majority of the samples plotted within the Within-Plate Basalt (WPB) field of the Zr versus TiO_2 plot of Pearce, while few plotted within the field of Mid-Oceanic Ridge Basalt.

3.3 Amphibole and Plagioclase Chemistry

Mainly of the calcic group, the amphiboles are predominantly magnesio-hornblende, with subordinate actinolite and accessory edenite, winchite, glaucophane, and barroisite. The plagioclases vary in composition from labradorite to albite, with An-content: 6.90–58.98.

An estimation of PT of formation (plagioclase-hornblende thermobarometer) yielded a temperature of 450–687 °C (Holland and Blundy 1994) and 561–666 °C (Blundy and Holland 1990), using an arbitrary pressure of 2 kbar. With the Holland and Blundy (1994) calibration, a temperature range of 456–683 °C with pressure 0.7–4.3 kbar were obtained. Blundy and Holland (1990) calibrations yielded temperature and pressure ranges of 578–642 °C and 0.5–4.3 kbar, respectively.

4 Discussion

It is believed that Basaltic suites spanning the MORB and WPB fields on the Zr versus TiO_2 plot were formed in environments transitional between the two settings. The amphiboles fall within the biotite zone and lower garnet zone, and are also of the medium pressure amphibole class. The An7—59 content of the plagioclases is suggestive of the temperature of formation $\geq 500^0$C. The calculated PT values

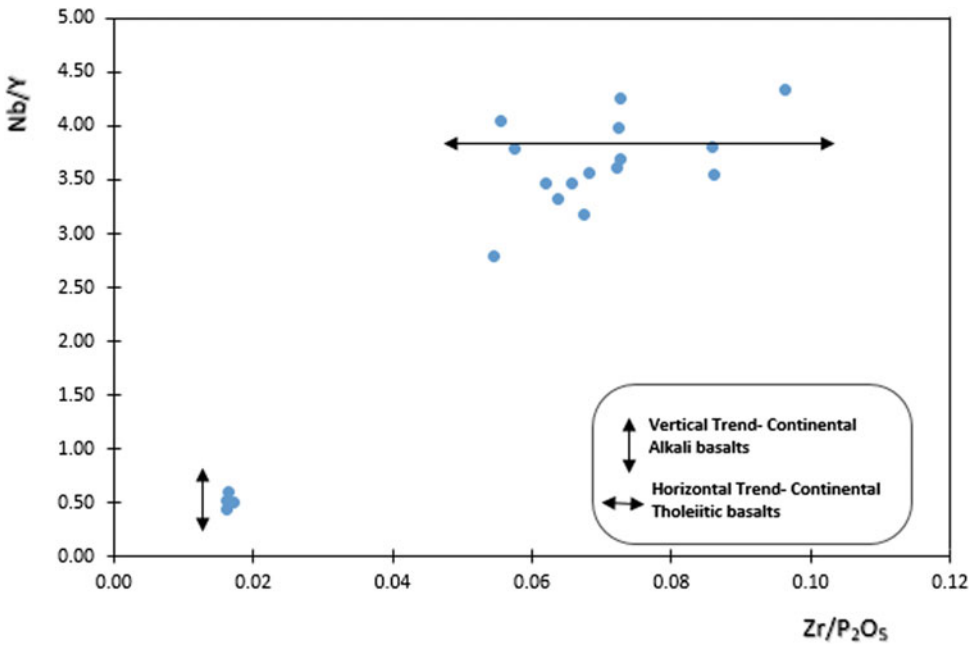

Fig. 1 Vertical and horizontal trends of Continental alkali and tholeiitic basalts on the Nb/Y–Zr/P_2O_5 plot

Table 1 Summary of major and trace element composition of Itagunmodi-Igun amphibolites

Oxide (%)	Range	Average
SiO_2	49.67–55.66	53.27
Al_2O_3	12.13–14.74	13.08
Fe_2O_3	7.75–11.15	10.13
MgO	6.42–7.24	6.70
CaO	5.70–10.96	8.90
Na_2O	***1.00–2.33***	***1.34***
K_2O	***0.66–6.66***	***2.22***
CaO + MgO	12.12–17.71	14.68
Trace elements (ppm)		
Rb	20–242	71.76
Sr	482–916	609.22
Y	21–31	26.83
Nb	10–115	83.15
Y/Nb	0.23–2.30	0.63
Rb/Sr	0.03–0.27	0.10

fall within the range of estimated values associated with the formation of rocks of the Amphibolite Facies. The average pressure of formation (i.e. 1.8kbar [Holland and Blundy 1994; Blundy and Holland 1990]) corresponds to an approximately 6.6–7.4 km depth of emplacement for the amphibolites.

5 Conclusions

The amphibolites contain magnesio-hornblende, actinolite, epidote, labradorite, albite with accessory titanite and opaques. They are ortho-amphibolites of tholeiitic and calc-alkalic affinities, likely derived from different source magmas and plotted in Within-Plate-Basalt tectonic field. Thermobarometric calculations constrained the temperature of their formation to 450-6870C and pressure 0.5–4.3 kbar, within the range of estimated values associated with the Amphibolite Facies.

References

Blundy, J.D., Holland, T.J.B: Calcic amphibole equilibria and a new amphibole-plagioclase geothermometer. Contrib. Miner. Petrol. **104**, 208–224 (1990)

Elueze, A.A.: Geology of the Precambrian Schist Belt in Ilesa Area, Southwest Nigeria. Precambrian Geology of Nigeria, pp. 77–82. Geological Survey of Nigeria Publication (1988)

Holland, T., Blundy, J.: Non-ideal interactions in calcic amphiboles and their bearing on amphibole-plagioclase thermometry. Contrib. Miner. Petrol. **116**, 433–437 (1994)

Sensibility of Tourmaline Chemistry to Granitic Magma Composition and Oxygen Fugacity

Isabel Ribeiro da Costa and Isabel Margarida Horta Ribeiro Antunes

Abstract

Extensive granitic magmatism is a dominant feature of the Central Iberian Zone (CIZ) of the Variscan Orogen. For the most part, these are S-type peraluminous granitic rocks exhibiting variable degrees of evolution and compositions ranging from granodiorites, through monzogranites and granites to leucogranites, bearing either biotite and muscovite, or just muscovite in the more evolved facies. Tourmaline is a common and essential accessory mineral in many of these peraluminous granitic rocks. Several granite-hosted tourmaline sets from the Castelo Branco, Idanha-a-Nova and Penamacor-Monsanto plutons were used to investigate how tourmaline chemistry reflects granitic magma composition and oxygen fugacity. Additionally, previously published data on tourmalines and their host-granites from Rebordelo (CIZ, Portugal) and the Alamo Complex and several Araya-type granitic batholiths (CIZ, Spain) were used to test the trends obtained. Most tourmaline components and component ratios, however, seem substantially impervious to granitic magma composition and oxygen fugacity. Exceptions are the Mg/(Mg + Fe) ratio and Ti contents of tourmaline, which show evident variation with the degree of evolution and oxygen fugacity of host granitic rocks. From both mineralogical and petrological point of view, it seems of interest that these compositional features of tourmaline may be used as indicators of the degree of evolution and of specific characteristics of the granitic magmas that produced them.

Keywords

Tourmaline • Granitic rocks • Central Iberian Zone

1 Introduction

Most peraluminous granitic rocks contain accessory tourmaline, besides micas. Tourmaline is stable over a sizeable P–T range and can accommodate a wide variety of primary and trace elements.

We have investigated how the degree of evolution of granitic magmas and their oxygen fugacity affect the composition of granite-hosted tourmalines using relevant components of tourmalines and bulk-rock parameters (e.g. MgO/(MgO + FeOT), Fe_2O_3/(FeO + Fe_2O_3), Rb/Ba ratio, P_2O_5 content and ASI index) from several granitic facies of the Castelo Branco (Antunes 2006; Martins et al. 2015), Idanha-a-Nova (Antunes 2006; Martins et al. 2015) and Penamacor-Monsanto (Costa et al. 2014) plutons. The trends obtained were tested with average compositions of tourmalines from other Variscan granitic rocks, namely from the Rebordelo pluton (CIZ, Portugal) (Neiva et al. 2007), from the Alamo Complex leucogranites and several Araya-type monzogranitic batholiths (CIZ, Spain) (Pesquera et al. 2013, 2005) (details in the legend of Fig. 1).

These previous studies have underlined the importance of tourmaline in the characterisation of Variscan granitic magmas.

2 Geological Setting and Analytical Methods

The Castelo Branco (Antunes 2006), Idanha-a-Nova (Antunes Mineralogia 2006) and Penamacor-Monsanto (Costa et al. 2014) granitic plutons intrude the ante-Ordovician Schist-Greywacke Complex (SGC), in the southern sector of the Central Iberian Zone (CIZ) of the Variscan orogenic belt.

I. Ribeiro da Costa (✉)
Department Geologia—Fac. Ciências, Universidade de Lisboa, 1749-016 Lisboa, Portugal
e-mail: imscosta@fc.ul.pt

I. M. H. R. Antunes
ICT Research Centre/Universidade Do Minho, Campus de Gualtar, 4710-057 Braga, Portugal

A. Çiner et al. (eds.), *Recent Research on Geomorphology, Sedimentology, Marine Geosciences and Geochemistry*, Advances in Science, Technology & Innovation, https://doi.org/10.1007/978-3-030-72547-1_72

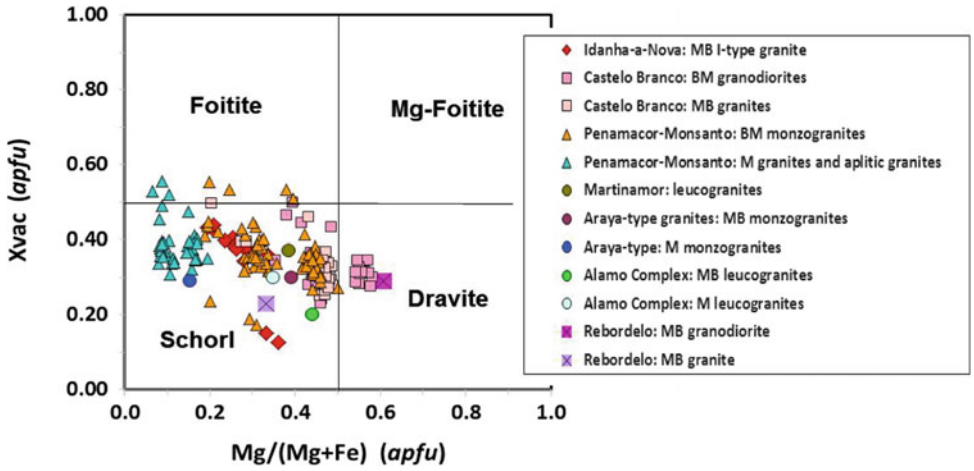

Fig. 1 Xvac versus Mg/(Mg + Fe) diagram for tourmaline classification. (M—muscovite, B—biotite, in granite facies designations)

Bulk-rock geochemistry for the Castelo Branco and Idanha-a-Nova granites (6 samples) was obtained by X-ray fluorescence at the Southampton Oceanographic Centre (UK); Fe titration was carried out at the Departamento de Ciências da Terra, Universidade de Coimbra (Portugal).

Whole-rock data for the Penamacor-Monsanto tourmaline-bearing granites (13 samples) were determined at ACTLABS (Canada), by Fusion-ICP-MS, INAA-Neutron Activation Analysis (REE), Fusion-ISE (F) and titration (ferrous iron).

Penamacor-Monsanto tourmalines were analysed on a JEOL JXA-8500 electron microprobe, at LNEG—Laboratório Nacional de Energia e Geologia (S. Mamede de Infesta, Portugal), under the following analytical conditions: 3–5 mm beam diameter, 15 kV accelerating voltage and counting times of the 20 s and 10 s for peak and background readings. Standards used were: orthoclase (Si, Al, K), albite (Na), apatite (Ca), MgO (Mg), Fe_2O_3 (Fe), Mn-standard (Mn), TiO_2 (Ti), Cr_2O_3 (Cr) and vanadinite (V). ZAF corrections were applied. The analytical error was £1% for the elements analysed.

Tourmalines from Idanha-a-Nova and Castelo Branco granitic rocks were analysed with a JEOL JXA-8200 electron microprobe, at the Departamento de Geologia, Faculdade de Ciências (ULisboa) under similar analytical conditions. Structural formulae of tourmalines were normalised for 15 (T + Z + Y) cations (Costa et al. 2014).

3 Results

Most granite-hosted tourmalines investigated occur as isolated grains, often showing some primary concentric zonation, and correspond to schorl compositions, only a few overlapping onto the dravite and foitite fields (Fig. 1).

4 Discussion

Although most tourmaline compositional variations seem unrelated to the degree of evolution of the studied granitic sets, components such as Ti and the Mg/(Mg + Fe) ratio definitely correlate with several parameters which are commonly considered good indicators of magmatic evolution, such as the MgO/(MgO + FeO^T) ratio (Fig. 2a, b, the Rb/Ba ratio, the P_2O_5 (Fig. 2c) and REE contents and the peraluminosity index (ASI = $[Al_2O_3]/([CaO] + [Na_2O] + [K_2O])$.

On the other hand, the Mg/(Mg + Fe) ratios in tourmaline tend to decrease with increasing oxygen fugacity in the granitic magma, indicated by the $Fe_2O_3/(FeO + Fe_2O_3)$ ratios of the granitic rocks (Fig. 2d).

5 Conclusions

Notwithstanding the relatively wide compositional range that tourmalines exhibit within each granitic facies, their Mg/(Mg + Fe) ratios and Ti contents correlate to geochemical features indicative of the degree of evolution of the host granitic magmas, such as their bulk MgO/(MgO + FeO^T) and Rb/Ba ratios, P_2O_5 contents and ASI index.

Oxygen fugacity in granitic magmas also affects the Mg/(Mg + Fe) ratio in tourmalines, which tends to decrease in more evolved granitic rocks, with typically higher Fe oxidation ratios.

Tourmalines from the I-type Idanha-a-Nova granite comply with the correlations found for S-type granite-hosted tourmaline sets, implying that magma composition, rather than genetic processes, is the main factor controlling tourmaline composition.

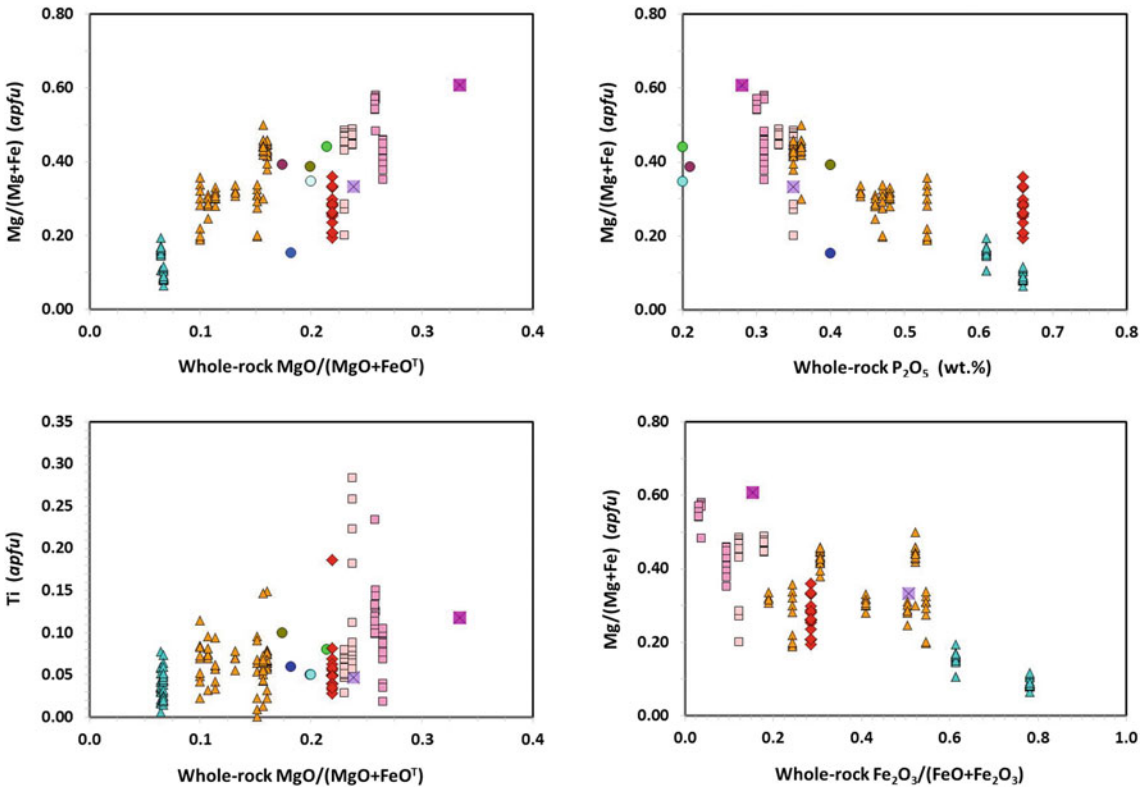

Fig. 2 Diagrams showing positive correlations between (A) Mg/(Mg + Fe) ratios and (B) Ti contents in tourmalines and host-rock MgO/(MgO + FeO^T) ratios, and negative correlations between Mg/(Mg + Fe) ratios in tourmalines and (C) P_2O_5 contents and (D) Fe_2O_3/(FeO + Fe_2O_3) ratios of host granitic rocks. (Graphic markers as in Fig. 1)

References

Antunes, I.M.H.R.: Mineralogia, Petrologia e Geoquímica de Rochas Granitóides da Área de Castelo Branco—Idanha-a-Nova. Unpubl, 453 p. Ph.D. Thesis, Univ. of Coimbra (2006)

da Costa, I.R., Mourão, C., Récio, C., Guimarães, F., Antunes, I.M., Farinha Ramos, J., Barriga, F.J.A.S., Palmer, M.R., Milton, J.A.: Tourmaline occurrences within the Penamacor-Monsanto granitic pluton and host-rocks (Central Portugal)—genetic implications of crystal-chemical and isotopic features. Contrib. Mineral. Petrol. **167**, 993–1015 (2014)

Martins, B., Morgado, C., Barbosa, J., Roseiro, J.: Um mistério a resolver—os granitos hiperaluminosos associados a orogenias diferentes contêm turmalinas quimicamente diferentes? p. 46. Unpubl. Project Report, ULisboa, (2015)

Neiva, A.M.R., Silva, M.M.V.G., Gomes, M.E.P.: Crystal chemistry of tourmaline from Variscan granites, associated tin-tungsten- and gold deposits, and associated metamorphic and metasomatic rocks from Northern Portugal. Neues Jahrb. Mineral. Abh. **184**, 45–76 (2007)

Pesquera, A., Torres-Ruiz, J., García-Casco, A., Gil-Crespo, P.P.: Evaluating the controls on tourmaline formation in granitic systems—a case study on peraluminous granites from the Central Iberian Zone (CIZ) Western Spain. J. Petrol. **54**, 609–634 (2013)

Pesquera, A., Torres-Ruiz, J., Gil-Crespo, P.P., Jiang, S.-Y.: Petrographic, chemical and B-isotopic insights into the origin of tourmaline-rich rocks and boron recycling in the Martinamor Antiform (Central Iberian Zone, Spain). J. Petrol. **46**(5), 1013–1044 (2005)

Compositional Evolution and Substitutions of Tourmaline from the Metamorphosed Sikait Pelitic Belt, Southern Eastern Desert (Egypt)

Hassan Z. Harraz and Mohamed Abd El Monsef

Abstract

Tourmaline in Sikait area is closely associated with stratiform metapelites schistose rocks. The distribution of tourmaline is confined to the Nugrus shear zone, along with leucocratic rock varieties (leucogranite, pegmatite and aplite dykes). Tourmaline occurs either as disseminated isolated clusters of crystals or as discontinuous tourmalinite bands within the metapelites rocks, pegmatites or quartz veins. Four mineral assemblages have been identified at Sikait area on the approach to the pegmatite contact, viz: (1) Quartz-biotite-K-Feldspar-chlorite, which consists mainly of the original metamorphic silicate plus anomalously high amounts of modal tourmaline; (2) Quartz-biotite-tourmaline-chlorite; (3) Tourmaline-quartz-muscovite; and (4) Tourmaline-quartz. The variations in the mineral assemblages and whole-rock chemistry within the mineralized zones appear to be a function of boron metasomatism and potash leaching. The normalized rare earth elements (REE) patterns of samples from the four assemblages suggest a partial alteration of the original pelitic rock pattern by the metasomatized magmatic fluids. The metasomatic/alteration zones represent an episode of (B-, Li-, Rb-enriched fluid) during pegmatite fluid-schist interactions. The aqueous fluid from the pegmatite reacts with the schist breaking down sheet silicate for leaching of Rb, Li and K and forming tourmaline-rich assemblages.

Keywords

Geochemistry • Boron metasomatism • Tourmaline • Metapelitic schist

H. Z. Harraz · M. Abd El Monsef (✉)
Geology Department, Faculty of Science, Tanta University, Tanta, 31527, Egypt
e-mail: monsef_egy@science.tanta.edu.eg

1 Introduction

The metasomatism of sediments commonly forms tourmalines by boron-rich hydrothermal fluids (Slack 1980). The chemistry of the tourmalines is also partly dependent on the bulk chemistry of the original sediments, where tourmalines grown in an Al-rich environment preferentially having high Al contents (Gallagher 1988). Replacement of original metamorphic and igneous minerals assemblages with boron enriched assemblages is a common feature of country rocks immediately adjacent to pegmatite. The fluid-mobile behaviour of boron plays an essential role in the origin of subduction-related magmas and metamorphism and crustal evolution. A Neoproterozoic metapelitic schist belt at the Sikait area of the Southern Eastern Desert of Egypt (SEDE) is a favourable environment for localization of tourmaline mineralization in the Pan-African in Egypt. The present study aims mainly to shed light on the origin and evolution mechanism of tourmaline deposits (as a semi-precious gemstone) in the Sikait area, Southern Eastern Desert of Egypt (SEDE).

1.1 Geologic Setting

The Sikait area consists mainly of metapelitic schist and gneiss that are forming the core of the Hafafit uplift which are intruded by granitoid masses and cut by several aplitic dykes and pegmatitic veins. The granitoid and pegmatite rocks intruded syntectonically along major ductile shear zones (Nugrus shear zone). Age determination of 610 ± 20 Ma was supposed to give the age of granite emplacement and connected pegmatites with various stages of hydrothermal quartz veins (Moghazi et al. 2004). A network to subparallel pegmatite veins (15–40 m length and 5–10 m width) dissected these rocks unites during the Pan-African tectono-thermal event, leading to the development of contact thermal aureoles of >10 cm width, the metasomatized or altered assemblage surrounding the

A. Çiner et al. (eds.), *Recent Research on Geomorphology, Sedimentology, Marine Geosciences and Geochemistry*, Advances in Science, Technology & Innovation, https://doi.org/10.1007/978-3-030-72547-1_73

pegmatite is discontinuous and of variable thickness. In the area surrounding the Sikait pegmatite, the metapelitic schist is predominantly a quartz-biotite-chlorite and quartz-biotite-potash feldspar-chlorite schist with accessory tourmaline, sillimanite and kyanite. Tourmaline occurs either as disseminated isolated clusters of crystals or as discontinuous tourmaline bands within the metapelitic rocks, pegmatites or quartz veins. The Sikait schist belt includes abundant xenoliths of supra-structure ophiolitic serpentinite rocks (El-Naby and Frisch 2006) (Fig. 1).

2 Petrography and Geochemistry

Based upon the modal mineralogy using microscopic examination for 28 samples, the metasomatic-altered zone around pegmatite bodies has been divided into four mineral assemblages: (1) Quartz-Biotite-Potassium Feldspar-Chlorite assemblage (Q-B-K-C); (2) Quartz-Biotite-Tourmaline-Chlorite assemblage (Q-B-T-C); (3) Tourmaline-Quartz-Muscovite assemblage (T-Q-M); and (4) Tourmaline-Quartz assemblage (T-Q). Whole-rock geochemistry of major and trace chemical analyses of tourmaline-rich metapelitic schist (14 samples), shows geochemical variations for some selected significant oxides and trace elements with B_2O_3 content (Fig. 2). Chondrite-normalized plots of REE concentrations of the four assemblages are shown in (Fig. 2).

3 Discussion and Conclusions

The variations in mineral assemblage and whole-rock chemistry within the four mineralized zone appear to be a function of the chemical potential of B_2O_3 (boron metasomatism) and K_2O (alkali leaching). The boron addition reacts with country rock forming tourmaline-rich zones. Hence, the alkali elements (Rb, Sr, K, Li), SiO_2 and CaO, show a substantial decrease from the Q-B-K-C to T-Q assemblages (Fig. 2). The breakdown of sheet silicate acts as "traps" for Rb, Ba, Sr and Li, results in the further enrichment of the pegmatitic fluid in these components. The mineralized zones surrounding the pegmatite may represent either a single or multiple episodes of interaction between the schistose rock and pegmatite-derived fluids.

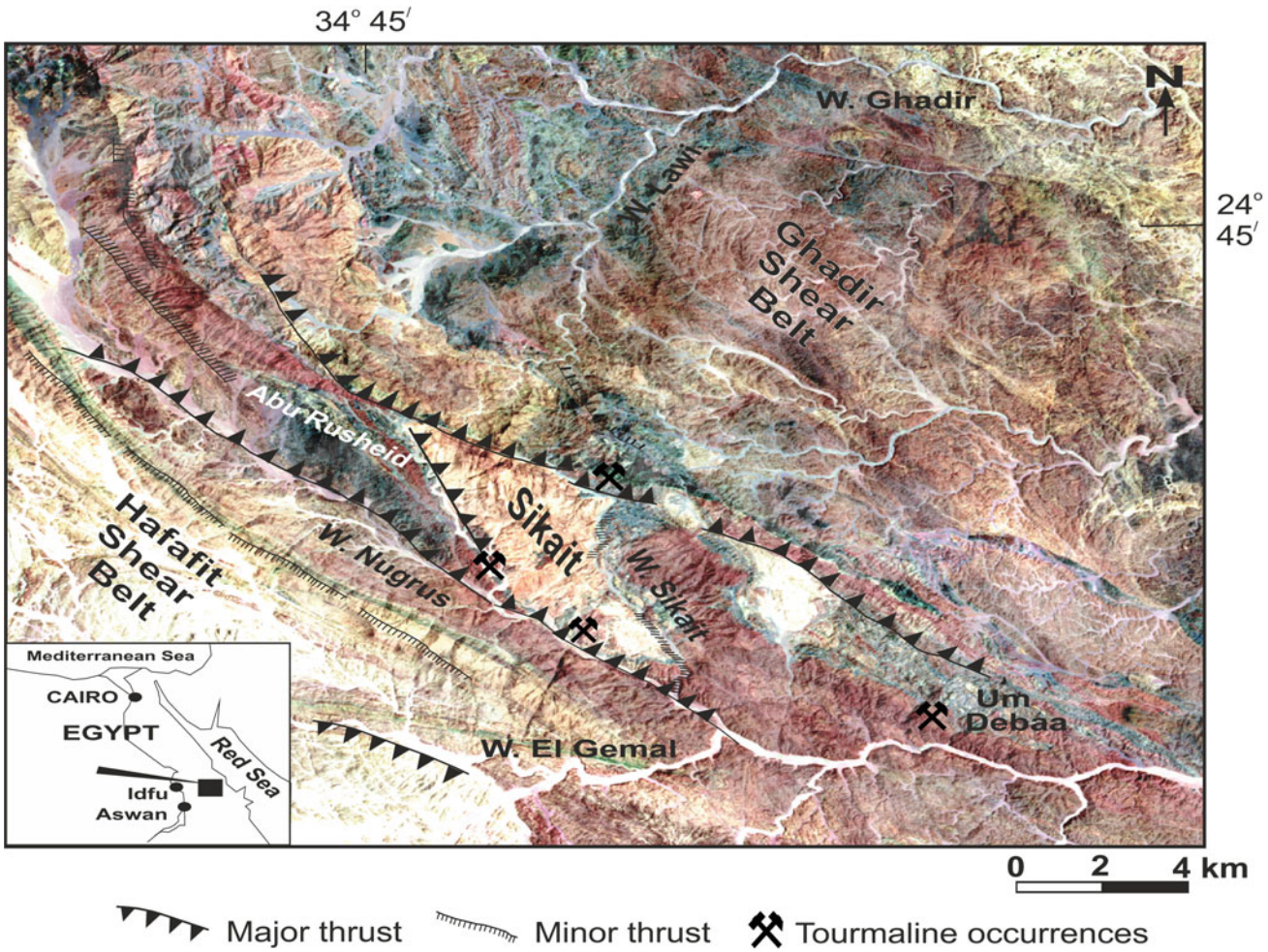

Fig. 1 Geologic map of the Sikait area showing sample locations (compiled and modified after, Greiling 1990; Takla et al. 1992) *Source* Google Earth satellite

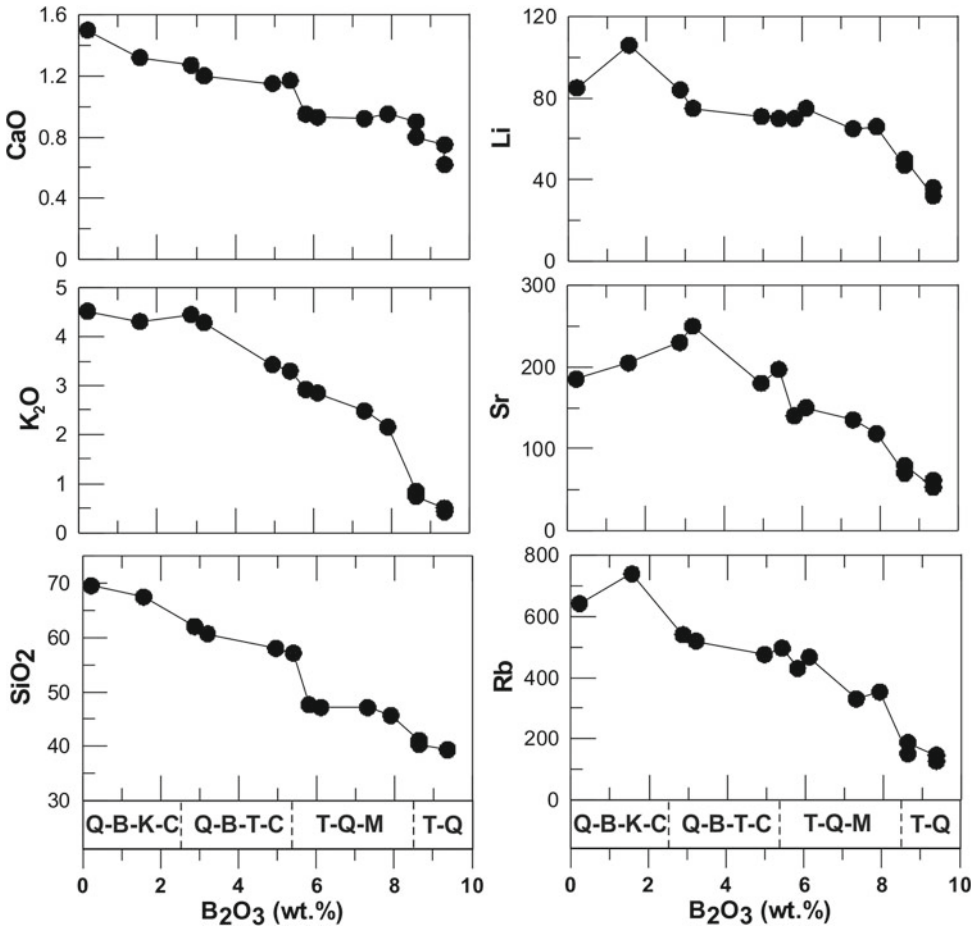

Fig. 2 Binary diagrams for selected major oxides and trace elements with B_2O_3 content

Where, H_2O and B_2O_3 may be derived from the pegmatitic aqueous magmatic fluid, and Al_2SiO_5 and SiO_2 may be transported out of the system or used in the reaction. Chondrite-normalized plots of REE concentrations of the four assemblages (Fig. 3) display different patterns reflecting the mixed petrogenetic affinities that suggest a partial alteration of the original sedimentary pattern by the metasomatized magmatic fluids. The unusual REE systematics of the T-Q assemblage may reflect hydrothermal alteration and loss of the LREE (Fig. 3d). A markable decrease in tourmaline concentrations was observed as far from the pegmatite bodies (Fig. 4).

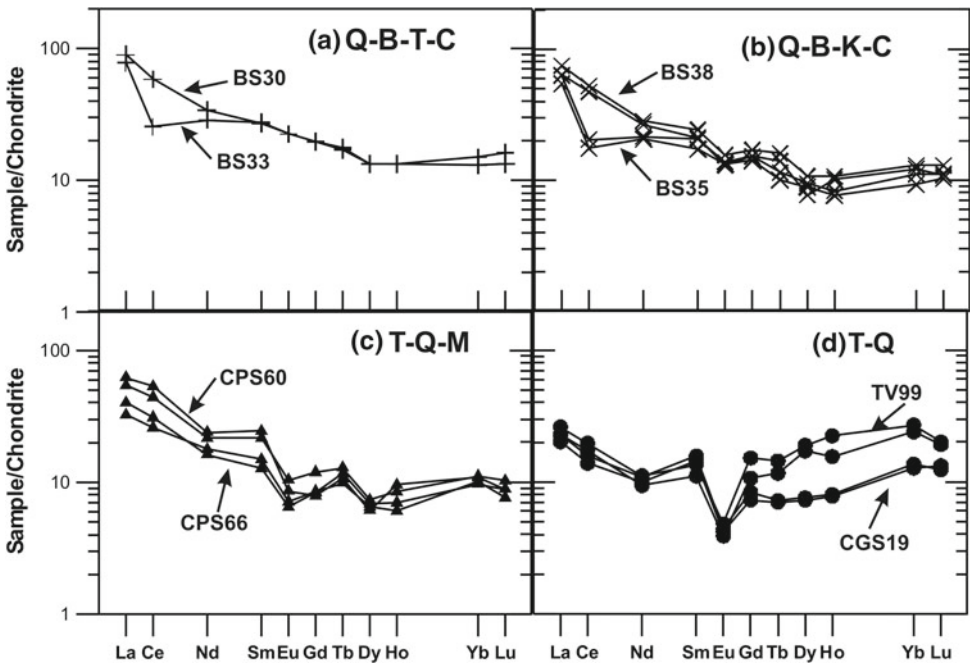

Fig. 3 Chondrite-normalized REE patterns for the four mineral assemblages

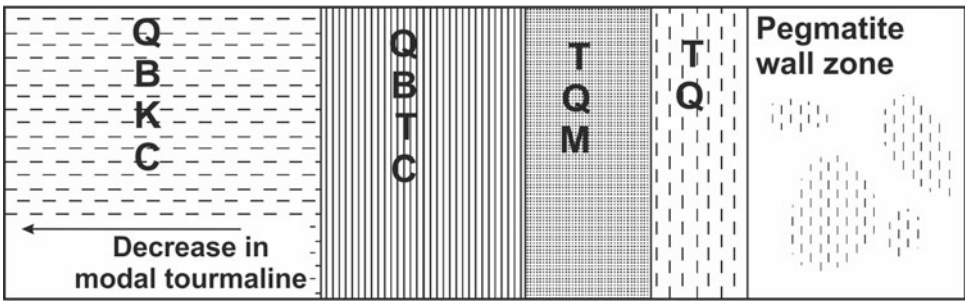

Fig. 4 Sketch model for tourmaline concentration in the four mineralized zones

References

El-Naby, H.A., Frisch, W.: Geochemical constraints from the Hafafit metamorphic complex (HMC): evidence of Neoproterozoic back-arc basin development in the central Eastern Desert of Egypt. J. Afr. Earth Sci. **45**(2), 173–186 (2006)

Gallagher, V.: Coupled substitutions in schorl-dravite tourmaline: new evidence from SE Ireland. Mineral. Mag. **52**, 637–650 (1988)

Greiling, R.O.: Structural and Geologic Map of Wadi Hafafit Area. TFH, Berlin (1990)

Moghazi, A.M., et al.: Late Neoproterozoic strongly peraluminous leucogranites, South Eastern Desert, Egypt–petrogenesis and geodynamic significance. Mineral. Petrol. **81**(1–2), 19–41 (2004)

Slack, J.F.: Tourmaline-a prospecting guide for massive base-metal sulfide deposits in the Penobscot Bay area, Maine (1980)

Takla, M.A., Basta, F.F., Surour, A.A.: Petrology and mineral chemistry of rodingites associating the Pan-African ultramafics of Sikait-Abu Rusheid area, South Eastern Desert, Egypt, pp. 491–507. In: 1st International Conference on Geology of the Arab World, Cairo University (1992)

Meteorites of Morocco: A Model of Science Development in the Arab Countries

Hasnaa Chennaoui Aoudjehane

Abstract

Meteorites are ultrabasic, basic or intermediate extraterrestrial rocks with most of them containing chondrules. They are crucial not only to the apparition of water and life on Earth but also to the mass extinction of species. Meteorites are mostly found in cold deserts such as Antarctica and hot ones such as Oman, Sahara and Chili. The Sahara, and especially the Moroccan one, provides a significant number of meteorites for researchers and collectors all over the world. Despite the richness of the Arab world in meteorites, there is a lack of interest in research on meteoritics and planetary science. This disinterest is a waste of opportunities to contribute to an innovative and promising field of research. It is also a waste of Geoheritage. In Morocco, since 2001, we started a strategy to develop and promote meteoritics and planetary science, based on three axes: research, education and communication. This strategy can be applied to other Arab countries allowing them to partake in the international scientific scene.

Keywords

Meteoritics and planetary sciences • Morocco • Arab countries • Geochemistry • Cosmochemistry

1 Introduction

During the last seventy years, meteorites have been a fantastic way to increase our knowledge about the origin of the solar system, the formation of planets including the Earth, and the massive impact-related extinctions during the geological times. Water on Earth, as well as the first life precursor elements, has an extraterrestrial origin (Lis et al. 2019) partly. Their study allowed scientists to have direct access to rocks from planets not yet directly explored. First ones represent the precursor of the actual solar system planets that have been fixed in the initial state of their formation as asteroids. Thousands of meteorites are collected in Morocco and most Arab countries (Chennaoui Aoudjehane 2018). They represent an essential source of improvement of meteoritics and planetary science in the world.

2 What is a Meteorite and How to Identify It?

Meteorites are extraterrestrial stones. They are mostly ultrabasic, basic or intermediate rocks. Analytical techniques used while studying them are the same as those used for earthly rocks, i.e. geochemistry and mineralogy. Macroscopic identification of a meteorite is based on presence of the fusion crust preserved on unweathered ones, chondrules (the first droplets crystallised in the early solar system), native metal and sulphides and magnetic properties. The second step is to describe the mineralogy and petrography under a microscope and then to analyse the minerals by XRD, EBDS or EMPA. The most important minerals to analyse for the first classification are olivine, pyroxenes and plagioclase. Native metal and sulphides, as well as accessory minerals, can also be analysed. Many other analytical techniques are used to have information on the formation and evolution of the rock and its parent bodies, such as noble gases, oxygen and other isotopes. The aim includes measurement of the cosmogenic ray exposure, identification of the original parent body or calculation of the crystallisation age of the rock. However, the first step is to classify the meteorite. Then, we submit it to the Nomenclature Committee (NomCom) of the Meteoritical Society (MetSoc) in order to make it official and to be able to publish in scientific journals after its acceptance.

H. Chennaoui Aoudjehane (✉)
GAIA Laboratory, Faculty of Sciences Ain Chock, Hassan II University of Casablanca, km8 Route d'El Jadida, 20150, Casablanca, Morocco
e-mail: hassna.chennaoui@univh2c.ma

A. Çiner et al. (eds.), *Recent Research on Geomorphology, Sedimentology, Marine Geosciences and Geochemistry*, Advances in Science, Technology & Innovation, https://doi.org/10.1007/978-3-030-72547-1_74

3 Meteorites of Morocco and Arab Countries

Collection of meteorites is mainly done in hot and cold deserts. Most of the Arabic countries contain large desert areas which are very rich in meteorite finds. Morocco has a vast and safe Sahara where many nomads are living. A big community of meteorite hunters is well established. Nomads and hunters are good observers; they learned by practising how to make the difference between terrestrial and extraterrestrial rocks that represent an essential source of revenue for them. Those meteorites are almost all exported. All classes of meteorites are found in the hot deserts including many rare and indispensable for scientific research ones. Most of Martian and lunar meteorites, angrites and other rare types are from the hot deserts (Chennaoui Aoudjehane 2018), (Table 1).

Morocco experienced eighteen meteorite falls in total (https://www.lpi.usra.edu/meteor/). Since 2004 falls have been classified and submitted to the NomCom by our team, including the exceptional fifth Martian meteorite fall in Morocco "Tissint" (Figs. 1 and 2). Many valuable papers have been published on these falls allowing Moroccan researchers to comfort their position on this topic (Chennaoui Aoudjehane et al. 2012). A similar effort was made with meteorite finds in Morocco, such as "Agoudal" (Chennaoui Aoudjehane et al. 2016). Most finds from the countries surrounding the Sahara (Morocco, Algeria, Tunisia, Mauritania Mali, Tchad, Niger…) are called by a serial name (Northwest Africa) followed by a number: NWAxxx. The exact origin of the samples is unknown, leading to the loss of valuable scientific and heritage information (Chennaoui Aoudjehane et al. 2014).

In Libya and Oman, there are large meteorite strewnfields with known geographic coordinates and a serial name plus a number such as Dar El Ghani (DAG xxx), Hamada Al Hamra (HAH xxx), Shisr xxx, … In Egypt, there is one famous Martian meteorite fall, Nakhla, as well as the most ancient meteoritic iron, found in the King Tut treasure (Comelli et al. 2016). In Saudi Arabia, there is a recent impact meteorite crater: the Wabar crater, while the black stone in the "Hajar Al Aswad" is said to be possibly a meteorite.

Despite this richness, most Arab countries do not have laboratories devoted to research on meteoritics and planetary science, nor do they have museums for the preservation of this patrimony that is lost quickly. However, a few exceptions do exist, such as the Sharjah Center of Astronomy and Space Sciences UAE and Emirates Mars Mission of the UAE Space Agency.

4 Strategy Adopted for Meteoritics Promotion in Morocco

Since 2001, research on meteoritics and planetary science in Morocco has sprung. A strategy for promoting these sciences and preserving meteorites was adopted based on

- Research development: Our team has published many valuable papers in dedicated journals (Chennaoui Aoudjehane 2018; Chennaoui Aoudjehane et al. 2012, 2016) as well as unwavering participation in scientific meetings. Ph.D. theses have been defended, and many are ongoing.

Table 1 Statistics of meteorites in Antarctica, Northwest Africa (NWA) and Morocco (Chennaoui Aoudjehane 2018). (Meteoritical bulletin database (https://www.lpi.usra.edu/meteor/) consulted on December 2018)

Meteorites types	Total number in the world	Number in Antarctica	Antarctica %	Morocco and NWA Number	Morocco and NWA %
Carbonaceous chondrites	2145	1158	54.0	797	37.2
Ordinary chondrites	48,814	33,747	69.1	5250	10.8
Enstatite chondrites	599	410	68.4	102	17.0
Angrites	28	4	14.3	24	85.7
Aubrites	73	44	60.3	21	28.8
Brachinites	41	4	9.8	37	90.2
Ureilites	448	128	28.6	244	54.5
HED	1868	723	38.7	1082	57.9
Martian meteorites	190	30	15.8	147	77.4
Lunar meteorites	297	35	11.8	210	70.7
Mesosiderite	234	58	24.8	103	44.0
Pallasites	111	34	30.6	23	20.7
Siderites	1159	155	13.4	106	9.1

Fig. 1 Location and names of all meteorite falls in Morocco, red stars are all meteorites classified and submitted by our team (Chennaoui Aoudjehane and Agee 2018). (Image BING satellite, Conception L. Zennouri and M. Karim)

Fig. 2 Samples of the exceptional Martian meteorite "Tissint" a fall of July 2011 in Morocco (Chennaoui Aoudjehane et al. 2012)

- Education: A specific cosmochemistry course has been introduced in the basic curricula of undergraduate students in the third year of Bachelor of Earth and Planetary Sciences in Morocco.
- Communication:
  - Towards Moroccan and Arab scientific community by organising scientific meetings in Morocco including the Arab Impact Cratering and Astrogeology Conference series AICAC II and III, and the 77th MetSoc meeting organised for the first time in an Arab country (Casablanca Morocco, September 2014);
  - Towards broad public: by organising many public lectures for students, youth and children in schools, participating in different media TV, radio, newspapers and magazines. An association named ATTARIK Foundation (www.attarikfoundation.org) was also created.

5 Results and Recommendations

This strategy allows Morocco to occupy a well-recognised international status and to have a community of young researchers integrated into the whole meteoritics community. All Moroccan citizens are now aware of the important geoheritage represented by meteorites and are proud of it. Moroccan authorities included meteorites in a new regulation with a win-win rule. The export is officially possible and regulated. Smart regulation is essential, and research centres and museums must be created in Arab countries. Significant

initiatives are already implemented and have promising results in UAE. ATTARIK foundation, as well as the African Initiative for Planetary and Space Sciences AFIPS (Baratoux et al. 2017), has been created to promote meteoritics and planetary sciences.

Every geologist interested in meteorites and impact craters can work on these fields after some training and an excellent bibliography. The Moroccan researchers are honoured to share their expertise with all interested geologists from Arab countries. We invite them to be more sensitive to meteoritics and planetary sciences and to include cosmochemistry in all undergraduate curricula for students on Earth and planetary science.

References

Baratoux, D., Chennaoui Aoudjehane, H., Gibson, R., Lamali, A., Reimold, W.U., Sepah, M.S., Chabou, M.C., Habarulema, J.B., Jessell, M., Mogessie, A., Benkhaldoun, Z., Nkhonjera, E., Mukosi, N.C., Kaire, M., Rochette, P., Sickafoose, A., Martínez-Frías, J., Hofmann, A., Folco, L., Rossi, A.P., Faye, G., Kolenberg, K., Tekle, K., Belhai, D., Elyajouri, M., Koeberl, C., Abdeem, M.: Africa initiative for planetary and space sciences. EOS Opinion 14 June 2017 (2017). https://eos.org/opinions/africa-initiative-for-planetary-and-space-sciences

Chennaoui Aoudjehane, H.: Les météorites du Maroc, état des lieux d'un patrimoine à préserver. In: Patrimoine Géologique du Maroc. Numéro spécial des Notes et Mémoires du Service Géologique du Maroc. Published by Ministère de l'Energie, des Mines et du Développement Durable of Morocco, 184 Pages (2018)

Chennaoui Aoudjehane, H., Agee, C.B.: Ksar El Goraane (H5): the latest Moroccan Meteorite fall on 2018. Meteorit. Planet. Sci. **54**, S1#6297 (2019)

Chennaoui Aoudjehane, H., Avice, G., Barrat, J.-A., Boudouma, O., Chen, G., Duke, M.J.M., Franchi, I.A., Gattacecca, J., Grady, M.M, Greenwood, R.C., Herd, C.D.K., Hewins, R., Jambon, A., Marty, B., Rochette, P., Smith, C.L, Sautter, V., Verchovsky, A., Weber, P., Zanda, B.: Tissint martian meteorite: a fresh look at the interior, surface and atmosphere of Mars. Science **338**(6108), 785–788 (2012)

Chennaoui Aoudjehane, H., El Kerni, H., Reimold, W.U., Baratoux, D., Koeberl, C., Bouley, S., Aoudjehane, M.: The Agoudal (High Atlas mountains, Morocco) shatter-cone conundrum: a recent meteorite fall onto the remnant of an impact site. Meteorit. Planet. Sci. **51**, 1497–1518 (2016)

Chennaoui Aoudjehane, H., Jambon, A., Larouci, N., Buhl, S., Bunch, T.: Meteorites from Northwest Africa (NWA) one step forward. Meteorit. Planet. Sci. **49**, S1#5289 (2014)

Comelli, D., D'orazio, M., Folco, L., El-Halwagy, M., Frizzi, T., Alberti, R., Capogrosso, V., Elnaggar, A., Hassan, H., Nevin, A., Porcelli, F., Rashed, M.G., Valentini, G.: The meteoritic origin of Tutankhamun's iron dagger blade. Meteorit. Planet. Sci. **51**, 1301–1309 (2016). https://doi.org/10.1111/maps.12664

Lis, D.C., Bockelée-Morvan, D., Güsten, R., Biver, N., Stutzki, J., Delorme, Y., Durán, C., Wiesemeyer, H., Okada, Y.: Terrestrial deuterium-to-hydrogen ratio in water in hyperactive comets. Astron. Astrophys. **625**, L5 (2019). https://doi.org/10.1051/0004-6361/201935554

Meteoritical bulletin search database. Homepage https://www.lpi.usra.edu/meteor/

Geochemistry and Metallogenesis: Processes and Products (T7): Origin and Exploration of Mineral Deposits

Mineralogy, Petrography, and Geochemical Studies of the Greenstone Belt Rocks and the Associated Gold Mineralization of Aoueouat at Tasiast Mine, Mauritania

Masbah Zeine, Abdoullah Soumary, Ahmedou Cherif, Moulay Mohamed, Iselmou Mouhamed, Abacar Sow, Zeidane Ahmed Vall, Mehfoudh Telmoud, and Mounir Medhioub

Abstract

The Reguibat Shield of North Mauritania represents the northern exposure of the West African Craton. Mesoarchean rocks of the Aoueouat greenstone belt host the Tasiast gold deposits. This work focus on mineralogical, petrographic, and geochemical studies of some samples collected from two drillings cores (05213DD and 05214DD) from the West Branch Pit linked to the shear zone and hosted in the greenstone belt "Aoueouat" at Tasiast mine in Mauritania. Diorite, felsite, greywacke, and siltstone represent the studied rock samples. These rocks are the seat of abundant silicate mineral and carbonate neoformations, reflecting mineralized flows. The petrography (observations), mineralogy (XRD), and geochemistry (XRF) were conducted in order to understand the process that controls the mineralization and the mineralogical phases. All these analyses allowed us to derive that the highest gold concentrations are hosted in the dioritic rock unit, within the creamy sulfide layer (pyrrhotite and pyrite) and the quartz veins. The observed minerals indicating metamorphism are amphiboles, micas, and neoformed minerals, such as chlorite and fuchsite, which generally crystallized in the hydrothermal veins. These observations reveal that this mineralization was related to the hydrothermal process.

Keywords

Tasiast mine • West Branch pit • Orogenic gold • Greenstone belt • Magmatic rocks • Metamorphic rocks • Neoformed minerals • Hydrothermal activity • BIF

1 Introduction

Mauritania is located in West Africa belonging to the West African Craton composed of Archaean formations >2.5 Ga (Maurin et al. 1996). These formations are cropping out in the Reguibat Shield area (part of the four significant geological assemblages of Mauritania, Fig. 2). It contains a greenstone belt of primary economic importance around the world. These rocks contain different resources, including gold deposits. The greenstone belts of Reguibat Shield was considerably explored. In recent years, gold has been the focus, especially in the Tasiast greenstone belts. Normandy Source NLSD (1996–2001) made the most important discovery in the Tasiast deposit, with a very high economic potential. This sector is located in Aoueouat greenstones belts where anomalies of gold were recorded over a length of about 20 km, which divided it into two sectors Piment and West Branch Pit. The latter has been operating in an open-pit mine for several years. Based on pit mapping (Fig. 3), the different lithostratigraphic units are greywacke (SGW), bent iron formations (BIF), siltstone (SVC), felsite (FVC), and granodiorite (GDI). Repetition of folds is evident in sediment intrusion. Much of this volcano-sedimentary ensemble, and this intrusion falls moderately (−40°) toward the east. The host sequence is cut with a set of younger post-mineralization mafic dykes. This volcano-sedimentary assembly is divided by a sub-parallel NNE-SSW shear direction (Figs. 1, 2 and 3).

This study aims to understand better the mechanisms of emplacement and genesis of gold mineralization in the geodynamic and structural framework using mineralogy, petrography, and geochemical data of samples from two mining drillings located in the West Branch pit Aoueouat greenstones belts.

M. Zeine (✉) · M. Medhioub
Department of Earth Sciences, Faculty of Sciences, University of Sfax, Sfax, Tunisia

A. Soumary · A. Cherif · M. Mohamed · I. Mouhamed · A. Sow · Z. A. Vall · M. Telmoud
Kinross Tasiast, Nouakchott, Mauritania

A. Çiner et al. (eds.), *Recent Research on Geomorphology, Sedimentology, Marine Geosciences and Geochemistry*, Advances in Science, Technology & Innovation, https://doi.org/10.1007/978-3-030-72547-1_75

Fig. 1 Geographical location of the Tasiast mine

2 Materials and Methods

More than 40 samples were collected from the two drilled cores. Thin sections and polished sections were made for determination of both mineralogy and texture of the rocks through the optical microscope and the metallographic microscope to observe the phases carrying the mineralization. The different samples studied were crushed and analyzed by X-ray diffraction (XRD: 30 mA, 40 kV, Cu Kα). This analysis aims to determine the nature of minerals and establish the mineralogical association of the rocks studied. X-ray fluorescence (XRF) chemical analysis was done in order to determine the major and trace elements content of the sample.

3 Results

The petrography (microscopic observations), mineralogy (XRD), and geochemistry (XRF for major and trace elements) studies were made in order to understand the conditions of implementation of the mineralization and the carrier phases. The XRD analysis reveals the presence, along the two holes, of some minerals like quartz, biotite, chlorite, muscovite, garnet, K-feldspar, amphibole, tourmaline, fuchsite, and cummingtonite whose associations depend on the type of the crossed facies. Results of the geochemical analysis show a high amount of SiO_2 (31–67%) associated with Al2O3 ranging from (1.3–20.5) with high percentages of Fe_2O_3 (0.5–48%) and lower percentages of CaO, MgO, and K_2O. The trace elements showed gold grades that vary from (1.3–7 ppm) and sulfur (pyrite and pyrrhotite) with values ranging from (0–265000 ppm). The results obtained from these different types of analysis allowed us to derive the following effects. Microscopic observations and X-ray diffractions analysis confirmed by a chemical analysis allowed us to determine the mineral parageneses made of quartz, feldspar, micas, amphiboles, garnets, oxides, and sulfide associated with gold. The various types of rocks encountered are magmatic rocks (diorite and felsite) and sedimentary rocks (siltstone, greywacke and BIF) which have undergone Catazonal metamorphism. The results of different analyses of the samples show that the dioritic rocks account most of the gold mineralization in addition to the quartz veins with the presence of sulfide minerals.

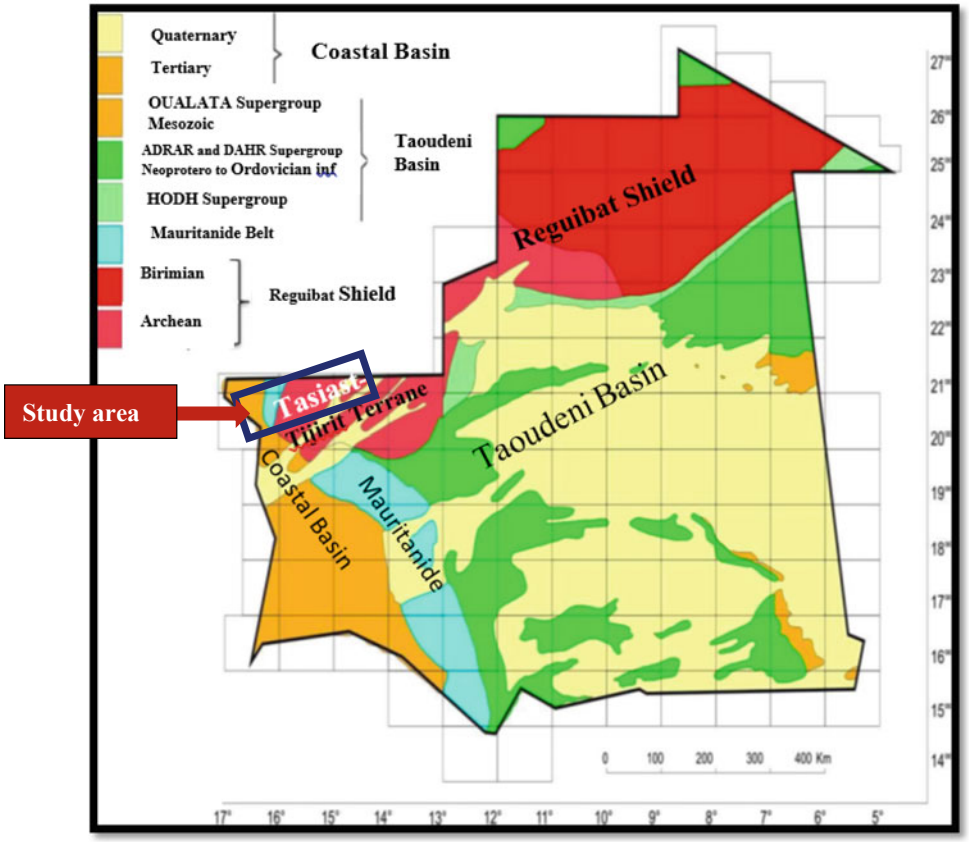

Fig. 2 Geological map of the main geological assemblages of Mauritania (After BGS 2004)

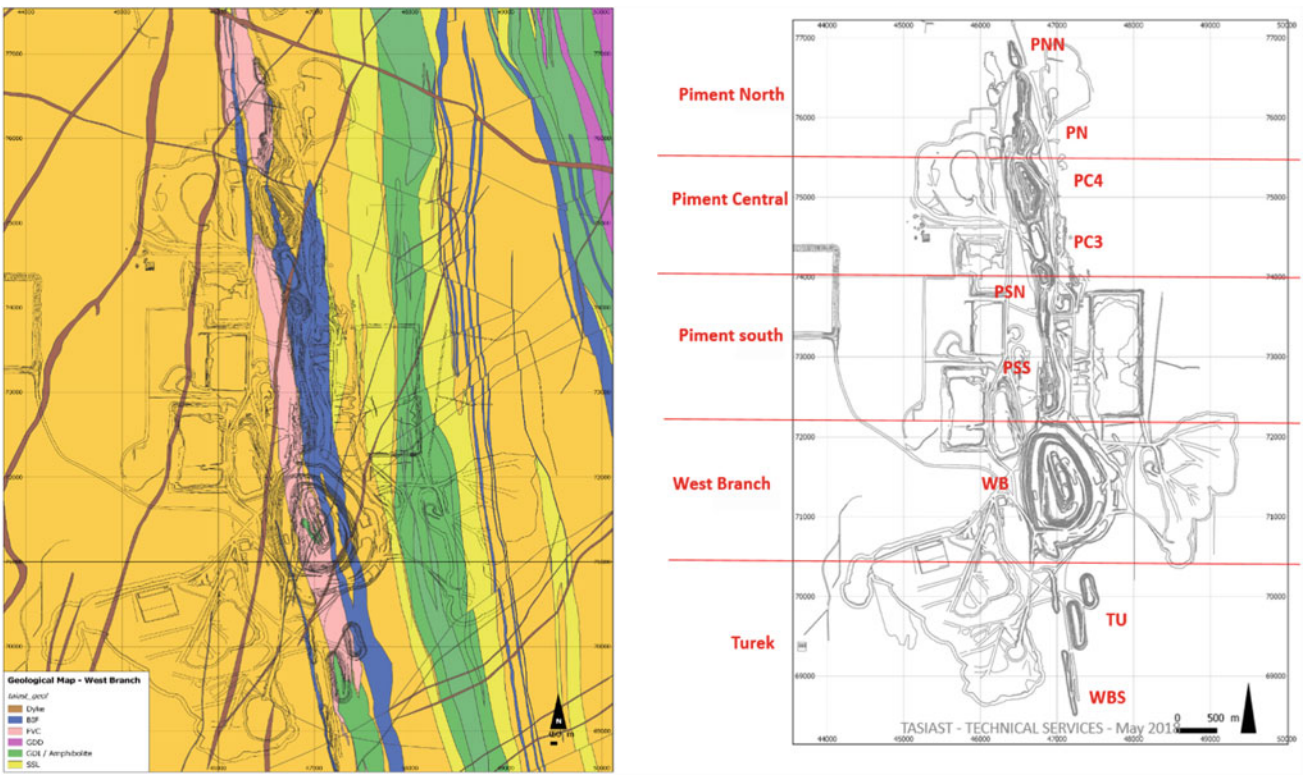

Fig. 3 Section showing the different lithological units in West Branch (Isselmou Eghlmbitt et al. 2018)

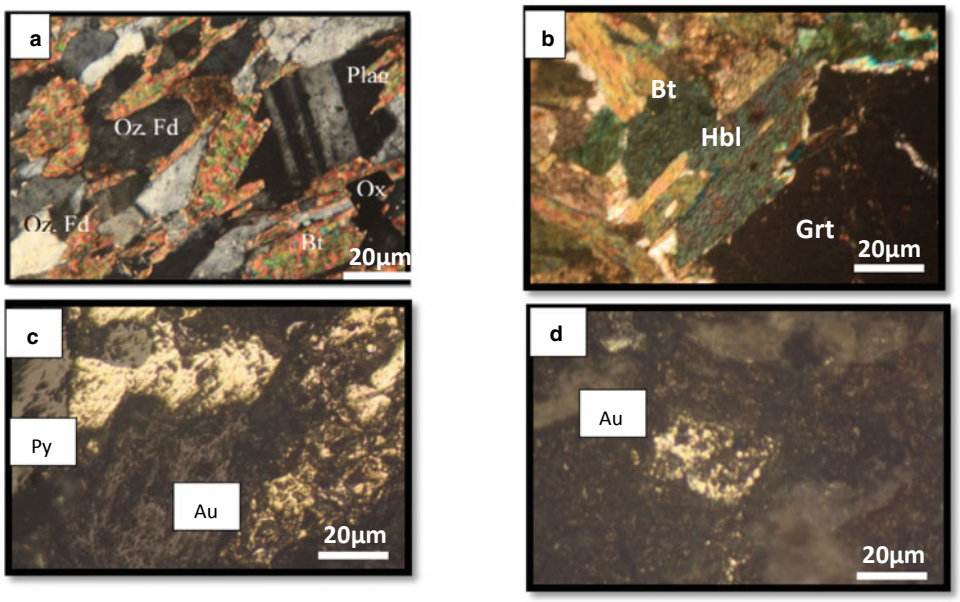

a-b: Photomicrographs of thin sections showing biotite (Bt), quartz (Qz), feldspar (Fsp), amphibole (Hbl), and garnet (Grt) in dioritic rocks.

c-d: Photomicrographs showing pyrite (Py) and gold (Au).

4 Discussion and Conclusion

The Archean Reguibat Shield is characterized by the presence of an old basement formed of gneiss, granitoids, and greenstone belts. For tectonic, ancient granitc-gneiss formations are characterized by early deformation of folds followed by a diapiric tectonic responsible for the establishment of structure type "mantled gneiss dome." This tectonic evolution is accompanied with a catazonal metamorphism evolving in the amphibolite facies. The Aoueouat formations are affected by a deformation that shows a gradual evolution with the opening of a sedimentary basin in first extensive episode during which the sedimentary units of Tasiast are deposited (Krus and Geo 2013). This basin reversed after a second compressive episode during the highest degree of metamorphism. The examined gold mineralization is hosted in the dioritic rocks with high content of sulfides and the quartz veins in a sequence of metamorphic mineral, with generally intense foliation defined by the presence of micas, amphiboles, and minerals neoformed, as chlorite and fuchsite that generally meet in the hydrothermal veins. Gold mineralization may be the result of a hydrothermal process associated with the circulation of hydrothermal fluids guided by structures acquired during major regional deformation.

This study has allowed us to derive important results, however, do not allow us to draw general conclusions because the number of drillings and sampling could not confirm or affirm these results. We focused to generate results that enable the discovery of the phenome that controls the mineralization, to determine the continuity of the rock carrying mineralization and their direction, and to understand where we can find another deposit of gold in this region which may have the same properties.

References

BGS: notice Explicative des Cartes Géologiques et Métallogéniques à 1/200 000 et 1/500 000 au Sud de la Mauritanie; Volume I—Géologie; Rapport final du PRISM, British geological survey, 580 p (2004)

Isselmou Eghlembit, Seyidna, A.L., Valentine: TASIAST from West branch to Piment geological mapping, pp. 3–8 (2018)

Key, R.M., Loughlin, S.C., Gillespie, M., Del Rio, M., Horstwood, M. S.A., Crowley, Q.G., Darbyshire, D.P.F., Pitfield, P.E.J., Henney: Two Mesoarchean terranes in the Reguibat shield of NW Mauritania: Geol. Soc. Lond. Spec. Pub. **297**, 33–52 P.J (2008)

Krus, S. Ph.D., Geo, P.: Terrane geosciences Inc—regional geometry and tectonic evolution of the Aoueouat greenstone belt and Tasiast metallogenic district for Tasiast Mauritanie limited S.A (2013)

Leroux, D.C., Roy, W.D., Orava, D.: Technical report on the Tasiast gold project, Islamic Republic of Mauritania, unpublished 43–101 report for red back mining Inc., 97 p. (2007)

Maurin, G., Bronner, G., Le Goff, E., and Chardon, D.: Châmi—notice explicative de la carte géologique à 1: 200,000; République Islamique de Mauritanie, Projet FED no. 7 ACP MAU 009 (MAU 7002), Prospection aurifère dans le Tasiast—Tijirit, N2459 (1996)

Normandy la source Mauritanie, Permis Tasiast, Tasiast Sud, N'Daouas, KattAtoui: Recherche d'anomalies aurifères et contrôle par sondage, Avancement des travaux Phase 5 (2000–2001). BRGM/RP-50941-FR—LaSource R00379 location (2000–2001) (2001)

Mineralogy and Paragenesis Associations of Polymetallic Deposits (Pb-Zn-Cu-Ag) of Boudoukha and Sidi Kambar—NE Algeria

Bouabsa Lakhdar, Kihal Hanna, and Hatert Frédéric

Abstract

The NE Algeria is mainly made of metamorphic rocks which are cut by massive granitic and microgranite intrusions. In the regions of Beni Toufout and Sidi Kambar, these formations are crossed by many veins of polymetallic mineralization. In the two fields, macroscopic and microscopic observations, show varied textures (disseminated, banded and massive). The metallographic study revealed the presence of a characteristic paragenesis, comprising sphalerite, galena, chalcopyrite, arsenopyrite, pyrite with traces of silver and gold. Micro textural relations between these different phases indicate that these mineralizations are the result of three stages. The results of preliminary chemical analysis (FRX, Atomic absorption and MEB) revealed the existence of two types of mineralization; one with a dominance of lead and the other with zinc. It should also be noted that these deposits have a lot of compatible trace elements: Ni, Co and Cr for Boudoukha; and Ni, Co and V for Sidi Kambar. They are also rich in gold, silver, arsenic and cadmium. This preliminary study shows that these deposits are associated with Miocene magmatism and can be considered as peri batholitic sulphide type hydrothermal mineralization.

Keywords

Polymetallic mineralization • Granitoids • Paragenesis • NE Algeria

B. Lakhdar (✉) · K. Hanna
Geodynamic and Natural Resources Laboratory, Department of Geology, Earth Sciences Faculty, Badji Mokhtar Annaba University, Annaba, Algeria
e-mail: lakhdar.bouabsa@univ-annaba.org

H. Frédéric
Mineralogy and Crystallochemistry Laboratory, Department of Geology, University of Liège, Liège, Belgium

1 Introduction

The history of the mineral deposits of northern Algeria results from the complex succession of very diverse geological events. During Tertiary times, in particular, numerous small deposits of non-uniform composition and morphology have formed. It is in eastern Algeria (from Bejaia to Annaba) that the granitoid and metamorphic rocks are the best represented and it is here also that the metalliferous deposits are the most abundant.

The studied regions of Boudoukha and Sidi Kambar are located in the massif of lesser Kabylia, and the mineralization is always spatially associated with Tertiary magmatism. Studies of metallogeny, gitology and geochemistry of this type of mineralization in this region are relatively rare; we can cite, Bolfa (1948), Touahri (1987), Bourahla (2015) and Touati et al. (2019). As a novel contribution provides by the present study, an initial attempt is made to highlight the mineralogical and geochemical features characterizing the ore body sulphides in this region of NE Algeria. Several geological observations and representative sampling of both the mineralized part and its immediate wall rock were made to make this study possible. Finally, to arrive at these preliminary results, qualitative and quantitative analyses were carried out using several analytical techniques (polished sections, analyses by DRX, FRX, Atomic Absorption and MEB).

2 Geology

The geographical area called "Kabylia of Collo" includes the regions of Boudoukha and Sidi Kambar occupies the central part of "Petite Kabylie" which stretches for about 150 km along the Mediterranean coast and is bordered by the city of Jijel in the West and the city of Skikda in the East. The geology of the "Kabylia of Collo" is characterized by a predominance of crystalline rocks, associated with primary

A. Çiner et al. (eds.), *Recent Research on Geomorphology, Sedimentology, Marine Geosciences and Geochemistry*, Advances in Science, Technology & Innovation, https://doi.org/10.1007/978-3-030-72547-1_76

and ultrabasic rocks (Tamanart—Collo). Moreover, an important Miocene magmatism generated granite (Beni—Toufout and Cap—Bougaroun), granodiorite, micro granodiorites, microgranites (Collo and El—Milia) and injections of acidic lava (Fig. 1).

2.1 The Boudoukha Deposit

It is characterized by an intrusive mass of granitoid and a small body of granodiorite (Ouabadi 1994). A large part of this body is hosted with microgranite points flush with the Oued Boudoukha level. The metamorphic formations (the basement) occupy the south and south-east part of the granodiorite; it is characterized by the predominance of mica schist, as well as biotite and muscovite gneiss. Several rhyolite veins intersect the metamorphic rocks.

This region is characterized by the presence of quartz veins with polymetallic sulphide mineralization (Cu, Zn, Pb, Ag) and iron oxide (hematite). These veins range between 50 and 1500 m lengths and from 10 cm up to 50 cm in the thickness. They are hosted in the granodioritic mass as well as in the metamorphic rocks. The macroscopic observations at the outcrop and on the samples show varied textures characteristic of the vein-type replacements: namely disseminated texture, ribbon texture and massive texture. According to the microscopic observations of the mineralization and their wall rock, we found three types of paragenetic successions; one is primarily associated with granular quartz and the second associated with quartz bipyramids, and the other micro-quartz associated with the oxidation and hydration of the first minerals (Table 1).

2.2 The Sidi Kambar Deposit

This region is characterized by the presence of barite veins with polymetallic sulphide mineralization (Zn, Cu, Pb and Ag) (Kihal 2009). These veins are hosted in the metamorphic rocks (gneiss and mica schist). This sulphide mineralization is associated with barite, quartz and calcite as accessories. Observations of polished sections allowed us to identify the following minerals: sphalerite, galena, pyrrhotite, chalcopyrite, pyrite, hematite and goethite. (Table 2).

3 Geochemical and Mineralogical Analyses

Several methods have been combined to highlight the mineralogical and geochemical characteristics of the deposit: Microscopic observation (Department of Geology—University of Annaba—Algeria), XRD, XRF spectrometry

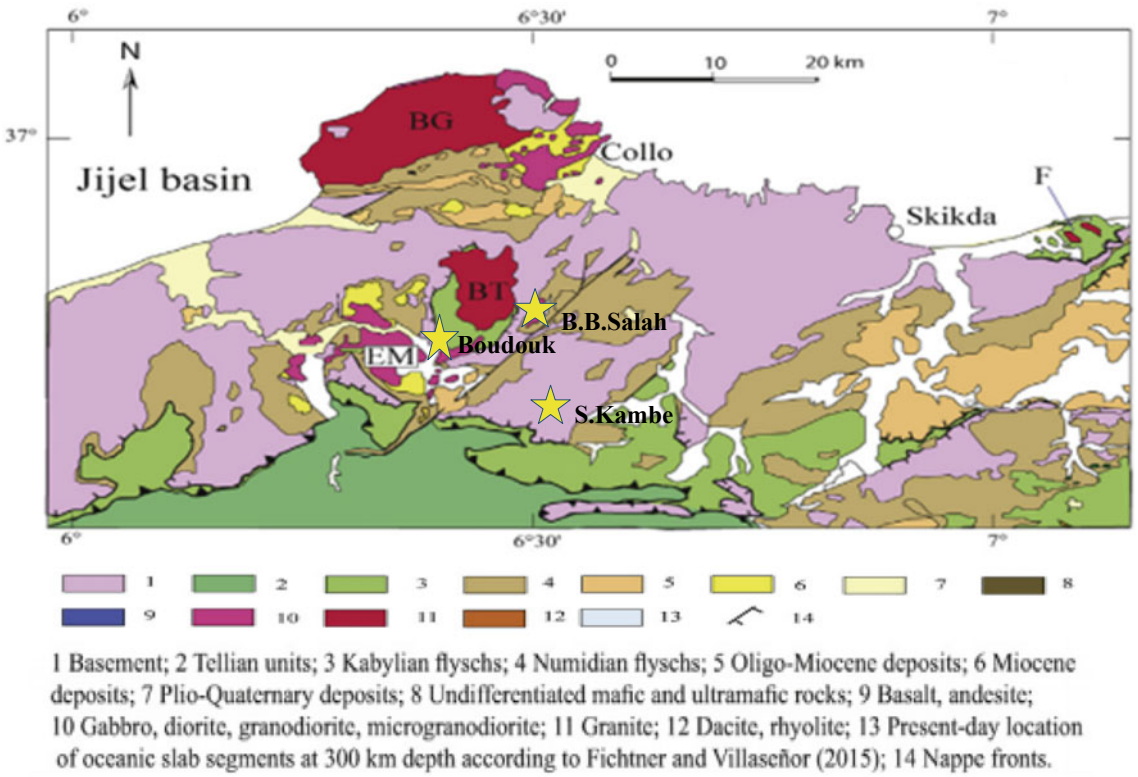

Fig. 1 Geological map of the Kabylia of Collo and El Milia (Bouillin, 1977) and location of studied zones (star)

Table 1 Paragenetic succession in Boudoukha

1st stage of sulphides and oxides depositions	2nd stage of sulphides depositions	Supergene weathering stage
Pyrite I Chalcopyrite I Sphalerite I Galena I Hematite I	Sphalerite II Galena II, Pyrite II Chalcopyrite II	Hematite II Goethite Cerusite

Table 2 Paragenetic succession in Sidi Kambar

1st stage of sulphides depositions	Supergene weathering stage
Sphalerite Pyrrhotite—Galena Chalcopyrite—pyrite	Hematite Goethite

and atomic absorption (Mineralogy Laboratory, Dpt of Geology—University of Liege—Belgium), scanning electron microscopy (School of Mines and Metallurgy—Annaba—Algeria). The results of chemical analyses carried out by "XRF" for the major elements and by atomic absorption for the trace elements confirm the petrographic and metallographic observations, in particular the presence of two types of mineralization: one rich in lead (32% Pb) and the other rich in zinc (23.22% to 25.4% Zn); the latter is relatively rich in Fe. The abundance of barite compared with quartz and calcite recognized in tin sections is well shown by the high levels of barium (BaO = 35.68%); the quartz matrix by the high content of SiO2 (27.73%). We also note that ore body of Boudoukha is rich in so-called compatible trace elements (Ni = 0.0126%, Co = 0.184% and Cr = 0.003%) and the Sidi Kambar ore (Ni = 0.01%, Co = 0.024% and V = 0.0133%). The scanning electron microscopy reveals the presence of Au, Ag and Cd associated with chalcopyrite and sphalerite. The arsenopyrite has also been identified associated with chalcopyrite.

4 Conclusion

The study of the geological context of the mineralization in Boudoukha and Sidi Kambar, the macroscopic and microscopic observations of the mineral associations, as well as the geochemical and mineralogical data, show that these deposits are spatially related to the magmatic formations (granitoïds). They also can be considered as hydrothermal mineralization, polymetallic sulphide type. The result of preliminary chemical analyses yielded two types of mineralization; the one rich in lead (32% Pb) and the other in zinc (24.3% Zn). Because of these preliminary results can we think of a hydrothermal system linked to geothermal activity during the alpine phase, as was the case for Ain Barbar? (Marignac 1988).

References

Bolfa, J. Contribution à l'étude des gites métallifères de la Kabylie de Collo et de la région de Bône.Bull.ser.de la carte géologique de l'Algérie. 6 séries de N1. (1948)

Bouillin, J.-P. Géologie alpine de la Petite Kabylie dans les régions de Collo et d'El Milia. Thèse Doctorat d'Etat, Univ. Paris VI, France, 511p (1977)

Bourahla Comparaison entre le district mineralise de Bir Beni Salah et celui de Boudoukha, Petite Kabylie centrale, (NE algerien). 9ème Colloque International du Magmatisme, Métamorphisme et Minéralisations Associées, Agadir, Maroc (2015)

Kihal, H. Contribution to the geological and gitological study of the polymetallic (Pb-Zn-Cu) peri-batholithic deposit of Boudoukha (W-Skikda). Engineering Memory (UBMA), p. 52. (2009)

Lyes, T., Omar, K., Abdelhak, B. Geology, petrography, and mineral chemistry of the Zn Pb-Cu-sulfide deposits of the Filfila Massif (East Algeria). Book: Petrogenesis and Exploration of the Earth's Interior. (2019)

Marignac, C. Les minéralisations filoniennes d'Ain-Barbar (Algérie): un exemple d'hydrothermalisme lié à l'activité géothermique alpine en Afrique du Nord.Thèse Doct. d'Etat INPL., Nancy. 1163 p. (1985)

Marignac, C.: A case of ore deposition associated with paleogeothermal activity: the polymetallic ore veins of Aïn Barbar (NE Constantinois, Algeria). Mineral. Petrol. **39**, 107–127 (1988)

Ouabadi, A. Pétrologie, géochimie et origine des granitoïdes péralumineux à cordiérite (Cap Bougaroun, Beni-Touffout et Filfila) Algérie nord-orientale. (1994)

Touahri, B. Géochimie et métallogénie des minéralisations à plomb et zinc du nord de l'Algérie. Thèse doct. Etat Paris VI. (1987)

Mineralogy and Geochemical Features of the Post-Gondwana Pedogenic North West Manganese Deposit in South Africa

Benedict Kinshasa Pharoe and Alexandr Nikolaevich Evdokimov

Abstract

The North West manganese ore deposit is comprised of supergene ores formed in a weathered crust of the Neoarchean manganiferous dolomites of the Transvaal Basin. The ores represent near-surface accumulation of black-powdered manganese wad and manganese nodules preserved in karstic depressions of the underlying Neoarchean manganiferous dolomites of the Malmani Subgroup, Transvaal Supergroup. The manganese wad forms part of the Waterval saprolite which lies immediately on top on the dolomites in a karstic system. The saprolite is in turn, overlain with a sharp erosional contact (Post-African Surface I) by West Wits alluvium hosting manganese nodules of various sizes. The alluvium thickness varies from 6 to 11 m. Secondary ore enrichment is attributed to surficial weathering and partial dissolution of the manganiferous Neoarchean dolomites of the Malmani Subgroup. Mining of the ore deposit around the area occurs in an open-cast mine setting. The mineralogical studies of the ore with X-ray diffraction analysis, petrographic and scanning electron microscope indicated the presence of a group of hollandite manganese mineral phases (i.e., cryptomelane and romanechite), vernadite, lithiophorite and pyrolusite. Other mineral components include hematite/goethite, clays, muscovite, quartz and calcite; and inclusions of detrital zircon and ilmenite. These accessory minerals occur as part of nodule grains (where quartz and calcite appear mostly as nuclear fragments and hematite both as concentric shell and cement between concentric shells) and as inclusions in authigenic cements. The geochemical and mineralogical data anomalies obtained in this study were used to develop a genetic classification of the North West manganese deposit. Based on ore mineral studies and geochemical anomalies, it was inferred that the ore is of supergene origin. Its formation took place due to continental weathering and dissolution of Neoarchean Malmani manganiferous dolomite in Late Mesozoic to Cenozoic period when the African land surface was uplifted and exposed to the action of meteoric fluids. Ore is precipitated from weathered colloids in an oxidized lacustrine environment. Such a setting is comparable with other supergene manganese ore deposits throughout Africa.

Keywords

North West Mn deposit • Mn wad • Supergene enrichment • Mn nodules • Neoarchean manganiferous dolomite

1 Introduction

Several small scale supergene ferromanganese wads and nodule deposits are developed on the Neoarchean Malmani carbonate platform of the Transvaal Supergroup. The Fe–Mn mineralization is widespread on top of the Malmani carbonate platform of the Transvaal Basin in the Highveld region of the North West Province of the Republic of South Africa. This platform stretches from the town of Krugersdorp in the east to Mafikeng in the west. After their discovery in 1960 by Dr Villiers of the former Geological Survey of the Union of South Africa, they were later studied in the late'90s by Beukes et al. (1999), Gutzmer and Beukes (1994), Pack et al. (2000), Niekerk et al. (1999) in Ryedale mine near Ventersdorp and West Wits mine near Krugersdorp, respectively. Villiers (1960) suggested that Fe–Mn deposits were derived from the supergene alteration of the underlying manganiferous dolomites of the Malmani Subgroup, which contain up to 4.5 wt % of FeO and MnO.

Further studies by Beukes et al. (1999), Gutzmer and Beukes (1994), Pack et al. (2000), Niekerk et al. (1999) led to the discovery of a new deposit being hosted by the Permian

B. K. Pharoe (✉) · A. N. Evdokimov
Saint Petersburg Mining University, 21 Line, No.2, Saint-Petersburg, Russian Federation199106

A. Çiner et al. (eds.), *Recent Research on Geomorphology, Sedimentology, Marine Geosciences and Geochemistry*, Advances in Science, Technology & Innovation, https://doi.org/10.1007/978-3-030-72547-1_77

Ecca strata of the Karoo Supergroup in Ryedale mine. The manganiferous deposit in Ryedale mine was described to contain well-preserved imprints of Glossopteris leaves on the bedding planes of the wad (Pack et al. 2000). Therefore, Villiers' (1960) ore classification had to be modified to include this newly discovered kind of ore deposit.

The manganese wad and nodule deposit studied under this work were recently reviewed and characterized stratigraphically by Pharaoh and Liu (2018). Due to lack of knowledge on the geochemical components, mineralogy, occurrence and mineral distribution and genetic model of the ore deposit; this research was therefore inspired to provide an understanding of the geological characteristics and genetic model of the ore deposit. The study was carried out in the region of North West Province between the towns of Ventersdorp, Carletonville and Boons. The study area under study is a farm that is currently under mine-development (General Manganese Mine) and contains several exploration pits which were opened during stages of exploration (Fig. 1). Similar to the Klipkuil and West Wits deposits (in Niekerk et al. 1999), this deposit was derived from and developed on the Early Proterozoic Malmani dolomite succession of the Transvaal Supergroup. Most of these secondary enriched deposits reported in the North West Province (Klipkuil, Ryedale, and West Wits) are composed predominantly of manganese dioxide (pyrolusite). The predominant manganese mineral composition in the area under study constitutes mainly of cryptomelane, romanechite and late stage diagenetic - lithiophorite. Early formed minerals such as vernadite and pyrolusite appears to have been transformed into cryptomelane and romanechite with change in chemistry (redox potential and pH) of basin waters.

2 Sampling and Methodology

An exploration grid (200m * 150m) comprising of 70 exploration pits was designed in the mine area during the 1st and 2nd stage of exploration. Ten of these pits were logged during this study to identify prominent features, such as mineral composition, nodule size distribution, nodule's shape and color change acrossthe profile section. Based on these features, the upper tier of the ore section was divided into eight zones (A to H, refer to Pharoe and Liu 2018). Samples of manganese nodules, manganiferous dolostones and manganese wad (manganese earth, Fig. 2c) were collected on each zone of the section and later analyzed for geochemical and mineralogical constituents at the Council for Geoscience laboratory in Pretoria, South Africa. The rock mineralogical analysis was carried out by X-ray diffraction (XRD), and the results were also compared with findings from the petrographic study. The XRD measurements were performed on a Bruker XRD Advance Model: V22.0.28 at room temperature of 25 °C. The finely powdered samples were spread on a glass slide and scanned at 2θ/minute stretching from 2° to 70° in the 2θ range (wavelength = 1.54058). Microscope investigation was carried out for 20 polished and 20 thin sections of various rock types. Manganese ore polished sections were examined under reflected light to identify ore minerals and their textures. The 20 thin sections of dolomites and Mn-bearing terrigenous clasts were studied under transmitted light. Images of interest were captured using an Olympus polarizing microscope with a built-in Leica camera, linked to a computer monitor at Saint Petersburg Mining University. The polarizing microscopic study was supplemented with scanning electron microscopic and energy dispersive spectroscopy link investigations performed on a JEOL JSM-6390 LV model. Major and trace elements were determined by X-ray Fluorescence (XRF) undertaken on a MagiX Fast, XRF spectrometer. For principal element analysis, the milled sample (<75 μm fraction) was roasted at 1000 °C for at least 3 h to oxidize Fe_2 + and S and to determine the loss of ignition (L.O.I.). Glass disks were prepared by fusing 1 g of roasted sample and 10 g flux consisting of 49.5% $Li_2B_4O_7$, 49.5% and 0.50% LiI at 1150 °C. Quality control/quality assurance was done by using an in-house amphibolite reference material (sample 12/76). Also, one in every ten samples was duplicated during sample preparation and analyses. For trace element analysis, 12 g milled sample and 3 g Lico wax was mixed and pressed into a powder briquette using a hydraulic press with an applied pressure at 25 ton. The glass disks and wax pellets were analyzed using a PANalytical wavelength dispersive Axios X-ray fluorescence spectrometer equipped with a four KW Rh tube.

3 Results

3.1 Mineralogy of Mn Oxides

Manganese mineral phases in the area consist mainly of a group of minerals with a common crystal structure A^+ ($^{2+}$) ($Mn_4{}^+{}_6Mn_3{}^+{}_2)O_{16}$), where A = K^+, Ba_{2+}, Pb_{2+}. This group of minerals include cryptomelane (K^+ [$Mn_4{}^+{}_6Mn_3{}^+{}_2]_8O_{16}$) and romanechite ((Ba, $H_2O)_2$ [Mn^{4+}, $Mn^{3+}]_5O_{10}$). Other manganese mineral phases include pyrolusite (MnO_2) and manganite (γ-MnOOH). Mn oxide minerals occur in the form of shell layers encircled around the nucleus of other rock fragments. Diagenetic features indicate the replacement of detrital grains and early formed mineral phases with manganese oxides. These include the replacement of detrital quartz grains in terrigenous sediments (Fig. 3a). Features of replacement of clay minerals by Mn oxides are also evident (Fig. 3b). Manganese mineral generation indicates the formation of manganese oxides from oxidative dissolution and replacement of primary manganese-bearing carbonate

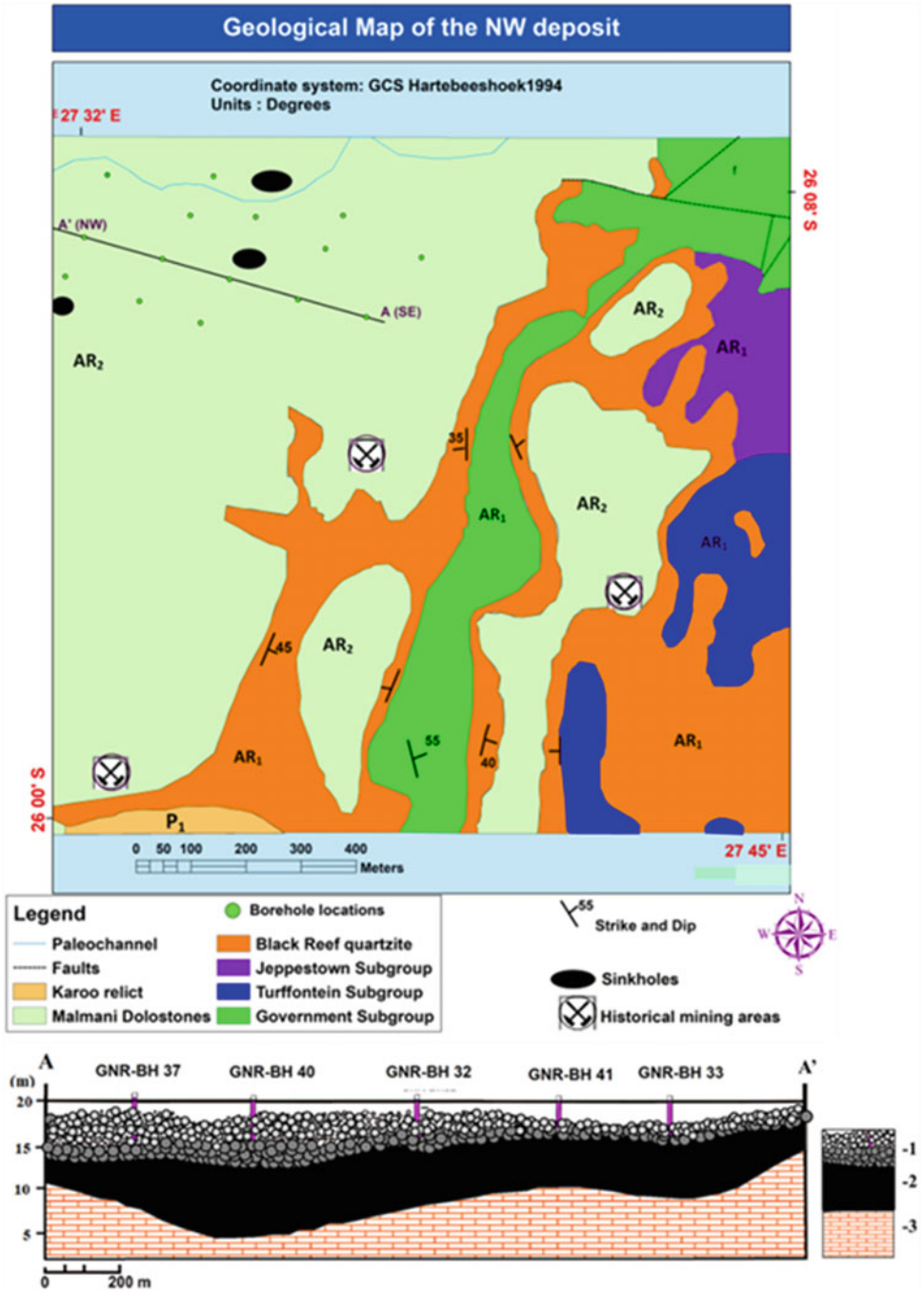

Fig. 1 Geological map of the Carletonville manganese ore deposit and a NW-SE geologic cross section of the area. Where: 1—Mn nodules, 2—manganese wad and 3—Malmani dolomite

minerals. Formation of manganite was characterized by direct precipitation of Mn colloids carried in water suspension. Formation of cryptomelane and romanechite was dominated by transformation of early formed manganese oxide phases as a result of increased degree of oxidation and pH values in an oxidative depository. Romanechite is present commonly as intergrowths with cryptomelane (Fig. 3c). The textural relations, especially the acicular morphology (Fig. 3h), suggest that hollandite minerals have good crystallinity, achieved by open-space filling. Pyrolusite is a widespread ore mineral, frequently exhibiting petrographic features, such as high reflectivity, yellow reflection color and strong anisotropism which make it easily recognizable under an optical microscope (Fig. 3g).

3.2 Geochemistry

Geochemical components show enrichment of MnO, Fe_2O_3, Al_2O_3 and SiO_2. Other major oxides have lower values

Fig. 2 Studied rock samples **a** Manganese nodule morphology, consisting of nucleus enclosed by Mn–Fe ring; **b** Occurrence of manganese in a weathered alluvial succession; **c** Mn WAD; **d** and **e** Malachite and Manganiferous stromatolite

ranging below 1 wt % (Fig. 4). The geochemical components of the lower zone (F, G and H) have MnO values in the range of 4.62–17.50 wt %, Fe_2O_3 ranges from 10 to 12 wt %. Al_2O_3 values are ranging between 11 and 14.82 wt % and SiO_2 values at 46.8–62.4 wt % (Fig. 4). This zone has elevated Mn content most probably due to the high mobility of Mn^{2+}in weathering crust and high concentration of Mn nodules. In the central zones (C, D and E), geochemical constituents include high values of SiO_2 (43–65 wt %), MnO (1.39–19 wt %), Al_2O_3 (12–13 wt %) and Fe_2O_3 (13–20 wt %). Values of Na_2O and K_2O and CaO are less than 1 wt % due to intense dissolution and leaching during meteoric water percolation. The uppermost zones (A and B) are composed of a negligible amount of manganese oxide (MnO ranges from 0.9 to 1.0 wt %) but have elevated content of SiO_2 (77–82 wt %) and Fe_2O_3 (6.4–9.32 wt %) and Al_2O_3 (5.6–8 wt %).

4 Genetic Model of the Ore Deposit

Rare and trace element geochemistry of manganese deposit plays a crucial role in the reconstruction of the genesis of the ore deposit. Different manganese classification schemes have been previously developed to constrain the genesis of particular types of manganese deposits of various geological ages. Such schemes (Achurra et al. 2009; Rio Salas et al. 2008; Heshmatbehzadi and Shahabpour 2010; Nath et al. 1997; Nicholson et al. 1997; Roy 1992; Sethumadhav et al. 2010; Toth 1980) make use of trace and major elements to constrain the genesis of a manganese deposit in a given environment. The use of trace elements in the identification of the mechanisms forming manganese oxide, and especially cryptomelane, proved to be one of the successful methodologies because of the adsorption of these elements into the K–Mn oxide tunnel structure in aqueous solution during precipitation (Mero 1962; Rendall et al. 1998). This study, therefore, used a combination of geological data to constrain the genesis of the North West manganese deposit. Based on the proposed classification schemes, it was inferred that the North West deposit formed in supergene and hydrogenous environment (Fig. 5) from the in situ weathering and dissolution of the underlying manganiferous Malmani dolomites in a humid, hot and oxidizing continental setting. The Mn/Fe ratio, as applied by Nicholson and others (Nicholson et al. 1997), indicates values of up to 0.53, suggesting manganese precipitation in a lacustrine environment. The increased values of Ce as attributed by less ratio of La/Ce, as indicated in Fig. 6 implies the adsorption of Ce and other REE elements in the ore crystal structure during hydrogenous precipitation.

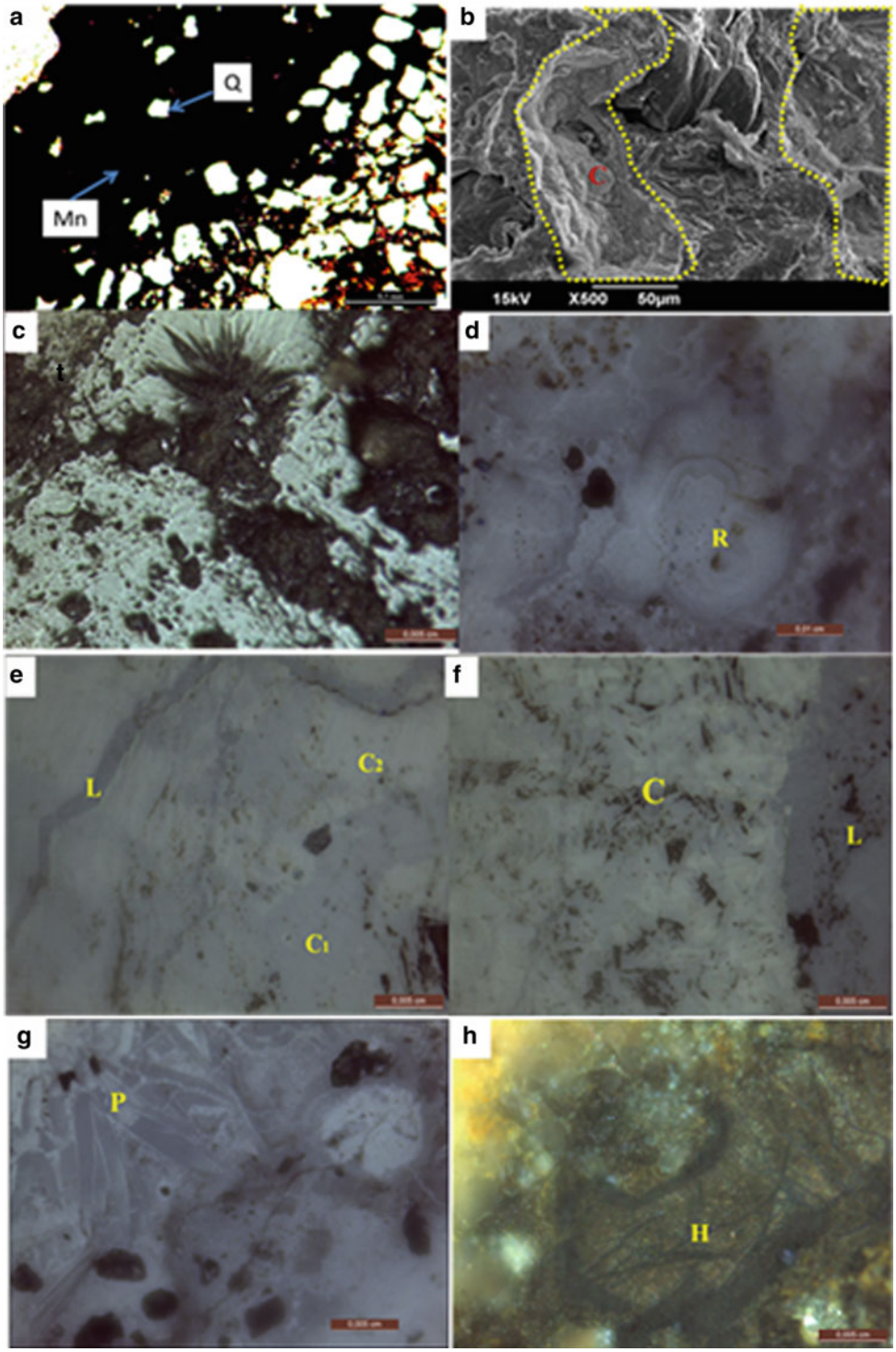

Fig. 3 Photomicrographs under both reflected and plane polarized light. **a** Replacement of detrital quartz grain by manganese oxides (viewed under plane polarized light); **b** SEM photomicrograph showing pseudomorphic texture of cryptomelane in cavities after replacement of smectite with original honeybox clay mineral texture preserved; **c** Crystalline Romanechite (white) and possibly lithiophorite (dark grey); **d** Botryoidal romanechite; **e** Cryptomelane generation (C1 and C2) with a vein filled by lithiophorite; **f** Paragenetic relationship of cryptomelane and lithiophorite. **g** Pyrolusite and **h** Hollandite manganese oxide showing acicular morphology

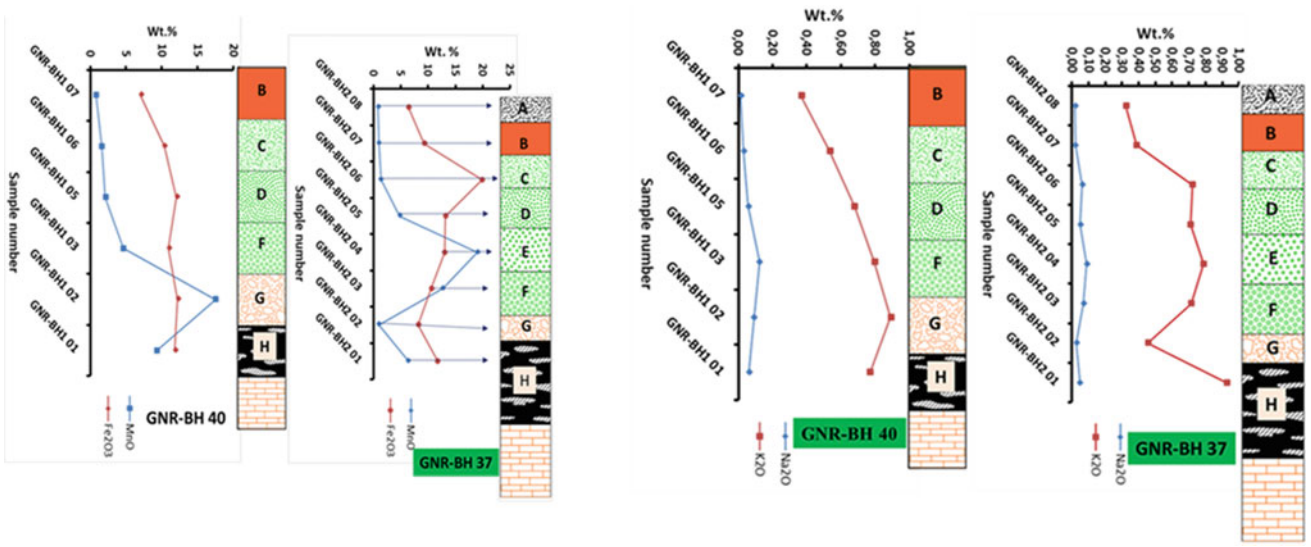

Fig. 4 The contents of major oxides (MnO, Fe_2O_3, Na_2O and K_2O) in different zones along the sections of GNR-BH 40 and GNR-BH 37

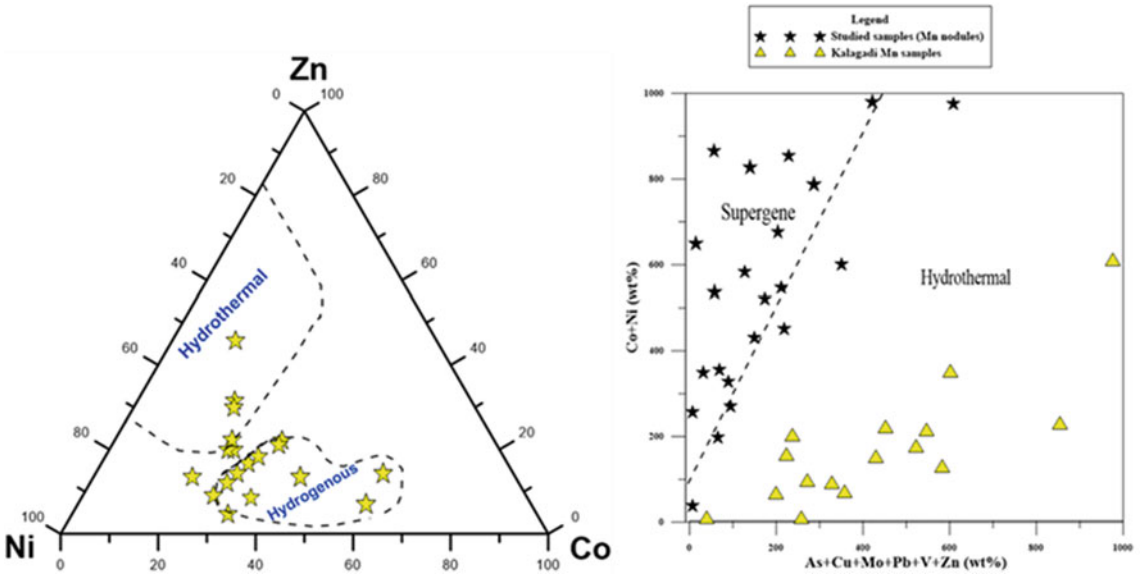

Fig. 5 Bivariate and ternary discrimination plots for trace elements indicating the possible sources of manganese based on (Rio Salas et al. 2008; Heshmatbehzadi and Shahabpour 2010; Sethumadhav et al. 2010)

5 Conclusions

The following findings and conclusions were made on this study: 1) Manganese ore samples are mineralogically characterized by a group of high valence state manganese oxides such as cryptomelane, hollandite, romanechite, pyrolusite and lithiophorite with vernadite. In addition, quartz, hematite and kaolinite are prevalent. 2) Application of geochemical data and associated classification schemes led to the reconstruction of the origin of the NW manganese ore. The latter indicated a supergene origin for manganese ores; their formation is attributable to hydrogenous precipitation as a governing ore formation mechanism. The ore substances released into the overlying water column from the dissolution and leaching of manganiferous dolomites gave rise to the formation of manganese nodules.

The chemical weathering and dissolution of the manganiferous dolomites produced manganese-rich residues and colloids, which later precipitated as manganese nodules lining up fragments of quartz, quartzite and sands. Romanechite, cryptomelane and lithiophorite are predominant manganese oxide in the mine area with pyrolusite (MnO_2) occurring at lesser degree due to it's transformation in the late

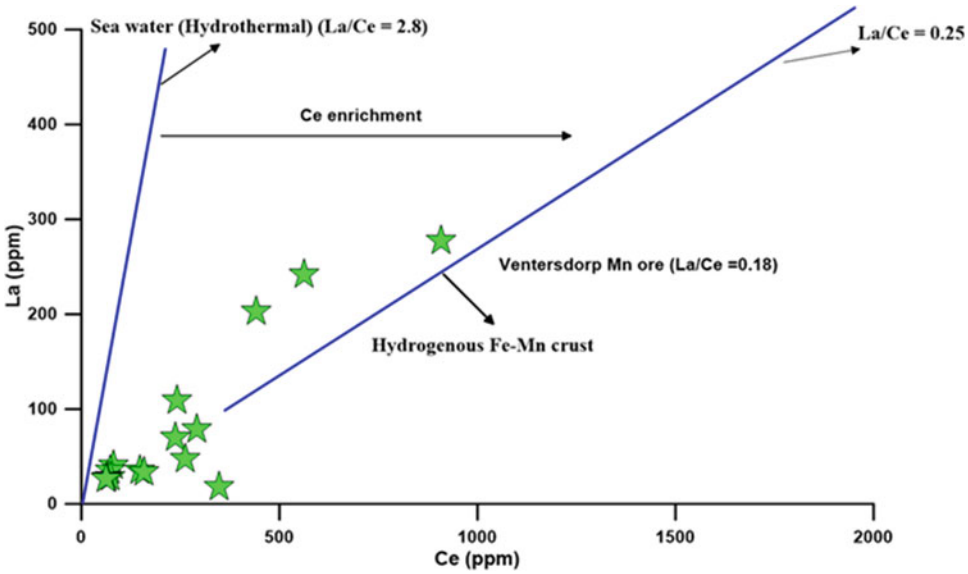

Fig. 6 Binary plot of La versus Ce concentration for the NW manganese nodules after (Nath et al. 1997; Toth 1980)

stage of mineral formation. The ore in NW deposit was formed and enriched at the expense of Paleoproterozoic manganese-rich Malmani dolomites, in a timespan tentatively linked with the Late Cretaceous to Mid-Cenozoic uplift of the African land surface. This setting is overall comparable with that of other manganese deposits elsewhere in Africa. Further age determination of the Carletonville ore, using Ar dating of cryptomelane and rare earth element anomalies should allow better correlation between Late Mesozoic to Cenozoic supergene manganese deposits across Africa.

References

Achurra, L.E., Lacassie, J.P., Le Roux, J.P., Marquardt, C., Belmar, M., Ruiz-del-Solar, J., Ishman, S.E.: Manganese nodules in the Miocene Bahia Inglesa Formation, north-central Chile: Petrography, geochemistry, genesis and palaeoceanographic significance. Sed. Geol. **217**, 128–139 (2009)

Beukes, N.J., Van Niekerk, H.S., Gutzmer, J.: Post-Gondwana African land surfaces and pedogenic ferromanganese deposits on the Witwatersrand at the West Wits gold mine. S. Afr. J. Geol. **102**, 65–82 (1999)

Burke, K., Gunnell, Y.: The African erosion surface: a continental-scale synthesis of geomorphology, tectonics, and environmental change over the past 180 million years. Geological Society of America, Memoir 201: p. 66, (2008)

De Villiers, J.: The manganese deposits of the Union of South Africa. Pretoria: Geological Survey of South Africa Handbook, vol. 2, p. 263. (1960)

Del Rio Salas, R., Ruiz, J., Ochoa-Landin, L., Noriega, O., Barra, F., Meza-Figueroa, D. and Paz-Moreno, F.: Geology, geochemistry and Re-Os systematics of manganese deposits from the Santa Rosalia Basin and adjacent area in Baja California Sur, Mexico. Int. J. Geol. Miner. Geochem. Mineral Deposits, **43**, 467–482 (2008)

Gutzmer, J., Beukes, N.J.: Karst control of the Ryedale Fe-Mn deposit in the Palaeozoic Karoo Supergroup, Western Transvaal, South Africa: Berichte der Deutschen Mineralogischen Gesellschaft, Beiheft zum. Eur. J. Miner. **6**(1), 333 (1994)

Heshmatbehzadi, K., Shahabpour, J.: Metallogeny of manganese and ferromanganese ores in Baft Ophiolitic Mélange, Kerman Iran. Aust. J. Basic Appl. Sci. **4**(2), 302–313 (2010)

Mero, J.L.: Ocean-floor manganese nodules. Econ. Geol. **57**, 747–767 (1962)

Nath, B.B., Pluger, W.L., Roelandts, I.: Geochemical constraints on the hydrothermal origin of ferromanganese incrustations from the Rodriguez triple junction, Indian Ocean. Geological Society, London, Special Publication **119**, 199–211 (1997)

Nicholson, K., Nayak, V.K., Nanda, J.K.: Manganese ores of the Ghoriajhor-Monmunda area, Sundergarh District, Orissa, India: geochemical evidence for a mixed Mn source. Geological Society of London, Special Publication **119**, 117–121 (1997)

Pack, A., Gutzmer, J., Beukes, N., Van Niekerk, H.: Supergene ferromanganese wad deposits derived from Permian Karoo Strata along the late Cretaceous-mid-Tertiary African land surface, Ryedale South Africa. Econ. Geol. **95**, 203–220 (2000)

Pharoe, B.K., Liu, K.: Stratigraphy of the pedogenic manganese nodules in the Carletonville area, North West Province of South Africa: a case study of the General Nice Manganese Mine. J. Afr. Earth Sci. **143**, 79–101 (2018)

Rendall, S.M., Serman, D.M., Ragnarsdottir, K.V.: An extended X-ray absorption fine structure spectroscopy investigation of cadmium sorption on cryptomelane (KMn8O16). Chem. Geol. **151**, 95–106 (1998)

Roy, S.: Environments and processes of manganese deposits. Econ. Geol. **87**, 1218–1236 (1992)

Roy, S.: Sedimentary manganese metallogenesis in response to the evolution of the Earth system. Earth-Sci. Rev. **77**, 273–305 (2006)

Sethumadhav, M.S., Yanni, G., Mohamed, M.A., Chinnaiah.: Late Archean manganese mineralization and younger supergene manganese ores in the Anmod-Bisgod region, western Dharwar Craton, southern India: Geological characterization, palaeoenvironmental history, and geomorphological setting. Ore Geol. Rev. **38**, 70–89 (2010)

Toth, J.R.: Deposition of submarine crusts rich in manganese and iron. Geol. Soc. Am. Bull. **91**, 44–54 (1980)

Van Niekerk, H.S., Beukes, N.J and Gutzmer, J.: Post-Gondwana pedogenic ferromanganese deposits, ancient soil profiles, African land surfaces and palaeoclimate change on the Highveld of South Africa. J. Afr. Earth Sci. **29**, 761–781(1999)

Origin of the Tala Hamza Igneous Rocks-Hosted Zinc-Lead Deposit, NE Algeria

Lekoui Abdelamalek, Laouar Rabah, Salmi-Laouar Sihem, Bouhlel Salah, and Adrian J. Boyce

Abstract

The Miocene igneous rocks that host the Tala Hamza Zn–Pb deposit are investigated in order to shed light on their petrogenesis and to provide a brief metallogenic description of associated sulphides mineralization. 800 m depth drill hole reveals from top to bottom the following succession: pyroclasitic rocks, andesite, volcanic tuff, microgranite, silicified tuff, kaolinized andesite cross-cut by aplite, metasomatized granodiorite and granodiorite. These rocks are composed of plagioclase, hornblende, biotite, alkali feldspar, sphene, apatite and zircon. Major elements geochemistry shows that these igneous rocks exhibit calc-alkaline, high K to shoshonitic, metaluminous to slightly peraluminous, I-type characters. Multi-elemental spectra, as well as chondrite-normalized rare earth spectra, show LILE and LREE enrichment relative to HFSE and HREE, respectively. The REE shows a slight negative anomaly in Eu. All these features indicate that the rocks originate from an igneous protolith, probably from a metasomatized mantle material that was contaminated by crustal material and emplaced in a post-collision context during the Miocene. Metallogenic study for both massive sulphides and stockworks reveals the presence of replacement textures, open-space-filling texture and pseudomorphism. These textural patterns, in addition to the presence of the anhydrite layer, are common in deposits of VHMS (volcanic-hosted massive sulphides) group formed in the submarine environment. They also indicate hydrothermal processes throughout two main stages: (1) an early stage in which disseminated pyrite and chalcopyrite hosted by metasomatized granodiorite were formed, and (2) a late-stage or mineralizing stage with the deposition of economic ore (mainly sphalerite and rare galena) along faults and fractures.

Keywords

Miocene magmatism • Geochemistry • Sulphides • Tala Hamza

1 Introduction

In northeastern Algeria, igneous complexes (11–17 Ma) (Chazot et al. 2017) intrude both the metamorphic basement and the sedimentary cover of the alpine belt. These post-collisional igneous rocks are believed to have been formed under a subduction-collision tectonic regime (Fig. 1). Previous studies (e.g., Laouar et al. 2005) reveal the existence of two types of magmas according to their origin: (1) a mantle-derived magma with variable crustal contamination (e.g. Edough, Cap de Fer) and (2) a magma originated from partial melting of meta-sedimentary rocks (e.g. Cap Bougaroune, Filfila). These two types of magmas (1) and (2) are qualified as I- and S-type, respectively according to the definition of Chappell and White (2001).

This magmatic activity has, often, been accompanied by hydrothermal alteration of variable degrees and the deposition of several types of mineralization, such as Pb–Zn–Cu, Sb–Au and As–W–Au. In this study, we report the genesis of both the Tala Hamza igneous rocks using significant trace and rare earth elements data and the associated Zn–Pb mineralization.

L. Abdelamalek (✉)
LGG Laboratory, Mohammed Seddik Ben Yahia University, Jijel, Algeria

L. Rabah · S.-L. Sihem
Faculté Des Sciences de La Terre, Département de Géologie, Université Badji-Mokhtar Annaba, B.P. 12, 23000 Annaba, Algeria

B. Salah
Faculté Des Sciences de Tunis, Département de Géologie, Université de Tunis el Manar, Tunis, Tunisia

A. J. Boyce
Isotope Geosciences Unit, S.U.E.R.C., East Kilbride, Glasgow, G75 0QU, Scotland, UK

A. Çiner et al. (eds.), *Recent Research on Geomorphology, Sedimentology, Marine Geosciences and Geochemistry*, Advances in Science, Technology & Innovation, https://doi.org/10.1007/978-3-030-72547-1_78

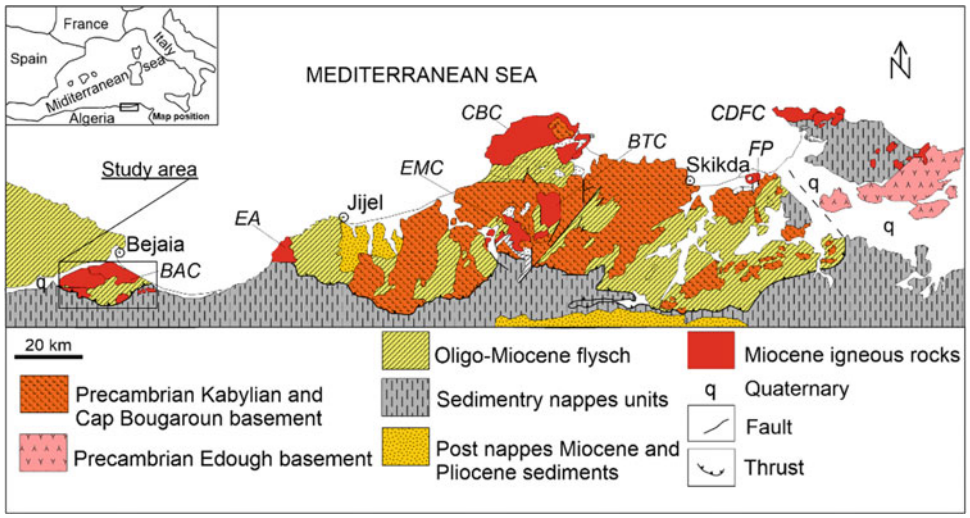

Fig. 1 Geological sketch map of northeastern Algeria showing the location of the igneous complexes. CBC: Cap Bougaroun, BTC: Beni Touffout and El Milia, FP: Filfila peraluminous plutons, BAC: Bejaia–Amizour, EA: El Aouana, CDFC: Chetaibi-Cap de Fer complex (Fourcade et al. 2001)

2 Materials and Methods

This study has been facilitated by the sampling of an 800 m deep drill hole. Twenty-two unaltered samples were sent to ALS Minerals, Spain, for major trace element analysis via ICP-AES and ICP-MS methods. Polished sections of different mineralization were prepared and studied using a reflected light microscope at "Laboratoire de Minéralogie et Géochimie Appliquée", Faculty of Sciences, El Manar University Tunis, Tunisia.

2.1 Results

The SiO_2 concentrations of igneous rocks range from 52.9 to 75.2 wt%. The Na_2O and K_2O contents are almost identical with a mean value of 3.54 and 3.57 wt%, respectively. Despite Na and K are mobile elements in the presence of aqueous fluids, it is expected that their concentrations still preserve the original magmatic behaviour in the least altered rocks. Al_2O_3 concentrations vary between 13.45 and 20.20% with a mean value of 15.88% (n = 22), while compatible elements such as Fe, Mg and Ca show more variable contents according to the lithology. Metallographic investigations show two zones of mineralization: (1) massive sulphides zone (consisting of sphalerite and galena with ubiquitous pyrite and subordinate chalcopyrite—black ore) representing the economic ore, hosted by kaolinized andesite and silicified tuff (from a depth of 400–600 m), (2) stockwork zone hosted by metasomatized granodiorite (from a depth of 600–750 m) and composed of yellow ore with chalcopyrite, pyrite and iron oxides. A 10 m anhydrite layer separates these two zones.

3 Discussion

The SiO_2 concentrations span a wide range that indicates felsic to intermediate compositions for the Tala Hamza igneous rocks. The variation of incompatible elements with SiO_2 contents shows the usual positive correlation while CaO, Al_2O_3, total iron (Fe_2O_3t) and MgO show a negative correlation ($r = -0.3$). All samples display a calc-alkaline highly potassic to shoshonitic character. These affinities have been highlighted for the majority of the Miocene magmatic complexes of northeastern Algeria. The majority of samples show ASI < 1, 1 (aluminium saturation index), which indicates a metaluminous to slightly peraluminous character. This observation, along with the mineralogical composition, may assign the rocks to I-type rocks.

In the chondrite-normalized multi-element and REE diagrams (Fig. 2), the Tala Hamza igneous rocks show enrichment in significant ion lithophile elements (LILE) and light rare earth elements (LREE) concerning high field strength elements (HFSE) and substantial rare earth element (HREE), respectively. These high-K calc-alkaline rocks also have pronounced Rb and Sr negative anomalies and slight negative Eu anomaly. These geochemical features indicate that the various igneous lithologies are genetically related. Sr, Eu and Rb anomaly could be explained by an early fractionation of plagioclase and biotite during the magma differentiation or ascension. Ta and Nb negative anomalies, as well as REE, behaviour advocate a subduction-related setting for these igneous rocks. Similarly, in the Nb + Y versus Rb diagram (Pearce et al. 1984) (not shown) these igneous rocks plot in the post-collisional field which is consistent with recent studies by Chazot et al. (2017) carried out on the Miocene igneous rocks of northeastern Algeria.

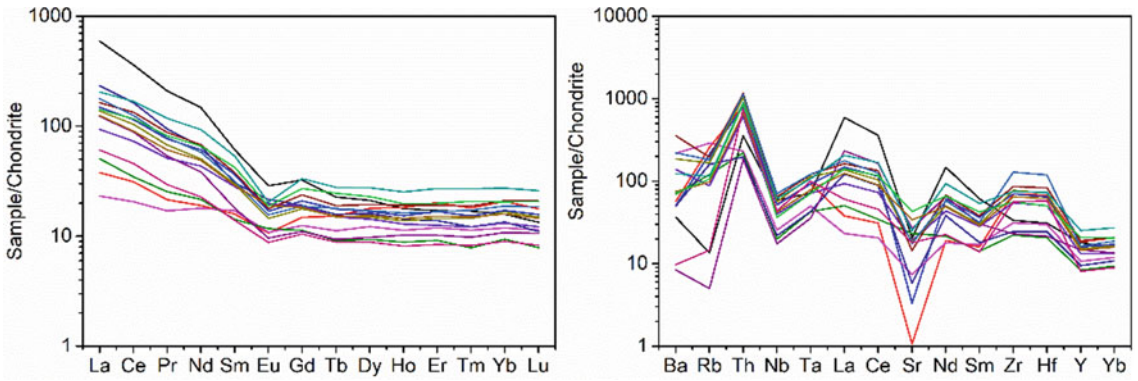

Fig. 2 Chondrite-normalized REE diagram (left) and multi-elements diagram (right) for the Tala Hamza granitoides

Textural patterns of the Zn–Pb ore in addition to the presence of the anhydrite layer are standard features of the VHMS deposit group that is formed in a submarine environment.

Metallographic observations also indicate hydrothermal processes throughout two main stages: (1) an early stage in with disseminated pyrite and chalcopyrite have been deposited within metasomatized granodiorite and (2) a late-stage or mineralizing stage with deposition of economic ore (sphalerite and galena mainly) along faults and fractures.

4 Conclusions

The geochemical characteristics of the Tala Hamza igneous rocks indicate that these rocks are calc-alkaline, highly potassic to shoshonitic rocks. They are metalouminous to slightly peraluminous assigned to I-type. Trace and REE elements behaviours confirm that they are post-collisional igneous rocks formed under the subduction-collision geotectonic regime. The magma source could be the Kabylian metasomatized lithospheric mantle. Zn–Pb mineralization associated with these granitoids exhibits many features of the VHMS group. Various sulphides minerals are believed to be deposited from hydrothermal fluids throughout two successive stages.

References

Chappell, B.W., White, A.J.R: Two contrasting granite types—25 years later. Aust.J. Earth Sci. 48, 489–499 (2001)

Chazot, G., Abbassene, F., Maury, R.C., Déverchère, J., Bellon, H., Ouabadi, A., Bosch, D.: An overview on the origin of post-collisional Miocene magmatism in the Kabylies (northern Algeria): evidence for crustal stacking, delamination and slab detachment. J. Afr. Earth Sci. **125**, 27–41 (2017)

Fourcade, S., Capdevila, R., Ouabadi, A., Martineau, F.: The origin and geodynamicsignificance of the Alpine cordierite-bearing granitoids of northern Algeria. A combinedpetrological, mineralogical, geochemical and isotopic (O, H, Sr, Nd) study (2001)

Laouar, R., Boyce, A.J., Arafa, M., Ouabadi, A., Fallick, A.E: Petrological, geochemical,and stable isotope constraints on the genesis of the Miocene igneous rocksof Chetaibi and Cap de Fer (NE Algeria). J. Afr. Earth Sci. **41**, 445–465 (2005)

Pearce, J.A., Harris, N.B.W., Tindle, A.G.: Trace element discrimination diagrams for the tectonic interpretation of granitic rocks. J. Petrol. **25**, 956–983 (1984)

Genesis of the Rift-Related Fe-Mn Sediment-Hosted Deposit, Masilah Basin (Yemen)

Laura Pinarelli and Mohamed Mattash

Abstract

The sedimentary Masilah Basin, in the southeastern Yemen, is a rift-basin linked to the Mesozoic breakup of Gondwanaland. Fe-Mn ore deposit occurs as variously oriented ore bodies, veins and alteration zones along a fault system inside Tertiary shallow marine carbonate rocks of the Masilah Basin. Massive hematite-rich veins have grades around 50% Fe. The manganese-rich veins mainly consist of hollandite-romanechite, cryptomelane or pyrolusite veins, and are high grade (47–51% Mn). Fe–Mn-rich ore (10–3.5% Fe and 6.7–2.0% Mn) occurs as disseminations and patches in the calcareous host rocks. Fe/Mn ratios and metal contents indicate that the ores in veins and lenses were generated by the circulation of hydrothermal fluids likely derived from Quaternary basic magmatic rocks, whereas the disseminated and patch ores have mixed hydrothermal-hydrogenetic origin.

Keywords

Masilah Basin • Fe-Mn ore • Mineralizing fluids • Geochemistry • Yemen

1 Introduction

Yemen forms the southwestern tip of the Arabian Peninsula (Fig. 1). The Masilah Basin (MB) is one of the Mesozoic sedimentary basins of Yemen and is located parallel to the Red Sea, with several small areas covered by Quaternary alkaline basalts. Its structural evolution is connected to the opening of the Gulf of Aden and the Red Sea rifts. It was developed in Late Jurassic to Early Cretaceous times, and hosts polymetallic Ba, Zn-Pb, Fe-Mn, V mineral deposits (Pinarelli and Mattash 2018). They represent examples of mineral deposits associated with extensional fault systems in continental environments and, as such, their investigation can shed light on the genesis and characteristics of this deposit type. Previous preliminary investigations on different geological aspects of MB Fe-Mn ores showed that they have been mostly formed as replacements and open space fillings (Mattash et al. 2007), along a fault system that cuts the altered calcareous host rocks and is connected to the syn- (late Oligocene-early Miocene) and post-rift (late Miocene-Recent) phases. In the present research, geological, mineralogical, and geochemical features of the MB Fe-Mn deposit are discussed to provide a better understanding of the mineralization processes.

2 Materials and Methods

In this paper, we report major trace elements, and rare earth elements (REE) on whole rock samples coming from Fe- and Mn-rich veins and lenses, as well as from calcareous host rocks. The specimens were sampled during fieldwork led by the Geological Survey and Minerals Resources of Hadramawt, Mukalla (Yemen). Mineralogical species were identified by X-ray diffraction (XRD) analysis at the University of British Columbia (Canada) using a Bruker D8 Focus (0–20, LynxEye detector) diffractometer. Whole rock chemical analyses of major and trace elements were carried out at AlsChemex Laboratory, Vancouver, Canada. Depending on the type of rock, the concentration of some elements may vary of several orders of magnitude, hence different analytical methods with appropriate sensitivity were used, as applicable. Accordingly, methods used are ICP (Inductively Coupled Plasma)-AES (Atomic Emission Spectrometry) and combined ICP-AES + ICP-MS (Mass

L. Pinarelli (✉)
CNR, Institute of Geosciences and Earth Resources—Section of Florence, Florence, Italy
e-mail: lapina@igg.cnr.it

M. Mattash
Geological Survey and Mineral Resources Board, Ministry of Oil and Minerals, Aden, Yemen

A. Çiner et al. (eds.), *Recent Research on Geomorphology, Sedimentology, Marine Geosciences and Geochemistry*, Advances in Science, Technology & Innovation, https://doi.org/10.1007/978-3-030-72547-1_79

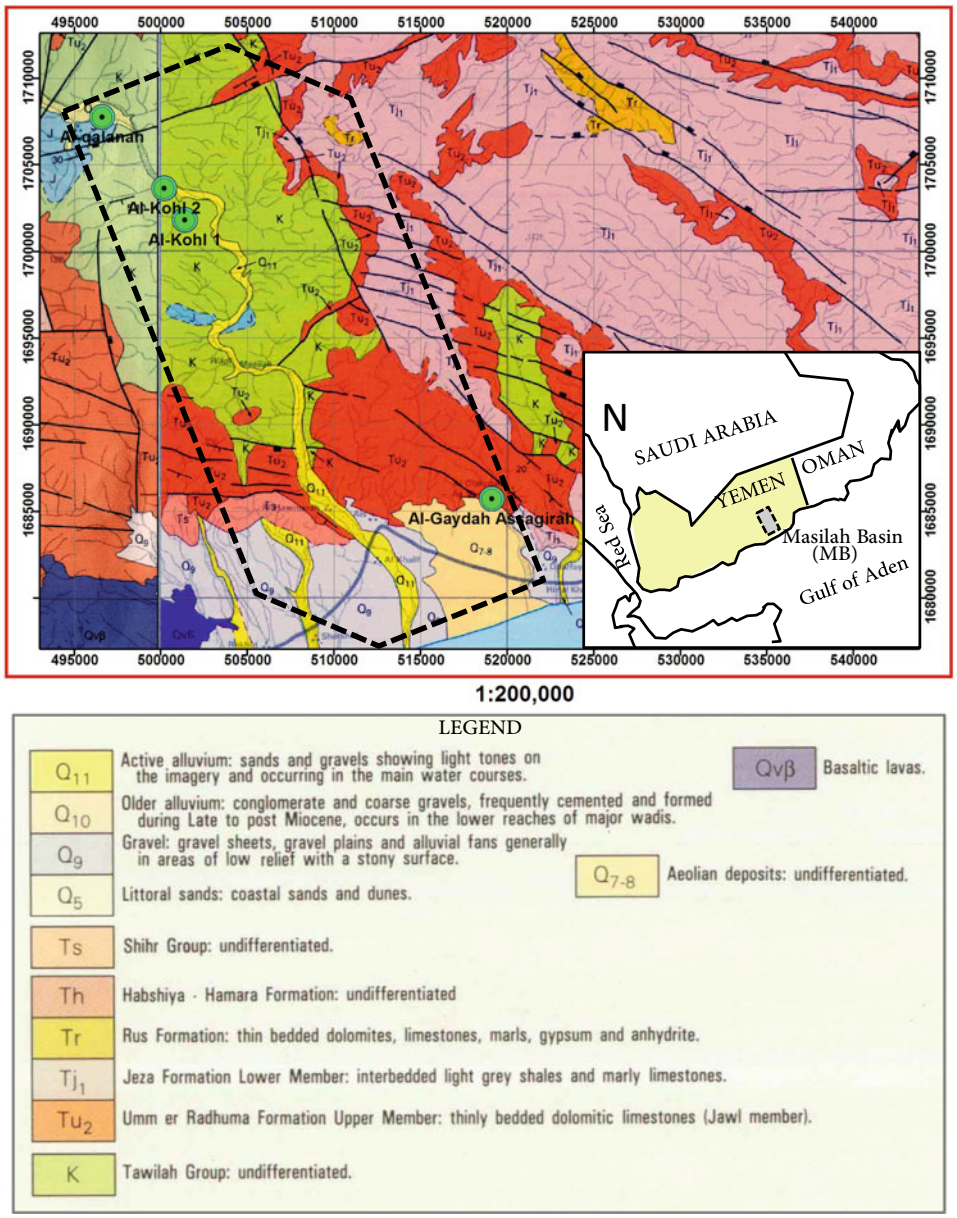

Fig. 1 Geological map illustrating the most important lithological units and the major structural patterns of the Masilah Basin (dashed box) at southeastern Yemen, with location of main occurrences of polymetallic mineral deposits (green circles). Inset sketch shows location of Yemen and the Masilah Basin

Spectrometry). Details on the analytical methods and detection limits can be found in the website of AlsChemex.

3 Results

3.1 Field Observations

The MB Fe-Mn ore deposit crops out et al.-Gaydah Assagirah prospect (Fig. 1) hosting in the Tertiary shallow marine carbonate that is associated with the base of Umm Er Radhuma limestone formation (Tu_2 in Fig. 1).

The Fe-Mn deposit consists of several discordant irregular veins striking NW-SE, near horizontal or in some cases steep dipping. Small massive veins of several meters, ranging in width from 1 to 1 m, are widespread. The investigated ores sometimes occur as stockwork breccia-filling and cavity and pores filling, characterized by botryoidal structure. Also, it is found as disseminations and patches in the calcareous rocks, associating with the hydrothermal alteration along the rift-related active fault system of MB. Fe-Mn nodules and spheroids were also observed. The mineralization style depends on the occurrence of sedimentary structures, such as cavities and vugs, as well as tectonic breccias.

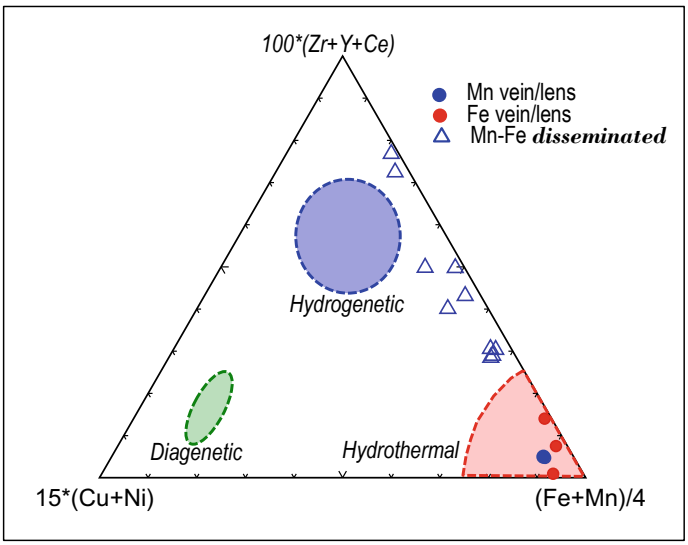

Fig. 2 Plot of MB Fe-Mn ore composition on ternary discriminative graph for genetic classification of Fe-Mn deposits after (Josso et al. 2017)

3.2 Mineralogy

The Fe-Mn ores at the Al-Gaydah Assagirah prospect consist mainly of hollandite, romanechite, cryptomelane, pyrolusite, hematite, limonite, and goethite.

Hollandite, romanechite, and cryptomelane form thin acicular (needle-like) crystals of spherulitic structure. Residual hollandite and pyrolusite fragments (up to 20 cm in diameter) are scattered and particularly associated with the debris carbonate sediments. In some cases, cryptomelane and pyrolusite occur as stockwork mineralization cementing brecciated carbonate rocks.

The Fe-rich ores occur at the vicinity of the Mn-rich ore occurrences. Hematite may occur as either massive veins attaining in some cases 2 m in width and more than 100 m in length, or in an intensively silicified breccia material, along with goethite. Limonite is found as pseudomorphous after hematite.

3.3 Major and Trace Element Geochemistry

Results of geochemical analyses classify the studied ores according to their grade. The high-grade manganese ore contains Mn of 47–51% in the cryptomelane and pyrolusite-rich veins, up to more than 50% in the hollandite-romanechite-rich veins. This ore type has Pb, Ba, Sr contents up to 1%, and Co, V, Mo, Zn, W, Ag concentrations up to 0.12%, 0.24%, 0.05%, 0.48%, 50 ppm, and 20 ppm, respectively. Low-grade ore veins have a Mn of 7–10%. The predominantly massive hematite-rich veins have grades of around 50% Fe. They have contents in Ba up to 0.46%, Cr up to 0.19%, Pb up to 0.11%, and Zn up 0.51%. In some cases, V contents up to 0.3% were found. Lower grade veins range in Fe contents from 32 to 7%. The disseminations in the calcareous rocks have Mn and Fe concentrations of 6.7–2.0% and 10–3.5%, respectively, and are depleted in Sr, Ba, V, REE, Cu, and Mo compared to the veins.

4 Discussion

Compared to the host calcareous rocks, the Fe-rich ores have analogous contents of Ba, Sr, REE, and Ni, whereas the Mn-rich ores are enriched in these trace elements. Fe-Mn ore deposits are generally classified in three main categories, related to different environments of formation: hydrogenetic, diagenetic, and hydrothermal (Nicholson 1992). The source of the mineralizing fluids affects the geochemical features of the deposits, like for instance the Fe/Mn ratio. Indeed, the intense differentiation of Fe and Mn within the transporting fluids in hydrothermal deposits produces very variable Mn/Fe ratios as a function of redox conditions and fluid temperature [4 and references therein]. Accordingly, the wide range of Mn/Fe ratios of MB deposits (0.001–50) agree with a hydrothermal origin. In addition, the contents, of trace elements such as Zr, Y, REE, Cu, Ni, and Ba, are indicators used to identify different genetic types of mineralization (Anaya-Gregorio et al. 2018). The rapid precipitation of the oxides in the hydrothermal processes commonly forms deposits with low-minor metal contents. Deposits influenced by hydrogenetic precipitation, instead, show higher contents of minor metals.

In the triangular discrimination diagram of Fig. 2, proposed by Josso et al. (2017), the MB Fe-Mn ore veins and lenses plot in the field of hydrothermal nature of the mineralizing fluid, whereas the disseminated ores are distributed along a trend between hydrothermal and hydrogenetic nature

of the mineralizing fluid. This evidence suggests that MB Fe-Mn veins and lenses are generated by the circulation of hydrothermal fluids. Besides, the fluids producing the disseminations in the calcareous rocks are the result of mixing between two main components of different origin: (1) hydrothermal and (2) hydrogenetic.

5 Conclusions

Based on the Fe/Mn ratio and trace element composition of the MB Fe-Mn deposit, the nature of its mineralizing fluids was deciphered. Ore veins and lenses were most probably generated due to circulation of hydrothermal fluids. Fe and Mn were plausibly sourced by the Quaternary alkaline basalts, as evidenced by similar enrichments of REE (up to 60 ppm La) and Ni (up to 200 ppm) in both volcanic rocks (Mattash and Pinarelli 2013) and ore samples. The Fe-Mn disseminations in the calcareous rocks, instead, describe a mixed source of the mineralizing fluid between a hydrothermal and a hydrogenetic (seawater) one.

References

Anaya-Gregorio, A., et al.: Textural and geochemical characteristics of late Pleistocene to Holocene fine-grained deep-sea sediment cores (GM6 and GM7), recovered from southwestern Gulf of Mexico. J. Palaeogeogr. **7**, 253–271 (2018)

Josso, P., et al.: A new discrimination scheme for oceanic ferromanganese deposits using high field strength and rare earth elements. Ore Geol. Rev. **87**, 3–15 (2017)

Mattash, M.A., Pinarelli, L., et al.: Continental flood basalts and rifting: geochemistry of Cenozoic Yemen Volcanic Province. Int. J. Geosci. **4**, 1459–1466 (2013)

Mattash M.A., Shaqra A.A., Al-Ameri A.A.: Geological survey and feasibility study of pyrolusite deposit in Yemen. Sixth International Symposium on Eastern Mediterranean Geology incorporating the Ninth International Conference of Jordanian Geologists Association. Extended Abstract, pp. 251–252. (2007)

Nicholson, K.: Constraining mineralogical-geochemical signatures of manganese oxides: guides to metallogenesis. Econ. Geol. **87**(5), 1253–1264 (1992)

Pinarelli, L., Mattash, M. A.: Mineral resources in the Red Sea/Gulf of Aden: polymetallic-barite mineralizations at Wadi Masilah Basin (Yemen). In: Robbins, D. (ed.) Red Sea: Historical Significance, Properties and Economic Importance. Series: Earth Sciences at the 21th Century, pp. 47–76. Nova Science Publishers, NY (2018)

Application of Multi-Element Soil Geochemistry and Particulate Gold Exploration in the Kambele Plain, Batouri Gold District, Southeast Cameroon

Mary Ewokolo Molua Etutu, George Teke Mafany, and Cheo Emmanuel Suh

Abstract

Soil geochemistry remains an essential tool in mineral exploration, especially in areas where the scarcity of outcrops and a thick lateritic overburden undermine the understanding of subsurface ore deposits. Thirty-five soil samples collected from six profiles within a 40 km^2 block around the Batouri gold district, southeast Cameroon were analyzed for major elements (Fe, K) and trace elements (Au, As, Ba, Hg, Sb, W, Cd, Cu, Mo, Mn, Ni, Pb, Zn, Ga, Ge, Se, Ta, Cs, Ti, Bi) using both inductively coupled plasma mass spectrometry (ICP-MS) and instrumental neutron activation analysis (INAA). Furthermore, a heavy mineral concentrate from the sampling point with the highest Au concentration (64 mg Kg^{-1} Au) was examined for the presence of particulate gold. The element concentrations obtained were plotted on element distribution maps and contoured to show the distribution patterns of the various elements in the soil. The results show that anomalous gold concentrations are found in the northeastern part of the study area. The data were analyzed using multivariate statistics and results from the principal component analysis (PCA) shows six components with components 2 (Au-As-Sb-W) and 3 (Cu-Ni-Zn-S) pointing to hydrothermal sulphide-related mineralization in the underlying rocks. As, Sb, W and S are identified in this study as potential pathfinder elements for gold mineralization in the Batouri gold district. Gold grains were recovered from the concentrate and this point to gold dispersal in the solid-state within the weathering cycle.

Keywords

Soil • Geochemistry • Principal component analysis (PCA) • Pathfinder elements • Particulate gold • Cameroon

1 Introduction

The search for ore deposits in recent times makes use of soil geochemistry, especially in areas of scarce outcrops and thick overburden which undermines the understanding of subsurface ore deposits (Nforba et al. 2011; Vishiti et al. 2015). Secondary dispersion is vital in exploring geochemistry as it results in the various elements present in an ore body being dispersed over a much wider target area, enabling the presence of mineralization to be detected as anomalous metal content in soils.

Soils derived from the weathering of underlying rocks with primary Au mineralization in savannah and rainforest areas are commonly enriched in gold, often with gold fragments that can even be extracted at a profit. Understanding the element composition, distribution and associations within a lateritic geochemical anomaly provides a better understanding of source rock geology and helps pinpoint favourable locations for drilling, especially where surface indications are lacking. Minimal studies have seen the use of soils as a tool in exploration and baseline studies, especially in the Central African Sub-region and Cameroon in particular (Nforba et al. 2011; Vishiti et al. 2015; Butt et al. 2000; Craig 2001). In this study, soil samples were collected from deep pits of between 2 and 4 m. The pits were placed over a wide Au-in-soil anomaly derived from a previous survey of

M. E. M. Etutu (✉) · C. E. Suh
Economic Geology Unit, Department of Geology, University of Buea, South West Region, P.O. Box 63 Buea, Cameroon

M. E. M. Etutu · C. E. Suh
Remote Sensing Unit, Department of Geology, University of Buea, South West Region, P.O Box 63 Buea, Cameroon

G. T. Mafany
South West Regional Centre for Scientific Research and Innovation, Southwest Region, Buea, Cameroon

C. E. Suh
Department of Geology, Mining and Environmental Science, The University of Bamenda, North West Region, P.O. box 39 Bambili, Cameroon

A. Çiner et al. (eds.), *Recent Research on Geomorphology, Sedimentology, Marine Geosciences and Geochemistry*, Advances in Science, Technology & Innovation, https://doi.org/10.1007/978-3-030-72547-1_80

shallow (<65 cm deep) 100 m spacing grid controlled soil programme carried out by African Aura Resources (AAR) Ltd (2009). Unlike the AAR survey, the samples were analyzed for a range of elements and the heavy mineral concentrate tested for the presence of particulate gold in the weathering profile.

The objective of this present study is to decipher through the use of soil geochemical anomalies, areas of high-gold potential as targets for further and more detailed exploration.

2 Geological Setting and Methodology

The Batouri gold district is situated in the equatorial rainforest belt of Cameroon and forms part of the Adamawa-Yade lithostructural unit (Vishiti et al. 2015) that constitutes the Pan African Fold Belt north of the Congo Craton (Fig. 1a). This fold belt is characterized mainly by metasedimentary and metaplutonic (metagabbros, metagranites, metadiorites, metasyenites) rocks (Fig. 1b). The location of the study area is shown in Fig. 1c.

A total of 35 bulk sediment samples were collected from six soil profiles across a 40km2block. Ten litres (~20 kg) of each sample were collected in a calibrated plastic bucket and subsequently quartered down to a 200 g fraction that was sent for analysis. The soil samples were analyzed at Activation Laboratories Canada (Actlabs) using combined Inductively Coupled Plasma/Mass Spectrometry (ICP-MS) and Instrumental Neutron Activation Analysis (INAA) techniques. In order to evaluate if particulate gold exists in the soil profiles, a heavy mineral concentrate was prepared for the soil sample that returned the highest gold concentration. This concentrate was examined under a binocular microscope and recovered gold grains by handpicking were further studied under a scanning electron microscope to elucidate their morphology and evolution within the weathering cover.

3 Results

3.1 Concentration of Elements in the Soil Samples

A total of 35 samples were analyzed for a suite of elements and 23 elements with concentrations (mg Kg^{-1}) above the detection limit are presented on element distribution maps (Fig. 2). The distribution shows two anomalous areas for Au with relatively high concentrations (>80 mg Kg^{-1}) around the northeastern part of the study area, which decreases to <5 mg Kg^{-1} towards the south. Other elements such as As, Sb, W, also have high concentrations around the northeastern part of the study area similar to S and Pb. Cu and Ni have a more-or-less uniform distribution.

3.2 Element Association

The raw data were log-transformed, and a Pearson's correlation matrix was computed for the elements in order to investigate their inter-element relationship. It is noticed that Au has a relatively high-correlation coefficient ® of 0.64, 0.52 and 0.55 with As, Sb and S, respectively. Other element pairs with relatively high-positive r values include As-Sb ($r = 0.77$), As-W ($r = 1.00$), Sb-W ($r = 0.89$), W-Cd ($r = 0.89$), W–Ni ($r = 0.71$). A few other elements such as W-Ge ($r = -0.76$) and Se-Cs ($r = -0.61$) are negatively correlated. The data were further subjected to principal component analysis (PCA) in order to investigate their elemental associations. Six components were generated. Each of these components represent a cluster of interrelated elements within the data set as follows: Component 1: As-Sb-Mn-Ga-Ge-Se-Ta-Fe, Component 2: Au-As-Sb-W, Component 3: Cu-Ni-Zn-S Component 4: Ge-Bi, Component 5: Mo, Component 6: Ni-Pb.

3.3 Particulate Gold

Samples of gold grains recovered from Sample number 28 with Au concentration of 90.5 mg Kg^{-1} are provided in Fig. 3. The gold grains vary from dendritic irregular to sub-rounded. Delicate structures on the surface of some of the grains such as dendrites are still well preserved, whilst the sub-rounded ones have blunt edges. The grains also have pitted surfaces. The aspect ratios of these gold grains are also plotted in Fig. 3 compared to grains from other parts of the world. The long measured axes and perpendicular short axes of the gold grains under study ranged between 480 and 750 µm and 240 and 700 µm, respectively. More than half of the gold grain population (80%) had long to short axes ratios between 1:0.5 and 1:0.98.

4 Discussion

The concentration of gold in the analyzed samples varies considerably ranging from 2.7 to 90.5 mg Kg^{-1}. According to Suh et al. (2006), considerable variations in gold concentration suggest the existence of high-grade ore shoots within a mainly low-grade gold system. Visible gold grains observed from panned samples imply that the gold occurs freely and is likely released by the oxidation of sulphides. This process usually leads to the release of gold that is held

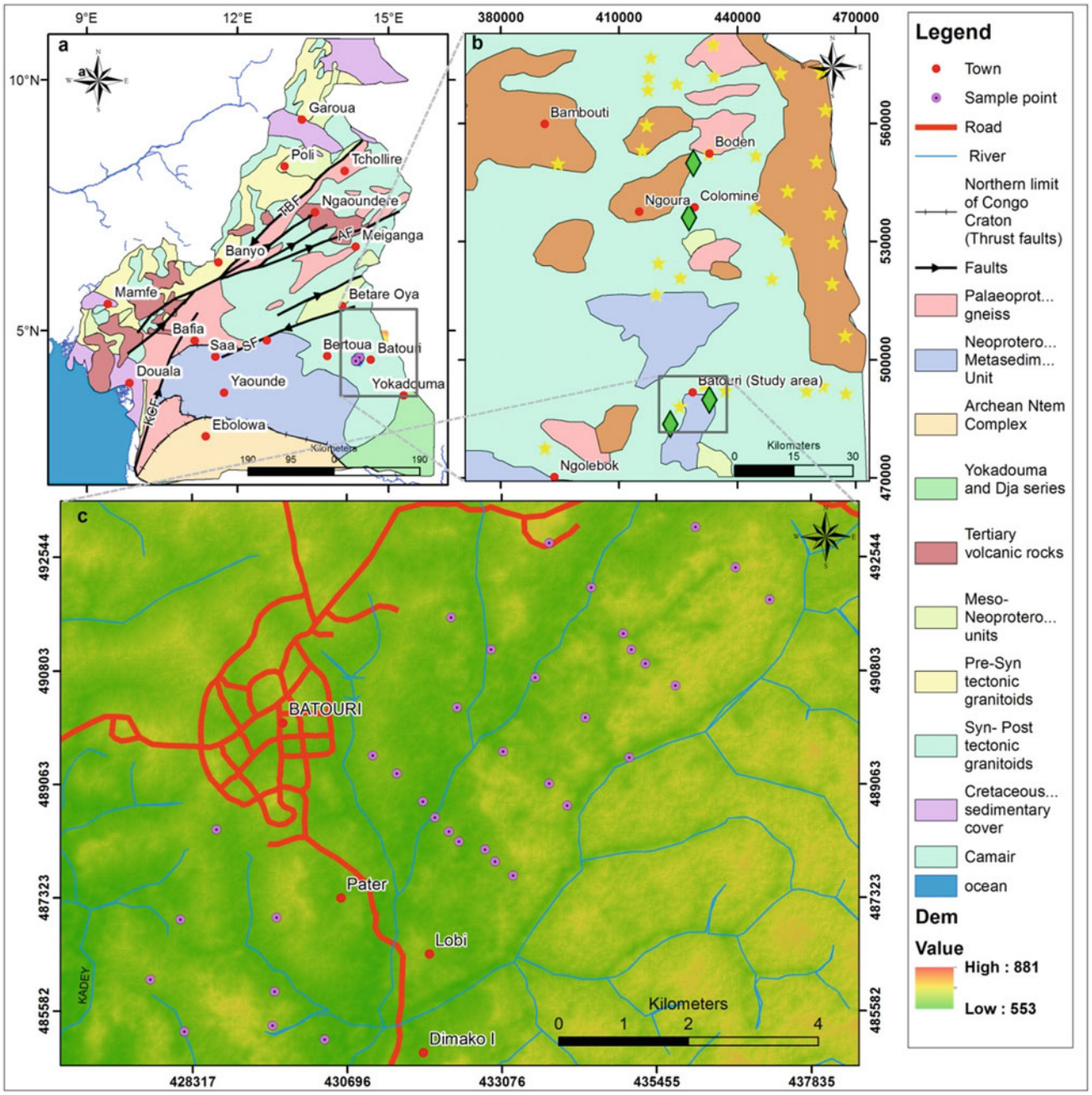

Fig. 1 Location of study area. **a** Geological map of Cameroon (modified after Vishiti et al. 2015) **b** Regional geological map of south eastern Cameroon showing artisanal gold mining sites (modified after Vishiti et al. 2015). **c** Topographic map of the study area showing sample collection points

in the sulphides as free gold and is attributed to deep weathering (Radtke 1985). The element distribution map for Au (Fig. 2) shows two anomalous areas with a promising prospect for gold occurrence in the northeastern part of the investigated block. The distribution pattern of gold in soils of the Batouri gold district shows a more extensive dispersion halo of about 2 km wide, with such distribution halo attributed to the extensive supergene lateral distribution of gold. The distribution pattern of Au in the investigated block also follows a NE-SW trend, and according to Suh et al. (2006), gold deposits in Cameroon are confined to a NE-SW trending shear zone. Principal components extraction method was applied, and the analysis indicated six components in the data accounting for 76.93% of the total variability. The geology of the area under study, particularly the rock formations can be associated with component 1

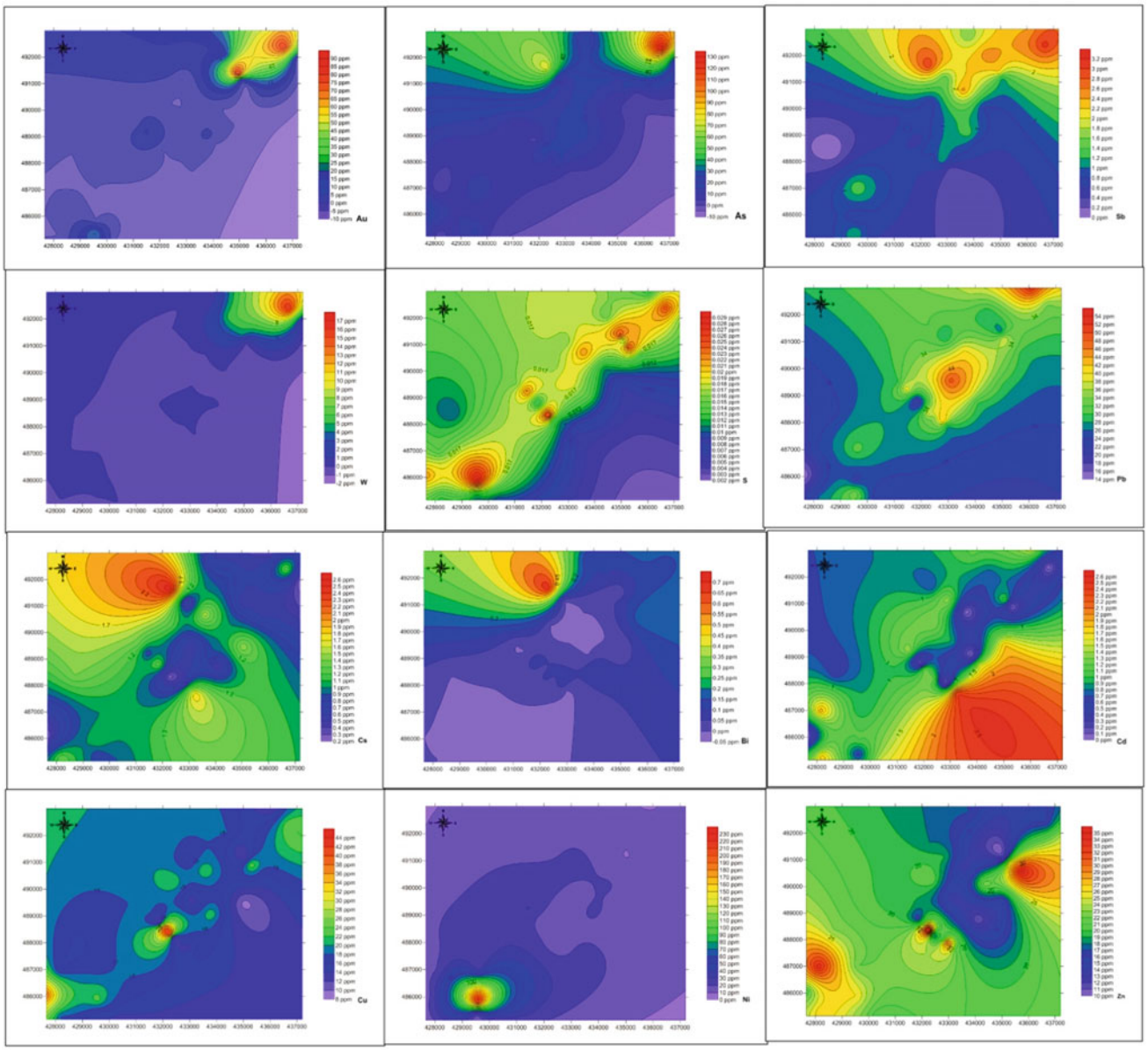

Fig. 2 Element distribution maps for Au, As, Sb, W, S, Pb, Cs, Bi, Cd, Cu, Ni and Zn concentrations determined by combined ICP-MS and INAA

(As-Sb-Mn-Ga-Ge-Se-Ta-Fe). The study area is known to be underlain by metagranites which are particularly rich in K-feldspars minerals. These granitic plutons have high-magnetic susceptibility values (Suh et al. 2006; Asaah et al. 2014) and belong to the magnetite series. This accounts for elevated Fe values and associated elements in the soil samples. The association of Au, As, Sb and W can be attributed to hydrothermal alteration of the wall rock resulting in the formation of arsenopyrite, stibnite and scheelite giving rise to this metal association. This sulphidation event may prove a greater possibility of finding primary gold mineralization in the region. It indicates that the primary gold mineralization is a product of wall rock sulphidation. The metal association of component 3 which is comprised of Cu, Ni, Zn and S is also a product of a possibly late and barren sulphidation event related to the formation of chalcopyrite. This late hydrothermal process might not be responsible for Au mineralization in the area. Weathering of rocks and oxidation of their sulphide minerals may have permitted As, Sb, S and W to be introduced within the soil profile in solution; thus these elements can assume the role of pathfinder elements for potentially economic deposits during a geochemical exploration using soil samples. The gold distribution pattern in this study shows a lateral SW extension. Where gold remobilization occurs from a quartz vein or stockwork system, secondary gold distribution is

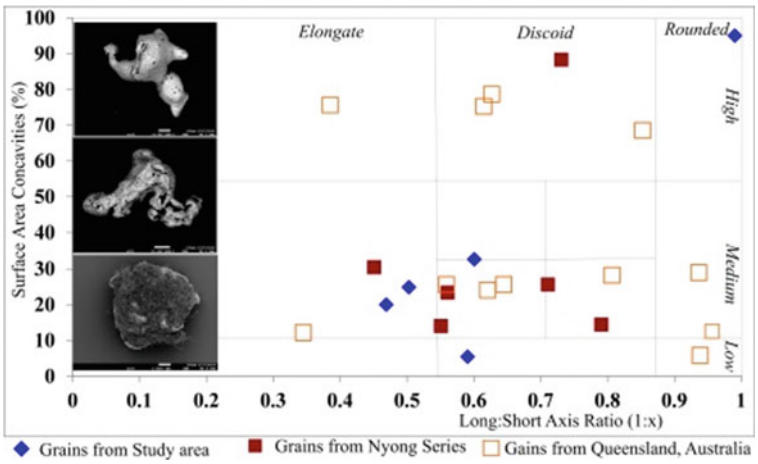

Fig. 3 A plot of long to short axis ratio of each grain and the percentages of surface area occurring as concavities. SEM images of some recovered gold grains in insert

primarily lateral at or near the palaeowater table with a characteristic T–shape. The gold grains recovered from sample number 28 possess delicate secondary gold structures such as dendrites which are common in authigenic gold. The presence of particulate gold with dendrites in the soil indicates proximity to the primary source. A predominance of dendritic shaped grains to circular grains indicates a short distance of transport as grains will be more circular with an increase in distance of transport (Townley et al. 2003). The elongated, discoid and rounded morphologies of the grains exhibit pitted surfaces which are corrosion features showing evidence of gold dissolution probably as a result of exposure to weathering solutions (Larizzatti et al. 2008). Au is usually dissolved from the higher horizons and reprecipitated from stable complexes to form mottled zone and saprolite haloes at depth especially in soil profiles where Au remobilization and chemical precipitation of authigenic gold is evident (Vishiti et al. 2015; Suh and Lehmann 2003).

5 Conclusions

This study shows that soil geochemical survey serves as a very effective method for gold exploration in this area as it is made up mainly of weathered overburden. Gold distribution in the area presents the potential of economic primary gold mineralization. Gold anomalies show an NW-SW trending direction. The application of factor analysis to multi-element soil geochemical data from the Batouri gold district showed that gold is associated with arsenic, antimony and sulphur and thus can be considered as pathfinder elements. The morphologies and surface features on the particulate gold grains indicate proximity to the primary source.

References

African Aura Mining Batouri gold project, Cameroon. African Aura Resources (UK) Ltd., London. http://www.african-aura.com/s/Batouri.asp. Accessed on 7 March 2009

Asaah, A.V., Zoheir, B., Lehmann, B., Frei, D., Burgess, R., Suh, C.E.: Geochemistry and geochronology of the ~620Ma gold associated Batouri granitoids, Cameroon. Int. Geol. Rev. 1–25 (2014)

Butt, C.R.M., Lintern, M.J., Anand, R.R.: Evolution of regoliths and landscapes in deeply weathered terrain—implication for geochemical exploration. Ore Geol. Rev. **16**(3–4), 167–183 (2000). https://doi.org/10.1016/S0169-1368(99)00029-3

Craig, M.A.: Regolith mapping for geochemical exploration in the Yilgran Craton, Western Australia. Geochem. Explor. Enviro. Anal. **1**, 383–390 (2001). https://doi.org/10.1144/geochem.1.4.383

Larizzatti, J.H., Oliveira, S.M.B., Butt, C.R.M.: Morphology and composition of gold in a lateritic profile, Fazenda Pison "Garimpo", Amazon, Brazil. J. s. Am. Earth Sci. **25**, 359–376 (2008)

Nforba, M.T., Kabeyene, V.K., Suh, C.E.: Regolith geochemistry and mineralogy of the Mbalam Itabirite-Hosted Iron Ore District, SE Cameroon. Open J. Geol. **1**, 17–36 (2011)

Radtke, A.S.: Geology of the Carlin gold deposit, Nevada. U.S. Geological Survey Professional Paper 1267, 124 p. (1985)

Suh, C.E., Lehmann, B.: Morphology and electron-probe microanalysis of residual gold grains at Dimako, Southeast Cameroon. Neues Jb. Mineral. Monat. **6**, 255–275 (2003)

Suh, C.E., Lehmann, B., Mafany, G.: Geology and geochemical aspects of lode gold mineralization at Dimako-Mboscorro, SE Cameroon. Geochem. Explor. Environ. Anal. **6**(4), 295–309 (2006)

Townley, B.K., Herail, G., Maksaev, V., Palacios, C., de Parseval, P., Sepuldeva, F., Orellana, R., Rivas, P., Ulloa, C.: Gold grain morphology and composition as an exploration tool: application to gold exploration in covered areas. Geoche. Explor. Environ. Anal. **3**, 29–38 (2003)

Vishiti, A., Suh, C.E., Lehmann, B., Egbe, J.A., Shemang, E.M.: Gold grade variation and particle microchemistry in exploration pits of the Batouri gold district, SE Cameroon. J. Afr. Earth Sc. **111**, 1–13 (2015)

Tailings are a Reliable Source of Mineral Reserves (Kazakhstan)

A. A. B. Baibatsha, G. M. Omarova, and Z. T. Baibatchayeva

Abstract

Kazakhstan, until recently, in the production of copper was among the top ten countries in the world. However, as the reserves of traditional ores are exhausted, the volume of copper produced has noticeably decreased. Currently, one of the reliable sources for the development of the resource base of processing enterprises is the tailings of the processing plants, which can be considered as technogenic deposits. According to a forecast, more than 1.5 billion tons of reserves of technogenic mineral raw materials are concentrated in the tails of only the Jeskazgan and Balkhash enrichment factories, when the content of the main component of ores, for example, copper is of the order of 0.1–0.3%, the total reserves of metals may be more than three million tons. The primary metals associated in tailings composition are (1) copper, lead and zinc; (2) gold and silver; (3) rare and scattered elements Zr, Se, Y and Yb. The content of Ni, Co, Mo, Bi, Sb, Be in tailings is of interest. According to the completed research works, results were obtained that ensure technological research related to the practical development of tailings as technogenic ore raw materials. The cost of processing tailings is usually 2–3 times less than the processing of natural raw materials. In the context of a growing shortage of raw materials, the stocked tailings of the processing plants can be an essential source of mineral resources replenishment.

Keywords

Tailings • Sulfides • Non-ferrous metals • Grinding • Copper concentrate • Technogenic materials

1 Introduction

According to official data, more than 20 billion tons of solid waste from the mining and smelting complex have been accumulated in Kazakhstan. A significant proportion of this waste is attributed to ore tailings, including copper-containing ores. Non-ferrous metallurgy is a leading industry, the development of which is based on various mineral resources and influences the formation of the socio-economic status of the Republic. In this regard, a comprehensive study of the conditions of formation and the material composition of the copper ore deposits tailings, which are considered as technogenic ore raw materials, has been carried out. Mineralogical studies of technogenic materials were carried out to assess the composition and properties for resource counting, which serve as the basis for technological research and the selection of a rational processing scheme for extraction of metals from the tailings. The initial sulfide ores for processing at the Balkhash enrichment factory (BEF) come mainly from the Konyrat copper-molybdenum mine. 83 samples of Jeskazgan and 35 samples of Balkhash tailings taken and studied.

2 Methods

Interest in the study of the tailings of the Balkhash enrichment factory (BEF) is because in it during 1937–2017 more than 630.0 million tons of tailings containing Cu, Zn, Pb, Mo and other metals and their compounds were accumulated. In agreement with the competent authorities, points were chosen for the location of the mapping wells, the drilling of which ensured the completeness of testing the tailings storage over its entire area and to the full depth. In general, the testing took place in the full volume of the tailings; the core output provided a full-fledged and complete sampling for representative laboratory studies. Evaluation of the material composition of the BEF tailings material aims to

A. A. B. Baibatsha (✉) · G. M. Omarova · Z. T. Baibatchayeva
Kazakh National Research Technical University named after K.I. Satpayev, Almaty, Republic of Kazakhstan

A. Çiner et al. (eds.), *Recent Research on Geomorphology, Sedimentology, Marine Geosciences and Geochemistry*, Advances in Science, Technology & Innovation, https://doi.org/10.1007/978-3-030-72547-1_81

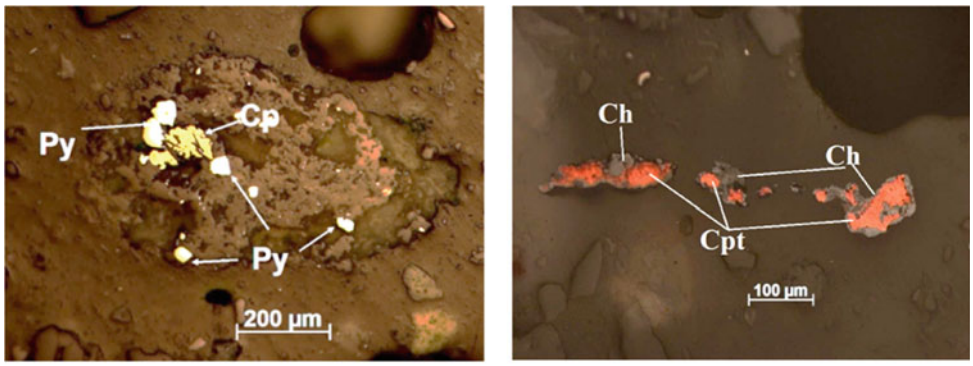

Fig. 1 **a** Chalcopyrite (Cp) and pyrite (Py) inside the rock grains, **b** Cuprite (Cpt) with a border of chalcocite (Ch)

establish their mineral and chemical composition. Based on these results, laboratory studies will be performed on the choice of the technological scheme of enrichment and processing of technogenic ore raw materials for the extraction of metals from them. A sample for spectral and chemical analyzes was taken from each sample, and from three samples, a sample was taken from each fraction. Such testing was carried out approximately in the upper, middle, and lower parts of the tailings storage.

3 Results and Discussion

According to the results of the study of the chemical composition of the Balkhash enrichment factory tailings, it was found that the average copper content (the main component of the ores) is 0.1–0.3%, increasing in some samples to 0.4–0.6%. There is a high content of zinc and lead, gold, silver, and rare metals.

After the corresponding sample preparation, sieve analysis of the samples was performed to assess the granulometric composition and determine the distribution of fractions by the depth and by weight of output of each class. The most common fractions are 250 (they are 33.06%) and 125 µm (41.16%), the sum of which in the total mass of tails is 74.22%. If the fraction larger than 0.5 mm is 8.18%, the smallest fraction smaller than 0.063 mm is only 3.56%.

According to the results of laboratory studies of tailings, the directions of studying the technology of enrichment and extraction of metals from them, which are based on advanced international and domestic scientific and practical experience, have been chosen (Golik et al. 2011; Schippers 2007; Rodriguez et al. 2003; Sand et al. 2001; Schippers and Sand 1999).

The mineral composition of tailings studied on cemented thin sections. According to the results, the micro-mineralogical description of the manufactured polished sections and the mineral composition of the tailings were established. Ore minerals are mainly chalcopyrite, covellin, bornite, sphalerite, rarely chalcocite, and very rarely cuprite. The studied tails in terms of their composition are similar to those of the Jeskazgan enrichment factory (Golik et al. 2011; Baibatsha et al. 2017; Baibatsha 2016, 2018). Chalcopyrite forms 18 grains (0.02–0.07 mm) along the outer edge of the grains of the host rocks; in a free form —one veinlet form (0.05 × 0.3 mm) and another— 0.02 × 0.05 mm; one selection of chalcopyrite (0.2 mm 0.25 mm) with small inclusions of pyrite grains; in the rock fragment together with the impregnation of magnetite 7 (0.01–0.06 mm) and in the other fragment 5 (0.01–0.04 mm) and another in the rock fragment in close germination with mica (0.01–0, 02 × 0.07 mm); (4) in intergrowths with quartz, 1 grain (0.05 × 0.15 mm) and 1 grain 0.2 mm in size; (5) in quartz grains—1 selection of chalcopyrite of veinlet form in accretion with magnetite, pyrite, and sphalerite (0.05 × 0.25 mm) and in the same grain of quartz small inclusions of chalcopyrite (15–20 inclusions of 0.01–0.05 mm in size), 5 more chalcopyrite grains (0.01–0.02 × 0.07 mm). Pyrite forms rather dense dissemination in free form Bornite is found along the edge of a grain of quartz with a size of 0.01 mm and in intergrowth with quartz —2 (0.01–0.02 mm). Covellin is in free form up to 5 grains with dimensions of 0.01–0.03 mm, in quartz up to 20 precipitates with a size of 0.01–0.02 mm and along the edge of a fragment of quartz with a size of up to 0.03 mm. There is also cuprite with chalcocite border (Fig. 1).

Ore minerals in the form of micrometric grains and inclusions, sometimes aggregates are often present in free form along the edges of the grains of siliceous host rocks, often in accretion or inside fragments of rocks. When positioned in the form of available grains along the edge of the debris can be easily retrieved. At the location of ore minerals inside the debris, they form a stop unit, for the opening of which requires the use of unique technological methods. In this case, the use of special reagents for the opening and further dissolution or flotation of ore aggregates is required. Based on the obtained research results, the best international and domestic scientific and practical experience, a

technological scheme for the enrichment and extraction of metals from the studied technogenic ore raw materials will be selected (Schippers 2007; Rodriguez et al. 2003; Sand et al. 2001).

4 Conclusions

The geological conditions of the formation and occurrence of technogenic ores of non-ferrous metals in the of the Balkhash enrichment factory tailings were studied. The material composition of technogenic mineral raw materials in tailings is estimated. Based on the results obtained, laboratory studies are currently being carried out on the choice of a technological scheme for the enrichment and processing of technogenic ore raw materials for the extraction of metals from them.

The results of laboratory mineralogical studies of hard sections made by cementation of loose material and particle-size analysis of the fractional composition of tails serve as reliable baseline data for technological research. They are taking into account advanced global and domestic scientific and practical choice of technological schemes for the enrichment and extraction of metals from these types of technogenic ore raw materials. The tailings of the processing plants can serve as technogenic ore raw materials to strengthen the resource base of existing processing plants and an additional source of metals.

Based on the results of this study, we conclude that of the enrichment of non-ferrous metal ores tailings as technogenic ore raw materials are the exact source of replenishment of the Kazakhstan mineral resource base.

Acknowledgements This work was supported by the scientific program «Comprehensive geological study of subsurface resources for the development of resource base and mining exploitation of new sources of ore raw materials in Kazakhstan».

References

Baibatsha, A.B., Dyussembayeva, K.Sh., Bekbotayeva, A.A.: Study of tails enrichment factory Zhezkazgan as a technogenic ore deposits, 16th international multidisciplinary scientific geoconference SGEM2016, 2016, pp. 579–586. Albena, Bulgaria, (2016)

Baibatsha, A.: Mineralogia hvostov Jeskasgan obogatitelnoi fabriki, p. 160. Almaty, (2018)

Baibatsha, A., Dyssembayeva, K., Bekbotayeva, A., Abdullayeva, T.: Tails of enrichment factories of DJezkazgan copper sandstone deposit are a source to replenish the mineral resource of non-ferrous metals, 21st International conference on non-ferrous minerals & metals-2017, p. 9/1. New Delhi, India, (2017).

Golik, V.I., Ismailov, T.T., Micik, M.F.: Universal'naja model' vyshhelachivanija metallov iz nekondicionnogo syr'ja s mehanohimicheskoj aktivaciej processov izvlechenija, Gornyj informacionno-analiticheskij bjulleten' (nauchno-tehnicheskij zhurnal). Moskwa **4**, 233–241 (2011)

Rodriguez, Y., Ballester, A., Blazquez, M.L., et al.: New information on the pyrite bioleaching mechanism at low and high temperature. Hydrometallurgy **71**, 37–46 (2003)

Sand, W., Gehrke, T., Jozsa, P.-G., Schippers, A.: (Bio)chemistry of bacterial leaching—direct versus indirect bioleaching. Hydrometallurgy **59**, 159–175 (2001)

Schippers, A.: Microorganisms Involved in Bioleaching and Nucleic Acid-based Molecular Methods for their Identification and Quantification, Microbial Processing of Metal Sulfides, pp. 3–33. Springer, Netherlands (2007)

Schippers, A., Sand, W.: Bacterial leaching of metal sulfides proceeds by two indirect mechanisms via thiosulfate or via polysulfides and sulfur. Appl. Environ. Microbiol. **65**(1), 319–321 (1999)

Evaluation of the Heat of Combustion of Ten Nigerian Coal Deposits and Their Potential as Alternative Energy Sources

Onoduku Usman, Thomas Ako, and Laminga Mohammed

Abstract

There are vast deposits of coals in Nigeria, and their particular physicochemical properties are not well studied and documented. The lack of literature has hindered the proper evaluation of this natural earth resource for their best uses, including their heating capacities and utilization as sources of energy. However, with the current dwindling power supply from hydropower and thermal power plants, coal is positioned to regain its recognition and place as an alternative source of energy in Nigeria. This study is intended to address part of the inadequacies posed by the utilization of the Country's coal resources. Forty coal samples (4 samples per deposit) from ten coal deposits that span over Anambra Basin and Benue Trough were sampled and analyzed for their heat of combustion, and the data generated were used in addition to those of the proximate and ultimate characteristics of the coal deposits earlier studied by the authors to evaluate their potentials as alternative sources of energy in Nigeria. These coal deposits include Onyema, Okpara, Ogboyoga, Okabe, Owukpa, Ibobo, Udane Biomi and Iva Valley in the Anambra Basin and Lafia Obi and Maiganga in the Benue Trough. Bomb calorimeter was used to determine the heat of combustion of the coals. The heat of combustion of the coals ranges from 5990 kJ/kg for the Iva Valley as the highest to 2220 kJ/kg for Ogboyoga coal as the lowest. Based on the analyzed heat of combustion, the proximate and ultimate characteristics of the studied coals, the coals are considered adequate for the generation of heat required for their uses as sources of alternative energies in Nigeria.

Keywords

Coal • Heat value • Benue trough • Anambra basin • Energy

1 Introduction

The Nigerian coal reserves are in the excesses of three billion (3,000,000,000) tons of indicated reserves spread over seventeen coal fields and over six hundred million (600,000,000) tons of proven reserves (Obaje 2009; Raw Material Research and Development Council 2015). These coal deposits and resources are spread over 13 states of the Federation but geologically restricted to the Benue Trough (Northern, Central-, and Southern-Benue Troughs) and the adjacent Anambra Basin. Some of the notable coal deposits in Nigeria include the Okaba, Owukpa, Inyi, Ogboyoga, Udane Biomi, Ibobo, Onyeama, Okpara, Iva Valley, Obi-Lafia along River Dep, Maiganga and Gidan Sidi coal deposits. Despite the vast coal resources in the Country, their particular physicochemical properties are not well studied and documented. This shortage has hindered the proper evaluation of this natural earth resource for their best uses, including their heat of combustion and utilization as sources of energy. This study attempted to address part of the inadequacies posed by the absence of detailed physicochemical characteristics of the Nigerian coals and their utilizations as alternative sources of energy.

2 Materials and Methods

Forty coal samples (4 per coal deposit) sampled by channel and grab methods from the coal seams and run-of-mine were used for analyses in this study. The coal samples include grab samples, channel samples and core samples.

O. Usman (✉) · T. Ako · L. Mohammed
Department of Geology, Federal University of Technology, Pmb, 65, Minna, Niger, Nigeria
e-mail: onoduku.usman@futminna.edu.ng

A. Çiner et al. (eds.), *Recent Research on Geomorphology, Sedimentology, Marine Geosciences and Geochemistry*, Advances in Science, Technology & Innovation, https://doi.org/10.1007/978-3-030-72547-1_82

2.1 Field Work and Samples Collection

During fieldwork, ten coal locations were selected within the country for this study. The ten locations were chosen to cover the whole length of Benue Trough and parts of the Anambra Basin. Coal samples from Ibobo, Udane Biomi and Ogboyoga (Kogi State), Iva Valley and Okpara (Enugu State) were obtained from coal seams exposed on the field either along river banks and beds, or in areas where the coal seams or beds have been exposed by erosion. Samples from Onyema (Enugu State), Owukpa (Benue State) and Kwaghshir (Lafia-Obi) (Nassarawa State) were obtained from old and abandoned coal mines, while in Okaba (Kogi State) and Maiganga (Gombe State) the samples were obtained from the recent mine sites.

Four representative coal samples were obtained at each of the ten study sites with the aid of a geological hammer. The sampling was done randomly, but in areas where the coal seams were well exposed as in Maiganga, and the samples were collected at the various coal seams seen in the mine site. During the sampling, a bulk sample of about 300 g each of coal was collected from four points within each of the study areas. The samples collected were sealed in polythene bags and were subsequently transferred into polyvinyl chloride (PVC) canisters and labeled appropriately for later transport to the laboratory for the various analyses. The coordinates of the sampling locations were taken with an Etrex Garmin model of GPS (Global Positioning Satellite). Location maps of the coal deposits were prepared from the GPS coordinates using ArcGis version 10.2.2.

2.2 Heat of Combustion, Proximate and Ultimate analyses of the Coals

Pulverized coal samples were analyzed for heat of combustion of forty samples (4 samples per coal deposit) from the ten studied coal deposits.

The heats of combustion of the coals were determined based on ASTM D5865 standards. The Ballistic Bomb Calorimeter was first standardized with benzoic acid of 6.32 kcal/g as its heat value. 0.5 g of each of the forty coal samples were placed in crucibles and the bomb body fastened and plugged to the thermocouple. The pressure discharge regulator was closed, and oxygen was supplied into the bomb until the pressure increased to 25 bars. The knob for firing was depressed and released for the bomb to be fired. The heat was given off, and the maximum deflection scale of the galvanometer was read and recorded. The maximum deflection obtained in the galvanometer was transformed to energy charge of the coal samples by contrasting the rise in galvanometer deflection with that achieved when a sample of identified heat amount of benzoic acid is combusted. The heat Q in KCal/g given off from the coal samples were calculated from Mason and Gandhi (1983) formula;

$$Q = \frac{G(\text{meter deflection} \times \text{calibration constant}}{\text{original mass of sample}} = \frac{(\partial_3 - \partial_1)\gamma}{Z} \quad (1)$$

where

∂_1 deflection of galvanometer without sample
∂_3 deflection of galvanometer with sample
Z mass of sample in gram
γ calibration constant

The results of the proximate and ultimate analyses carried out in a previous study by Mohammed et al. (2017) in conjunction with the results of the heat of combustion determined were used in this study to evaluate the energy potentials of the coals. The laboratory analyses were carried out at the Engineering Materials Development Institute (EMDI) of the National Agency for Science and Engineering Infrastructure (NASENI), Akure, Nigeria.

3 Results and Discussions

3.1 Field Results

The coal samples were obtained from ten studied coal deposits. Figure 1 shows the locations of the sampled coal deposits, while Table 1 indicates the information on the sample origins.

3.2 Heat of Combustion of the Coals

The heat of combustion of the coals as determined are indicated in Table 2.

On the basis of coal classification based on their respective heatof combustion according to Kumar and Saxena (2014), the analyzed coals are classified as indicated in Table 3.

3.3 Proximate and Ultimate Characteristics of the Coals

The proximate characteristics of the studied coal deposits are as shown in Table 4.

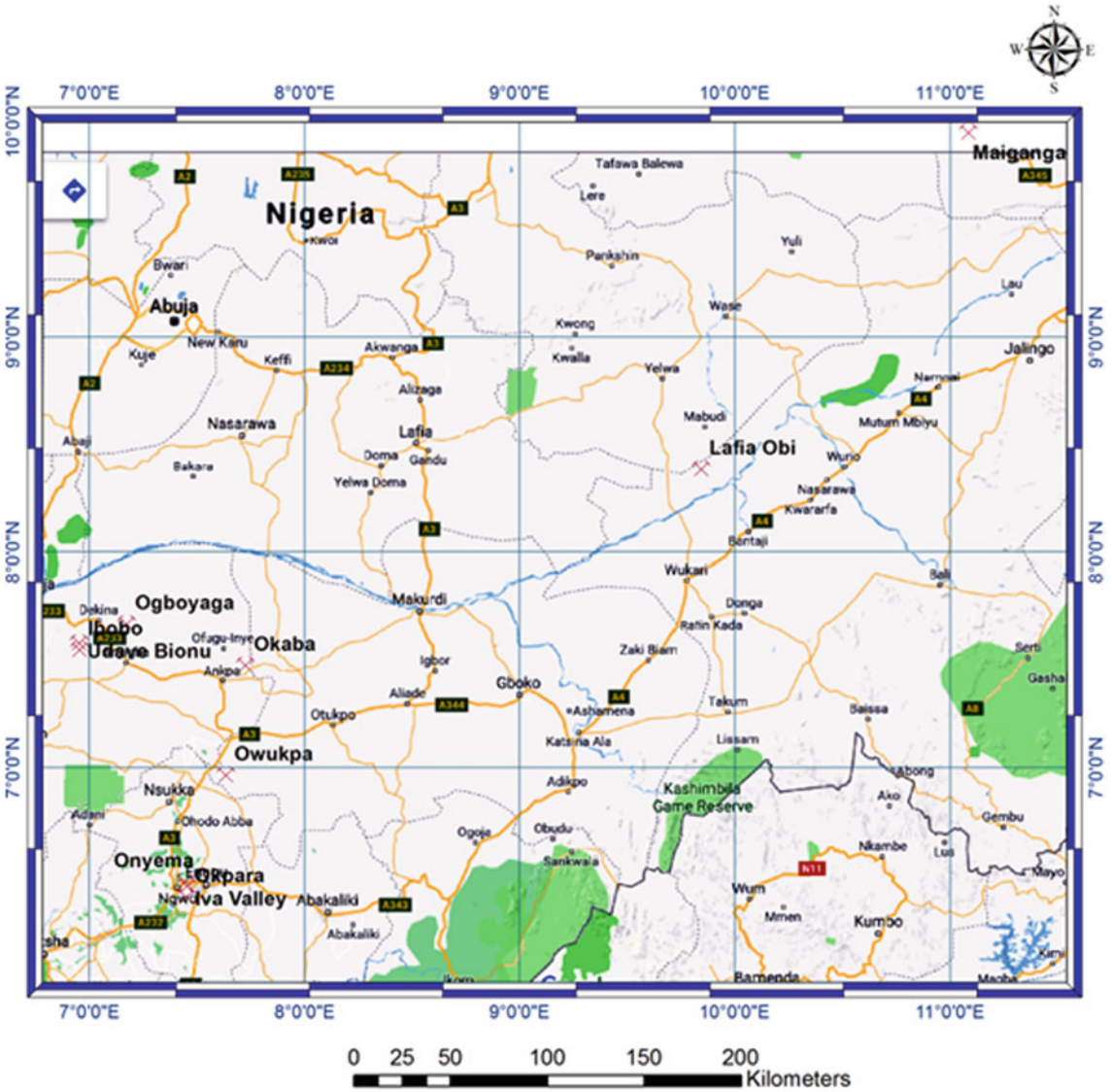

Fig. 1 Location map of the coal deposits where samples were obtained for the study

Table 1 Information on the coal samples origin

Coal deposit	Sample origin
Ibobo	Run-off-mine
Udane Biomi	River channel
Ogboyoga	River bank
Okaba	Mine face
Owukpa	Abandoned mine
Onyema	Coal outcrop
Okpara	Coal outcrop
Iva Valley	Coal outcrop
Maiganga	Mine face
Lafia Obi	Core sample

Table 2 Mean values of four measurements of heat of combustion for the coals

Coal deposit	Mean heat of combustion (Kcal/kg)
Iva valley	5990
Okaba	4723
Ibobo	4640
Obi–Lafia	4345
Owukpa	3780
Onyema	3742
Okpara	3569
Maiganga	2861
Udane–Biomi	2625
Ogboyoga	2220

Table 3 Classification of the analyzed coals based on heatof combustion

Grade	Analysed coal deposits
B	Iva valley
C	Okaba
D	Ibobo
D	Obi-Lafia
E	Owukpa
E	Onyema
E	Okpara
F	Maiganga
F	Udane-Biomi
G	Ogboyoga

3.4 The Potentials of the Coals as Sources of Energy

The Maiganga coal, having the highest moisture content of 11.01% (Table 4) which is far more than the acceptable value is considered least matured than the rest studied coals, while Udane Biomi coal deposit with the least moisture content of 2.45% is considered most matured. Hence, the rate of combustion of the coals increases in the same order because moisture content influences the heat of combustion of coals (Akinyemi et al. 2012). Also, the Lafia Obi, Udane Biomi, Okpara, Ibobo, Owukpa and Ogboyoga coal deposits have markedly high ash contents than the 10% generally considered for excellent metallurgical coke making (Ryemshak and Jauro 2013). In contrast, Onyema, Okaba, Maiganga and Iva Valley coals have ash contents that are considered optimum or below the specified value for coke making. The values of the volatile matters for the coals suggest that only Lafia Obi, Udane Biomi and Okpara coal deposits with volatile matter contents that fall within the specified range are suitable for metallurgical coke making. At the same time, Onyema, Okabe, Maiganga, Ibobo, Owukpa, Iva Valley and Ogboyoga coals are not good coke forming coals. The trend in the fixed carbon content suggests that the Udane Biomi coal with the highest fixed carbon content has most carbon for coke formation, followed by Obi-Lafia, Okpara, Owukpa, Onyema, Okaba, Iva Valley, Maiganga, Ibobo and Ogboyoga with the least fixed carbon content. From the results of the organic carbon content, the Iva Valley coal can be considered most matured of all the analyzed coals, while the Lafia Obi is considered the least matured. The nitrogen values for all the analyzed coals are generally low. The phosphorous contents of the coals fall within the acceptable limits for their uses, but those of sulfur concentrations exceed the acceptable limit of 1.5% to 1.6% (Mason and Gandhi 1983; Ryemshak and Jauro 2013). The heat combustion of the ten coal deposits (Table 2) are sufficiently high and can be utilized for the generation of power. The Iva Valley coal deposit with the highest heat of combustion of 5,990 kcal/kg could be the most excellent for heating and generation of power.

4 Conclusions

The selected ten studied Nigerian coals are situated within the Benue Trough and Anambra Basin. Based on the (Kumar and Saxena 2014) classification based on calorific value, the analyzed coals are grouped as Iva Valley–grade B, Okaba–grade C, Obi- Lafia–grade D, Ibobo–grade D, Onyema-grade E, Owukpa–grade E, Okpara–grade E, Udane Biomi-grade F, Maiganga-grade F and Ogboyoga G.

In terms of the technological applications of the studied coals, the heat of combustion of the coal deposits are sufficiently high and indicate their suitability for the generation of power.

The heat combustion of the ten coal deposits is sufficiently high and can be utilized for the generation of power. The Iva Valley coal deposit with the most significant heat of combustion of 5,990 kcal/kg could be the most excellent for heating and generation of power.

Table 4 Mean Proximate and ultimate characteristics of four measurements for the studied coal deposits

Locations	Lafia obi	Onyema	Okaba	Maiganga	Udane biomi	Okpara	Ibobo	Owukpa	Iva valley	Ogboyoga
Moisture Content (%)	6.62	5	7.98	11.01	2.45	7.03	9.23	7.23	4.07	3.62
Ash Content (%)	40.65	8.52	10.85	7.82	20.1	42.47	15.42	14.7	7.3	40.27
Volatile Matter (%)	11.12	67.6	63.9	67.35	19.6	22.5	62.97	56.6	74.22	45.57
Fixed Carbon (%)	41.6	18.87	17.26	13.81	57.85	27.98	12.36	21.46	14.4	10.52
Organic Carbon (%)	2.08	3.16	3.23	2.91	2.91	2.95	2.86	2.82	3.29	3.01
Total Nitrogen (%)	0.42	0.63	0.65	0.58	0.58	0.59	0.57	0.57	0.66	0.61
Phosphorus (%)	0.47	0.93	0.77	0.73	0.63	0.87	0.85	0.77	0.87	0.75
Sulfur (%)	0.74	1.27	1.9	0.96	1.58	1.24	2.03	1.74	1.9	1.36

References

Akinyemi, S.A., Akinlua, A., Gitari, W.M., Nyale, S.M., Akinyeye, R. O., Petrik, L.F.: An investigative study on the chemical, orphological and mineralogical alterations of dry disposed fly ash during sequential chemical extraction. Energy Sci. Technol. **3**(1), 28–37 (2012)

Kumar, V., Saxena, V.K.: Studies of the variation in coal properties of low volatile coking coal after beneficiation. Int. J. Comput. Eng. Res. **4**(1), 39–57 (2014)

Mason, D.M., Gandhi, K.N.: Formulas for calculating the calorific value of coal and coal chars: development, tests and uses. J. Fuel Process. Technol. **7**(1), 11–22 (1983)

Mohammed, L. M, Onoduku, U. S, Ako, T. A, Ogunbajo, M. I., & Musa, R.T. O.: Proximate and ultimate characteristics of some Nigerian coal deposits in benue trough and Anambra basin. Research journal of the department of geology, federal university of technology, Minna, Nigeria. Minna J. Geosci. **1**(2) (2017)

Obaje, N.G.: Geology and Mineral Resources of Nigeria, p. 221. Springer, Dordrecht Heidelberg London, New York (2009)

Raw Material Research and Development Council. Brief on Nigerian Coals (2015)

Ryemshak, S.A., Jauro, A.: Proximate analysis, rheological properties and technological applications of some Nigerian coals. Int. J. Ind. Chem. **4**(7), 1–7 (2013)

Acid Activation of Ypresian Clay from Central Tunisia, Synthesis of Porous Materials and Clarification of Soybean Oils

Mohamed Mosbahi, Mahmoud Khlifi, Fakher Jamoussi, and Ali Tlili

Abstract

The central objective of the present study is the investigation of acid activation of Ypresian clays by HCl. The studied clay samples are taken from the Paleocene-Eocene transition between El Haria and Chouabine formations of lithological sections made in the Ypresian series from Meknassy-Mezzouna basin (Central Tunisia). This clay was subjected to chemical and mineralogical characterizations. The mineralogical study showed that the studied clay is composed of smectite associated with sepiolite, palygorskite and kaolinite. The accessory minerals are quartz and dolomite. The raw sample shows a specific surface that is about 30.41 m^2/g, which improves by HCl activation. The optimal activation conditions were obtained at a temperature of 75 °C for 4 h at a concentration of 3 N of the added HCl. These conditions increased the specific surface area up to 100 m^2/g, enhanced the crystal growth of quartz, gypsum and feldspar, yielded partial dissolution of the clay particles especially smectite and fibrous clay and the total dissolution of dolomite. Regarding the clarification of neutral soybean oils, the acid activation of Ypresian clays provides better results compared to those given by primary activation and by the Tonsil product used for by many refinery companies. Indeed, the bleaching capacity of the acid-activated clay is 78.08%, compared to 71.48% from the primary activation and the Tonsil (56.12%).

M. Mosbahi (✉) · A. Tlili
College of Sciences, Department of Earth Sciences, Sfax University, GEOGLOB Laboratory, Sokra road 3.5 Km, Sfax, Tunisia

M. Khlifi
National School of Engineers of Sfax, 3E Laboratory, Sfax, Tunisia

F. Jamoussi
Laboratory of Georesources, CERTE, CNRSM BP 273, 8020 Soliman, Tunisia

Keywords

Acid activation • Ypresian clay • Bleaching capacity • Soybean oils • Meknassy-Mezzouna region

1 Introduction

This study aims at the industrial exploitation of the Paleocene-Eocene clays of the Meknassy-Mezzouna basin in centre western Tunisia. Specifically, the goal is to determine the optimal conditions for the acid activation of the Ypresian clay by HCl and deliver the conditions of the Soybean oils clarification. Raw clays were selected according to the relatively high-specific surface (about 30.41 m^2/g), the smectite richness and the presence of the fibrous clay (palygorskite and sepiolite). The clay minerals are often used in the vegetable oils purification and clarification (Christidis et al. 1997; Gannouni et al. 1999; Mosbahi et al. 2007). The bentonites activation is commonly performed by sulfuric acid or hydrochloric acid with heating for a few hours (Mosbahi 2007; Benguella and Yacouta-Nour 2009; Didi et al. 2009). On the one hand, previous studies have shown that hydrochloric acid is the best clay activating agent (Mathers et al. 1954; Pesquera et al. 1992). Moreover, acid activations trough HCl allows the increase in the specific surface, thus enhancing the formation of active sites in the crystal lattice of the clay minerals. The mineralogical and chemical analyses, the specific surface and the bleaching capacity of the natural and activated clays of the basin will be compared with those of imported bleaching earth (Tonsil) used in the SATHOP and SOZITEX industry.

2 Materials and Methods

The studied clay was collected from the Paleocene-Eocene transition (Ypresian) of the Meknassy-Mezzouna basin (centre western Tunisia). The raw samples were suspended

A. Çiner et al. (eds.), *Recent Research on Geomorphology, Sedimentology, Marine Geosciences and Geochemistry*, Advances in Science, Technology & Innovation, https://doi.org/10.1007/978-3-030-72547-1_83

in water for a few days, and sieved through a sieve of 40 µm to remove impurities, and then dried in an oven at 60 °C for several days. All these samples were characterized by XRD, X-ray fluorescence and SEM observations.

3 Results

3.1 Specific Surface of the Samples Before and After Acid Activation

The results are summarized in Table 1. The best activation results obtained with HCl (3 N) correspond to clays activated for four hours. For the different times (2 h, 4 h, 6 h), the most interesting result of the specific surface of the treated clay samples obtained in a temperature of 75 °C.

3.2 X-ray Diffraction of Raw and Activated Clay (Fig. 1 a-b-c)

Figure 1 shows that the studied sample corresponds to smectite rich clay with minor kaolinite, palygorskite and sepiolite contents. After acid activation (HCl (3 N)) at 75 °C during four hours (Fig. 1a), most clay minerals, especially smectite and fibrous clay, are partially dissolved, whereas dolomite disappeared completely. The signals of quartz crystals, gypsum and feldspar are enhanced.

3.3 Chemical Analysis

The amount of SiO_2 measured in the raw clay from the Ypresian series is 48.68 wt% against 60 wt% in the acid-activated clay and 89% in the Tonsil (Table 2). The concentration of Al_2O_3 in the raw clay, which is related to smectite, sepiolite, palygorskite and kaolinite as observed from SEM analysis and confirmed by XRD, is of 15.51 wt %. The concentration of Al_2O_3 varied between 13.54, 11.20 and 10.30 wt% and decreased with the activation times 2, 4 and 6 h, respectively. However, the concentration of Al_2O_3 in the Tonsil is much less in the investigated clays. The concentration of Al_2O_3 decreases with the activation time as the concentration of SiO_2 increased. The concentration of MgO in the raw clay is 2.54 wt% due to the presence of fibrous clays, smectite and dolomite. However, the weight percentages of MgO decreases with the activation time in consequence of the total dissolution of dolomite.

3.4 SEM Investigations Before and After Treatment

Before activation, the SEM images of the selected raw clays from the Ypresian series (Figs. 2a–d) revealed the foliated smectitic clays containing weathered dolomite, which is confirmed by signals related to Ca and Mg in the EDX analysis of this rhombohedral dolomite crystal (Fig. 2a). This dolomite is more or less the altered forms embedded in the smectic matrix. In Fig. 2b, we observed clay in the thorny shape and thread-like facies of palygorskite. The fibrous clays are Mg-rich as revealed by the EDX analysis, which can be due to sepiolite. After acid activation (HCl, 3 N), the SEM images (Figs. 2c–d) reveal angular edges of smectite platelets resulting from partial dissolution. The total dissolution of rhombohedral dolomites is also observed, the remaining traces of rhombohedral cavities.

3.5 Bleaching Tests of Soybean Oils

In the best conditions of acid activation, treated Soybean oil with activated clay shows an optical density (0.515) which is inferior to that of untreated oil (2.35), oil-treated by raw clay (1.110), oil-treated by Tonsil (1.031), and oil-treated by primary activation (0.67) (Mosbahi et al. 2017). Similarly, the bleaching capacity is increasing using activated clay (78.08%) rather than using raw clay (52.76%) and Tonsil (57.73%).

Table 1 Specific surface and porosity of raw clay, of tonsil, of basic-activated clay (Mosbahi et al. 2017) and its activated equivalents for different HCl amounts at different times, under 75 °C

Samples	Raw clay	Tonsil	Basic-activated clay (5% Na_2CO_3, 75 °C, 1 h) (Mosbahi et al. 2017)					Acid-activated clay		
				Activated clays at different proportions of HCl (75 °C, 1 h)				Activated clays by HCl (3 N) at different times at 75 °C		
				1 N	2 N	3 N	4 N	2 h	4 h	6 h
Ss (m^2/g)	30.41	51	58.63	50.9	52	56	53	76	100	98
P (%)	17.26	28.95	33.71	28.89	29.51	31.78	30.08	42.87	56.76	55.63

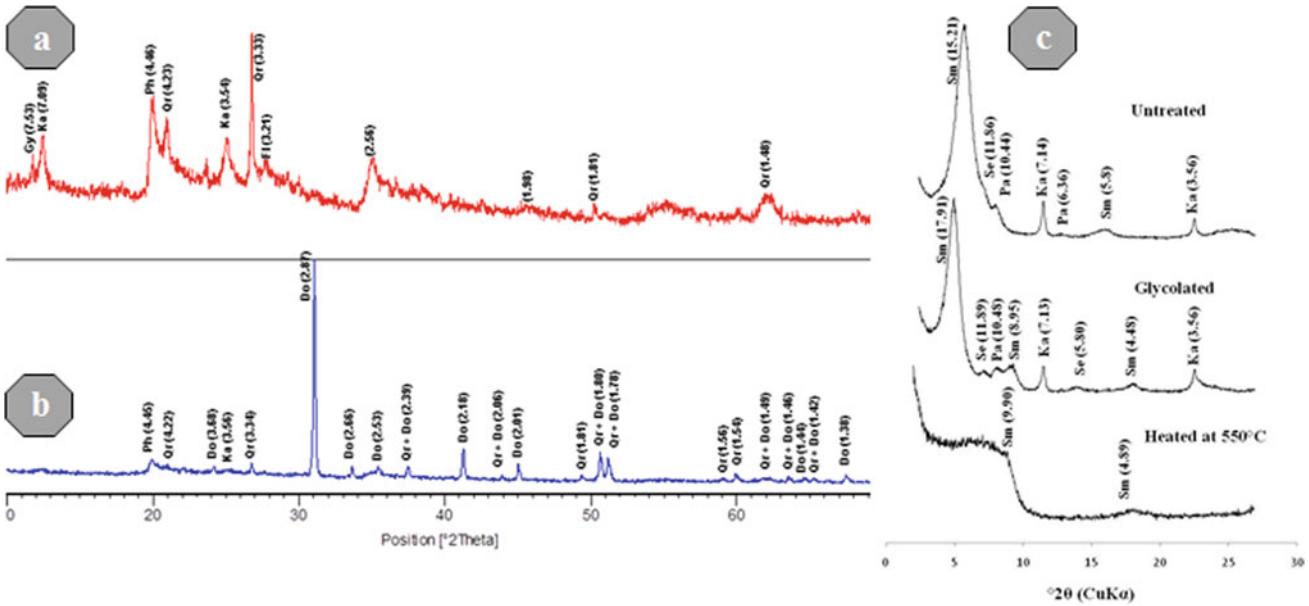

Fig. 1 XRD patterns (CuKα radiation) of the raw clay (**a**), the activated clay (**b**) and of three oriented clay fractions (**c**). (Sm) smectite; (Pa) palygorskite; (Se) sepiolite; (Ka) kaolinite; (Fl) feldespar; (Do) dolomite; (Qr) quartz; (Gy) gypsum

Table 2 Chemical analysis of the Tonsil, the raw clay, activated clay, and rate of clays destruction (%) as a function of time (2 h–4 h–6 h)

Oxydes (%)	Tonsil	Raw clay	Acid-activated clay (2 h)	Acid-activated clay (4 h)	Acid-activated clay (6 h)
SiO_2	89	48.68	54.1	60.02	61.03
Al_2O_3	3.5	15.51	13.54	11.20	10.30
Fe_2O_3	0.3	5.65	3.56	1.02	0.53
MgO	0.18	2.54	2.0	1.55	1.36
CaO	–	1.41	0.41	0.35	0.27
K_2O	0.2	0.95	1.03	0.66	0.43
SO_3	0.2	0.38	0.10	0,08	0.07
Na_2O	0.2	0.29	0.29	0.09	0.15
P_2O_5	1	1.2	1.2	0	0
LOI	4 0.8	23.4	23.39	24.35	24.77
Total %	99.38	100.01	99.6	99.32	98.91

4 Discussion

The results of X-ray diffraction (Fig. 1a–c) showed that the raw clay is composed of a higher percentage of smectite of about 82% in the presence of a small amount of sepiolite, palygorskite, kaolinite, dolomite and quartz, (Fig. 1b–c). After acid-activation, mineralogical transformations following to dissolution and recrystallization (Figs. 1a and 2) have been noted through X-ray diffraction and SEM analyses. The crystallization of the pre-existing minerals and the synthesis of porous materials have been observed mainly after acid activation by HCl in optimal conditions (3 N, 75 °C, 4 h) (Fig. 2a–d). The total disappearance of dolomite is caused by a severe dissolution of Mg^{2+} and Ca^{2+}.

The moderate dissolution of Al^{3+}, Ca^{2+}, Mg^{2+}, Fe^{2+} has advanced significantly in the mid-existing crystals (smectite, sepiolite, palygorskite and kaolinite), which acted as a filter against organic micelles. Al_2O_3, Fe_2O_3, MgO, CaO corresponded to the significant elements, whose dissolution is progressive and hardly released (Srasra and Ayadi-Trabelsi 2000; Mosbahi 2007). The results of the clay activation of

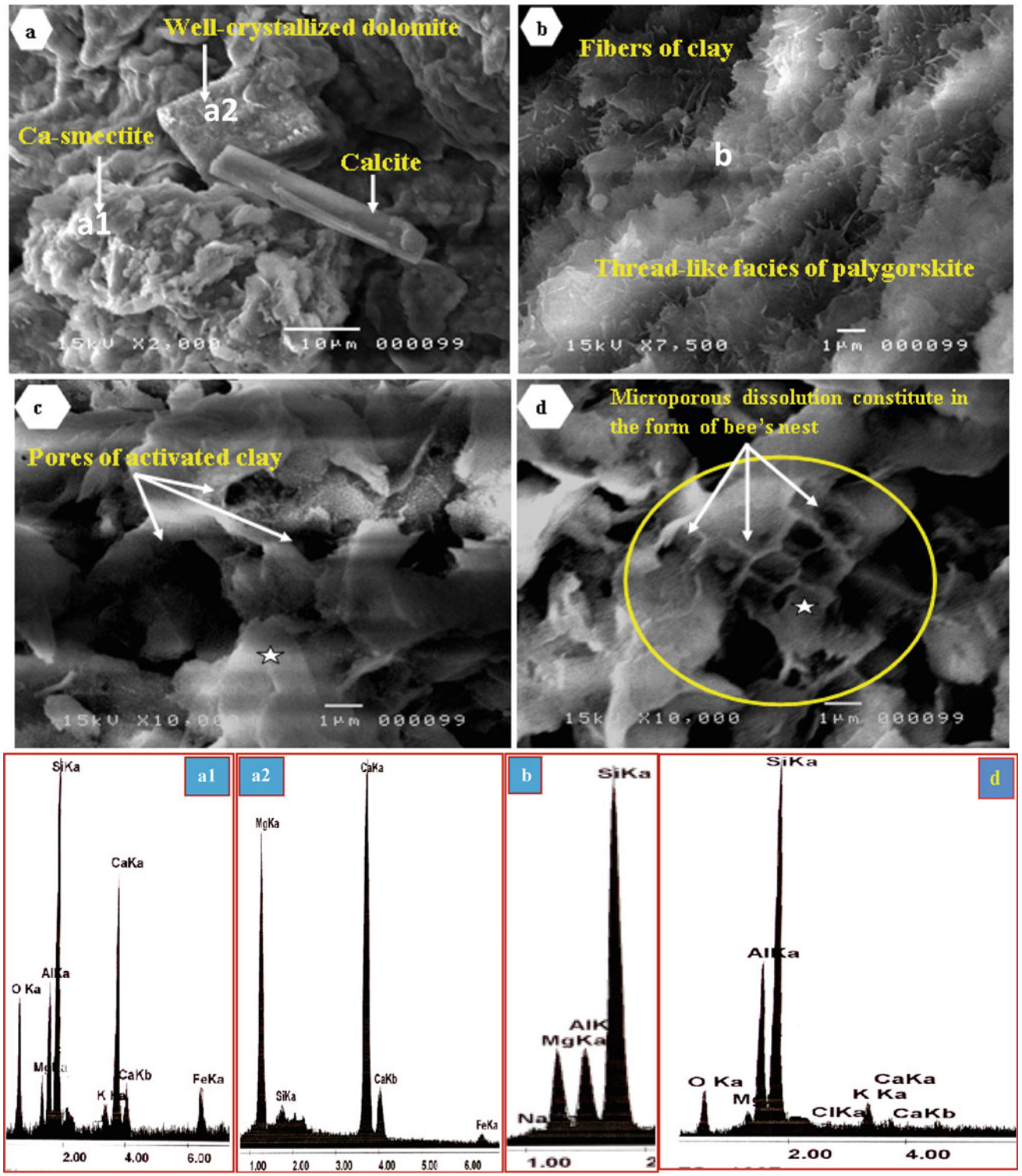

Fig. 2 SEM observation of raw clay samples (**a**–**b**) and activated clay (**c**–**d**). (**a**1) EDX of the clay reveals the presence of Ca, Si and Al; (**a**2) Microanalyses X reveals two strong peaks of Mg and Ca; **b** EDX of the fibrous clay reveals the presence of Mg, Si and Al

the Meknassy-Mezzouna basin have shown that the best activation conditions were obtained with HCl (3 N) at 75 °C for 4 h. Under these conditions, the specific surface area increased from 30.41 m2 g-1 in the raw clay to 100 $m^2\ g^{-1}$ in the activated clay (Table 1).

5 Conclusions

The acid activation of the Ypresian clays from the Meknassy-Mezzouna basin shows that the best results are obtained with HCl (3 N) for 4 h at 75 °C. In these conditions, the activated clays give comparable results of neutral soybean oil clarification to the Tonsil industrial product used in the clarification of oils by SATHOP and SOZITEX companies. Therefore, the acid activation of these Ypresian clays increases the specific surface from 30.41 to 100 m^2/g and promotes the formation of porous materials. Besides, raw clays give bleaching power of soybean oils slightly below the Tonsil. Nevertheless, once activated (HCl (3 N), 75 °C, 4 h), they give significantly better results than the Tonsil. Then, satisfactory clarification of soybean oils can be obtained by 0.75% of activated clay.

References

Benguella, B., Yacouta-Nour, A.: Adsorption of bezanyl red and nylomine green from aqueous solutions by natural and acid-activated bentonite. Desalination **235**, 276–292 (2009)

Christidis, G.E., Scott, P.W., Dunham, A.C.: Acid activation and bleaching capacity of bentonites from the Islands of milos and chios, Aegean. Greece. Appl. Clay Sci. **12**, 329–347 (1997)

Didi, M.A., Makhoukhi, B., Azzouz, A., Villemin, D.: Colza oil bleaching through optimized acid activation of bentonite; a comparative study. Appl. Clay Sci. **42**, 336–344 (2009)

Gannouni, A., Bellagi, A., Bagane, M.: Préparation d'une argile activée pour la décoloration de l'huile d'olive. Ann. Chim. Sci. Mat **24**, 407–416 (1999)

Mathers, A.C., Weed, S.B., Coleman, N.T.: The effect of acid heat treatment on montmorillonites. Clay Clay Miner. **3**(1), 403–412 (1954)

Mosbahi, M.: Caractérisation minéralogique des argiles de la formation El Haria du bassin Meknassy-Mezzouna: Essais de clarification des huiles végétales de soja, p. 85. Master GAREN, Sfax-University, Tunisia (2007)

Mosbahi, M., Tlili, A., Khlifi, M., Jamoussi, F.: Basic activation of lower eocene clay from Meknassy-Mezzouna basin (centerwestern Tunisia), synthesis of zeolite and clarification of soybean oils. Appl. Clay Sci. **138**, 1–11 (2017)

Pesquera, C., Gonzalez, F., Benito, I., Blanco, C., Mendioroz, S., Pajares, J.: Passivation of a montmorillonite by the silica created in acid activation. J. Mat. Chem. **2**, 907–912 (1992)

Srasra, E., Ayadi-Trabelsi, M.: Textural properties of acid actived glauconite. Appl. Clay Sci. **17**, 71–84 (2000)